11.3.64

THE FLOW OF GASES THROUGH REACTOR GRAPHITES.

by

G. J. Field, B.E. (Hons.)

(Department of Mining, Metallurgical, and Chemical Engineering).

A Thesis
Submitted for the Degree of
Doctor of Philosophy
in the
Faculty of Engineering
of the
University of Adelaide.

February
1963

TABLE OF CONTENTS

Section	Item	Page
1	INTRODUCTION	1
2	LITERATURE REVIEW	7
2.1	Gas Flow Through Porous Media	8
2.1.1	Introduction	8
2.1.1.1	Darcy's Law	9
2.1.1.2	The General Flow Equation	10
2.1.1.3	Particular Solutions to the Flow Equation	11
2.1.1.4	Distribution of Pressure for Flow Through Porous Media	14
2.1.1.5	The Concept of Permeability	18
2.1.1.6	Integration of the Permeability Equations	20
2.1.2	The Use of Models to Describe Pore Structures	22
2.1.2.1	Gas Flow Through Capillary Tubes	22
2.1.2.2	The Capillary Pore Model	26
2.1.2.3	Statistical Pore Models	28
2.1.2.4	Constriction-Type Pore Models	28
2.1.2.5	Miscellaneous Pore Models	29
2.1.3	The Viscous Flow Region	30
2.1.3.1	Viscous Flow Correlations	31
2.1.3.2	The Kozeny Theory	34
2.1.4	The Slip Flow Region	40
2.1.4.1	The Permeability Equations	41
2.1.4.2	Adzumi Equation	43
2.1.4.3	The Modified Kozeny Equation	45
2.1.4.4	Consolidated Porous Media	46
2.1.4.5	Other Correlations	49
2.1.5	The Knudsen Flow Region	49
2.1.5.1	The Transition Region	51

Section	Item	Page
2.1.5.2	Minima in the K-p_m plots	53
2.1.5.3	The Time-Lag Method	61
2.1.6	The Flow of Adsorbable Gases	73
2.1.6.1	The Calculation of Surface Diffusion Coefficients	75
2.1.6.2	Experimental Observations	76
2.1.6.3	Criticism of the Surface Flow Theory	78
2.1.7	The Turbulent Flow Region	79
2.1.7.1	The Mechanism of Turbulent Flow	80
2.1.7.2	Turbulent Flow Correlations	82
2.1.8	The Measurement of Permeability Coefficients	93
2.1.8.1	The Theory of Permeability Measurements	93
2.1.8.2	The Methods Used for Determining Permeability Coefficients	94
2.1.9	Summary	108
2.1.9.1	Introduction	108
2.1.9.2	The Use of Models to Describe Pore Structures	109
2.1.9.3	The Viscous Flow Region	109
2.1.9.4	The Slip Flow Region	110
2.1.9.5	The Knudsen Flow Region	110
2.1.9.6	The Flow of Adsorbable Gases	111
2.1.9.7	The Turbulent Flow Region	111
2.1.9.8	The Measurement of Permeability Coefficients	112
2.2	The Porosity of a Porous Medium	112
2.2.1	Theory	112
2.2.2	The Measurement of the Porosity	113
2.2.2.1	The Helium Displacement Method	114
2.2.3	Summary	115
2.3	The Surface Area of a Porous Medium	115
2.3.1	Theory	115

Section	Item	Page
2.3.2	The Measurement of the Surface Area	116
2.3.2.1	The Gas Adsorption Methods	117
2.3.2.2	The Permeability Method	123
2.3.2.3	Comparison of the Adsorption and Permeability Methods	124
2.3.3	Summary	127
2.4	The Pore Size Distribution of a Porous Medium	128
2.4.1	The "Size" of the Pores	128
2.4.2	The Pore Size Distribution	130
2.4.3	The Pore Size Distribution and the Permeability	131
2.4.3.1	Equations Based on Capillary Models	131
2.4.3.2	Equations Based on Statistical Models	133
2.4.3.3	Other Expressions	134
2.4.3.4	Experimental Verification	135
2.4.4	The Measurement of the Pore Size Distribution	136
2.4.4.1	The Capillary Pressure Methods	136
2.4.4.2	The Capillary Condensation Method	141
2.4.4.3	Comparison Between the Capillary Pressure and Capillary Condensation Methods	142
2.4.5	Summary	143
2.5	The Tortuosity of a Porous Medium	144
2.5.1	Definition of the Tortuosity	144
2.5.2	The Tortuosity in Permeability Studies	148
2.5.3	The Tortuosity in Electrical Resistivity Measurements	149
2.5.4	The Tortuosity in Gaseous Diffusion Experiments	153
2.5.5	The Relation Between the Tortuosity Factors	154
2.5.5.1	The Electrical and Permeability Tortuosity Factors	154

Section	Item	Page
2.5.5.2	The Electrical and Diffusion Tortuosity Factors	157
2.5.6	Tortuosity Measurements by Electrical Resistivity Methods	158
2.5.6.1	Methods for Non-conducting Porous Media	159
2.5.6.2	Methods for Conducting Porous Media	160
2.5.6.3	Recommended Measuring Method	162
2.5.7	Summary	163
3	APPARATUS AND EXPERIMENTAL PROCEDURE	165
3.1	Gas Flow Measurements	166
3.1.1	Materials for the Permeability Determinations	166
3.1.1.1	Sample Preparation	166
3.1.1.2	Gases	169
3.1.2	Description of the Low Pressure (Vacuum) Permeability Apparatus	171
3.1.2.1	The Permeability Cells	171
3.1.2.2	Pressure Measurement	175
3.1.2.3	The Vacuum System	176
3.1.2.4	The Gas System	177
3.1.2.5	Volume Calibration	177
3.1.3	Experimental Procedures for the Low Pressure Apparatus	178
3.1.3.1	The Pressure Increase and Time-Lag Method	178
3.1.3.2	The Pressure Decay Method	181
3.1.3.3	The Pressure Equalization Method	183
3.1.3.4	The Low Pressure Flow Method	184
3.1.4	Description of the High Pressure Permeability Apparatus	185
3.1.4.1	The Permeability Cells	188
3.1.4.2	Pressure Measurement	189
3.1.4.3	Flow-rate Measurement	190
3.1.4.4	The Gas Introduction System	193
3.1.4.5	The Vacuum System	194

Section	Item	Page
3.1.5	Experimental Procedure for the High Pressure Apparatus	195
3.1.6	The Measurement of the Pressure Distribution	198
3.1.6.1	Sample Preparation	198
3.1.6.2	Gases	198
3.1.6.3	Description of the Apparatus	200
3.1.6.4	Experimental Procedure	200
3.2	The Porosity Measurements	202
3.2.1	Materials	202
3.2.1.1	Sample Preparation	202
3.2.1.2	Gases	202
3.2.2	Description of the Apparatus	203
3.2.2.1	Pressure Measurement	203
3.2.2.2	Volume Calibrations	205
3.2.2.3	Temperature Measurement and Control	206
3.2.3	Experimental Procedure	206
3.2.3.1	Outgassing of the Sample	206
3.2.3.2	Measurement of the Dead Space Volume	207
3.2.3.3	Measurement of the Bulb Volume	207
3.3	The Surface Area Determinations	208
3.3.1	Materials	208
3.3.2	Description of the Apparatus	209
3.3.2.1	Pressure Measurement	209
3.3.2.2	Temperature Measurement	210
3.3.3	Experimental Procedure	210
3.3.3.1	Outgassing of the Sample	210
3.3.3.2	Calibration of the Free Space and Dead Space Volumes	211
3.3.3.3	Isotherm Determination	211
3.4	The Pore Size Distribution Measurements	212
3.4.1	The C.S.I.R.O. Measurements	213
3.4.1.1	Materials	213

Section	Item	Page
3.4.1.2	Description of the Apparatus	213
3.4.1.3	Experimental Procedure	214
3.4.2	The A.A.E.C. Measurements	215
3.4.2.1	Materials	215
3.4.2.2	Description of the Apparatus	215
3.4.2.3	Experimental Procedure	216
3.5	The Electrical Resistivity Measurements	216
3.5.1	Materials	217
3.5.1.1	Sample Preparation	217
3.5.1.2	Electrolytes	217
3.5.2	Description of the Apparatus	217
3.5.2.1	The Formation Factor Cell	218
3.5.2.2	The Arrangement for Evacuating and Filling the Cell	219
3.5.2.3	The Electrical Equipment	222
3.5.2.4	The Conductivity Bridge	223
3.5.3	Experimental Procedure	223
3.5.3.1	Measurement of the Decomposition Potential	224
3.5.3.2	Preparation of the Cell and Sample	226
3.5.3.3	Electrical Resistivity Measurements	227
4	RESULTS	229
4.1	The Gas Flow Measurements	229
4.1.1	P.G. 60 Graphite	229
4.1.2	Acheson "A" Graphite	235
4.1.2.1	The Low Pressure Determinations	236
4.1.2.2	The High Pressure Determinations	245
4.1.3	Morgan "EY9" Graphite	248
4.1.3.1	The Low Pressure Determinations	249
4.1.3.2	The High Pressure Determinations	258
4.1.4	Impregnated Graphite	262
4.1.4.1	The Low Pressure Determinations	262
4.1.4.2	The High Pressure Determinations	271

Section	Item	Page
4.1.5	Pressure Distribution Measurements	276
4.1.5.1	P.G. 60 Graphite	279
4.1.5.2	Acheson "A" Graphite	280
4.1.5.3	Morgan "EY9166" Graphite	286
4.2	The Porosity Measurements	289
4.3	The Surface Area Measurements	292
4.4	The Pore Size Distribution Measurements	297
4.4.1	The C.S.I.R.O. Measurements	298
4.4.2	The A.A.E.C. Measurements	301
4.4.3	The Estimation of Pore Properties from the Pore Size Distribution	306
4.5	The Electrical Resistivity Measurements	307
4.5.1	P.G. 60 Graphite	308
4.5.2	Acheson "A" Graphite	309
4.5.3	Morgan "EY9" Graphite	314
4.5.4	Impregnated Graphite	316
5	DISCUSSION OF RESULTS	318
5.1	The Gas Flow Measurements	319
5.1.1	P.G. 60 Graphite	319
5.1.1.1	The Curvature of the K-p_m plots	319
5.1.1.2	The Flow Phenomenon	325
5.1.1.3	The Values of B_o and K_o	327
5.1.1.4	The Values of β	328
5.1.1.5	Anisotropy of P.G. 60 Graphite	329
5.1.2	Acheson "A" Graphite	329
5.1.2.1	The Experimental Methods	329
5.1.2.2	The Values of B_o and K_o	332
5.1.2.3	Anisotropy of Acheson "A" Graphite	335
5.1.2.4	The High Pressure Flow Phenomenon	337
5.1.3	Morgan "EY9" Graphite	359
5.1.3.1	The Experimental Methods	359

Section	Item	Page
5.1.3.2	The Values of B_o and K_o	362
5.1.3.3	Anisotropy of Morgan "EY9" Graphite	365
5.1.3.4	Transient Flow Measurements	366
5.1.3.5	Minima in the K-p_m Plots	395
5.1.3.6	The High Pressure Determinations	410
5.1.4	Impregnated Graphite	414
5.1.4.1	The Low Pressure Experimental Methods	414
5.1.4.2	The Values of B_o and K_o	422
5.1.4.3	Transient Flow Measurements	424
5.1.4.4	Minima in the K-p_m Plots	434
5.1.4.5	Flow at High Pressures	435
5.1.4.6	The Freon High Pressure Determination	437
5.1.5	Pressure Distribution Measurements	441
5.1.5.1	Equations for the Pressure Distribution Curves	442
5.1.5.2	Consequences of the Pressure Distribution Equations	445
5.1.5.3	The Experimental Pressure Distributions	447
5.1.5.4	Comparison Between the Experimental and "Ideal" Pressure Distributions	450
5.1.5.5	The Determination of the a/b Values	451
5.1.5.6	The Inhomogeneity of the Graphite	453
5.1.5.7	Accuracy of the Distribution Measurements	454
5.2	The Porosity Measurements	457
5.2.1	The Accuracy of the Measurements	457
5.2.2	The Values of the Pore Properties	458
5.3	The Surface Area Measurements	460
5.3.1	The Accuracy of the Method of Measurement	460
5.3.2	The Surface Area of Acheson "A" Graphite	462
5.3.3	The Surface Area of Impregnated Graphite	463

Section	Item	Page
5.4	The Pore Size Distribution Measurements	465
5.4.1	Comparison Between the C.S.I.R.O. and A.A.E.C. Measurements	465
5.4.2	Significance of the Measurements	466
5.4.3	The Estimation of the Pore Properties from the Pore Size Distribution	468
5.5	The Electrical Resistivity Measurements	470
5.5.1	The Method of Measurement	470
5.5.2	The Values of F and q	473
5.5.3	Correlation of F with ε and K	476
5.6	Permeability and the Pore Structure	478
5.6.1	Calculation of the Pore Properties from the Permeability	479
5.6.1.1	The Carman-Arnell Equation	479
5.6.1.2	The Hutcheon, Longstaff, and Warner Method	480
5.6.1.3	The Adzumi Method	482
5.6.1.4	The Transient Flow Method	483
5.6.1.5	The Pore Size Distribution Method	484
5.6.2	Comparison of the Pore Properties	485
5.6.2.1	The Bulk Density ρ_b	485
5.6.2.2	The Porosity ε	486
5.6.2.3	The Mean Pore Radius r_m	488
5.6.2.4	The Surface Area S_g	490
5.6.2.5	The Tortuosity Factor τ	491
5.6.3	Deductions Concerning the Pore Structure	494
6	CONCLUSIONS	496
6.1	The Permeability Measurements	496
6.2	High Pressure Flow Results	498
6.3	Low Pressure Flow Phenomena	500
6.4	The Pressure Distribution Measurements	501
6.5	The Pore Properties	503
6.6	Recommendations	505

Section	Item	Page
Appendix		
A	THE GRAPHITE SAMPLES	507
A.1	Details of the Reactor Graphites	507
A.2	The Graphite Samples for Permeability Determinations	507
A.2.1	Details of the Permeability Samples	507
A.2.2	Description of the Sample Holders	507
A.3	The Graphite Specimens for the Pressure Distribution Measurements	513
A.4	The Graphite Samples for the Porosity and Surface Area Determinations	513
A.5	The Graphite Samples for the Pore Size Distribution Measurements	513
A.6	Details of the Graphite Samples for the Electrical Resistivity Determinations	514
B	GAS PROPERTIES	519
C	THE PERMEABILITY DETERMINATIONS	520
C.1	Volume Calibrations for the Low Pressure Apparatus	520
C.2	The Pressure Increase/Time-Lag Method	520
C.2.1	The Theory of the Pressure Increase Method	520
C.2.2	Type Calculation for the Pressure Increase Method	523
C.2.3	Experimental Accuracy	529
C.3	The Pressure Decay Method	530
C.3.1	The Theory of the Pressure Decay Method	530
C.3.2	Type Calculation for the Pressure Decay Method	532
C.3.3	Experimental Accuracy	535
C.3.4	The Pressure Equalization Method	536
C.4	The Low Pressure Flow Method	537
C.5	The High Pressure Flow Method	537

Section	Item	Page
C.5.1	The Theory of the High Pressure Flow Method	537
C.5.2	Type Calculation for the High Pressure Flow Method	539
C.5.3	Experimental Accuracy	543
D	CORRELATION OF THE HIGH PRESSURE FLOW RESULTS	545
D.1	Theory of the Green and Duwez Method	545
D.2	Type Calculation of the f-N_{Re} Plot	546
D.3	The Deviations Due to Slip Flow	550
E	THE DISTRIBUTION OF PRESSURE FOR GAS FLOW IN POROUS MEDIA	553
E.1	Derivation of the Equations for the Pressure Distribution	553
E.2	Comparison of the Pressure Distributions	559
E.3	Reprint of a Published Paper	566
F	THE POROSITY DETERMINATIONS	567
F.1	The Theory of the Porosity Determinations	567
F.2	Type Calculation of the Porosity	568
G	THE SURFACE AREA DETERMINATIONS	571
G.1	The Theory of the Krypton Surface Area Determinations	571
G.2	Type Calculation of the Surface Area	572
H	THE PORE SIZE DISTRIBUTION MEASUREMENTS	576
H.1	Theory	576
H.2	Estimation of Pore Properties from the Pore Size Distribution	576
J	THE ELECTRICAL RESISTIVITY MEASUREMENTS	580
J.1	The Theory of the Electrical Resistivity Measurements	580
J.2	Type Calculation of the Electrical Tortuosity Factor	580
K	DETAILED PERMEABILITY RESULTS	583

Section	Item	Page
K.1	List of the Permeability Determinations	583
K.2	The Low Pressure Determinations	587
K.3	The High Pressure Determinations	615
K.4	The Pressure Distribution Measurements	630
	BIBLIOGRAPHY	636
	GLOSSARY OF SYMBOLS	652

LIST OF TABLES

Table	Title	Page
2.1-1	Values of τ^2 and $\sigma_1/k_1\tau^2$ for Consolidated Media	48
3.1-1	Reactor Graphites	166
4.1-1	Permeability Results for P.G. 60 Graphite Samples	233
4.1-2	Permeability Results for Acheson "A" Graphite Samples	242
4.1-3	Permeability Results for Morgan "EY9" Graphite Samples	252
4.1-4	Permeability Results for Impregnated Graphite Samples	268
4.1-5	Values of a and b for Detmns. No. G:4 and No. G:5	289
4.2-1	Summary of the Results of the Porosity Measurements	293
4.3-1	Summary of the Results of the Krypton Surface Area Determinations	293
4.4-1	Values of the Pore Properties Estimated from the Pore Size Distribution Data	304
4.5-1	Results of the Electrical Resistivity Measurements	312
4.5-2	Summary of Electrical Resistivity Results	313
5.1-1	Summary of the Permeability Results	320-2
5.1-2	Critical Mean Pressures for P.G. 60 Determinations	324
5.1-3	Values of B_o and β Obtained by the $\alpha-\beta$ Method for the High Pressure Permeability Determinations	347
5.1-4	Limiting Values of the Time-Lags for Morgan "EY9" Samples	368
5.1-5	Calculated Values from Time-Lag Measurements on Morgan "EY9" Samples	368
5.1-6	Minima Details for Morgan "EY9" and Impregnated Graphites	396
5.1-7	Intercept Values of the Time-Lags for Impregnated Graphite Sample No. K42	426

Table	Title	Page
5.1-8	Calculated Values from Time-Lag Measurements on Impregnated Graphite Sample No. K42	426
5.6-1	Pore Properties Calculated from the Permeability Results	481
5.6-2	Pore Properties Calculated by the Adzumi Method	483
5.6-3	The Properties Calculated from Transient Flow Results	483
5.6-4	Values of the Bulk Density ρ_b (g/cm^3)	486
5.6-5	Values of the Porosity ε (cm^3/cm^3)	487
5.6-6	Values of the Mean Pore Radius r_m (microns)	488
5.6-7	Values of the Surface Area S_g (m^2/g)	490
5.6-8	Values of the Tortuosity Factor τ (cm/cm)	492
A.1-1	Details of the Reactor Graphites	508
A.2-1	Details of the Graphite Samples for the Permeability Determinations	509
A.3-1	Details of the Graphite Specimens for Pressure Distribution Measurements	515
A.4-1	Details of the Graphite Samples for Porosity and Surface Area Measurements	516
A.5-1	Details of the Graphite Samples for the C.S.I.R.O. Pore Size Distribution Measurements[240]	517
A.6-1	Details of the Graphite Samples for Electrical Resistivity Determinations	518
B.1-1	Properties of the Gases	519
C.1-1	Volumes of Sections of the Low Pressure Permeability Apparatus	521
C.2-1	Experimental Results for a Pressure Increase Determination (No. L:49)	524-6
C.2-2	Permeability Results for a Pressure Increase Determination (No. L:49)	526
C.3-1	Experimental Results for Detmn. No. L:53	533
C.3-2	Permeability Results for a Pressure Decay Determination (No. L:53)	533

Table	Title	Page
C.5-1	Experimental Results for a High Pressure Flow Determination (No. H:20)	540
C.5-2	Permeability Results for a High Pressure Flow Determination (No. H:20)	541
D.2-1	Typical Calculation of Values of N_{Re} and f for Detmn. No. H:20	548
E.2-1	Theoretical Pressure Distributions (in cm Hg)	560
E.2-2	Examination of the Pressure Distribution Equations by means of Experimental Results	564
F.2-1	Typical Results of Helium Displacement Measurements (Detmn. No. D:1)	569
G.2-1	Typical Results of a Krypton Surface Area Determination (Detmn. No. S:5)	574
H.2-1	Summary of the Pore Size Distribution Results	578-9
J.2-1	Experimental Results of a Typical Tortuosity Determination (No. T:3)	581
K.1-1	The Low Pressure Determinations	583-4
K.1-2	The High Pressure Determinations	585
K.1-3	The Pressure Distribution Measurements	586

LIST OF FIGURES

Figure	Title	Page
2.1-1	Parabolic Distribution Curve Calculated from Equation (2.1.1-13) for p_i = 100 cm Hg, p_o = 20 cm Hg, a/b = 20	15
2.1-2	Schematic Representation of the Methods for Determining Permeability Coefficients for Gas Flow in Porous Media	96
3.1-1	Line Diagram of Low Pressure Permeability Apparatus	172
3.1-2	Photograph of Low Pressure Permeability Apparatus	173
3.1-3	Line Diagram of High Pressure Permeability Apparatus	186
3.1-4	Photograph of High Pressure Permeability Apparatus	187
3.1-5(a)	Diagram of Pressure Distribution Specimen	199
3.1-5(b)	Photograph of Pressure Distribution Specimen	199
3.2-1	Line Diagrams of (a) Helium Displacement Apparatus, (b) Krypton Surface Area Apparatus	204
3.5-1	Diagram of Formation Factor Cell	220
3.5-2	Photograph of Formation Factor Cell	220
3.5-3	Diagram of Evacuating and Filling Arrangement	221
3.5-4	Diagram of Electrical Circuit for Electrical Resistivity Measurements	221
3.5-5	Decomposition Potential Graphs of E_d against I for the Graphite/0.5 N K_2CO_3 and the Graphite/N KCl Half Cells	225
4.1-1	K-p_m Plots for Flow of Different Gases through P.G. 60 Graphite at High Pressures	232
4.1-2	K-p_m Plots for Nitrogen Flow in Acheson "A" Graphite Samples for Different Measuring Methods	240
4.1-3	K-p_m Plots for Nitrogen and Argon Flow through Acheson "A" Graphite Samples with Axes Perpendicular to the Extrusion Direction	240

Figure	Title	Page
4.1-4	$K-p_m$ Plots for Flow of Different Gases through Acheson "A" Graphite Rod No. K2A (Determined by the Pressure Decay Method).	241
4.1-5	$K-p_m$ Plots for Nitrogen and Hydrogen Flow through Acheson "A" Graphite Rod No. K2A at High Pressures	247
4.1-6	$K-p_m$ Plots for Flow of Different Gases through Morgan "EY9" Graphite Rod No. K21 (Determined by the Pressure Increase Method).	251
4.1-7	$K-p_m$ Plots for Nitrogen Flow through Morgan "EY9" Graphite Rod No. K21 for Different Measuring Methods	251A
4.1-8	$K-p_m$ Plots for Nitrogen and Argon Flow through Morgan "EY9" Graphite Samples with Axes Perpendicular to the Extrusion Direction	251A
4.1-9	$\phi-p_m$ Plots for Gas Flow through Morgan "EY9" Graphite (a) Sample No. K21 (b) Samples No. K23 and No. K24	257
4.1-10	$K-p_m$ Plots for Nitrogen Flow through Morgan "EY9" Graphite Samples No. K22 and No. K23 at High Pressures	260
4.1-11	$K-p_m$ Plots for Flow of Different Gases through Impregnated Graphite Sample No. K42 (Determined by the Pressure Increase Method)	265
4.1-12	$K-p_m$ Plots for Nitrogen Flow through Impregnated Graphite Sample No. K42 for Different Measuring Methods	266
4.1-13	Approach to Equilibrium Nitrogen Flow in Impregnated Graphite Sample No. K42 (Detmn. No. L:31)	266
4.1-14	$\phi-p_m$ Plots for Gas Flow through Impregnated Graphite Sample No. K42	267
4.1-15	$K-p_m$ Plots for High Pressure Gas Flow through Impregnated Graphite Sample No. K41	273
4.1-16	$K-p_m$ Plots for High Pressure Nitrogen and Hydrogen Flow through Impregnated Graphite Sample No. K42	273

Figure	Title	Page
4.1-17	Typical Dimensionless Pressure Distributions for Nitrogen and Hydrogen Flow through P.G. 60 Graphite Specimen No. G31 with p_i about 155 cm Hg	282
4.1-18	Pressure Distribution Curves for Nitrogen Flow through Acheson "A" Graphite Specimen No. G1	282
4.1-19	Typical Dimensionless Pressure Distribution for Nitrogen and Carbon Dioxide Flow through Acheson "A" Graphite Specimen No. G1 with p_i about 120 cm Hg	283
4.1-20	Typical Dimensionless Pressure Distributions for Nitrogen Flow through Morgan "EY9" Graphite Specimen No. G21 with p_i about 135 cm Hg	283
4.1-21	Corrected K-p_m Plot and K_{ow}-p_m Values for Nitrogen Flow through Acheson "A" Graphite Specimen No. G1	284
4.1-22	K-p_m Plots for Nitrogen Flow in Each Disc and in the Overall Morgan "EY9" Graphite Specimen No. G21	284
4.4-1	Pressurizing Curves of V(r) against p_c for the C.S.I.R.O. Pore Size Distribution Measurements	302
4.4-2	Pore Size Distribution Curves of D(r) against r for P.G. 60, Acheson "A", and Morgan "EY9" Graphites as Determined by the C.S.I.R.O.	302
4.4-3	Pressurizing Curves of ε(r) against p_c for the A.A.E.C. Pore Size Distribution Measurements	303
4.4-4	Pore Size Distribution Curves of $D(r)/V_t$ against r for Morgan "EY9" (No. 100) and Impregnated Graphite Samples Calculated from the A.A.E.C. Data	303
5.1-1	The f-N_{Re} Graph for the High Pressure Flow Results for P.G. 60, Acheson "A", and Morgan "EY9" Graphites (Green and Duwez Correlation)	348

Figure	Title	Page
5.1-2	The β-B$_8$ Plot of Stutzman and Thodos,[146] showing the Experimental Results for the Reactor Graphite Samples and the Results of Other Authors[125,126]	355A
5.1-3	Graph of b against $1/\mu$ for the Low Pressure Permeability Results for Morgan "EY9" Graphite Rod No. K21	364
5.1-4	Graph of a against $\sqrt{(\mathcal{J}/M)}$ for the Low Pressure Permeability Results for Morgan "EY9" Graphite Rod No. K21	364
5.1-5	Graphs of H against p_m for Helium, Nitrogen, and Freon-12 Adsorption on Morgan "EY9" Graphite Rod No. K21 Derived from the Time-Lag Results	386
5.1-6	Adsorption Isotherms of y against p_m for Helium, Nitrogen, and Freon-12 Adsorption on Morgan "EY9" Graphite Rod No. K21 at Room Temperature	386
5.1-7	Adsorbed-Phase Concentration Distributions in a Morgan "EY9" Graphite Sample (a/b = 50) for Various Pressure Conditions	390
5.1-8	Graphs of H against p_m for Hydrogen, Nitrogen, and Xenon Adsorption on Impregnated Graphite Sample No. K42 Derived from the Time-Lag Results	432
5.1-9	Adsorption Isotherms of y against p_m for Hydrogen, Nitrogen, and Xenon Adsorption on Impregnated Graphite Sample No. K42 at Room Temperature	432
5.5-1	Correlations of F with ε and F with K Obtained from Electrical Resistivity Measurements on the Graphite Samples	477
A.2-1	Diagrams of Permeability Cells and Sample Holders for the Low Pressure Permeability Apparatus (a) Permeability Cell Type I with Sample Holder Type (a); (b) Permeability Cell Type II; (c) Sample Holder Type (c); (d) Sample Holder Type (d)	511

Figure	Title	Page
A.2-2	Diagrams of Permeability Cells and Sample Holders for the High Pressure Permeability Apparatus (a) Permeability Cell Type I; (b) Permeability Cell Type II; (c) Sample Holder Type (e); (d) Sample Holder Type (b)	512
C.2-1	Pressure Increase Plots of p_e against t for Detmn. No. L:49 (Carbon Dioxide Flow through Morgan "EY9" Rod No. K21)	528
C.2-2	K-p_m Plot for Carbon Dioxide Flow through Morgan "EY9" Rod No. K21 (Detmn. No. L:49 - Pressure Increase Method)	528
C.3-1	Pressure Decay Plot of p_i against t for Detmn. No. L:53 (Carbon Dioxide Flow Through Acheson "A" Rod No. K2A)	534
C.3-2	K-p_m Plot for Carbon Dioxide Flow through Acheson "A" Rod No. K2A (Detmn. No. L:53- Pressure Decay Method)	534
C.5-1	K-p_m Plot for Nitrogen Flow through Acheson "A" Rod No. K4 (Detmn. No. H:20 - High Pressure Flow Method)	542
D.2-1 (a)	The Cornell-Katz Plot of $p_m \Delta p/Q_a p_a$ against $Q_a p_a$, and	
(b)	The $\alpha - \beta$ Plot of $p_m \Delta p/(Q_a p_a)^2$ against $1/Q_a p_a$ for Results of Detmn. No. H:20 (Nitrogen Flow through Acheson "A" Rod No. K4)	549
D.2-2	The Uncorrected and Corrected f-N_{Re} Graphs for Results of Detmn. No. H:20	549
E.2-1	Theoretical Pressure Distribution Curves Showing Variation of Curvature with a/b	561
F.2-1	Plot of $(pV_s/\mathcal{I}_s) + (pV_F/\mathcal{I}_a)$ against $(p/\mathcal{I}_b)$ for Calculating the Porosity of Acheson "A" Sample No. S2 (Detmn. No. D:1) from Helium Displacement Measurements	570
G.2-1	Krypton Isotherm of V against p/P_o for Morgan "EY9" Sample No. S21 (Detmn.No.S:5)	575
G.2-2	B.E.T. Plot of $p/V(P_o - p)$ against p/P_o for Determining the Krypton Surface Area of Morgan "EY9" Sample No.S21 (Detmn.No.S:5)	575
J.2-1	Plot of ΔE against I for Determining the Formation Factor for Acheson "A" Sample No. T2 (Detmn. No. T:5)	582

SUMMARY

In this research project, the flow of gases through porous reactor graphites has been studied. The graphites supplied by the Australian Atomic Energy Commission were P.G. 60 (porosity $\varepsilon = 0.54$), Acheson "A" ($\varepsilon = 0.28$), Morgan "EY9" ($\varepsilon = 0.15$), and Impregnated graphite ($\varepsilon = 0.11$).

Permeability coefficients K were determined for the flow of hydrogen, helium, nitrogen, argon, carbon dioxide, freon-12, and xenon through the four graphites at room temperature (about 20°C) and at mean pressures p_m from 0.02 cm Hg to 1236 cm Hg (16.3 atm). The main measuring methods were the pressure increase and the pressure decay methods in a low pressure (vacuum) apparatus and the flow method in a high pressure apparatus.

Several flow phenomena, which previously had not been reported or were only observed and discussed to a limited extent, occurred during the flow measurements.

(1) In the high pressure flow phenomenon, K varied with p_{out} at any p_m when the Reynolds number N_{Re} was above 0.01 because of the effect of inertial resistance. The flow results were satisfactorily correlated by the Green and Duwez method, modified for slip flow, to give a single f-N_{Re} plot. An equation

for K covering gas flow in porous media from Knudsen to complete turbulent flow was derived, e.g.,

$$K = \left[a + \frac{B_o\, p_m}{\mu} \right] \Big/ \left[1 + \beta G \left(\frac{B_o}{\mu} + \frac{a}{p_m} \right) \right] ,$$

where a, B_o, and β were flow coefficients, μ the gas viscosity, and G the mass flow-rate.

(2) Definite evidence of minima in the $K-p_m$ plots at very low pressures was obtained for the fine-pored graphites. Interaction of the gas molecules at the pore walls, surface flow effects, Knudsen flow in long flow paths, and the particular pore structure of the medium were considered to influence the occurrence of a minimum.

(3) The low pressure transient behaviour, when the time-lag increased sharply with decreasing p_m, was due to adsorption effects, a longer time being necessary at low pressures to establish the equilibrium adsorbed-phase concentration distribution in the graphite. Isotherms for gas adsorption on the fine-pored graphites at room temperature were derived; even helium was slightly adsorbed.

(4) Pressure distribution curves, measured for equilibrium gas flow through graphite specimens for pressures below two atmospheres, were approximately parabolic in shape but deviated from theoretical

distributions because of the graphite inhomogeneity. Theoretical equations for the pressure distributions for simultaneous slip, viscous, and turbulent flow were derived; consequently, Darcy's law could be validly integrated for large Δp.

At the critical N_{Re} (0.01), slip flow constituted about 10% of the total flow for the coarse-pored graphites because of their extremely wide pore size distributions.

Pore properties calculated from the permeability results differed from independently measured values because of the occurrence of dead-end pores and the inadequacy of pore models. Porosities and helium densities of the graphites were measured by the helium displacement method, surface areas by the krypton adsorption method, pore size distributions by the mercury penetration method (by outside research organizations), and electrical formation factors by a new refined d.c. resistivity method. The high tortuosity factors indicated that the graphite pore structure consisted of voids and constrictions.

I certify that this Thesis contains no material which has been accepted for the award of any other Degree or Diploma in any University and that, to the best of my knowledge and belief, this Thesis contains no material previously published or written by any other person except when due reference is made in the text of the Thesis.

G. J. Field.

Dept. of Mining, Metallurgical, and Chemical Engineering,
Univ. of Adelaide,
South Australia.

ACKNOWLEDGEMENTS

The author wishes to express thanks to Professor E.C.R. Spooner for his support of this project, and to acknowledge the ready guidance and encouragement of Dr. H. Watts, who supervised the research work. The continued interest of Dr. R.V. Culver is also appreciated.

The author is further indebted for the help given by the following: Dr. W.T. Denholm of the South Australian Institute of Technology for helpful discussions concerning the electrochemical aspect of the electrical resistivity measurements; the staff of the Chemical Engineering Section of the Australian Atomic Energy Commission, Lucas Heights, N.S.W., for providing the graphite samples and relevant information about the graphite grades, and for useful discussions concerning the permeability determinations; and the Division of Coal Research of the Commonwealth Scientific and Industrial Research Organization, Chatswood, N.S.W., for determining the pore size distributions for a number of graphite samples.

The financial assistance provided by the Australian Atomic Energy Commission in the form of a Postgraduate Research Studentship and an Equipment Grant is gratefully acknowledged.

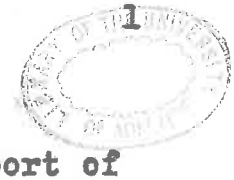

1. INTRODUCTION

In many branches of technology, the transport of gases and liquids through porous bodies is of vital practical importance. Thus petroleum technologists are concerned with the movement of ground waters, oil, and natural gas through porous gas- and oil-bearing formations beneath the earth's surface, civil engineers wish to know the extent of seepage through the subsoil of dams and large buildings, and soil scientists are interested in the distribution of moisture in soils. Chemical engineering operations involving transport in porous materials include the filtration of slurries and suspensions, the flow of fluids through packed columns for mass transfer by absorption or distillation, the drying of porous solids, and the diffusion of reacting gases into porous catalyst particles. The transport characteristics of many industrial products such as textiles, rubbers, plastic membranes, metals, refractories, and glass may be important for certain applications. Porous barriers are used to separate gas mixtures, while the specific surfaces of industrial powders are measured by gas flow techniques.

With the advent of the nuclear age, many new problems have arisen with the design of atomic power reactors. A major difficulty for the Australian

Atomic Energy Commission (A.A.E.C.) in their development of a high-temperature gas-cooled graphite-moderated reactor for Australian conditions is the high permeability of commercial reactor-grade graphites. These graphites, if used as canning material for the fuel elements, would allow the highly radioactive gaseous fission products from the fuel elements to escape through the graphite cans and contaminate the reactor cooling gas. The use of graphite in the proposed reactor otherwise would be most advantageous since graphite has very good moderating, structural, and heat transfer properties[1] and would enable the reactor to operate at temperatures much higher than are possible with metal-clad fuel elements.[2,3] A reduction in the permeability of the commercial graphites to about 10^{-6} cm^2/sec would be necessary for successful operation of the reactor.[3,4] A number of workers, including the A.A.E.C., have been investigating methods to reduce the permeability of graphite, and subsequently measuring the gas transport through the resulting products. This research project was initiated for the study of the flow of gases through porous reactor graphites with the two-fold purpose of providing permeability data on various fine-pored reactor graphites supplied by the A.A.E.C., and extending the fundamental knowledge of gas

transport through porous media in general and graphite in particular.

The monographs by Carman[5] and Scheidegger[6] are excellent reviews of the theory and literature for flow through porous media. Early investigations were mainly confined to liquid flow in porous materials and later to gas flow through unconsolidated powders; the application of the derived theories to gas flow in consolidated porous media has generally proved unsatisfactory and has led to some confusion concerning this subject. The experimental work on consolidated media is rather limited, especially at pressures greater than a few atmospheres and at temperatures above 100°C.

No satisfactory flow equation is available to describe the flow for all possible conditions from Knudsen flow at very low pressures to completely turbulent flow at very high pressures. Correlations between the permeability and the pore properties of a medium are only of limited application, an indeterminate portion of the pore space in consolidated media often being unavailable for flow. Very little consideration has been given to the distribution of pressure in a porous medium during flow. At low pressures, the minima in the permeability curves and the transient flow behaviour have not been satisfactorily explained, the experimental evidence being limited. The concept of the surface flow of

adsorbable gases is rather doubtful.

Therefore, there are a number of controversial aspects of gas flow in porous media that still remain to be clarified; further experimental and theoretical studies are necessary in order to understand these problems fully. An investigation of the flow of a range of gases through the different grades of reactor graphites of varying porosities and pore sizes over a wide range of pressures should yield results which would permit the extension of the present knowledge of gas transport in consolidated porous media.

By the independent measurement of the pore properties of the graphites such as the porosity, surface area, tortuosity factor, and pore size distribution, the effect of the pore structure on the permeability could be examined and the published correlations tested; special attention should be given to the relation between the permeability coefficient and the electrical tortuosity factor as measured by electrical resistivity methods. Investigations into the permeability of the graphites at high temperatures and the diffusion of gases through the graphites under zero pressure gradient have been conducted by other workers concurrently with this research project.

In section 2 of this thesis, the literature, theory,

and methods of measurement of the various gas transport and pore properties of a porous medium are reviewed. In section 2.1, the flow of gases through porous media is considered; the basic theory of the permeability concept and the distribution of pressure is presented, the use of models to represent porous media is examined, the various types of flow (viscous, slip, Knudsen, surface, and turbulent flow) are discussed in detail with the different correlations and flow phenomena being described, and the methods of measuring the permeability are mentioned. Section 2.2 gives the theory and measuring methods for the porosity of a porous medium, while, in section 2.3, the surface area of a porous medium is discussed with the relation between the area and permeability measurements being mentioned. The pore structure of a porous medium is discussed in section 2.4, the pore size distribution is defined and introduced into the permeability equations, and the methods of measuring the distribution are described. In section 2.5, the tortuosity is defined, its relation to the permeability, the electrical resistivity, and the diffusion coefficient mentioned, and the methods of its measurement considered.

Except for section 6, each section is divided into five parts in the same way as in section 2; part 1 is

concerned with the permeability and pressure distribution measurements, part 2 the porosity measurements, part 3 the surface area measurements, part 4 the pore size distribution measurements, and part 5 the electrical resistivity and tortuosity measurements. In section 3, the apparatus employed for each type of measurement is described and the experimental procedure is given; the details concerning the graphite samples and other necessary materials are also mentioned. The overall results of the various determinations are reported in section 4, the results in detail being confined to the Appendices. The results are discussed in section 5 with special attention being given to the various flow phenomena observed; in section 5.6 values of the various pore properties estimated from the results of the permeability determinations are compared with the values obtained by independent measurements. Finally, in section 6, the conclusions drawn from the results of this research project are presented and recommendations are made for future investigations on gas flow in porous media.

2. LITERATURE REVIEW

A porous medium is a solid body in which pores or void spaces are distributed fairly evenly (ref.6,p.5). If some of the pores are interconnected, gases or liquids can flow through the medium (see section 2.1). A porous medium may be either unconsolidated or consolidated (ref.5,p.7); an unconsolidated medium is made up of discrete particles, e.g., a bed of powder or sand grains, while a consolidated medium is formed either by the welding together of solid particles in some way as in porous rocks and synthetic ceramics or by the removal of a part of a continuous solid material, e.g., charcoal and Vycor porous glass.

The pore structure of a consolidated medium is generally more complex than that of an unconsolidated bed and may be anisotropic in that the various physical properties of the medium vary with direction. The pore structure of a porous medium is characterized by various pore properties, viz., the porosity, the surface area, the pore size distribution, and the tortuosity; these properties are discussed and their relation to the permeability considered in sections 2.2, 2.3, 2.4, and 2.5, respectively.

Synthetic reactor graphites are inherently porous because of their mode of manufacture. They are usually

manufactured from petroleum coke particles and coal-tar pitch by the Acheson process;[7-9] the desired mixture of the raw materials is either extruded or moulded to form rods or bars which are then graphitized at temperatures of 2500 to 3000°C. Various impregnation processes[9-12] have been developed to reduce the porosity and permeability of these graphites, the method used by the Australian Atomic Energy Commission[13] involving repeated impregnations with furfuryl alcohol.

2.1 Gas Flow Through Porous Media

2.1.1 Introduction

For gas flow through a porous medium, a number of types of flow can occur, viz., turbulent or inertial flow, viscous or laminar flow, slip flow, Knudsen or molecular flow, and surface flow. The type of flow depends upon the pressure and flow-rate conditions and the pore diameter.

Because the pores available for gas flow in a porous medium often cover a wide range of pore sizes from fine capillaries to large voids, more than one type of flow can occur in the pore space at any time. Thus, slip flow nearly always occurs simultaneously with viscous flow, a fact that is not always appreciated, while turbulent flow may commence in the larger pores when viscous flow still predominates in the smaller pores. The non-uniformity

of the pore sizes therefore leads to a gradual transition from one flow type to the next (cf. the sharp transitions in flow observed for gas flow in capillary tubes), the extent of the transition region depending upon the width of the pore size distribution. Gas flow in a porous medium is further complicated in that the type of flow in a certain pore may change as the pressure decreases when the pressure drop is large, or as the pore diameter varies for a pore of irregular cross-section.

2.1.1.1 Darcy's Law

The theory of the flow of fluids through porous media is based on experiments originally performed by Darcy,[14] who deduced that the rate of flow of a fluid through a porous medium was directly proportional to the pressure gradient causing flow. If Q is the total volume of fluid flowing in unit time in the x-direction through a porous medium of length L and cross-sectional area A, then Darcy's law states that

$$Q = B_1 A \partial p/\partial x , \qquad \ldots (2.1.1\text{-}1)$$

where p = pressure at any point x in the medium,

and B_1 = permeability coefficient. Other forms of Darcy's law, and further permeability coefficients B_o, B, and K are given in section 2.1.1.5.

Darcy's law as expressed by equation (2.1.1-1) is the equation of motion for a fluid through a porous medium in

the viscous flow region. It is employed to derive a general equation of flow in a porous medium.

2.1.1.2 The General Flow Equation

Three kinds of physical conditions or equations, viz., the equation of continuity, the equation of motion, and the rheological equation of state, determine the motion of a fluid (ref.6,p.23). In addition to these equations, a set of initial or boundary conditions fully specifies any particular flow system.

For fluid flow through a porous medium in the direction of the x-axis, a mass balance across a small element of unit cross-section and thickness δx over a period of time δt gives an equation of continuity (ref.5,p.4), i.e.,

$$\frac{\partial(\rho v)}{\partial x} = -\varepsilon \frac{\partial \rho}{\partial t} , \qquad \ldots (2.1.1\text{-}2)$$

where ρ = density of the fluid,

v = velocity of fluid flow, and

ε = porosity of the medium. Darcy's law in a generalized form

$$Q\rho/A = v\rho = -B_1 \rho ((\partial p/\partial x) - \rho g) \qquad \ldots (2.1.1\text{-}3)$$

expresses the equation of motion of a fluid through a porous medium, where g is the gravitational acceleration. The non-ideality and compressibility of the fluid are covered by the equation of state (ref.15,p.131), viz.,

$$\rho = \rho_0 p^m e^{bp}, \qquad \ldots (2.1.1\text{-}4)$$

where ρ_0 = fluid density at unit pressure, and m and b are constants.

For gas flow through a porous medium under isothermal conditions, m = 1, b = 0, g = 0, and $B_1 = K/p$ (equation 2.1.1-21). Then, by the combination of the above equations, the equation of flow is

$$\varepsilon \frac{\partial p}{\partial t} = \frac{\partial}{\partial x}\left(K \frac{\partial p}{\partial x}\right) . \qquad \ldots (2.1.1 - 5)$$

Solutions of this equation with the appropriate boundary conditions give p as a function of t and x. Corresponding flow equations are available for flow in three dimensions and for different coordinate systems.

2.1.1.3 Particular Solutions to the Flow Equation

For steady state flow conditions, the pressure at any point in the porous medium remains constant with time, i.e., $\partial p/\partial t = 0$. Then equation (2.1.1 - 5) becomes

$$\frac{\partial}{\partial x}\left(K \frac{\partial p}{\partial x}\right) = 0 . \qquad \ldots (2.1.1 - 6)$$

If the permeability coefficient K is a constant, equation (2.1.1 - 6) can be solved (see Appendix E.1, Condition 1) for the boundary conditions

$$\begin{cases} p = p_i \text{ (inlet pressure) at } x = L, \\ p = p_o \text{ (outlet pressure) at } x = 0, \\ p = \Phi(x) \quad 0 < x < L \text{ for all time,} \end{cases} \qquad \ldots (2.1.1 - 7)$$

to give $$p - \frac{\Delta p\, x}{L} - p_o = 0, \quad \ldots (2.1.1-8)$$

where $$\Delta p = p_i - p_o . \quad \ldots (2.1.1-9)$$

In the viscous flow region, the coefficient K in equation (2.1.1 - 6) can be replaced by $B_o p/\mu$ (equation 2.1.1-23), where B_o is the viscous flow permeability coefficient and is a constant, and μ is the viscosity of the gas and is assumed independent of pressure[16] (see Appendix E.1, Condition 2). Then

$$\frac{\partial}{\partial x}\left(p \frac{\partial p}{\partial x}\right) = \frac{1}{2} \frac{\partial^2 (p^2)}{\partial x^2} = 0. \quad \ldots (2.1.1-10)$$

The differential equation (2.1.1-10) may be solved for the boundary conditions (2.1.1-7) to give (ref.15,p.680)

$$p^2 - 2p_m \Delta p \frac{x}{L} - p_o^2 = 0 \quad \ldots (2.1.1-11)$$

where $$p_m = \tfrac{1}{2}(p_i + p_o). \quad \ldots (2.1.1-12)$$

Similarly when slip as well as viscous flow occurs and K is a linear function of pressure (see section 2.1.4.1) i.e., $K = a + bp$, where a and b are constants, the more general solution:

$$p^2 + \frac{2a}{b} p - \left(\frac{a}{b} + p_m\right) 2\Delta p \frac{x}{L} - p_o^2 - \frac{2a}{b} p_o = 0 \quad \ldots (2.1.1-13)$$

can be obtained from equation (2.1.1-6), (see Appendix E.1, Condition 3). This expression for the pressure distribution for one-dimensional gas flow through a porous

medium in the viscous and slip flow regions apparently has not been mentioned previously in the literature; consequently a short communication has been published[17] (a reprint is included as Appendix E.3). Equation (2.1.1-13) can also be derived from the general solution given by Barrer[18] for the distribution of concentration in a porous medium when the diffusion coefficient D is a function of concentration. The corresponding solution for viscous flow in a radial system has been discussed by Muskat (ref.15, p.682) with particular reference to the production of gas by oil wells.

When the pressure at any point in the medium varies with time ($\partial p / \partial t \neq 0$), transient or unsteady state flow conditions occur. Analytical solutions of the differential equation (2.1.1-5) for transient flow are not easy since p is a function of both t and x. A number of references to solutions of the flow equation for specific transient systems are listed by Scheidegger (ref.6,p.86).

By replacing the non-linear differential equation (2.1.1-5) by a difference equation and solving by means of a high speed electronic digital computer, Aronofsky and co-workers[16,19-21] obtained numerical solutions to a number of transient systems involving gas flow through porous media. These systems were one-dimensional flow in the viscous flow region,[19,21]

one-dimensional flow corrected for slip flow,[16] and radial viscous flow.[20]

2.1.1.4 Distribution of Pressure for Flow through Porous Media

The particular solutions of the one-dimensional flow equation under steady state conditions express the pressure p in terms of the position x within a porous medium. When K is dependent upon p, the solutions are of the form of the general equation for a parabola, viz.,

$$p^2 + Ax + Bp + C = 0.$$

The general solution for the distribution of pressure (equation 2.1.1-13) is the equation for a family of parabolas which is dependent upon the inlet and outlet pressures, and has a vertex at

$x = -L(a + b\,p_o)^2 / 2\Delta p\, b(a + b\,p_m)$, $p = -a/b$

(see Fig. 2.1-1). The observation that the pressure distribution curves are a family of parabolas apparently has not been mentioned in the literature.

Indeed, the literature concerning the pressure distribution for gas flow through a porous medium is limited. Muskat (ref.15,p.77) noted that p^2 varied linearly with x for isothermal one-dimensional flow of an ideal gas (cf. equation 2.1.1-11). (For liquid flow, p changed linearly with x).

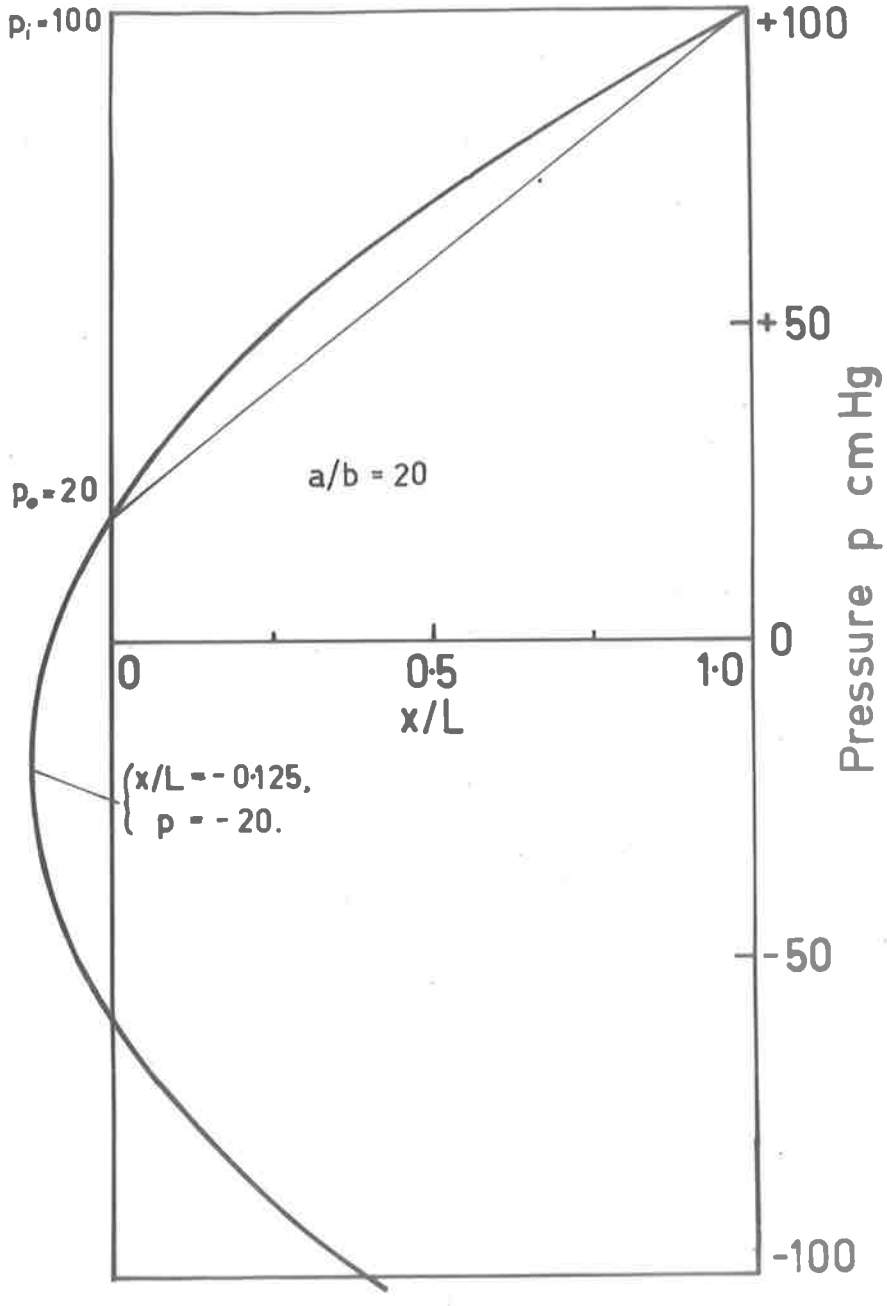

Fig. 2.1-1 Parabolic Distribution Curve Calculated from Equation (2.1.1-13) for p_i = 100 cm Hg, p_o = 20 cm Hg, a/b = 20.

Theoretical pressure distributions, plotted dimensionlessly as p/p_o against x/L, were presented for linear gas flow (ref.15,p.681); under isothermal flow conditions (m = 1), the amount of gas flowing through a porous sample would be 14% less, and the parabolic distribution more curved than that for adiabatic flow (m < 1) under otherwise identical conditions.

Aronofsky and Jenkins[19] have presented a method of solving the basic flow equation for one-dimensional unsteady state gas flow through porous media and thereby computed dimensionless pressure distributions for various ratios of p_o to p_i when the pressure at one end (x = 0) of a porous sample was suddenly changed from p_o to a constant p_i. At infinite time, when steady state conditions were attained, the distributions of $(p - p_o) / (p_i - p_o)$ against x/L were parabolic for p_i/p_o greater than unity. The distributions were more curved and steady state flow was approached more rapidly for larger values of p_i/p_o than for smaller values. At p_i/p_o = 10/1, the pressure at the centre of the sample was about 30% greater than p_m.

The analysis of Aronofsky and Jenkins[19] applied to flow in the viscous region where B_o was independent of pressure. The effect of slip was considered[16] for a different transient flow system, but no steady state pressure distributions were presented.

However, their results indicated that the transient pressure distributions were markedly influenced by the gas slip for absolute pressures below 2 to 4 atm.

Barrer[18] has derived an equation for the steady state distribution of concentration in a porous medium when the diffusion "constant" D was a known function of concentration, i.e.,

$$D = D_o \ (1 + \bar{\Phi} \ (c)). \qquad \ldots (2.1.1\text{-}14)$$

As p is proportional to c, the pressure distribution equation (2.1.1-13) can be derived from Barrer's equation. For various functions $\bar{\Phi}$ (c), Barrer plotted concentration distributions of c/c_1 against x/L; in general, the distribution curves were convex away from the x/L-axis when D increased as c increased, and were convex towards that axis when D decreased for increasing c. From an experimentally determined distribution, D_o and $\bar{\Phi}$ (c) could be derived.

Very few workers have determined the pressure distribution for steady state gas flow through a porous medium experimentally. Muskat and Botset,[22] and Heatherington et al.[23] measured the pressure at several points within unconsolidated sand beds for steady state viscous gas flow and found that p^2 was linear with x . Consideration of the general pressure distribution equation (2.1.1-13) shows that a plot of p^2 against x/L is

only linear when a/b = 0, i.e., when no slip flow occurs. Pressure distributions for unsteady state gas flow in a sand bed were determined by Vetrov et al.[24]

Because of the limited theoretical considerations and general lack of experimental confirmation concerning the pressure distribution for gas flow in porous media, especially when slip and turbulent flow occur, further experimental work was considered necessary. Accordingly, pressure distributions have been determined for gas flow through various graphite samples.

2.1.1.5 The Concept of Permeability

The permeability coefficient B_1 has been defined by Darcy's law, viz.,

$$Q = - B_1 A \partial p / \partial x. \qquad \ldots (2.1.1\text{-}1)$$

As B_1 depends on the properties of both the flowing fluid and the porous medium, another constant B_o, termed the specific permeability coefficient for viscous flow, can be introduced (ref.5,p.1) by the equation

$$Q = \frac{- B_o A}{\mu} \frac{\partial p}{\partial x}, \qquad \ldots (2.1.1\text{-}15)$$

where μ is the viscosity of the fluid. In the c.g.s. system, this new constant has the unit of cm^2 which has been called the "perm" by German ceramic workers.[25] Petroleum technologists (ref.15,p.76) have employed a

mixed unit called the "darcy", in which the pressure is expressed in atm/cm^2.

For the flow of gases through a porous medium, the volumetric flow-rate Q varies with pressure and hence changes from point to point in the medium. However the mass rate of flow $G = Q\rho/A$ remains constant; its introduction into equation (2.1.1-15) gives

$$G = -\frac{B_o}{\mu}\,\rho\,\frac{\partial p}{\partial x} \quad . \qquad \ldots (2.1.1\text{-}16)$$

Carman (ref.5,p.2) introduces further permeability coefficients B and K which can be used outside the viscous flow region. These coefficients are defined by the equations

$$G/M = -B\,\partial p/\partial x, \qquad \ldots (2.1.1\text{-}17)$$

and

$$\frac{G}{M} = -K\frac{\partial C}{\partial x} = -\frac{K}{\mathcal{R}\mathcal{T}}\frac{\partial p}{\partial x}, \qquad \ldots (2.1.1\text{-}18)$$

where C = concentration of the gas at the pressure p

$$= p/\mathcal{R}\mathcal{T} = \rho/M, \qquad \ldots (2.1.1\text{-}19)$$

$\mathcal{R}$ = universal gas constant,

$\mathcal{T}$ = absolute temperature of the gas, and

M = molecular weight of the gas.

Hence $$B = B_1\,\rho_m/M = B_1\,p_m/\mathcal{R}\mathcal{T}, \qquad \ldots (2.1.1\text{-}20)$$

and $$K = B\,\mathcal{R}\mathcal{T} = B_1\,p_m \quad . \qquad \ldots (2.1.1\text{-}21)$$

For viscous flow only,

$$B_1 = B_o/\mu \qquad \ldots (2.1.1\text{-}22)$$

and $$K = B_o\,p_m/\mu. \qquad \ldots (2.1.1\text{-}23)$$

2.1.1.6 Integration of the Permeability Equations

The permeability coefficients B_1, B_o, B, and K are defined by equations (2.1.1-1), (2.1.1-16), (2.1.1-17), and (2.1.1-18), respectively. With the provision that the permeability coefficients are independent of pressure or Δp is small enough so that variations in the coefficients can be ignored, Carman (ref.5,p.2) directly integrates these permeability equations over the length of the sample L to give the expressions

$$Q = B_1 A \Delta p/L, \quad \ldots (2.1.1\text{-}24)$$

$$G = \frac{B_o \rho_m \Delta p}{\mu L}, \quad \ldots (2.1.1\text{-}25)$$

$$\frac{G}{M} = \frac{B \Delta p}{L}, \quad \ldots (2.1.1\text{-}26)$$

and

$$\frac{G}{M} = \frac{K}{\mathcal{R}\mathcal{T}} \frac{\Delta p}{L}, \quad \ldots (2.1.1\text{-}27)$$

where ρ_m = density of the gas at the mean pressure p_m.

As the coefficients B and K are both dependent on pressure, the latter two integrations are apparently not valid when Δp is large. However, differentiation of the general expression for the pressure distribution through the medium (equation 2.1.1-13) shows that the slope of the tangent to the distribution curve at $p = p_m$ is equal

to the mean pressure gradient in the medium, i.e., at $p = p_m$, $\partial p/\partial x = \Delta p/L$ (see Appendix E.1, Condition 3). This means that equations (2.1.1-26) and (2.1.1-27) can be applied respectively to calculate B and K at the mean pressure in the medium even where Δp is large provided K is a linear function of pressure.[17] If B and K are neither constant nor linear functions of pressure, as may occur at high flow-rates (turbulent flow) and at very low pressures, then the respective integrations may not be valid.

Petroleum technologists, when investigating gas flow through sedimentary rock formations, generally have calculated the permeability coefficient B_o. However, the calculation of the coefficient K is often advantageous since this coefficient has the dimensions of cm^2/sec and can then be readily compared with the diffusion coefficient D which has the same dimensions. The coefficient K can be employed outside the viscous flow region so that correction for slip flow is avoided (section 2.1.4.1).

A combination of equations (2.1.1-27) and (2.1.1-19) shows that K can be calculated from the equations

$$K = \frac{G L p_m}{\Delta p \rho_m} = \frac{Q_m p_m L}{\Delta p A}, \qquad \ldots (2.1.1\text{-}28)$$

where Q_m = volumetric flow-rate through the medium at the mean pressure p_m.

2.1.2 The Use of Models to Describe Pore Structures

The permeability of a porous medium can usually be measured readily, but it is often desirable to relate it to the pore properties of the pore structure (ref.5,p.6). As this is difficult because of the complexity of the pore space, models are adopted to represent the pore structure of the medium. If the model is simple enough so that it can be treated mathematically, theoretical correlations between the permeability and the pore properties can be established.

In the most commonly employed pore model, the pore space is assumed to be equivalent to a bundle of straight parallel capillary tubes, since then the well-known equations for gas flow in capillaries can be applied. This is a reasonable assumption since the flows in porous media and in capillary systems are analogous and similar equations should apply. The basic equations for the flow of gases through capillary tubes will be therefore mentioned; the main characteristics of the various types of flow will be also noted.

2.1.2.1 Gas Flow Through Capillary Tubes

(a) Viscous or Laminar Flow

The general equation for the flow-rate of a gas through a circular capillary tube of diameter d_c in the

laminar flow region is the Hagen-Poiseuille equation,[26]

$$Q_{mo} = \frac{\pi}{128} \frac{d_c^4}{\mu} \frac{\Delta p}{L_c} \quad \ldots (2.1.2\text{-}1)$$

$$\text{or } G_c = \frac{d_c^2}{32} \frac{\rho_m}{\mu} \frac{\Delta p}{L_c} \quad \ldots (2.1.2\text{-}2)$$

where Q_{mo} = volumetric flow-rate through the tube at the mean pressure p_m,

G_c = mass flow-rate through the tube,

Δp = pressure difference across the tube causing flow, and

L_c = length of the tube.

These equations show that the flow-rate through any capillary tube is directly proportional to the pressure difference causing the flow, with the resistance to flow arising solely from the internal friction or viscosity of the gas.

(b) Turbulent Flow

Above a certain critical flow-rate, the linear relation between Q_{mo} and Δp no longer holds.[26] With increasing flow-rate, the flow passes through a transition region until complete turbulence has developed; the resistance to flow then results mainly from the roughness of the tube.

The flow of gases through straight tubes is often characterized[26] by a dimensionless group known as the Reynolds number

$$N_{Re} = d_c \, v \, \rho_m / \mu$$
$$= d_c \, G_c / \mu \, , \qquad \ldots (2.1.2\text{-}3)$$

while the resistance to flow is expressed by a friction factor

$$f = \frac{2 \, d_c \, \Delta p}{\rho_m \, v^2 \, L_c} \, , \qquad \ldots (2.1.2\text{-}4)$$

where v is the average velocity of flow through the tube. The Reynolds number and the friction factor are generally plotted against each other as a friction factor chart,[26] which is linear in the laminar flow region ($f = 64 / N_{Re}$) but is curved above the critical Reynolds number at which turbulence commences. The critical N_{Re} for straight tubes is about 2000.

(c) Slip Flow

When the mean absolute pressure of a gas flowing through a circular capillary tube is decreased until the mean free path λ of the gas molecules approaches the tube diameter d_c, the flow-rate exceeds that calculated from Poiseuille's formula (ref.5,p.62). To account for this effect, which is attributed to slippage at the tube walls, an extra term is added to Poiseuille's law (equation 2.1.2-2), which then becomes

$$G_c \frac{L_c}{\Delta p} = \frac{d_c^2 \, \rho_m}{32 \, \mu} + \frac{d_c}{2 \, \bar{v}} \frac{(2 - f_1)}{f_1} \, . \qquad (2.1.2\text{-}5)$$

where $\bar{v}$ = mean thermal molecular velocity of the gas

$= \sqrt{(8\mathcal{R}\mathcal{T}/\pi M)}$, and . . . (2.1.2-6)

f_1 = fraction of gas molecules diffusely reflected on impinging with the tube walls.

(d) Knudsen Flow

If the mean absolute pressure is further decreased until λ is much greater than d_o, the molecules collide only with the tube walls and not with one another (ref.5,p.62). This flow is called Knudsen or free molecule flow. Flow in the transition region between pure slip flow (λ / d_o less than 0.1) and pure Knudsen flow (λ / d_o tends to infinity) can be summarized by the equation

$$\frac{G_o L_o}{\Delta p} = \frac{d_o^2 \rho_m}{32\mu} + \frac{\delta d_o \bar{v} \rho_o}{3}, \quad \ldots (2.1.2\text{-}7)$$

where ρ_o = gas density at unit pressure

$= M/\mathcal{R}\mathcal{T}$. . . . (2.1.2-8)

The dimensionless factor δ allows for the proportion of diffuse to specular reflections of the gas molecules at the tube walls. It approaches constant values δ_1, which ranges between 0.69 and 0.90 depending on the particular gas-surface system, and $\delta_o \simeq 1$ for slip and Knudsen flow, respectively, but varies in a complex way with λ / d_o in the transition region (ref.5,p.64). Equations (2.1.2-5) and (2.1.2-7) show that a plot of $G_o / \Delta p$ against $p_m = \rho_m \mathcal{R}\mathcal{T}/M$ is linear for λ / d_o less than unity but passes through a

minimum of about $d_o \simeq \lambda$ before approaching the limiting value for pure Knudsen flow (ref.5,p.65).

For non-circular capillary tubes, $d_o/4$ is replaced by the hydraulic radius m_o, and shape factors k_o and k_1, tabulated for various cross-sectional shapes by Carman (ref.5,pp.12,66), are introduced into equation (2.1.2-7), which then becomes

$$\frac{G_o L_o}{\Delta p} = \frac{m_o^2 \rho_m}{k_o \mu} + \frac{4 \delta m_o \rho_o \bar{v}}{3 k_1} \quad \ldots (2.1.2\text{-}9)$$

2.1.2.2 The Capillary Pore Model

A great number of investigators have employed the capillary pore model in which the porous medium is represented by a bundle of parallel capillaries. The capillaries may be of uniform size[27] and either circular (diameter d_o) or non-circular (hydraulic radius m_o). When the capillaries have varying cross-sections, the mean capillary size can be expressed either in terms of the pore size distribution[28-30] (see section 2.4.3), or as the mean hydraulic radius m_i in these latter models, termed hydraulic radius models (ref.6,p.99), the internal surface and volume of the capillaries equals the internal surface area and pore volume of the porous medium.[31,32] The length of the capillaries L_o can equal or be greater

than the geometric length of the porous medium L so that the tortuosity $T = L_e/L$ (see section 2.5.1). Adzumi[33] adopted a more complex model pore space which consisted of short circular capillaries of various diameters in series and parallel.

For the equations for gas flow in capillary tubes (section 2.1.2.1) to apply to the capillary pore model, the quantities G_c and L_c, which refer to a single capillary tube, must be replaced by measurable quantities G and L, and the porosity ε and tortuosity L_e/L introduced.[34] Then

$$G_c L_c = \frac{G L}{\varepsilon}\left(\frac{L_e}{L}\right)^2. \qquad \ldots (2.1.2\text{-}10)$$

For porous media with interconnected and tortuous pores, the various capillary pore models are gross over-simplifications of the pore structure since the permeability would be zero in the direction normal to the capillary axis (ref.5,p.6). The equations derived from these models have failed to describe the observed flow behaviour, any agreement between theory and observation having been achieved by inserting parameters of doubtful physical significance[35] (section 2.1.3.1). Pore models based on beds of spheres are more realistic than capillary models but do not permit simple mathematical treatment. Other more complex models have therefore been suggested.

2.1.2.3 Statistical Pore Models

Because the pore structure of a porous medium is generally extremely disordered, it would seem more logical to represent the medium by a disordered model based on statistics rather than the regular and ordered capillary pore model (ref.6,p.113). A number of workers[36-39] have considered such statistical models; from pore size distribution data, they estimated the probability of the occurrence of pore constrictions of all sizes and evaluated the contribution made by each constriction to the permeability. Flood[40,41] has also described a statistical model for a pore. Scheidegger (ref.6,p.120) considered that the use of statistical models was the only sensible method of describing porous media.

2.1.2.4 Constriction-Type Pore Models

In the above statistical models,[36-39] the effect of constrictions in the pores was examined statistically. Other workers[42] considered that the resistance to flow was mainly due to energy losses near constrictions in the pores and accordingly proposed a model to account for this effect.

Owen[43] has described a model pore structure consisting of void-spaces connected by capillary tubes; with this pore model, he was able to explain experimental results for consolidated porous media (section 2.5.3).

The model of Flood[41] was similar to that of Owen. Peterson[44] has examined an idealized hyperbolic pore model containing periodic pore constrictions.

2.1.2.5 Miscellaneous Pore Models

Several authors[45,46] have derived equations for gas transport in a porous medium by considering a "dusty gas" model, i.e., they visualized the medium as a collection of spherical particles randomly and rigidly fixed in space with the spheres being treated as a gas of large molecular weight in a multi-component gas mixture (section 2.1.5.2(c)). Other authors[47-49] have used models based on the drag theory of permeability (section 2.1.3.1(c)).

Fatt[35] has considered four types of network models in which the porous medium was represented by a geometric network of short interconnected capillary tubes of varying radii; by means of an analog computer, he showed that these network models gave pore size distributions, relative permeabilities, and electrical resistivities similar to those obtained experimentally for real media. Rose et al.[50] have used an analog representation of the pore structure of a porous medium to examine the effect of dead-end pore volume.

Everett[51] has theoretically considered various geometric pore models and obtained values for the pore volume,

solid volume, surface area, and shape factor for each model in terms of two characteristic parameters.

2.1.3 The Viscous Flow Region

For the viscous flow of a gas through a porous medium, Darcy's law states that the flow-rate is directly proportional to the pressure gradient causing flow (see section 2.1.1.1); it is thus analogous to Poiseuille's law for flow in capillary tubes (equation 2.1.2-2). In the integrated form, Darcy's equation is

$$B_0 = \frac{\mu G L}{\rho_m \Delta p}, \qquad \ldots (2.1.1-25)$$

where B_0 = viscous flow permeability coefficient.

Darcy's law is only valid for fluid flow in the viscous flow region. Above a certain critical flow-rate, it ceases to be valid due to the commencement of turbulent flow (see section 2.1.7). For gas flow, there is a lower limit to the validity of the law due to the effect of slippage at the pore walls (see section 2.1.4). Because of the non-uniformity of the pore sizes, slip flow frequently occurs in conjunction with viscous flow. Unfortunately, many of the correlations reported in the literature for gas flow in porous media were derived neglecting slippage and are therefore of limited application.

2.1.3.1 Viscous Flow Correlations

Many attempts have been made to obtain empirical and theoretical correlations between the viscous flow permeability coefficient B_o and the various properties of a porous medium such as the porosity, pore size, pore size distribution, and internal surface area. From such correlations, it should be possible to calculate the permeability of a given porous material from its pore properties, or conversely to estimate the properties of the material from a permeability determination.

Scheidegger (ref.6,p.89) has summarized the many empirical correlations suggested in the literature to relate B_o separately with the pore properties, but concluded that no satisfactory empirical correlations existed.

Theoretical considerations have also been applied to this problem to find satisfactory correlations. By representing the porous medium by a theoretical model which can be treated mathematically (see section 2.1.2), correlations between B_o and the pore properties have been established. The permeability theories so developed can be divided into four groups (ref.6,part 6), viz., capillary model theories, hydraulic radius theories, drag theories, and statistical theories.

(a) Capillary Model Theories

The simplest pore models are those consisting of capillaries, since then the Hagen-Poiseuille equation (equation 2.1.2-2) can be applied to express the flow through each capillary. Scheidegger (ref.6,p.92) has reviewed the use of capillary models. By means of different models, equations have been derived relating B_0 to the porosity ε, the pore diameter d, the pore size distribution function D(r), the internal surface area S_v, and an arbitrary factor τ termed the tortuosity factor. However, these equations are quite unsatisfactory since it is difficult to define a pore diameter for a porous medium (see section 2.4.1), and the value of τ can be altered to make the experimental results fit the equations. Equations relating B_0 to the pore size distribution on the basis of capillary pore models are mentioned in section 2.4.3.1.

(b) Hydraulic Radius Theories

In order to understand the theory of viscous flow in porous media, more elaborate pore models than the capillary models mentioned above must be used. The hydraulic radius theories are based on such models. These theories will be discussed in more detail in the next section since they include the very important Kozeny theory, upon which much of the theory of gas flow in porous media is based.

(c) Drag Theories

In a different approach, initiated by Emersleben[47] and called the "drag theory" of permeability, the solid particles of the porous medium are treated as obstacles to the flow of a viscous fluid and the total frictional drag as estimated from Stoke's law is equated to the resistance of the porous medium to flow. The drag theory gives good results for highly porous media such as beds of fibres, but fails at low porosities (ε less than 0.5).[49]

On the basis of the drag theory, equations for the permeability coefficient have been derived by Iberall,[49] who considered that the porous medium was equivalent to an array of uniform circular cylinders in parallel, and by Brinkman,[48] who assumed that the porous medium was a bed of fluidized spheres. Iberall's correlation[49] showed that B_0 apparently varied very slowly with flow even at low Reynolds numbers because of fluid inertia effects; he also extended his equation to include slip flow.

(d) Statistical Theories

Porous media have been represented by disordered models (see section 2.1.2.3) and the methods of statistical mechanics applied to obtain flow equations. Childs and Collis-George,[36] and later Marshall,[37] Wyllie and Gardner,[38] and Millington and Quirk[39] applied statistical

models based on the pore size distribution to obtain equations describing flow in porous media; these equations are discussed in greater detail in section 2.4.3.2.

Scheidegger[52] has rigidly applied statistics to flow through porous media and has introduced a new quantity, the "dispersivity", to indicate the sideways dispersion of a fluid stream. In his treatment, he assumed the porous medium to be isotropic and homogeneous, and showed that Darcy's law must be modified slightly to account for the dispersivity effect. According to Scheidegger (ref.6,p.120) the statistics of disorder seem to be the only sensible approach to the phenomenon of flow through porous media.

2.1.3.2 The Kozeny Theory

The Kozeny theory[31] is the most widely accepted explanation of the permeability of a porous medium for viscous flow. It is an hydraulic radius theory (section 2.1.3.1 (b)) since the permeability coefficient B_0 is expressed in terms of the hydraulic radius m by an equation of the form

$$B_0 = c \frac{m^3}{\Phi(\varepsilon)}, \qquad \ldots (2.1.3\text{-}1)$$

where c = a dimensionless constant, and

$\Phi(\varepsilon)$ = porosity function. The problem with

the hydraulic radius theories is to find the physical significance of m and $\Phi(\varepsilon)$ (ref.6,p.99).

The assumptions on which the hydraulic theories are based are listed by Carman[53] and are:

(i) no pores are sealed off,

(ii) the pores are distributed at random,

(iii) the pores are reasonably uniform in size,

(iv) the porosity is not too high,

(v) diffusion (or slip) phenomena are absent,

(vi) fluid motion through the pores occurs in the same way as through a batch of capillaries.

(a) The Kozeny Equation

In the Kozeny theory,[31] the porous medium is represented by a bundle of parallel capillaries of various cross-sections but of definite length such that the internal surface and volume of the capillaries equals the internal surface area and pore volume of the medium, respectively. The permeability coefficient is then given by the Kozeny equation

$$B_o = \frac{\varepsilon m^2}{k} = \frac{\varepsilon^3}{k S_v^2}, \qquad \ldots (2.1.3\text{-}2)$$

where S_v = internal surface area/unit bulk volume of the medium, and

k = factor called the Kozeny constant,

which theoretically should not vary.

Carman[32] has modified the Kozeny equation by the introduction of the tortuosity factor $\tau = L_p / L$ and the specific surface $S_o = S_v / (1 - \varepsilon)$ to give an equation which is now known as the Kozeny-Carman equation, e.g.,

$$B_o = \frac{\varepsilon^3}{k_o \tau^2 S_o^2 (1 - \varepsilon)^2} . \qquad \ldots (2.1.3\text{-}3)$$

The Kozeny constant is expressed by

$$k = k_o \tau^2, \qquad \ldots (2.1.3\text{-}4)$$

where k_o is a shape factor which equals 2.0 for a capillary of circular cross-section (ref.5,p.12). Sullivan[54] further modified the Kozeny equation by introducing an orientation factor.

Carman (ref.5,p.14) has discussed the value of the Kozeny constant k, and concluded that it approximately equalled 5.0 for most unconsolidated porous media with random packings and ε less than 0.80. Wyllie and Spangler[30] considered that $k = 5.0 \pm 10\%$. With $k = 5.0$, and taking $\tau = \sqrt{2}$, Carman[32] deduced that the shape factor k_o was about 2.5 for unconsolidated beds. Unfortunately, neither k_o nor τ can be determined directly; the approximate constancy of k possibly results from the variations in k_o and τ tending to cancel (ref.5,p.46).

(b) Limitations and Applications of the Theory

The Kozeny theory has been severely criticised because of the assumptions made in its derivation. Many workers have claimed to have substantiated the theory (ref.6,p.105), but no valid check can be made unless all the quantities involved can be determined independently; this may be difficult since it is often doubtful if the independently measured value of S_0 is actually the area of surface involved in flow (section 2.3.2.3), or the value of τ can be precisely determined. The limitations of the theory have been discussed by Carman (ref.5,p.13) and Scheidegger (ref.6,p.107). Generally, the assumptions listed by Carman[53] are valid only for isotropic unconsolidated media with random but uniform pore structures. Non-uniformity of the pore sizes leads to measured permeabilities that are higher than those expected from the theory while the high tortuosity factors often found in consolidated media (section 2.5.1) give lower permeabilities (ref.5,p.34).

The Kozeny-Carman equation has been widely used to calculate the specific surface of unconsolidated porous media, especially industrial powders, from permeability measurements,[55] good agreement being often observed between these permeability areas and those obtained by other methods (see section 2.3.2.2). Several workers[56,57]

have determined the apparent densities of porous particles of charcoal and coke by the application of the Kozeny equation (2.1.3-2). However, as Scheidegger (ref.6,p.107) noted, not too much confidence should be placed on the values of the various geometrical properties calculated from permeability measurements.

(c) Consolidated and Anisotropic Porous Media

As mentioned above, the Kozeny theory does not strictly apply for anisotropic consolidated porous media with non-uniform and tortuous pore structures. Actually the verification of the Kozeny-Carman equation for consolidated media is not easy since an independent measurement of the specific surface S_0 by the nitrogen adsorption method, for example, leads to an area value which includes the area of blind pores and so is much higher than that involved in flow (see section 2.3.2.3). Small cracks and fissures in a consolidated medium will lead to unduly high permeabilities.[53]

In an endeavour to apply the Kozeny equation to flow in consolidated porous media with high tortuosity factors, which lead to experimental permeability values lower than those expected, Wyllie and co-workers[58,30] assumed that the shape factor k_0 was a constant (= 2.5) for all media, and the permeability tortuosity factor τ was equal to the tortuosity factor q obtained from

electrical resistivity measurements on the saturated porous medium. Then the Kozeny "constant" k, expressed as

$$k = k_o q^2, \qquad \ldots (2.1.3\text{-}5)$$

could be much greater than the value of 5.0 obtained for unconsolidated beds. Wyllie and co-workers[30,58,59] found good agreement between measured permeabilities and those calculated from the modified Kozeny equation using measured values of q. However, as discussed in section 2.5.5.1, there is considerable disagreement in the literature as to the actual relation between q and τ.

In a consolidated porous medium, a non-uniform pore structure may counteract the effect of a large tortuosity to give a permeability of about the value expected from the Kozeny equation. Non-uniformity of the pore structure can be accounted for by introducing a pore size distribution function into the equation as well as the electrical tortuosity factor;[28-30,38] this is discussed in greater detail in section 2.4.3 .

In an anisotropic consolidated porous medium, the value of the permeability coefficient varies with the direction of flow. Marked permeability anisotropy has been observed in sedimentary rocks,[76,30] and in extruded graphites.[8,9] Walker, Rusinko, and Raats[61] obtained anisotropy of the effective diffusion coefficient for extruded carbon rods because of the different tortuosities

in the different directions.

Wyllie and Spangler[30] indicated that the ratio between the permeabilities in the x and y directions in an anisotropic porous medium was

$$B_{ox} / B_{oy} = q_y^2 / q_x^2, \qquad \ldots (2.1.3\text{-}6)$$

where q_x and q_y were the tortuosity factors in the two directions, and it was assumed that $\varepsilon_x = \varepsilon_y = \varepsilon$, $m_x = m_y = m$, and $k_{ox} \simeq k_{oy}$. Their results for five sandstones approximately correlated with this equation. Scheidegger (ref.6,p.63) has given equations for the permeability coefficient B_{on} in any direction n in terms of the angles the direction n made with the principal axes and the permeabilities corresponding to these axes; a plot of $1 / \sqrt{B_{on}}$ on polar coordinates gave an ellipsoid.

2.1.4 The Slip Flow Region

It has not always been clearly recognized that there is a lower limit to the validity of Darcy's law for gas flow in porous media. However, when several investigators (ref.6,p.125) observed that the values of B_o for gas flow were not independent of the mean pressure and were higher than the B_o values for liquid flow in the same porous medium, it was presumed that molecular effects caused the differences. Adzumi,[33] by analogy with the equation for gas flow through a circular capillary in the transition region between Knudsen and

viscous flow (equation 2.1.1-7), suggested a similar equation for gas flow in porous media with a molecular slip flow term accounting for the observed high gas permeabilities. Later, Klinkenberg[62] also explained the observed gas flow anomalies in terms of slip flow effects.

When the gas pressure in a porous medium is low enough so that the mean free path λ of the gas molecules approaches the diameter d of a pore, i.e., the Knudsen number $N_{Ku} = \lambda/d$ tends to unity, slippage takes place at the pore walls and viscous flow undergoes a transition to slip flow in that pore. At higher values of N_{Ku} when λ is much greater than d, the flow undergoes a further transition to molecular streaming or Knudsen flow (section 2.1.5). Because of the distribution of pore sizes in a porous medium, slip flow generally occurs simultaneously with viscous flow; therefore both types of flow must be discussed together.

2.1.4.1 The Permeability Equations

To account for the slip effect for gas flow through fine-pored media, an extra term is added to the flow equation (Darcy's law) so that a linear relation of the form

$$K = a + b\,p_m \qquad \ldots (2.1.4\text{-}1)$$

is obtained (ref.5,p.68), where K is the permeability coefficient defined by equation (2.1.1-28). The term

a represents the slip flow contribution and, by analogy with flow in capillaries, should be proportional to the mean thermal molecular velocity $\bar{v}$ given by

$$\bar{v} = \sqrt{(8 \mathcal{R} \mathcal{T} / \pi M)}. \qquad \ldots (2.1.2\text{-}6)$$

Since for viscous flow alone, $K = B_o \, p_m / \mu$ (equation 2.1.1-23), the viscous flow contribution $b = B_o / \mu$. A plot of K against p_m yields a as the intercept and b as the slope. Carman (ref.5,p.69) has written equation (2.1.4-1) as

$$K = \frac{B_o \, p_m}{\mu} + \frac{4 \, K_o \, \bar{v}}{3}, \qquad \ldots (2.1.4\text{-}2)$$

where K_o is the slip flow permeability coefficient and, like B_o, should be a specific property of the porous medium.

A number of investigators[34,62-68] have confirmed that $b\mu = B_o$ and $a \sqrt{(M / \mathcal{T})} = K_o$ were constants for any given porous sample, either consolidated or unconsolidated, and were independent of the gas used; then plots of b against $1/\mu$ and of a against $\sqrt{(\mathcal{T}/M)}$ yielded straight lines.[63,65] The values of $B_o = b\mu$ for gas flow agreed with the liquid permeabilities.[69] Schwertz[63] and Hutcheon et al.[34] tested equation (2.1.4-2) over a range of temperatures from room temperature up to 300°C and 1000°C, respectively, and found that the values of B_o and K_o were independent of temperature.

Most investigators, following Adzumi,[33] expressed their equations for combined viscous and slip flow in the

form of equation (2.1.4-1). However, many petroleum technologists in U.S.A.[16,70] have preferred to use the equation derived by Klinkenberg,[62] viz.,

$$K_a = B_o + \frac{a\,\mu}{p_m}, \qquad \ldots (2.1.4\text{-}3)$$

where K_a = apparent permeability coefficient

$$= \frac{G\,L\,\mu}{\Delta p\, p_m}. \qquad \ldots (2.1.4\text{-}4)$$

Then a plot of K_a against $1/p_m$ gave B_o as the intercept. These workers generally required a value of B_o (in daroys) to characterise their porous oil well formations, and occasionally have neglected to correct for slip flow (i.e., K_a was equated to B_o).

As for viscous flow in porous media (see section 2.1.3.1) attempts have been made to relate B_o and K_o to the pore properties of the medium and a number of models have been employed. These correlations are discussed below.

2.1.4.2 Adzumi Equation

Adzumi[33] adopted a model pore space consisting of uniform circular capillaries in series and parallel and obtained the equation

$$K = \frac{\pi}{8\mu}\, p_m E_o + \frac{2}{3}\,\pi\,\delta_1\,\bar{v}\,F_o \qquad \ldots (2.1.4\text{-}5)$$

where δ_1 = Adzumi constant (= 0.9),

$E_o = n r^4$,

$F_o = n r^3$, and

n = number of capillaries of radius r per unit area of cross-section.

By the experimental evaluation of E_o and F_o from the slope/intercept of the K-p_m plot, respectively, and the quantities $n = F_o^4 / E_o^3$, $r = E_o / F_o$, $\varepsilon = n \pi r^2$, and $S_v = 2\pi rn$ could be obtained.

Barrer and Grove,[65] and Ash and Grove[67] found that the values of ε and S_v calculated from the permeability by means of the Adzumi method were much lower, while the values of r were higher than those obtained by other methods; their results revealed the inadequacy of a model based on parallel circular capillaries especially for a porous medium in which blind pores occurred. Barrer and Grove[65] attempted to allow for the tortuosity of the pores but without much success. Flood, Tomlinson, and Leger[71] have pointed out that r in the Adzumi equation was really an average value r_m for which it was not generally true that $r_m^4 / r_m^3 = r_m$; without a knowledge of the pore size distribution (cf.equation 2.4.2-4, section 2.4.2), values of the pore properties could not be accurately obtained by the Adzumi method. O'Neill, Hey, and Livey[68] have generalized the Adzumi equation by including the pore size distribution in the manner suggested by Flood et al.[71] (see equation 2.4.3-6 , section 2.4.3.3).

2.1.4.3 The Modified Kozeny Equation

Adzumi's model has been refined by many authors[64,69,72-75] to account for non-circular pores and the tortuosity. Rigden[69] and Arnell[72] independently derived a modified Kozeny equation containing a correction term for slip as well as the viscosity term; such an equation is subject to the same criticisms as the Kozeny-Carman equation (section 2.1.3.2(b)), and only applies to unconsolidated media with uniform pore textures. Carman and Arnell[75] reviewed the modified equations and arrived at the equation

$$K = \frac{\varepsilon m^2 p_m}{k \mu} + \frac{4 \delta_1 \varepsilon m \bar{v}}{3 k'} \quad \ldots (2.1.4\text{-}6)$$

where $k = k_0 \tau^2$ (viscous flow), $\ldots (2.1.3\text{-}4)$

$k' = k_1 \tau^2$ (slip flow), $\ldots (2.1.4\text{-}7)$

k_1 = shape factor for slip flow, and

δ_1 = parameter accounting for the type of molecular reflection at the pore walls (cf. equation 2.1.2-7).

Comparison of the Carman-Arnell equation (2.1.4-6) with equation (2.1.4-2) shows that $B_0 = \varepsilon m^2 / k$ as in the unmodified Kozeny equation (2.1.3-2), while

$$K_0 = \frac{\delta_1 \varepsilon m}{k'} . \quad \ldots (2.1.4\text{-}8)$$

Later workers[76] have replaced δ_1/k' by a single structure factor $\mathcal{K}_1$. The specific surface area S_0 of

fine powders has been estimated from flow experiments by means of equation (2.1.4-6), m being equated to $\varepsilon / (1 - \varepsilon) S_o$ (see section 2.3.2.2).

In equation (2.1.4-6), it is assumed that the tortuosity factor τ is the same for both viscous and slip flow (ref.5,p.70). For slip flow, $k_1 = 1$ so that $k' = \tau^2 \simeq 2$ for unconsolidated beds. As δ_1 should theoretically be between 0.6 and 0.9, $\mathcal{K}_1$ should fall in the range 0.3 to 0.5.[64] Carman (ref.5,p.71) has considered the experimental results available for unconsolidated beds, viz., $\mathcal{K}_1$ was about 0.4 for beds of closely sized spheres,[66,77] but ranged from 0.27 to 0.53 for powders[66,75] covering a wide range of porosities; experimental evidence favoured the value of about 0.4 for $\mathcal{K}_1$ for slip flow in unconsolidated beds.

2.1.4.4 Consolidated Porous Media

Equation (2.1.4-2) has proved applicable to consolidated porous media,[34,67,68] but the modified Kozeny equation (2.1.4-6) is not valid because of the limitations of the Kozeny theory. However, by modifying the slip term according to the Wyllie and Rose approach[58] (see section 2.1.3.2 (c)), equation (2.1.4-6) becomes

$$K = \frac{\varepsilon m^2 p_m}{\mu k_o q^2} + \frac{4 \delta_1 \varepsilon m \bar{v}}{3 k_1 q^2} \quad \ldots (2.1.4\text{-}9)$$

where $k_o \simeq 2.5$ and $k_1 = 1$.

For slip flow in consolidated porous media, the use of equation (2.1.4-9) and the determination of the structure factor $\mathcal{K}_1 = \delta_1 / k_1 \tau^2$ is quite difficult since q^2 or τ^2 can be much greater than 2.0 and can be different for each porous medium. Carman (ref.5,p.77) has assumed that $\delta_1 \simeq 0.8$ for consolidated media; then $\mathcal{K}_1$ can be much less than 0.4. In Table 2.1-1, some results for gas flow in consolidated materials are analysed with $k_o = 2.5$ and $\delta_1 = 0.8$; the surface area S_v was estimated from $\varepsilon K_o / B_o k_o \delta_1$ and the tortuosity factor τ^2 from $\varepsilon^3 / S_v^2 B_o k_o$. These calculations showed that τ was about $\sqrt{2}$ for the bed of analcite spheres[65] and medium grade fritted glass,[63] but ranged up to about 6 and 20 for graphite[34] and beryllia,[68] respectively. These large values of τ confirmed the high values obtained previously by other methods (section 2.5.1). The calculated values of S_v were all less than the B.E.T. surface areas.

Table 2.1-1

Values of τ^2 and $\delta_1 / k_1 \tau^2$ for Consolidated Media

($S_v = \varepsilon K_o / B_o k_o \delta_1$, $\tau^2 = \varepsilon^3 / S_v^2 B_o k_o$,

$k_o = 2.5$, $\delta_1 = 0.8$).

Porous Sample	ε	S_v cm^2/cm^3	τ^2	$\frac{\delta_1}{k_1 \tau^2}$	Ref. No.
Fritted glass:					
Medium grade	0.30	1480	2.21	0.36	63
Fine grade	0.27	2610	2.47	0.32	
Ultrafine grade	0.25	9860	3.54	0.23	
Analcite spheres	0.50	1310	2.09	0.38	65
Graphite	0.17	5850	35.2	0.023	34
Ceramic	0.30	4040	4.28	0.19	67
Beryllia	0.002	58	390	0.002	68

Generally, as for the above calculations, the surface areas involved in viscous flow and slip flow are considered to be the same; however, Kraus et al.[66] calculated separate surface areas. The values of ε employed in the above calculations were the open porosity values. For unconsolidated beds, all of the open pore volume is probably involved in the flow, but for consolidated media, the pore volume actually concerned in

the flow is usually much smaller because of the effect of dead-end pores. Hence a smaller porosity value ε_s should be used for consolidated porous media instead of ε ; then the calculated values of S_v and τ would be lower by the ratio $\varepsilon_s / \varepsilon$ than those listed in Table 2.1-1 .

2.1.4.5 Other Correlations

The correlations mentioned above come under the classification of capillary model theories and hydraulic radius theories (section 2.1.3.1). The drag and statistical theories of permeability have also been extended to include slip flow.

Thus, Iberall[49] extended the drag theory of permeability and obtained an equation similar to that given by Klinkenberg.[62] Scheidegger[78] has applied statistical considerations to slip flow in porous media in an analogous manner to that for viscous flow. Flood[41] has shown that the constants a and b in equation (2.1.4-1) could be determined from a statistical pore model characterized by two parameters α and β a distribution function N.

2.1.5 The Knudsen Flow Region

Knudsen[79] observed that there was a transition from slip flow to molecular streaming for flow in fine capillaries when N_{Ku} was about unity; a similar

transition occurs for flow in fine-pored media. When the pressure in a porous medium is reduced so that the mean free path λ of the gas molecules becomes much greater than the pore diameter d in any pore, i.e., N_{Ku} tends to infinity, molecules no longer collide with each other but only with the pore walls. This Knudsen flow or molecular streaming is believed to be the same process as Knudsen diffusion, which occurs when there is no total pressure gradient but only a partial pressure gradient across the porous medium (ref.5,p.62).

For flow in the Knudsen region, the permeability coefficient is given by the equation (ref.5,p.71)

$$K = \frac{4}{3} \frac{\delta_o}{k'} \varepsilon m \bar{v}, \qquad \ldots (2.1.5\text{-}1)$$

where $k' = k_1 \tau^2$. In this equation, the Knudsen flow parameter δ_o, which allows for the proportion of diffuse to specular reflections of the gas molecules at the pore walls, approximates to unity. The value of the shape factor k_1 for Knudsen flow is difficult to assess and it is uncertain whether the tortuosity factor τ has the same value as for viscous-slip flow. Carman (ref.5,p.71) expected k_1 to be about 1.5 so that for unconsolidated beds ($\tau^2 = 2$), $\delta_o / k' = \mathcal{K}_o \simeq 0.35$. The experimental evaluation of $\mathcal{K}_o$ for Knudsen flow is rather inconclusive (ref.5,p.74), with values ranging from 0.39 to 0.48 for unconsolidated

beds. For consolidated porous media, Carman (ref.5,p.77) assumed that $\delta_o / k_1 \simeq 0.8$.

2.1.5.1 The Transition Region

It is difficult to express mathematically the transition from slip to Knudsen flow in a porous medium (ref.80,p.33). Because of the non-uniformity of the pore sizes, Knudsen flow may occur in the porous medium at the same time as slip flow. The only way in which this transition region can be expressed at the present time for a porous medium with a wide distribution of pore sizes is by the use of the rather unsatisfactory empirical factor $\mathcal{K} = \delta / k_1 \tau^2$. By analogy with flow in capillaries,[81] Carman[64] considered that the value of δ for flow in a porous medium should increase as p_m decreased, but found experimentally that $\mathcal{K}_o$ decreased or remained constant in this low pressure region. Any deviation above the straight K-p_m plot at low pressures would cause $\mathcal{K}$ to increase in the transition region with decreasing p_m as Carman expected.

According to equation (2.1.5-1), K should be independent of p_m when the flow is completely in the Knudsen flow region, i.e., the flow-rate G should vary linearly with Δp. The constancy of K with p_m has been observed over a large pressure range by a number of workers for gas flow through materials with extremely fine

pores (r_m of the order of 10 to 30 Å), viz., porous glasses,[82-84] and carbon powders.[76,85,86] For media with larger pores, the K-p_m plots above N_{Ku} = 1 have been variously observed to either flatten out, curve upwards and give a minimum, or curve downwards as p_m decreased; this varied behaviour in the transition region will be examined in detail in the next section (2.1.5.2).

Equations (2.1.4-2) and (2.1.5-1) predict that the permeability coefficient K at vanishingly small pressures is proportional to $\sqrt{(\mathscr{T}/\ M)}$, i.e., the permeability coefficient K_o for a porous medium is independent of the gas and temperature but depends upon the medium itself (cf. section 2.1.4.1). However, Berman and Lund[87] have shown by precise measurements that the permeability of several porous samples was gas- and temperature-dependent when molecule-wall collisions contributed to the total gas transport; the values of K_o were consistently lower than expected by as much as 5% . Other authors[34,65,67] have noticed abnormal values of K_o for one or two of the gases which they studied. When surface flow does not occur (section 2.1.6), i.e., K_o is not greater than expected, it is possible that Knudsen's law at zero pressure as expressed by equation (2.1.5-1) is not always valid.

2.1.5.2 Minima in the K-p_m plots

(a) Low Pressure Flow in Capillaries

It has been definitely observed [79,81] that a plot of $G / \Delta p$ against p_m for flow in circular capillaries is no longer linear at low pressures where λ is of the same order as the capillary diameter d_o, but passes through a minimum at about $N_{Ku} = 1$ and approaches the limiting value for molecular flow as p_m is decreased (see section 2.1.2.1 (d)). A marked minimum was also observed by Gaede[88] for the flow of hydrogen between parallel plates.

The complete explanation of this low pressure flow phenomenon in capillaries is still far from clear.[89] According to Carman,[64] the minimum arises from the variation of the parameter δ with pressure in the transition region between slip and Knudsen flow since nearly all of the gas molecules undergo diffuse (or random) reflection at the capillary walls for Knudsen flow while a certain fraction $1 - f_1$ undergoes specular reflection for slip flow. Pollard and Present[90] have offered the explanation that when λ is greater than d_o but less than $\frac{1}{2} L_o$, the number of gas phase collisions among molecules directed more or less along the direction of flow decreases as the pressure decreases so that an increase in K results; when λ is much greater than $\frac{1}{2} L_o$, K

approaches a limit corresponding to molecule-wall collisions only.

(b) Low Pressure Flow in Porous Media

In a porous bed, which is equivalent to a series of kinked tubes with no straight path much longer than d, Pollard and Present[90] and Eberhardt[91] considered that there would be no significant increase in K at very low pressures, i.e., no minimum was to be expected. Hiby and Pahl[92] deduced that no minimum was possible for a capillary when L_c / d_c was less than 4. However experimental evidence has shown that permeability minima are sometimes obtained for flow in porous media although a flattening or a curving downwards of the $K-p_m$ plot have also been observed.

By analogy with gas flow through capillaries, Carman[64] expected a minimum at about $N_{Ku} = 1$ for the flow of different gases in a number of powders of different particle sizes, but found for N_{Ku} up to as high as 25 ($d/\lambda = 0.04$) that the $K-p_m$ plot was linear or underwent a small and very gradual increase in gradient in the transition region. Hirsch[93] observed that the $K-p_m$ plot curved sharply downwards at p_m less than about 5 mm Hg for gas flow through porous glass discs. Monroe and Gaffee[94] also observed that the permeability suddenly decreased at low pressures for the flow of hydrogen and

helium through silica powder; however, for air and freon flow, the K-p_m plots each showed a minimum.

Barrer and Grove[65] found that the K-p_m plots for the flow of a number of gases through a bed of analcite spheres flattened below about p_m = 1.5 cm Hg, i.e., K became independent of p_m , but no evidence of a minimum was obtained. The tendency of K to become constant correlated with λ since the range of constancy of K was greatest for helium (largest λ) and least for carbon tetrachloride vapour (smallest λ). Wicke and Vollmer[95] also observed a flattening of the K-p_m plots at low pressures. Arnell and Henneberry[85] considered that the constant value of K obtained for fine-pored carbon blacks was due to the flow occurring in the pressure region at the base of the minimum in the K-p_m plot. Other investigators (see section 2.1.5.1) observed that K was independent of p_m over a large pressure range for extremely fine-pored media.

Although permeability minima have been reported by several investigators,[71,94,96] it was Grove and Ford[97] who first gave definite evidence of minima for low pressure gas flow in porous media. They observed quite marked minima for the flow of inert gases in a porous ceramic and a relatively impermeable graphite while a flattening was obtained at low pressures for other grades

of ceramic and graphite. The mean pressure corresponding to the minimum varied with the gas used, with N_{Ku} at this pressure being about 3½ for the ceramic and 25 for the graphite sample. The minimum was most marked for helium flow. The results suggested that the pore size distribution might be a factor which determined whether or not a minimum was observed.

Further results of Ash and Grove[67] for a porous ceramic showed that a minimum in the K-p_m plot was obtained at low pressures for the flow of hydrogen and helium and a flattening for some of the other gases. These authors found that N_{Ku} at the pressure at which the permeability plot deviated from the straight line was about 3 for most of the permanent gases but roughly unity for carbon dioxide and sulphur dioxide, possibly because of surface flow.

O'Neill, Hey, and Livey[68] obtained a definite minimum in the K-p_m plot at about p_m = 4 cm Hg (N_{Ku} about unity) for nitrogen flow in a relatively impermeable fabricated beryllia sample (ε = 0.0019). They suggested that the capillaries in a porous medium for which a minimum was observed were sufficiently long (approximately the grain diameter in length) for the Knudsen effect of Pollard and Present[90] to be noted. For a medium with a wide pore size distribution, they

reasoned that successive pore sizes would come into the Knudsen range as p_m was decreased and a minimum would occur on the K-p_m plot if δ_o/k_1 was greater than δ_1. If the pore size distribution was narrow, or there was a negligible difference between the values of δ_1 and δ_o/k_1, a horizontal plot would result at low pressures. O'Neill et al.[68] tested this explanation by assuming that $\delta_1 = 0.6$ and $\delta_o/k_1 \simeq 0.9$ and calculating the permeability at various p_m from pore size distribution results for a beryllia sample by means of a generalized form of the Adzumi equation (equation 2.4.3-6, section 2.4.3.3). Good agreement was obtained between the experimental and calculated permeability curves despite the assumptions made in the calculations, and the latter curve showed a minimum as suggested by their reasoning.

(c) Theoretical Considerations

By means of the "dusty gas" model (see section 2.1.2.5) Derjaguin and Bakanov[45] have shown theoretically by considering the probability of gas-phase and molecule-wall collisions that the K-p_m curve for a porous medium with a high porosity must have a minimum, no matter whether the gas molecules were specularly or diffusely reflected at the pore walls. The expression derived for K as a first approximation was of the form

$$K = \frac{3\pi\varepsilon^2 \bar{v}}{8 S_v} \frac{(A\alpha + B) D}{(A\alpha + B - C)} \quad \ldots (2.1.5\text{-}2)$$

where $$\alpha = \lambda_w / \lambda_g , \quad \ldots (2.1.5\text{-}3)$$

λ_w = mean free path of a gas molecule between collisions with the pore walls

$$= 4\varepsilon / S_v , \quad \ldots (2.1.5\text{-}4)$$

λ_g = mean free path of a gas molecule at p_m, and

A,B,C,D = constants which had different values for specular and diffuse reflection.

The dimensionless quantity α of Derjaguin and Bakanov corresponded to $1/N_{Ku}$. Talaev[98] showed that minima were observed for air flow in highly porous materials in accordance with the Derjaguin-Bakanov theory.

Equation (2.1.5-2) is similar to the semi-empirical equation of Knudsen[79] for flow through a "long" capillary, for which the parameter δ was given[81] by

$$\delta = \frac{1 + c_1/N_{Ku}}{1 + c_2/N_{Ku}} , \quad \ldots (2.1.5\text{-}5)$$

where c_1 and c_2 were constants (1.25 and 1.55, respectively). Wicke and Vollmer[95] have shown that an equation analogous to Knudsen's equation could be derived by considering laminar and molecular flow to occur in series in a capillary.

Recently, Maidanik[99] has developed a semi-empirical theory which resulted in a complex equation expressing K

in terms of λ_w / λ_g and p_m. This equation showed that a flattening or a minimum in the K-p_m plot was obtained at low pressures depending upon the values of various constants in the theory; a curving downwards resulted if adsorption of the gas molecules had taken place on the surface of the medium.

(d) Discussion about Permeability Minima

The above review of the literature on minima in K-p_m plots at low pressures shows that minima have definitely been observed for gas flow in consolidated porous bodies,[67,68,71,96-98] especially porous ceramics and graphites. For flow in unconsolidated porous media, a few claims have been made for minima,[94] while a flattening in the K-p_m plot has also been obtained.[65,95] The K-p_m plot has been observed to curve downwards at low pressures by some authors.[64,93,94]

Some authors[90-92] considered that no minimum could be expected for flow in a porous medium, but others[45,68,99] have shown theoretically that a minimum could occur. It appears that the surmise of Pollard and Present[90] that a straight flow path in a porous body is not much longer than the pore diameter d is frequently in error, especially for consolidated porous media as noted by O'Neill et al.[68] Unconsolidated beds often have fairly uniform pore structures whereas consolidated media can have a wide

distribution of pore sizes. The general observation of a flattening of the K-p_m plot for unconsolidated beds and a minimum for consolidated porous materials is probably accounted for by the different ranges of pore sizes in the two types of media as pointed out by O'Neill et al.[68]

The actual mechanism occurring in the pore space at low pressures to give the increase in K is difficult to visualize, but apparently the observed behaviour results from the decrease in gas-phase collisions by the molecules as the pressure decreases with a corresponding decrease in the proportion of specular reflections of the molecules at the pore walls. The transition in flow can be expressed mathematically by the change of δ with p_m, as given by Derjaguin and Bakanov[45] and Knudsen,[79] or by the more complex expression given by Maidanik.[99] The occurrence of surface flow of adsorbable vapours (see section 2.1.6) further complicates the position at low pressures, while the nature of the surface of the medium influences the type of molecular reflection at the pore walls.

It must not be ruled out that the phenomena observed at low pressures were due to faulty experimental techniques. The measurement of values of the permeability coefficient as the mean pressure is decreased become increasingly more

difficult with the greater significance of minute leaks, adsorption effects, pressure differences due to thermal effects, and inaccurate measurement of the flow-rate and pressure. These problems could depend on the method of measurement.

The most marked minima have been obtained[67,68,97] by the pressure increase method of measuring permeability coefficients (see section 2.1.8.2). Berman and Lund[87] observed no minima in K-p_m plots up to N_{Ku} = 200 for the flow of noble gases through a porous metal and a porous glass; their experiments were performed by a pressure equalization method. Minima and a flattening of the K-p_m plot have also been observed for the pressure equalization method,[95,96] while ex minima and a curving downwards of the K-p_m plot have been obtained by flow methods.[64,71,93,98] Thus the observed behaviour at low pressures is apparently not dependent upon the method of measuring K.

2.1.5.3 The Time-Lag Method

For gas flow in the Knudsen region, Barrer[27] has described a method of calculating diffusion coefficients based on transient flow measurements. If gas at a pressure p_1 is suddenly applied at zero time to one side of an initially evacuated porous sample, transient flow occurs and a certain time elapses before steady state

flow is attained. Provided the outlet pressure p_0 remains much less than p_1, a plot of p_0 against time t approaches asymptotically a straight line characteristic of steady state flow; extrapolation of the straight line back to cut the t-axis gives an intercept ϕ, which is the "time-lag" and is a measure of the time required to attain steady flow conditions. The time-lag method was introduced by Daynes[100] and has been employed widely by Barrer and co-workers for gas flow in porous plugs[76,82,101-103] as well as for permeation studies in metals[104] and polymer membranes.[105] Experimental details of the method are given in section 2.1.8.2(c).

(a) Theoretical Considerations

For Knudsen flow or molecular streaming, where the diffusion constant D can often be assumed reasonably constant, the general differential equation of flow in a porous medium is

$$\frac{\partial c}{\partial t} = D \frac{\partial^2 c}{\partial x^2} , \qquad \ldots (2.1.5\text{-}6)$$

where c = gas concentration at any point x in the medium.

Barrer[27] has given the solution of equation (2.1.5-6) for transient flow in a porous medium for the boundary conditions:

$$\begin{cases} c = c_i \text{ at } x = 0 \text{ for all } t, \\ c = 0 \text{ at } t = 0 \text{ for } 0 < x < L, \\ c \simeq 0 \text{ at } x = L \text{ for all } t \end{cases} \quad . . . (2.1.5\text{-}7)$$

The solution shows that the intercept on the t-axis or time-lag ϕ is given by

$$\phi = \frac{L^2}{6 D_t'} = \frac{\tau^2 L^2}{6 D_t} , \quad . . . (2.1.5\text{-}8)$$

where D_t' = diffusion coefficient in the actual porous medium,

D_t = diffusion coefficient in the capillaries of the porous medium

$= D_t' \tau^2$, and . . . (2.1.5-9)

τ = tortuosity factor,

Although D_t can be directly related to the gas phase diffusion coefficient D_{gt} for transient flow, adsorption and surface diffusion effects (see section 2.1.6) greatly modify the expression for D_t.[76,82] If the flowing gas is adsorbed according to Henry's law to give a mobile film, D_t is given by the equation[101]

$$D_t = \frac{D_{gt} + D_{st} H}{1 + H} , \quad . . . (2.1.5\text{-}10)$$

where D_{st} = surface diffusion coefficient for transient flow,

$H = S_v k_s / \varepsilon$, and . . . (2.1.5-11)

k_s = Henry's law constant, i.e., the ratio of the number of molecules per cm^2 of the surface to the number per cm^3 of the gas phase.

For an immobile film, $D_{st} = 0$, while for no adsorption, $H = 0$, i.e., $D_t = D_{gt}$. Thus, unless D_{st} is large, the time-lag will be increased by adsorption.[67] Adsorption can only be neglected when H is much less than unity. The diffusion coefficient D_{gt} for an adsorbed gas is estimated[101] from the time-lag for a non-sorbed gas such as helium or neon by the relation

$$D_{gt} = \frac{\tau^2 L^2}{6\phi} = \frac{\tau^2 L^2}{6} \frac{\sqrt{M_{He}}}{\phi_{He}\sqrt{M}} \quad \ldots (2.1.5\text{-}12)$$

Barrer and Grove[101] calculated the mean pore radius r_m and the internal surface area S_v of a porous bed of analcite crystals by considering that the medium was equivalent to a set of uniform parallel cylindrical capillaries. They employed the equations

$$D_{go} = \frac{4\delta\varepsilon\bar{v}}{3 k_1 S_v} \quad \ldots (2.1.5\text{-}13)$$

and

$$r_m = 2\varepsilon / S_v , \quad \ldots (2.1.5\text{-}14)$$

where D_{go} = gas phase diffusion coefficient for the capillary pore model and was equated to D_t when adsorption was negligible (with τ assumed to be $\sqrt{2}$ and δ / k_1 unity). Later workers[76,82] used independent values of $r_m = 2\varepsilon / S_v$ to calculate values of τ. These authors considered that D_{gt} for non-sorbed gases could be directly related to the permeability coefficient for steady state Knudsen flow $K_k = 4 K_o \bar{v} / 3$.

The surface area obtained from steady state flow measurements was generally much less than that calculated by the transient flow method because blind pores contributed to the latter area but not to the former[67,101,106] (see section 2.3.2.3(c)). Barrer and Gabor[102] therefore extended the analysis of time-lag results by considering different area and porosity values (S_t and S_s, $\mathcal{E}_t$ and $\mathcal{E}_s$, respectively) for transient and steady state flow such that

$$\frac{\mathcal{E}_s}{S_s} = \frac{\eta \mathcal{E}_t}{S_t} = \frac{\eta \mathcal{E}}{S_v} . \qquad \ldots (2.1.5\text{-}15)$$

They introduced structure factors $\mathcal{K}$ relating the gas diffusion coefficients D_{gt} and D_{gs} for transient and steady state flow, respectively, to the diffusion coefficient D_{go} for the capillary model (equation 2.1.5-13), e.g.,

$$D_{gt} = \mathcal{K}_{gt} D_{go}$$

and

$$D_{gs} = \mathcal{K}_{gs} \eta D_{go} ; \qquad \ldots (2.1.5\text{-}16)$$

two similar expressions were proposed for the corresponding surface diffusion coefficients, D_{st} and D_{ss}. The permeability coefficient K_k was then related to the diffusion coefficients by the equations

$$K_k / \mathcal{E} = D'_{gs} + D'_{ss} H / \eta \qquad \ldots (2.1.5\text{-}17)$$

$$= \frac{\mathcal{K}_{gs}}{\mathcal{K}_{gt}} \eta D'_{gt} + \frac{\mathcal{K}_{ss}}{\mathcal{K}_{st}} H D'_{st} , \qquad \ldots (2.1.5\text{-}18)$$

where $D' = D / \tau^2$.

By comparison with equation (2.1.5-1), the factor $\mathcal{K}_{gs}\eta / \mathcal{K}_{gt}$ is equivalent to $\varepsilon_s \eta / \varepsilon$ and is readily evaluated experimentally for the flow of a non-sorbed gas.

For a non-sorbed gas[67] (H = 0),

$$K_k \phi = \mathcal{K}_{gs} \eta L^2 \varepsilon / 6 \mathcal{K}_{gt}, \quad \ldots (2.1.5\text{-}19)$$

i.e., the quantity $6 K_k \phi \mathcal{K}_{gt} / \mathcal{K}_{gs} \eta L^2 \varepsilon$ should equal unity. Adsorption, and perhaps surface diffusion, was indicated when this quantity was greater than 1.0, the difference equalling the adsorption coefficient H[67,76,82] when $D_{st} = 0$.[102]

(b) Concentration and Time-Dependence of D

Barrer's time-lag method only applies when the diffusion coefficient D is effectively constant with concentration (or pressure), i.e., when Knudsen flow predominates. Ash and Grove[67] have noted that the theoretical treatment of transient state flow would have to be extended to explain their experimental results in the viscous-slip flow region. Carman and Raal[107] have applied the method for the diffusion of n-butane in Linde silica plugs; they ensured that Δc was small enough so that the diffusion equation (2.1.5-6) was applicable even though D varied considerably with concentration.

Frisch[108,109] considered the concentration- and time-dependence of the diffusion coefficient and obtained a general expression for the time-lag ϕ when D was a function of concentration. His expressions however did not allow for adsorption and surface flow effects.

For a porous medium containing dead-end pores, Fatt[110] demonstrated by means of a laboratory pore model that pressure transients were influenced by the amount of dead-end pore volume. Goodknight, Klikoff, and Fatt[111] allowed for dead-end pores in the diffusion equation (2.1.5-6) by the addition of a source function and derived expressions for transient flow in a porous medium. Goodknight and Fatt[112] extended the treatment by obtaining an expression for the time-lag in terms of the flow channel volume V_c and the dead-end pore volume V_v. Barrer's time-lag theory was inapplicable when restrictions occurred between V_v and V_c but applied when restrictions were negligible;[110] the dead-end pores only influenced the early portion of the transient flow as the flow did not "see" the volume V_v initially (i.e., effective volume = V_c) but later this volume became accessible (effective volume = $V_c + V_v$) as if there were no

restrictions between V_v and V_o.[110,112] Rose, Tung, and Newman[50] showed by means of an analog network model that pressure transients depended on the number and location of dead-end pores, and the resistance of the dead-end pore.

If the dead-end and open pores differed in size and shape, Barrer and Gabor[103] considered that the diffusion coefficient could vary with time since the dead-end pores would have a decreasing influence on gas-phase flow but an increasing influence on surface flow as steady state was approached. They suggested that the time-lag ϕ could be expressed as

$$\phi = \frac{a}{h} + \frac{L^2}{6 D_s} , \qquad \ldots (2.1.5\text{-}20)$$

where D_s = diffusion coefficient for steady state flow, and

$a/h = \phi (1 - D_{gt}/ D_{gs})$ for a non-sorbed gas; a positive value of a/h could mean that the dead-end pores were on the average of smaller diameter than the open pores. Kraus and Ross[106] also considered that dead-end or blind pores would produce a time-dependent diffusion coefficient.

(c) Experimental Observations

Barrer and Grove[101] found that the time-lag ϕ was fairly constant with pressure for the flow of inert and permanent gases through a bed of analcite crystals

(ε / S_v = 1.4 microns), although a close examination of the typical experimental results given showed that ϕ possibly increased slightly as p_m decreased. For the flow of the polar gases ammonia and sulphur dioxide, ϕ increased sharply as p_m decreased; these gases were suspected to be adsorbed as immobile films in the porous medium. For microporous media with ε/S_v between 3 and 14 Å, Barrer and co-workers[76,82,102,103] generally found that ϕ was independent of p_m although ϕ increased slightly as p_m decreased in several experiments; the corresponding K-p_m plots showed that Knudsen flow predominated since K was independent of or increased slightly with p_m.

Ash and Grove[67] observed that ϕ increased as p_m decreased for the flow of a range of gases through a porous ceramic (ε /S_v = 0.102 microns), the plots for sulphur dioxide and, to a lesser extent, carbon dioxide curving upwards very sharply possibly because of surface flow. These authors employed the limiting value ϕ_i at zero pressure to calculate pore properties. The product $K\phi$ remained substantially constant (cf. equation 2.1.5-19) over the pressure range of the experiments for all gases except hydrogen and sulphur dioxide even though the flow was in the viscous-slip region above about p_m = 4 cm Hg. The diffusion coefficient D_t' approximately equalled K_k/ε for most

non-sorbed gases.

For non-sorbed gases, $\phi_1\sqrt{(\mathscr{J}/\mathbb{M})}$ was observed to be constant and equation (2.2.5-19) obeyed.[67,76,82] For gas flow in Vycor porous glass, Barrer and Barrie[82] found that adsorption effects were very marked except for the gases helium, neon, and hydrogen and $\phi_1\sqrt{(\mathscr{J}/\mathbb{M})}$ and $K_k/D_t'\varepsilon$ increased with adsorption. However K_o (= 3 K_k / 4 $\bar{v}$) remained relatively constant showing that surface flow was negligible for steady state flow but made a considerable contribution to flow in the transient state; this difference was because all the accessible micropores and crevices were penetrated and filled by gas molecules during the transient period whereas those pores which were blind did not contribute to the flow when steady state was established. Barrer and Strachan,[76] and Carman and Raal[107] found that the transient flow and steady flow results were in agreement for Carbolac and Linde silica plugs, respectively. The former authors discovered that even helium and neon showed surface diffusion effects.

(d) Discussion about the Time-Lag Theory

The simple theory originally developed by Barrer for determining diffusion coefficients for gas flow in porous media from transient state measurements is only applicable to systems where D is independent of both

concentration and time, i.e., when Fick's second law of diffusion is obeyed. However, when either a minimum occurs in the K-p_m plot at low pressures so that K increases with decreasing p_m in the Knudsen flow region, or the flow is in the viscous-slip flow region, K (≡ D) is a function of pressure (or concentration). When blind pores occur in the porous medium, every evidence indicates that D is time-dependent during transient flow so that Fick's law is invalid.

Barrer has extended the time-lag theory to allow for the adsorption and surface flow of the gas molecules in the porous medium. This theory only applies in the Henry's law adsorption region, i.e., for very dilute adsorbed films, since at higher concentrations D_{st} is strongly dependent upon concentration and the transport can not be considered a diffusion process.[107,113] As mentioned in section 2.1.6, the whole concept of surface diffusion in porous media is doubtful thus suggesting that Barrer's approach may be questionable. According to Babbitt,[114] the use of Fick's law as the fundamental equation for diffusion in porous media is not valid when adsorption occurs.

The use of a capillary pore model to describe a porous medium is a gross over-simplification (see section 2.1.2.2), and in the time-lag theory leads

to many obscurities[82] which have tended to confuse the understanding of flow processes in porous media. The improved approach of Barrer and Gabor[102] is more rigorous than the original theory of Barrer, but tends to make the analysis more complex since it is difficult to appreciate the significance of the four structure factors.

It is necessary that further mathematical approaches similar to those of Frisch[108,109] and Fatt[110-112] be considered. The flow equation should be extended to allow for all possible flow phenomena, e.g., it should contain a term for viscous-slip flow, a source function to account for time effects, adequate treatment of adsorption and surface flow effects, and a means of allowing for the variation of the diffusion coefficients with concentration. The final expression for ϕ could be very complex and require an electronic computer for calculations.

No complete explanation of the observed variation of ϕ with p_m has been given although adsorption[101] and surface flow [67] effects were suggested as possible reasons for the sharp increase of ϕ at low p_m. No attempts have been made to analyse time-lag results obtained in the viscous-slip flow region where Barrer's theory does not apply.

2.1.6 The Flow of Adsorbable Gases

Equation (2.1.4-2), viz.,

$$K = \frac{B_o P_m}{\mu} + \frac{4}{3} K_o \sqrt{\frac{8 \mathcal{R} T}{\pi M}} \quad \ldots (2.1.4\text{-}2)$$

shows that the limiting permeability at $p_m = 0$ should be proportional to $\sqrt{(T/M)}$, i.e., at a given temperature the intercepts of the K-p_m plots for the flow of different gases in a porous medium should vary with $1 / \sqrt{M}$. However, a number of investigators[115-118] have observed that the flow of adsorbable gases through porous media did not obey this law since the flow-rates were much greater than those expected. Gilliland, Baddour, and Russell[83] found that the permeabilities for ethylene, propylene, and isobutane flowing through Vycor glass were up to seventeen times larger than the values predicted from equation (2.1.4-2).

The most widely accepted explanation for this enhanced flow is that there is a flow of adsorbed gas at the pore walls of the porous medium in addition to the normal flow in the gas phase (ref.5,p.105). This flow in the adsorbed phase is known as surface diffusion. Most gases and vapours are physically adsorbed onto porous materials to a significant extent and even helium, which is generally considered to be non-sorbed at room temperatures, has been shown to be slightly adsorbed[76,119]

on some materials and to give surface flow effects.[76] When a gas is caused to flow through a porous material under a pressure gradient, each molecule, on colliding with a solid surface, is adsorbed for a certain finite time τ before it is evaporated or desorbed (ref.5,p.104). Such adsorption would not be expected to influence the steady gas phase flow through the porous medium provided the adsorbed layer is immobile and is a negligible part of the total pore volume.

As the surface concentration of the adsorbed molecules depends upon the pressure (presumably according to the adsorption isotherm), there is a surface concentration gradient corresponding to the pressure gradient through the porous medium. If the time of residence τ of the adsorbed molecules at the surface is long enough and the molecules possess a certain mobility, then this concentration gradient causes a diffusion of the molecules in the surface layer in addition to the gas phase flow due to the pressure gradient.

Carman (ref.5,Chapt.5) and Timofeev[89] have reviewed surface flow phenomena. Carman and Malherbe[118] considered that surface flow made a significant contribution to the total transport when the surface to volume ratio of the porous medium was large, e.g., when the specific surface S_0 was greater than 10^6 cm^2/cm^3. The mechanism of

surface diffusion has been discussed by Carman (ref. 5, p.118). At low surface concentrations, the gas molecules adsorbed on energetically smooth surfaces may behave as a two-dimensional gas with a gas-like mobility characterized by a very small activation energy. Alternatively, a definite activation energy may be required for strongly adsorbed molecules to jump from one adsorption site to the next. However, the activation energy is no criterion for distinguishing between the two mechanisms of surface flow.[89]

2.1.6.1 The Calculation of Surface Diffusion Coefficients

Surface flow can be assumed[118,120] to take place in parallel with the flow in the gas phase and an extra term added to the flow equation (2.1.4-2) as the contribution due to surface flow, e.g.,

$$K = K_g + K_s \qquad \ldots (2.1.6\text{-}1)$$

$$\text{or } -\frac{G}{M} = D'_{gs}\frac{\partial c_g}{\partial x} + D'_{ss}\frac{\partial c_s}{\partial x}, \qquad \ldots (2.1.6\text{-}2)$$

where K_g = permeability coefficient for gas phase flow (equation 2.1.4-2),

K_s = permeability coefficient for surface flow,

D'_{gs} = gas phase diffusion coefficient,

D'_{ss} = surface diffusion coefficient,

c_g = gas phase concentration/unit bulk volume

$$= \varepsilon p / RT, \qquad \ldots (2.1.6\text{-}3)$$

c_s = adsorbed phase concentration/unit bulk volume

$$= \rho_b \, y, \qquad \ldots (2.1.6\text{-}4)$$

p = pressure of the gas,

ρ_b = bulk density of the porous medium, and

y = adsorbed phase concentration/unit weight of the medium.

If K_g can be estimated from the permeability of a non-sorbed gas (helium), then the difference between the measured permeability K and the estimated K_g is the excess flow attributed to surface diffusion.
The surface diffusion coefficient then becomes

$$D'_{ss} = (K - K_g) / \varepsilon H, \qquad \ldots (2.1.6\text{-}5)$$

where H = adsorption coefficient

$$= \partial c_s / \partial c_g \, . \qquad \ldots (2.1.6\text{-}6)$$

For the satisfactory evaluation of D'_{ss}, both D'_{ss} and H should be constants or Δp should be small enough so that these quantities can be assumed constant (ref.5,p.110). The calculation of surface diffusion coefficients for transient or unsteady state flow has been discussed previously under the time-lag method (section 2.1.5.3 (a)).

2.1.6.2 Experimental Observations

Carman and Malherbe[118] and Carman and Raal[107,113] have found that the surface diffusion coefficient D'_{ss}

was strongly dependent upon the surface coverage or adsorbate concentration y. Three adsorption regions were observed. At low concentrations less than the monolayer concentration, D'_{ss} increased rapidly with increasing y. Above the monolayer concentration, at which a slight maximum in D'_{ss} occurred, multilayers were formed and D'_{ss} was approximately constant. As y approached the saturation value, D'_{ss} increased rapidly due to capillary condensation. Similar results were observed by Ross and Good,[121] and Gilliland et al.[83]

At relative vapour pressures near unity, when the pore space became almost completely filled with capillary condensate, Carman[122] found that the driving force producing flow of the capillary condensate through a porous medium was not the measured gas pressure difference, but a much larger capillary pressure difference resulting from the action of surface tension on the liquid-vapour interfaces in the pores. The capillary condensate then behaved as if it were a bulk liquid in viscous flow through the pores and caused the very high values of D'_{ss}. Experimental results of Carman[122] agreed within 20% with the theoretical deductions. The permeability showed a hysteresis effect similar to that observed for an adsorption isotherm as it depended upon whether the gas was being adsorbed or

described.[83,122] If the saturation pressure was exceeded, the permeability decreased sharply since the condensed liquid hindered flow.[118,123,124]

The theoretical treatments of Carman (ref.5,p.108) and Barrer (see section 2.1.5.3 (a)) are based upon Fick's laws of diffusion, which may not strictly apply when the diffusion coefficient varies with concentration.[83,114,123] By contrast, Gilliland et al.[83] and Rutz and Kammermeyer[123] considered that the adsorbed layer acted as a two-dimensional fluid such that surface flow could be described as a hydrodynamic phenomenon. The derived correlations relating the surface flow to the adsorption isotherm data satisfactorily fitted the experimental results for a wide range of conditions.

2.1.6.3 Criticism of the Surface Flow Theory

A number of the assumptions made in the theoretical considerations of surface flow tend to be dubious. As helium can sometimes be adsorbed and even show surface flow effects, the method of calculating D'_{ss} as the flow in excess of the gas phase flow is not completely satisfactory. In the microporous media (d = 13 to 60 Å) in which surface flow has been observed,[76,82-84,86,113] a molecule of about 4 Å diameter would reduce the cross-sectional area of a pore by about 25% to 85% when a

monolayer was completed; such an adsorbed layer would surely considerably influence the gas phase flow-rate. There is no direct evidence that the equilibrium between the gas phase and the adsorbed layer in the pores during flow is identical with that obtained from adsorption measurements. The surface transport can not really be described as a diffusion process since D'_{ss} varies considerably with concentration.

2.1.7 The Turbulent Flow Region

For gas flow through a tube, the Hagen-Poiseuille equation ceases to describe the flow when the flow-rate exceeds a certain critical value (see section 2.1.2.1). Similarly, for gas flow in porous media, Darcy's law ceases to be valid at high flow-rates (ref.6,p.123). Although this departure from Darcy's law has been often attributed to the commencement of turbulence within the pores, other mechanisms have been suggested as mentioned below in section 2.1.7.1. In straight tubes, the transition between viscous and complete turbulent flow is quite sharp. However, in porous media, the transition to "turbulent" flow is gradual because of the wide size distribution of the pores and their tortuous nature (ref.15,p.58).

As with viscous flow (section 2.1.3.1), a large number of correlations, both empirical and theoretical,

have been proposed to relate the pressure drop to the flow-rate for flow through porous media in the transition or quasi-turbulent and turbulent flow regions. Scheidegger (ref.6,section 7.2) has reviewed these correlations in detail; they are discussed in section 2.1.7.2.

2.1.7.1 The Mechanism of Turbulent Flow

Several explanations for the deviation from Darcy's law at high flow-rates have been advanced in the literature. By analogy with flow through straight tubes, it can be assumed that this deviation is due to the onset of turbulence within the pores of the medium, i.e., the instantaneous velocity of flow at a given point begins to fluctuate rapidly with time in both magnitude and direction. This explanation was maintained by Cornell and Katz,[125] who considered that turbulence was only present in the larger pores at first while viscous flow occurred in the bulk of the moving stream; this turbulence was responsible for the extra pressure drop required for flow.

This explanation generally appears unsatisfactory[126] since the value of the "critical" Reynolds number, above which Darcy's law ceases to hold, is much lower for porous media than for straight tubes (about 2000) and apparently ranges from 0.1 to 75 (ref.6,p.124).

Carman (ref.5,p.155) has suggested that flow in porous media could be more closely analogous to flow in a curved tube than in a straight tube.

Another explanation[127] attributes the deviation from Darcy's law to the drag resulting from the separation and local eddies which attend the growth of inertia forces in a fluid as it flows through a medium. Lapple[128] considered that the kinetic energy losses due to contractions and expansions of the cross-sectional area of the pores as the fluid moved through the porous medium were responsible for nearly all the pressure drop; the roughness of the surface of the medium had little effect on the flow.

Green and Duwez[126] considered that the latter two mechanisms should be combined so that both constrictions and drag effects contributed to the total resistance to flow, which was termed "inertial resistance". Then the flow could be described by a quadratic resistance equation (cf.equation 2.1.7-2). Their experimental results for gas flow through porous metals supported their argument.

The different explanations proposed for the deviation from Darcy's law at high flow-rates indicate that the detailed mechanism of the flow process in the interstices of a porous medium at these flow-rates is

not greatly understood. The departure from viscous flow may possibly be due to both the onset of turbulence and the gradual increase of inertia effects in the pores.

2.1.7.2 Turbulent Flow Correlations

(a) Forchheimer-type Equations

Forchheimer[129] in 1901 suggested that a second-order or a third-order velocity term added to Darcy's law would correlate experimental results for flow through porous media at high flow velocities. Thus

$$\Delta p/L = av + b v^2 + cv^3, \quad \ldots (2.1.7\text{-}1)$$

where $\Delta p/L$ = pressure gradient across the porous medium,

v = superficial linear velocity of flow based on the cross-sectional area of the medium, and

a,b,c = factors, presumably constant.

The Forchheimer relations are valid only at very high velocities.

Other investigators (ref.6,p.127) have proposed relations between $\Delta p/L$ and v^n. The value of the exponent n was between 1 and 2 but varied with the system investigated so that no consistent correlation was achieved.

If the transition to turbulent flow is caused by an increase in kinetic energy losses due to the inertia forces in the fluid, the inertial resistance can be

regarded as superimposed upon the viscous resistance (ref.5,p.155) so that a second-order Forchheimer-type equation results, e.g.,

$$\Delta p/L = \alpha \mu v + \beta \rho v^2. \qquad \ldots (2.1.7\text{-}2)$$

Rearrangement of this equation gives

$$\frac{p_m \Delta p}{L G} \frac{\rho_o}{} = \frac{\mu}{B_o} + \beta G, \qquad \ldots (2.1.7\text{-}3)$$

where $\rho_o = M/z\mathcal{R}T$,

B_o = viscous flow permeability coefficient

$= 1/\alpha$, $\qquad \ldots (2.1.7\text{-}4)$

α = viscous resistance coefficient,[126] and

β = inertial resistance coefficient.[126]

The coefficients α and β, of dimensions L^{-2} and L^{-1} respectively, are characteristic properties of a porous medium. A plot of $p_m \Delta p/L G$ against G is linear, with μ/B_o and β as the intercept and slope, respectively. Such a plot has been shown to be applicable to unconsolidated beds by Lindquist,[130] and Ergun and Orning,[131] and to consolidated porous media by Green and Duwez,[126] Cornell and Katz,[125] and Greenberg and Weger.[132]

By extending the Kozeny-Carman equation (2.1.3-3) to the turbulent flow region by the addition of a second term corresponding to the kinetic energy losses, Ergun and Orning,[131] and Ergun[133] theoretically deduced

the equation

$$\frac{\Delta p}{L} = 5\alpha_E \frac{(1-\varepsilon)^2}{\varepsilon^3}\mu S_o^2 v + \beta_E \frac{(1-\varepsilon)}{8\varepsilon^3}\rho v^2 S_o \quad \ldots (2.1.7\text{-}5)$$

where α_E and β_E expressed the parts of the pressure drop due to viscous and kinetic energy losses, respectively. Several authors[134,135] have tested the correlations of Ergun,[133] Chilton and Colburn,[136] Carman,[32] Brownell et al.,[137] and Leva[138] (see section 2.1.7.2(c)) with experimental results for gas flow through beds of particles; Ergun's correlation was found to give the most consistent prediction of the pressure drop across the bed.

(b) <u>The Reynolds Number - Friction Factor Representation</u>

The representation of flow through porous media by means of the Reynolds number N_{Re} and the friction factor f is extremely popular. These dimensionless groups are defined as (cf. section 2.1.2.1 (b))

$$N_{Re} = \frac{d\, v\, \rho_m}{\mu}, \quad \ldots (2.1.2\text{-}3)$$

and

$$f = \frac{2\, d\, \Delta p}{\rho_m v^2 L}, \quad \ldots (2.1.2\text{-}4)$$

where d = a diameter associated with the porous medium, which is considered equivalent to an assemblage of straight capillary tubes.

This representation is thus dependent on both the choice of the quantity d and the limitations of the capillary model (ref.6,p.123). As there is no rigid definition of the pore diameter d (section 2.4.1), the use of the Reynolds number concept as defined above fails to describe flow in porous media satisfactorily.

Nevertheless, with appropriate modifications of the groups, better correlations have been obtained. The particle diameter[136,137] and the mean surface diameter[139] have been employed as a measure of d for granular unconsolidated beds, but these diameters are unsatisfactory for consolidated media where the particles have generally lost their individual identity. Often the dimensionless groups have been modified in various ways by the introduction of the various pore properties; correlations involving these modified groups are considered in section (2.1.7.2(c)).

Because of the lack of consistency among investigators in defining the properties of porous media, and the variance between the methods of modifying the dimensionless groups, the "critical" Reynolds number varies by a factor of 750. For this reason, no universally applicable $f - N_{Re}$ correlation has apparently been found; each correlation is valid only for the particular system for which it was derived (ref. 6, p.132).

(e) Modifications to N_{Re} and f

Most investigators found that the Reynolds number and friction factor defined by equations (2.1.2-3) and (2.1.2-4) did not account for variations in the properties of porous media. The porosity ε was considered especially significant and modified friction factors

$$f' = f \times \Phi(\varepsilon)$$

were proposed to correlate experimental results, generally for unconsolidated beds. The various porosity functions $\Phi(\varepsilon)$ employed in these modifications have been reviewed by Hudson and Roberts,[140] and Scheidegger (ref.6,p.129), and include ε^2, ε^n, $\varepsilon^3/(1-\varepsilon)$, and $1/(1-\varepsilon)^3$. The friction factor was also modified by the introduction of d^2 or d^n in to equation (2.1.2-4). These modified friction factors have been correlated in various ways with the Reynolds number by different authors to fit their experimental results (ref.6,p.130), each author claiming that his particular correlation was valid for a certain range of N_{Re}.

The shape and surface area of the particles of the porous bed were considered by some workers (see Leva et al.)[141].

Blake,[142] and Burke and Plummer[143] introduced a modified Reynolds number

$$N_{Re}' = \frac{\rho v}{\mu S_v} , \qquad \ldots (2.1.7\text{-}6)$$

and a modified friction factor

$$f' = \frac{\Delta p \, \varepsilon^3}{L \rho v^2 S_v} , \qquad \ldots (2.1.7\text{-}7)$$

in terms of the surface area S_v of the bed per unit bulk volume. Carman[32] employed Blake's modified groups to propose the relation

$$f' = c/(N_{Re}')^{0.1} \qquad \ldots (2.1.7\text{-}8)$$

where c depended upon the particle shape. For a large number of experimental results, the critical Reynolds number occurred at $N_{Re}' \simeq 1$. Leva[138] obtained a similar relation to that of Carman.

Brownell et al.[137] obtained empirical correction factors F_{Re} and F_f from charts of the correction factor against the porosity with the particle sphericity as a parameter. Then N_{Re} and f were corrected by means of these factors. The prepared charts were inaccurate at low sphericities and high porosities.[135] For beds of uniformly-sized spheres consolidated with resin, Brownell et al.[144] obtained an f-N_{Re} plot in terms of the corrected N_{Re} and f.

As an extension of their investigations on viscous flow through porous media, MacMullin and Muccini[145] suggested that N_{Re} and f could be modified to include the hydraulic radius and the electrical tortuosity factor. Their groups have not been tested experimentally.

(d) The Green-Duwez Approach

A number of the authors[136,137,140,141,144] mentioned previously presented their experimental results by means of an f-N_{Re} plot. Often, a large scatter was observed about the plot in the quasi-turbulent and turbulent flow regions with the porosity[140] or surface roughness[141] as a parameter.

Green and Duwez[126] overcame this problem of scatter and found that their experimental results for the flow of gases through porous metals fell along a single curve of equation

$$f'' = 2 + 2/N_{Re}'' \qquad \ldots (2.1.7\text{-}9)$$

by employing the dimensionless groups

$$N_{Re}'' = \frac{\beta v \rho}{\alpha \mu} \qquad \ldots (2.1.7\text{-}10)$$

and

$$f'' = \frac{2 \Delta p}{\beta \rho v^2 L} . \qquad \ldots (2.1.7\text{-}11)$$

The two coefficients α and β were the viscous and inertial resistance coefficients of the medium, respectively, and were determined from the intercept

and slope of a plot of $p_m \Delta p/LG$ against G (see equation 2.1.7-3).

Cornell and Katz[125] also obtained a satisfactory $f-N_{Re}$ plot for their results for gas flow through samples of sandstone, limestone, and dolomite by using these modified groups. They expressed α and β in terms of the electrical formation factor F, the porosity ε, the hydraulic radius m, and two empirical constants. Greenberg and Weger[132] also employed these groups to correlate their experimental results for flow in porous metals.

For flow in the transition region between viscous and complete turbulent flow, where no satisfactory analytical expressions were available, Stutzman and Thodos[146] suggested that the Cornell and Katz $f-N_{Re}$ plot was particularly advantageous for predicting the flow of fluids through consolidated formations for engineering purposes. They presented a plot of β against B_o, due to Katz and Cornell,[147] so that β could be readily estimated.

(e) Theoretical Correlations

Some authors have applied dimensional analysis in considering the many variables that might influence flow through porous media (ref.6,p.133). Thus Rose[148] made a thorough study of the possible variables and

obtained a complex dimensionless equation. Unfortunately the values of the exponents in the equation must be determined experimentally.

Other investigators have endeavoured to extend the viscous flow theories (see section 2.1.3.1) to the turbulent flow region (ref.6,p.135). Ergun and Orning,[131] and Cornell and Katz[125] have extended the Kozeny-Carman theory (section 2.1.3.2) to the turbulent region. Such approaches are subject to the limitations of the original viscous flow theory and may depend on the critical value of the Reynolds number.

The application of the concepts of statistical hydrodynamics to turbulent flow in porous media has been considered by Scheidegger.[78] The flow was shown to consist of two effects, viz., an average turbulent flow portion and a dispersivity effect.

(f) Discussion on Turbulent Flow Correlations

Scheidegger (ref.6,p.132), in reviewing the numerous correlations for turbulent flow, has stated that "they cannot all be universally valid, as practically any one of them contradicts the others". The frequently used correlations based upon the Reynolds number concept were subject to the limitations mentioned in section (2.1.7.2(b)). Scheidegger considered that there was no such thing as a "universal"

critical Reynolds number at which turbulence would commence. There was apparently no physical basis to expect that flows should be identical in two different systems even if the Reynolds numbers were the same.

In nearly all the attempts to obtain a correlation between the pressure drop and flow-rate for flow through a porous medium in the quasi-turbulent and turbulent flow regions, some property of the medium such as the pore diameter d, the particle diameter d_p, the porosity ε, or the surface area S is involved. Although it is desirable to be able to predict the flow through a medium from its pore properties, no satisfactory correlation applicable to all systems has been found. Because of the lack of an adequate definition for d, and the uncertainty whether the experimental values of ε and S are a true measure of the pore volume and surface actually involved in flow, this apparently desirable approach becomes unacceptable for flow in consolidated media. The dimensionless groups defined by equations (2.1.2-3) and (2.1.2-4), and those proposed by Blake,[142] Brownell et al.,[137] and MacMullin and Muccini[145] are therefore unsuitable for consolidated media.

For these reasons, the procedure proposed by

Green and Duwez[126] and developed by Cornell and Katz,[125] and Stutzman and Thodos[146] is the most satisfactory method of correlating experimental results for flow through porous media at high flow-rates. This procedure is suitable for both liquids and gases for linear or radial flow,[146] and should also be applicable to flow in unconsolidated materials.[125] As noted in section (2.1.7.2 (a)), a similar treatment by Ergun and Orning[131] has given a fairly reliable correlation for flow through granular beds.

The criticism of Scheidegger concerning the use of the Reynolds number concept in correlating flow through porous media does not apply to N_{Re}'' and f'' since the definitions (equations 2.1.7-10 and 2.1.7-11) are not dependent upon any pore model and β/α, of dimensions L, represents a characteristic length of the medium which can be readily determined.

It is probably a disadvantage[149] that several flow experiments must be performed under transition or turbulent flow conditions for each flow system in order to evaluate α and β. If B_o is known, e.g., from low pressure experiments, β can be estimated from the graph[147] of β against B_o. However, on evaluating α and β, it should be possible to estimate from the f'' - N_{Re}'' plot the flow through a porous medium over a

wide range of Reynolds numbers from viscous to turbulent flow.[146]

Although Cornell and Katz[125] expressed α and β in terms of F, ε, m, and empirical constants k_1 and k_2, the values of m and k_2 were calculated from the experimental values of α and β (k_1 was assumed to equal 0.5). Thus, at the present time, no satisfactory prediction of the flow can be obtained by the Green and Duwez method from a knowledge of the properties of the pore structure of the medium. It may be possible to relate the coefficient β to the properties of a medium by the choice of a suitable pore model (cf. $\alpha = 1/B_0 = k/\varepsilon m^2$ for a capillary pore model).

2.1.8 The Measurement of Permeability Coefficients

2.1.8.1 The Theory of Permeability Measurements

The definitions of the various permeability coefficients given in sections 2.1.1.5 and 2.1.1.6 show that these coefficients can be determined experimentally by the measurement of the volumetric flow-rate Q_m or the mass flow-rate G of the gas flowing through the porous medium due to a pressure difference Δp. Generally, the inlet pressure p_i and the outlet pressure p_o are measured and p_m and Δp obtained respectively from the relations

$$p_m = \tfrac{1}{2}(p_i + p_o) \qquad \ldots (2.1.1\text{-}12)$$

and $$\Delta p = (p_i - p_o). \qquad \ldots (2.1.1\text{-}9)$$

From the measured dimensions of the sample, the flow length L and the cross-sectional area to flow A are calculated. The viscosity of the gas μ at the temperature of the determination $\mathcal{T}_s$ is obtained from published viscosity data.[150]

2.1.8.2 The Methods Used for Determining Permeability Coefficients

In all the methods mentioned in the literature for determining permeability coefficients for gas flow through porous media, the measurement of the pressures p_i and p_o follows a relatively standard pattern. Pressures from a few cm Hg absolute up to 2 atm are measured by means of mercury manometers, and pressures above 1 atm absolute by Bourdon-type pressure gauges. For very low pressures, suitable vacuum gauges such as the McLeod gauge, the Pirani gauge, or the ionization gauge are employed. Often, the pressure difference across the medium Δp is measured by means of a differential manometer or gauge.

The measurement of the gas flow-rate is more varied than the pressure measurement. The range of flow-rates encountered for flow through porous media is extremely large, the magnitude of the flow-rate

depending upon the porosity and pore size of the medium under investigation, the gas studied, and the pressure and temperature conditions. Different methods of flow-rate measurement are necessary for flow in very porous sandstones at high pressures and for flow in fine-pored glasses under vacuum conditions. Hence a number of methods have been applied to measure the flow-rate and have led to the variety of methods available for determining permeability coefficients. Both direct and indirect methods of flow-rate measurement have been used, the direct methods generally applying to steady state flow measurements and the indirect methods to unsteady state measurements.

The methods of determining permeability coefficients for the flow of gases through porous materials can conveniently be subdivided into the following classifications:

(a) the flow method,

(b) the variable volume flow method,

(c) the pressure increase method (and the time-lag method),

(d) the pressure equalization and decay methods.

These methods are described below. They are represented schematically in Fig. 2.1-2.

(a) Flow Method

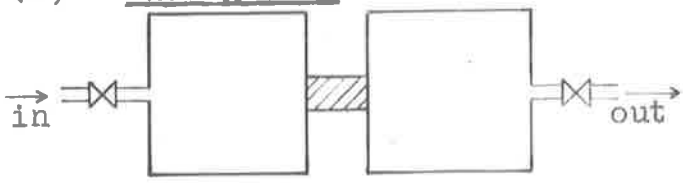

p_i const. p_o const.

Measure gas flow-rate with flow-meter.

(b) Variable Volume Flow Method

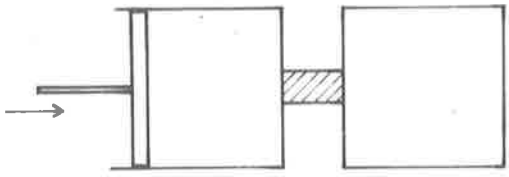

V_i is decreased with time to keep p_i const.

p_o const. $V_o \simeq$ const.

Flow-rate obtained from rate of volume change, dV_i/dt.

(c) Pressure Increase Method

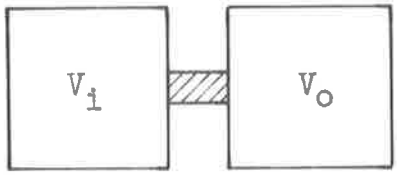

$p_i \simeq$ const. V_i large

$p_o = 0$ at $t = 0$. p_o increases with time.

Flow-rate obtained from rate of increase of p_o in V_o, dp_o/dt.

(d) Pressure Decay Method

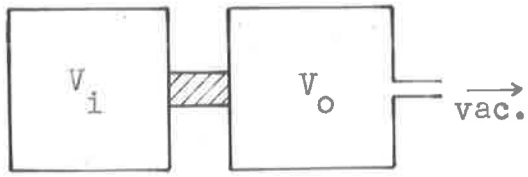

p_i decreases with time.

$p_o \simeq 0$.

Flow-rate obtained from rate of decay of p_i in V_i, dp_i/dt.

▨ = Graphite Sample.

Fig. 2.1-2 Schematic Representation of the Methods for Determining Permeability Coefficients for Gas Flow in Porous Media.

(a) The Flow Method

Permeability coefficients can be determined by a flow method, in which gas at a constant inlet pressure p_i flows through the porous sample under a constant pressure difference Δp and the gas flow-rate is measured directly by means of a suitable flow-meter (see Fig. 2.1-1 (a)). The flow method is a steady state method and is particularly suitable for permeability determinations at pressures above atmospheric pressure where viscous and turbulent flow occur. A number of types of flow-meters have been used to measure the gas flow-rate, the type depending mainly on the range of flow-rates occurring. At low flow-rates, the volume of gas flowing in a given time interval can be measured directly at the pressure and temperature of the gas stream by displacement in a calibrated tube or vessel.

For low flow-rates of the order of 0.001 to 0.1 cm^3/sec, several investigators[84,85,123] timed the volumetric displacement of a mercury slug moving along a length of calibrated capillary tubing. For accurate flow measurement by a mercury slug meter, the mercury and capillary surface must be scrupulously clean so that the slug moves uniformly through the

capillary. Other workers[63,66] have measured the rate of collection of gas by displacement of water in a graduated vessel. Cornell and Katz[125] measured gas flow-rates by means of a soap-bubble flow-meter,[151] in which the time was observed for a soap film moving up a burette to cover a certain volume. The burette must be completely wetted by the soap solution for the soap films to remain stable.

Wall[152] of the Australian Atomic Energy Commission has measured the flow-rate of methane labelled with radioactive C^{14} through impregnated graphites. A sample of the outflowing gas was collected for a small time interval and its radioactivity (and hence the volume) measured. As leaks into the outflowing gas have no effect on the flow-rate measurement, this flow method is very favourable for the measurement of low flow-rates under vacuum conditions provided the necessary facilities are available for handling isotopes, and the gases to be investigated can be labelled. For the measurement of large gas flow-rates, the pressure difference across a constriction can be measured instead of the volume directly. For greatest accuracy, flow-meters of this type require calibration for each gas as well as for temperature and pressure, although any changes in the flow

conditions can be allowed for by theoretical factors of questionable accuracy. It is advisable to operate these flow-meters at constant pressure and temperature conditions to avoid the need of any correction. Both capillary flow-meters[74,132,153] and orifice flow-meters[136] have been frequently used. These meters are unreliable if the constriction coefficient varies with the Reynolds number. Higher flow-rates have been measured with rotameters.[34] In these flow-meters, the height of a float indicates the flow-rate, which for various meters can range from 0.5 cm^3/sec to 20 l./sec.

In wet gas test meters, the volume of gas passing in a given time interval is measured by the displacement of water in a revolving sectioned drum and must be corrected for the water vapour in the gas. These meters have been used at high flow-rates for direct flow-rate measurement[125] or for calibration of pressure differential flow-meters.[153]

Several investigators have applied the flow method for permeability determinations below atmospheric pressure. The flow-rates in such determinations have been measured either by capillary flow-meters placed on the inlet side of the sample so that the pressure in the capillary remained at one atmosphere,[93,98]

by mercury slug meters under vacuum conditions,[84,85] or by the collection of the gas discharged from the vacuum pump.[63,66]

Of the flow-meters that have been used to measure the flow of gases through porous media, those in which the volume of gas at a known pressure and temperature is measured directly are preferable to the other meters which require calibration. Flow measurement at low flow-rates and under vacuum conditions by means of a flow-meter is generally difficult and not entirely satisfactory. By variation of the size of the calibrated vessel or constriction, a range of flow-rates can be measured by any type of flow-meter.

(b) The Variable Volume Flow Method

A variation of the steady state flow method has been used to determine permeability coefficients at pressures lower than one atmosphere, where simple flow-rate measurement is relatively difficult. A device is included in the apparatus whereby the volume of the isolated apparatus can be varied to keep a constant Δp across the sample, and the flow-rate obtained directly from the rate of volume change (see Fig. 2.1-2 (b)).

A number of investigators have applied this variable volume flow method for permeability measurements on fine-pored media. Generally, either p_i or Δp was

controlled by causing mercury to rise in a gas burette and so decrease the inlet volume V_i as the gas flowed through the porous sample. Carman and Malherbe[154] controlled p_i manually and maintained p_o at a constant value by a manostat. This technique was modified by Carman and co-workers[64,118] who automatically controlled p_i; when p_i decreased, mercury in a manometer broke electrical contact causing a small electrolytic cell to generate gas and raise mercury in the burette until p_i was at the desired value again. Flood, Dacey, and co-workers[86,116,155] maintained p_i constant by an electric contact mercury manometer; this manometer operated a magnetic valve admitting mercury to the gas burette at a rate such that p_i remained constant. Other workers[83,121] used motors to cause movement of the mercury column in the burette. If the outlet volume of the apparatus was much larger than V_i, p_o could be kept constant manually.[83,86,155]

By employing their respective versions of the variable volume flow method, the investigators mentioned above have satisfactorily measured flow-rates of the order of 0.001 to 1.0 cm^3/sec under low pressure conditions. Either the diameter of the burette or the inlet volume of the apparatus can be

varied to extend the range of flow-rates that can be measured by this method. As manual control of the pressure can be tedious, especially during a long experiment, some method of automatic control is desirable; however the apparatus required is complex and can not be simply constructed. For experiments which may require a long period of time to reach steady state flow, the variable volume flow method may not be entirely satisfactory.

(c) The Pressure Increase Method (and Time-Lag Method)

The flow-rate of a gas through a porous medium at low pressures has been successfully determined by measuring the rate of increase of the pressure p_o in an isolated volume V_o on the outgoing side of the previously evacuated medium while applying a constant gas pressure p_i on the ingoing side (see Fig.2.1-2(c)). This is essentially a non-steady state method since Δp and hence the flow-rate decrease with time; however, if p_i is very much greater than p_o during an experiment, steady state flow conditions can be assumed and a steady flow-rate is observed (as shown by a straight line plot of p_o against time t) after an initial unsteady state flow period. When p_i is only slightly greater than p_o, a curved pressure increase

plot is obtained as steady state conditions are not approximated.

Barrer and co-workers[65,76,82] controlled the inlet pressure by means of a Toepler pump and measured p_o as a function of time with a McLeod gauge. The outlet volume was sufficiently large so that p_o was negligible compared with p_i throughout an experiment. Kraus and Ross[106] found it unnecessary to control p_i if the gas flow was small and V_i was large. Besides the McLeod gauge, a thermocouple vacuum gauge[106] and an ionisation gauge[156] have been used to measure the increase in p_o. For graphites of very low permeability ($K = 10^{-7}$ to 10^{-10} cm^2/sec), helium flow-rates have been measured[157] by means of a helium leak detector or a mass spectrometer attached to V_o.

With the pressure increase method, every care must be taken to ensure that leakage around the sample or into the outlet volume does not occur. A choice of vacuum measuring gauges and a series of possible outlet volumes permit the measurement of a large range of flow-rates. For extremely low flow-rates, when ultra-high vacuum apparatus and techniques are necessary[156] and an ionisation gauge or mass spectrometer must be used to measure the pressure increase rate, the pressure increase method may be the only one possible

for determining permeability coefficients.

When, in the pressure increase experiments described above, gas is suddenly applied at zero time to the inlet side of the initially evacuated sample, unsteady state or transient flow occurs and a certain time elapses before a constant flow-rate is observed. Extrapolation of the straight line portion of the $p_o - t$ plot back to zero pressure gives an intercept on the t-axis known as the time-lag ϕ. By measuring the values of ϕ, a number of investigators[67,76,82,101,106] have calculated diffusion coefficients D for transient flow in porous media. The theoretical considerations of this time-lag method are discussed in section 2.1.5.3; it is only valid when D is constant and not a function of concentration (pressure) as is often observed.

(d) The Pressure Equalization and Decay Methods

The flow-rate of a gas through a porous medium has been measured by following the rate of pressure equalization as gas flows through the sample from a confined volume V_i at a high pressure p_i into a chamber (V_o) at a lower pressure p_o (see Fig.2.1-2(d)). This method is a non-steady state method since Δp and the flow-rate decrease as p_i decreases.

A number of investigators[72,87,95,158,159] have

used the pressure equalization method to determine permeability coefficients for various types of porous media. Often the time was measured for the pressure to change a fixed amount and the measured value inserted into a given expression; otherwise complex calculations were necessary to calculate the flow-rate.[72,95] The techniques developed by several workers[158,159] provided a simple means of determining comparative and routine flow data.

When p_o is kept effectively constant during a pressure equalization experiment, e.g., by removing the gas by vacuum, and the rate of decay of p_i is fairly slow, steady state conditions can be assumed with little error. This is the pressure decay method. If the decay experiment is continued until p_i is very low, values of the permeability coefficient can be determined at a series of mean pressures. The pressure decay method should give more accurate values of the permeability coefficient than the pressure equalization method because it approximates to steady state conditions. (The satisfactory application of the decay method is demonstrated by the agreement observed between the permeability results determined by this and other methods for coarse-pored graphites - see section 4.1.2).

When the pressure decay method was first considered and applied(1959), the author was not aware of any similar experimental techniques. However, since then, Whiteway,[160] and Davies and Booth[161] have described similar experimental methods in which the pressure equalization method was modified by maintaining p_o at zero and at atmospheric pressure, respectively.

(e) Recommended Measuring Methods

Of the methods previously used to determine permeability coefficients for gas flow through porous media, the flow method is particularly suitable for determinations above atmospheric pressure, especially when very high flow-rates are observed (e.g., in coarse-pored media). By the use of a series of different flow-meters, a considerable range of flow-rates can be measured; direct volume-measuring flow-meters are preferable to pressure differential meters and rotameters which require calibration for different gases and correction for pressure and temperature.

All the other methods described are generally used for permeability determinations at pressures less than one atmosphere. The variable volume flow method is more positive than the approximate steady state methods, but the apparatus required is complex. The pressure increase method gives satisfactory values of K

provided p_1 is much greater than p_0. Transient flow results, which are obtained from the commencement of pressure increase experiments, permit the calculation of diffusion coefficients and yield information regarding adsorption and surface flow. Whereas only one value of K at a certain mean pressure is calculated from a pressure increase experiment, values at a series of mean pressures can be determined by the pressure decay method. By varying the volume of the apparatus by the addition or removal of reservoir bulbs so that the rate of pressure change is convenient, it is possible to measure a large range of low flow-rates by the pressure increase and decay methods. The pressure equalization method is suitable for simple routine measurements. Because the reactor graphites to be studied in this research project (see section 3) cover a wide range of pore sizes, thus encompassing a great spread of flow-rates, it seems desirable to construct two apparatus for low pressure (vacuum) and high pressure permeability determinations, respectively. In the low pressure apparatus, permeability coefficients can then be determined by the pressure increase/time-lag method and the decay method. If this apparatus does not give satisfactory K values by these methods, it can

be modified for the more complex variable volume flow measurements. In the high pressure apparatus, permeability coefficients can be determined by the flow method at high pressures, various types of flow-meters being employed as required. This apparatus should be constructed so that permeability coefficients below atmospheric pressure can be determined by the flow method, i.e., the pressure ranges of the two apparatus should overlap.

With these two versatile apparatus, it should be possible to determine the permeability coefficients of the reactor graphites for a series of gases at room temperature and covering a wide range of pressures from a few millimetres of mercury up to about 30 atmospheres.

2.1.9 Summary

2.1.9.1 Introduction

The basic flow equation for isothermal one-dimensional gas flow through a porous medium was derived from first principles. The steady state solution for combined viscous and slip flow, which has apparently not been reported previously, shows that the distribution of pressure in a porous medium during flow is represented by a family of parabolas. In general, the theoretical and experimental aspects

of the pressure distribution mentioned in the literature are limited, being confined to the viscous flow region; further considerations are therefore necessary.

The various permeability coefficients B_1,B_0,B, and K were defined. As a consequence of the pressure distribution theory, the integration of Darcy's law is valid even when $\triangle p$ is large and the permeability coefficient varies with pressure.

2.1.9.2 The Use of Models to Describe Pore Structures

The representation of the pore structure of a porous medium by models was discussed. Capillary pore models are the most amenable to mathematical treatment but generally fail to give satisfactory correlations which describe the observed flow behaviour. Other pore models have been used but are generally difficult to apply. The statistical approach is the most logical.

2.1.9.3 The Viscous Flow Region

Of the various theories developed to explain viscous flow in porous media, the Kozeny theory is the most important. It has been successfully used for unconsolidated powders with uniform pore structures, but otherwise has proved inapplicable since non-uniformity of the pore sizes leads to high permeabil-

ities while high tortuosity factors give low permeabilities. The theory has been modified for consolidated porous media but may still be unsatisfactory.

2.1.9.4 The Slip Flow Region

Because of the distribution of pore sizes in most porous media, slip flow generally occurs simultaneously with viscous flow. The permeability coefficients B_o and K_o are determined from a plot of K against p_m. The Adzumi correlation is not adequate for evaluating the pore properties of a medium, while the Carman-Arnell equation is subject to the same limitations as the Kozeny theory. For consolidated media, the tortuosity factor is high; the porosity value ε_s should be used in calculating pore properties instead of the open porosity ε.

2.1.9.5 The Knudsen Flow Region

There is an indication that Knudsen's law for flow in porous media at very small pressures may not always be valid. It is difficult to express mathematically the transition from slip to Knudsen flow. Above about $N_{Ku} = 1$, the K-p_m plots have been observed to either flatten out, curve downwards, or give a minimum. These low pressure phenomena apparently result from the interaction of the gas molecules with the porous medium, but no clear

explanation is available. Experimental evidence and theoretical considerations show that minima can definitely occur, especially for consolidated porous media.

The calculation of diffusion coefficients from transient flow measurements by Barrer's time-lag theory is not always valid because of the many limitations of the theory. Extension of the theory is necessary to allow for all possible flow phenomena. The reason for the observed variation of ϕ with p_m is not clear.

2.1.9.6 The Flow of Adsorbable Gases

The assumptions made in the derivation of the theory of surface flow in porous media are questionable. The surface diffusion coefficient varies considerably with the adsorbate concentration, while, at high relative vapour pressures, capillary condensate flow may occur. More experimental work is required before surface flow is completely understood.

2.1.9.7 The Turbulent Flow Region

The mechanism of the flow process occurring in a porous medium when Darcy's law becomes invalid is not greatly understood; turbulence and inertial effects may occur. Of the various correlations proposed to

relate Δp to the flow-rate, the Green and Duwez approach is the most satisfactory since it does not depend on any pore model or the definitions of the pore properties. Although empirical coefficients are necessary to correlate experimental results, a satisfactory f-N_{Re} correlation is obtained.

2.1.9.8 The Measurement of Permeability Coefficients

Four methods, viz., the flow method, the variable volume flow method, the pressure increase (and time-lag) method, and the pressure equalization and decay method, are available for determining permeability coefficients for gas flow in porous media. The flow method and the pressure increase and decay methods are suitable for the permeability determinations above atmospheric pressure and at low pressures, respectively.

2.2 The Porosity of a Porous Medium

2.2.1 Theory

The porosity or void fraction ε of a porous medium is defined as the ratio of the volume of the pore space V_p to the total or bulk volume of the medium V_t (ref.6,p.6), i.e.,

$$\varepsilon = V_p / V_t . \qquad \ldots (2.2.1\text{-}1)$$

When the density ρ_s of the material of which the medium

is composed and the bulk density ρ_b of the medium are known, then

$$\varepsilon = 1 - \rho_b / \rho_s . \qquad \ldots (2.2.1\text{-}2)$$

Porosities of consolidated media are usually in the range 2 to 35%, while for powders and granular beds they range generally between 30 and 60% (ref.6,p.12).

The porosity generally measured is the interconnected or "open" porosity and does not include any pores which are totally enclosed or blocked off. Of the open porosity, only a portion ε_s takes part in flow when dead-end or blind pores occur in the medium (cf. Zagar[162]).

2.2.2 The Measurement of the Porosity

The various methods of measuring the porosity of a porous medium have been summarized by Scheidegger (ref.6,p.8). The bulk volume V_t of a sample can be obtained by measuring the dimensions of the sample, or, more accurately, by volumetric displacement of a non-wetting fluid such as mercury. The most commonly employed method of measuring the pore volume V_p of a porous sample is the helium displacement method, in which the volume of helium contained in or required to fill the interconnected pore space is measured directly.

For any plane section taken randomly through a

porous medium, the ratio of the area of pore mouths to the total area of the section is equal to ε. Thus the porosity can be estimated by visual measurement of this ratio by means of a microscope. Generally, the area of the pore mouths does not equal ΣA_p, but $\Sigma(A_p/\cos\Phi)$, where A_p is the cross-sectional area of a pore and Φ is the angle at which the pore meets the plane section.[163]

2.2.2.1 The Helium Displacement Method

In the helium displacement or helium density method, the sample of known weight and bulk volume is placed in a bulb of known volume, evacuated, and a known quantity of helium expanded into the bulb.[164] From the decrease in pressure, the volume and hence the density ρ_s of the solid material of the medium can be calculated. Then ε results from the equation (2.2.1-2). Often[165,166] a calibrated burette is included in the apparatus so that the helium trapped in the bulb and burette can be compressed or expanded several times to give an accurate mean value of the dead space in the bulb. Relatively accurate and rapid measurements of ε can be made by the helium displacement method.

Helium is the most suitable gas since the molecules are so small that they can penetrate the pore system of

the medium completely, and because they are adsorbed on carbonaceous surfaces at room temperatures to a negligible extent.[166,167] However, Maggs, Schwabe, and Williams[119] have shown that carbonaceous materials (including graphite) apparently adsorbed a small amount of helium at room temperature so that the observed helium densities were too high by 6 to 12%. Wall[164] considered that there was negligible adsorption of helium on graphite surfaces.

2.2.3 Summary

Generally, the methods of mercury and helium displacement are employed to determine the open porosity ε of a porous medium. The pore volume involved in flow through a medium may be less than the interconnected pore volume.

2.3 The Surface Area of a Porous Medium

2.3.1 Theory

The internal surface area of a porous medium consists of the total area of the walls of all the pores and may be many times greater than the external geometric area of the medium.[163] It can be expressed as either the area per unit mass S_g, the area per unit bulk volume of the medium S_v, or the area per unit volume of the solid material S_o (specific surface). These three areas are related by the equations

$$S_v = S_g \rho_b \quad \ldots (2.3.1\text{-}1)$$

$$= S_o(1 - \varepsilon), \quad \ldots (2.3.1\text{-}2)$$

where ρ_b = bulk density of the medium, and

ε = porosity.

Large diameter pores contribute very little to the total surface area of the medium compared with the contribution made by pores of smaller diameter. Generally, the internal surface area of natural graphites ranges[168] between 0.47 and 0.87 m^2/g. For synthetic nuclear grade graphites, Davidson[9] reported that S_g was about 0.5 m^2/g. Roberts et al.[169] found that the area of bulk reactor graphite ranged between 0.9 and 1.3 m^2/g; the area increased to about 3 m^2/g on grinding the graphite to a -110/ +200 mesh powder and on oxidation at 400 to 500°C to a 6% weight loss.

2.3.2 The Measurement of the Surface Area

Recently, Connor[170] has reviewed the methods available for measuring the internal surface areas of porous media. The gas adsorption methods are the most widely used, although the methods based on fluid flow through the media have found considerable application for unconsolidated beds. Other methods such as the photo-extinction method, the photo-micrograph method, and the dye adsorption method have

only a limited application and are not of very great importance. The gas adsorption methods and the fluid flow or permeability method are discussed and compared in the following sections.

2.3.2.1 The Gas Adsorption Methods

The gas adsorption methods consist of measuring the adsorption isotherm of a suitable inert gaseous adsorbate on the internal surface of the medium at temperatures near the boiling point of the gas and determining the point on the isotherm corresponding to the volume of gas required to form a single close-packed layer on the surface, i.e., the mono-layer capacity.[171] The internal surface area can then be calculated if the area occupied by a single adsorbate molecule is known. Emmett[171] states that absolute values of the surface area of solids can be measured by gas adsorption techniques with an uncertainty of ± 30%, while relative surface area values can be estimated to within a few per cent.

The main theories advanced in order to explain the adsorption of gases on porous solids are the B.E.T. theory[172,173] and the Harkins and Jura theory.[174] From these theories, the internal surface area of the solids can be calculated. Although the B.E.T. theory has been criticised severely[175] mainly because of the

assumptions made in its derivation, it still offers the most convenient and accurate means of calculating surface areas from adsorption isotherm data.

(a) The B.E.T. Theory

Brunauer, Emmett, and Teller,[172] and Brunauer, Deming, Deming, and Teller[173] developed an adsorption theory which allowed for the formation of adsorbed layers more than one molecule thick on the adsorbent surface and covered the five types of isotherms of the Brunauer classification.[176] Mathematical considerations resulted in the following equation, known as the B.E.T. equation:

$$\frac{p}{V(P_o - p)} = \frac{1}{V_m C} + \frac{C - 1}{V_m C}\frac{p}{P_o}, \quad \ldots (2.3.2\text{-}1)$$

where V = volume of gas adsorbed by the adsorbent at the pressure p,

V_m = monolayer capacity, or the volume of adsorbate required to cover the surface of the adsorbent with a unimolecular layer,

P_o = saturation vapour pressure of the adsorbate, and

C = constant.

Generally, the B.E.T. theory describes the adsorption isotherm satisfactorily over a limited relative pressure range, viz., p/P_o = 0.05 to 0.35.[175]

For any particular system, the quantities V_m and C

are determined by plotting the experimental adsorption results as $p/V\,(P_o - p)$ against p/P_o (the B.E.T.plot).[175] Then $V_m = (\text{slope} + \text{intercept})^{-1}$ and $C = (V_m \times \text{intercept})^{-1}$. From the value determined for V_m (cm^3), the surface area S_g (cm^2/g) can be calculated by means of the equation

$$S_g = \frac{V_m N_L \sigma}{\mathcal{V} w} \quad , \qquad \ldots (2.3.2\text{-}2)$$

where N_L = Avogadro's number
= 6.023×10^{23} mol/g-mol,

σ = cross-sectional area of the adsorbate molecule (cm^2/mol),

$\mathcal{V}$ = molar volume of gaseous adsorbate
= 22,400 cm^3/g-mol, and

w = weight of the adsorbent (g).

Surface areas of adsorbents are frequently calculated by measuring the adsorption of nitrogen at -195.8°C and applying the B.E.T. equation. The widely accepted value for the cross-sectional area of the nitrogen molecule σ_{N_2} to be used in equation (2.3.2-2) is 16.2 Å ^{2}.

The point "B" method suggested by Emmett and Brunauer[177] is also used to estimate values of V_m when the adsorption isotherm is sigmoid-shaped (Type II[176]). This method may be especially applicable when the B.E.T. plot is curved.[169]

(b) The Krypton Adsorption Method

Satisfactory values of the surface area of adsorbents from several hundred down to a few square metres per gram have been measured by the B.E.T. method with nitrogen as the adsorbate.[178] For smaller areas, conventional nitrogen adsorption techniques lead to very inaccurate area values since the volume of gas adsorbed at any pressure may be smaller than the volume of gas in the apparatus. As the precision required for accurate adsorption measurements on adsorbents of small area was practically impossible,[179] it was necessary to select an adsorbate whose saturation pressure at the operating temperature was relatively small.[178]

For the measurement of small surface areas at low temperatures, ethylene, ethane, and butane have been used effectively;[170] however krypton, since first employed by Beebe, Beckwith, and Honig,[180] has found considerable application[178-185] for the rapid and accurate measurement[179] of areas down to as low as 50 cm^2.

As for nitrogen adsorption experiments, B.E.T. plots are prepared and V_m determined as described above. Generally, the adsorption measurements are made in a conventional volumetric apparatus with the

sample bulb in a liquid nitrogen bath; since the saturation vapour pressure P_o of krypton at liquid nitrogen temperatures is about 4 mm Hg, an accurate gauge such as the McLeod gauge[178,181] or thermistor[179,185] is required for measuring low pressures. Because of the temperature difference between the pressure gauge and the sample bulb, and the small diameter of the inlet capillary to the bulb, thermal transpiration may cause the pressure in the bulb to be less than the measured pressure;[178,179] correction of the pressure is then required. Correction may also be necessary for the adsorption of krypton on the apparatus walls.[178,185]

(c) The Values for P_o and σ_{Kr}

Although krypton is solid at liquid nitrogen temperatures, a number of investigators[179-181,185] have evaluated their adsorption results from the extrapolated vapour pressure of liquid krypton (supercooled). Others[178,183] used the experimentally determined saturation pressure. Recent practice[170] has been to follow the example of Beebe et al.[180] and use the extrapolated liquid vapour pressure as given by the formula of Meihuitzen and Crommelin.[186] Haynes[187] showed that the use of the liquid vapour

pressure gave straighter B.E.T. plots and more consistent values of V_m than if the solid vapour pressure was used.

From theoretical considerations, Beebe et al.[180] estimated that the value of the cross-sectional area of the krypton molecule σ_{Kr} should be either 14.0Å^2 or 15.2Å^2; however, they found that σ_{Kr} must equal 19.5Å^2 so that surface areas obtained by krypton adsorption might agree with those determined by nitrogen adsorption. While some workers[183] have used σ_{Kr} = 14.6Å^2, most investigators[179-182,184,185] have ascribed the value of 19.5Å^2 to σ_{Kr}. Gaines and Cannon[188] have indicated that surface areas from krypton adsorption measurements reported in recent years in the literature were in reasonable agreement with values determined by other methods for a wide range of materials if $\sigma_{Kr} = 19.5 \pm 1$Å^2.

(d) Suitability of the Krypton Adsorption Method

There is some doubt concerning the suitability of the krypton adsorption method for the determination of small surface areas. Malden and Marsh[189] found that the krypton method was liable to yield curved B.E.T. plots which were convex to the p/P_0 axis and which greatly reduced the accuracy of determining V_m. Similar curved plots were observed for krypton

adsorption on polycrystalline graphite by Gulbransen and Andrew.[182] Thomas[190] recently obtained anomalous B.E.T. plots for krypton adsorption on freshly sintered silver films, possibly because of phase-changes in the adsorbed film. McDermot and Lawton[184] observed two discontinuities (phase-changes) in the isotherm for krypton adsorption on graphite at 78°K, but were able to obtain a satisfactory area value.

Gaines and Cannon,[188,191] on the basis of a large number of area determinations and on theoretical grounds, considered that the criticism of the use of krypton for area measurements was unfounded since valid and useful results could be obtained by the method even when discontinuities appeared in the isotherm.

2.3.2.2 The Permeability Method

In the permeability method of measuring the surface area of a porous medium, the area can be estimated by means of an equation relating the specific surface S_0 to the permeability coefficient K determined from steady state fluid flow measurements.
The Kozeny-Carman equation (2.1.3-3) applies for gas flow in the viscous region, while the Carman-Arnell equation (2.1.4-6) with m equated to $\varepsilon / (1 - \varepsilon) S_0$ must be used when slip flow also occurs.

This latter equation is

$$K = \frac{\varepsilon^3}{k S_0^2 (1-\varepsilon)^2} \frac{p_m}{\mu} + \frac{4}{3} \frac{\sigma_1}{k'} \frac{\varepsilon^2 \bar{v}}{S_0 (1-\varepsilon)} . \quad \ldots (2.3.2\text{-}3)$$

Carman (ref.5,p.84) has demonstrated the use of equation (2.3.2-3) to calculate values of S_0 for fine powders. The permeability method has been applied extensively to the routine measurement of the specific surface of industrial powders and other unconsolidated beds.[55]

The methods of measuring the permeability coefficients for porous media have been discussed in section 2.1.8.2.

Values of the surface area can be determined for porous media from transient gas flow measurements (see section 2.1.5.3); the time-lag ϕ in setting up steady state flow is determined and the area S_v estimated by means of equation (2.1.5-13).[67,101]

2.3.2.3 Comparison of the Adsorption and Permeability Methods

(a) Steady State Measurements

Carman (ref.5,p.82) has discussed the relative merits of the gas adsorption and permeability methods. Generally, for unconsolidated porous materials with random but uniform pore structures, the Kozeny-Carman

equation is valid. Values of S_o computed from permeability measurements by means of this equation satisfactorily agreed with those calculated from electron microscope measurements,[72,85] but were often greater than those computed from the B.E.T. adsorption method.[77,85,154]

Mathews[192] found that the areas obtained from the B.E.T. method for a series of powders were 2 to 12 times greater than those measured by the air permeability method. The higher adsorption surfaces were usually attributed to an appreciable internal surface in the particles which was not exposed to the gas flow in permeability surface area measurements. For consolidated porous media, the Kozeny-Carman equation does not apply because of the non-uniform and tortuous pore structure (section 2.1.3.2 (c)). On modification of the equation to account for high tortuosity factors as suggested by Wyllie and co-workers,[30,58] the values of the area determined from permeability experiments are generally smaller than those obtained by nitrogen adsorption.[34] Brooks and Purcell[193] found that gas adsorption areas for porous sandstones and limestones were 5 to 100 times greater than areas measured by the permeability method. The difference between the two areas was attributed

to non-uniformity of the pore structure, so that the Kozeny theory was not applicable, and also to a considerable proportion of the surface not taking part in the flow.

Thus, for both unconsolidated and consolidated porous media, the surface area determined by the gas adsorption method is often greater than that measured by the permeability method. In permeability determinations, only the surface actually exposed to the gas flow is measured; additional surface due to roughness of the surface, blind pores, cracks, and the internal porosity of the solid material is not measured. In the adsorption of gas on the surface, the total accessible surface, including that due to surface roughness and blind pores, is covered with gas molecules; it is the number of molecules of gas required to cover this surface with a monolayer, and hence the area of the surface, that is estimated by the B.E.T. method.

(b) The Time-Lag Method

Values of the internal surface area of porous media determined by the time-lag method are much greater than those determined by the steady state permeability method, because of the effect of dead-end pores.[67,101] Ash and Grove[67] have shown that the transient state area value for a ceramic was much

nearer the B.E.T. surface area than the steady state permeability area. Similar agreement was observed by Kraus and Ross.[106] During the transient state flow before steady state conditions are attained, gas molecules must flow into all accessible parts of the previously evacuated porous medium. The surface area resulting from the time-lag measurements should therefore approach the B.E.T. adsorption area[67,101] as the same surfaces are involved.

2.3.3 Summary

The B.E.T. method is the most convenient of the gas adsorption methods for measuring the surface areas of porous media. As the area of graphites ranges between 0.5 and 3 m^2/g, the krypton adsorption method must be used for surface area measurements on reactor graphites instead of the less accurate nitrogen adsorption method. Generally, the krypton adsorption results are evaluated from the extrapolated vapour pressure of liquid krypton and $\sigma_{Kr} = 19.5$ Å^2. Even when curved B.E.T. plots are observed, the krypton method can result in valid and useful results.

Values of the surface areas of porous media can be determined from steady state gas flow experiments by means of the Kozeny-Carman equation, and also from transient state (time-lag) measurements.

The permeability and gas adsorption methods generally do not give area values which agree since the total accessible surface is measured in the gas adsorption and time-lag methods but only the surface actually involved in the flow is measured in the permeability method.

2.4 The Pore Size Distribution of a Porous Medium

2.4.1 The "Size" of the Pores

In any porous medium, the pore structure is generally very complex; pores vary irregularly in cross-section and shape and intersect each other in their tortuous path through the medium. Thus it is impossible to assign a "pore diameter" to a porous medium and truly describe the "size" of the pores. Apparently no satisfactory solution to this problem has been mentioned in the literature (ref.6,p.6), although several mean pore "sizes" have been proposed.

When the pore space is represented by a capillary pore model (see section 2.1.2.2), the mean pore diameter d or the mean hydraulic radius m (ref.5,p.10) of the capillary tubes can be considered a measure of the "average pore size" for capillaries of circular or non-circular cross-section, respectively.

Then

$$d = 4 V_p / S_g \qquad \ldots (2.4.1\text{-}1)$$

and

$$m = \varepsilon / S_v . \qquad \ldots (2.4.1\text{-}2)$$

Expression (2.4.1-1) can be modified to allow for the roughness of the pore walls and the interconnection of the pores in an actual medium.[163]

Scheidegger (ref.6,p.7) has suggested that the "diameter" of any one point in the pore space can be rigorously defined as the diameter of the largest sphere which contains this point and remains wholly within the pore space. Then the pore structure can be described effectively in terms of the distribution of this "pore diameter". Unfortunately, no method is known of measuring this diameter.[38]

Thus, although a mean pore "size" may be assigned to a porous medium, it only serves to indicate the approximate average size of the pores, and may be greatly in error because of the disparity of the assumed pore model with the pore structure of the actual medium. The pore structure of a consolidated porous medium can not be described in terms of the particle size distribution (ref.6,p.7) since the individual particles are bonded together and so have lost their identity.

2.4.2 The Pore Size Distribution

The pore size distribution for a porous medium usually has a limited meaning because of the lack of a useable definition of the pore "size". However, the application of Scheidegger's definition of the pore diameter (see above) enables a consistent pore size distribution function to be defined.

The pore size distribution function $D(r_i)$[194] is a measure of the volume δV_{pi} of all pores with radii between r_i and $r_i + \delta r$, i.e.,

$$\delta V_{pi} = D(r_i)\, \delta r, \qquad \ldots (2.4.2\text{-}1)$$

$$V(r_i) = \int_{r_i}^{r_{max.}} D(r)\, dr, \qquad \ldots (2.4.2\text{-}2)$$

and $$V_p = \int_{0}^{r_{max.}} D(r)\, dr, \qquad \ldots (2.4.2\text{-}3)$$

where $V(r_i)$ = cumulative pore volume for pores of radius $\geq r_i$, and V_p = total pore volume.
Then the mean pore radius is given by

$$r_m = \frac{\int_{0}^{r_{max.}} r\, D(r)\, dr}{\int_{0}^{r_{max.}} D(r)\, dr}. \qquad \ldots (2.4.2\text{-}4)$$

A plot of $D(r_i)$ against r_i yields the differential pore size distribution curve, while a cumulative pore size distribution curve is obtained when the cumulative pore volume $V(r_i)$ is plotted against r_i. The general

shape of the peaks of the differential curve often closely resembles a Gaussian or a Maxwellian distribution curve.

2.4.3 The Pore Size Distribution and the Permeability

The Kozeny-Carman equation, which relates the viscous flow permeability coefficient B_0 to the various properties of a porous medium, is only applicable to media with reasonably uniform pore sizes (see section 2.1.3.2). A number of authors have attempted to extend the Kozeny theory for non-uniform pore structures by the inclusion of a pore size distribution term in the equation instead of the unsatisfactory "average" pore size term (cf. section 2.4.1). These authors were mainly soil physicists[36,37,39] and petroleum technologists[28-30,38] and their expressions were specifically for liquid flow. None of the authors have modified their expressions to account for slippage during gas flow (see section 2.1.4.1); hence, for gas flow, the permeability values calculated from their expressions were lower than those observed experimentally.

2.4.3.1 Equations Based on Capillary Models

Purcell,[28] Burdine et al.,[29] and Wyllie and

Spangler[30] have proposed equations accounting for the pore size distribution based upon the Kozeny-Carman capillary model. If δV_{pi} is the volume of all pores with radii between r_i and $r_i + \delta r$, and τ_i is the incremental tortuosity factor of the pores in this interval, then the equations can be written in the form

$$B_o = \frac{1}{4\, k_o\, V_t} \sum \frac{\delta V_{pi}\, r_i^2}{\tau_i^2} \qquad \ldots (2.4.3\text{-}1)$$

$$\text{or } B_o = \frac{1}{4\, k_o\, V_t} \int_o^{V_p} \frac{r^2}{\tau^2}\, d\, V_p . \qquad \ldots (2.4.3\text{-}2)$$

These equations can be simplified[195] if it is assumed that each set of pores i has the same tortuosity factor τ. Often the substitution $\delta \mathcal{E}_i = \delta V_{pi} / V_t$ and also the introduction of the saturation s_i and the capillary pressure p_{ci} (section 2.4.4) are made into the equations so that B_o can be computed directly from the experimental capillary pressure distribution results. When expressed in terms of the distribution function $D(r_i)$, equation (2.4.3-2) becomes

$$B_o = \frac{1}{4\, k_o \tau^2 V_t} \int_o^{r_{max.}} r^2 D(r)\, dr. \qquad \ldots (2.4.3\text{-}3)$$

The above equations apply only to gas flow in the viscous flow region. To generalize them so that they apply to the slip-flow region also, the derivations of the above authors[28-30] have been repeated to include the slip term by following a similar procedure to that by which Carman modified the Kozeny-Carman equation (ref.5,p.70). Then equation (2.4.3-3) becomes

$$K = \frac{p_m}{k_o \mu \tau^2 V_t} \int_o^{r_{max.}} r^2 D(r)\, dr + \frac{4}{3} \frac{\delta_1 \bar{v}}{k_1 \tau^2 V_t} \int_o^{r_{max.}} r\, D(r)\, dr. \quad \ldots (2.4.3\text{-}4)$$

2.4.3.2 Equations Based on Statistical Models

Childs and Collis-George,[36] Marshall,[37] Wyllie and Gardner,[38] and Millington and Quirk,[39] applied statistical pore models based upon the distribution of the pore sizes (see section 2.1.2.3) to obtain permeability equations for gas flow through porous media in the viscous flow region; for fine-pored media, these equations must be corrected to allow for slip flow.

The expression derived by Marshall[37] was

$$B_o = \frac{\varepsilon^2}{8 n^2}\left[r_1^2 + 3 r_2^2 + 5 r_3^2 + \ldots + (2n-1) r_n^2\right], \quad \ldots (2.4.3\text{-}5)$$

where r_1, r_2, ... r_n represented the mean radius of the pores in each of n equal fractions of the total pore volume. Millington and Quirk[39] extended the theory of Childs and Collis-George,[36] and Marshall;[37] their theory was of limited value for computing the permeability of consolidated media because of anisotropy, cementation, and incomplete dispersion of the pore sizes.

Wyllie and Gardner,[38] who considered a statistical model similar to that of Marshall,[37] derived an equation of similar form to that of Wyllie and Spangler[30] (equation 2.4.3-2). Because the additional parameters introduced to allow for the constrictions in the pores were difficult to estimate, this theory was more applicable to two-phase relative flow than to single-phase flow.

2.4.3.3 Other Expressions

O'Neill et al.[68] have generalized the Adzumi equation (section 2.1.4.2) by including the pore size distribution, e.g.,

$$K = \frac{\pi}{10 \mu \tau}(n_1 r_1^4 + n_2 r_2^4 + \ldots) p_m + \frac{2\pi \sigma_1 \bar{v}}{3\tau}(n_1 r_1^3 + n_2 r_2^3 + \ldots), \quad \ldots (2.4.3\text{-}6)$$

where n_1, n_2, ... were the number of pores of tortuosity τ and radius r_1, r_2, . . . per cm^2, respectively. Wiggs[196] estimated two mean diameters characterizing viscous and molecular flow from the cumulative pore size distribution data, and calculated the permeability for samples of reactor graphite. Later Wiggs[197] concluded that there was no unique relationship between the pore size distribution as measured by fluid displacement and the gas permeability, but that a semi-empirical relation could be found for any class of materials having similar pore textures.

2.4.3.4 Experimental Verification

Experimental verification of the expressions mentioned above relating the gas flow through consolidated porous media to the pore size distribution is rather limited. Henderson[198] has indicated that permeability values calculated from pore size distribution data on the basis of the capillary model theory were not satisfactory. Several workers[28,29] have applied their theoretical expressions to determine the value of the tortuosity factor τ or formation factor F for porous sedimentary rocks. Millington and Quirk,[39] and Wiggs[196] have shown that their respective methods gave satisfactory agreement between

measured and calculated permeabilities. The most satistactory verification[38] of the theoretical expressions is that by Faris, Gournay, Lipson, and Webb.[195] Wyllie and Gardner[38] considered that further experimental work was necessary in order to verify completely the permeability-pore size distribution equations.

2.4.4 The Measurement of the Pore Size Distribution

The pore size distributions of porous media have most frequently been determined by means of capillary pressure methods (of which the mercury penetration method is the most important), or from capillary condensation studies. Optical methods and methods based on the principles of X-ray scattering have also been employed to a lesser extent (ref.6,p.14). The capillary pressure and the capillary condensation methods will be discussed in the following sections.

2.4.4.1 The Capillary Pressure Methods

When a capillary in a porous medium is partly filled with a liquid, a pressure difference exists across the curved air-liquid interface because of surface tension forces; for a capillary of radius r, this pressure difference or capillary pressure p_c is expressed by the equation (ref.5,p.40)

$$p_c = 2\sigma \cos\theta / r, \qquad \ldots (2.4.4\text{-}1)$$

where σ = surface tension at the air-liquid interface, and

θ = angle of contact.

The pressure p_c is the pressure of air required to displace liquid from a saturated capillary of radius r. As no pore space is uniformly sized, any pressure p_{ci} will correspond to displacement of liquid from pores of radius r_i or larger. If the volume of unfilled pores $V(r_i)$ can be measured at each p_{ci} for $V(r_i)$ from 0 to V_p, then a curve of $V(r_i)$ against r_i (the cumulative pore size distribution curve) can be prepared by means of equation (2.4.4-1). This is the basis of the capillary pressure methods. The same principles hold when any fluid phase displaces a different immiscible fluid phase from the pore space of the medium (ref.5,p.41).

Carman (ref.5,p.42) has outlined the methods available for the measurement of capillary pressures. The column and diaphragm methods have often been applied by soil physicists and petroleum technologists; in these methods, water in the pore space is displaced by air and $\theta = 0^\circ$. As the mercury penetration method is important, it will be considered in more detail.

(a) The Mercury Penetration Method

When an evacuated sample is contacted with mercury, surface tension forces oppose the entrance of the mercury into the pores because the contact angle is about 140°. Therefore an external pressure must be applied to the mercury.[194] The pressure P_{oi} required to fill pores of radius r_i is given by equation (2.4.4-1), viz.,

$$P_{oi} = 2\gamma \cos\theta / r_i \quad . \quad . \quad . \quad (2.4.4\text{-}1)$$

As the pressure is increased, smaller and smaller pores are filled. By measurement of the quantity of mercury δV_{pi} entering the pores at each pressure P_{oi}, the pressurizing curve of the cumulative volume $V(r_i)$ against P_{oi} is obtained.

The mercury penetration method was first suggested by Washburn,[199] and was greatly popularized by Ritter and Drake.[194,200] Since then, the method has been widely adopted for pore size distribution studies on cracking catalysts,[201] sedimentary rocks,[28,29] cokes,[202] and graphites.[203]

Ritter and Drake[194] have discussed the sources of possible error in measurements by this method. The contact angle θ has been generally taken[28,194,200] as 140°, although some workers[202,204] used the value of 130°. An error of 1° in θ would mean a 1.5% error

in r_i and a shift of the pore size distribution curve[194]. The accepted value of the surface tension of mercury γ is 480 dyn/cm. The values for θ and γ were assumed to be independent of pressure[201] and the method was considered to apply down to very small pore sizes ($r = 20\text{Å}$) where the concepts of θ and γ might break down.[194]

The pore radius calculated from the mercury penetration measurements is the radius of the largest opening into the pore.[194] If a pore of large radius has only capillary entrances (an "ink-bottle" pore), then the whole volume of this pore will be allotted to the radius of the largest capillary entrance and the distribution curve will be weighted towards the lower radii. Meyer[205] has attempted to correct experimental pore size distributions to account for this difficulty, but the method involved tedious trial and error calculations.

After penetration measurements to 10,000 p.s.i., Drake and Ritter[200] found that the distribution curve obtained on the release of the pressure did not follow the curve for the increase in pressure, about 80% of the macropore volume of a carbon sample remaining filled with mercury after release of the pressure. This hysteresis effect was due to the large number of "ink-bottle" pores in the carbon.

(b) The Mercury Porosimeter

Because of the high surface tension of mercury (480 dyn/cm), extremely high pressures must be applied to the mercury to force it into the very finest pores; hence a special high pressure porosimeter must be employed. Such an apparatus must include[29] a system for the evacuation of the sample and admittance of mercury to the cell, a means whereby the pressure can be increased in increments from a vacuum to high pressure, and a method of measuring the quantity of mercury forced into the pores of the sample.

Various types of porosimeters have been described; several[201,206] have been designed for operation at pressures up to 50,000 to 60,000 p.s.i. (lowest pore radius about 20Å). The amount of mercury forced into the sample at each pressure was generally obtained by measuring the fall in the mercury level in the capillary stem of a dilatometer by resistance[29,201,204,206] or direct[202,203] methods.

A number of workers[28,29,206] commenced their penetration measurements at pressures much less than one atmosphere so that pores of radius greater than 70,000Å were not immediately filled but their distribution was determined. Generally, sufficient time

was allowed at each pressure for the mercury to penetrate all possible pores and attain an equilibrium. Corrections were generally made[202,206] to the measured mercury volumes penetrating the sample to allow for compression of the mercury and the sample. For cokes, Cameron and Stacy[202] observed that the compression above 5000 p.s.i.a. was between 8 and 12 x 10^{-12} cm^2/dyn.

2.4.4.2 The Capillary Condensation Method

At a curved liquid-vapour interface in a capillary of radius r_i, there is a reduction in the vapour pressure of the liquid at the meniscus from the normal value P_o to p_{vi} (ref.5,p.44). Then the relative pressure p_{vi}/P_o is given by the Kelvin equation

$$\ln (P_o/p_{vi}) = \frac{2 \gamma M \cos \theta}{r_i \rho_l \mathcal{R} \mathcal{T}}, \qquad \ldots (2.4.4\text{-}2)$$

where γ = surface tension,
M = molecular weight of the liquid,
θ = contact angle, and
ρ_l = density of the liquid.

The assumptions upon which the Kelvin equation is based have been discussed by Carman.[208]

By means of the Kelvin equation, the pore size distribution of a porous medium can be derived from

the desorption isotherm in the region of capillary condensation. Because multilayer adsorption and capillary condensation occur simultaneously within a pore, the Kelvin equation must be corrected to allow for the decrease in the effective radius of the capillary by the adsorbed layers.[208-210]

2.4.4.3 Comparison Between the Capillary Pressure and Capillary Condensation Methods

Pore size distributions have been determined in the range of pore radii from about 50Å up to the order of 500,000Å (50 microns) by the mercury penetration method and between 10Å and 300Å by the application of the Kelvin equation (capillary condensation method).[209] Joyner, Barrett, and Skold,[204] and Cochran and Cosgrove[211] found that in the overlapping radii range, the mercury penetration and capillary condensation methods gave concordant distribution results. Thus a fairly reliable pore size distribution for a porous solid can be determined by a combination of these two methods.[171] With both methods, the radius measured is that of the largest entrance to the pore.

Generally, the column and diaphragm capillary pressure methods, with water as the wetting fluid, yield distribution results which closely agree with

those measured by the mercury penetration method;[28,29] however, the last method is more advantageous since the distribution of a wider range of pore sizes can be measured.

2.4.5 Summary

It is impossible to assign a rigorous geometrical quantity to a consolidated porous medium as a measure of the pore "size" because of the complex pore structure. For a medium with a wide range of pore "sizes", the pore size distribution may effectively describe the pore structure.

For gas flow through porous media, the Kozeny theory has been extended for non-uniform pore structures by the inclusion of the pore size distribution; the derived expressions must be modified for viscous-slip flow. The experimental verification of the theoretical expressions is limited, further experimental work being necessary.

The mercury penetration method is now widely employed for pore size distribution measurements. As the pore radius calculated from this method is the radius of the largest entrance to a pore, the distribution will be in error if "ink-bottle" pores occur in the medium. The values generally accepted for γ and θ for mercury are 480 dyn/cm and 140° ,

respectively. Because of the high value of γ, extremely high pressures must be applied to force the mercury into the finest pores. By means of a corrected form of the Kelvin equation, a cumulative distribution curve for a porous medium can also be derived from the results of desorption measurements (capillary condensation method). A combination of the two main measuring methods should give a fairly reliable pore size distribution for a porous medium. For reactor graphites, satisfactory distributions can be obtained by the mercury penetration method for pores of radius greater than about 50Å .

2.5 The Tortuosity of a Porous Medium

2.5.1 Definition of the Tortuosity

In any porous medium, the pore structure is generally very complex with the pores following tortuous or crooked paths through the medium. To take account of this tortuous nature of the pore structure, a factor has been introduced into studies on porous media; this factor, called the tortuosity T by Rose and Bruce,[212] is defined by the equation

$$T = (L_p/L)^2, \qquad \ldots (2.5.1\text{-}1)$$

where L_p = average length of a flow path through a porous medium, and

L = geometric length of the medium.

As each tortuous flow path through the medium is of a different length, T is a statistical average value.[213] The tortuosity may also be defined[43] in terms of the average angle Θ which the flow paths make with the overall direction of flow in the medium, i.e.,

$$T^{\frac{1}{2}} = 1/\cos\Theta. \qquad \ldots (2.5.1\text{-}2)$$

Carman[32] has demonstrated that the angle Θ was 45° for flow through a bed of large glass spheres. Hence $L_p/L = \sqrt{2}$ has been used[32,163] for unconsolidated beds. Carman (ref.5,p.46) has discussed the values of T employed by various authors, and concluded that T was between 1.5 and 2.5 for unconsolidated media.

For consolidated media, higher tortuosities than those encountered for unconsolidated beds can be expected because of the blockage of some of the pores. However, the very large values of T observed experimentally (see later) are difficult to visualise and indeed are extremely unlikely on the basis of the definition expressed as equation (2.5.1-1).

The tortuosity is important for several aspects of flow through porous media. In permeability studies, a tortuosity factor τ is included in the equations correlating gas flow through porous media (see sections 2.1.3.2 and 2.5.2). This factor is combined with an indeterminate shape factor k_o to give

the Kozeny "constant" k, i.e.,

$$k = k_o \tau^2. \qquad \ldots (2.1.3\text{-}4)$$

As any reasonable value can be ascribed to τ so that the experimental results fit the permeability equation, this tortuosity factor is little more than a factor of ignorance.

For a porous medium in which the pore space is filled with an electrically conducting fluid, petroleum technologists[30,214] have introduced an electrical tortuosity factor q defined as

$$q = F \varepsilon , \qquad \ldots (2.5.1\text{-}3)$$

where ε = porosity of the medium, and

F = formation resistivity factor

determined by electrical resistance measurements on the saturated medium (see section 2.5.3). For diffusion of gases through porous media, a tortuosity or labyrinth factor χ has been defined[44,215] as

$$\chi = \varepsilon / \psi , \qquad \ldots (2.5.1\text{-}4)$$

where ψ = diffusibility obtained from diffusion experiments (see section 2.5.4).

The relation between the various tortuosity factors defined above is not always clear; this is pointed out in the discussion in section 2.5.5. Because of the number of different tortuosity factors, the uncertain relation between these factors, and the high values

observed for consolidated porous media, considerable confusion has arisen concerning the concept of tortuosity. Experimental evidence has not completely elucidated the difficulties.

Recently it has been recognized that high values of τ, q, and χ were due to constrictions and variations in the cross-sectional area of the pores.[43,44,213] On this basis, the tortuosity factors can be expressed more adequately by equations of the form[44,216]

$$\tau = T^{1/2}/P_p \qquad \ldots (2.5.1\text{-}5)$$

$$q = T^{1/2}/P_e \qquad \ldots (2.5.1\text{-}6)$$

and

$$\chi = T^{1/2}/P_d. \qquad \ldots (2.5.1\text{-}7)$$

The quantities P_p, P_e, and P_d are constriction or convergence factors[44] to account for constrictions in the pores for permeability, electrical conductivity, and diffusion studies, respectively. The best value to take for T is probably 2($\theta = 45^0$ or $L_p/L = \sqrt{2}$) as for unconsolidated beds; then high values of the tortuosity factors are obtained when the convergence factors are less than unity.

The term "impedance factor", as suggested by Wyllie and Gardner,[38] is preferred for τ, q, and χ instead of the term "tortuosity factor", and should be distinguished from the term "tortuosity" defined by equations (2.5.1-1) and (2.5.1-2).

2.5.2 The Tortuosity in Permeability Studies

In the application of the Kozeny-Carman capillary pore model to describe flow through porous media, the term $(L_p/L)^2$ arises in the flow equation to account for the tortuous nature of the pore structure (ref.5,p.13). Experimental evidence shows that generally the use of the tortuosity T (=2) in the permeability equation is valid and $T = \tau^2$ for unconsolidated porous media since the average value of the Kozeny constant k ($= k_o \tau^2$ - equation 2.1.3-4) is about 5.0 and $k_o = 2.5$ (see section 2.1.3.2).

However, for consolidated porous media, the experimental permeability values are often much lower than those expected from the Kozeny-Carman equation with k = 5.0; these low values are ascribed to a high permeability tortuosity factor τ(ref.4,p.50) such that τ^2 is much greater than T. The calculations presented in Table 2.1-1, section 2.1.4.4, demonstrated that values of τ for consolidated ceramic materials[34,67,68] ranged from about 2 up to 20 ($k_o = 2.5$). For porous glasses,[63,82,86] τ ranged from 2.2 to 3.5. As the Kozeny-Carman equation is therefore not valid for flow through consolidated porous media, it has been modified by Wyllie and co-workers[30,58] as described in section 2.5.3.1.

Since the permeability tortuosity factor τ can be greater than $T^{\frac{1}{2}}$, it can be expressed by the equation

$$\tau P_p = P_p(k/k_o)^{\frac{1}{2}} = T^{\frac{1}{2}}, \qquad \ldots (2.5.1\text{-}5)$$

where P_p is a convergence factor to allow for constrictions in the pore structure. For unconsolidated beds with uniform pore structures, $P_p \simeq 1.0$ and $\tau = T^{\frac{1}{2}} \simeq 2$; for consolidated media, higher values of τ are obtained if P_p is less than unity.

2.5.3 The Tortuosity in Electrical Resistivity Measurements

Electrical log determinations have been employed by petroleum technologists for a number of years to differentiate between porous rock formations penetrated on drilling during the exploitation of oil and gas reservoirs, and to permit an estimation of the nature of the fluids contained in these formations.[217] The electrical log is obtained by lowering a system of electrodes down a drill hole and measuring the electrical resistivity of the saturated or partially saturated formation as a function of depth.

In the interpretation of these electrical logs to evaluate the characteristics of the reservoir rocks, Archie[217] introduced the concept of a formation resistivity factor or formation factor F, which was defined as the ratio of the resistivity R of the porous

rock formation 100% saturated with a conducting fluid to the resistivity R_o of the fluid, i.e.,

$$F = R/R_o , \qquad \ldots (2.5.3\text{-}1)$$

where the resistivity is the resistance of a unit cube. It was assumed that the porous material itself was non-conducting. Archie[217] proposed that F was related to the porosity ε of the material by the relation

$$F = \varepsilon^{-m} \qquad \ldots (2.5.3\text{-}2)$$

where the exponent m, termed the cementation factor,[214] ranged generally from 1.4 to 3.0.

Wyllie and co-workers[30,58,214] have postulated that an electrical tortuosity factor q could be obtained from electrical resistivity measurements on a porous medium saturated with an electrically conducting solution. They have shown that the formation factor

$$F = q/\varepsilon \qquad \ldots (2.5.1\text{-}3)$$

since $F(= R/R_o)$ is much greater than unity because only the liquid-filled fraction ε of the total cross-sectional area is available for the passage of an electric current and also the current must follow a tortuous path through the medium.

Electrical resistivity measurements on porous media saturated with electrically conducting fluids have been performed by a number of workers and values of q calculated according to equation (2.5.1-3). For uncon-

solidated beds of glass spheres and sand particles, values of q varied between 1.4 and 2.0 (ref.5,p.48). However, for consolidated materials, the observed values of q were much greater than those for unconsolidated beds and ranged from 2 up to about 10 for sandstones and other sedimentary rocks,[125,145,217] and up to 22 for artificially consolidated media.[218]

In order to explain the high electrical tortuosity values observed for consolidated porous media, Owen[43] assumed that a porous medium could be built of a number of identical unit cubes, each of which contained a centrally located cubic void-space joined to each face of the cubic unit by connecting tubes at angles θ to the axes; the tortuosity T was defined by equation (2.5.1-2). Then, depending upon the ratio of the size of the void-space compared with that of the connecting tubes (the constriction factor C), values of F were calculated for various porosities ε and tortuosities of 1.0 ($\theta = 0^{\circ}$), 1.08 ($\theta = 22\frac{1}{2}^{\circ}$), and 1.41 ($\theta = 45^{\circ}$); F ranged from 6 up to about 200 for C between 1 and 6. For example, for $\varepsilon = 0.20$, and $T^{\frac{1}{2}} = 1.0$, F increased from 10 at C = 1 (three intersecting straight capillaries) to 55 at C = 6, i.e., $F\varepsilon = q$ ranged between 2 and 11, while, for $T^{\frac{1}{2}} = 1.41$, $F\varepsilon$ similarly ranged between 3.5 and 14.

Thus Owen's analysis shows that the electrical

tortuosity factor q ($= F\varepsilon$) can be much greater than the tortuosity $T^{\frac{1}{2}}$ ($= 1/\cos\theta$), the magnitude of the difference between q and $T^{\frac{1}{2}}$ depending upon the size of the constrictions (C). Even for a pore structure containing no constrictions ($C = 1$), q is greater than $T^{\frac{1}{2}}$ because of the intersection of the capillaries. Almost identical results can be calculated for a similar model described by Flood.[41] Although these models are theoretical, they do show that high values of F, and hence q, can result because of the intersection of the pores, dead-end pores, and the enlargements and constrictions in the pores. These high values are not due entirely to tortuous pore paths through the medium as has often been presumed, although the tortuous nature of the pore structure does contribute towards the value of q.[38]

To allow for the effect of constrictions on the electrical tortuosity factor, a correction analogous to that for the diffusion tortuosity factor (see section 2.5.4) can be made, i.e.,

$$q P_e = \varepsilon F P_e = T^{\frac{1}{2}}, \qquad \ldots (2.5.1\text{-}6)$$

where P_e is a constriction factor which approximates to unity for unconsolidated beds, but becomes less than unity when pore constrictions occur.

The relation of the electrical tortuosity factor q to the permeability and diffusion tortuosity factors

τ and χ is discussed in section 2.5.5. The methods of determining F and q by electrical resistivity measurements are described in section 2.5.6.

2.5.4 The Tortuosity in Gaseous Diffusion Experiments

Since the diffusion of a gas through a porous material is closely analogous to electrical current flow through a liquid-filled pore space, a similar relation to that for electrical resistivity measurements (equation 2.5.1-3) should apply.[219] Thus, Hoogschagen[215] has calculated a diffusion tortuosity factor χ (labyrinth factor) from the equation

$$\chi = \varepsilon / \psi , \qquad \ldots (2.5.1\text{-}4)$$

where ψ, termed the diffusibility, is the ratio of the effective or apparent diffusion coefficient D_e of a gas diffusing through the porous medium to the true diffusion coefficient D_b of the free gas, i.e.,

$$\psi = D_e/D_b . \qquad \ldots (2.5.4\text{-}1)$$

The diffusibility ψ is analogous to 1/F. The coefficients D_e and D_b can be determined by measuring the rate at which the gas diffuses through the porous medium and through the bulk gaseous phase, respectively.

The values of χ obtained for diffusion in unconsolidated beds[215,220] were about 1.5, while higher values up to 12.5 were observed for consolidated porous media.[215,221]

In order to account for these high values of χ, Peterson[44] has examined an hyperbolic pore model containing periodic pore constrictions, and has shown that χ was not equal to the tortuosity $T^{1/2}$ but must be corrected by a convergence factor P_d to allow for the reduction in D_e due to constrictions in the pores. Then

$$\chi P_d = \frac{\varepsilon}{\nu} P_d = T^{1/2} . \qquad \ldots (2.5.1\text{-}7)$$

For loosely packed beds where ε is greater than 0.4, $P_d \simeq 1$ and $\chi \simeq \sqrt{2}$; however, when the beds were compacted, Peterson postulated that pore constrictions were produced and P_d became less than unity. Michaels[222] has given a simplified treatment of Peterson's mathematical analysis.

2.5.5 The Relation Between the Tortuosity Factors

2.5.5.1 The Electrical and Permeability Tortuosity Factors

Wyllie and Rose[214] contended that the electrical path through a porous medium was identical to the path of a flowing fluid; however, they did not infer that the mechanisms were the same. The tortuosity factor pertaining to electrical flow was therefore equal to the tortuosity factor appearing in the permeability equations (see section 2.5.2), i.e., $q = \tau$. The equivalence of q and τ apparently depended to some extent on the degree

of uniformity of the pore structure; evidence showed that any empirical constant connecting the two tortuosity factors, if it existed, was very close to unity. A fundamental difference[38,214] between the processes of current flow and fluid flow in a porous medium is that the resistance to current flow depends on the pore radius squared (r^2), while that for fluid flow is proportional to the fourth power of r (r^4).

By means of this assumed equivalence, and the assumption that the shape factor k_o in permeability studies was a constant (= 2.5), Wyllie and co-workers[30,58] modified the Kozeny-Carman equation (2.1.3-3) to apply it to consolidated porous media (see section 2.1.3.2(c)).

There has been considerable disagreement in the literature concerning the actual relation between q and τ. Wyllie and co-workers[30,58,59,214] have maintained that

$$q = F\varepsilon = L_p/L = \tau, \quad \ldots(2.5.5\text{-}1)$$

while others[125] assumed that

$$q = F\varepsilon = (L_p/L)^2 = \tau^2. \quad \ldots(2.5.5\text{-}2)$$

Wyllie,[38,59] and Street[223] have pointed out that the definition of q, and hence F, depends upon the model chosen for the pore structure of the porous medium. If capillary pore models are used, equation (2.5.5-1) follows[223] when the cross-sectional area to flow $A_1 = \varepsilon A$,

but the equation

$$q = F\varepsilon = \tau^{4/3} \qquad \ldots (2.5.5\text{-}3)$$

results[223] when $A_2 = \varepsilon A(L/L_p)$. Wyllie and Gardner[38] indicated that equation (2.5.5-2) of Cornell and Katz[125] was inconsistent.

Wyllie and Gregory[59] performed extensive experimental work on beds of regularly shaped particles in order to check the $q-\tau$ relation. They determined values of the Kozeny constant $k(= k_o \tau^2)$ from permeability studies,[59] and values of F by electrical resistivity measurements on the same beds.[218] Their results fitted equation (2.5.5-1) more satisfactorily than equation (2.5.5-2), although some $F\varepsilon$ values were between $F\varepsilon = \tau$ and $F\varepsilon = \tau^{4/3}$.

Other experimental work does not really elucidate the relation between q and τ. Winsauer et al.[213] found that $F\varepsilon = \tau^{1.67}$ for a series of sandstones, although later more accurate experiments[224] showed that in fact $F\varepsilon = \tau^2$. Faris et al.,[195] by measuring the permeability, the pore size distribution, the formation factor F, and the porosity ε for a series of sandstones and limestones, obtained equations relating τ to $F\varepsilon$; Wyllie[38,225] subsequently pointed out that these equations would conform to $\tau = F\varepsilon$ if different but realistic values were given to certain constants involved in the calculations.

Carman (ref.5,p.47) has suggested that the true

relation between q and τ probably lay between the two extremities expressed by equations (2.5.5-1) and (2.5.5-2). The consideration of more complex models than the capillary pore models does not assist in relating q and τ. Lorenz[226] has considered a conically-shaped pore section and has shown that $T = (L_p/L)^2$ could be greater or less than $F\varepsilon$ depending upon the mean area of the pore chosen, viz., the arithmetical or the harmonic mean.

The only real test[38] of the validity of any assumed relation between q and τ depends upon the agreement between experimental values of q and τ obtained for the same medium by electrical resistivity and permeability determinations, respectively. Further experimental work is necessary to supplement the previous investigations. It is possible that a separate relation between q and τ may exist for each particular porous medium. Greater differentiation between values for consolidated and unconsolidated media is required since τ does not always equal $T^{\frac{1}{2}}$.

2.5.5.2 The Electrical and Diffusion Tortuosity Factors

Klinkenberg[219] has indicated the analogy existing between the diffusion and electrical conduction processes in the pore space of a porous medium. Hence, the definitions for the diffusion tortuosity factor χ and the

electrical tortuosity factor q are similar (see section 2.5.4).

Klinkenberg[219] and Hedley[216] have demonstrated that within experimental error, values of χ obtained from diffusion experiments agreed with values of q from electrical resistivity measurements performed on the same material. Hedley[216] has shown that the constriction factors P_d and P_e were identical. Because the values of χ and q are equal, the diffusibility Ψ can be estimated readily from electrical resistivity measurements.[216,219]

The relation between the diffusion tortuosity factor χ and the permeability tortuosity factor τ has not been specifically investigated, but should be very similar to that between q and τ (section 2.5.5.1).

2.5.6 Tortuosity Measurements by Electrical Resistivity Methods

In the electrical resistivity methods, either an a.c. or a d.c. current is passed through the saturated sample and the voltage drop across the sample is measured. The resistance R' of the saturated sample can be calculated from these measurements. Then the formation factor results from the equation

$$F = R'/R'_0 , \qquad \ldots(2.5.6\text{-}1)$$

where

$$R'_0 = R_0(L/A) \qquad \ldots(2.5.6\text{-}2)$$

= resistance of the conducting fluid,

R_o = specific resistance of the conducting fluid, and

L, A = dimensions of the sample.

Since graphite is an electrically conducting porous material, special techniques are necessary in order to measure the electrical resistance of the saturated material. The resistivity methods employed for non-conducting media will therefore only be briefly mentioned.

2.5.6.1 Methods for Non-conducting Porous Media

For non-conducting porous media, e.g., porous sedimentary rocks, electrical resistivity measurements have been made by a.c. conductivity methods. Rust[227] specified two fundamental techniques, viz., the two-electrode method, in which the saturated sample is mounted between two electrodes serving as both current-carrying and potential-measuring electrodes, and the four-electrode method, where additional electrodes along the length of the sample are used to measure the potential drop. The four-electrode method is often employed to overcome high contact resistances at the current electrodes.[228]

Several workers[213,224] calculated tortuosities by employing a d.c. ionic mobility method in which the time for an ion to migrate through a saturated sample was measured.

2.5.6.2 Methods for Conducting Porous Media

Both a.c.[229-231] and d.c.[145,232] methods have been applied for resistivity measurements on electrically conducting media. Patnode and Wyllie[229] have shown how ideally a correction could be made for the presence of conducting solids in a saturated porous medium so that formation factors could be calculated from a.c. measurements. Wyllie and Southwick[230] considered that an aggregate of conductive particles saturated with a conducting electrolyte was compatible with an equivalent resistance model comprising of three conducting elements in parallel, viz., an electrolyte conducting path, a solid conducting path, and a particle/electrolyte conducting path.

Sauer, Southwick, Spiegler, and Wyllie[231] examined the conductance of a plug of conductive ion-exchange resin particles saturated with various electrolytes; the electrical conductance of the resin plug was measured by means of a 1000 cycles/sec conductivity bridge at 0.35 V a.c. for progressively more concentrated solutions of each electrolyte. From the curve of the measured conductance against the conductance of the saturating solution, and the theory resulting from the assumed model,[230] the formation factor and the relative

proportions of each element in the model could be calculated.

On the other hand, MacMullin and Muccini[145] applied a d.c. technique to measure the resistivity of electrically conducting carbon and graphite samples because the porous material itself would conduct a.c. much more than the electrolyte so that erroneous resistances would result. As long as the potential difference across the sample was less than the decomposition potential of the solution, then the sample provided no path for the current (except for a small leakage current at very low current densities). The sample was mounted in the centre of a cell with current-carrying and potential-measuring platinized platinum electrodes at each end and could be evacuated and saturated while in the cell. The resistance between the electrodes was measured with (R_1') and without (R_2') the sample in the cell, and the formation factor calculated from

$$F = R'/R_o' = (R_1' - R_2' - R_o')/R_o' \quad \ldots(2.5.6\text{-}3)$$

This d.c. method generally was not as accurate as a.c. methods and gave resistivity values which were up to 10% lower.

Stender and Ksenzhek[232] employed a similar d.c. technique for graphite samples; they used a four-

electrode system in which the potential drop across the sample was measured independently of the current-carrying electrodes by means of potential probes and calomel electrodes.

2.5.6.3 Recommended Measuring Method

Of the methods available for measuring the electrical resistivity of conducting porous media, the d.c. method is preferable to the a.c. method. In the a.c. method, complicated and probably inaccurate corrections must be made for the current flow through the solid; erroneous resistance values may be obtained because of condenser effects and double-layer capacity effects in the pores.

A refinement of the d.c. method of MacMullin and Muccini[145] is suggested for electrical resistivity measurements on the reactor graphite samples. The use of a four-electrode system, with "Luggin" capillary probes in conjunction with calomel reference electrodes to sense the potential drop across the sample (cf. Winsauer et al.[213]), will avoid the need of correction for electrode polarization or the resistance of the electrolyte between the sample and the electrodes. As long as the potential difference across the sample is less than the decomposition potential of the electrolyte at the graphite surface, no polarization of

the graphite occurs and no current flows through the solid material. The justification of this refined d.c. method for conducting porous media will be published shortly.[233]

This method of measuring the potential drop across the sample is very similar to that described by Stender and Ksenzhek.[232] The method was independently developed on the suggestion of Dr. W.T.Denholm,* and measurements were commenced before the paper of Stender and Ksenzhek became available.

2.5.7 Summary

Much confusion exists in the literature concerning the concept of the tortuosity of a porous medium. Care has been therefore taken to distinguish between the tortuosity T $\left[= (L_p/L)^2 \text{ or } \cos^2\theta\right]$ and the tortuosity factors τ, q, and χ for permeability, electrical resistivity, and diffusion measurements, respectively; these quantities were defined and the relation between them discussed. The relation between q and τ is not clear but q and χ are analogous.

For unconsolidated porous media, $T = \tau^2 \simeq 2.0$; for

---

*Senior Lecturer in Physical Metallurgy, South Australian Institute of Technology.

consolidated media, the tortuosity factors are much higher. Owen[45] has demonstrated that these high values could be due to the enlargements and constrictions in the pores. The use of convergence or constriction factors may give satisfactory relations between the tortuosity (or impedance) factors and the tortuosity T (= 2).

The d.c.method is preferable to the a.c. method for measuring the electrical resistivity of a conducting porous medium. A refined d.c. method is suggested.

3. APPARATUS AND EXPERIMENTAL PROCEDURE

The methods for the measurement of the permeability, the porosity, the surface area, the pore size distribution, and the electrical resistivity of a porous medium have been discussed in sections 2.1.8, 2.2.2, 2.3.2, 2.4.4, and 2.5.6, respectively, and the methods considered the most satisfactory for measurements on reactor graphites have been chosen. In accordance with these recommendations, various apparatus were constructed and experimental techniques were developed.

In this section, the experimental details are described for:

1) permeability determinations in a low and a high pressure apparatus by the pressure increase, pressure decay, and flow methods, and also steady state pressure distribution measurements in the high pressure apparatus,
2) porosity measurements by the helium displacement method,
3) surface area determinations by the krypton adsorption method,
4) pore size distribution measurements by the mercury penetration method, and
5) electrical resistivity (formation factor) measurements by the d.c. method.

A number of grades of reactor graphite were supplied by the Australian Atomic Energy Commission (A.A.E.C) for this research project. The graphites which have been used in the investigations are listed in Table 3.1-1 with their respective average pore diameters. Further details concerning the manufacture and composition of these graphites are given in Table A.1-1,Appendix A.1. Several other grades of coarse-pored Porous Graphites (Grades 10, 30, and 40) were available but were not used.

Table 3.1-1

Reactor Graphites

Graphite Grade	Average pore diameter, microns.
Porous Graphite 60	33
Acheson "A" Graphite	10 - 20
Morgan "EY9" Graphite	1 - 2
Morgan "EY9166" Graphite	1 - 2
Impregnated Morgan "EY9166" Graphite	?

3.1 Gas Flow Measurements

3.1.1 Materials for the Permeability Determinations

3.1.1.1 Sample Preparation

Samples for the permeability determinations were

prepared as rods (approximately 7 cm long x 1.3 cm diameter) whose axes were either parallel or perpendicular to the axis of extrusion of the graphite, or as hollow cylinders (approximately 8 cm long x 2.5 cm o.d. x 0.7 cm i.d.) with their axes parallel to the extrusion axis. The samples were machined to size on a lathe and their dimensions measured (to $\pm$ 0.005 cm) with either vernier calipers or a micrometer.

For the rod samples, where flow occurred along the axis of the sample, the flow length L and the cross-sectional area to flow A were identical with the length and the cross-sectional area of the sample, respectively. However, for the hollow cylindrical samples, where flow occurred radially, the flow length L equalled the thickness of the walls of the hollow cylinder ($=\frac{1}{2}(d_o-d_i)$, where d_o and d_i were the external and internal diameters, respectively) and the flow area A was taken as the logarithmic mean of the external and internal areas of the hollow cylinder. The samples and their dimensions are listed in Table A.2-1, Appendix A.2.

So that gas could not flow out from the sides of the graphite rods, these samples were coated mostly with Epoxy resin; several samples were coated with Shellac, while paraffin-wax followed by Epoxy resin, and red sealing wax were used successfully to coat the

P.G.60 graphite samples. Care was taken that the coatings did not soak into the pores. The coating for each sample is listed in Table A.2-1, Appendix A.2.

The graphite samples were attached to sample holders in order to support them in the permeability cells (see sections 3.1.2.1 and 3.1.3.1). The various types of sample holders employed are described in detail in Appendix A.2.2 and shown diagrammatically in Figs. A.2-1 and A.2-2. They are mentioned briefly here.

Type (a): The graphite rod was held between glass tubing with rubber hose for measurements in the low pressure permeability cell type I.

Type (b): The graphite rod was attached to a brass holder with rubber hose enabling it to be supported in the high pressure permeability cells or the low pressure type II cell.

Type (c): The cylindrical sample was sealed to a dural sample holder for low pressure determinations in the type II permeability cell.

Type (d): The cylindrical sample was attached to an FG 10 flat joint for measurements carried in both the low pressure type II permeability cell and the high pressure cells.

Type (e): The cylindrical sample was held in the high pressure permeability cell type I by means of a clamp.

The sample holder employed for each graphite sample is given in Table A.2-1, Appendix A.2.

3.1.1.2 Gases

The gases hydrogen H_2, helium He, nitrogen N_2, argon A, carbon dioxide CO_2, freon-12 CF_2Cl_2, and xenon Xe have been used in the permeability determinations.

Generally, nitrogen (molecular weight M = 28.02) was used as a preliminary gas to establish a technique for determinations where a new grade of graphite or a new method was to be investigated. The nitrogen, as industrial gas, was supplied in cylinders by the Commonwealth Industrial Gases, Ltd. (C.I.G). The suppliers claimed that the nitrogen was about 99.7% pure with about 0.2% oxygen, 0.1% rare gases, and 0.03% moisture as impurities.

Hydrogen (M = 2.02), similarly supplied in cylinders by C.I.G., was over 99.5% pure, the impurities consisting of about 0.4% nitrogen, 0.1% oxygen, 0.03% moisture, and 0.05% carbon compounds.

Helium (M = 4.00) was obtained in a cylinder from Air Reduction, U.S.A., at over 99.8% purity with about 50 p.p.m. by volume of neon and lesser quantities of

hydrogen and oxygen as impurities.

Argon (M = 39.94) was about 99.7% pure and contained about 0.1% nitrogen and 0.03% moisture as impurities. It was supplied in cylinders by C.I.G.

Carbon dioxide (M = 44.01) for the high pressure permeability determinations was obtained with a purity of 99.7 to 99.9% (dew point = -20°F) from cylinders of liquid carbon dioxide supplied by Carba Dry Ice Ltd. Carbon dioxide for low pressure permeability determinations was prepared from dry ice supplied by Carba Dry Ice Ltd., and purified by double distillation.

Freon-12 (M = 120.92), containing a maximum of 10 p.p.m by weight of moisture and 1.5% by volume of non-condensables, was obtained from 15 oz "Can-O-Gas" refrigerant charger cans manufactured by Virginia Smelting Co., U.S.A., and available commercially.

Xenon (M = 131.3), of 99 to 100% purity with the balance krypton, was available in 1 l. pyrex flasks from the British Oxygen Co.Ltd. (agents C.I.G).

All the gases were investigated for determinations in the low pressure apparatus and were stored in reservoir bulbs attached to the apparatus (see section 3.1.2.4). Helium and xenon were not used in the high pressure permeability experiments; the other gases were supplied directly from the gas cylinders (section 3.1.4.4).

The properties of the gases are listed in Table B.1-1, Appendix B.

3.1.2 Description of the Low Pressure (Vacuum) Permeability Apparatus

The apparatus for the determination of permeability coefficients at pressures between zero and one atmosphere by the pressure increase/time-lag and pressure decay methods is shown diagrammatically in Fig.3.1-1 and by photograph in Fig.3.1-2. It consisted essentially of a permeability cell N (see Fig.3.1-1), which contained the graphite sample and separated two calibrated volumes (sides 1 and 2), a high vacuum pumping system ABCDE to evacuate the apparatus and sample, pressure measuring devices (manometers J and M, McLeod gauge O, and Pirani gauge G), and a gas introduction U and storage system S.

The apparatus was constructed of English Pyrex glass; Quickfit and Springham high vacuum stopcocks and Quickfit conical and spherical joints were used. All stopcocks were greased with Apiezon "N" grease. Leaks in the evacuated apparatus were detected with an Edwards high frequency spark tester.

3.1.2.1 The Permeability Cells

The permeability cell N contained the graphite sample held by a sample holder (see section 3.1.1.1). The cell

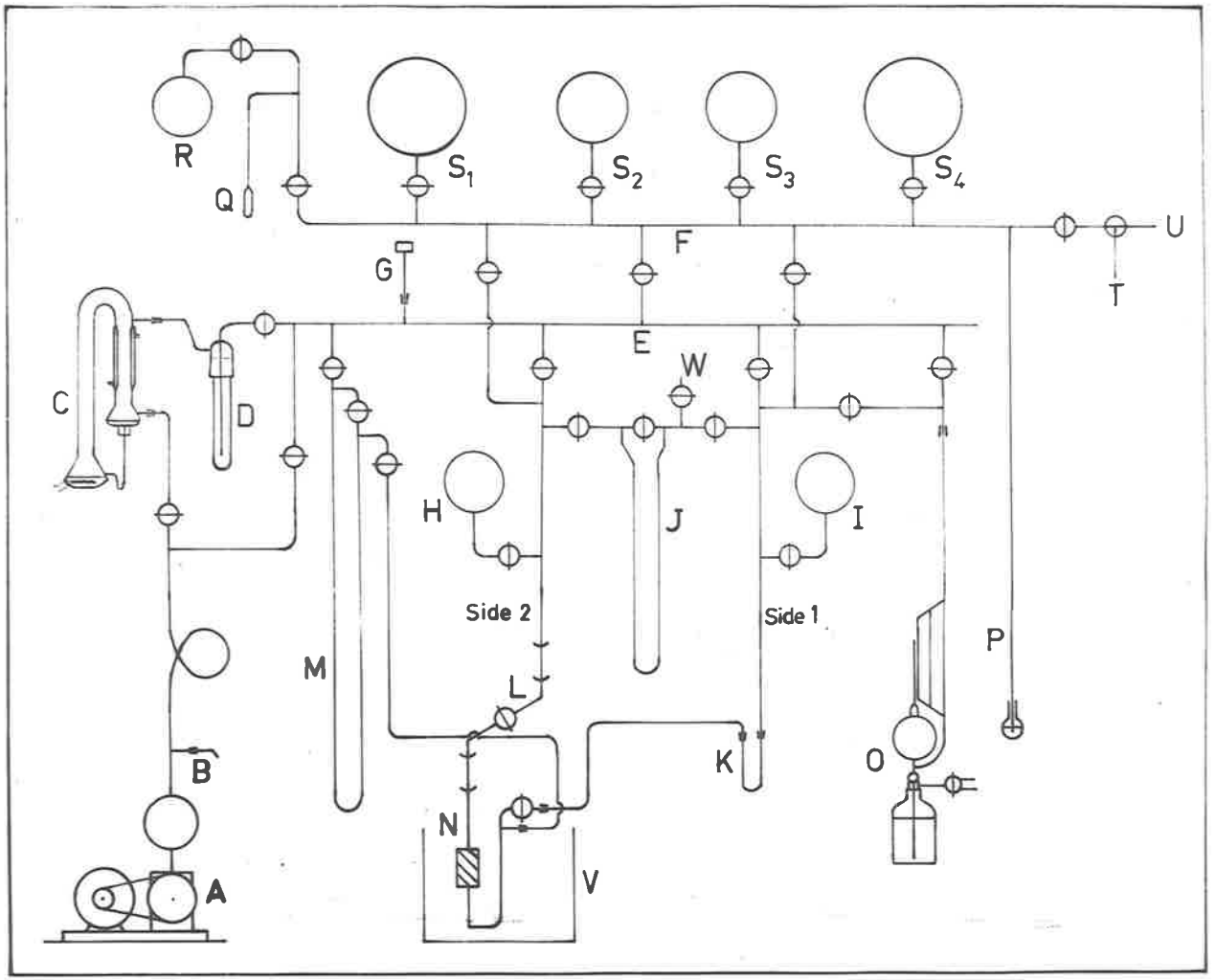

Fig. 3.1-1 Line Diagram of Low Pressure Permeability Apparatus.

LEGEND FOR FIG. 3.1-1

A	Edwards "Speedivac" 2SC20 vacuum pump	M	Mercury manometer, 0 to 76 cm Hg
B	Air admittance B7 joint	N	Permeability cell
C	Jena 3Q6 mercury diffusion pump	O	Jena McLeod gauge, 10^{-5} to 3 mm Hg
D	Liquid air trap	P	Mercury blowoff
E	High vacuum line	Q	Freezing trap for Xenon recovery
F	Gas line	R	Flask of Xenon
G	Pirani gauge head	S	Gas storage reservoirs
H	Calibrated volume, side 2	T	To manostat
I	Calibrated volume, side 1	U	Gas introduction line
J	Mercury manometer, 0 to 30 cm Hg	V	Townson and Mercer X27 thermostated water bath
K	Freezing trap	W	Vent to atmosphere
L	Spherical joint system		

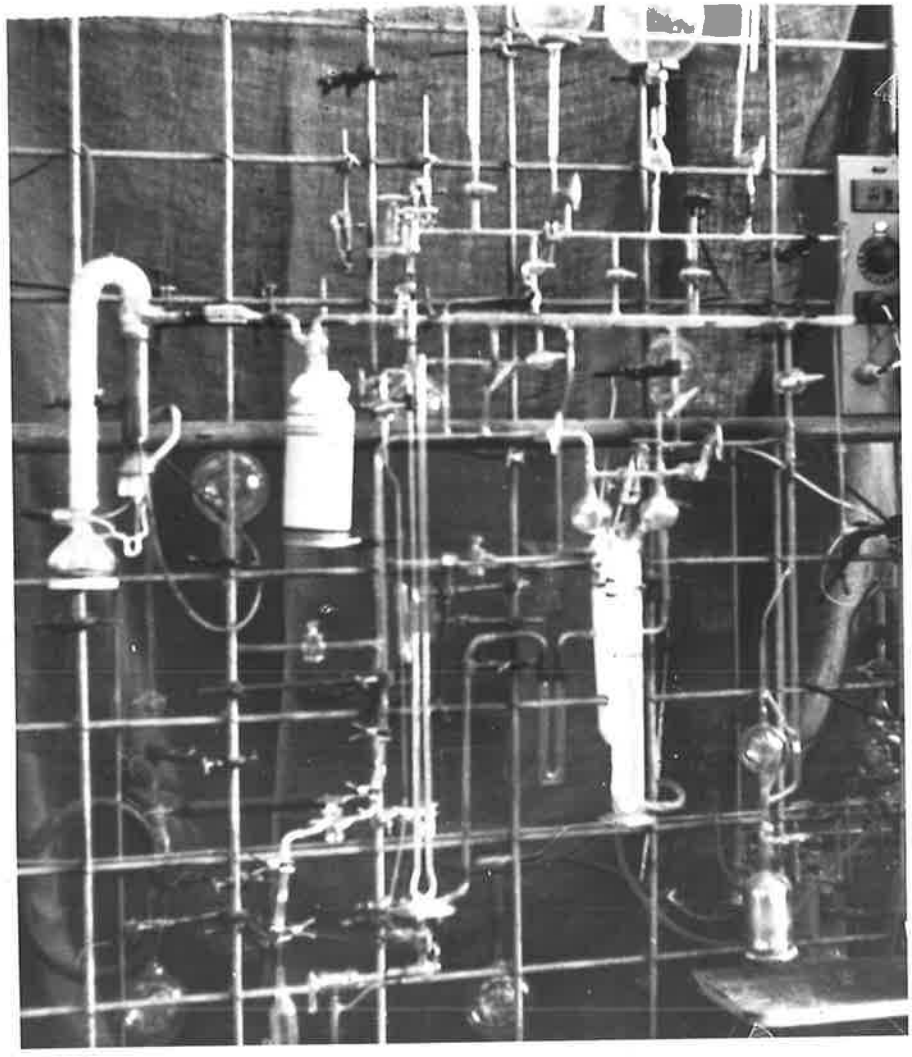

Fig. 3.1-2 Photograph of Low Pressure Permeability Apparatus.

was attached to side 1 of the apparatus by a B16 conical joint and to side 2 by a system of 9/18 spherical joints L so that it could be removed readily from the apparatus for replacement of the graphite sample. A stopcock was included in the spherical joint system to isolate the sample from the inlet side of the apparatus before commencing a pressure increase experiment (section 3.1.3.1). The cell was supported in a Townson and Mercer X27 thermostatted water bath V to ensure a uniform temperature in the cell.

The type I permeability cell was an adaption of that used by Barrer and Barrie.[82] The coated graphite rod, held in a type (a) sample holder (see Appendix A.2.2), was supported in a special test tube container through a B14 conical joint (see Fig.A.2-1(a), Appendix A.2.2). Mercury was placed in this container to prevent air leakage into the apparatus.

The type II permeability cell was initially constructed for hollow cylindrical graphite samples held in type (c) sample holders, but was later used for graphite rods attached to type (b) holders (see Appendix A.2.2). The cell, shown in Fig.A.2-1(b), consisted of a container into which the sample holder was sealed through an SCB19 socket. A B40 conical joint in the container permitted the sample holder to be removed. A stopcock

on side 1 of the cell allowed pressure decay experiments to be performed with a small decay volume, the pressure being followed with manometer M attached via a B7 conical joint.

3.1.2.2 Pressure Measurement

The gas pressure in the apparatus was measured with mercury manometers J and M for pressures up to 76 cm Hg, a calibrated Jená McLeod gauge O to cover the low pressure range 10^{-5} to 3 mm Hg, and an Edwards Pirani gauge (model B2, head type G-6) G attached to the high vacuum line E to indicate the vacuum in the apparatus.

The 0 to 30 cm Hg manometer J was used to measure the gas pressure on side 1 for pressure decay experiments or on side 2 for pressure increase experiments. A vent to the atmosphere W permitted the range of the manometer to be extended up to 1 atm. The 0 to 76 cm Hg manometer M was also used to measure pressures for decay experiments, especially when only a small decay volume was required. Both manometers were constructed of approximately 10 mm bore tubing to reduce the capillary depression of the mercury.

The head of mercury indicated on the manometer was measured by means of a cathetometer (The Precision Tool and Instrument Co.Ltd.) which could be read to 0.001 cm.

The error in a pressure reading was 0.06 cm Hg owing to the inaccuracies in measuring the mercury levels.

A Jená calibrated McLeod gauge with three scales covering the range 10^{-5} to 3 mm Hg was used to measure the vacuum in the apparatus, and the pressure on side 1 of the apparatus for pressure increase experiments. The three scales covered the ranges 10^{-5} to 2×10^{-2} mm Hg, 0 to 6×10^{-1} mm Hg, and 0 to 3 mm Hg, respectively. Pressure readings on the third scale were corrected (x 1.011) to allow for the gas pressure above the mercury in the limb of the gauge leading to the apparatus. In the range 10^{-2} to 10^{-1} mm Hg, pressures recorded on the gauge were found to be greatly in error (up to 20%) and were therefore corrected from a calibration curve. After these corrections had been made, a maximum calibration error of 1% and a reading error of less than 1% were involved in pressure measurements above 10^{-2} mm Hg.

3.1.2.3 <u>The Vacuum System</u>

The high vacuum system for evacuating the graphite sample consisted of a Jená type 306 mercury diffusion pump C backed by a two stage air ballasted rotary oil vacuum pump A (Edwards "Speedivac" 2SC20). A liquid air trap D prevented mercury vapour from entering the apparatus. The diffusion pump could be bypassed when initially

evacuating the apparatus. A vacuum of 10^{-6} mm Hg could be produced in the apparatus with this system.

3.1.2.4 The Gas System

The gases (see section 3.1.1.2) were stored in reservoirs S attached to the gas line F. Cylinder gas was admitted through a previously evacuated and purged gas admittance line U into the evacuated reservoir flask. A mercury blowoff P prevented the pressure from increasing beyond one atmosphere in the reservoir flask and also served as an indicator of the gas pressure in the gas line or a reservoir. The flask of Xenon R was joined directly to the gas line F with a freezing trap Q attached for the recovery of the Xenon.

3.1.2.5 Volume Calibration

The volumes of various sections of the apparatus were accurately calibrated by gas expansion from a flask I of known volume using the McLeod gauge and applying Boyle's law. The volumes of other sections of the apparatus, including the gas reservoirs S and the flasks H and I, were calibrated before attachment to the apparatus by weighing empty and full of distilled water. The volumes of the permeability cells N and the various adaptors and sample holders were also calibrated by the weighing method. The volume of the sections of the apparatus, and the standard deviations are listed in Table C.1-1, Appendix C.1.

3.1.3 Experimental Procedures for the Low Pressure Apparatus

The low pressure apparatus was designed so that permeability coefficients could be determined at pressures less than one atmosphere by the pressure increase/time-lag and pressure decay methods (see section 2.1.8.2 (e)). Several determinations were also performed in the apparatus by the pressure equalization and the low pressure flow methods. In the following sections, the experimental procedures for all these methods will be described.

3.1.3.1 The Pressure Increase and Time-Lag Method

A brief description of the pressure increase/time-lag method for determining permeability coefficients for porous media has been given in section 2.1.8.2 (c). Essentially the pressure increase method consisted of measuring the rate of increase of the pressure p_o in an isolated volume V_o on the outlet side of a previously outgassed sample while the inlet side pressure p_i was kept effectively constant. Then the flow-rate Q through the sample was calculated from the observed rate of increase of p_o, i.e., dp_o/dt (see Appendix C.2.2), provided p_i remained very much greater than p_o throughout the experiment so that steady state flow conditions could be assumed. The plot of p_o against t, when extrapolated to zero pressure, yielded the time-lag $\emptyset$ as

the intercept on the time axis. The combined method has been applied successfully to determine permeability coefficients for Morgan "EY9" and Impregnated graphite samples, and to a lesser extent for Acheson "A" graphite samples.

The sample, held in the permeability cell N, was evacuated to a pressure of less than 10^{-5} mm Hg for at least 24 hours before commencing a determination. A blank experiment was performed first by observing the rate of pressure increase in the isolated outlet side volume V_o (side 1 of the apparatus) by means of the McLeod gauge O in order to determine the rate of leakage and degassing from the apparatus and sample; the degassing rate was considered negligible if p_o was less than 10^{-3} mm Hg after 20 minutes (0.01×10^{-4} mm Hg/sec). The evacuated sample was then isolated from side 2 and gas was introduced into the inlet volume (side 2) from the gas storage system S until the desired p_i, indicated on manometer J, was obtained. At time $t = 0$, V_o was isolated, the stopcock in the spherical joint system L opened to initiate the gas flow through the sample, and a stop-clock started.

Using the McLeod gauge, the outlet pressure was measured as a function of time, about 6 to 8 p_o values being measured so that a satisfactory p_o-t plot was

obtained. The volume V_o could be adjusted with the calibrated flask I so that a suitable rate of pressure increase was observed (15×10^{-4} to 0.1×10^{-4} mm Hg/sec). The time interval between successive pressure readings and the volume V_o were made as large as practicable for each experiment so that the flow-rate was measured accurately (see Appendix C.2.3). As p_i decreased by less than 2% during an experiment because of the fairly large inlet side volume, the average inlet pressure as measured with the manometer J was generally used in the calculations. For p_i below about 4 mm Hg, the McLeod gauge was used to measure the initial pressure. The ambient and water bath temperatures were recorded at the beginning and at the end of the experiment and the averages taken.

The value of the permeability coefficient K at the mean pressure p_m in the sample was calculated from the observed steady rate of pressure increase dp_o/dt (slope of the p_o-t plot) as shown in Appendix C.2.2. Further values of K at different p_m were obtained by repeating the above experimental procedure for different inlet pressures. The time-lag ϕ was also obtained from the p_o-t plot.

For Acheson "A" graphite, the pressure increase method was unsatisfactory because p_o increased so quickly

that it passed beyond the range of the McLeod gauge in a very short time when p_i was greater than 8 cm Hg. The procedure was therefore modified in that the experiment was repeated several times at the same p_i (variation 1½%) and values of p_o were measured at different intervals of time after commencing the flow to give the p_o-t plot. Although experiments by this modified procedure did not approximate to steady state, satisfactory results were obtained as shown in section 4.1.2.

3.1.3.2 The Pressure Decay Method

The pressure decay method for determining permeability coefficients for porous media has been mentioned in section 2.1.8.2 (d). When pressure decay experiments were first commenced, the method had apparently not been reported previously in the literature, although the non-steady state pressure equalization method had been frequently applied.

In the pressure decay method, the rate of decay of the pressure p_i in an isolated volume V_i on the inlet side of the porous sample was measured while the outlet side pressure p_o was kept effectively constant. The flow-rate Q through the sample was calculated from the observed rate of pressure decay, i.e., dp_i/dt, as shown in Appendix C.3.2, steady state flow conditions being approximated if dp_i/dt was relatively slow. This method

has been used with success to determine permeability coefficients for Acheson "A" graphite samples. However, for Morgan "EY9" and Impregnated graphite samples, the method has generally proved unsatisfactory.

The graphite sample, placed in the permeability cell N, was evacuated to a pressure of less than 10^{-5} mm Hg for at least 24 hours prior to the commencement of a determination. The sample was then isolated from the inlet side volume V_i (side 1 of the apparatus), which was filled to the desired starting inlet pressure p_i with gas from the gas storage S. At time t = 0, the stopcock isolating the sample from V_i was opened to allow gas to flow through the sample and a stop-clock was started. The outlet side volume (side 2) was continually evacuated by means of the diffusion pump to keep p_o approximately zero; the magnitude of p_o was indicated by the Pirani gauge G.

At various time intervals during the experiment, the inlet pressure p_i was measured using the manometer M, which was isolated from V_i during the measurement so that the value of p_i recorded on the manometer remained constant. The manometer J and the McLeod gauge O were also used to measure the pressure. When the rate of pressure change became too slow (less than 0.03 cm Hg/min), the volume V_i was reduced successively by removing various

portions of the apparatus. The ambient and water bath temperatures were recorded at approximately hourly intervals and the average values calculated.

The slope dp_i/dt of the best fit curve through the experimental p_i-t points was measured at a series of pressures by means of a straight-edge or the numerical procedure of Douglass and Avakian,[234] the accuracy in the values of dp_i/dt being about 4% (see Appendix C.3.3). Values of the permeability coefficient K were calculated from the values of dp_i/dt at the series of mean pressures as shown in Appendix C.3.2.

3.1.3.3 The Pressure Equalization Method

Several pressure equalization experiments, discussed in section 2.1.8.2 (d), were attempted for Acheson "A" graphite samples in the low pressure apparatus. Gas flowed through the graphite sample from a volume V_i at a high pressure to an isolated low pressure volume V_o and the pressure difference Δp across the sample was measured by means of manometer J at various times after the commencement of the experiment. From a plot of Δp against t, the rate of change in Δp, viz., $d(\Delta p)/dt$, was obtained at various Δp and values of the permeability coefficient calculated knowing the initial inlet pressure p_i and the volumes V_i and V_o of the two sides of the apparatus (see Appendix C.3.4). Because the permeability

coefficients calculated from these pressure equalization determinations were quite scattered (see section 4.1.2.1), the pressure decay method was preferred to the pressure equalization method.

3.1.3.4 The Low Pressure Flow Method

A few determinations were performed in the low pressure apparatus by a steady state flow method (cf. section 2.1.8.2(a)). Permeability coefficients were determined for Acheson "A", Morgan "EY9", and Impregnated graphite samples, and the approach to an equilibrium flow-rate was observed by this method.

In the low pressure flow method, gas was continuously supplied to the inlet side (side 2) of the graphite sample from a gas cylinder fitted with a regulating valve. The inlet pressure p_i, measured by means of manometer J, was controlled to within 1% by a Cartesian manostat[235] attached to the apparatus at T. The gas flowed through the sample to the outlet volume V_o (side 1 of the apparatus) where it was continuously evacuated. The flow-rate Q at any time t after the commencement of the flow was determined by measuring with the McLeod gauge O the increase in pressure p_o in the volume V_o over a certain time interval (2 minutes) after V_o was isolated from the vacuum pump. Provided p_i was much greater than p_o, the steady state flow conditions were negligibly affected by

the collection of the gas sample. The calculation of the permeability coefficient K is discussed in Appendix C.4.

3.1.4 Description of the High Pressure Permeability Apparatus

The apparatus for the determination of permeability coefficients at high pressures up to about 30 atm by a flow method is shown diagrammatically in Fig.3.1-3 and by photograph in Fig. 3.1-4. The apparatus consisted of a supply of gas from cylinder A (see Fig.3.1-3), a permeability cell H containing the graphite sample, pressure gauges E, F, and G and a manometer J for measuring the inlet and outlet pressures, and various flow-meters, viz., rotameters N and O, a soap-bubble flow-meter P, a capillary flow-meter Q, and a wet gas test meter R, for measuring the gas flow-rate. Permeability determinations could be performed with the outlet pressure p_o either greater than or less than atmospheric pressure, the gas stream being bypassed through a vacuum pump K for the latter determinations.

The high pressure portion of the apparatus was constructed from high pressure fittings and Foxboro high pressure needle valves, all joints being sealed with pipe-joining compound. Leaks, found by applying

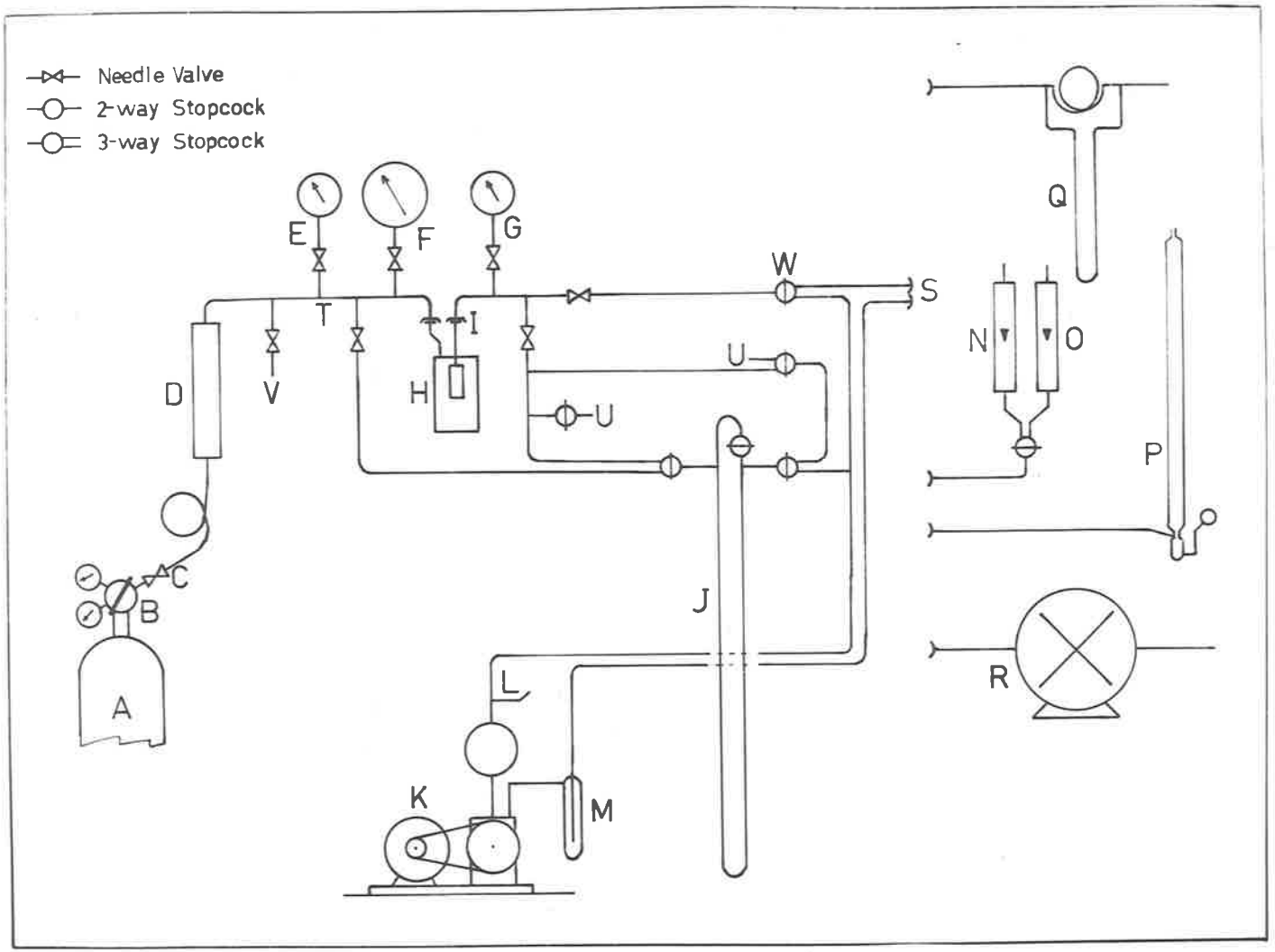

Fig. 3.1-3 Line Diagram of High Pressure Permeability Apparatus.

LEGEND FOR FIG. 3.1-3

A Cylinder of gas

B Regulating valve

C Needle valve

D Drying tower

E A.N.A. pressure gauge, 0 to 100 p.s.i.g.

F Foxboro pressure gauge, 0 to 600 p.s.i.g.

G A.N.A. pressure gauge, 0 to 150 p.s.i.g.

H Permeability cell

I Hexagonal unions

J Mercury manometer, 0 to 2 atm

K Edwards "Speedivac" 1SP30 vacuum pump

L Air admittance B7 joint

M Activated charcoal trap

N,O Brooks rotameters

P Soap-bubble flow-meters

Q Capillary flow-meter

R Wet gas test meter

S Spherical joints

T High pressure inlet manifold

U Air vents

V Manostat attachment

W Bypass stopcock to vacuum pump

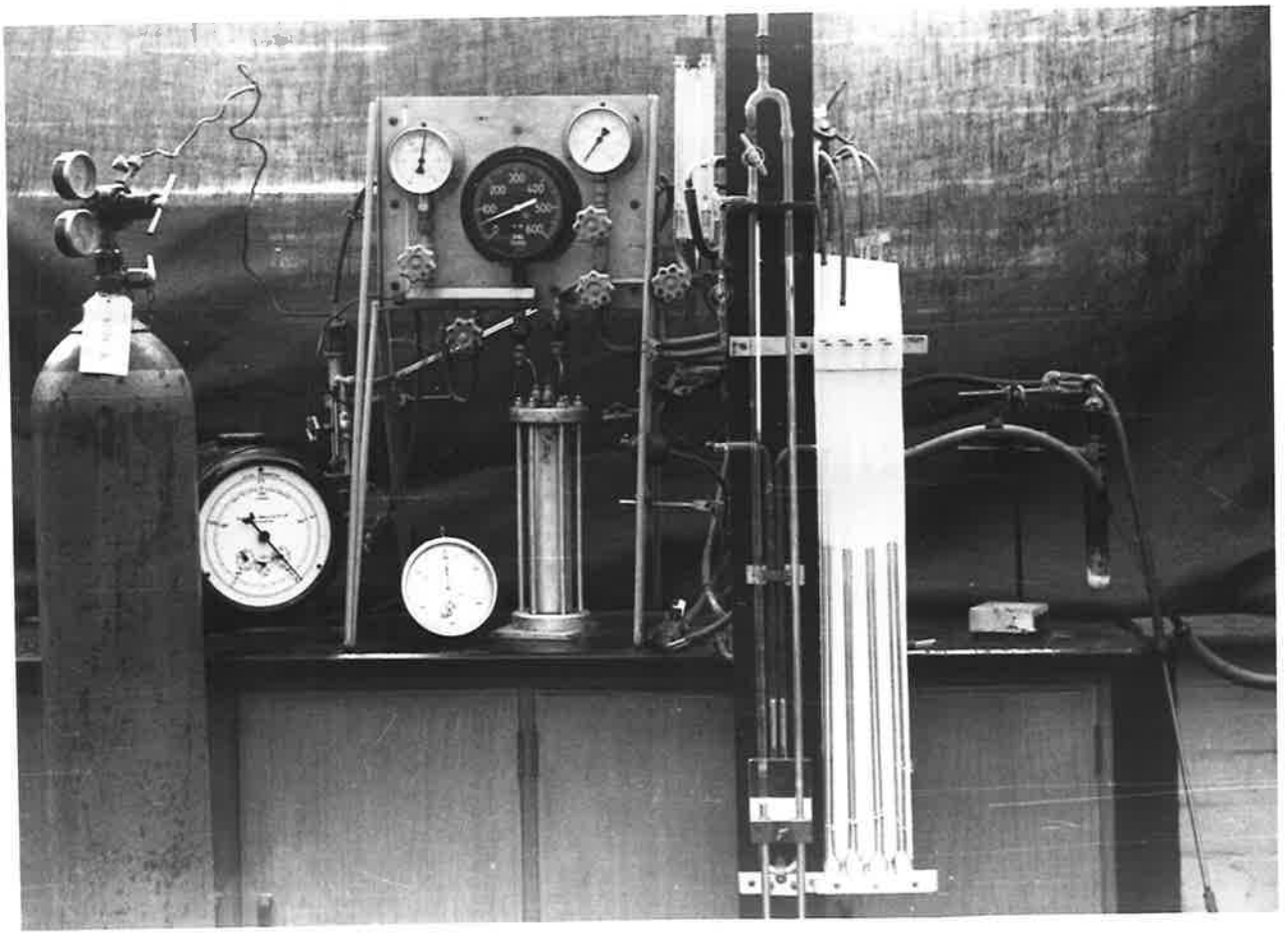

Fig. 3.1-4 Photograph of High Pressure Permeability Apparatus.

soap solution to the joints when under pressure, were repaired with Epoxy resin. The manometer J and the flow measuring equipment N to R were connected together with glass and rubber tubing sealed with wire clips and Apiezon black wax "W". Glass stopcocks were used in this low pressure portion of the apparatus.

3.1.4.1 The Permeability Cells

The graphite sample was held by a sample holder in the permeability cell H. For easy removal, the cell was attached to the inlet and outlet manifolds with Peal ¼ in. hexagonal high pressure unions I whose faces were machined to hold neoprene washers. These seals in the unions and also those in the tops of the cells have withstood pressures of 500 p.s.i.g. without leaking.

Cell type I was constructed from an old bomb calorimeter (see Fig. A.2-2(a)). The modified top screwed onto the calorimeter base with a gas-tight seal being obtained by means of a neoprene washer. At high flow-rates, excessive pressure drops occurred between the pressure tappings and the permeability cell because of the small diameter lines; corrections to the pressure measurements were therefore necessary.

Cell type II was constructed from a 2¾ in. o.d. x 12 in. long x 10 gauge drawn welded steel tube with 1 in. thick steel end discs sealed to the tube with rubber rings

and held by six ⅜ in. bolts (see Fig.A.2-2(b)). As no pressure drop corrections were required at high flow-rates, permeability cell type II was preferred for the high pressure permeability determinations.

3.1.4.2 Pressure Measurement

The inlet gas pressure was measured by means of either a 0 to 100 p.s.i.g. A.N.A. Bourdon gauge E, a 0 to 600 p.s.i.g. Foxboro Bourdon gauge F, or a 0 to 2 atm mercury manometer J, depending on the magnitude of the pressure to be measured. The manometer and gauge E could be isolated at pressures above 17 and 100 p.s.i.g., respectively, by Foxboro needle valves. Pressures below 17 p.s.i.g. were measured more accurately by means of the manometer J than by the 0 to 100 p.s.i.g. gauge E; the manometer pressures, read with a cathetometer, were in error by up to 0.06 cm Hg. Pressure measurements with the 0 to 100 p.s.i.g. gauge involved a calibration and reading error of 1% (5 cm Hg) for full scale deflection, while the error for the 0 to 600 p.s.i.g. gauge decreased with increasing pressure from 2% (10 cm Hg) at 100 p.s.i.g. For each series of pressure measurements, the atmospheric pressure was measured with the manometer J with a vacuum applied to one arm; this pressure was then added to the observed gauge pressures.

The outlet gas pressure p_o was measured by means of either a 0 to 150 p.s.i.g. A.N.A. Bourdon gauge G or the 0 to 2 atm mercury manometer J. As the mercury manometer was used to measure both p_i and p_o for determinations with p_i less than 2 atm, p_i was measured before p_o to avoid disturbing the flow through the graphite sample.

3.1.4.3 Flow-rate Measurement

Because of the considerable range of gas flow-rates encountered for the series of graphite samples, a number of methods of flow-rate measurement were employed. Flow-rates were measured by means of a wet gas test meter R, rotameters N and O, soap-bubble flow-meters P, and a capillary flow-meter Q. These flow-meters were interchangeable as each could be connected to the end of the apparatus by the 9/18 spherical joints S. All flow measurements were made at approximately atmospheric pressure and room temperature so that no corrections were required (see section 2.1.8.2(a)).

The wet gas test meter R (Alexander Wright and Co.Ltd.), with a capacity of 2.5 l. per revolution, was used to measure flow-rates in the range 10 to 200 cm^3/sec at N.T.P. The time for a certain volume of gas to pass through the meter was measured with a Pye stop-clock, the average of several readings being taken (variation = $\pm$ 0.25 sec). The measured gas flow-rate

was corrected to allow for the water vapour in the gas.

The range of flow-rates from 1 to 25 cm^3/sec at N.T.P. was covered by two Brooks glass laboratory rotameters N and O, viz., tube 1A-15-1 (stainless steel float) and tube 2-15-3 (glass and stainless steel floats). The rotameters were calibrated by displacement of water; then the gas flow-rate through the meters was obtained from calibration charts of the rotameter float height against the flow-rate Q.

Soap-bubble flow-meters P were employed to measure lower flow-rates from 0.0005 to 5 cm^3/sec at N.T.P. A series of soap-bubbles were formed at the base of a calibrated burette or pipette by allowing the gas stream to bubble through soap solution (a mixture of approximately 1 part of "Teepol" and 1 part of glycerine boiled in 3 parts of water) raised from a small reservoir by a rubber bulb. The time taken for a soap film to traverse a certain volume of the burette tube was measured with a Pye stop-clock, the average of several readings being taken.

The flow tubes used for the flow-meters were a 100 cm^3 burette graduated in 0.2 cm^3 (flow range 0.015 to 5 cm^3/sec at N.T.P), a 2 cm^3 pipette graduated in 0.02 cm^3 (0.005 to 0.025 cm^3/sec), and a 1 cm^3 pipette graduated in 0.01 cm^3(0.0005 to 0.006 cm^3/ sec).

Care was taken to ensure that the walls of a flow-meter tube were thoroughly wetted before a flow-rate measurement was made. The flow-rate was not corrected for the water vapour added to the gas from the soap solution because it was probably less than 1% of the gas volume.

Before the low volume (1 and 2 cm^3) soap bubble flow-meters were used, other methods of low flow-rate measurement were tried. Flow-rates measured by timing the movement of a mercury slug along a horizontal calibrated glass capillary tube (2 mm i.d.) were not consistent because the glass surface and the mercury could not be cleaned sufficiently to permit uniform motion of the mercury slug. A capillary flow-meter Q, consisting of a 30 ft length of 0.015 in. i.d. copper capillary tubing across a 0 to 30 cm Hg manometer, was used to measure flow-rates in the range 0.005 to 0.2 cm^3/sec at N.T.P. Because the capillary flow-meter needed recalibration for each different gas, and the measurement of very low flow-rates below 0.03 cm^3/sec was inaccurate, low flow-rates of all gases have been measured preferably with the soap-bubble flow-meters.

The range of flow-rates that could be measured with each flow-meter is summarized below:

	cm^3/sec at N.T.P.
Wet gas test meter	10 - 200
Rotameter No.2-15-3	6 - 25
Rotameter No.1A-15-1	1 - 7
Soap-bubble flow-meter,100 cm^3	0.015 - 5
Soap-bubble flow-meter, 2 cm^3	0.005 - 0.025
Soap-bubble flow-meter, 1 cm^3	0.0005 - 0.006
Capillary flow-meter	0.03 - 0.2

Calibration showed that the error involved in the measurement of the flow-rate was generally less than 2% if the flow-rate occurred in the middle portion of the flow-meter range.

3.1.4.4 The Gas Introduction System

The gas, supplied from cylinder A through a C.I.G. regulating valve B and a C.I.G. type T398 needle valve C, entered the high pressure inlet manifold T through a 4 ft length of 1/8 in. copper tubing, which allowed the gas to equilibrate to ambient temperature. The flow was regulated by means of either a C.I.G. type T328 high pressure regulator (nitrogen and argon), a type T285 regulator (hydrogen), or a low pressure CO_2 regulator (carbon dioxide and freon-12). The gas (e.g.carbon dioxide) could be dried by passing it through tower D packed with

silica gel and magnesium perchlorate held on glass wool.

For pressures below 2 atm, it was difficult to control p_i accurately with the regulating valve and needle valve. However, by means of a glass or metal Cartesian manostat[235] attached to the apparatus at V, p_i has been effectively controlled to within ½%.

3.1.4.5 The Vacuum System

For permeability determinations with the outlet pressure p_o less than one atmosphere, the gas stream was bypassed by a 3-way stopcock W to an Edwards "Speedivac" 1SP30 single stage rotary vacuum pump K. The discharge gas from the outlet of the pump passed through a trap M (packed with activated charcoal held on glass wool to remove the oil mist) to the flow-meter by way of the spherical joints S. Originally a liquid air trap packed with glass wool was used to remove the oil mist in the discharge gas, the gas being reheated to room temperature in a copper coil; however, the activated charcoal trap proved more effective than the liquid air trap and required renewal of the contents less often.

The vacuum system was checked frequently to ensure that no leakage occurred so that the flow-rate of the discharge from the pump agreed with the gas flow-rate into the pump to within ± 1%. At very low flow-rates,

the discharge flow-rate was often high by 0.003 to 0.01 cm^3/sec because of degassing or a small undiscoverable leak; this leakage rate was therefore calibrated and the measured flow-rates corrected.

The flow-meters were placed after the pump so that flow-rate measurements were always made at approximately atmospheric pressure. If the flow-meter was placed before the pump, the mean pressure in the meter varied so that a pressure correction was necessary for each flow-rate measurement, and the flow coefficient of the meter could possibly vary.

3.1.5 Experimental Procedure for the High Pressure Apparatus

The high pressure apparatus has been designed for the determination of permeability coefficients at pressures from less than 1 atm up to about 30 atm by the flow method. A brief description of the flow method for determining permeability coefficients for porous media has been given in section 2.1.8.2 (a). In the flow method, gas at a constant inlet pressure p_i flowed through the graphite sample under a constant pressure difference Δp and the flow-rate was measured by means of a suitable flow-meter. Permeability coefficients were determined for all graphite grades by this method.

The permeability cell H, containing the graphite sample supported by its sample holder, was attached to the apparatus by means of the unions I, the seals being tested with soap solution when pressure was applied. Gas was supplied from the cylinder A, and its flow regulated with the regulator B and the needle valve C, or controlled by the manostat at V, so that p_i remained at the desired value. The gas passed from the inlet manifold T through the sample to the outlet side where it was directed via stopcock W and the spherical joints S to the appropriate flow-meter N to R. For experiments with p_o less than 1 atm, the gas stream was bypassed through the vacuum pump K. Most permeability determinations have been made with p_o at about 0 or 76 cm Hg; for other p_o values, the desired pressure was obtained by restricting the outflow of gas with a needle valve.

When steady state flow was attained, p_i and p_o were measured by means of the gauges E or F or the manometer J, and the flow-rate measured by means of the flow-meter, the choice of pressure and flow measuring devices depending on the magnitudes of p_i and Q, respectively. (Steady state flow was reached after a few minutes for P.G.60 and Acheson "A" graphites, but about 5 minutes and one hour were required for Morgan "EY9" and Impregnated graphites to attain equilibrium flow, respectively).

Several flow-rate readings were made, the average value being taken (maximum variation = 2%). The permeability coefficient K was then calculated as shown in Appendix C.5.2. Further experiments at different values of p_i and p_o were performed by repeating the above procedure. The temperature at the sample (ambient temperature), the temperature at the flow-meter, and the atmospheric pressure were measured for each experiment.

It was desirable to measure flow-rates in the middle portions of each flow-meter range for maximum accuracy in the flow measurement. With the wet gas test meter and the soap-bubble flow-meter, the time was measured for a certain volume of gas to pass through the meter, as indicated by the revolving pointer and the moving soap film, respectively. In the rotameter, the height of the float was recorded, while for the capillary flow-meter, the pressure differential across the capillary was measured when equilibrium flow was reached; for both these meters, the value of the flow-rate was obtained from calibration charts.

3.1.6 The Measurement of the Pressure Distribution

3.1.6.1 Sample Preparation

For the pressure distribution measurements, special composite graphite specimens were prepared so that the pressure could be measured at several points within each specimen during gas flow. Each specimen was prepared from a rod of graphite, which was machined on the lathe, coated on the side with Epoxy resin or red sealing wax (see section 3.1.1.1), and cut into four equally-sized graphite discs (approximately 1.25 cm diameter x 1.0 to 2.5 cm thick). The dimensions of the discs were measured (to $\pm$ 0.005 cm) with either vernier calipers or a micrometer.

To make a continuous specimen, the four discs were connected together with rubber sleeves, each of which held a glass tube to enable the pressure to be measured between the discs during flow (see Fig.3.1-5). All joins were carefully sealed with Epoxy resin to prevent the leakage of gas around a disc or to the atmosphere. Each specimen was supported in a metal tube for strength. The details of the specimens are listed in Table A.3-1, Appendix A.3.

3.1.6.2 Gases

The gases nitrogen, hydrogen, carbon dioxide, and freon-12 were used for the pressure distribution

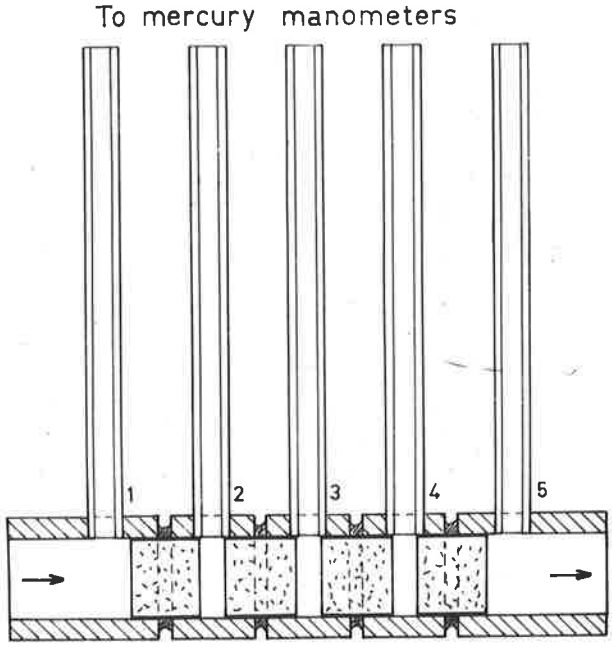

Fig. 3.1-5(a) Diagram of Pressure Distribution Specimen.

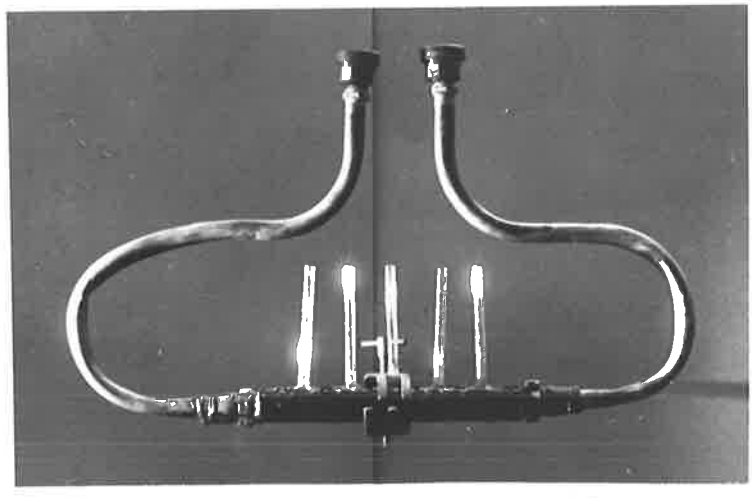

Fig. 3.1-5(b) Photograph of Pressure Distribution Specimen.

measurements. The composition and supply of these gases has been mentioned in section 3.1.1.2.

3.1.6.3 Description of the Apparatus

The pressure distributions in the composite graphite specimens were determined during steady state flow measurements performed in the high pressure apparatus. Accordingly, only the additional apparatus will be mentioned here as the description of the high pressure apparatus has been detailed in section 3.1.4.

The graphite specimen, with copper connecting tubing fastened to its ends, was attached to the high pressure apparatus by means of the hexagonal unions I (see Fig. 3.1-3).

The intermediate pressures along the specimen were measured by means of four mercury manometers (see Fig.3.1-4), one arm of each being connected by rubber hosing to the pressure tappings in the specimen. The second arm of each manometer was open to the atmosphere, thus necessitating the measurement of the atmospheric pressure for each flow experiment. Although the small bore (4 mm) of these manometers caused a large capillary depression for mercury, it was assumed that the depression was equal in both arms and so cancelled out.

3.1.6.4 Experimental Procedure

The pressure distribution in the specimen was

measured when steady state flow conditions were attained. Besides measuring the pressures along the sample, the flow-rate was also obtained. The experimental procedure was therefore similar to that described in section 3.1.5.

When any leaks in the apparatus and specimen had been repaired, gas was admitted from cylinder A (see Fig. 3.1-3) and its flow-rate regulated to give the desired value of p_i. Generally p_i was controlled to a steady value by means of either a glass or a metal Cartesian manostat (section 3.1.4.4). The required value for p_o, either greater or less than atmospheric pressure, was obtained as mentioned in section 3.1.5. After passing through the sample, the gas stream was directed to the appropriate flow-meter.

When equilibrium flow was attained, the pressures and flow-rate were measured. The inlet pressure p_i was measured by means of either gauge E or manometer J, while the intermediate pressures and p_o were measured with the four small mercury manometers (section 3.1.6.3). The cathetometer was used to measure all manometer pressures.

Further experiments at different values of p_i and p_o were performed by repeating the above procedure. Because the intermediate pressures were measured on manometers, the maximum value of p_i was limited to about

165 cm Hg (17 p.s.i.g). For each experiment, the temperatures and the atmospheric pressure were measured. The permeability coefficients K for each disc and for the total specimen were calculated as shown in Appendix C.5.2, and the pressure distribution curves were plotted.

3.2 The Porosity Measurements

3.2.1 Materials

3.2.1.1 Sample Preparation

The graphite samples for the porosity measurements by the helium displacement method were prepared as small cylinders (about 3 cm long x 1.2 cm diameter) by machining to size on a lathe. Their dimensions were measured to ± 0.005 cm with vernier calipers or a micrometer, and their weight determined to ± 0.001 g. The details of the samples are summarized in Table A.4-1, Appendix A.4.

Each sample was placed in a glass bulb, previously prepared for attachment to the apparatus by means of a B7 conical joint, and the end was sealed to give only a small dead space volume in the bulb.

3.2.1.2 Gases

"Spectrally pure" helium supplied in 1 l. pyrex flasks by the British Oxygen Co.Ltd. was available for the displacement measurements.

3.2.2 Description of the Apparatus

The apparatus in which the helium displacement measurements were made was constructed originally for nitrogen adsorption measurements; it is shown diagrammatically in Fig. 3.2-1(a). Essentially it consisted of a calibrated gas burette S (see Fig. 3.2-1(a)) joined through capillary tubing to a detachable sample bulb B and a constant volume mercury manometer M, and connected to a high vacuum system and a helium supply. The gas burette and sample bulb were water jacketted to maintain the gas at a constant temperature.

The original apparatus has been described in detail by Culver[236] and Ward;[237] only the important aspects of pressure, volume, and temperature measurement will be mentioned here.

3.2.2.1 Pressure Measurement

The pressure in the gas burette was measured by means of a constant volume mercury manometer[238] M, in which the mercury level could be adjusted to a tungsten reference point P so that the free space volume remained constant. A fine adjustment control C and a "magic eye" indicator[238] I, the "eye" of which closed when an electric circuit was completed by the contact of the point P with with the mercury, permitted the mercury level to be set with an error of about 0.01 mm (or less than 0.001 cm^3 volume variation). The mercury levels in the manometer

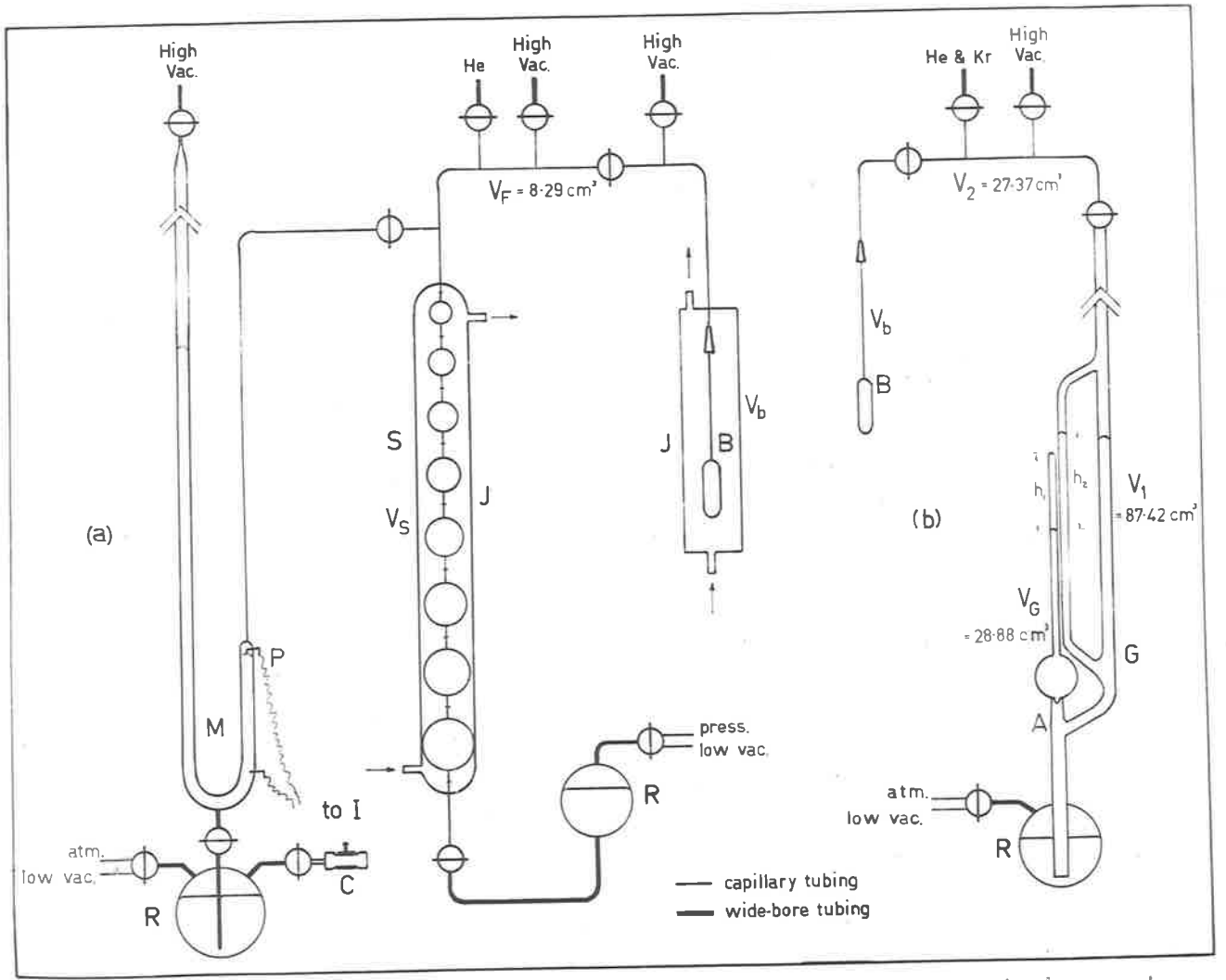

Fig. 3.2-1 Line Diagrams of (a) Helium Displacement Apparatus.
(b) Krypton Surface Area Apparatus.

LEGEND FOR FIG. 3.2-1

(a) Helium Displacement Apparatus

B Sample bulb (volume V_b)

C Fine adjustment control

I Magic "eye" indicator

J Water jackets

M Manometer, 0 to 76 cm Hg

P Tungsten reference point in manometer

R Mercury reservoirs

S Gas burette (volume V_S)

(b) Krypton Surface Area Apparatus

A Cut off point in McLeod gauge

B Sample bulb (volume V_b)

G McLeod gauge (volume V_G)

R Mercury reservoirs

were measured with a cathetometer with a maximum error of 0.03 cm Hg.

3.2.2.2 Volume Calibrations

(a) Gas Burette Volumes

The values of the cumulative volume V_S of the gas burette S from the top reference mark to the successive marks between the bulbs were 2.638, 6.536, 13.003, 19.590, 32.183, 44.521, 73.856, and 104.883 cm^3, respectively; these values had been obtained by direct calibration with mercury before the burette was joined to the apparatus.[236] The errors involved were less than 0.005 cm^3.

(b) Free Space Volume

The free space volume V_F was the volume of the capillary tubing bounded by the top reference mark in the gas burette S, the mercury level in the manometer M, the stopcocks to the vacuum and gas systems, and the top of the B7 conical joint to which the sample bulb B was attached (see Fig.3.2-1(a)). As this volume had to be calibrated indirectly and was subject to ambient temperature fluctuations, it was kept as small as possible.

The volume V_F was determined by admitting helium to the apparatus and measuring the pressure p when the mercury level in the burette was adjusted to each successive calibration mark.

Then $$\frac{p V_S}{\mathcal{T}_S} = \text{constant} - \frac{p V_F}{\mathcal{T}_a} , \qquad \ldots (3.2.2\text{-}1)$$

where $\mathcal{T}_S$ and $\mathcal{T}_a$ were the burette jacket and ambient temperatures, respectively. The slope of a plot of $p V_S/\mathcal{T}_S$ against $p/\mathcal{T}_a$ yielded V_F as 8.29 cm^3.

3.2.2.3 Temperature Measurement and Control

The temperatures of the water jackets J around the gas burette and sample bulb were maintained to $\pm$ 0.02°C by water circulating from a constant temperature bath controlled by a Techne "Tempunit" thermostat unit. The temperatures $\mathcal{T}_S$ and $\mathcal{T}_b$ were measured by thermometers to 0.05°C, and the ambient temperature $\mathcal{T}_a$ to 0.1°C.

3.2.3 Experimental Procedure

The method employed for the helium displacement measurements was similar to that of Smith[166] (see section 2.2.2.1); the calibrated burette S enabled a number of expansions to be made to give an accurate mean value of the dead space volume.

3.2.3.1 Outgassing of the Sample

The sample bulb B containing the sample (see 3.2.1.1) was attached to the apparatus, evacuated, and tested for leaks. The sample was outgassed for about 16 hr at a temperature of approximately 300°C and a pressure

of 10^{-5} mm Hg. A small furnace, controlled by a Sunvic type TYB energy regulator, was used to heat the graphite sample during outgassing. The jacket J was placed over the bulb before the dead space volume was measured.

3.2.3.2 Measurement of the Dead Space Volume

The dead space in the bulb V_D was determined in a similar way to the calibration of the free space volume (section 3.2.2.2). Helium was admitted to the evacuated gas burette S and sample bulb B, and the pressure was measured when the mercury level in the burette was successively adjusted to each calibration mark, sufficient time being allowed at each pressure for the gas to penetrate the sample completely. Then the volume V_D could be calculated as shown in Appendix F. Alternatively, the volume of helium at S.T.P. admitted to the gas burette could be determined by successive expansions in the burette prior to its introduction into the evacuated sample bulb.

3.2.3.3 Measurement of the Bulb Volume

Generally the bulb volume V_b has been measured by helium expansion as described above before the sample was placed in the sample bulb. However, as the graphite samples were enclosed in glass bulbs sealed to minimize the dead space volume (see section 3.2.1.1), V_b could not be measured by this means.

Two methods were used to measure V_b. For the fine-pored graphites, the bulb, still containing the sample, was filled with mercury; the increase in weight gave the bulb volume less the graphite volume. For the coarse-pored graphites, the glass bulb was carefully cracked in halves, the sample removed, and the bulb rejoined firmly with adhesive tape. Then the weight and hence the volume of mercury to fill the bulb was measured.

From the above measurements and the weight and bulk volume of the graphite sample, the porosity, the helium density, the bulk density, and the percentage of unopen pores were calculated as shown in Appendix F.

3.3 The Surface Area Determinations

3.3.1 Materials

The krypton adsorption surface area determinations were performed on the same graphite samples that were used for the porosity measurements, each sample being sealed into a glass bulb (see section 3.2.1.1). The initial determinations on Acheson "A" graphite were performed on the -14/+18 B.S.S. mesh fraction of the crushed graphite, contained in a glass bulb.

For the krypton adsorption measurements, the helium for calibration purposes and the krypton were obtained in 1 l.pyrex flasks from the British Oxygen Co.Ltd.

The helium was "spectrally pure", while the krypton was 99 to 100% pure with xenon as the main impurity. The flasks were sealed on to the apparatus and were opened by breaking the glass tip by means of a magnetic hammer.

3.3.2 Description of the Apparatus

The volumetric adsorption apparatus for determining krypton isotherms for solid adsorbents has been described by Ward.[237] The apparatus (see Fig.3.2-1(b)) was similar to that used by Bloecher.[181] It consisted of a manifold to which were attached the sample bulb E and a low sensitivity McLeod gauge G for pressure measurement. The manifold was connected to the same high vacuum system and gas reservoirs that were employed for the helium displacement apparatus.

3.3.2.1 Pressure Measurement

The McLeod gauge G was so designed that pressures between 0.05 and 4.5 mm Hg could be measured accurately. The volume V_G of the capillary and the bulb above the cut-off point A of the gauge was 28.88 cm^3, the calibration error being about 0.1%. To measure the pressure, the heights of the end of the closed capillary and the mercury levels in the open and closed capillaries were measured by means of a cathetometer; the pressure p was calculated from these three cathetometer readings according to Boyle's law, e.g.,

$$p = \frac{A\, h_1\, h_2}{V_G - A\, h_1} , \qquad \ldots (3.3.2\text{-}1)$$

where A = cross-sectional area of the capillary

$= 0.01\,\pi$ cm^2 ,

h_1 = length of the closed capillary not filled with mercury (see Fig. 3.2-1(b)),

and h_2 = height of mercury in the open capillary above the level in the closed capillary.

The estimated maximum error involved in any pressure reading was $\pm$ 0.5%.

3.3.2.2 Temperature Measurement

The temperature of the liquid nitrogen bath in which the sample bulb B was placed was measured with an oxygen vapour pressure thermometer. The vapour pressures were converted to temperatures according to the expression given by Yost and Russell.[239] The vapour pressure of krypton P_o at the measured temperature was obtained from tables prepared from published data.[186]

3.3.3 Experimental Procedure

To determine an isotherm, the amount of gas adsorbed at different pressures must be measured (section 2.3.2.1). In the following procedure, such measurements are outlined.

3.3.3.1 Outgassing of the Sample

The samples were outgassed at about 300°C in the same manner as described for the helium displacement measurements (section 3.2.3.1).

3.3.3.2 Calibration of the Free Space and Dead Space Volumes

As the volume V_G of the bulb of the McLeod Gauge G was the only known volume in the apparatus, the volume V_1 from the cut-off point A to the manifold, and the manifold volume V_2 were calibrated by the expansion of a known quantity of helium from the McLeod gauge into the apparatus using the McLeod gauge to measure the pressures. These volumes were respectively 87.42 and 27.37 cm^3, the error being less than $\pm$ 0.4%.

For each isotherm determination, the volume of the dead space in the sample bulb V_D was similarly calibrated by expansion of helium trapped in the capillary of the McLeod gauge into the evacuated apparatus. The average of several measurements was taken, the variation generally being $\pm$ 0.5%.

3.3.3.3 Isotherm Determination

After calibration of the dead space in the sample bulb, the apparatus was evacuated for about an hour. The sample bulb was then surrounded by a liquid nitrogen bath, which was contained in a Dewar flask and agitated by a slow stream of dried nitrogen gas.

A small amount of krypton was admitted to the McLeod gauge G and its pressure measured. The krypton trapped in the capillary of the gauge (volume V_G at pressure p_1)

was expanded into the evacuated apparatus. After allowing some time for the krypton to equilibrate with the sample, the sample bulb was isolated, the liquid nitrogen bath temperature $\mathcal{T}_b$ and the ambient temperature $\mathcal{T}_a$ recorded, and the new pressure p_2 measured. Then the amount of gas adsorbed could be calculated as shown in Appendix G.2.

This procedure was repeated by successively admitting more krypton to the sample as described above until p/P_o was about 0.25 after an adsorption. At this pressure, the volume of gas in either V_2 or V_a ($= V_1 + V_2 + V_G$) was pumped out and the sample allowed to desorb gas. Successive quantities of krypton were removed and the equilibrium pressures measured until sufficient points on the isotherm had been determined.

The surface area was then determined as shown in Appendix G.2. No correction was necessary for deviations from the ideal gas law,[180] but a correction for thermal transpiration (see section 2.3.2.1(b)) was possibly required.

3.4 The Pore Size Distribution Measurements

The pore size distribution measurements were not performed by the author as a high pressure mercury porosimeter was not available locally. The distributions

for samples of P.G. 60, Acheson "A", and Morgan "EY9" graphites were determined at the laboratories of the Division of Coal Research of the Commonwealth Scientific and Industrial Research Organization (C.S.I.R.O.), Chatswood, N.S.W., while the distributions for the Impregnated graphite samples were supplied by the Australian Atomic Energy Commission (A.A.E.C.), Lucas Heights, N.S.W. from measurements performed during investigations in their laboratories.

The apparatus and experimental procedure used at each laboratory will be briefly outlined.

3.4.1 The C.S.I.R.O. Measurements

3.4.1.1 Materials

Samples of the P.G. 60, Acheson "A", and Morgan "EY9" graphites were sent to the laboratories of the Division of Coal Research. The samples were machined into cylinders (approximately 5/8 in. diameter x 1 in. long) and their volumes determined by micrometer measurements.[240] The weights of the samples were obtained after drying in an oven at 200°C for 2 hr. The details[240] of these cylinders are given in Table A.5-1.

3.4.1.2 Description of the Apparatus

The mercury porosimeters employed by the Division of Coal Research of the C.S.I.R.O. have been mentioned by Cameron and Stacy.[202,207] The high-pressure instrument[202]

was similar to that described by Ingles;[206] however, the volume of mercury penetrating the sample at each pressure was determined by measuring the fall in the mercury level in the neck of the dilatometer (to 0.005 in.) with a probe in conjunction with a vernier scale. With this apparatus, the distribution of pores within the pore radius range 20 to 70,000Å could be obtained. A low pressure porosimeter,[207] operating at pressures below one atmosphere, enabled the range of the high pressure instrument to be extended to radii beyond 70,000Å.

3.4.1.3 Experimental Procedure

In the procedure described by Cameron and Stacy,[202] a dilatometer containing the sample was filled with mercury after being evacuated to a pressure of 10^{-4} mm Hg. With the dilatometer fitted into the porosimeter, the pressure on the sample was increased progressively and the volume of mercury penetrating the sample at each pressure was measured. An interval of 15 min was allowed to elapse after each pressure increment before a volume measurement was made.

From the experimental results, the pressurizing curve of $V(r_i)$ against p_{ci} was plotted. Then the pore entrance size distribution function D(r) was obtained as indicated in Appendix H.1, with the surface tension γ

of mercury being 480 dyn/cm and the contact angle θ between graphite and mercury being taken[240] as 140° (cf. section 2.4.4.1(a)). The results were corrected for compression of the sample and the mercury at pressures above 6000 p.s.i.[240]

3.4.2 The A.A.E.C. Measurements

3.4.2.1 Materials

The pore size distribution results[241] supplied by the A.A.E.C. were for a series of Impregnated graphites which had been prepared by the A.A.E.C. from Morgan "EY9" stock.[13] No details are available of the size or weight of the samples for the distribution measurements.

3.4.2.2 Description of the Apparatus

The mercury porosimeters employed at the laboratories of the A.A.E.C. have been described by Thurstan and Wall.[203] Two instruments were used, viz., a high pressure porosimeter for the pore radius range 35 to 1250 Å and a low pressure porosimeter for the pore radius range 1250 to 12,500 Å. The high pressure porosimeter was of similar design to that of Ingles;[206] the volume of mercury penetrating the sample was determined by measuring the movement of a plunger in a precision syringe (0.2 cm^3/ cm) by means of a differential transformer. With the low pressure instrument, the fall in the mercury level in a glass capillary was observed by

means of a cathetometer, the error in measuring a level being ± 0.1 mm.

3.4.2.3 Experimental Procedure

In the procedure adopted by Thurstan and Wall,[203] the cylindrical graphite sample was placed in a small bottle and outgassed at 2×10^{-4} mm Hg and 300°C for 8 hr. The bottle was filled with mercury under vacuum, attached to the low pressure apparatus, and pressurized in suitable increments. At each pressure, sufficient time was allowed for equilibrium to be attained (up to 8 hr) before the change in mercury volume was measured.

When the pressure had been increased to 800 p.s.i.g., the sample container was inserted in the high pressure porosimeter and the pressure progressively increased to 30,000 p.s.i.g. From these results, the pressurizing curve of $V(r_i)$ or $\mathcal{E}(r_i)$ against p_{ci} was plotted. Compressibility of the graphite sample was considered negligible.

3.5 The Electrical Resistivity Measurements

The method suggested in section 2.5.6.3 for the measurement of the formation factors of saturated graphite samples was a refinement of the d.c. method of MacMullin and Muccini.[145] The apparatus and experimental techniques developed for such measurements are described in this section.

3.5.1 Materials

3.5.1.1 Sample Preparation

The graphite samples for the electrical resistivity determinations were prepared in the form of cylinders (approximately 2.5 cm diameter and from 1.8 to 5.6 cm long) whose axes were either parallel or perpendicular to the extrusion axis of the graphite. The samples were machined to size on a lathe and their dimensions measured (to $\pm$ 0.005 cm) with vernier calipers or a micrometer. The dimensions of the samples are given in Table A.6-1, Appendix A.6. The cylindrical surfaces of the samples were coated with Epoxy resin generally, although paraffin-wax was applied to the P.G. 60 samples (cf. section 3.1.1.1).

3.5.1.2 Electrolytes

Normal potassium chloride (N KCl) was the electrolyte used to saturate the graphite samples for most of the electrical resistivity experiments; 0.5N potassium carbonate (K_2CO_3) and approximately 3N potassium chloride were each used in one experiment. The solutions were prepared from A.R. grade chemicals and distilled water. The electrolyte was degassed (see section 3.5.3.2) before being introduced into the formation factor cell.

3.5.2 Description of the Apparatus

The apparatus for the determination of electrical

resistivity factors or formation factors consisted essentially of a formation factor cell into which the graphite sample was sealed, and a four-electrode system (with the necessary electrical equipment) for passing a d.c. current through the saturated sample and measuring the voltage drop across the sample. Auxiliary apparatus included an arrangement for evacuating the cell and filling it with electrolyte, and a conductivity bridge for measuring the conductivity of the electrolyte.

3.5.2.1 The Formation Factor Cell

The formation factor cell, shown diagrammatically in Fig. 3.5-1 and by photograph in Fig. 3.5-2, consisted of two Quickfit B29 sockets A between which the coated graphite sample H was held. The B14 sockets B attached to the sides of the cell enabled the cell and sample to be evacuated and filled with electrolyte when blank rubber stoppers were inserted into the ends of the sockets. For the electrical measurements, the blank ends were replaced with rubber stoppers E each carrying the electrode assembly D and F (see section 3.5.2.3). The cell arrangement was held on a rigid metal base-plate by means of Terry clips and was placed in a Townson and Mercer thermostatted water bath for the resistivity measurements.

Originally, the graphite sample was sealed into

the cell with B29 PTFE sleeves and secured with springs; however, such seals allowed considerable leakage and were unsatisfactory. A large number of measurements were performed with the sample sealed into the B29 sockets with Apiezon "Q" Wax, the middle portion of the cell being coated with shellac and celluloid solution to prevent leakage. Finally, red sealing wax was used to seal the sample into the cell. Although rather messy to apply, the sealing wax was proved very satisfactory as the resulting seal was stronger and less susceptible to leaks into the cell and between the two sides of the cell than the Apiezon wax/shellac seals.

3.5.2.2 The Arrangement for Evacuating and Filling the Cell

In order to evacuate the sample and fill the cell with electrolyte, the cell was attached to the arrangement shown diagrammatically in Fig. 3.5-3. Both sides of the cell could be evacuated when the arrangement was connected at J to a high vacuum system consisting of a mercury diffusion pump and an Edwards backing pump. Degassed electrolyte could be admitted to the evacuated system from a storage funnel I.

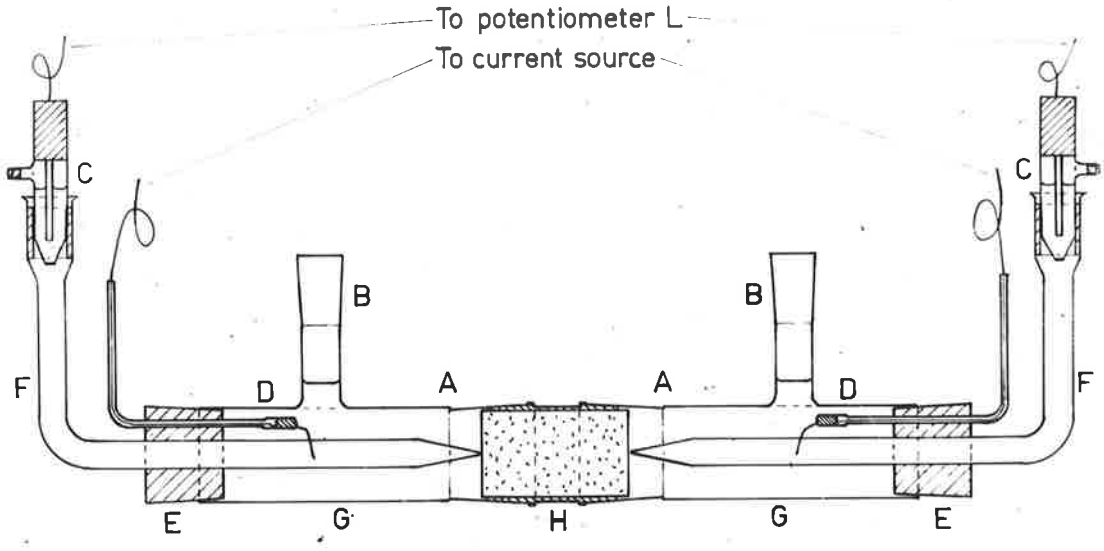

Fig. 3.5-1 Diagram of Formation Factor Cell.

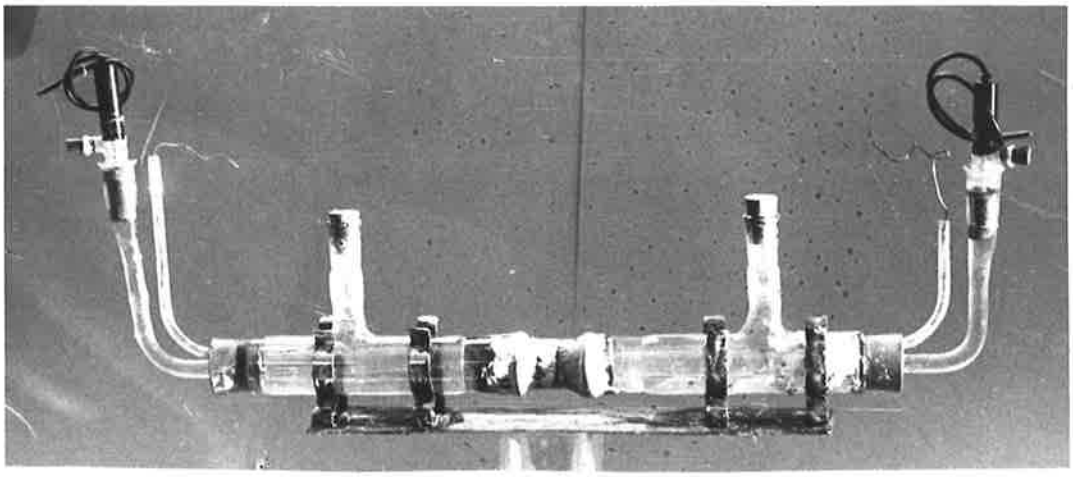

Fig. 3.5-2 Photograph of Formation Factor Cell.

LEGEND FOR FIGURES

Fig. 3.5-1 The Formation Factor Cell

A Quickfit B29 sockets

B Quickfit B14 sockets for evacuating and filling the cell

C Beckman saturated calomel reference electrodes

D Current-carrying electrodes

E Rubber stoppers

F "Luggin" capillary probe

G Electrolyte in the cell

H Graphite sample

Fig. 3.5-3 Evacuating and Filling Arrangement

I Electrolyte storage funnel

J Connection for high vacuum

K 3-way stopcock

Fig. 3.5-4 The Electrical Circuit

L Yew d.c. potentiometer

M Dry cell voltage source, 140 V max.

N Decade resistance box, 10^3 to 2×10^8 ohms

O Shunt

P Cambridge spot galvanometer, 1 μA f.s.d.

Q Reversing switch

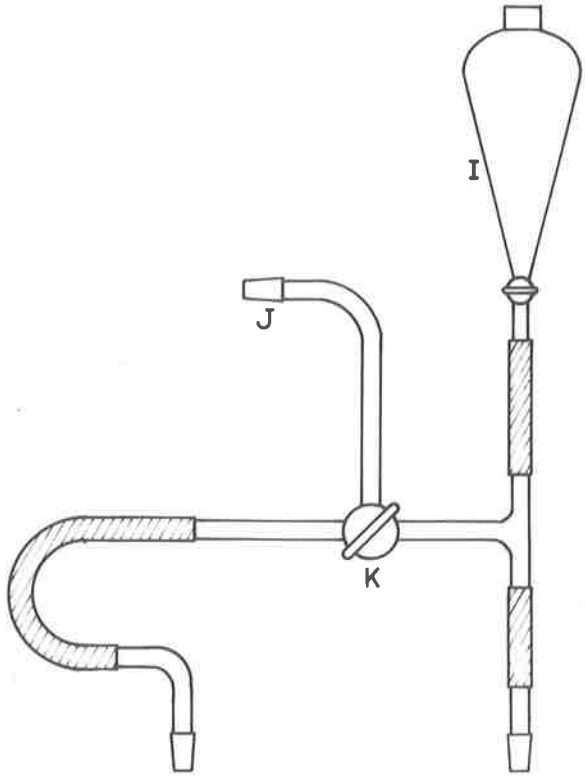

Fig. 3.5-3 Diagram of Evacuating and Filling Arrangement.

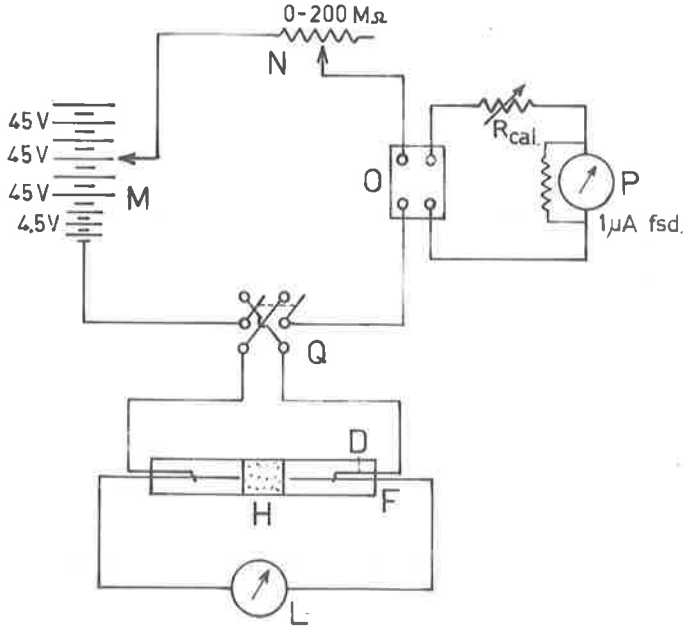

Fig. 3.5-4 Diagram of Electrical Circuit for Electrical Resistivity Measurements.

3.5.2.3 The Electrical Equipment

A d.c. current, which could be kept constant at any desired value down to as low as 0.1 μA, was supplied to the current carrying electrodes D in the cell by the circuit shown in Fig. 3.5-4. This circuit consisted of a dry cell source M of 140 V maximum in series with a decade resistance box N (range 10^3 to 2 x 10^8 ohms), a shunt O, and a reversing switch Q. The current flowing through the cell was measured by means of a Cambridge spot galvanometer P (sensitivity 1 μA full scale deflection) in parallel with the shunt O.

When the sample was saturated with 0.5NK_2CO_3, spiral platinized platinum electrodes carried the current to the cell. However, for the KCl electrolyte, the current electrodes D were silver wire coated with silver chloride; these electrodes were sealed into glass tubes in the rubber stoppers E and were connected to the constant current supply.

Beckman saturated calomel reference electrodes C supported by "Luggin" capillary probes F enabled the potential drop ΔE across the graphite sample to be measured by an accurate potentiometer L (see Fig.3.5-1). These "Luggin" probes were filled with the electrolyte solution and were located in the formation factor cell by the rubber stoppers E so that they reached right up

to the graphite surfaces and could sense the potentials close to the graphite/electrolyte interfaces.

The potential difference ΔE was originally measured with a Jones pH meter (0 to 1300 mV). Later, a Yew d.c. potentiometer (Model P-1) together with a Pye "Scalamp" galvanometer (1400 ohms resistance), a 2V battery, and a Weston standard cell were employed to measure ΔE.

3.5.2.4 The Conductivity Bridge

The specific resistance R_o of the electrolyte in the cell was measured independently by a 1000 cycles/sec Kohlrausch Universal Conductivity Bridge using a cathode ray oscilloscope as the null point detector. The sample of electrolyte solution in the conductivity cell was placed in a water bath at the same temperature at which the electrical resistivity measurements had been made.

3.5.3 Experimental Procedure

The determination of the electrical resistivity factor for a graphite sample involved the saturation of the evacuated sample with the electrolyte and the measurement of its resistance R'. The resistance R_o' of the electrolyte was measured independently with the conductivity bridge. Before the resistivity measurements were commenced, the preliminary determination of the decomposition potential for each graphite/electrolyte

half cell was essential.

3.5.3.1 Measurement of the Decomposition Potential

The decomposition potential E_d of a graphite/electrolyte half cell is the electrical potential at which an appreciable discharge of the electrolyte at a graphite electrode commences for any current flow I. Decomposition potentials were determined by means of a cell equivalent to a half of the formation factor cell with the graphite as one electrode. For any constant current I, E_d was the potential difference between the graphite and the electrolyte/graphite interface, measured relative to the calomel reference electrode.

By the measurement of E_d at a series of current densities, graphs of E_d against I, shown in Fig. 3.5-5, were prepared for the graphite/0.5N K_2CO_3 and the graphite/NKCl half cells. No graph was prepared for the graphite/3N KCl half cell as the potential was only slightly different from that for the graphite/N KCl half cell.

During the electrical resistivity measurements, no current would be conducted by the graphite itself, but only by the electrolyte within the graphite pores if the voltage drop ΔE across the graphite sample at any current I was much less than the decomposition potential E_d at that current.

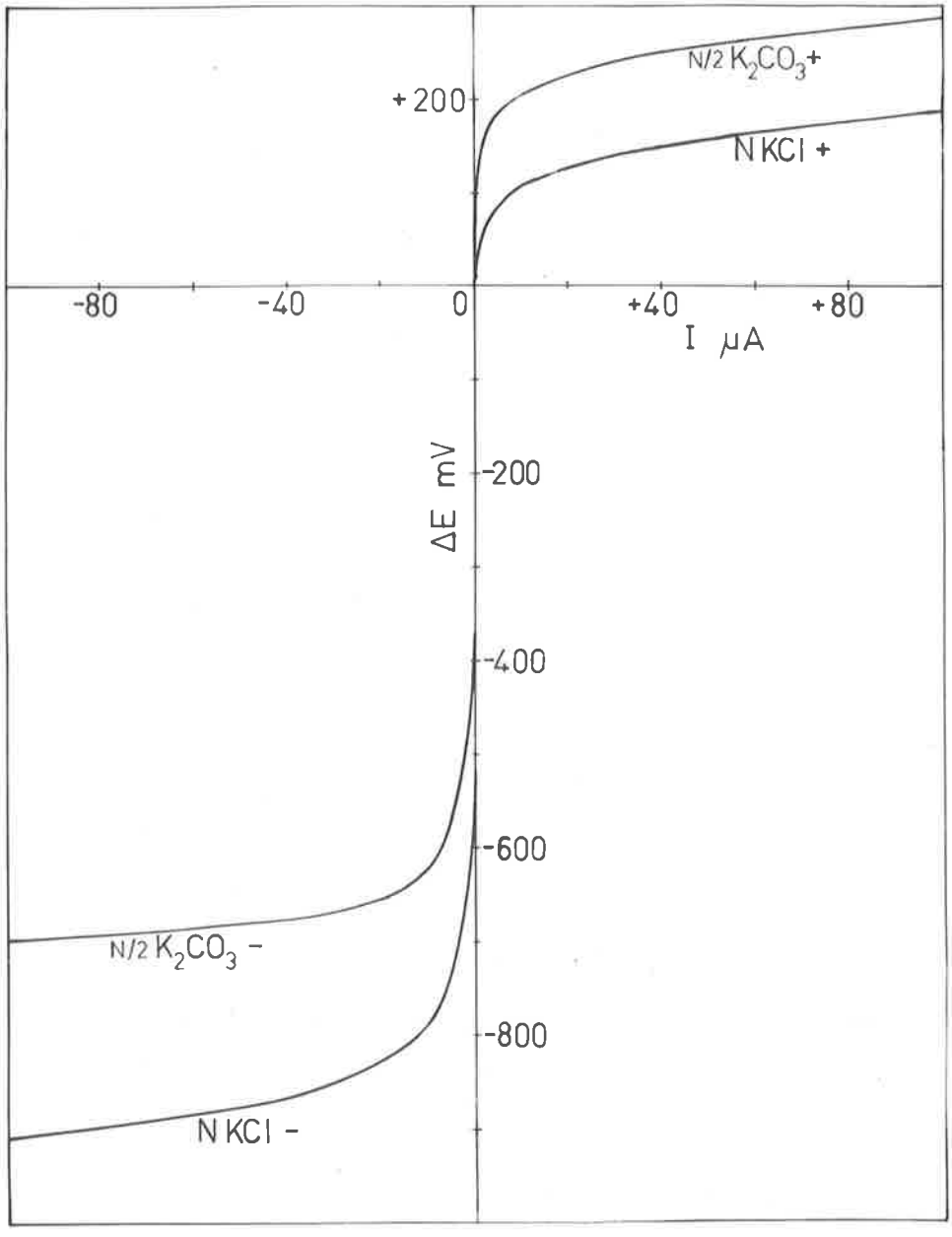

Fig. 3.5-5 Decomposition Potential Graphs of E_d against I for the Graphite/0.5 N K_2CO_3 and the Graphite/N KCl Half Cells.

3.5.3.2 Preparation of the Cell and Sample

The coated graphite sample was sealed into the cleaned formation factor cell (see section 3.5.2.1). With blank rubber stoppers inserted in its ends, the cell was attached to the arrangement shown in Fig. 3.5-3 and evacuated for about 2 days by the backing pump, and then for several hours with the diffusion pump to a vacuum of about 10^{-4} mm Hg as indicated on a Pirani gauge. Any leaks detected in the cell with an Edwards high frequency spark tester were sealed with shellac.

The required amount of electrolyte (approximately 300 cm^3) was degassed by heating in a flask under low vacuum produced by a water jet pump, cooled under vacuum, and quickly transferred to the storage funnel I. When the cell had been evacuated at 10^{-4} mm Hg for several hours, it was isolated from the vacuum system by the 3-way stopcock K and degassed electrolyte was admitted slowly from funnel I, care being taken to ensure that the graphite sample was completely saturated. When the cell and the graphite sample were full of electrolyte, low vacuum was applied to each side of the cell in turn to remove any gas bubbles. With the coarser-pored graphites, the electrolyte could be sucked through the sample to assist in its penetration of all the pores.

The cell was removed from the evacuating and filling apparatus, and the blank stoppers were each replaced carefully in turn by the stoppers E carrying the prepared electrode assemblies CDF. The current-carrying electrodes D and the standard calomel electrodes C were connected respectively to the current supply M to Q and the potentiometer L, and the cell was placed in the thermostatted water bath ready for resistivity measurements.

3.5.3.3 Electrical Resistivity Measurements

The potential difference ΔE across the sample was measured with the potentiometer L for a number of values of the current I, set by adjusting the resistance of the decade box N; I was not altered until a steady ΔE value was obtained. Provided ΔE was very much less than the decomposition potential E_d at the preset current I, no current was conducted by the graphite itself (see section 3.5.3.1). The resistance R' of the saturated graphite sample was obtained as the slope of the graph of ΔE against I (see Appendix J.2).

When the resistivity measurements for any determination were completed, a representative sample of the electrolyte was withdrawn from the cell and placed in the conductivity cell for which the cell constant was known. By means of the conductivity bridge, the

specific resistance R_o of the electrolyte was measured. As the degassing of the electrolyte concentrated the solution by a slight but variable amount, the value of R_o obtained for different determinations was not constant.

The formation factor F and the electrical tortuosity factor q were calculated as shown in Appendix J.2.

4. RESULTS

4.1 The Gas Flow Measurements

In this section, the experimental results of the permeability determinations and the pressure distribution measurements on the reactor graphites are presented. The permeability results are considered in the order of decreasing pore size of the graphites, viz., P.G. 60 graphite, Acheson "A" graphite, Morgan "EY9" graphite, and Impregnated graphite, and are tabulated in Tables 4.1-1 to 4.1-4, respectively. The average values of the permeability coefficients B_o and K_o calculated from the permeability results are summarized in Table 5.1-1, section 5.1.

The experimental permeability results for each determination are detailed in Appendix K. Particular comments about experimental observations for each determination are also included.

4.1.1 P.G. 60 Graphite

Permeability coefficients were determined for two samples of P.G. 60 graphite. For Rod No. K31, whose axis was parallel to the extrusion axis of the graphite block, the flow of nitrogen, hydrogen, argon, and freon was investigated, while for the perpendicular sample, Rod No. K32, only nitrogen flow was examined. All the determinations were performed

in the high pressure apparatus since the flow-rate through the samples under vacuum conditions was much too high for a low pressure permeability method to be employed.

The results of these determinations (Nos. H:15 to H:19) are summarized in Table 4.1-1, while the K-p_m plots for the determinations are shown in Fig. 4.1-1.

The wet gas test meter was employed to measure high flow-rates, and the rotameter and soap-bubble flow-meter for low flow-rates. Above flow-rates of about 50 cm^3/sec, the revolving of the wet gas test meter caused fluctuations in the flow through the sample; restriction of the outflow from the permeability cell to counteract these flucuations meant that p_o did not remain approximately constant at 0 or 76 cm Hg but varied quite considerably (see Detmn.No.H:15). For freon flow (Detmn. No. H:17), some difficulty was encountered since the gas supply and the maximum gas pressure available from the cans of freon were limited.

The K-p_m plots for all the P.G. 60 determinations (Fig.4.1-1) were curved above about p_m = 15 cm Hg. The plot for freon flow through Rod No. K31 (Detmn. No. H:17) was the most curved, while that for hydrogen flow (Detmn. No. H:16) was only slightly

curved. Because p_o varied considerably for any determination, the plots were less curved than if p_o was kept constant at 0 and 76 cm Hg (the dashed line in Fig. 4.1-1 for nitrogen flow in Rod No. K31 represents the plot for $p_o = 96 \pm 1$ cm Hg).

The scatter of the K-p_m values about the plots was generally less than $\pm$ 5 cm^2/sec (less than $\pm$ 1% above p_m = 76 cm Hg). For the experiments at the lowest mean pressures when p_o was about zero, the flow-rate was corrected for the leakage (0.01 cm^3/sec) into the vacuum system (section 3.1.4.5). Any error in this correction resulted in inaccurate K values at low p_m.

For the high pressure flow determinations on the P.G. 60 graphite samples, the K-p_m plots obtained when p_o was about 80 cm Hg were higher than those when p_o was near zero. Similar variations of K with p_o at any p_m were observed for the high pressure flow determinations on Acheson "A" samples (see section 4.1.2.2). For Rod No. K31, the variation in K at p_m = 80 cm Hg was lower for hydrogen flow than for nitrogen or argon flow (4% cf. 25% and 20%), but was much larger for freon flow (100%) as shown in Fig. 4.1-1. The corresponding variation for nitrogen flow through Rod No. K32 was 18%.

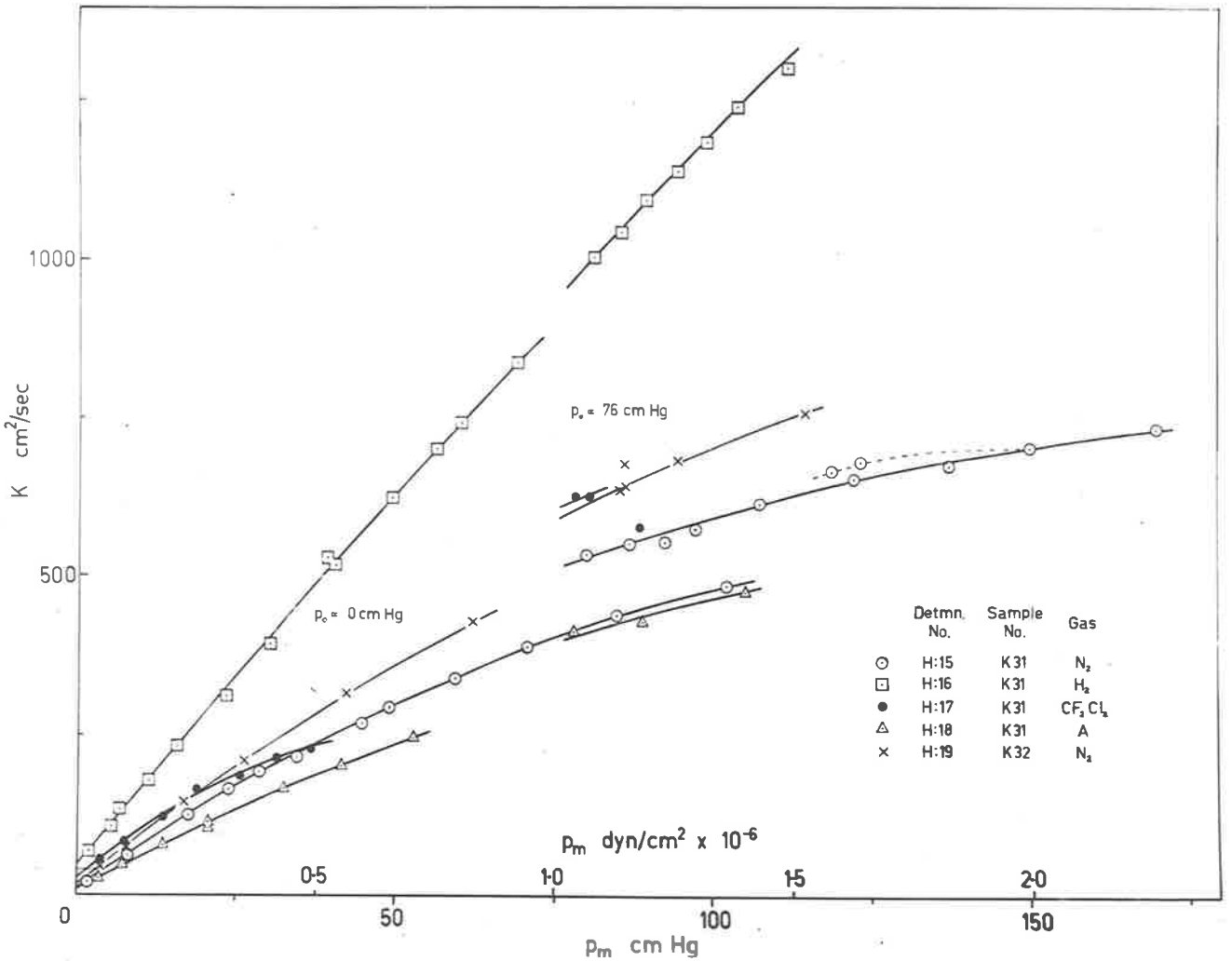

Fig. 4.1-1 K-p_m Plots for Flow of Different Gases through P.G. 60 Graphite at High Pressures.

Table 4.1-1

Permeability Results for P.G. 60 Graphite Samples

Detmn. No.	Gas	$\mathcal{T}_s$ (av) °C	Range of p_m cm Hg	Slope b cm²/sec, cm Hg	B_o cm² x 10^8	Intercept a cm²/sec	K_o cm x 10^4
Sample No. K31, L/A = 5.67 cm^{-1}							
H:16	H_2	16.4	1.7 – 111.5	11.7	7.7	48	2.07
H:15	N_2	16.6	1.7 – 170.2	6.6	8.7	8.4	1.35
H:18	A	16.4	3.4 – 105.4	5.2	8.7	7.1	4.30
H:17	CF_2Cl_2	17.6	3.5 – 88.6	7.1	6.6	29	9.64
Sample No. K32, L/A = 6.58 cm^{-1}							
H:19	N_2	16.6	3.8 – 114.7	7.9	10.3	12	1.92

For flow through Rod No. K31, the K-p_m plots for hydrogen flow (Detmn. No. H:16) were higher than those for all the other gases investigated (see Fig. 4.1-1). While the argon plots (Detmn.No. H:18) were lower than those for nitrogen flow (No. H:15), the plots for freon flow (Detmn. No. H:17) were higher.

The values of the slope and intercept of the straight portion of the K-p_m plots below about p_m = 15 cm Hg were determined by the method of least squares; the values of B_o and K_o calculated respectively from the slope and intercept values are recorded in Table 4.1-1. Because of the small number of points below p_m = 15 cm Hg for each determination, the curvature of the plots, and the inaccurate correction of the K values, these values of B_o and K_o were not very accurate, the errors observed in any value being about 4% and 10%, respectively.

For Rod No. K31, the average value of B_o was 7.9×10^{-8} cm^2 with a standard deviation of $\pm 0.5 \times 10^{-8}$ cm^2 (maximum variation = 2.1×10^{-8} cm^2). For nitrogen and argon flow, B_o was 8.7×10^{-8} cm^2, but was lower for hydrogen and freon flow. Greater variation (8.3×10^{-4} cm) was observed between the values of K_o for Rod No. K31; the average value was $(4.34 \pm 1.64) \times 10^{-4}$ cm. The K_o value for argon

agreed with the average value, the nitrogen and hydrogen values were lower, while the freon value was much higher (9.64×10^{-4} cm).

The K-p_m plot for nitrogen flow through Rod No. K32 (axis perpendicular to the extrusion axis) was about 20% higher than the plot for nitrogen flow through Rod No. K31 (axis parallel to the extrusion axis) (cf, Detmn. No. H:15 with Detmn. No. H:19). The values of B_o and K_o were also higher than the respective values for nitrogen flow in Rod No. K31. Greater flow in the direction perpendicular to the extrusion axis of the graphite than in the parallel direction was also observed for Acheson "A" samples (section 4.1.2.1).

4.1.2 Acheson "A" Graphite

For Acheson "A" graphite samples, permeability coefficients were determined by all methods, viz., the pressure increase, the pressure decay, the pressure equalization, and the low pressure flow methods in the low pressure apparatus, and the high pressure flow method in the high pressure apparatus. All of the gases mentioned in section 3.1.1.2 with the exception of helium were investigated by the decay method; nitrogen was employed for the determinations by the other methods with xenon and hydrogen also being examined by the pressure increase and high pressure flow methods, respectively. The decay method was the

most suitable of the low pressure methods for determinations below one atmosphere, while satisfactory results were obtained by the flow method at higher pressures.

The results of the determinations are summarized in Table 4.1-2, while the K-p_m plots for the determinations are shown in Figs. 4.1-2 to 4.1-5.

4.1.2.1 The Low Pressure Determinations

By means of the pressure increase method, satisfactory values of K were determined for nitrogen flow in Rod No. K3 (Detmns. No. L:18 and No. L:21) when p_m was less than about 4 cm Hg (see Fig. 4.1-2) even though dp_o/dt was greater than the suggested maximum rate, viz., 15×10^{-4} mm Hg/sec. Although the p_o-t plots were slightly curved, thus resulting in some inaccuracy in calculating K, the experimental scatter about the K-p_m plot was very small ($\pm$ 0.005 cm^2/sec). Above p_m = 4 cm Hg, the modified pressure increase method (see section 3.1.3.1) was employed (Detmn. No. L:18) and reasonable values of K were obtained.

In Detmn. No. L:52, permeability determinations were made at extremely low pressures by the pressure increase method in order to observe whether a minimum was obtained in the K-p_m plot for xenon flow through

Acheson "A" graphite; xenon was chosen for these experiments because of its high molecular weight and hence small flow-rate through the graphite, permitting accurate measurement of dp_o/dt. Above p_m = 0.023 cm Hg, there was no indication of the values of K increasing at the lowest mean pressures.

In the pressure increase determinations No. L:21 and No. L:52, small time-lags were observed ranging from a few seconds up to 0.33 and 2.14 min, respectively. Generally, they were too small to measure accurately.

Detmns. No. L:17 and No. L:21B showed that the pressure equalization method was not very accurate as the values of K were scattered about the mean K-p_m plot by $\pm$ 0.1 cm^2/sec or $\pm$ 10% (see Fig. 4.1-2). This scatter was due to the difficulty in determining the slope $d(\Delta p)/dt$ of the Δp-t plot accurately (section 3.1.3.3). Because of this inaccuracy, and the small range of p_m covered in any experiment when V_i and V_o were of the same order of magnitude, no further determinations were performed using this method after the initial trial experiments.

The values of K determined in the low pressure flow determination (No. L:34) agreed within experimental error with those calculated from decay measurements on the same sample (Rod No. K2A).

Except at the highest flow-rates when dp_i/dt was greater than 20 cm Hg/hr, and at the lowest flow-rates (dp_i/dt less than 0.2 cm Hg/hr), good $K-p_m$ plots were obtained by the pressure decay method, the values of K being scattered about the plots by less than $\pm$ 0.05 cm^2/sec ($\pm$ 5% at p_m = 10 cm Hg for nitrogen flow). The relative experimental error was estimated as 4½% (see Appendix C.3.3); generally the standard deviations in any values of the slope and intercept were about 5% and 1%, respectively.

The reproducibility between the $K-p_m$ plots resulting from different determinations for the same gas and the same sample was generally quite good (see Fig. 4.1-2). For repeat pressure decay determinations on Rod No. K2 (Detmns. No. L:7 to No. L:10), the differences between the values of the slope and intercept were 1% and 5%, respectively. Excluding the pressure equalization determinations, the total variation in K between determinations for Rod No. K3 was 0.03 cm^2/sec (5% at p_m = 5 cm Hg). Although less accurate, the values of K determined by the high pressure flow method for p_m below 30 cm Hg agreed closely with the low pressure results (see Figs. 4.1-3 and 4.1-4).

A comparison of the pressure decay determinations

performed on Acheson "A" Rod No. K2A for the flow of different gases is presented graphically in Fig. 4.1-4. With the exception of hydrogen (Detmn. No. L:50), the K-p_m plots below p_m = 30 cm Hg for all the other gases (nitrogen, argon, carbon dioxide, freon-12, and xenon) were grouped together; at p_m = 15 cm Hg, the variation in K for these gases was 0.64 cm^2/sec or about 50% whereas K for hydrogen flow (3.3 cm^2/sec) was three times larger. Table 4.1-2 gives the respective values for B_o and K_o for each gas in this series of determinations. The values were calculated at the appropriate sample temperature T_s as shown in Appendix C.3.2.

Excluding the value of B_o for hydrogen (11.65×10^{-10} cm^2), the values for gas flow through Rod No. K2A agreed quite closely and averaged 8.64×10^{-10} cm^2 (standard deviation $\pm$ 0.11×10^{-10} cm^2). With K_o, the values for carbon dioxide (4.62×10^{-6} cm) and freon (5.31×10^{-6} cm) were higher than the average value of (4.06 ± 0.14) $\times 10^{-6}$ cm for the flow of the other four gases. The average for the six determinations was (4.36 ± 0.23) $\times 10^{-6}$ cm.

At any p_m, the total variation of K values determined for nitrogen flow through different samples of Acheson "A" graphite cut parallel to the extrusion

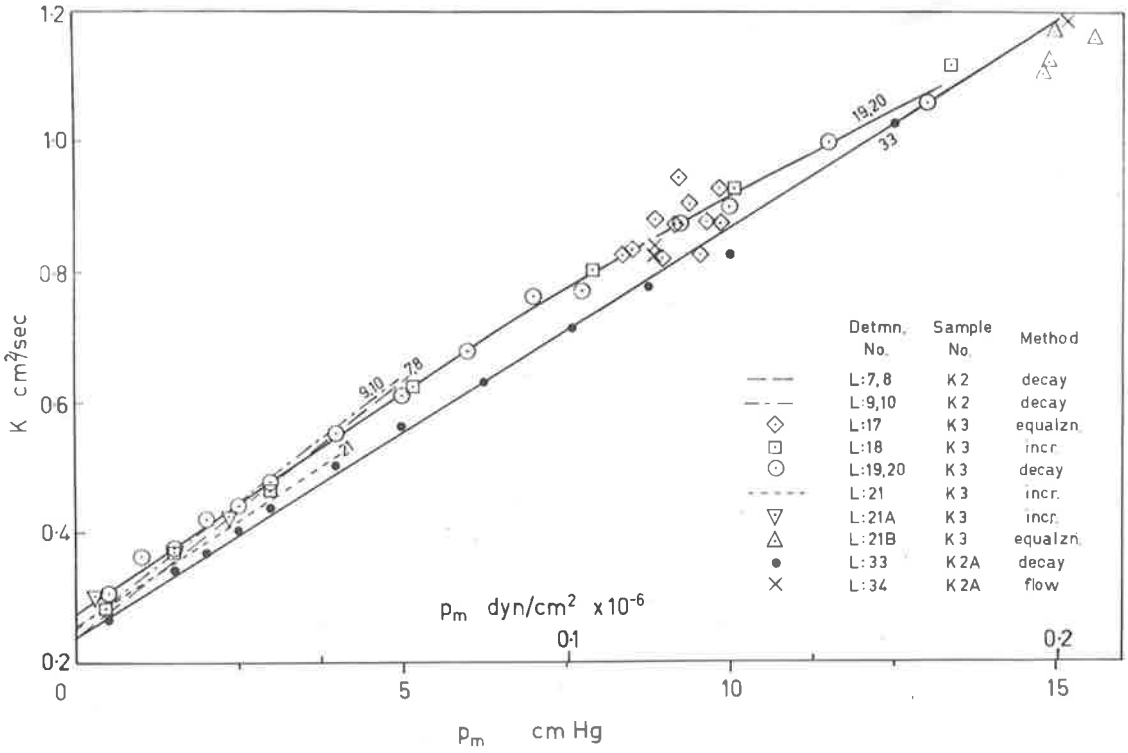

Fig. 4.1-2 K-p_m Plots for Nitrogen Flow in Acheson "A" Graphite Samples for Different Measuring Methods.

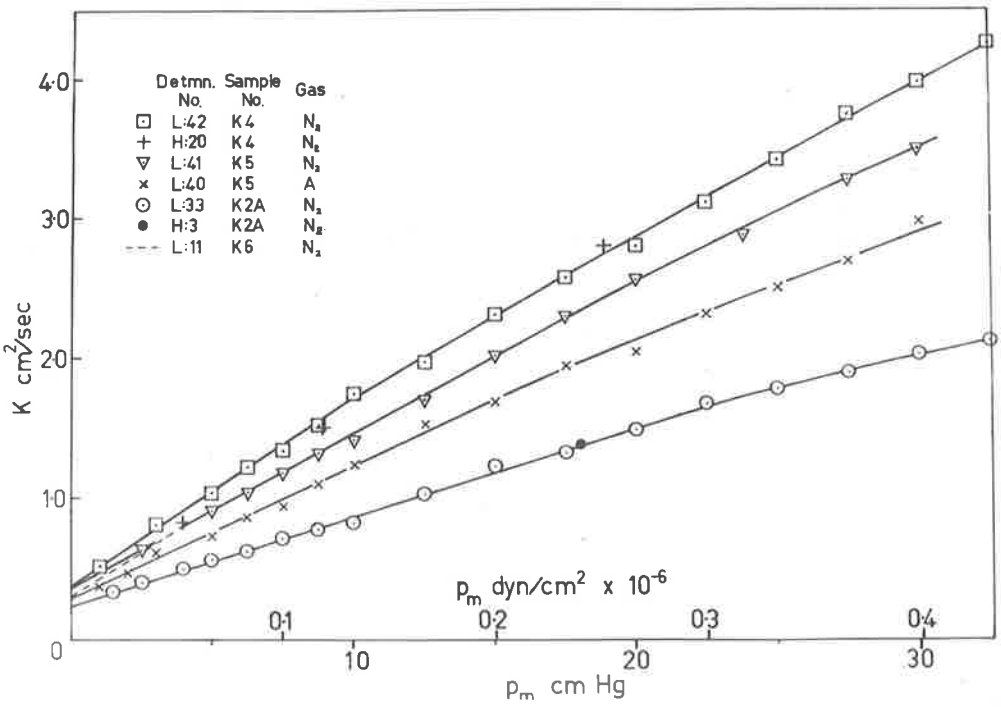

Fig. 4.1-3 K-p_m Plots for Nitrogen and Argon Flow through Acheson "A" Graphite Samples with Axes Perpendicular to the Extrusion Direction.

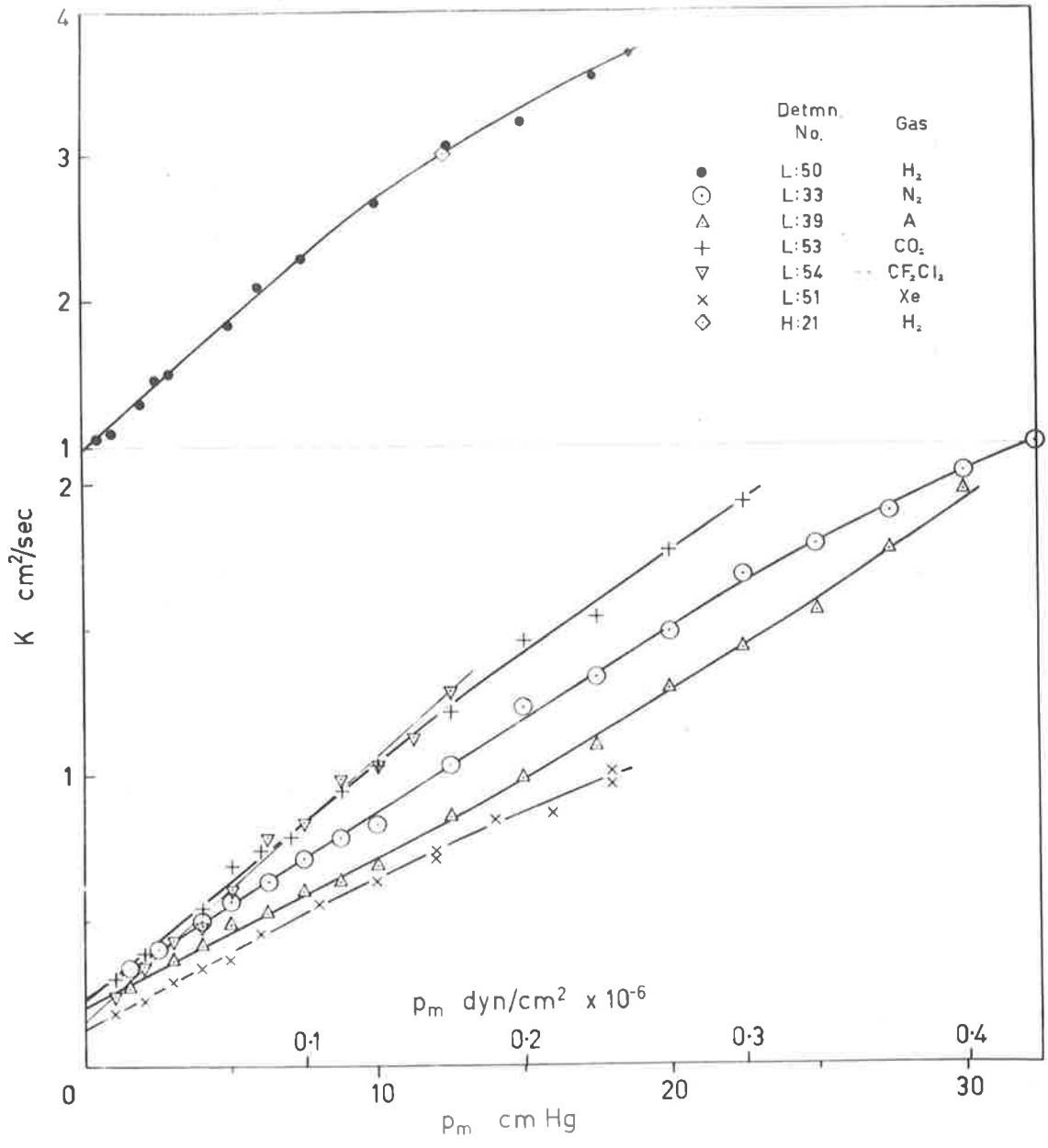

Fig. 4.1-4 K-p_m Plots for Flow of Different Gases through Acheson "A" Graphite Rod No. K2A (Determined by the Pressure Decay Method).

Table 4.1-2

Permeability Results for Acheson "A" Graphite Samples

Detmn. No.	Method	Gas	$\mathcal{T}_s$ (av) °C	Range of p_m cm Hg	Slope b cm²/sec cm Hg	B_o cm² x 10^{10}	Intercept a cm²/sec	K_o cm x 10^6	Comments
	Sample No. K2, L/A = 5.95 cm^{-1}								
L:7	L.p.decay)	N_2	19.6	0.05 - 5.5	0.0784	10.31	0.241	3.84	
L:8	L.p.decay)								
L:9	L.p.decay)	N_2	20.7	0.10 - 5.0	0.0776	10.24	0.253	4.03	
L:10	L.p.decay)								
	Sample No. K2A, L/A = 5.46 cm^{-1}								K-p_m plots began curving
L:33	L.p.decay	N_2	27.1	0.25 - 35.0	0.0631	8.48	0.240	3.77	down at: p_m = 22 cm Hg
L:34	L.p.flow	N_2	25.0	8.8 & 15.1	–	–	–	–	2 values
H:3	H.p.flow	N_2	16.1	18 - 476	(0.058)	(7.20)	(0.36)	(5.77)	
L:50	L.p.decay	H_2	18.8	0.20 - 18.8	0.1760	11.65	0.982	4.21	p_m = 8 cm Hg
H:21	H.p.flow	H_2	16.0	12.3 - 232	(0.125)	(8.30)	(1.44)	(6.16)	
L:39	L.p.decay	A	26.3	0.25 - 30.0	0.0509	8.69	0.206	3.87	Curved up, p_m = 15 cm Hg
L:53	L.p.decay	CO_2	16.6	1.00 - 22.5	0.0810	8.82	0.230	4.62	p_m = 12 cm Hg
L:54	L.p.decay	CF_2Cl_2	16.5	0.50 - 12.5	0.0901	8.32	0.159	5.31	No curvature
L:51	L.p.decay	Xe	18.6	1.00 - 18.0	0.0528	8.89	0.127	4.38	p_m = 8 cm Hg
L:52	L.p.increase	Xe	16.9	0.02 - 2.17	–	–	–	–	No minimum
	Sample No. K3, L/A = 4.16 cm^{-1}								
L:18	L.p.increase	N_2	26.3	0.44 - 13.3	0.0650	8.72	0.271	4.27	p_m = 8 cm Hg
L:21	L.p.increase	N_2	15.8	0.15 - 16.3	0.0657	8.56	0.254	4.08	
L:21A	L.p.increase	N_2	35.5	0.50 & 2.35	–	–	–	–	2 values
L:19	L.p.decay)	N_2	23.9	0.25 - 13.0	0.0676	9.01	0.276	4.38	p_m = 7 cm Hg
L:20	L.p.decay)								
L:17	L.p.equalzn.	N_2	24.7	8.4 - 9.8	–	–	–	–	2 experiments
L:21B	L.p.equalzn.	N_2	15.6	14.75 - 15.53	–	–	–	–	1 experiment
	Sample No. K4, L/A = 5.22 cm^{-1}								
L:42	L.p.decay	N_2	24.0	0.50 - 32.5	0.1337	17.8	0.375	5.94	p_m = 10 cm Hg
H:20	H.p.flow	N_2	16.8	4.0 - 276	(0.130)	(17.0)	(0.37)	(5.87)	
	Sample No. K5, L/A = 5.20 cm^{-1}								
L:41	L.p.decay	N_2	24.8	0.50 - 30.0	0.1095	14.6	0.364	5.75	p_m = 20 cm Hg
L:40	L.p.decay	A	24.4	0.50 - 32.5	0.0952	15.8	0.281	5.30	p_m = 17 cm Hg
	Sample No. K6, L/A = 0.026 cm^{-1}								
L:11	L.p.decay	N_2	25.2	0.50 - 3.7	0.1239	16.6	0.314	4.96	Inaccurate

axis, viz., Rods K2, K2A, and K3, was 0.07 cm^2/sec, which was less than the maximum scatter observed for individual K values about any K-p_m plot ($\pm$ 0.05 cm^2/sec). For Rod No. K2, the B_o value of (10.27 $\pm$ 0.04) x 10^{-10} cm^2 was about 20% higher, while the value of K_o ((3.93 $\pm$ 0.10) x 10^{-6} cm) was slightly lower than the corresponding average values for Rod No. K2A (see Table 4.1-2). For Rod No. K3, the B_o and K_o values were (8.76 $\pm$ 0.13) x 10^{-10} cm^2 and (4.24 $\pm$ 0.09) x 10^{-6} cm, respectively; these values agreed quite closely with the average values for Rod No. K2A.

Permeability values for the flow of nitrogen and argon perpendicular to the extrusion axis of the graphite (Rods K4 and K5) were over 1½ times greater than those for flow parallel to the direction of extrusion (Rods K2, K2A, and K3) (cf. Detmns. No. L:41 and No. L:42 with Detmn. No. L:33 for nitrogen flow and Detmn. No. L:40 with Detmn. No. L:39 for argon flow - Fig. 4.1-3). For the two samples, Rods K4 and K5, whose axes were at right angles to the extrusion axis of the graphite in perpendicular directions, the values of the slopes of the K-p_m plots for nitrogen flow were different by 15% although the intercepts were almost identical.

For the hollow cylindrical sample, Cylinder No. K6, in which flow occurred radially and perpendicular to the extrusion axis, the permeability values (Detmn.No.L:11)

agreed with those obtained in Detmn. No. L:41 for Rod No. K5 even though the rate of pressure decay was too fast for steady state conditions to be assumed and the K values were scattered below p_m = 2 cm Hg.

The values of B_o and K_o for nitrogen and argon flow in Rod No. K5 each varied by about 8%, the average values being $(15.2 \pm 0.6) \times 10^{-10}$ cm^2 and $(5.52 \pm 0.22) \times 10^{-6}$ cm, respectively (see Table 4.1-2). These average values were 15% and 7% lower than the corresponding values for Rod No. K4, but were respectively 75% and 35% greater than the average values for the samples whose axes were parallel to the extrusion direction.

The K-p_m plots were linear at the lowest mean pressures, but generally curved slightly towards the p_m-axis above about p_m = 8 cm Hg (see Figs.4.1-3 and 4.1-4). The mean pressure at which a plot commenced to curve was not definite because of the scatter of the K-p_m points about the plot; the approximate values of p_m are noted in Table 4.1-2. No particular pattern was observed in these values of p_m as K-p_m plots for nitrogen determinations curved at about 8 cm Hg (Detmn. No. L:18) and 22 cm Hg (No. L:33). For Detmn. No. L:39 (argon flow through Rod No. K2A), the K-p_m plot tended to curve upwards; this anomaly was

possibly due to a faulty experimental or analytical technique as the plots for no other determinations were observed to curve upwards.

4.1.2.2 The High Pressure Determinations

Three satisfactory high pressure determinations were performed on Acheson "A" graphite rods after two initial determinations (No. H:1 and No. H:2) on hollow cylindrical samples proved unreliable. In Detmn. No. H:1, only rough values of K were calculated, while, for Detmn. No. H:2, the values of K were of questionable accuracy as a leak might have occurred through the seals of the sample holder (type (e)).

For the high pressure permeability determinations for nitrogen and hydrogen flow through Rod No. K2A (Detmns. No. H:3 and No. H:21, respectively) and for nitrogen flow through Rod No. K4 (Detmn. No. H:20), the calculated values of K when p_m was less than 30 cm Hg agreed closely with the respective K-p_m plots obtained from the pressure decay measurements (see Figs.4.1-3 and 4.1-4). The values of the slope and the intercept of the line drawn through the low pressure points for a high pressure determination were generally lower and higher, respectively, than those reported in Table 4.1-2 for determinations by the low pressure methods.

Above about 30 cm Hg, the K-p_m plots definitely

curved towards the p_m-axis (cf. the low pressure determinations). The actual pressure at which this curvature commenced was difficult to judge because the change in the slope of the plot from linear to curved was very gradual.

Besides the curvature of the K-p_m plots, the results of the high pressure permeability determinations on Acheson "A" graphite showed that a separate plot could be drawn for each set value of the outlet pressure p_o. At any p_m, the value of K increased with increasing p_o. In Detmn. No. H:3, over 150 experiments for the flow of nitrogen through Rod No. K2A were performed for five set values of p_o (0, 37, 78, 109, and 128 cm Hg) and various p_i between 36 cm Hg and 11 atm in order to investigate this variation fully. The K-p_m graph for this determination is shown in Fig. 4.1-5. For a plot at any set value of p_o, the observed scatter of the K values was less than $\pm$ 0.3 cm^2/sec, or $\pm$ 3% at p_m = 250 cm Hg. While the estimated relative error between values of K from different experiments was 4% (see Appendix C.5.3), the observed total variation in K at any p_m was from 1.0 to 1.2 cm^2/sec (10% at p_m = 250 cm Hg). Thus a definite phenomenon occurred for flow through Acheson "A" graphite at mean pressures above 100 cm Hg. When the K-p_m graph was replotted with Δp as the parameter, the

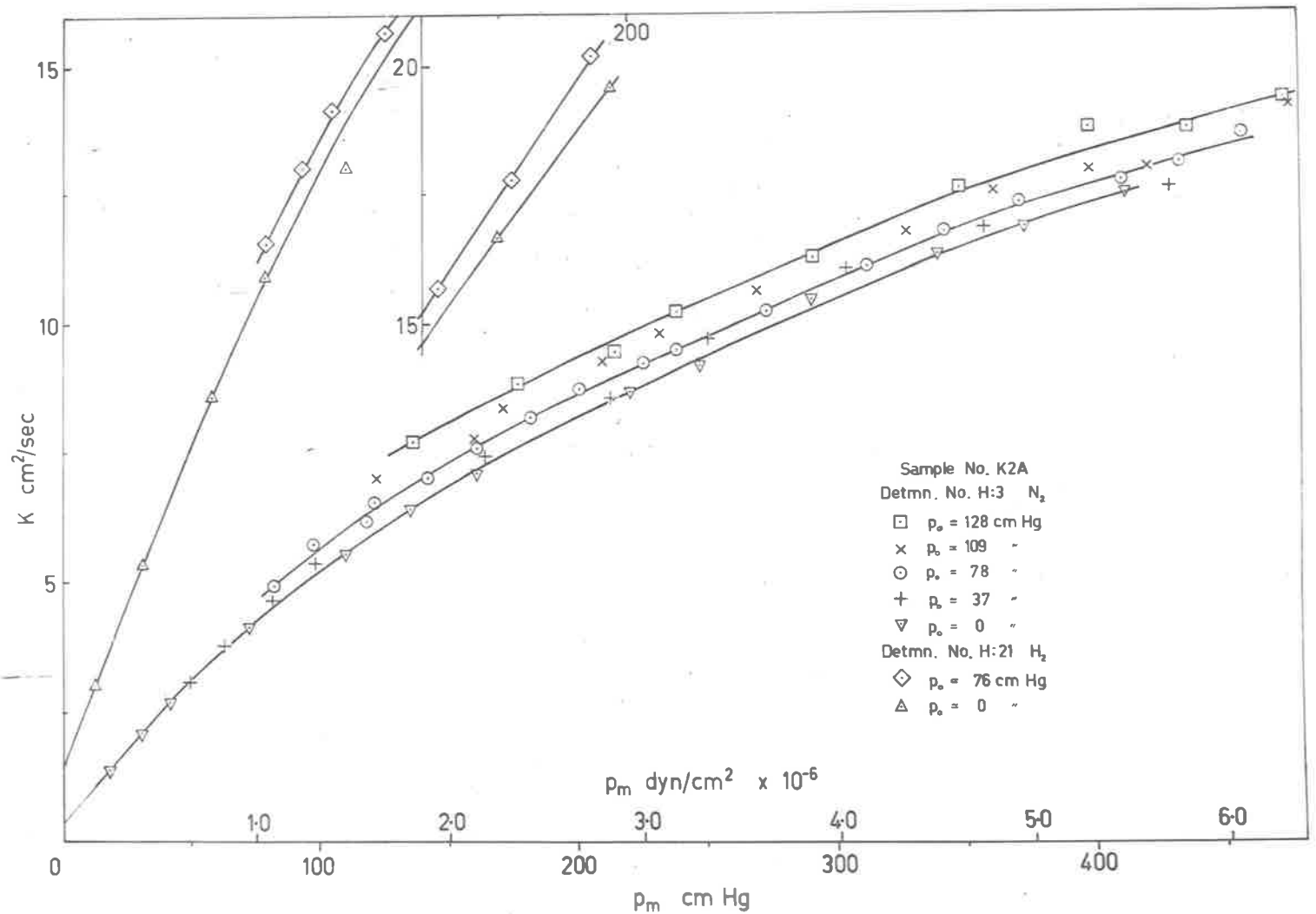

Fig. 4.1-5 K-p_m Plots for Nitrogen and Hydrogen Flow through Acheson "A" Graphite Rod No. K2A at High Pressures.

values of K and the slope of the plots both decreased at any p_m as Δp increased.

For hydrogen flow through Rod No. K2A (Detmn. No. H:21), separate K-p_m plots were observed (Fig. 4.1-5) for p_o at about 0 and 76 cm Hg. The variation in K was 0.6 cm^2/sec (3½% at p_m = 150 cm Hg) compared with the corresponding variation of 0.4 cm^2/sec (6%) for nitrogen flow (Detmn. No. H:3). Similar plots were obtained for nitrogen flow through Rod No. K4 (Detmn. No. H:20); the difference between the p_o = 0 and p_o = 76 cm Hg plots was 1.4 cm^2/sec or 9.3% at p_m = 150 cm Hg (see Fig. C.5-1, Appendix C.5.2). The observed scatter of the results for Detmn. No. H:2 showed the same type of variation as observed in the later determinations although it was not obvious at the time of measurement.

4.1.3 Morgan "EY9" Graphite

All of the methods of determining permeability coefficients except the low pressure equalization method were employed for investigating gas flow through Morgan "EY9" graphite samples. For Rod No. K21, the range of seven gases mentioned in section 3.1.1.2 were studied, but for the other samples, only the flow of nitrogen and argon (for one determination) was investigated. Generally, the pressure increase method proved

the most suitable for determining permeability coefficients in the low pressure apparatus, while the flow method gave satisfactory results at high pressures.

The results of the determinations are summarized in Table 4.1-3, while the $K-p_m$ and $\phi-p_m$ plots are shown in Figs. 4.1-6 to 4.1-10.

4.1.3.1 The Low Pressure Determinations

Two determinations were performed on Rod No. K21 by the pressure decay method for nitrogen (Detmn.No. L:14) and hydrogen flow (Detmn. No. L:48), and on both occasions the $K-p_m$ plots were about 5% lower than the corresponding plots obtained by the pressure increase method (see Figs. 4.1-6 and 4.1-7). The scatter of the values of K about the plots ($\pm$ 3%) was greater than for the pressure increase determinations (generally less than $\pm$ 1%). For nitrogen flow through Cylinder No. K25, three pressure decay determinations were made; Detmn. No. L:26 was a repeat of Detmn. No. L:25 and gave very good reproducibility of the results, while Detmn. No. L:27, which was conducted with a much larger inlet volume, gave values of K 9% higher than those for the previous determinations possibly because of the slower gas flow-rate (see Fig. 4.1-8).

Although the decay of the pressure was followed down to less than 0.5 cm Hg in several determinations,

and values of K were calculated for p_m down to 0.2 cm Hg, no sign of a minimum in the K-p_m plot was evident; below p_m = 2 to 4 cm Hg, the values of K were extremely scattered about the plot ($\pm$ 10 to 12%) and tended to be low.

For Rod No. K23, two low pressure nitrogen flow experiments were conducted (Detmn. No. L:36). The values of K were about 2% higher than the K-p_m plot obtained in Detmn. No. L:35 for the same sample by the pressure increase method.

Satisfactory values of K and good K-p_m plots were obtained for the permeability determinations on Morgan "EY9" graphite samples by the pressure increase method, the scatter of the points about the plots being generally between $\pm$ 0.5 to 1%. In several determinations curved p_o-t graphs were obtained, but values of K were calculated as mentioned in Appendix C.2.2. Greater scatter of the values of K was occasionally noticed at low p_m (less than 2 cm Hg) because of inaccuracies resulting from the curvature of the p_o-t plots and an inaccurate portion of the McLeod gauge scale.

Detmns. No. L:13 and No. L:24 for nitrogen flow in Rod No. K21 showed very good reproducibility between different pressure increase determinations for the same gas and the same sample, since the difference between the K-p_m plots was about 0.0002 cm^2/sec (less than 1%) (see Fig. 4.1-7).

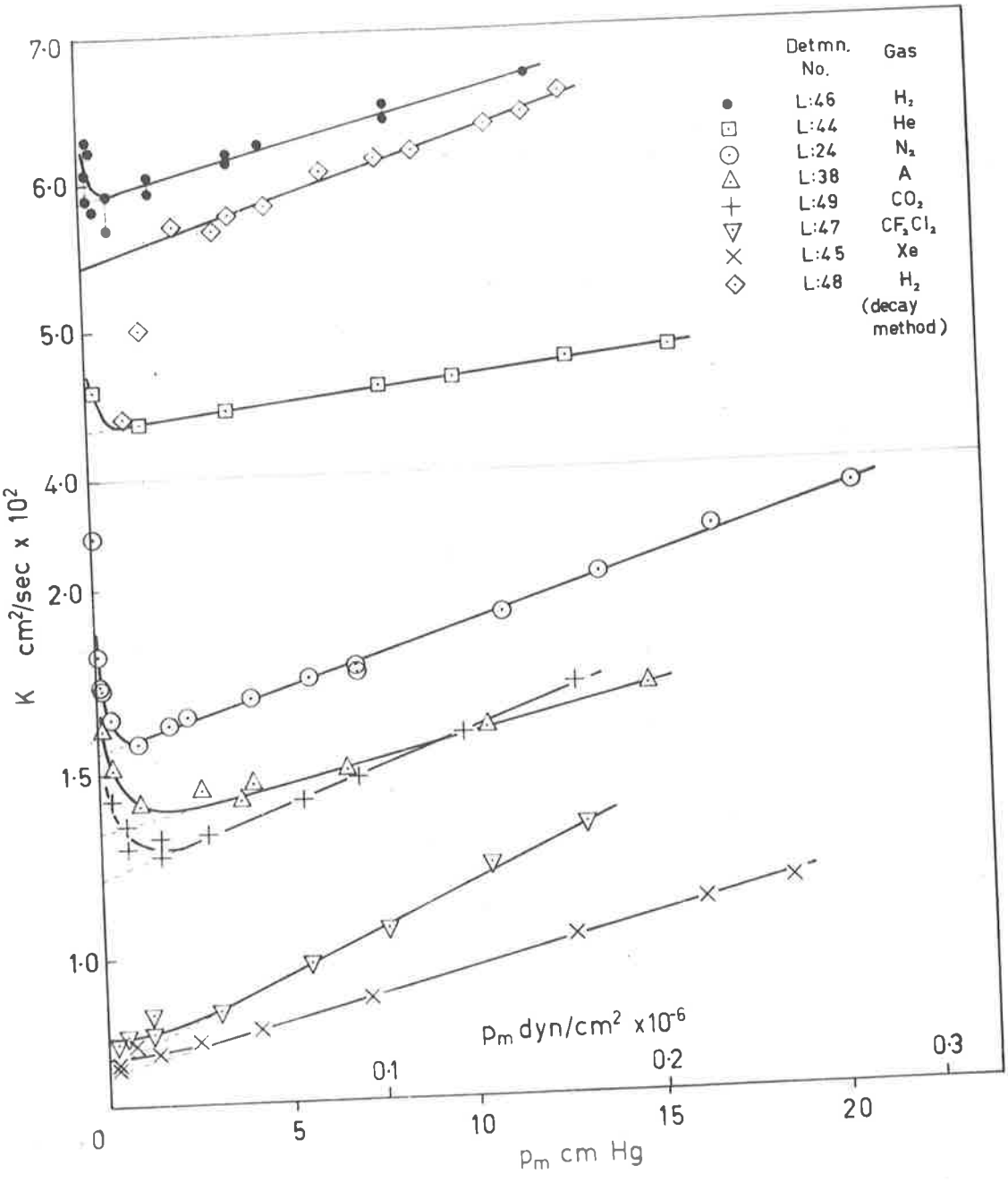

Fig. 4.1-6 K-p_m Plots for Flow of Different Gases through Morgan "EY9" Graphite Rod No. K21 (Determined by the Pressure Increase Method).

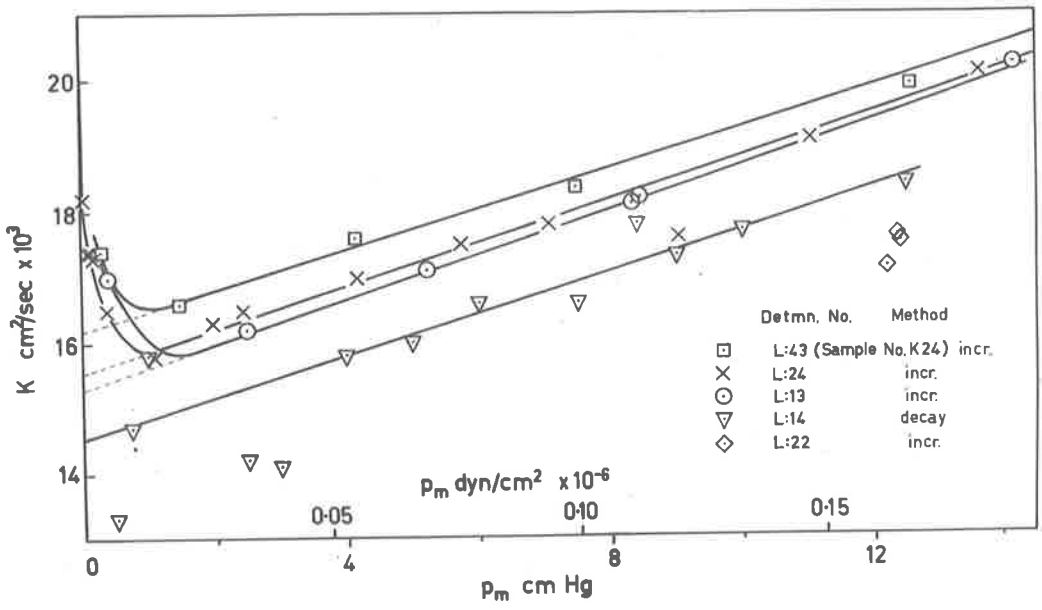

Fig. 4.1-7 K-p_m Plots for Nitrogen Flow through Morgan "EY9" Graphite Rod No. K21 for Different Measuring Methods.

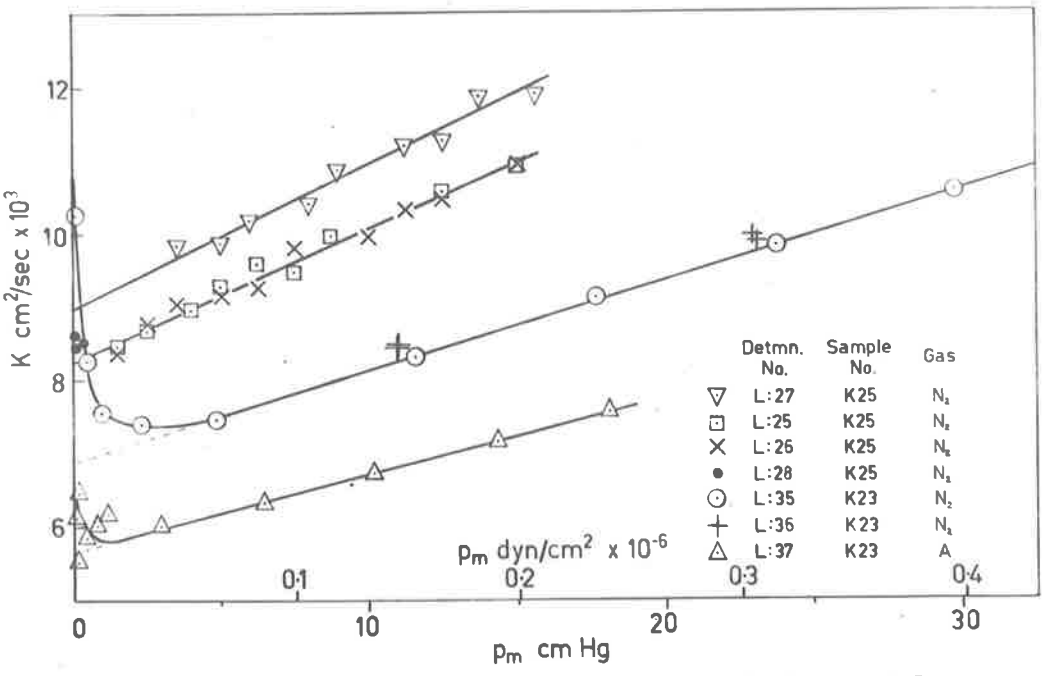

Fig. 4.1-8 K-p_m Plots for Nitrogen and Argon Flow through Morgan "EY9" Graphite Samples with Axes Perpendicular to the Extrusion Direction.

Table 4.1-3

Permeability Results for Morgan "EY9" Graphite Samples

Detmn. No.	Method	Gas	$\mathcal{T}_s$ (av) °C	Range of p cm Hg	Slope b cm²/sec, cm Hg x 10⁴	B_o cm² x 10¹²	Intercept a cm²/sec	K_o cm x 10⁷	Comments
	Sample No. K21, L/A = 6.18 cm⁻¹								
L:13	L.p.increase	N_2	18.5	0.43 – 14.2	3.41	4.48	0.0153	2.45	Minm. 1.4 cm Hg
L:22	L.p.increase	N_2	15.9	12.2 to 12.4	–	–	–	–	3 expts.
L:24	L.p.increase	N_2	16.4	0.18 – 31.2	3.36	4.38	0.0155	2.49	Minm. 1.0 cm Hg
L:24A	L.p.increase	N_2	27.2	0.03 – 0.14	–	–	–	–	
L:14	L.p.decay	N_2	20.4	0.50 – 12.5	3.16	4.17	0.0146	2.32	
L:46	L.p.increase	H_2	18.1	0.23 – 12.1	6.75	4.46	0.0587	2.52	Minm. 0.7 cm Hg
L:48	L.p.decay	H_2	18.7	1.00 – 13.0	8.38	5.55	0.0543	2.33	
L:44	L.p.increase	He	19.7	0.19 – 15.7	3.13	4.60	0.0432	2.60	Minm. 1.0 cm Hg
L:38	L.p.increase	A	26.9	0.17 – 14.8	2.46	4.21	0.0134	2.52	Minm. 2.0 cm Hg
L:49	L.p.increase	CO_2	18.2	0.30 – 12.9	3.86	4.23	0.0121	2.42	Minm. 2.0 cm Hg
L:47	L.p.increase	CF_2Cl_2	18.8	0.27 – 13.1	4.77	4.36	0.00706	2.34	Flattens
L:45	L.p.increase	Xe_2	17.6	0.27 – 18.6	2.58	4.32	0.00693	2.40	Flattens
	Sample No. K22, L/A = 4.27 cm⁻¹								
H:5A	H.p.flow	N_2	19.1	253 – 872	2.85	3.75	0.0155	2.47	Plot curves slightly
H:5B	H.p.flow	N_2	19.8	62 – 290					
H:5C	H.p.flow	N_2	28.3	811 – 1216					
	Sample No. K23, L/A = 4.94 cm⁻¹								
L:35	L.p.increase	N_2	26.1	0.15 – 38.2	1.22	1.63	0.00690	1.09	Minm. 2.5 cm Hg
L:36	L.p.flow	N_2	27.7	10.9 & 23.0	–	–	–	–	2 expts.
H:4A	H.p.flow	N_2	19.6	279 – 851	1.19	1.57	0.00600	0.956	Plot curves slightly
H:4B	H.p.flow	N_2	19.9	67 – 294					
H:4C	H.p.flow	N_2	25.9	384 – 1236	1.03	1.75	0.00568	1.07	Minm. 1.0 cm Hg
L:37	L.p.increase	A	25.0	0.07 – 18.1					
	Sample No. K24, L/A = 4.21 cm⁻¹ (Morgan "EY9166" graphite)								
L:43	L.p.increase	N_2	22.0	0.30 – 21.4	3.09	4.09	0.0162	2.57	Minm. 0.8 cm Hg
	Sample No. K25, L/A = 0.0234 cm⁻¹								
L:25	L.p.decay	N_2	26.4	1.50 – 15.0	1.83	2.45	0.00824	1.30	
L:26	L.p.decay	N_2	24.7	1.50 – 15.0	1.79	2.39	0.00825	1.30	
L;27	L.p.decay	N_2	24.3	3.50 – 15.6	1.94	2.59	0.00899	1.42	
L:28	L.p.increase	N_2	22.5	0.02 – 0.38	–	–	–	–	Slight minm.

However, for Detmn. No. L:22 the values of K were 10% lower than those for Detmn. No. L:24, possibly because a slightly different experimental technique was employed.

A comparison of the K-p_m plots determined by the pressure increase method for the flow of different gases in Morgan "EY9" Rod No. K21 is presented in Fig. 4.1-6. The flow of hydrogen gave the highest permeability and xenon flow the lowest. The values of B_o and K_o for the flow of each gas in this series of determinations are presented in Table 4.1-3.

For Rod No. K21, the values of B_o and K_o obtained in the pressure increase determinations agreed quite closely and averaged 4.38×10^{-12} cm^2 (standard deviation $\pm 0.05 \times 10^{-12}$ cm^2) and 2.47×10^{-7} cm (deviation $\pm 0.03 \times 10^{-7}$ cm), respectively. The decay determinations on Rod No. K21 noted previously gave values of B_o and K_o which differed from the average values.

The values of B_o and K_o obtained for Rod No. K24, which was a sample of the Morgan "EY9166" graphite cut parallel to the extrusion axis, were 6½% lower and 4% higher, respectively, than the average values for the Morgan "EY9" graphite Rod No. K21. This was quite good agreement between the two grades of Morgan graphite.

The permeability values for the flow of nitrogen and argon perpendicular to the extrusion axis of the

graphite (Rod No. K23 and Cylinder No. K25) were approximately a half of those for flow parallel to the extrusion axis (Rods K21, K22, and K24). For Rod No. K23, the average values of B_o and K_o from two low pressure determinations (Nos. L:35 and L:37) were $(1.69 \pm 0.06) \times 10^{-12}$ cm^2 and $(1.08 \pm 0.01) \times 10^{-7}$ cm, respectively. If the lower values obtained for this sample from the high pressure determination (No. H:4) were also included (section 4.1.3.2), the average values became $(1.65 \pm 0.05) \times 10^{-12}$ cm^2 and $(1.04 \pm 0.04) \times 10^{-7}$ cm, respectively. The values of B_o and K_o obtained for the hollow cylindrical sample (No. K25) for nitrogen flow by the pressure decay method (Detmns. L:25, L:26, and L:27) were about 50% and 30% higher than the values for Rod No. K23. The average values were respectively $(2.48 \pm 0.06) \times 10^{-12}$ cm^2 and $(1.34 \pm 0.04) \times 10^{-7}$ cm.

A minimum or a flattening was observed at low p_m (below 4 cm Hg) for each K-p_m plot obtained by the pressure increase method for the Morgan "EY9" graphite samples (see Figs. 4.1-6 to 4.1-8). For some determinations (Nos. L:24, L:35, and L:38), the minimum was well defined as the points obtained below the mean pressure of the minimum gave a smooth curve which approached the K-axis asymptotically; the value of K at the lowest p_m for these determinations was of the same order as that

calculated when p_m was 20 to 30 cm Hg. In other determinations (Nos. L:13, L:43, and L:44), only one low pressure K value was determined but it was adequate to show that the plot did curve upwards. Because of the difficulty in obtaining accurate values of dp_o/dt for the low pressure experiments (curved p_o-t plots), some variation of the K values was observed for Detmns. L:37, L:46, and L:49 but a minimum in the K-p_m plots was still indicated. For Detmns. No. L:45 and No. L:47 (xenon and freon flow in Rod No. K21), there was no definite evidence of a minimum; although the low pressure points showed some scatter, the K-p_m plots tended to flatten out. In Detmn. No. L:28 only a small range of p_m (0.02 to 0.38 cm Hg) was examined for Cylinder No. K25 but an upward curving of the K-p_m plot was noticed.

The mean pressure at which the minimum occurred in any K-p_m graph was fairly difficult to determine precisely because of the scatter of the points. The approximate values indicated by the graphs are noted in Table 4.1-3. As far as could be observed for Rod No. K21, the minima for hydrogen and helium flow occurred at the lowest p_m (0.7 to 1.0 cm Hg), while those for argon and carbon dioxide flow occurred at about p_m = 2 cm Hg; for freon and xenon flow, the

flattening of the curves commenced at about p_m = 3 cm Hg. The hydrogen graph was apparently the most curved at the minimum, while the freon and xenon graphs were the least curved.

Time-lags ϕ were observed in all experiments conducted on Morgan "EY9" graphite samples by the pressure increase method except those in Detmn. No. L:13, when the stopcock to isolate the sample from the inlet side volume had not been added to the apparatus. For Detmn. No. L:28 (nitrogen flow in Cylinder No. K25 at very low pressures), the time-lags observed were very small and were not considered further. The value of ϕ obtained for each experiment is listed in the detailed results in Appendix K.

Graphs of ϕ against p_m for each determination are shown in Fig. 4.1-9. For flow in Rod No. K21 (see Fig. 4.1-9(a)), the graphs for freon and xenon were the highest, and those for hydrogen and helium the lowest. The values of ϕ above about p_m = 4 cm Hg decreased only slightly as p_m increased and so were almost constant with p_m. However, at lower p_m, the graphs curved sharply upwards. The graphs for hydrogen and helium flow (Detmns. No. L:46 and No. L:44) commenced curving at about p_m = 2 cm Hg but apparently did not curve to the same extent as the graphs for the other determinations. For nitrogen, argon, and

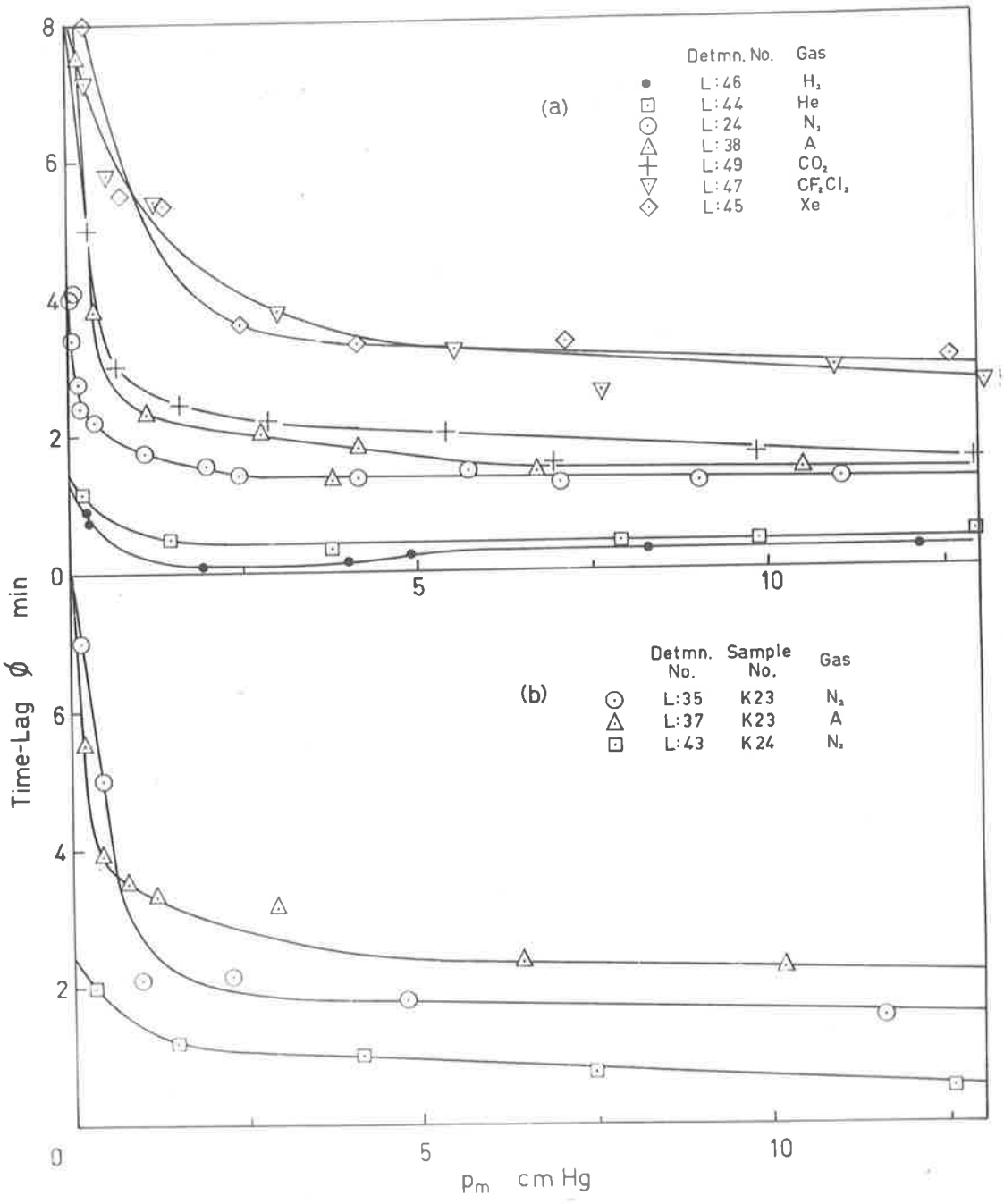

Fig. 4.1-9 ϕ-p_m Plots for Gas Flow through Morgan "EY9" Graphite.
(a) Sample No. K21.
(b) Samples No. K23 and No. K24.

carbon dioxide flow, the curvature of the graphs commenced in the vicinity of p_m = 3 cm Hg and was very sharp at about 0.5 cm Hg. The curvature was more gradual for freon and xenon flow (Detmns. No. L:47 and No. L:45) and started at about p_m = 4 cm Hg.

The value of ϕ for any experiment was obtained from the p_o-t plot as shown in Appendix C.2.1. Often it was difficult to get an accurate value from the plot when the pressure measurements at small times were inaccurate and the plot was slightly curved. For small time-lags of less than 2 min, the ϕ values were calculated more accurately by means of equation (C.2-4), Appendix C.2.1. The scatter of the ϕ values about the ϕ-p_m plots was due to the inaccuracy of determining the ϕ values. For hydrogen flow in Rod No. K21 (Detmn. No. L:46), the values of ϕ between p_m = 2 and 6 cm Hg were about 50% lower than those at higher pressures, possibly because of the inaccuracy of measuring small time-lag values (0.3 min above p_m = 6 cm Hg).

4.1.3.2 <u>The High Pressure Determinations</u>

Only two determinations (Nos. H:4 and H:5) were made on Morgan "EY9" graphite samples in the high pressure apparatus, but each determination was performed in three parts. In part A, the flow-rates

were measured by means of the soap-bubble flow-meter and the experiments were confined to the mean pressure range from 250 to 870 cm Hg (p_i from 100 to 300 p.s.i.g). With the construction and calibration of the capillary flow-meter for measuring flow-rates below 0.1 cm^3/sec (section 3.1.4.3), the determinations were continued (part B) at lower pressures (p_m = 60 to 290 cm Hg). The determinations were extended (part C) to higher pressures up to p_i = 450 p.s.i.g. (31.6 atm) or p_m = 1240 cm Hg in order to show whether the K-p_m plots were curved at higher pressures.

Permeability coefficients were determined for nitrogen flow through Rod No. K22 and Rod No. K23 (axes respectively parallel and perpendicular to the extrusion axis of the graphite). For Rod No.K22 (Detmn. No. H:5), the high pressure K-p_m plot extrapolated back to zero pressure was slightly lower than that obtained in the low pressure determination (No. L:24) on a similar sample (Rod No. K21). The value of B_o was 15% lower while the K_o value was the same as that for Rod No. K21. For nitrogen flow in Rod No. K23, the extrapolated high pressure K-p_m plot (Detmn. No. H:4) was lower (0.001 cm^2/sec) and the values of B_o and K_o were respectively 7% and 11% lower than those obtained in Detmn. No. L:35.

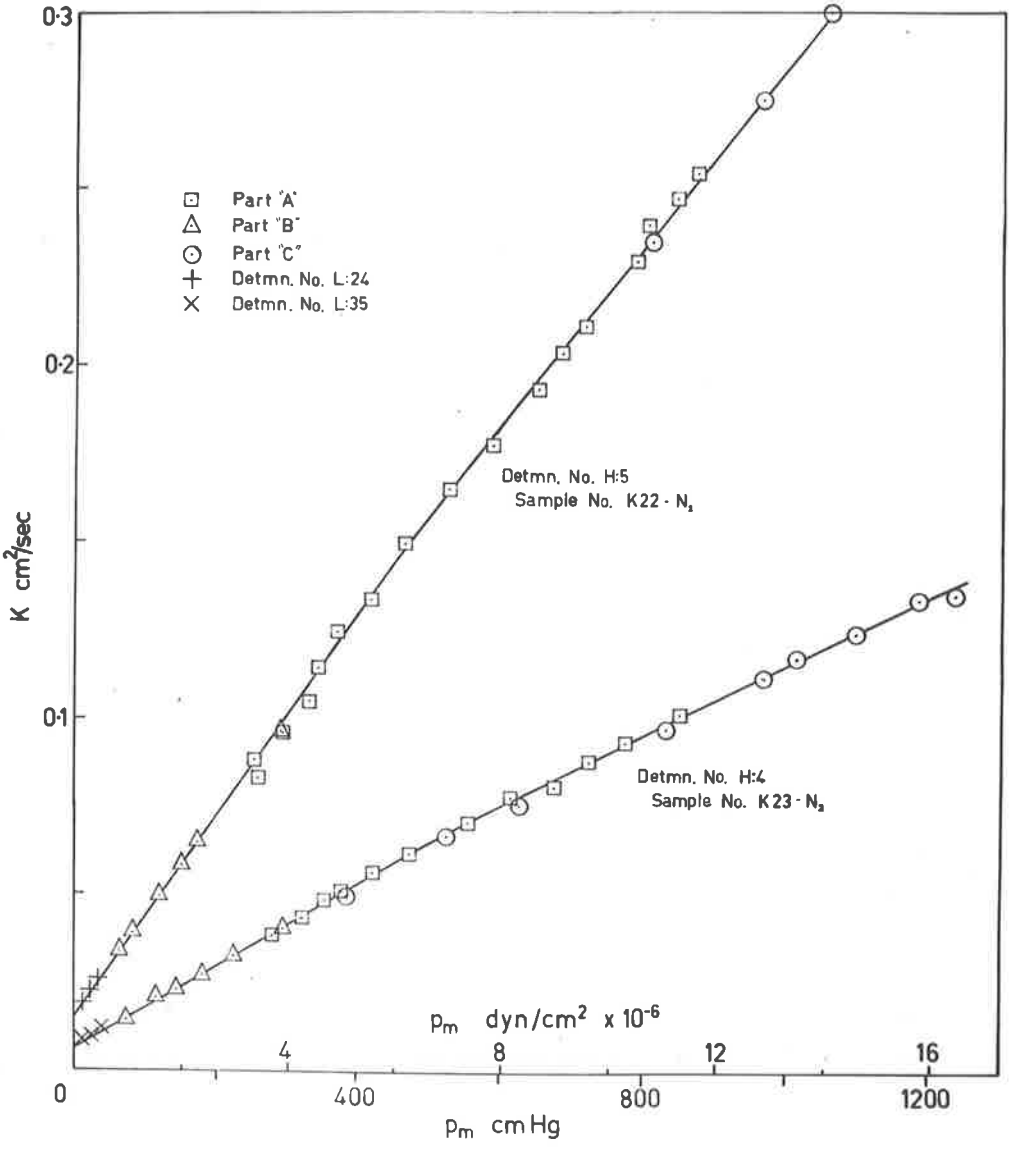

Fig. 4.1-10 K-p_m Plots for Nitrogen Flow through Morgan "EY9" Graphite Samples No. K22 and No. K23 at High Pressures.

The K-p_m plots for the two high pressure determinations are shown in Fig. 4.1-10. The plots were near enough to straight up to about p_m = 550 cm Hg but then commenced to curve slightly towards the p_m-axis; at p_m = 1000 cm Hg, the deviation from the straight line through the low pressure points was about 7%. The curvature was much less than that observed in the high pressure plots for Acheson "A" graphite (section 4.1.2.2).

The flow phenomenon observed for the Acheson "A" and P.G. 60 graphite high pressure determinations (sections 4.1.1 and 4.1.2.2), when a separate K-p_m plot could be drawn for each value of p_o, was not noticed at high pressures for either Morgan "EY9" rod. In both determinations, several experiments were performed with p_o either about zero or 150 cm Hg but the resulting values of K agreed within the experimental scatter ($\pm$ 2.5% at p_m = 600 cm Hg) with the values obtained when p_o was approximately atmospheric pressure. For the experiments with p_o near zero and p_m less than 250 cm Hg, the flow-rate values were corrected for the leakage rate of 0.003 cm^3/sec into the vacuum system.

4.1.4 Impregnated Graphite

Permeability coefficients were determined for two samples of Impregnated graphite. For Cylinder No. K41, the flow of a range of gases (nitrogen, hydrogen, argon, carbon dioxide, and freon) was investigated by the high pressure flow method, while for Cylinder No. K42, the high pressure flow method and all the low pressure methods except the pressure equalization method were employed to determine permeability coefficients for the flow of nitrogen, hydrogen, helium, argon, and xenon. The pressure increase method proved the most favourable of the low pressure methods. The samples were in the form of hollow cylinders since the ratio L/A for radial flow was smaller and the gas flow-rate at any mean pressure was larger than that for a rod; then more accurate measurement of the expected low flow-rate was possible.

The results of the determinations are summarized in Table 4.1-4, and are shown graphically in Figs. 4.1-11 to 4.1-16.

4.1.4.1 The Low Pressure Determinations

For Cylinder No. K41, a trial low pressure determination was made by the pressure decay method (Detmn. No. L:23); however, the values of K differed considerably from the corresponding high pressure

results for the same sample (Detmn. No. H:14) and a curved K-p_m plot was obtained. Further low pressure determinations by the pressure increase method were planned for Cylinder No. K41, but were not possible as the graphite sample was ruined during the high pressure measurements (Detmn. No. H:11A).

A pressure decay determination was performed on Cylinder No. K42 (Detmn. No. L:30); the values of K remained approximately constant at 1.13 x 10^{-4} cm^2/sec over most of the pressure range investigated (see Fig. 4.1-12) and were 10 to 25% lower than the corresponding K-p_m plot obtained for the sample by the pressure increase method (Detmn. No. L:29). Below about p_m = 5 cm Hg, the values of K were quite scattered but increased slightly at low p_m and possibly indicated a minimum in the K-p_m plot.

For six pressure increase determinations on Cylinder No. K42, good K-p_m plots were obtained with the scatter about the plots generally being about $\pm$ 2 to 3% although for several determinations it was less than $\pm$ 1%. In some determinations, a large scatter was observed at pressures below p_m = 1.5 cm Hg, because of the curvature of the p_o-t plots.

The length of the pressure increase experiments was influenced by the time required to reach

equilibrium flow, about 2 hr being necessary for nitrogen flow experiments (Detmn. No. L:29) where the time to reach equilibrium was up to 50 min. For xenon flow, where from 5 to 10 hr were required to reach equilibrium conditions, experiments were continued until an apparently straight p_o-t plot was obtained or p_o was beyond the range of the McLeod gauge; the calculated values of K could have been low if equilibrium had not been reached completely.

In Fig. 4.1-11, the K-p_m plots for the flow of different gases in Cylinder No. K42 are compared. Hydrogen flow gave the highest permeability and xenon the lowest. The values of B_o and K_o calculated for the flow of each gas are tabulated in Table 4.1-4. For B_o, the low pressure values varied between 1.0 and 1.8 x 10^{-14} cm^2, the average value being 1.36 x 10^{-14} cm^2 (standard deviation $\pm$ 0.15 x 10^{-14} cm^2); the four low values gave an average of (1.12 $\pm$ 0.08) x 10^{-14} cm^2. Except for xenon flow (K_o = 1.13 x 10^{-9} cm), the values of K_o agreed fairly well, with the average being (1.89 $\pm$ 0.05) x 10^{-9} cm.

Several low pressure flow experiments (section 3.1.3.4) were made on Cylinder No. K42 (Detmn. No. L:31). By determining the flow-rate Q at various times after the commencement of flow

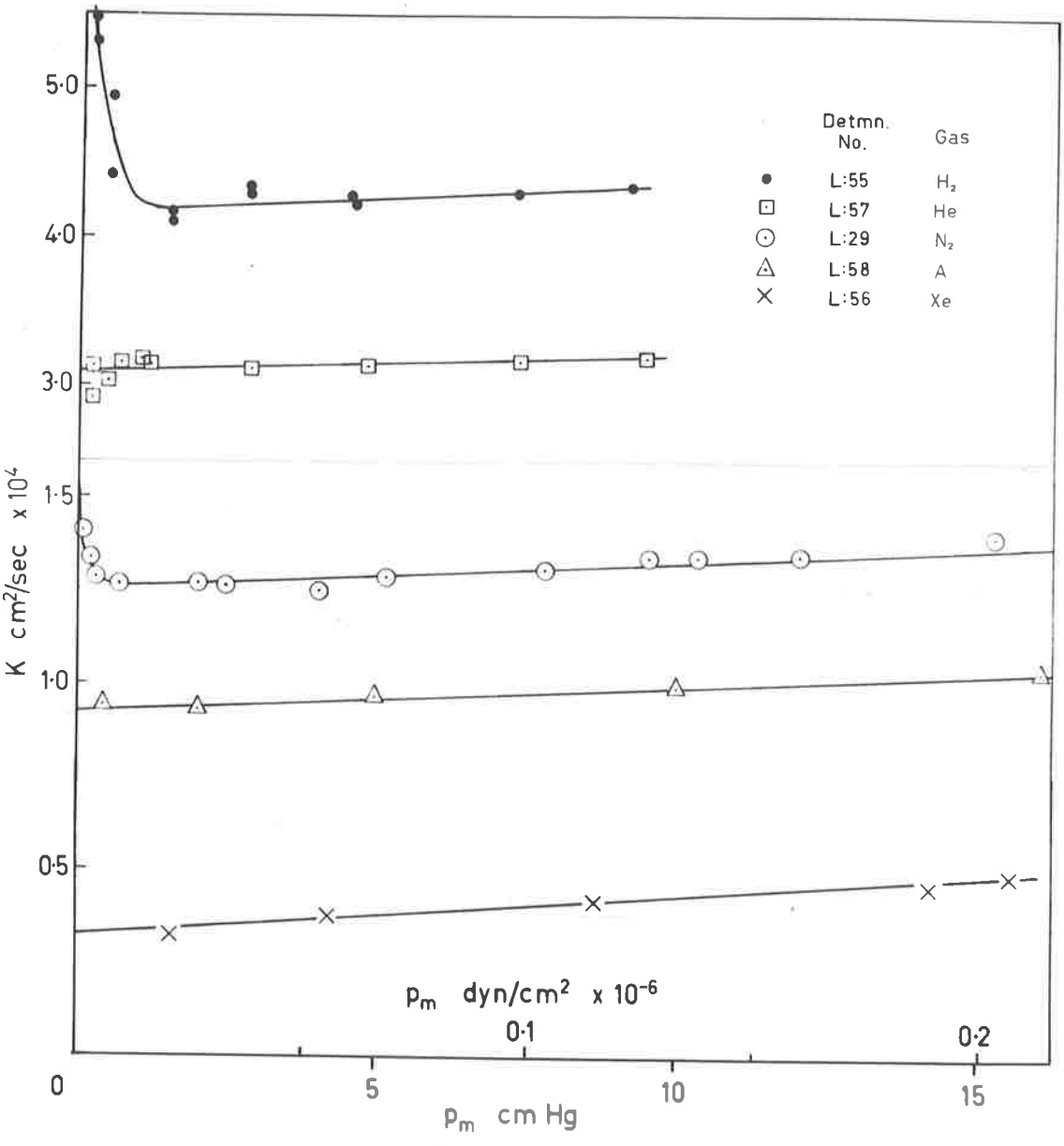

Fig. 4.1-11 K-p_m Plots for Flow of Different Gases through Impregnated Graphite Sample No. K42 (Determined by the Pressure Increase Method).

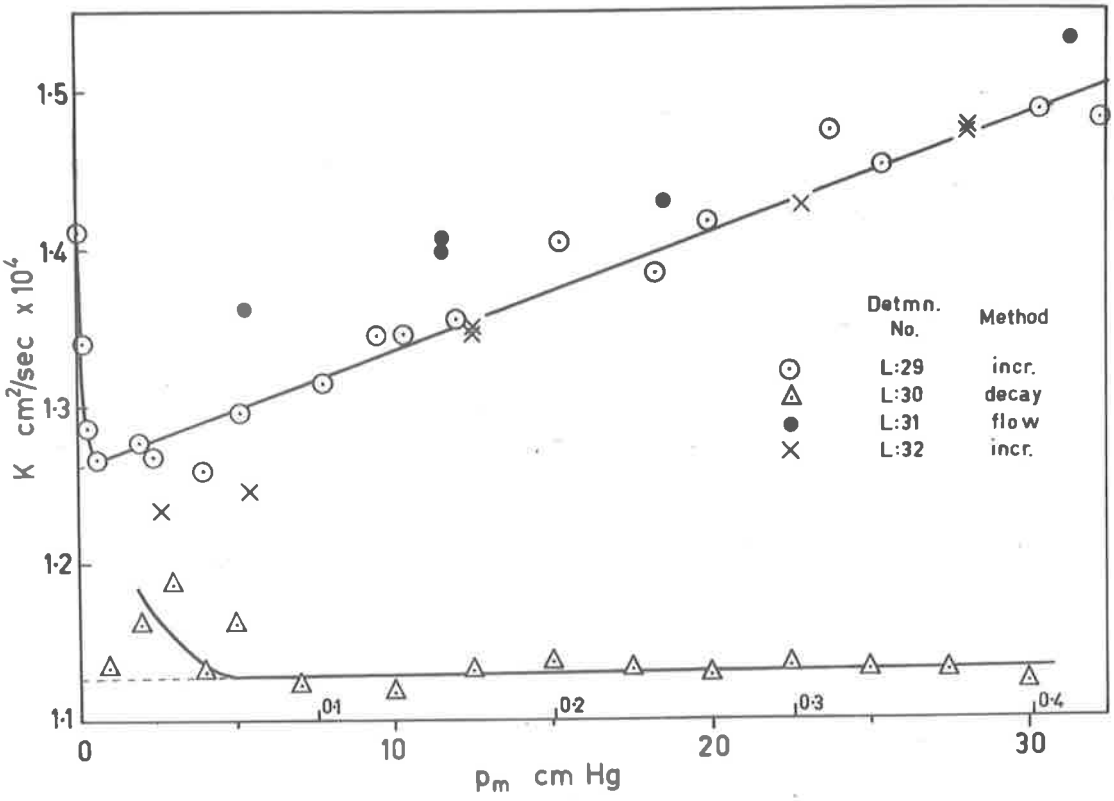

Fig. 4.1-12 K-p_m Plots for Nitrogen Flow through Impregnated Graphite Sample No. K42 for Different Measuring Methods.

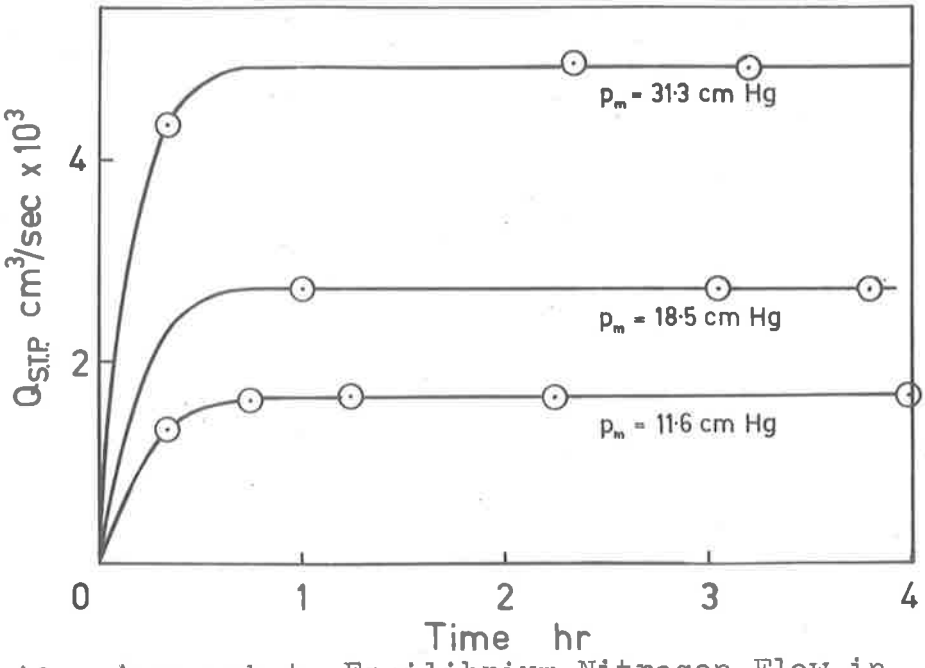

Fig. 4.1-13 Approach to Equilibrium Nitrogen Flow in Impregnated Graphite Sample No. K42 (Detmn. No. L:31).

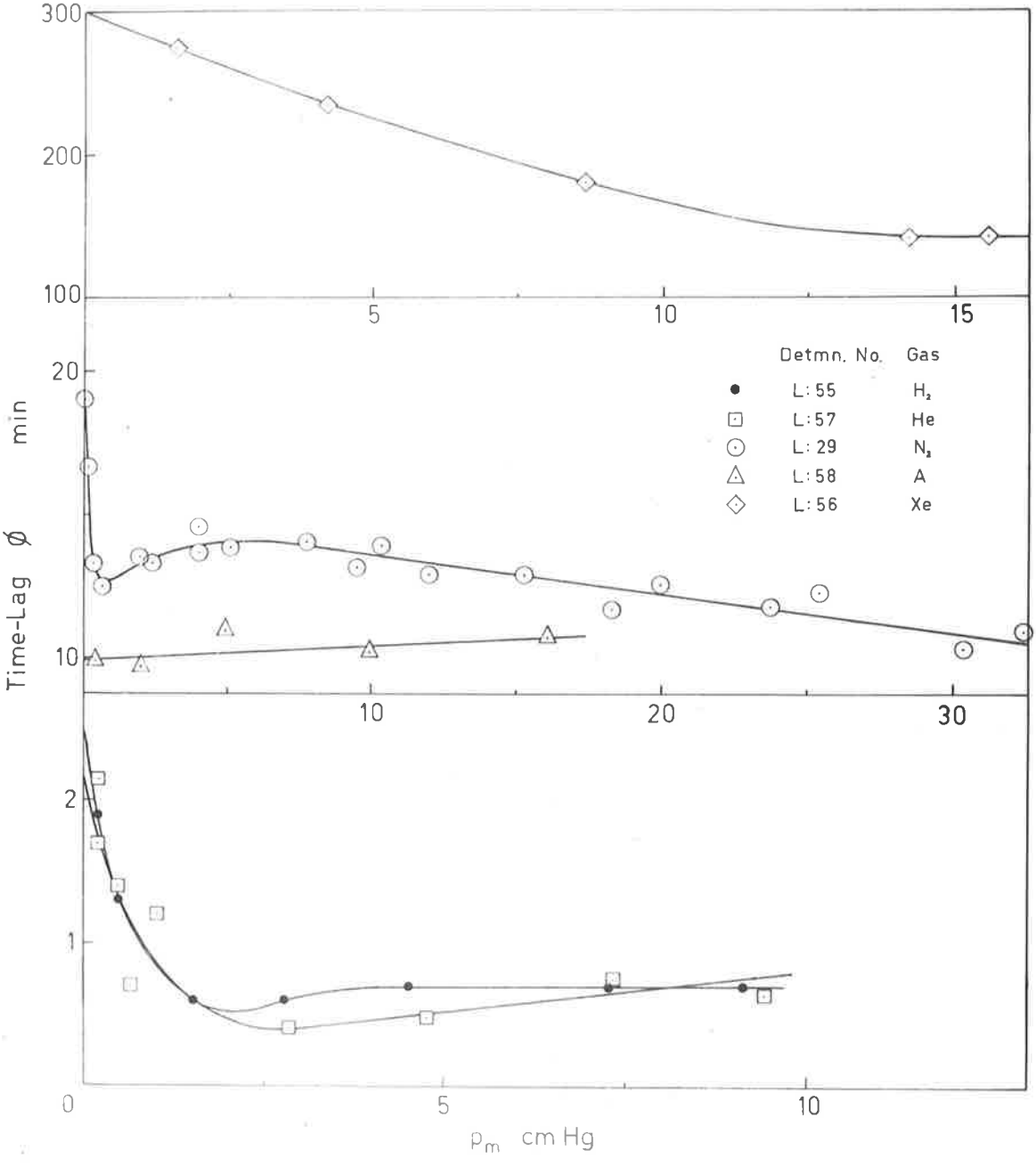

Fig. 4.1-14 ϕ-p_m Plots for Gas Flow through Impregnated Graphite Sample No. K42.

Table 4.1-4

Permeability Results for Impregnated Graphite Samples

Detmn. No.	Method	Gas	$\mathcal{J}_s$ (av) °C	Range of p_m cm Hg	Slope b cm²/sec, cm Hg x 10⁶	B_o cm² x 10¹⁴	Intercept a cm²/sec x 10⁴	K_o cm x 10⁹	Comments
	Sample No. K41, L/A = 0.0261 cm^{-1}								
H:7	H.p.flow	N_2	28.0	106 - 792	-	-	-	-	Plot curved down
H:14	H.p.flow	N_2	20.0	194 - 701	0.0715	0.0941	0.413	0.658	
H:9A	H.p.flow	N_2	19.2	163 - 426	0.1992	0.132	1.31	0.560	
H:8A	H.p.flow	A	19.8	218 - 576	0.0626	0.105	0.310	0.591	
H:10	H.p.flow	CO_2	21.5	129 - 432	(0.105)	(0.116)	(0.280)	(0.558)	Estimated values Leakage
H:11	H.p.flow	CF_2Cl_2	18.5	102 - 220	(0.120)	(0.111)	(0.022)	(0.731)	
H:11A	H.p.flow	CF_2Cl_2	19.9	244 - 377	-	-	-	-	Sample blocked
	Sample No. K42, L/A = 0.0240 cm^{-1}								
L:29	L.p.increase	N_2	23.4	0.06 - 38.0	0.746	0.991	1.26	2.00	Minm. 0.5 cm Hg
L:32	L.p.increase	N_2	17.5	5.40 - 36.9	0.767	1.004	1.25	2.01	
L:30	L.p.decay	N_2	22.2	1.50 - 32.5		Approx.	1.13		Minm. ?
L:31	L.p.flow	N_2	18.0	5.30 - 36.5	-	-	-	-	5 expts.
H:6	H.p.flow	N_2	28.7	180 - 655	0.424	0.566	1.99	3.15	
H:22	H.p.flow	N_2	24.8	128 - 687					
L:55	L.p.increase	H_2	16.8	0.20 - 9.1	1.99	1.31	4.18	1.80	Minm. 1.2 cm Hg
H:23	H.p.flow	H_2	23.6	231 - 540	0.917	0.615	5.94	2.55	
L:57	L.p.increase	He	20.1	0.20 - 9.4	1.26	1.85	3.10	1.87	
L:58	L.p.increase	A	23.1	0.41 - 16.1	0.702	1.19	0.928	1.76	
L:56	L.p.increase	Xe	18.5	1.59 - 15.6	1.065	1.79	0.328	1.13	Large ϕ values

(see Fig. 4.1-13), it was demonstrated that steady state flow was attained in less than one hour; the flow-rate then remained constant with time within experimental error. The values of K calculated from these flow experiments were 3 to 4½% higher than the K-p_m plot obtained in Detmn. No. L:29 by the pressure increase method (see Fig.4.1-12). Detmn. No. L:32, in which values of K were measured by both the pressure increase and flow methods, was performed to explain this difference.

In Detmn. No. L:32, the values of K decreased as the sample time Δt (the time of collection of a gas sample in the McLeod gauge) increased; for Δt = 2 min (a flow experiment), the K values agreed with those from Detmn. No. L:31, while for Δt longer than 10 min, the K values agreed with the K-p_m plot obtained in Detmn. No. L:29. The error in calculating the flow-rate for the short time interval was 5% and the error for the longer time interval was 3%, i.e., the relative error between the two techniques was 2% or less than the observed difference of 3 to 4½%.

In two of the pressure increase determinations on Cylinder No. K42, a well-defined minimum in the K-p_m plot was observed at low pressures (Fig.4.1-11). The minimum occurred at about p_m = 1.2 cm Hg for

hydrogen flow (Detmn. No. L:55), and p_m = 0.5 cm Hg for nitrogen flow (Detmn. No. L:29). For argon and xenon flow, experiments were not continued to low enough pressures for a minimum to be observed. For helium flow (Detmn. No. L:57), there was insufficient evidence for a minimum in the K-p_m plot since faulty experimental technique caused a large scatter of the low pressure points.

Time-lags ϕ were measured in all pressure increase experiments conducted on Cylinder No. K42 except those in Detmn. No. L:32. The values of ϕ obtained for each determination are listed in Appendix K and graphs of ϕ against p_m are shown in Fig. 4.1-14. The graph for xenon flow was the highest, with those for hydrogen and helium flow the lowest. Above p_m = 5 cm Hg, ϕ was observed to decrease with increasing p_m for nitrogen flow (Detmn. No. L:29) and xenon flow (Detmn. No. L:56), but was constant for hydrogen flow (Detmn. No. L:55) and increased slightly for helium and argon flow (Detmns. No. L:57 and No. L:58). Below p_m = 5 cm Hg, the ϕ-p_m graphs for nitrogen, hydrogen, and helium flow dipped downwards and then curved sharply upwards to give a minimum at about p_m = 2 cm Hg. The nitrogen graph was the most sharply curved. The values of ϕ for xenon flow were extremely

large compared with those for the other gases and ranged from about 2.5 to 4.5 hr. The scatter of the ϕ values about the ϕ-p_m plot for nitrogen flow (Detmn. No. L:29) was $\pm$ 0.5 min ($\pm$ 4%) and was due to the inaccuracy of determining the values of ϕ.

4.1.4.2 The High Pressure Determinations

For cylinder No. K41, values of K were determined in the high pressure apparatus for the flow of hydrogen, nitrogen, argon, carbon dioxide, and freon-12. When this series of determinations (Nos. H:7 to H:11) had been completed, a repeat nitrogen determination (No. H:12) showed that the graphite sample holder at some stage during the series had developed a leak as the nitrogen permeability results were not reproducible with those of Detmn. No. H:7. The presence of the leak meant that the results of some or all of the determinations in the series were in error. The determinations were therefore repeated when the sample holder had been repaired.

The repeat determinations showed that the size of the leak had increased with time since the redetermined K-p_m plots at p_m = 300 cm Hg were lower than the original plots by 6% for argon flow (Detmn. No. H:8A cf. No. H:8), 9% for hydrogen flow (No.H:9A cf. No. H:9),

and 13% for nitrogen flow (No. H:14 cf. No. H:12). In the initial hydrogen determination (No. H:9), the values of K were observed to increase by 100% over four days and then remain constant and give a straight K-p_m plot. Detmn. No. H:9A showed that leakage accounted for only a small portion of this increase. Therefore the increase was suspected to be mainly due to the slow displacement of argon from the sample and apparatus; care was accordingly taken for all further determinations to ensure that the graphite sample was completely evacuated between determinations.

When the freon determination was repeated (No. H:11A), experiments were attempted at high relative partial pressures p/P_o from 0.6 to 0.9 in order to observe whether enhanced flow-rates would occur due to capillary condensate flow (cf. the experiments of Carman[122]). When p_m was about 250 cm Hg (p_m/P_o = 0.59), the values of K were 30% lower than the K-p_m plot for Detmn. No. H:11; however, at higher pressures (p_m = 370 cm Hg, p_m/P_o = 0.87), the values of K were only about 15% of those expected from Detmn. No. H:11 (see Fig. 4.1-15).

The sample was removed from the permeability cell and examined for an explanation of these low results; on replacement of the sample for further flow

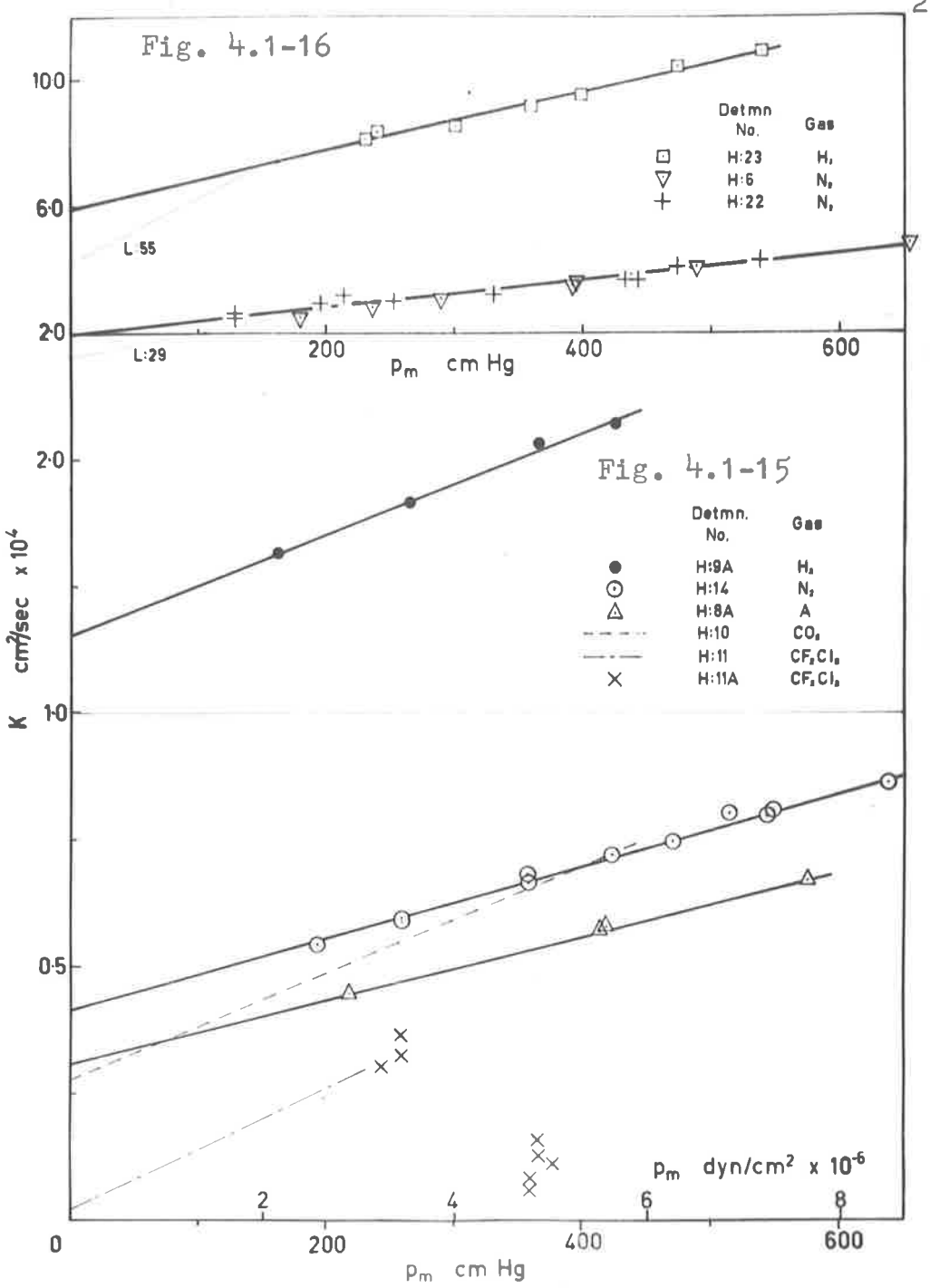

Fig. 4.1-15 K-p_m Plots for High Pressure Gas Flow through Impregnated Graphite Sample No. K41.

Fig. 4.1-16 K-p_m Plots for High Pressure Nitrogen and Hydrogen Flow through Impregnated Graphite Sample No. K42.

measurements, it was found that no flow was obtained, even when the graphite was heated and when pressure or vacuum was applied. No further permeability determinations were possible for this sample as it was apparently blocked. Accordingly, for carbon dioxide and freon flow through Cylinder No. K41, the equations of the $K-p_m$ plots for no leakage were estimated from the plots obtained in Detmns. No. H:10 and No. H:11, respectively.

Gas flow-rates in all the determinations performed on Cylinder No. K41 were measured by means of soap-bubble flow-meters. At very low flow-rates (less than 0.02 cm^3/sec at N.T.P.), difficulty was often experienced in obtaining accurate values of the flow-rate because of the sticking of bubbles in the flow-meters, the variation of the inlet gas pressure, and the limited supply of gas; this difficulty resulted in a large scatter (about $\pm$ 10%) of the K values about the $K-p_m$ plots for carbon dioxide and freon flow (Detmns. H:10 and H:11). For the other gases (hydrogen, nitrogen, and argon), a scatter of less than $\pm$ 2% was observed since the higher flow-rates were measured with greater accuracy.

After a change in the pressure conditions, a minimum of an hour was allowed for equilibrium flow

as indicated by a constant flow-rate to be reached in the sample. For Detmn. No. H:7, several experiments were performed with p_o corresponding to 0 or 225 cm Hg; the resulting values of K agreed within experimental error with those obtained when p_o was atmospheric pressure, thus indicating that the flow phenomenon obtained in the high pressure determinations for Acheson "A" and P.G. 60 graphites (sections 4.1.1 and 4.1.2.2) was not evident for Impregnated graphite.

The straight $K-p_m$ plots for gas flow in cylinder No. K41 at high pressures are shown in Fig. 4.1-15, the estimated plots for carbon dioxide and freon flow being dashed. The values of B_o and K_o calculated from these plots for each determination are given in Table 4.1-4. For hydrogen, nitrogen, and argon flow, the values of B_o and K_o showed reasonable agreement, the average values being $(1.10 \pm 0.11) \times 10^{-15}$ cm^2 and $(6.03 \pm 0.29) \times 10^{-10}$ cm, respectively. The estimated values of B_o and K_o for carbon dioxide and freon were quite close to the respective average values, the estimated K_o value for freon flow being 20% high owing to the greater inaccuracy of estimating small intercept values.

For Cylinder No. K42, high pressure flow determinations were conducted for nitrogen and hydrogen flow.

The K-p_m plots for these determinations are shown in Fig. 4.1-16. The scatter of the K values about the plots was $\pm$ 0.2 x 10^{-4} cm^2/sec (5½% and 2% for nitrogen and hydrogen flow, respectively, at p_m = 400 cm Hg).

The values of B_o and K_o for these determinations are reported in Table 4.1-4. For B_o, the average value was 0.590 x 10^{-14} cm^2, which was about a half of the average low pressure value for this sample (1.36 x 10^{-14} cm^2); for K_o, the average value of 2.84 x 10^{-9} cm was about 50% greater than the average low pressure value (1.89 x 10^{-9} cm). The values of B_o and K_o for Detmn. No. H:6 were closer to the corresponding values for Detmn. No. H:23 than to those of Detmn. No.H:22.

4.1.5 Pressure Distribution Measurements

Pressure distributions were determined in the high pressure apparatus for nitrogen and carbon dioxide flow through the Acheson "A" graphite pressure distribution specimen, nitrogen, carbon dioxide, and freon flow through the Morgan "EY9166" graphite specimen, and nitrogen and hydrogen flow through the P.G. 60 graphite specimen. For each determination, several experiments were performed for various pressure conditions, viz., p_i from 40 cm Hg up to 168 cm Hg and p_o generally either 0 or 76 cm Hg.

The detailed pressure values for each experiment are reported in Appendix K.4. Typical pressure

distributions, plotted dimensionlessly as $(p - p_o)/(p_i - p_o)$ against x/L, are presented in Figs. 4.1-17, 4.1-19, and 4.1-20. The distributions were concave to the x/L-axis as expected and were approximately parabolic in shape. For each experiment, values of p at the points x/L = 1/4, 1/2, and 3/4 were calculated from the theoretical equation (2.1.1-13) for the pressure distribution for gas flow through a porous sample and were compared with the experimentally determined values. In all experiments except those in Detmn. No. G:1, the "ideal" pressure distribution lay below the experimental distribution.

As the flow-rate Q_a was measured in all experiments, permeability values were calculated for both the overall specimen (K_{ov}) and the individual discs in the specimen ($K_{\text{disc 1}}, \ldots . K_{\text{disc 4}}$). These results are also reported in Appendix K.4. The values of $K_{av} = (\sum_{i=1}^{4} K_{\text{disc } i})/4$ and $(p_m)_{av} = (\sum_{i=1}^{4}(p_m)_{\text{disc } i})/4$ averaged for the graphite discs in a specimen were greater than the overall values of K_{ov} and p_m, which were derived from the values of p_i and p_o for each experiment. Except for Detmn. No. G:1, the experimental values of K_{av} and $(p_m)_{av}$ were also larger than the average values calculated from the theoretical

distribution.

When K-p_m plots were prepared (see Fig. 4.1-22), a separate graph was obtained for each graphite diso in a specimen; the maximum variation between the plots at p_m = 100 cm Hg was about 35% for P.G. 60 and Acheson "A" graphites, but was 55% for Morgan "EY9166" graphite. In order to calculate the theoretical pressure distribution for each experiment by means of equation (2.1.1-13), a value of a/b was obtained from the K_{ov} - p_m plot for each determination. As turbulent flow caused scatter of the values of K for the Acheson "A" and P.G. 60 graphite specimens, the K_{ov} - p_m plots had to be corrected. For each determination on these graphites, values of K_v, the permeability contribution due to viscous-slip flow (= $a + bp_m$), were estimated from the values of K_{ov} and G by means of a rearranged form of equation (5.1.2-7), viz.,

$$K_v = p_m K/(p_m - \beta G K), \qquad \ldots (4.1.5\text{-}1)$$

and the K_v-p_m plot drawn. The individual K_{diso} values were not corrected. The value of β for each graphite is given in Table 5.1-1; calculations were relatively insensitive to errors in the value of β when the flow was almost viscous (see section 5.1.2.4).

4.1.5.1 P.G. 60 Graphite

Five pressure distribution experiments were performed for nitrogen flow through the P.G. 60 graphite specimen No. G31 (Detmn. No. G:7), and two experiments for hydrogen flow (Detmn. No. G:8). Flow-rates were measured by means of the wet gas test meter; the inlet pressure was kept constant for each experiment with the manostat.

Typical dimensionless pressure distributions are shown in Fig. 4.1-17. Generally, the distribution curves were almost linear over the first half of the specimen. For nitrogen and hydrogen flow, the experimental distributions for p_i = 155.7 cm Hg and p_o about 80 cm Hg (Fig. 4.1-17) were quite close and within experimental error; the "ideal" distributions for these experiments were almost the same. The distributions for p_o = 22 cm Hg were higher than those when p_o was about 1 atm. For a series of experiments for nitrogen flow (Detmn. No. G:7) with p_i about 154 cm Hg and p_o varying between 22 and 100 cm Hg, the curvature of the distributions increased as Δp increased.

Permeability coefficients were calculated for each disc and for the overall specimen. Disc. no. 2 had the highest permeability while disc. no. 3 had

the lowest, the variation in the permeability at p_m = 100 cm Hg being 32%. The overall K-p_m values were quite scattered because of the effects of turbulent flow and no satisfactory K-p_m plot could be drawn. Accordingly, values of K_v were calculated (see section 4.1.5), β being taken as 5.70×10^3 cm^{-1}.

For nitrogen flow (Detmn. No. G:7), the values of a and b obtained from the K_v-p_m plot were respectively 26 and 7.36, i.e., a/b was 3.53. These values of a and b were consistent with those obtained for the high pressure nitrogen determinations on P.G. 60 graphite samples (Detmns. No. H:15 and No. H:19). For hydrogen flow (Detmn. No. G:8), the values of a and b were estimated to be 40 and 13.8 respectively, (a/b=2.9) by a comparison with the results of Detmn. No. H:16.

4.1.5.2 Acheson "A" Graphite

A number of pressure distributions were determined for nitrogen flow in the Acheson "A" graphite specimen No. G1, eleven experiments being performed in one direction (discs in order 4 to 1 - Detmn. No. G:1), and six in the reversed direction (order 1 to 4 - Detmn. No. G:2). For carbon dioxide flow (Detmn. No. G:3), six experiments were made. The gas flow-rate was measured by means of the soap-bubble

flow-meter or the rotameter, and the inlet pressure was held constant for each experiment by means of the manostat. Leaks found in the apparatus and specimen were repaired with Epoxy resin.

Some of the distribution curves are shown in Figs. 4.1-18 and 4.1-19. A series of distribution curves for Detmn. No. G:2 (Fig. 4.1-18) with p_i about 125 cm Hg and p_o varying between 12 and 83 cm Hg showed that the curvature of the distributions increased as Δp increased. For two experiments (nos. 4 and 6) with about the same Δp (71 cm Hg), the curvature was greater for the experiment with the lower p_m.

In Fig. 4.1-19, typical experimental and "ideal" pressure distribution curves for p_i about 120 cm Hg and p_o either about 76 cm Hg or 1 cm Hg are plotted dimensionlessly. The curves for p_o = 76 cm Hg were lower than those for p_o = 1 cm Hg. For flow in Specimen No. G1 with disc no. 1 at the inlet end, the distributions for carbon dioxide flow (Detmn. No. G:3) and nitrogen flow (Detmn. No. G:2) were the same showing that the pressure distribution for given pressure conditions was not significantly altered on changing the flowing gas.

Comparison of the distributions for nitrogen flow

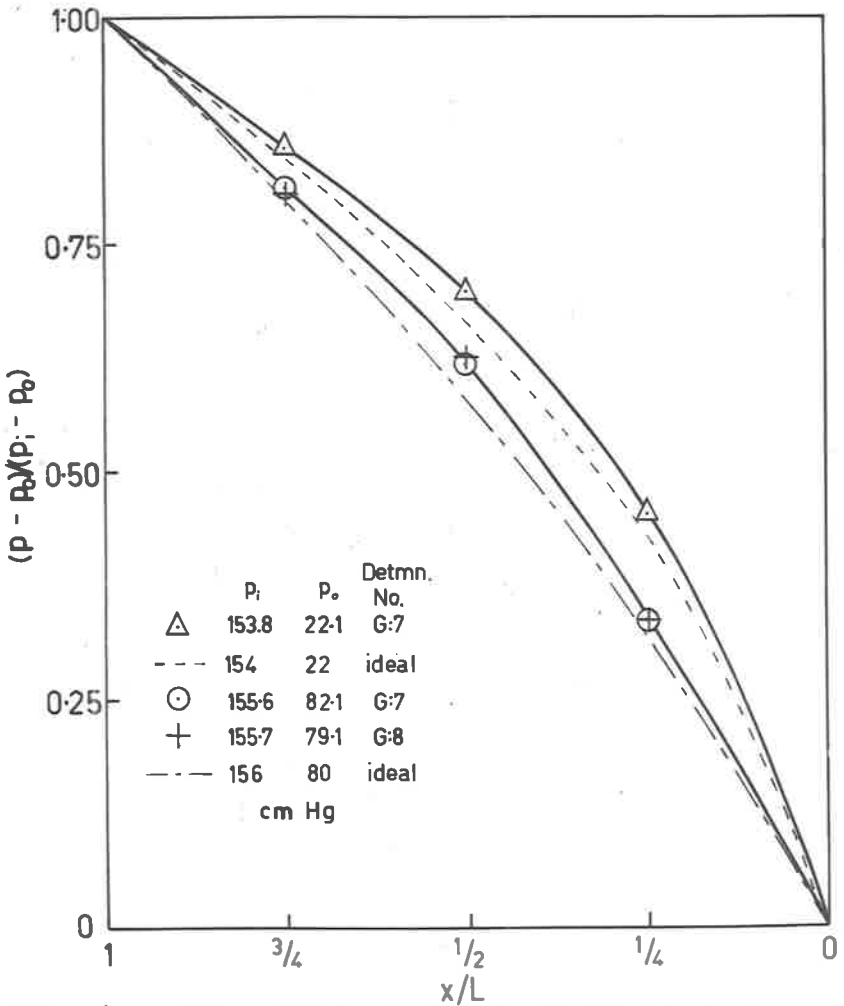

Fig. 4.1-17 Typical Dimensionless Pressure Distributions for Nitrogen and Hydrogen Flow through P.G. 60 Graphite Specimen No. G31 with p_i about 155 cm Hg.

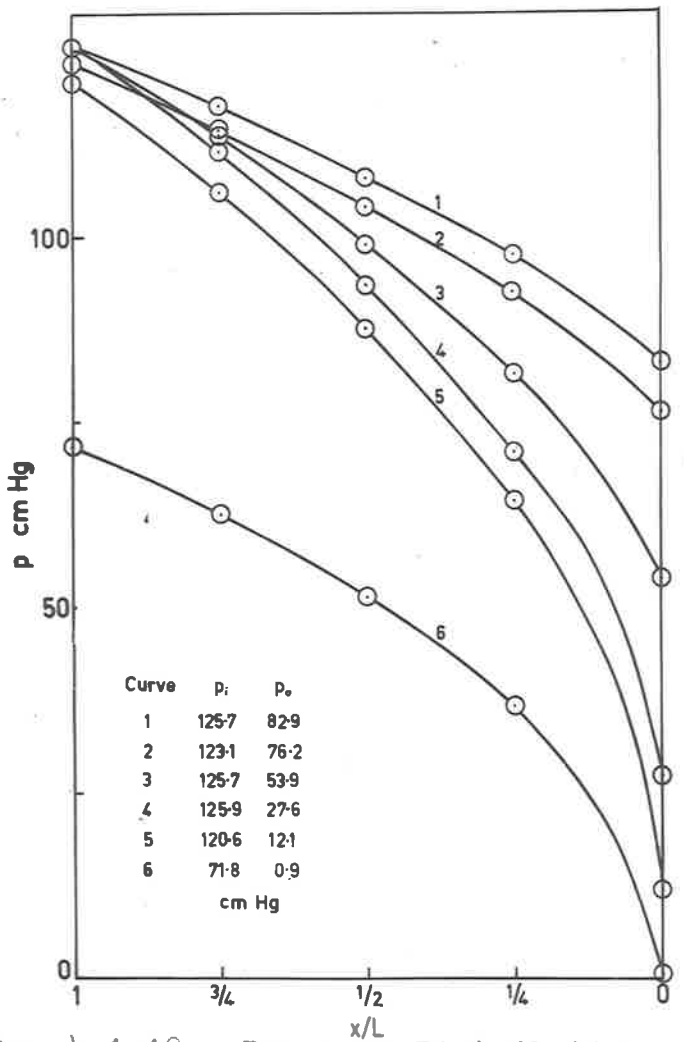

Fig. 4.1-18 Pressure Distribution Curves for Nitrogen Flow through Acheson "A" Graphite Specimen No. G1.

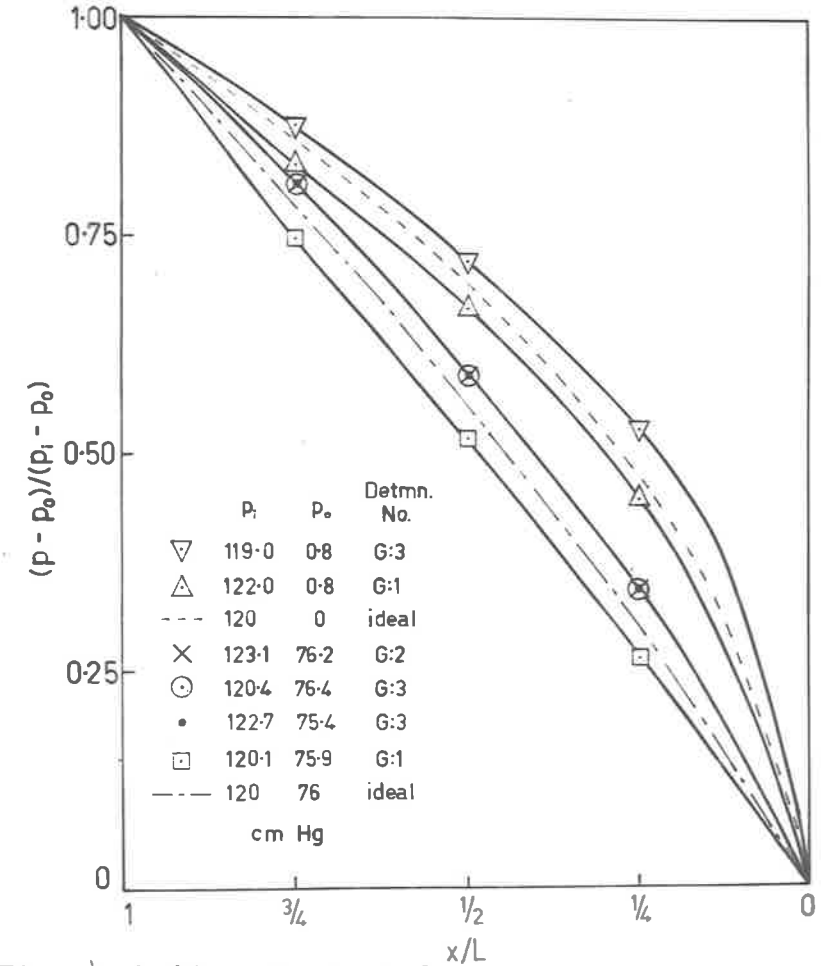

Fig. 4.1-19 Typical Dimensionless Pressure Distribution for Nitrogen and Carbon Dioxide Flow through Acheson "A" Graphite Specimen No. G1 with p_i about 120 cm Hg.

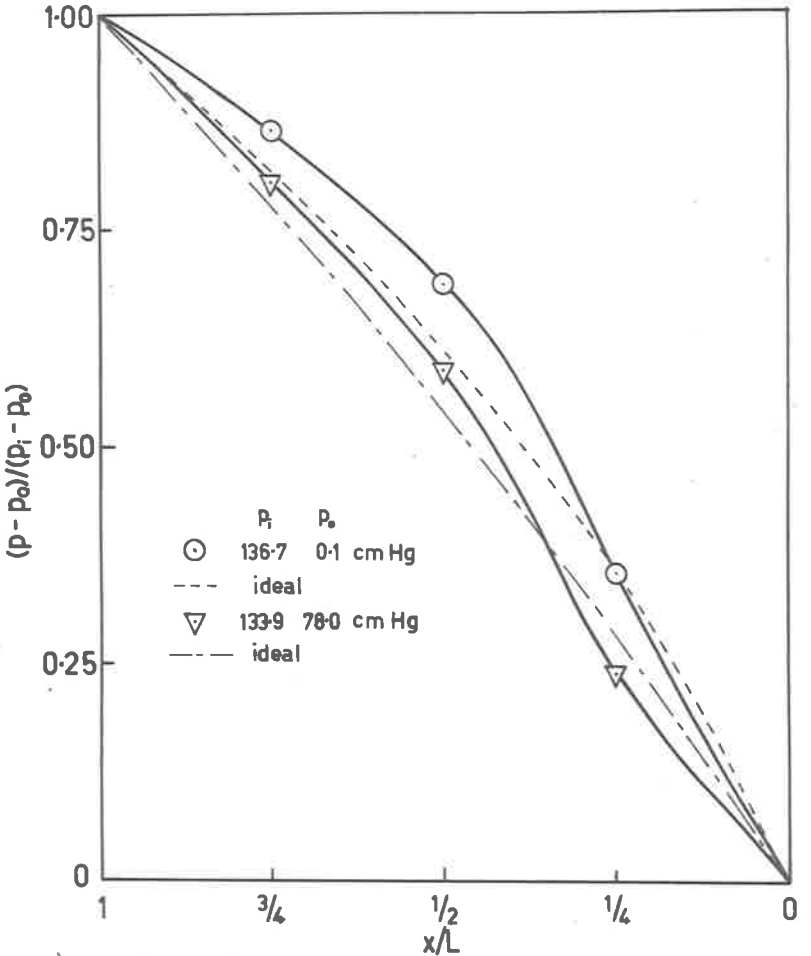

Fig. 4.1-20 Typical Dimensionless Pressure Distributions for Nitrogen Flow through Morgan "EY9" Graphite Specimen No. G21 with p_i about 135 cm Hg.

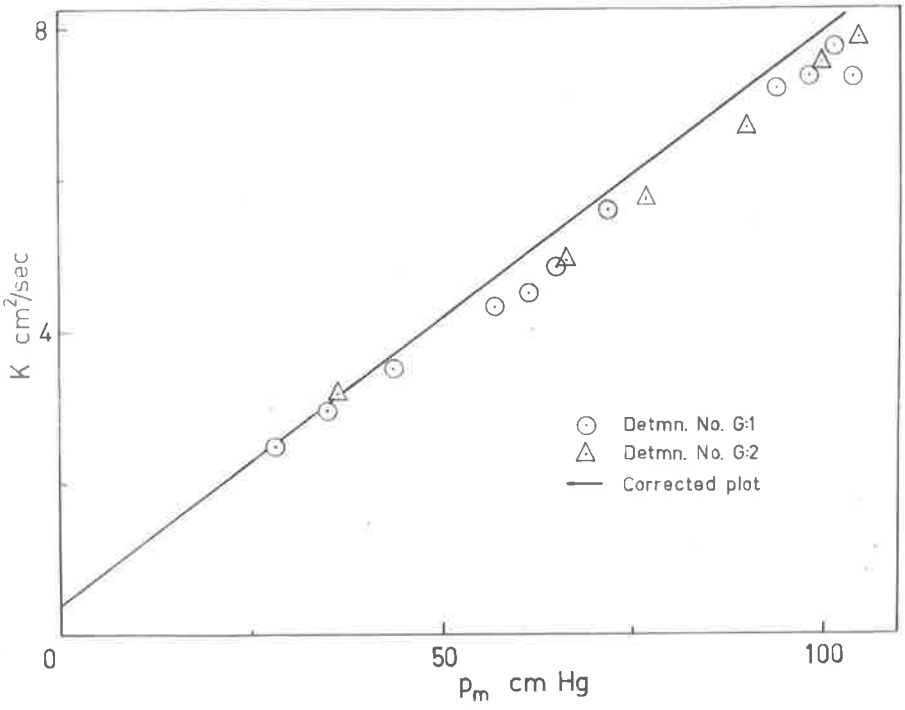

Fig. 4.1-21 Corrected K-p_m and K_{ov}-p_m Values for Nitrogen Flow through Acheson "A" Graphite Specimen No. G1.

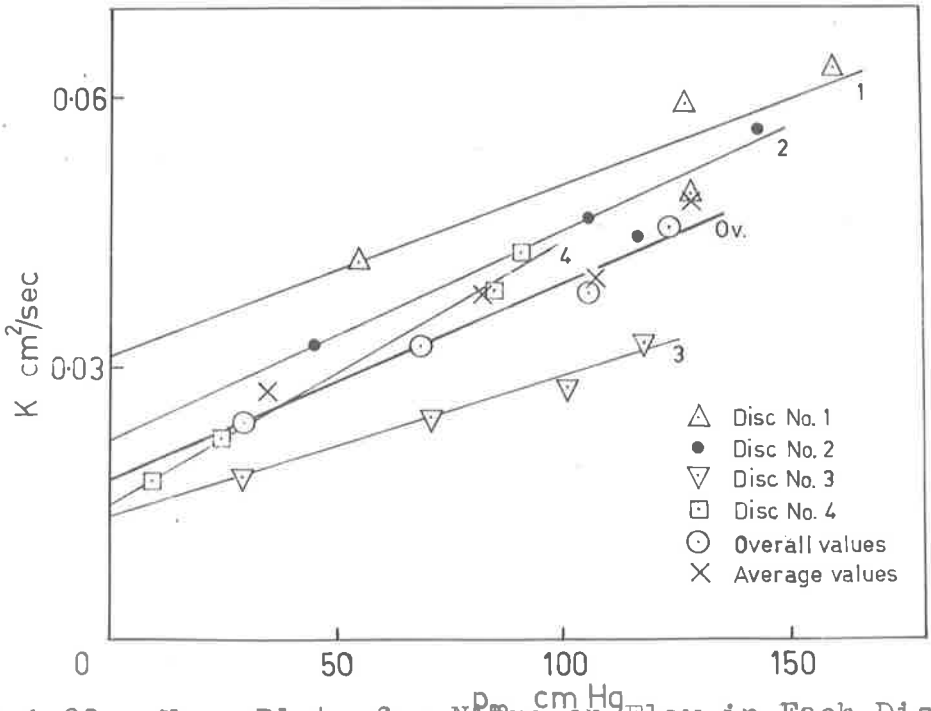

Fig. 4.1-22 K-p_m Plots for Nitrogen Flow in Each Disc and in the Overall Morgan "EY9" Graphite Specimen No. G21.

in both directions in the specimen showed that, for flow in the direction from disc no. 4 to disc no. 1 (Detmn. No. G:1), the pressure distribution curves were lower (see Fig. 4.1-19) than both the "ideal" distributions and those for flow in the reversed direction (Detmn. No. G:2); the initial portion of the curves was not parabolic, but tended to be linear or slightly convex. The experimental distributions for both Detmns. No. G:2 and No. G:3 were higher than the "ideal" curve.

From the measured pressures and flow-rate for each experiment, values of K were calculated for each disc and for the overall specimen. Disc no. 1 had the highest permeability and disc no. 4 had the lowest. At p_m = 100 cm Hg, the total variation in the K values was 35%.

Satisfactory K-p_m plots could not be prepared since a separate curved graph resulted for each value of p_o for Acheson "A" graphite because of the effects of inertial or turbulent flow above the critical Reynolds number (see 5.1.2.4).

Therefore values of K_v were estimated for each determination by means of equation (4.1.5-1), the value of β being taken as 6.76×10^6 cm^{-1}. The K_v-p_m plot for nitrogen flow is shown in Fig. 4.1-21

together with the K_{ov}-p_m points from which the K_v-p_m points were calculated; the points for both Detmn. No. G:1 and Detmn. No. G:2 lay on the same K_v-p_m plot.

The values of a and b obtained from the K_v-p_m plot were respectively 0.40 and 0.076 for nitrogen flow, and 0.67 and 0.083 for carbon dioxide flow, i.e., the values of a/b were 5.26 and 8.07. From the low pressure determinations on Rod No. K2A, the values of a and b were respectively 0.24 and 0.063 for nitrogen flow, and 0.23 and 0.081 for carbon dioxide flow. Although the values of a from the estimated plots were higher than those for the low pressure measurements, the agreement was fairly good.

4.1.5.3 Morgan "EY9166" Graphite

For the Morgan "EY9166" graphite specimen (No. G21), four pressure distribution experiments were performed for nitrogen flow (Detmn. No. G:4) and three each for carbon dioxide and freon flow (Detmns. No. G:5 and No. G:6). The gas flow-rates were measured by means of the capillary flow-meter; for carbon dioxide and freon flow, the flow-meter calibration constant X (4.64×10^{-3} cm^3/sec, cm Hg for nitrogen flow) was corrected by multiplying by the ratio of viscosities μ_{N_2} / μ_{gas}. For experiments with p_o a

vacuum, the flow-rate was corrected to allow for a leakage rate of 0.003 cm^3/sec into the vacuum system. For the freon experiments (Detmn. No. G:6), some difficulty was encountered because of the limited gas supply in the freon cans.

Two typical dimensionless pressure distributions for nitrogen flow through the Morgan "EY9166" specimen are given in Fig. 4.1-20 together with the respective "ideal" pressure distributions. The distributions were generally sigmoid-shaped. The distributions when p_o was a vacuum were more curved than when p_o was about atmospheric pressure. Comparison of the distributions for carbon dioxide and freon flow with p_i about 125 cm Hg and p_o either 77 or 0 cm Hg showed that the distribution curves for freon flow (Detmn. No. G:6) tended to be higher (more curved) than those for carbon dioxide flow (Detmn. No. G:5). No definite comparison could be made, however, because it was suspected that the freon distributions (especially that for experiment no. 3, Detmn. No. G:6) were inaccurate possibly because of non-equilibrium flow or an air leak into the apparatus.

From the calculated values of K, straight K-p_m plots were drawn for nitrogen and carbon dioxide flow (Detmns. No. G:4 and No. G:5) even though only a few

experiments were performed in each determination and the points showed some scatter. For freon flow (Detmn. No. G:6), a K-p_m plot was not drawn because of the irregular variation and inaccuracy of the K values. The K-p_m plots were not corrected for turbulent flow effects (cf. P.G. 60 and Acheson "A" graphites) since the flow was considerably below the critical Reynolds number.

The K-p_m plots for each disc and for the overall specimen, together with the K_{av}- $(p_m)_{av}$ points, are shown in Fig. 4.1-22 for nitrogen flow. The average points were higher than the overall K-p_m plot. In Table 4.1-5, the values of the intercept a and slope b of the K-p_m plots are recorded for both nitrogen and carbon dioxide flow. Disc no. 1 had the highest permeability while disc no. 3 had the lowest; the variation between the K values for these discs at p_m = 100 cm Hg was 55%.

The values of a/b chosen to calculate the theoretical distributions for nitrogen and carbon dioxide flow in Specimen No. G21 were the values obtained from the overall K-p_m plots, viz., 81.1 and 170, respectively (see Table 4.1-5). These average values were 16% and 35% higher than the overall values, repectively, and considerably higher than the values obtained from deter-

minations on different samples in the low pressure apparatus. The a/b value for freon flow was assumed equal to that for nitrogen because of the lack of adequate flow results for freon.

Table 4.1-5

Values of a and b for Detmns. No. G:4 and No. G:5

	Nitrogen - No.G:4			Carbon Dioxide - No.G:5		
	a	b x 10^4	a/b	a	b x 10^4	a/b
Disc no.1	0.0313	1.90	165	0.0372	0.95	392
Disc no.2	0.0220	2.32	94.9	0.0300	0.93	323
Disc no.3	0.0136	1.53	89.0	0.0175	0.63	278
Disc no.4	0.0149	2.92	51.0	0.0137	1.79	77
Average	0.0204	2.17	94.0	0.0246	1.08	229
Overall	0.0176	2.17	81.1	0.0214	1.26	170
Permeability Detmn.*	0.0162	3.09	52.5	0.0121	3.86	31.4

* Detmn. No. L:43 for nitrogen flow and Detmn. No. L:49 for carbon dioxide flow.

4.2 The Porosity Measurements

By means of the measurements described in section 3.2.3, values of the porosity ε, the bulk density ρ_b, the helium density ρ_s, and the percentage of unopen pores were calculated for each graphite sample. A type calculation of these quantities for

Acheson "A" Sample No. S2 (Detmn. No. D:1) is presented in Appendix F.2. The calculated results for the various samples are summarized in Table 4.2-1.

The error in obtaining the bulk density ρ_b of a sample from its bulk volume V_t and weight w was about 1%. The average values obtained were 0.96 g/cm^3, 1.51 g/cm^3, 1.72 g/cm^3, and 1.79 g/cm^3 for P.G. 60, Acheson "A", Morgan "EY9", and Impregnated graphites, respectively.

The determination of the dead space volume in the bulb V_D by helium displacement measurements was made with little difficulty, the uncertainty in any value of V_D being less than $\pm$ 0.5%. The accuracy of the measurements and the excellent volume control obtained by the constant volume manometer system were demonstrated by the very small variation ($\pm$ 0.05%) in the total volume of gas (at S.T.P.) in the apparatus for any determination. The value of V_D was obtained more accurately by the method of least squares than by graphical means. In all determinations, equilibrium was attained very quickly after each gas expansion.

The determination of the volume of the empty bulb V_b proved quite difficult. Because V_b could not be determined by helium displacement measurements, other methods were employed (see section 3.2.3.3). When

mercury was added to the sample bulb with the sample still in place, it was difficult to remove all the air from the bulb or to ensure that no mercury entered any large pores in the sample; if these effects occurred, then high or low values of the porosity would result, respectively. When the volume of the sample bulb was measured after the sample had been removed (by cracking the bulb in halves and then rejoining with adhesive), a low value of ε was possible if the bulb was not rejoined satisfactorily.

For Morgan "EY9" and Impregnated graphites, V_b was measured by both methods, the second method generally giving the more accurate value of V_b. For the coarse-pored graphites, only the second method could be used.

The average values of the porosity ε were:

P.G. 60 graphite	54%
Acheson "A" graphite	28%
Morgan "EY9" graphite	15%
Impregnated graphite	11.5%

The helium densities ρ_s of these graphites ranged between 1.97 and 2.10 g/cm^3, while the percentage of unopen pores in the graphites was between 16 and 36%. The finer-pored graphites had the smaller

densities and the greater percentage of unopen pores. For P.G. 60 and Impregnated graphites, the values of ε and ρ_s calculated from two separate determinations agreed quite closely (see Table 4.2-1). However, for Morgan "EY9" graphite, the two values of ε and ρ_s differed by about 27% and 5%, respectively. The error in the porosity values could be quite large, especially for the fine-pored graphites with small pore volumes V_p, since inaccuracies in the volume measurements were magnified on taking the difference between the volumes V_t and V_s (see Appendix F).

4.3 The Surface Area Measurements

The values of the surface areas of the various graphite samples as determined from the krypton adsorption measurements are summarized in Table 4.3-1. The calculation of the area for Morgan "EY9" Sample No. S21 (Detmn. No. S:5) is given in detail in Appendix G.2, together with the krypton isotherm up to $p/P_o = 0.3$ (Fig. G.2-1) and the B.E.T. plot (Fig. G.2-2) for this sample.

For solid graphite samples, the average values of S_g were:

P.G. 60 graphite	1.1 m^2/g
Acheson "A" graphite	0.71 m^2/g
Morgan "EY9" graphite	0.50 m^2/g
Impregnated graphite	2.5 m^2/g.

Table 4.2-1

Summary of the Results of the Porosity Measurements

Graphite Grade	Detmn. No.	Sample No.	w g	V_t cm^3	V_D cm^3	V_b cm^3	V_p cm^3	ε	ρ_b g/cm^3	ρ_s g/cm^3	%age unopen pores	Outgassing Conditions
P.G. 60	D:3	S31	5.370	5.633	7.720	10.278	3.075	0.546	0.952	2.097	18.3	5 hr at 320°C
	D:5	S32	5.012	5.150	8.066	10.459	2.757	0.535	0.973	2.094	17.5	4½ hr at 300°C
Acheson "A"	D:1	S2	5.588	3.701	4.076	6.745	1.032	0.279	1.510	2.093	16.1	15 hr at 310°C
Morgan "EY9"	D:2	S22	5.148	2.999	4.609	7.102	0.505	0.168	1.716	2.069	21.0	15 hr at 320°C
	D:6	S21	5.464	3.177	5.511	8.278	0.410	0.129	1.720	1.974	35.5	18 hr at 330°C
Impregnated	D:4	S41	4.370	2.446	3.160	5.338	0.268	0.109	1.787	2.006	24.5	16 hr at 310°C
	D:7	S42	6.517	3.624	7.421	10.610	0.435	0.120	1.794	2.044	31.1	19 hr at 300°C

Table 4.3-1

Summary of the Results of the Krypton Surface Area Determinations

Graphite Grade	Detmn. No.	Sample No.	w g	V_m cm^3	S_g m^2/g	S_v m^2/cm^3	T_b(av) °K	Outgassing Conditions
P.G. 60	S:7	S31	5.370	1.168	1.140	1.093	80.0	15 hr at 330°C
Acheson "A"	S:1[a]	S1	4.276	1.129	1.38	2.08	79.5	15 hr at about 300°C
	S:2[a]	S1	4.237	0.998	1.24	1.87	80.6	
	S:3	S1	4.079	0.333	0.428	0.645	82.7[b]	20 hr at 310-340°C
	S:4	S2	5.588	0.752	0.706	1.067	79.9	18 hr at 300-330°C
Morgan "EY9"	S:5	S21	5.464	0.568	0.545	0.937	80.7	20 hr at 300°C
	S:6	S22	5.148	0.637	0.649	1.115	79.7	16 hr at 290-310°C
Impregnated	S:8	S41	4.370	1.760	2.11	3.78	80.7	14 hr at 330°C
	S:9	S42	6.517	3.564	2.87	5.14	77.7[c]	14 hr at 340°C

Notes: a Detmns. S:1 and S:2 were performed approximately three years prior to the remainder of the determinations. During this interval, the krypton adsorption apparatus was reconstructed. All details given in the experimental section refer to the present apparatus; for the measurements on the old apparatus, the volumes were different and the temperature of the liquid nitrogen bath was measured with a platinum resistance thermometer.

b Liquid air bath used.

c High purity liquid nitrogen bath used.

On the first adsorption of krypton by the sample, over 99.5% of the original quantity of gas was adsorbed and p decreased from about 4 mm Hg to about 0.005 mm Hg. At p = 0.005 mm Hg, thermal transpiration was significant (section 2.3.2.1(b)) and the pressure correction[178] required was 0.55 (i.e., $p_{actual} = 0.55 \times p_{measured}$). However, because such a large quantity of gas was adsorbed, non-correction of the pressure resulted in less than a 0.2% error in $(pV/\mathscr{V})_{ads.}$ for all determinations (see Appendix G.2).

The krypton isotherms were sigmoid-shaped in the relative pressure range up to about 0.3 (cf. Fig. G.2-1); they flattened out for the straight middle portion at about $p/P_o = 0.05$ but commenced curving upwards again at about $p/P_o = 0.28$. Above $p/P_o = 0.25$, the experimental points were very scattered about the B.E.T. plots because of the upward trend of the isotherms; desorption was therefore commenced before this relative pressure.

Unfortunately, too much krypton was often added to the sample at a time so that, after the first adsorption point at very low p/P_o, only one or two more adsorption points were obtained for the B.E.T. plot below $p/P_o = 0.25$. Further points obtained

on desorption served to show that the B.E.T. plot was straight. Desorption points were frequently slightly lower than the adsorption plot and often gave a negative intercept. The scatter of the points about the average plot led to a variation of about 6% in the resulting surface area value. Generally, the value of the intercept of the B.E.T. plot was almost zero and less than 1% of the slope value.

Except for Detmns. No. S:3 and No. S:9, when liquid air ($83^{o}K$) and very pure liquid nitrogen ($78^{o}K$) baths were used, respectively, the temperature $\mathcal{T}_b$ of the liquid nitrogen bath was approximately $80^{o}K$. During any determination, $\mathcal{T}_b$ generally increased by less than $0.4^{o}K$; frequent additions of liquid nitrogen and agitation of the bath by a nitrogen stream kept the change in temperature to a minimum.

Although the oxygen vapour pressure thermometer, which was used to measure the liquid nitrogen bath temperature, should give accurate temperature values, it was considered that the measured temperature could be high by up to $0.3^{o}K$ because of difficulties which arose during construction of the thermometer. An error in $\mathcal{T}_b$ of this order meant that P_o was in error by 6% at $80^{o}K$. As p/P_o and $p/V\,(P_o-p)$ were both therefore in error by about 6%, very little error was

involved in the value of V_m.

The initial values of the area S_g determined for the -14/+18 mesh fraction of Acheson "A" graphite were about three times greater than the area determined on the same sample approximately three years later (see Table 4.3-1). For the later determination (No. S:3) on the crushed sample, the B.E.T. plot was anomalous since the intercept was not about zero as was observed for the other measurements and hysteresis effects occurred. For a solid sample of Acheson "A" graphite(Sample No. S2), the area was between the other two values.

For Detmn. No. S:8, a leak to vacuum evidently occurred after the adsorption points had been obtained; the reported area value was calculated from the B.E.T. plot through the adsorption points.

In Detmn. No. S:9, adsorption was very slow as over 6 hr were required for the krypton to equilibrate with the sample after krypton addition to the sample bulb. Frequently, more krypton was added before equilibrium was attained for the previous quantity of krypton. On each adsorption, nearly all the krypton was adsorbed so that p/P_o was still very low (less than 0.01) after eight additions of krypton to the bulb in 30 hr. At this low relative pressure, the total volume of gas adsorbed was much greater than

in previous determinations (3.6 cm^3 or 0.55 cm^3/g at S.T.P. compared with about 0.2 cm^3/g for Detmns. No. S:7 and No. S:8 at the same p/P_o). Because a B.E.T. plot could not be obtained from the adsorption points, a number of which did not represent equilibrium conditions, the final adsorption was continued for 7½ hr when equilibrium was assumed; V_m was then calculated by assuming that the intercept of the B.E.T. plot was zero.

4.4 The Pore Size Distribution Measurements

Pore size distributions were determined by the C.S.I.R.O. for two samples of P.G. 60 graphite, four samples of Acheson "A" graphite, and two samples of Morgan "EY9" graphite. The pressurizing curves of V(r) against p_o (Fig.4.4-1) and the distribution curves of D(r) against r (Fig. 4.4-2) were received from the C.S.I.R.O.[240] as the results of the determinations on these samples. These distributions are considered in section 4.4.1.

For the Impregnated graphites, a series of pore size distribution results, tabulated as the cumulative porosity $\mathcal{E}(r)$ for pores of radius greater than r against d(= 2r), were provided by the A.A.E.C.[241] These distribution results had been determined during an investigation by the A.A.E.C.

into the effect of the different variables arising in the impregnation process (see Appendix A.1) on the pore structure of the final graphite. No details were supplied concerning the particular impregnation treatment of each graphite. The results for graphites No. 100 (probably Morgan "EY9166" base stock), No. 101, No. 107, and No. 112 were chosen as representative of the graphites. From the data provided for these graphites, the pressurizing curves of $\mathcal{E}(r)$ against p_c (see Fig.4.4-3), and the distribution curves of $D(r)/V_t$ against r (Fig.4.4-4) were derived as shown in Appendix H.1. These results are considered in section 4.4.2.

4.4.1 The C.S.I.R.O. Measurements

The pressurizing curves (see Fig.4.4-1) received from the C.S.I.R.O. covered the pressure range from 1 to 30,000 p.s.i.a. The experimental points for all the samples of each graphite were presented and the mean line drawn through the points; only the mean lines are reproduced in Fig.4.4-1. The scatter of the points about the mean line was less than $\pm$ 0.005 cm^3/g showing that good reproducibility was obtained between different samples of the same graphite.

The pore size distribution plots (Fig.4.4-2) were derived from the mean cumulative plots by the C.S.I.R.O.

Two distinct peaks were observed in the distribution plots at r = 200,000 Å and 2000 Å for P.G. 60 graphite, and at r = 24,000 Å and 200 Å for Acheson "A" graphite. For Morgan "EY9" graphite, a sharp peak at r = 4000 Å and a smaller peak at r = 1600 Å were observed.

Above approximately 6000 p.s.i.a., the upward trend of the pressurizing curves was believed to be due to the compression of the graphite sample and of the mercury;[240] in calculating D(r) (see Appendix H.1), the slope of the pressurizing curve $dV(r)/dp_c$ was corrected for this compression. The corrections made represented a compression of about 10×10^{-12} cm^2/dyn, which was of the same order as the compression observed by Cameron and Stacy.[202]

Because no tabulated figures were supplied with the C.S.I.R.O. plots, the accuracy of the distribution results was unknown. Some error was no doubt involved in obtaining the slope of the pressurizing curve at any p_c. A comparison of the cumulative pore volume $\Sigma D(r_i)\,\delta r_i$ estimated from the area under the distribution plot (see Appendix H.2) with the cumulative pore volume $V(r_i)$ obtained from the pressurizing curve provided a check on the accuracy of the distribution plots.

For Acheson "A" graphite, the total estimated volume of 0.215 cm^3/g compared with V_p = 0.190 cm^3/g (0.208 cm^3/g when uncorrected for compression) from the pressurizing curve, a 13% difference. For Morgan "EY9" graphite, a similar difference was observed; however, on reducing the volume contribution of the pores at the sharp peak (r = 4000Å), good agreement was obtained. (This correction was justifiable since the plotting and estimation of the area under such a sharp peak was quite inaccurate). Compared with the reasonable agreement observed for Acheson "A" and Morgan "EY9" graphites, the total estimated volume for P.G. 60 graphite was about twice the value recorded on the pressurizing curve. However, on checking the graphical differentiation of the pressurizing curve, the distribution curve reported by the C.S.I.R.O. was found to be in error; the corrected plot was similarly shaped to the C.S.I.R.O. curve but was plotted with a different ordinate scale. The area under this new curve gave a total pore volume which agreed satisfactorily with that obtained from the pressurizing curve (see Table 4.4-1).

Because of the correction for compression at high pressures, the distribution curves sloped down below r = 200Å and ended at about 100Å even though

there were probably some pores of radius less than 100Å. For the coarse-pored P.G. 60 graphite, the curve ended at 1000Å. The maximum radius to which the distribution curves were plotted was about 600,000Å for P.G. 60 and Acheson "A" graphites, and 7000Å for Morgan "EY9" graphite. However, additional pore volume, which was not shown on the distribution curves because of the small value of D(r), was indicated by the pressurizing curves since V(r) at the pressures equivalent to the maximum pore sizes was not zero. This extra volume was added to the volume estimated from the distribution curve.

4.4.2 The A.A.E.C. Measurements

The pressurizing curves of $\mathcal{E}(r)$ against p_o shown in Fig.4.4-3 were plotted from the tabulated distribution data supplied by the A.A.E.C. The curves for graphites No. 107 and No. 112 showed two steps during the sharp increase in $\mathcal{E}(r)$ at about 1000 p.s.i.a. compared with only one for graphite No. 101; the curve for the base material, No. 100, increased sharply at about 160 p.s.i.a. and was much higher than the other three curves.

By graphical differentiation of the distribution data (see Appendix H.1), values of $D(r_i)/V_t$ as a function of r_i were computed and plotted to give the distribution curve (Fig.4.4-4).

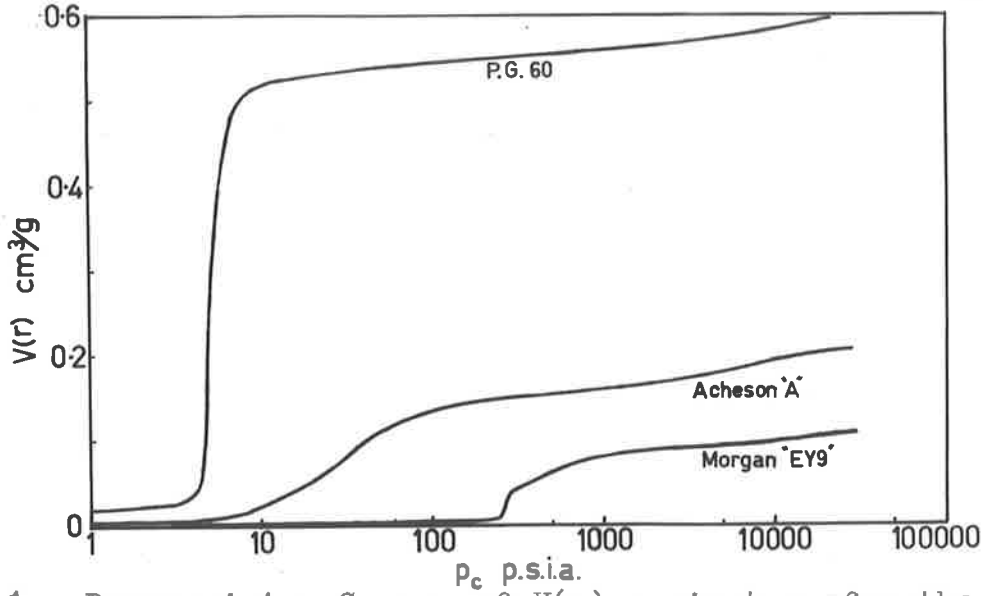

Fig. 4.4-1 Pressurizing Curves of V(r) against p_c for the C.S.I.R.O. Pore Size Distribution Measurements.

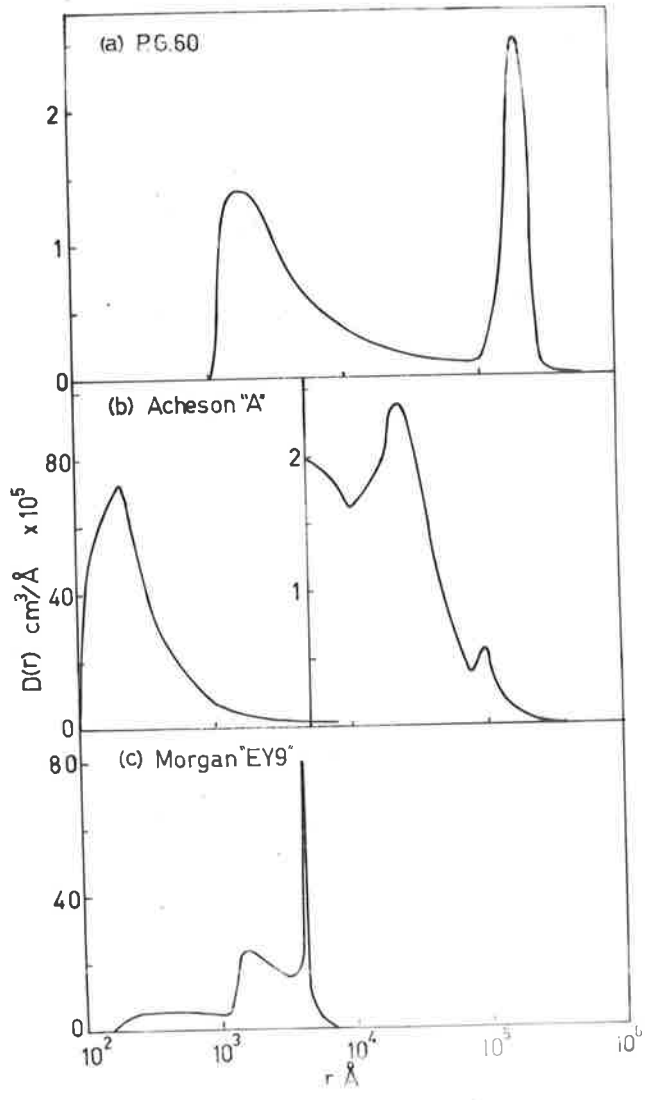

Fig. 4.4-2 Pore Size Distribution Curves of D(r) against r for P.G. 60, Acheson "A", and Morgan "EY9" Graphites as Determined by the C.S.I.R.O.

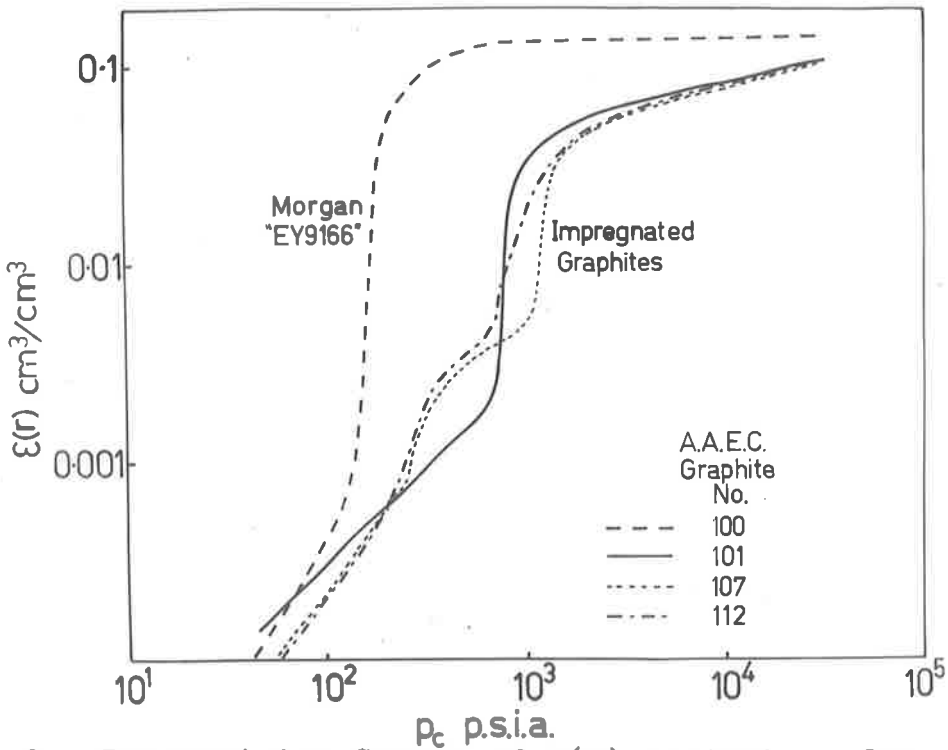

Fig. 4.4-3 Pressurizing Curves of $\varepsilon(r)$ against p_c for the A.A.E.C. Pore Size Distribution Measurements.

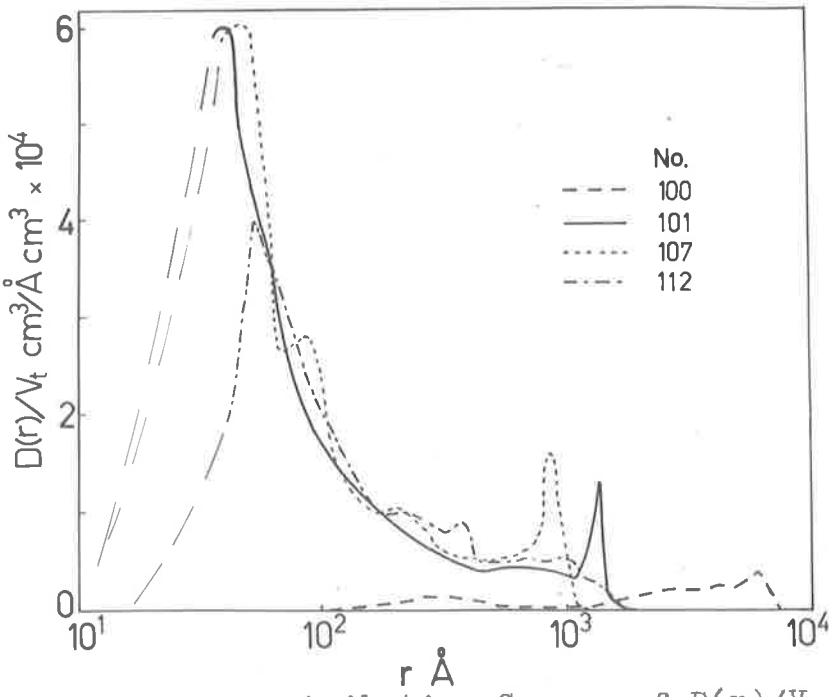

Fig. 4.4-4 Pore Size Distribution Curves of $D(r)/V_t$ against r for Morgan "EY9" (No. 100) and Impregnated Graphite Samples Calculated from the A.A.E.C. data.

Table 4.4-1

Values of the Pore Properties Estimated from the Pore Size Distribution Data

Graphite Grade	Laboratory	Sample Nos.	ε from pressurizing curve	ε corrected for compression	ε estimated	r_m microns	S_g m^2/g	$K\tau^2$(nitrogen) cm^2/sec (p_m in cm Hg)
P.G. 60	C.S.I.R.O.	P31,P32	0.580	0.541	0.545	18.9	0.147	$70.2\ p_m + 51.8$
Acheson "A"	C.S.I.R.O.	P1 to P4	0.321	0.293	0.332	4.46	2.52	$4.86\ p_m + 7.44$
Morgan "EY9"	C.S.I.R.O.	P21,P22	0.183	0.157	0.158	0.310	0.827	$0.00532\ p_m + 0.240$
Morgan "EY9166"	A.A.E.C.	P23	0.143	0.140*	0.141	0.440	0.596	$0.0103\ p_m + 0.312$
Impregnated No. 101	A.A.E.C.	P41	0.108	0.106*	0.110	0.0706	9.61 (4.30)**	$1.12 \times 10^{-4}\ p_m + 0.0391$
Impregnated No. 112	A.A.E.C.	P43	0.106	0.104*	0.105	0.0707	6.14 (4.89)**	$5.82 \times 10^{-5}\ p_m + 0.0375$

* estimated 2% correction

** area for pores of radii greater than 100Å .

For the Morgan "EY9166" base material, a peak was observed at r = 6000Å. For the Impregnated samples, sharp peaks occurred at 1400Å and 900Å for graphites No. 101 and No. 107, respectively, while a plateau was observed between 500Å and 1000Å for graphite No. 112; all these graphites showed very large peaks at about r = 50Å.

Thurstan and Wall[203] reported that the correction for compression effects at the maximum pressure was 0.2% of the total porosity. However it was suspected that the compression above 10,000 p.s.i.a. was greater than 0.2%$\mathcal{E}$ because large increases were observed above this pressure when the pressurizing curves were plotted on linear coordinates. In plotting the distribution curves, correction was made for this compression for the Morgan "EY9166" graphite. For the Impregnated samples, no correction was made; such a correction would only reduce the height of the peaks at r = 50Å by an uncertain amount.

With the distribution curves for the A.A.E.C. samples, the pore volume determined from the area under the curve agreed to about 2% with the total volume filled with mercury at 30,000 p.s.i.a. (see Table 4.4-1).

4.4.3 The Estimation of Pore Properties from the Pore Size Distribution

By graphical integration of the pore size distribution functions, i.e., by summing the areas of a number of small elements (width δr_i) under the distribution curve as described in Appendix H.2, the pore properties such as the porosity ε, the mean pore radius r_m, the surface area S_g, and the permeability $K\tau^2$ (for nitrogen flow at 20°C) were estimated for each graphite sample except Impregnated graphite No. 107. The summations required to calculate these properties, viz., $\Sigma D(r_i)\delta r_i$, $\Sigma r_i D(r_i)\delta r_i$, $\Sigma r_i^2 D(r_i)\delta r_i$, and $\Sigma D(r_i)\delta r_i/r_i$, are summarized for each graphite in Table H.2-1, Appendix H.2; summations over about six intervals of pore radii are included to show the contribution of each interval of pore sizes to the individual properties. The estimated properties and the porosities obtained from the pressurizing curves are tabulated in Table 4.4-1. Comparison of these results with those obtained by other methods will be considered in section 5.6.

With the exception of Acheson "A" graphite, the estimated porosity agreed closely with the value obtained from the pressurizing curve after correction

for compression. With P.G. 60 and Morgan "EY9" graphites, this agreement was only obtained after recalculating the distribution curve, and correcting the area under the distribution curve, respectively (see section 4.4.1).

The agreement between values of the pore properties estimated from the distribution curves for different samples of the same graphite was reasonably good; for Impregnated graphite, excellent agreement was obtained for values of r_m for graphites No. 101 and No. 112. As already mentioned, each C.S.I.R.O. distribution plot represented the mean for penetration tests on several samples of each graphite; hence average pore properties were estimated from these C.S.I.R.O. measurements.

4.5 The Electrical Resistivity Measurements

The graphs of the decomposition potential E_d against the current I for the graphite /0.5N K_2CO_3 and the graphite /N KCl half cells were presented in Fig. 3.5-5. In the resistivity determinations on the P.G. 60 and Acheson "A" graphite samples, the voltage drop ΔE across the saturated graphite sample was certainly much less than E_d for the range of currents studied; however, for the determinations

on the Morgan "EY9" graphite samples (see section 4.5.3), some difficulty was experienced in preventing the graphite from becoming polarized (ΔE greater than E_d).

A type calculation of the formation factor F and the electrical tortuosity factor q for Detmn. No. T:3 (Acheson "A" Graphite Sample No. T2 saturated with N KCl) is presented in Appendix J.2. The values of F and q obtained for each determination are listed in Table 4.5-1, while the average values for each graphite (parallel and perpendicular to the extrusion axis) are summarized in Table 4.5-2.

The first few determinations were performed at 25°C, but all later determinations were made at 30°C since the thermostatted bath was then easier to control during hot weather. The value of the formation factor should not depend significantly upon the temperature of measurement.

4.5.1 P.G. 60 Graphite

Electrical resistivity measurements were performed on two samples of P.G. 60 graphite saturated with N KCl (Detmns. No. T:14 and No. T:15) for I in the range between ± 10,000 μA (ΔE between ± 250 mV); the scatter in ΔE at any I was less than ± 8 mV.

The values of F for the samples whose axes were parallel (No. T31) and perpendicular (No. T32) to the

axis of extrusion were 3.09 and 2.76, respectively. As the 10% difference between these values was of the order of accuracy of the measurements, the anisotropy of P.G. 60 graphite was quite small.

4.5.2 Acheson "A" Graphite

Fifteen electrical resistivity determinations were conducted on eleven Acheson "A" graphite samples. For the first determination (Detmn. No. T:1), the sample (No. T1) was saturated with 0.5 N $K_2 CO_3$, but N KCl was used as the electrolyte for all other determinations. Several determinations were made on reconditioned samples (i.e., the electrolyte was removed from the pores by sucking water through the sample until no electrolyte was found in the discharge and then by distilling the water from the pores into a liquid air trap under vacuum).

Generally, I ranged between $\pm$ 1000 μA (ΔE between $\pm$ 200 mV); at any I, the scatter in ΔE was generally less than $\pm$ 2 mV. After a step change in the current, ΔE reached its new value in a few minutes and then varied slightly about this value because of small fluctuations in the current.

Values of F for Acheson "A" graphite were quite scattered, varying between 18 and 41. For samples whose axes were parallel to the extrusion axis of the

graphite, values of F between 35.5 and 40.9 (average 38.9) and between 18.2 and 23.8 (for Samples No. T6 and No. T8) were obtained. However, the low F values were incorrect since Sample No. T6 was shown by permeability measurements (see later) to have been cut accidentally from the graphite block in the perpendicular direction, while a leak around Sample No. T8 was suspected. Thus, for parallel samples, the average values of F and q were respectively 38.9 and 10.9, with a variation of $\pm$ 8%.

For the samples with their axes perpendicular to the direction of extrusion, values of F ranged between 26.9 and 33.9 with that for Sample No. T6 at about 20. The lower values of F (26.9, 23.8, and 18.2, average 23.0, variation $\pm$ 20%) were presumably for samples cut in one perpendicular direction (2), while the higher values (average 32.2, variation $\pm$ 6%) were for samples cut in the other perpendicular direction (1). The particular perpendicular direction in which the samples were cut was generally not noted when the perpendicular samples were prepared.

The accuracy of both determinations on Sample No.T6 was questionable; in Detmn. No. T:13, the rough degassing of the sample possibly led to only partial saturation with electrolyte and a low value of F, while,

for Detmn. No. T:14, the reconditioning of the sample could have been unsatisfactory. For these reasons, F = 26.9 (Detmn. No. T:24) was considered a more reliable value than F = 23.0 for perpendicular (2) samples of Acheson "A" graphite.

After several determinations had been performed, the results apparently indicated that the value of F was dependent upon the length of the sample. Accordingly, the length of Sample No. T2 was decreased by 16% and a repeat determination (No. T:4) made; however the new value of F was only about 3% lower. Samples No. T3 and No. T4 when joined together gave F = 38.3, but on separation gave F = 39.3 and 33.9, respectively. These determinations, backed by later experiments, showed that the value of F was not dependent on the sample length.

As the F values were scattered with some values being apparantly anomalous, nitrogen permeability determinations were made on a number of the samples. At first, the permeability was determined on the reconditioned samples; however, as the reconditioning process could be unsatisfactory even though care was taken to remove all the electrolyte and water, the permeability of Samples T9, T10, and T11 was determined prior to the resistivity measurements.

Table 4.5-1

Results of the Electrical Resistivity Measurements

Detmn. No.	Sample No.	L/A cm^{-1}	Relation to Extrusion Axis	Solution	R' ohm	Temp. °C	R_o ohm-cm	R_o' ohm	F	q	K (N_2) at p_m = 120 cm Hg cm^2/sec i
P.G. 60 Graphite (ε = 0.54)											
T:15	T31	0.827	Par.	N KCl	20.5	30	8.04	6.64	3.09	1.67	(660 - H:15)
T:14	T32	0.991	Perp.	N KCl	22.8	30	8.33	8.25	2.76	1.49	(770 - H:19)
Acheson "A" Graphite (ε = 0.28)											
T:1	T1	0.983	Par.	N/2 K_2CO_3	482	25	11.98	11.78	40.9	11.43	(6.4 - H:3)
T:2 a	T1	0.983	Par.	N KCl	348	25	8.88	8.74	39.8	11.13	-
T:3	T2	0.357	Perp.	N KCl	102	25	8.75	3.12	32.7	9.15	(13.7 - H:20)
T:4 b	T2A	0.299	Perp.	N KCl	84	25	8.80	2.63	31.9	8.94	-
T:5 c	T3 + T4	0.724	-	N KCl	211	30	7.62	5.52	38.3	10.72	-
T:7 c	T3	0.325	Par.	N KCl	100	30	7.82	2.54	39.3	11.00	6.7 g
T:6 c	T4	0.400	Perp.	N KCl	106	30	7.83	3.13	33.9	9.49	-
T:11	T5	0.862	Perp.	N KCl	228	30	8.34	7.19	31.7	8.87	10.8 g
T:13d	T6 e	0.478	Par.	N KCl	95	30	8.33	3.98	23.8	6.66	14.1 g
T:16a	T6 e	0.478	Par.	N KCl	70	30	8.09	3.87	18.2	5.10	
T:12	T7	0.780	Perp.	N KCl	198	30	8.37	6.53	30.3	8.49	12.5 g
T:17	T8	0.675	Par.	N KCl	116	30	7.76	5.24	22.1	6.19	8.5 g
T:22	T9	0.968	Par.	N KCl	271	30	7.89	7.64	35.5	9.94	10.4 h
T:23	T10	0.760	Perp.(1)	N KCl	195	30	7.88	5.98	32.6	9.13	13.6 h
T:24	T11	1.096	Perp.(2)	N KCl	210	30	7.11	7.79	26.9	7.54	13.4 h
Morgan "EY9" Graphite (ε = 0.15)											
T:10f	T21	0.348	Par.	N KCl	2490	30	4.15	1.44	1720	258	0.083 g
T:19f a	T21	0.348	Par.	N KCl	3340	30	7.78	2.71	1230	184	
T:18f	T23	0.292	Perp.≃	3N KCl	2175	30	3.29	0.96	2270	341	-
T:20	T24	0.467	Par.	N KCl	3246	30	7.96	3.72	874	131	(0.049- H:5)
T:21	T25	0.440	Perp.	N KCl	3200	30	7.55	3.32	964	144	(0.021- H:4)
Impregnated Graphite (ε = 0.11)											
T:25	T41	0.378	-	N KCl	2500	30	7.57	2.86	875	96	(2.5×10^{-4} - H:6) (0.5×10^{-4} - H:14)

Notes: see next page

Notes for Table 4.5-1

a The repeat determination was made on the reconditioned sample.

b The length of Sample No. T2 was decreased while still saturated and Detmn. No. T:4 performed.

c Samples No. T3 and No. T4 were joined with adhesive tape and Detmn. No. T:5 made. While still saturated, the samples were separated and repeat determinations made.

d The sample was only roughly degassed by means of the backing pump.

e Permeability measurements on this sample showed that it was cut perpendicular to the graphite extrusion axis.

f This determination was unfortunately performed at too high a current so that ΔE was greater than E_d and the graphite became polarized.

g The permeability was determined on the reconditioned sample.

h The permeability was determined prior to the resistivity measurements.

i The permeability at p_m = 120 cm Hg as determined during the permeability investigations (section 4.1) is included for comparison.

Table 4.5-2

Summary of Electrical Resistivity Results

Graphite Grade	F (av.)	q (av.)	Percent Variatn.	No. of Detmns.
P.G. 60 Par.	3.09	1.67	-	1
Perp.	2.76	1.49	-	1
Acheson "A" Par.	38.9	10.90	± 8	4
Perp.(1)	32.2	9.01	± 6	6
Perp.(2)	27.0	7.56	-	1
Morgan "EY9" Par.	874	131	-	1
Perp.	964	144	-	1
Impregnated	875	96	-	1

The permeability determinations were made in the high pressure permeability apparatus by the flow method (see section 3.1.4) for p_i between 90 and 290 cm Hg and p_o = 1 atm. The resistivity sample was attached by a rubber sleeve and red sealing wax to a glass adaptor and inserted into the high pressure permeability cell type II for the permeability determinations.

In Table 4.5-1, the nitrogen permeability K at p_m = 120 cm Hg is recorded for those samples on which permeability determinations were made. The values of K at p_m = 120 cm Hg as determined in the high pressure permeability determinations (Nos. H:3 and H:20) for Acheson "A" graphite samples with axes parallel and perpendicular to the extrusion axis were 6.4 and 13.7 cm^2/sec, respectively (see section 4.1.2.2). The permeability measurements indicated that the F values for Samples No. T6 and No. T8 were unreliable as discussed above.

4.5.3 Morgan "EY9" Graphite

In the first three determinations (Nos. T:10, T:18, and T:19) on the Morgan "EY9" and Morgan "EY9166" graphite samples, the graphite was inadvertently polarized as the voltage drop ΔE across the sample was much greater than the decomposition potential E_d at the current I applied to the cell. This meant that the graphite as well as the electrolyte in the pores was conducting current.

In Detmn. No. T:10, ΔE continually changed with time for a given current I, at first increasing very rapidly and reaching a peak after about 20 hr, but then slowly decreasing and approaching a constant value asymptotically (the resistance R' decreased from 10,000 to 3,000 ohm in 30 days). The value of F calculated from the asymptotic value of R' was 1720. It was thought that the change in ΔE was due to the rapid absorption of electrolyte by the graphite surface followed by the slow diffusion of electrolyte into the graphite pores to raise the concentration back to its original value. In order to counteract any absorption effect, Sample No. T23 was impregnated with almost saturated KCl for Detmn. No. T:18. Again ΔE changed with time, R' decreasing from 18,000 to 4,000 ohm in 14 days.

However, when it was observed that ΔE was much greater than E_d at the currents applied (+ 70 μA and + 47 μA), I was reduced to between $\pm$ 20 μA so that ΔE (between $\pm$ 100 mV) was less than E_d. Then ΔE still decreased slightly at any I probably because the graphite was recovering from polarization. Although the resistance R' was decreasing slowly (about 200 ohm (10%) in a week), a value of F (= 2270) was calculated.

In a repeat determination (T:19) on the reconditioned Sample No. T21 saturated with N KCl, ΔE again changed with time because the sample was polarized at + 6 μA,

a current at which ΔE (about 290 mV) was much higher than expected. With I reduced to between $\pm$ 1.2 μA so that ΔE (between + 2 and - 9mV) was less than E_d, the resistance again slowly decreased, the final value of F being 1230.

Extreme care was taken in the next two determinations to prevent polarization. In Detmn. No. T:20 on Sample No. T24, I was kept between $\pm$ 5.6 μA (ΔE between + 12 and - 18 mV) and the value of F = 874 was obtained. At any current, ΔE drifted slightly about the average value, the scatter being $\pm$ 0.5mV at the lowest currents but less at higher currents. When the sample was polarized at 216 μA for 26 min, the value of F remained unchanged. In Detmn. No. T:21, resistance measurements were made in the current range between - 1.2 and + 1.0 μA (ΔE between -34 and +29mV) and a value of F = 964 was obtained for Sample No. T25.

As the accuracy of the results of the first three determinations on Morgan "EY9" graphite was questionable due to the polarization effects, the values of F (874 and 964) for Samples No. T24 and No. T25 were taken as the values for samples whose axes were parallel and perpendicular to the graphite extrusion axis, respectively.

4.5.4 Impregnated Graphite

Because of the difficulty experienced with the

resistivity measurements on Morgan "EY9" graphite by the d.c. method (section 4.5.3), only one electrical resistivity determination (No. T:25) was attempted on an Impregnated graphite sample. Low currents between $\pm$ 7.8 μA were employed and the sample was saturated with N KCl. The potential drop ΔE across the sample continually drifted with time between about $\pm$ 60mV and yet the resistance remained approximately constant at 2500 $\pm$ 300 ohm over a 2 week period. The same behaviour was observed at all currents from 0.45 μA to 7.8 μA. The value of F calculated for this determination was 875.

5. DISCUSSION OF RESULTS

The experimental results, which were presented in section 4, are discussed in this section. The results for gas flow through the reactor graphites indicated the occurrence of several flow phenomena which had apparently not been noted in the literature previously or had only been observed on several occasions. In section 5.1, in addition to a general discussion concerning the gas flow measurements, these phenomena are considered in detail and explanations are attempted.

These special phenomena are:

(i) the high pressure flow effect or the variation of K with p_o (or Δp) at a constant p_m;

(ii) the low pressure transient flow behaviour, when values of the time-lag ϕ increased sharply with decreasing p_m;

(iii) the minima in the K-p_m plots at low pressures;

(iv) the distribution of pressure within a porous medium during gas flow.

In sections 5.2 to 5.5, the measurement of the various pore properties of the reactor graphites is discussed, and the values of the properties obtained for each graphite are compared in section 5.6 with those values calculated from the permeability results.

The main observations and conclusions of the discussion are summarized in section 6.

5.1 The Gas Flow Measurements

The values of the permeability coefficients B_o and K_o for the various graphites were presented in Tables 4.1-1 to 4.1-4. In Table 5.1-1, the average values of these coefficients and of the coefficient β are summarized, together with the standard deviations. These average values are used to estimate values of the pore properties (see section 5.6.1).

5.1.1 P.G. 60 Graphite

In this section, reference is frequently made to the discussion of the high pressure flow phenomenon given in section 5.1.2.4. This phenomenon is considered in detail under Acheson "A" graphite since it was first observed and fully investigated experimentally for this graphite.

5.1.1.1 The Curvature of the K-p_m Plots

The K-p_m plots for the permeability determinations on P.G. 60 graphite samples in the high pressure apparatus were definitely curved towards the p_m-axis. The curvature was more pronounced than that observed for the K-p_m plots for Acheson "A" graphite (section 4.1.2.2).

The curvature of the plots was due to the transition in the flow from viscous to turbulent flow.

Table 5.1-1

Summary of the Permeability Results

Graphite Sample	B_o cm^2 Low Pressure	B_o cm^2 High Pressure $K-p_m$	B_o cm^2 High Pressure $\alpha-\beta$	K_o cm Low Pressure	K_o cm High Pressure	β cm^{-1}
P.G. 60 Graphite		x 10^8		x 10^4		x 10^{-3}
K31 (Parallel)	-	7.90 ± 0.50 (4)	8.57 ± 0.17 (4)	-	4.34 ± 1.64 (4)	5.70 ± 0.26 (4)
		8.24 ± 0.27 (8)				
K32 (Perp.)	-	10.28	10.62	-	1.92 (1)	3.84 (1)
		10.45 ± 0.17 (2)				
Acheson "A" Graphite		x 10^{10}		x 10^6		x 10^{-6}
K2 (Par.)	10.27* ± 0.04 (2)	-	-	3.93 ± 0.10 (2)	-	-
K2A (Par.)	8.64 ± 0.11(5)	7.75* ± 0.55(2)	{8.65* {6.00*	4.06 ± 0.14 (4)	5.97 ± 0.20 (2)	{22.4 { 6.76
K3 (Par.)	8.76 ± 0.13(3)	-	-	4.24 ± 0.09 (3)	-	-
	8.69 ± 0.08 (8)			4.09 ± 0.07 (9)		

Table 5.1-1 Continued

Summary of the Permeability Results

Graphite Sample	B_o cm^2 Low Pressure	B_o cm^2 High Pressure $K-p_m$	B_o cm^2 High Pressure $\alpha-\beta$	K_o cm Low Pressure	K_o cm High Pressure	β cm^{-1}
K4 (Perp.)	17.8(1)	17.0(1)	15.6(1)	5.94(1)	5.87(1)	3.15(1)
K5 (Perp.)	15.2 ±0.6(2)	-	-	5.52 ±0.22(2)	-	-
K6 (Perp.)	16.6(1)	-	-	4.96(1)	-	-
	16.2 ± 0.5 (6)			5.56 ± 0.19 (5)		
Morgan "EY9" Graphite	x 10^{12}			x 10^{7}		x 10^{-10}
K21 (Par.)	4.38 ±0.05(8)	-	-	2.47 ±0.03(8)	-	-
K22 (Par.)	-	3.75(1)*	-	-	2.47(1)	-
	4.38 ± 0.05 (8)			2.47 ± 0.03 (9)		
K24 (Par.) ("EY9166")	4.09(1)	-	-	2.57(1)	-	-
K23 (Perp.)	1.69 ±0.06(2)	1.57(1)	1.61(1)	1.08 ±0.01(2)	0.96(1)	1.35(1)
	1.64 ± 0.04 (4)			1.04 ± 0.04 (3)		

Table 5.1-1 Continued

Summary of the Permeability Results

Graphite Sample	B_o cm^2 Low Pressure	B_o cm^2 High Pressure $K-p_m$	B_o cm^2 High Pressure $\alpha-\beta$	K_o cm Low Pressure	K_o cm High Pressure	β cm^{-1}
K25 (Perp.)	2.42(2) 2.59	-	-	1.30(2) 1.42	-	-
Impregnated Graphite		x 10^{14}		x 10^9		
K41	-	0.110 ±0.011(3)	-	-	0.603 ± 0.029(3)	-
K42	1.12 ± 0.08(4)	0.590 ± 0.025(2)	-	1.89 ± 0.05(5)	2.84 ± 0.31(2)	-

Notes: The values of the coefficients summarized above for each sample are the averages of the values reported in Tables 4.1-1 to 4.1-4 for B_o and K_o, and in Table 5.1-3 for B_o and β. The Standard deviation and the number of determinations taken for each average value are also given.

Where values of B_o and K_o have been determined either for the same sample by different methods, e.g., by low pressure and high pressure measurements, or for different samples of the same graphite, overall averages have been calculated. Not all values are included in the averages; only the more accurate values have been preferred, with values marked with an asterisk* being left out.

Similar curvature in K-p_m or Δp-flow-rate plots for gas flow through coarse-pored consolidated media has been attributed to the transition to turbulent flow by Carlson and Eastman,[153] Leva et al.,[141] Eusner and Shapland,[242] Davidson,[9] and Truitt et al.[243] When Darcy's law ceases to be valid, the resistance to flow increases at a faster rate than does the flow-rate or mean pressure, causing the plots to be curved. Whereas the transition to turbulent flow occurs quite sharply at about N_{Re} = 2000 for flow through straight pipes, it is gradual in porous media because of the wide size distribution of the pores (section 2.1.7).

For the flow of the different gases through Rod No. K31, the curvature was the greatest for the freon plot and decreased as the molecular weight of the gas decreased. This variation in the curvature of the plots was examined by considering the critical Reynolds number at which deviations from Darcy's law commenced. With the critical value of N_{Re} taken as 0.01 (see section 5.1.2.4(g)), the mean pressures at which this Reynolds number occurred for the P.G. 60 determinations were estimated from interpolation of the experimental results, values of N_{Re} having been calculated as shown in section 5.1.2.4. These "critical" values of p_m are given in the following table:

Table 5.1-2
Critical Mean Pressures for P.G. 60 Determinations

Detmn. No.	Gas	Mean Pressures (cm Hg) at: N_{Re}= 0.01	N_{Re}= 0.1	$Q_a p_a$ (cm^3, cm Hg/sec) N_{Re}= 0.01	M/μ at 20°C
H:16	H_2	12.3	62.1	782	0.0023
H:19	N_2	10.9	44.1	319	0.016
H:15	N_2	10.3	41.1	266	0.016
H:18	A	11.2	43.6	228	0.018
H:17	CF_2Cl_2	< 3.5	10.4	38	0.098

The critical p_m (at N_{Re} = 0.01) was the lowest for freon and the highest for hydrogen and indicated that the K-p_m plot for freon would commence curving at the lowest p_m. Comparison of the critical p_m with the p_m estimated at N_{Re} = 0.1 showed that complete turbulence would be reached at a much lower pressure and the pressure range for the transition region would be much smaller for freon flow than for the flow of the other gases. The flow of hydrogen would be completely turbulent only at very high mean pressures. Thus the variation in the curvature of the K-p_m plots for different gases was due to the different rates at which the transition from viscous to turbulent flow occurred, i.e., the different rates at which the

flow-rate (proportional to N_{Re}) changed with pressure in the transition region.

Since the Reynolds number $N_{Re} = B_o \beta \rho_o Q_a p_a / \mu A$ (slip flow neglected) (see 5.1.2.4(c)), the flow-rates $Q_a p_a$ at the critical N_{Re} and at the N_{Re} when turbulent flow was fully developed were both proportional to μ/M. That is, the flow of the gas with the highest value of M/μ (viz., freon) should deviate from Darcy's law and also attain complete turbulence at the lowest flow-rates (and also mean pressures) compared with the flow of other gases. This comparison is demonstrated quite well by the experimental results presented in Table 5.1-2 even though the values of p_m and $Q_a p_a$ for nitrogen (N_2) and argon (A) flow are slightly scattered.

5.1.1.2 The Flow Phenomenon

For gas flow through a sample of P.G. 60 graphite, a separate $K-p_m$ plot was obtained for each set value of the outlet pressure p_o. This phenomenon was also observed for Acheson "A" graphite and is discussed in detail in section 5.1.2.4. For P.G. 60 graphite, the variation in K between the plot for p_o about 80 cm Hg and that for p_o near zero was much greater than for Acheson "A" graphite (for nitrogen flow, 20% cf. 6 to 9%).

The experimental results were examined according to the Green and Duwez approach[126] (section 5.1.2.4(c)).

The values of N_{Re} (slip-corrected) and f, when plotted, gave a good f-N_{Re} graph which agreed with that for Acheson "A" graphite. This graph is shown as Fig. 5.1-1. The values of N_{Re} and f for the P.G. 60 determinations are listed with the detailed results in Appendix K.3. The values of the constants B_o and β (Table 5.1-3) employed to calculate the values of N_{Re} and f for each determination were obtained from a plot of $\Delta pp_m/G^2$ against 1/G (the α-β plot, see 5.1.2.4(d)), while the value of a was obtained as the intercept of the K_v-p_m plot (see Table 4.1-1).

In general, the scatter of the experimental results about the f-N_{Re} plot for the P.G. 60 determinations was quite small. For Detmns. H:15, H:18, and H:19, the f-N_{Re} points agreed very closely with the theoretical curve. However, for freon flow through Rod No. K31 (Detmn. No. H:17), the f-N_{Re} points all lay above the plot (see Fig. 5.1-1). Better agreement with the theoretical f-N_{Re} curve was obtained if the constant a was reduced from 29 to about 17. Consideration of the accuracy of the K-p_m plot for Detmn. No. H:17 showed that the intercept value a could be lower than observed, e.g., about 20; then a = 17 was a plausible value. For hydrogen flow through Rod No. K31 (Detmn. No. H:16), the f-N_{Re}

points below N_{Re} = 0.05 were slightly high but not to the same extent as those for freon flow. A slightly lower value of a, viz., 40 instead of 48, caused better agreement of the results with the f-N_{Re} curve.

5.1.1.3 The Values of B_o and K_o

The average value of B_o determined for Rod No. K31 from the low pressure portion of the K-p_m plots was (7.9 ± 0.5) x 10^{-8} cm^2 (section 4.1.1). The values of B_o obtained for this sample from the α-β plots (see 5.1.2.4(d)) were less scattered, the average value being (8.57 ± 0.17) x 10^{-8} cm^2 (Table 5.1-3). This latter value was the more accurate since the former was susceptible to the inaccuracies of the K-p_m plot at low pressures, viz., the curvature of the plot, the small number of experimental points, and the inaccurate correction of the K values. The K-p_m plot values of B_o for hydrogen and freon flow were low probably because of these inaccuracies but the values of B_o for both nitrogen and argon flow were quite good (8.7 x 10^{-8} cm^2). For nitrogen flow in Rod No. K32, the values of B_o calculated from the K-p_m and α-β plots were quite close, with the average value being (10.45 ± 0.17) x 10^{-8} cm^2.

The values of K_o for Rod No. K31 were very scattered (section 4.1.1). The extremely high value for freon (9.64 x 10^{-4} cm) probably resulted because

of the very large curvature of the K-p_m plot and the inaccuracy of the low pressure K values for Detmn.No. H:17. Consideration of the f-N_{Re} plot for this determination confirmed that the intercept value was high (see 5.1.1.2); the more plausible intercept value (= 17) led to K_o = 5.65 x 10^{-4} cm. Even with this lower value, the K_o values were still scattered.

Because of the general inaccuracy in obtaining the intercepts of the K-p_m plots, the further examination of the K_o values to discover whether K_o was actually a constant or varied for some reason was not worthwhile. Experimental determination of K-p_m plots for gas flow in P.G. 60 graphite samples by a low pressure method (if possible) should give more accurate values of B_o and K_o than high pressure measurements.

5.1.1.4 The Values of β

The values of the inertial resistance coefficient β for Rod No. K31 were fairly close and averaged 5.70 x 10^3 cm^{-1} (standard deviation = $\pm$ 0.26 x 10^3 cm^{-1}); the value for Rod No. K32 was lower at 3.84 x 10^3 cm^{-1} (see Table 5.1-3). The good agreement between the β values for Rod No. K31 showed that β could be taken as a characteristic coefficient of a porous medium (see section 5.1.2.4(i)).

The values of B_o and β for the determinations on

P.G. 60 graphite samples (see Table 5.1-3) were plotted on the $\beta - B_o$ plot of Katz and Cornell[147] (Fig.5.1-2). All of the $\beta - B_o$ points agreed quite closely with this plot, the scatter being much less than that observed for the results of Cornell and Katz.[125]

5.1.1.5 Anisotropy of P.G. 60 Graphite

For nitrogen flow determinations on P.G. 60 graphite samples, greater flow occurred in the direction perpendicular to the extrusion axis of the graphite than in the parallel direction. The values of B_o and K_o were higher while β was lower for the perpendicular sample, Rod No. K32. Similar anomalous results observed for Acheson "A" graphite samples are discussed in section 5.1.2.3. For Acheson "A" graphite, the difference in the values of K for the two directions was 150% compared with only about 20% for P.G. 60 graphite. Thus, the anisotropy of P.G. 60 graphite was less than that for Acheson "A" graphite.

5.1.2 Acheson "A" Graphite

5.1.2.1 The Experimental Methods

The permeability results in section 4.1.2 showed that the pressure decay method was the most suitable of the low pressure methods for determining permeability coefficients for Acheson "A" graphite samples. Although this method was really an unsteady state method

(section 2.1.8.2(d)), the agreement between values of K determined by the low pressure flow and pressure decay methods indicated the validity of the assumption that steady state conditions were closely approximated in the decay experiments on Acheson "A" graphite provided dp_1/dt was relatively small. The values of B_o and K_o obtained by the decay method were considered quite accurate (standard deviations for any determination were 5% and 1%, respectively), even though the scatter of the K values about the K-p_m plot was fairly high ($\pm$ 0.05 cm^2/sec or about $\pm$ 5%) because of the inaccuracies arising during the calculation of these values (see Appendix C.3.3).

Although the pressure increase method proved satisfactory at mean pressures less than about 4 cm Hg, the modified pressure increase method (section 3.1.3.1) had to be employed above this pressure (e.g., Detmn. No. L:18). Although the results obtained in Detmn. No. L:18 were reasonable, the modified pressure increase method was unsatisfactory since it was unlikely that steady state conditions were approximated at the high flow-rates observed. Alteration of the apparatus to include a much larger buildup volume on the outlet side of the sample would enable pressure increase experiments to be performed

at much higher mean pressures for Acheson "A" graphite without resorting to the modified method. Because of the inaccuracy of the pressure equalization method (see section 4.1.2.1), and the difficulty of measuring flow-rates under vacuum conditions for flow determinations (section 2.1.8.2(a)), the pressure decay method was the only really satisfactory method of determining K in the low pressure apparatus above p_m = 4 cm Hg for Acheson "A" graphite.

The good reproducibility of the K-p_m plots determined by different methods for nitrogen flow in the one graphite sample was due to the coarse pore structure of the Acheson "A" graphite, which permitted equilibrium flow to be attained almost immediately after a change in pressure for the unsteady state methods.

Although the values of K determined by the high pressure method for p_m less than 30 cm Hg agreed closely with the low pressure results (see 4.1.2.2), the high pressure slope and intercept values differed from the corresponding low pressure values probably because of the curvature of the K-p_m plots and the small number of experimental points at low pressures for the high pressure determinations. The curvature of the plots was due to the gradual transition from viscous to turbulent flow (see section 5.1.1.1).

5.1.2.2 The Values of B_o and K_o

The good agreement between the low pressure values of B_o for Rod No. K2A showed that B_o was independent of the gas employed and was a constant coefficient of a porous medium. The values of K_o for this sample were more scattered. Hutcheon et al.[34] also observed better agreement between B_o values than for K_o values when investigating the flow of different gases in the one graphite sample.

The variation of the low pressure values of B_o and K_o for the different determinations was due to inaccuracies in the $K-p_m$ plots arising from small experimental errors and errors in measuring the slope of the pressure decay plot (the relative error between different experiments on the same sample was generally less than 4%, but was as great as 9% below p_m = 5 cm Hg). Errors due to non-equilibrium flow were considered negligible (see section 5.1.2.1). The gradual curvature of the $K-p_m$ plots might have caused a small error in the low pressure values of B_o and K_o but would lead to greater errors in the high pressure values.

The B_o and K_o values obtained for Rod No. K2A by the high pressure determinations differed from the low pressure values because of the inaccuracies of the

high pressure plots at low pressures (see 5.1.2.1). While the B_o values obtained from the high pressure $K-p_m$ plot and the $\alpha-\beta$ plot (see 5.1.2.4(d)) for hydrogen flow both agreed with the average low pressure value, the values for nitrogen flow differed widely (section 5.1.2.4(f)). The high pressure K_o values for Rod No. K2A were about 45% higher than the low pressure values.

For hydrogen flow in Rod No. K2A (Detmn. No. L:50), the value of B_o was 35% higher than the average value for the other gases (11.65×10^{-10} cm^2 cf. 8.64×10^{-10} cm^2) but the K_o value agreed with the average K_o value. As the high pressure values of B_o for hydrogen flow (Detmn. No. H:21) agreed quite closely with the average B_o value, it was suspected that a leak from the inlet side of the apparatus occurred during the determination so that the K values at high pressures were too great.

The high values of K_o for carbon dioxide and freon flow through Rod No. K2A (14% and 32%, respectively) were possibly due to the curvature of the $K-p_m$ plots. They were not considered to be caused by surface diffusion or non-ideal behaviour of the gases.

The good agreement generally for the B_o and K_o values obtained for low pressure nitrogen flow through

the different samples where flow occurred parallel to the graphite extrusion axis, viz., Rods K2, K2A, and K3, indicated that the Acheson "A" graphite was apparently homogeneous in this direction. An examination of the K-p_m plots in Fig. 4.1-2 showed that the high value of B_o for Rod No. K2 (Detmns. No. L:7 to No. L:10) was due to the particular scatter of the K values; extension of the determinations to higher p_m may have resulted in a plot of lower slope (and hence a lower value of B_o).

The average low pressure values of B_o and K_o for nitrogen flow through Rods K2, K2A, and K3 were $(8.69 \pm 0.12) \times 10^{-10}$ cm^2 and $(4.06 \pm 0.10) \times 10^{-6}$ cm, respectively. The overall average values for all determinations on these samples were $(8.69 \pm 0.08) \times 10^{-10}$ cm^2 and $(4.09 \pm 0.07) \times 10^{-6}$ cm (see Table 5.1-1). In calculating these average values, the results of doubtful accuracy mentioned above were excluded. For both B_o and K_o, the average values for Rod No. K2A, the average values for nitrogen flow, and the overall average values were almost identical.

The values of B_o and K_o for the samples (Nos. K4, K5, and K6) whose axes were perpendicular to the direction of extrusion were more scattered than those for samples parallel to the extrusion direction.

The high pressure values of B_o and K_o determined for Rod No. K4 (Detmn. No. H:20) agreed with the low pressure values within the observed scatter. The variation of about 20% in the values of B_o and K_o for different samples indicated that Acheson "A" graphite was probably not isotropic in the plane perpendicular to the extrusion axis. If the graphite was considered isotropic, the average values of B_o and K_o were $(16.2 \pm 0.5) \times 10^{-10}$ cm^2 and $(5.56 \pm 0.19) \times 10^{-6}$ cm, respectively (see Table 5.1-1).

5.1.2.3 Anisotropy of Acheson "A" Graphite

For the samples in which flow occurred perpendicular to the extrusion axis of the graphite (Nos. K4, K5, and K6), the values of B_o and K_o were respectively 70 to 100% and 20 to 45% higher than the average values for Rods K2, K2A, and K3 (axes parallel to the extrusion axis). This result was apparently anomalous since, for extruded graphites, the permeability (and also other physical properties) has been reported as greater in the direction of extrusion than in the perpendicular directions.[8,9] This anistropy occurs in graphites because the splintery particles of petroleum coke tend to align with their longest dimension parallel to the direction of extrusion during the graphite manufacturing process.[8]

Similar anomalous results were observed for P.G. 60 graphite samples (section 5.1.1.5).

Because of the anomalous directional variation of the permeability results for Acheson "A" graphite, it was suspected that the graphite was formed by a moulding process, when the coke particles would tend to line up with their longest dimension perpendicular to the moulding pressure.[8] Then the permeability in the direction parallel to the moulding force would be lower than that in the perpendicular directions. However, a communication with the A.A.E.C.,[244] who had supplied the graphites, confirmed that the Acheson "A" graphite had been manufactured by extrusion.

An examination of the extrusion process shows[245] that a billet is distorted during extrusion; the outer layers are held back and much internal shearing occurs after the billet passes through the die. Such internal shearing would surely tend to align the graphite particles parallel to the extrusion direction unless only a small pressure was necessary to force the coke-pitch mixture through the die in the manufacture of the graphite. During the plastic deformation of a metal, the polycrystal grains rotate so that they approach a preferred orientation and the metal is rendered anisotropic.[246]

The directional variation of the results was considered to be due to anisotropy and not to any random inhomogeneity of the graphite. The reproducibility of the permeability results for different samples of the graphite has been good, with 8% and 15% variation in the values of B_o and K_o for the parallel direction, and about 20% variation in these values in the plane perpendicular to the extrusion axis. The permeability determinations on the electrical resistivity samples (see section 4.5.2) indicated greater inhomogeneity of the graphite; however the samples still showed that the permeability in the perpendicular direction was greater than in the parallel direction. As it was most unlikely that any of the permeability samples had been cut from the graphite block in the wrong direction, the anomalous anisotropy of Acheson "A" graphite must be due to some abnormality in the extrusion process.

5.1.2.4 The High Pressure Flow Phenomenon

For gas flow through Acheson "A" graphite at mean pressures above about 100 cm Hg, a separate $K-p_m$ plot could be drawn for each set value of the outlet pressure p_o (see section 4.1.2.2). This phenomenon was also observed for P.G. 60 graphite, the variation in K at any p_m being much greater than

for Acheson "A" graphite (section 5.1.1.2). The phenomenon was definite since the relative error was about 4% whereas the observed total variation in K at p_m = 250 cm Hg for Acheson "A" graphite was 10%.

The variation of K (or G) with p_o or Δp at any p_m has apparently not been observed previously for gas flow in porous media. Most workers either have preferred to correlate their experimental results for flow in the transition region by the Reynolds number-friction factor method or have measured their results over limited ranges of pressures so that the flow phenomenon was not observed. Wallick[247] observed a similar effect for gas flow in capillaries and intimated that Calhoun and Yuster[248] had obtained a similar flow behaviour for fluid flow in ideal porous media.

(a) Possible Explanations of the Phenomenon

Several possible explanations of the phenomenon were considered. Any leakage into or out of the outlet side of the apparatus when p_o was less than or greater than atmospheric pressure would increase or decrease the flow-rate respectively; such changes were contrary to the observed variation in the results. The deviation from ideal gas behaviour for the gases was negligible under the maximum pressure conditions occurring in the determinations. In the transition

between viscous and turbulent flow, the wide distribution of pore sizes in the graphite had no other effect than to cause the curvature of the $K-p_m$ plot.

Because of the high pressure drops encountered in many of the experiments, the validity of the permeability equation $K = Q_m\ p_m\ L/\ \Delta p\ A$ . . .(2.1.1-28) was examined. Carman (ref.5,p.2) indicated that the particular form of Darcy's equation could be integrated to give equation (2.1.1-28) provided K was independent of pressure or Δp was very small. A consideration of the distribution of pressure in a porous medium during flow (see section 2.1.1.6) showed that the equation could be applied in the slip and viscous flow regions where K was a linear function of pressure (= a + bp) even when Δp was large.[17]

In the transition region to turbulent flow, the high pressure experiments have shown that K was not a linear function of pressure. Therefore the use of the permeability equation was apparently invalid at high flow-rates and large Δp. Examination of the high pressure $K-p_m$ plots for Acheson "A" graphite (Fig.4.1-5) showed that the values of K at the commencement of each separate p_o plot (i.e., when Δp was very small) lay on the straight portion of the plot when extrapolated from low to higher mean pressures. This

observation confirmed the invalidity of the permeability equation.

As Darcy's law was therefore not valid when turbulent flow commenced, it was necessary to know the manner in which K varied with p (and perhaps the flow-rate G) in the transition region so that Darcy's law, viz., $$\frac{G}{\rho_o} = K \frac{\partial p}{\partial x} = \Phi (p,G) \frac{\partial p}{\partial x} , \qquad \ldots (5.1.2\text{-}1)$$ in which K was a function of p and G, $\Phi (p,G)$, could be extended to yield a new flow relation. As no satisfactory relation describing flow in the transition region had been previously obtained, an attempt was made to find such a relation which would explain the observed flow phenomenon.

(b) Kinetic Energy Effects

For gas flow through glass capillaries (d_o = 0.07 cm), Wallick[247] observed deviations from Poiseuille's law which could not be attributed to slip flow or turbulence. His results, which varied in a similar manner to those of Detmn. No. H:3, showed that the flow-rate Q_c decreased by about 15% when the mean pressure in the capillary increased from 1 to 6 atm for Δp = 3.0 cm Hg. Wallick intimated that similar deviations had been observed for fluid flow through ideal porous media by Calhoun and Yuster,[248] who explained

the results on the basis of kinetic energy effects. Wallick was able to describe his observed flow behaviour by adding a kinetic energy correction term to Poiseuille's equation.

A consideration of the kinetic energy losses for flow through porous media in the transition region (see section 2.1.7.2(a)) yielded the equation

$$\frac{\rho_o \, p_m \, \Delta p}{LG} = \frac{\mu}{B_o} + \beta G. \qquad \ldots (2.1.7\text{-}3)$$

When this equation was rearranged and a slip correction term included, the expression for K was of the general form

$$K = a + bp_m - c\,G^2/\Delta p, \ldots (5.1.2\text{-}2)$$

where a and b were the intercept and slope of the linear portion of the K-p_m plot, respectively, and $c = b\beta L/\rho_o$. After the constants a, b, and c were determined from the experimental results for Detmn. No. H:3, equation (5.1.2-2) was found to agree fairly well with the experimental K-p_m plot up to about p_m = 150 cm Hg and to give the observed variation of K with p_o at any p_m. Thus, the consideration of kinetic energy effects partially explained the observed flow phenomenon.

The addition of further terms to equation (5.1.2-2) in order to obtain the complete equation of the K-p_m graph proved in vain; all attempted equations resulted

in considerable deviations from the experimental graph over some range of p_m mainly because the form of the additional term was unknown.

(o) The Green and Duwez Correlation

Correlations based upon the Reynolds number concept were considered in order to describe the flow phenomenon. As discussed in section 2.1.7.2(f), the Reynolds number and friction factor were generally unsuitable to represent turbulent flow in consolidated media. The Green and Duwez procedure[125,126,146] was considered the most satisfactory method of correlating experimental results and was accordingly tested upon the Acheson "A" high pressure flow results. This method was based upon kinetic energy losses since it required the calculation of the coefficients α and β from equation (2.1.7-3).

As originally defined by Green and Duwez[126] (see section 2.1.7.2(d)),

$$f = \frac{2\,\Delta p}{\beta \rho\, v^2\, L} = \frac{2\,\rho\,\Delta p}{\beta G^2\, L} . \qquad \ldots (2.1.7\text{-}11)$$

Other authors[125,146] have defined f with different constants. However, for the purposes of correlating the flow through the reactor graphites, the Reynolds number and friction factor were defined by the equations

$$N_{Re} = \frac{\beta G}{\alpha \mu} \qquad \ldots (2.1.7\text{-}10)$$

and $$f = \frac{\rho \Delta p}{\beta G^2 L} \quad . \qquad \ldots (2.1.7\text{-}11a)$$

The Reynolds number as expressed above represented the ratio of the inertial resistance to the viscous resistance,[132] since these resistances respectively equalled $\beta G^2/\rho_m$ and $\propto \mu G/\rho_m$ (see equation 2.1.7-2).

(d) The $\propto - \beta$ Plot

Cornell and Katz[125] determined the coefficients $\propto$ and β from a plot equivalent to $\Delta p\ p_m/LG$ against G (see equation 2.1.7-3). Because of the scatter of the points and the curvature of the graph, the determination of $\propto$ and β from this plot was not accurate (see Appendix D.3). However, a plot of $\Delta p\ p_m/LG^2$ against 1/G (the $\propto - \beta$ plot), which gave $\propto$ as the slope and β as the intercept, was found to be more satisfactory as less scatter was observed between the experimental values for p_o about 0 cm Hg and p_o about 76 cm Hg and more accurate values of $\propto$ and β were determined.

A typical example of the Cornell and Katz and $\propto - \beta$ plots for Detmn. No. H:20 is shown in Fig. D.2-1, Appendix D.2. The curvature observed in the plots at low flow-rates was due to the occurrence of slip flow; the values of $\propto$ and β were determined from the straight line plot through the points for which slip flow was neglibible, i.e., at high flow-rates. When the

flow-rates were not high enough for slip flow to be negligible and separate $\alpha-\beta$ plots were obtained for p_o at 0 and 76 cm Hg, the p_o = 76 cm Hg plot gave the better values of α and β (see Appendix D.3).

(e) Correction for Slip Flow

Values of α and β were determined by means of the $\alpha-\beta$ plot for Detmns. No. H:3, No. H:20, and No. H:21; after calculating values for N_{Re} and f, a logarithmic plot of f against N_{Re} was prepared. Above N_{Re} = 0.1, the f-N_{Re} values for the three determinations lay on a single curve. However, below N_{Re} = 0.1, where viscous flow occurred, the values were scattered below the theoretical line whose equation was f x N_{Re} = 1.

The deviation from the theoretical line increased as N_{Re} decreased, and was greater for the values with p_o near 0 cm Hg than those with p_o about 76 cm Hg. Fig. D.2-2, Appendix D.2, shows the scatter of values in the viscous region for Detmn. No. H:20. The high pressure flow results for P.G. 60 graphite (section 5.1.1.2) similarly deviated from the theoretical line below N_{Re} = 0.1, but the deviations were generally less than for Acheson "A" graphite as the percentage of slip flow at any N_{Re} was less.

When a slip flow correction term was added to N_{Re}, the deviation in the results was eliminated. The

terms $1/(\alpha\mu) = B_o/\mu = b$ in the definition for N_{Re} (equation 2.1.7-10) were replaced by K_v/p_m, where K_v, the permeability coefficient for viscous-slip flow, was expressed by $K_v = a + bp_m$; . . .(2.1.4-1) then N_{Re} was given by the equation

$$N_{Re} = \beta G \left(\frac{a}{p_m} + \frac{B_o}{\mu} \right). \quad . . . (5.1.2-3)$$

The values of the constants a and B_o were obtained from the linear K_v-p_m plot, while β and B_o were determined from the $\alpha - \beta$ plot.

The other authors[125,126,132] who have employed this method of correlating results for flow in the transition region have not found it necessary to correct for slip flow. The experimental results for Acheson "A" and P.G. 60 graphite are apparently the first reported instance where slip flow and inertial flow have been observed to occur in a porous medium simultaneously. Because of the extremely wide pore size distributions in the graphites, slip flow was still occurring in the smallest pores when inertial flow commenced in the largest pores. Examination of Table E.2-2, Appendix E.2, showed that the percentage of slip flow to total flow at $N_{Re} = 0.01$ (the critical N_{Re} at which Darcy's law became invalid - see section 5.1.2.4(g)) was about 10% even for P.G. 60 graphite.

In previous investigations on coarse-pored media with relatively narrow pore size distributions, the contribution of slip flow at the critical N_{Re} was either so small that it could not be observed or was neglected, perhaps erroneously, without any confirmation.

(f) The $f-N_{Re}$ plot

A type example of the determination of values of α and β, the calculation of the values of N_{Re} (slip-corrected) and f, and the plotting of the $f-N_{Re}$ graph for the high pressure flow results of Detmn. No. H:20 is given in Appendix D.2. The values of B_o and β determined by means of the $\alpha-\beta$ plot for gas flow through Acheson "A" graphite (Detmns. H:3, H:20, and H:21) are summarized in Table 5.1-3 together with the appropriate constants for calculating N_{Re} and f. Values of a are recorded in Table 4.1-2. The values of N_{Re} and f for these determinations are listed in the detailed results presented in Appendix K.3.

The results of Detmns. H:3, H:20, and H:21, when plotted as an $f-N_{Re}$ graph (Fig. 5.1-1), gave a curve which was linear in the viscous flow region and curved in the transition region. The $f-N_{Re}$ results for flow through P.G. 60 and Morgan "EY9" graphites also lay on the same curve (see sections 5.1.1.2 and 5.1.3.6 , respectively). Since the results of nine determinations

Table 5.1-3

Values of B_o and β Obtained by the $\alpha-\beta$ Method for the High Pressure Permeability Detmns.

Detmn. No.	Gas	Range of N_{Re}	Slope Y/B_o	B_o cm^2	Intercept βYZ	β cm^{-1}	l^*	m^*	n^*
(a)	Acheson "A"			$\times 10^{10}$		$\times 10^{-6}$	$\times 10^{4}$	$\times 10^{3}$	
	Sample No. K2A								
H:3	N_2	0.0029 - 0.56	118	6.00	0.0345	6.76	2.92	2.28	28.3
H:21	H_2	0.0031 - 0.29	41.6	8.65	0.00845	22.4	1.99	2.18	120.9
	Sample No. K4								
H:20	N_2	0.0008 - 0.53	43.7	15.6	0.0143	3.15	3.28	1.02	69.9
(b)	P.G. 60			$\times 10^{8}$	$\times 10^{5}$	$\times 10^{-3}$	$\times 10^{5}$	$\times 10^{5}$	$\times 10^{4}$
	Sample No. K31								
H:16	H_2	0.0004 - 0.06	0.460	8.12	0.180	5.06	0.39	1.46	55.6
H:15	N_2	0.0006 - 0.52	0.861	8.60	2.80	5.65	3.25	4.14	3.58
H:18	A^2	0.0014 - 0.15	1.107	8.50	4.00	5.67	3.62	5.01	2.50
H:17	CF_2Cl_2	0.028 - 0.60	0.580	9.06	13.5	6.34	23.7	70.4	0.726
	Sample No. K32								
H:19	N_2	0.0017 - 0.20	0.811	10.62	2.20	3.84	2.71	4.01	4.54
(c)	Morgan "EY9"			$\times 10^{-4} \times 10^{12}$		$\times 10^{-10}$	$\times 10^{3}$	$\times 10^{2}$	$\times 10^{2}$
	Sample No. K23								
H:4	N_2	0.0009 - 0.09	4.28	1.61	59.0	1.35	1.43	7.18	1.69

* $N_{Re} = l\, Q_a p_a + m\, Q_a p_a / p_m$ $\qquad f = n\, \Delta p\, p_m / (Q_a p_a)^2$

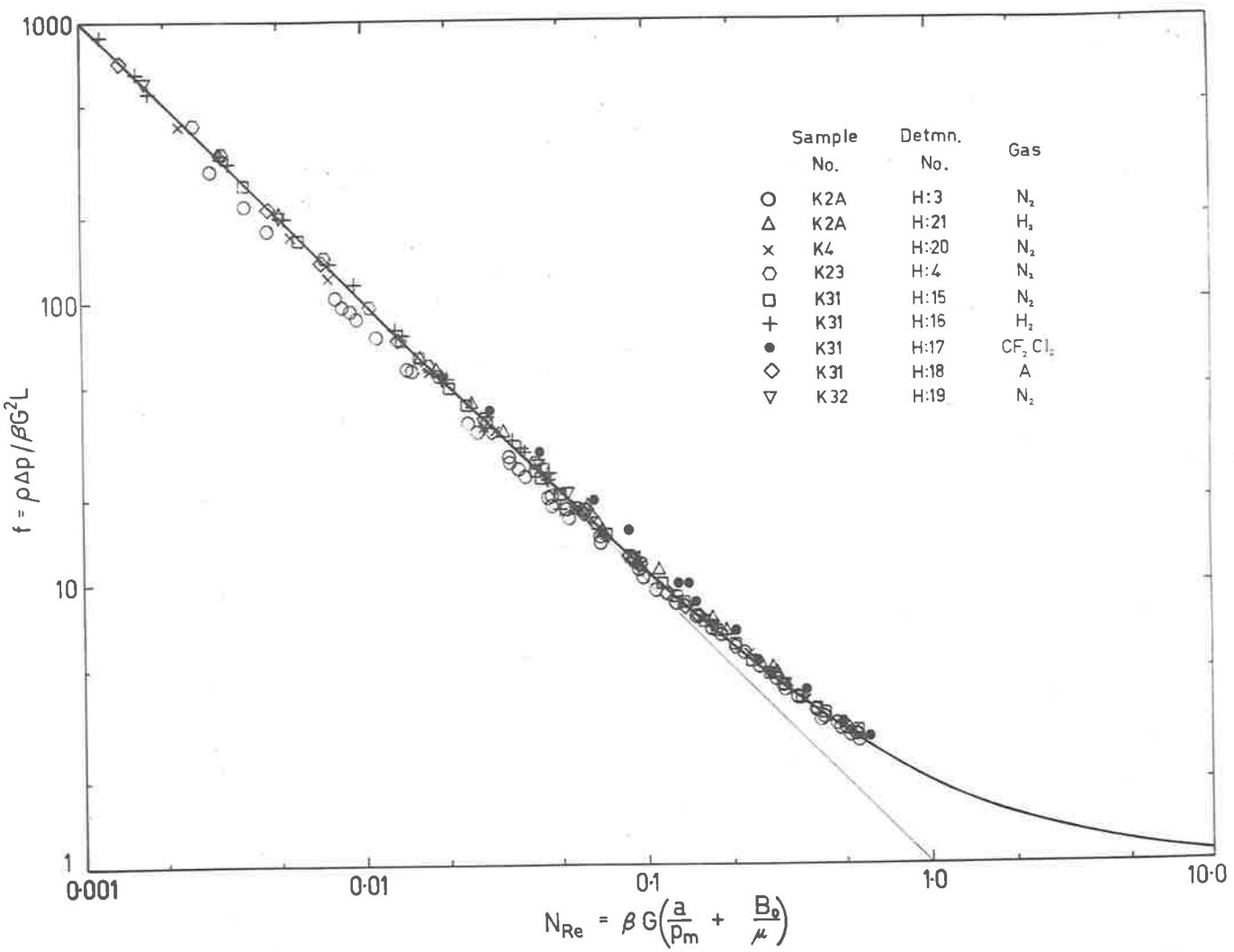

Fig. 5.1-1 The f-N_{Re} Graph for the High Pressure Flow Results for P.G. 60, Acheson "A", and Morgan "EY9" Graphites (Green and Duwez Correlations).

on five graphite samples all closely fitted the one $f\text{-}N_{Re}$ plot, and other authors have obtained similar satisfactory plots by the Green and Duwez method for gas flow in porous metals,[126,132] and in sandstones, limestones, and dolomites,[125] it was established that gas flow through different consolidated porous media could be satisfactorily correlated by this method. Experimental results for various values of p_o all agreed with the $f\text{-}N_{Re}$ graph and showed that the observed high pressure flow phenomenon was satisfactorily described by this method.

For Detmns. No. H:20 and No. H:21, the scatter about the $f\text{-}N_{Re}$ plot was quite small. However, for nitrogen flow through Rod No. K2A (Detmn. No. H:3), the experimental values deviated from the plot because of the choice of the value for B_o. Whereas the value of B_o determined from the high pressure results of Detmn. No. H:3 by means of the $\alpha\text{-}\beta$ plot was 6.0×10^{-10} cm^2, the value of B_o estimated from the slope of the low pressure linear portion of the $K\text{-}p_m$ plot was 7.2×10^{-10} cm^2. As the low pressure value was considered the more inaccurate of the two (see Appendix D.2), $B_o = 6.0 \times 10^{-10}$ cm^2 (with $\beta = 6.76 \times 10^6$ cm^{-1}) was used to calculate values of N_{Re} and f; these values fitted the $f\text{-}N_{Re}$ curve at

high flow-rates when N_{Re} was greater than 0.1. If $B_o = 7.2 \times 10^{-10}$ cm^2 was employed, the experimental results fitted the curve in the low pressure (viscous) region but deviated in the transition region. Both these B_o values were much lower than the value obtained for Rod No. K2A in the low pressure determinations (8.48×10^{-10} cm^2 - Detmn. No. L:33).

Thus B_o apparently changed as the pressure was raised; no such change was observed in other determinations. The 20% change in the value of B_o was possibly due to the compression of the graphite at high pressures, causing the pores to become smaller in size and the permeability to decrease accordingly. In Detmn. No.H:3, the maximum p_m was 476 cm Hg or about 6 atm, which was much higher than the maximum pressures in other determinations on Acheson "A" and P.G. 60 graphites (less than 300 cm Hg for Detmns. H:20 and H:21 for Acheson "A" samples, and less than 200 cm Hg for the determinations on the P.G. 60 graphite samples). For the Morgan "EY9" high pressure determinations (section 5.1.3.6), the maximum p_m was about 1200 cm Hg, but this graphite was less susceptible to compression effects because of the more compact pore structure.

(g) Equation of the Curve

The equation which expressed the f-N_{Re} curve was

$$f = 1 + 1/N_{Re} \qquad \ldots (5.1.2\text{-}4)$$

(compare with the equation given by Green and Duwez[126] for their curve). This equation is plotted in Fig. 5.1-1 as the theoretical curve. The equation tended towards Darcy's law, i.e., $f = 1/N_{Re}$, at low N_{Re} and towards $f = 1$ at high N_{Re}. At $N_{Re} = 0.01$, the difference between the values of f calculated from Darcy's law and equation (5.1.2-4) was 1%. Similarly, at $N_{Re} = 100$, the difference between $f = 1$ and the value from equation (5.1.2-4) was 1%.

Therefore, with the Green and Duwez correlation, it can be assumed that viscous flow occurs below $N_{Re} = 0.01$ (the critical N_{Re}) and complete turbulent flow is reached at $N_{Re} = 100$; between these two Reynolds numbers, a transition from viscous to turbulent flow takes place. At $N_{Re} = 0.01$, Darcy's law ceases to be valid because some of the resistance to flow arises from inertia effects, while complete turbulence occurs at $N_{Re} = 100$ when the viscous resistance is negligible.

By substitution of equations (5.1.2-3) and (2.1.7-11a) into equation (5.1.2-4), various expressions were derived. The pressure gradient $\Delta p/L$ was given by the expression

$$\frac{\Delta p}{L} = \frac{\beta G^2}{\rho_o p_m} + \frac{G}{\rho_o K_v} , \qquad \ldots (5.1.2\text{-}5)$$

where $K_v = a + bp_m$; on rearrangement of equation (5.1.2-5), an equation analogous to the kinetic energy equation (2.1.7-3) was obtained, e.g.,

$$\frac{\rho_o p_m \Delta p}{L G} = \frac{p_m}{K_v} + \beta G , \qquad \ldots (5.1.2\text{-}6)$$

The equation for the permeability coefficient K was

$$K = \frac{p_m K_v}{p_m + \beta G K_v} . \qquad \ldots (5.1.2\text{-}7)$$

Equation (5.1.2-7), which expressed K in terms of p and G for flow in the transition region, was the relation sought after in section 5.1.2.4(a). Previously, no satisfactory expression for K was available for flow in this region. By means of this new equation, the permeability equation (2.1.1-28) was shown to be valid for large Δp when the flow was in the transition and turbulent flow regions (see section 5.1.5.2).

At very high pressures and flow-rates, equation (5.1.2-7) showed that

$$K = K_t = p_m / \beta G , \qquad \ldots (5.1.2\text{-}8)$$

where K_t was the permeability coefficient for turbulent flow, while at very low pressures and flow-rates, $K = K_v = a + bp_m$. In the transition region, viscous and turbulent (inertial) flow occurred in parallel.

Equations (5.1.2-5) to (5.1.2-7) showed that for flow through a porous medium, the pressure drop could be predicted for any flow-rate and mean pressure, while the flow-rate could be calculated when the inlet and outlet pressure conditions were known provided the constants B_o, a, and β could be evaluated for the particular porous medium. Both B_o and β were independent of the gas employed; however, the value of a varied with the temperature and the gas according to equation (2.1.2-6).

For the high pressure Acheson "A" determinations, values of K calculated by means of equation (5.1.2-7) using the experimentally determined values of the constants (see Table 5.1-3) agreed to within 5% with the values of K given by the experimental $K-p_m$ plot. This agreement was very good for predicting the pressure drop for engineering purposes; better agreement would be possible if the constants could be determined with greater accuracy.

(h) Determination of the Values of the Constants B_o, a, and β

As has been previously noted, two plots, viz., the K_v-p_m plot and the $\alpha-\beta$ plot, were required to obtain the constants B_o, a, and β. Unfortunately, experimental results in both the low flow-rate (non-turbulent)

and the high flow-rate (non-slip) regions were necessary so that these graphs could be respectively drawn.

If a slip-corrected α-β plot of $\Delta p \quad p_m/G^2$ against p_m/GK_v (see equation 5.1.2-7) was drawn instead of the previously described α-β plot, a straight line was expected over the whole range of flow-rates with β being obtained from the intercept. Then β could be determined from the low flow-rate results as well as B_o and a. However, a slip-corrected α-β plot, prepared from the results of Detmn. No. H:20, was found to depend upon the accuracy with which the values of B_o and a had been determined from the K_v-p_m plot; inaccurate values led to a curved plot and an error in the value of β of up to 20%. A slip-corrected Cornell-Katz plot resulted in an even more inaccurate value of β as there was considerable scatter about the plot besides the dependence upon the values of B_o and a.

When N_{Re} was less than about 0.5, i.e., when the flow was viscous or almost viscous, f approximately

equalled $1/N_{Re}$; the prediction of the pressure drop or flow-rate by means of either equation (5.1.2-7) or the $f-N_{Re}$ plot was then relatively insensitive to errors in the value of β since both f and $1/N_{Re}$ were proportional to $1/\beta$. For example, at $N_{Re} = 0.2$ for Detmn. No. H:20, a 15% error in β gave less than a 1% error in the calculated flow-rate for flow under known pressure conditions. However, above $N_{Re} = 0.5$, an error in β was of greater consequence as the 15% error in β when $N_{Re} = 1.0$ then resulted in a 6% error in the calculated flow-rate.

Thus the relatively inaccurate values of β, as determined from low flow-rate results by means of the slip-corrected $\alpha-\beta$ plot, were sufficient for calculating Δp or G when N_{Re} was less than about 0.5. Values of β which were accurate enough for most engineering purposes could also be estimated from the $\beta - B_o$ plot of Katz and Cornell[147] (see section 5.1.2.4(i) and Fig. 5.1-2) provided the value of B_o had been obtained from the K_v-p_m plot.

When N_{Re} was greater than 0.5, more accurate values of β obtained from the $\alpha-\beta$ plot were required for accurate predictions of Δp or G. Then experiments were necessary in the regions where turbulent and slip flow were negligible so that the K_v-p_m and $\alpha-\beta$

plots could be prepared, respectively. For rough calculations, the values of β obtained from the slip-corrected $\alpha-\beta$ plot or the $\beta - B_o$ plot were probably adequate.

In the viscous and transition regions, inaccurate values of B_o and a meant that the calculated values of Δp or G were considerably in error.

(i) The $\beta - B_o$ Plot

Stutzman and Thodos[146] presented a plot of the inertial resistance coefficient β against the viscous permeability coefficient B_o; this plot, originally prepared by Katz and Cornell,[147] is shown in Fig.5.1-2 with c.g.s. units for β and B_o. As no individual points were included in the plot of Stutzman and Thodos, the experimental results of Green and Duwez,[126] and Cornell and Katz[125] were plotted in Fig. 5.1-2. These points were scattered about the plot and indicated that the dashed line might be more correct as the mean line than that drawn by Katz and Cornell.[147] However, further experimental data, which were not available to the present author, were probably employed by the latter authors to give the $\beta - B_o$ plot.

The $\beta - B_o$ points obtained from the three flow determinations on the Acheson "A" graphite samples

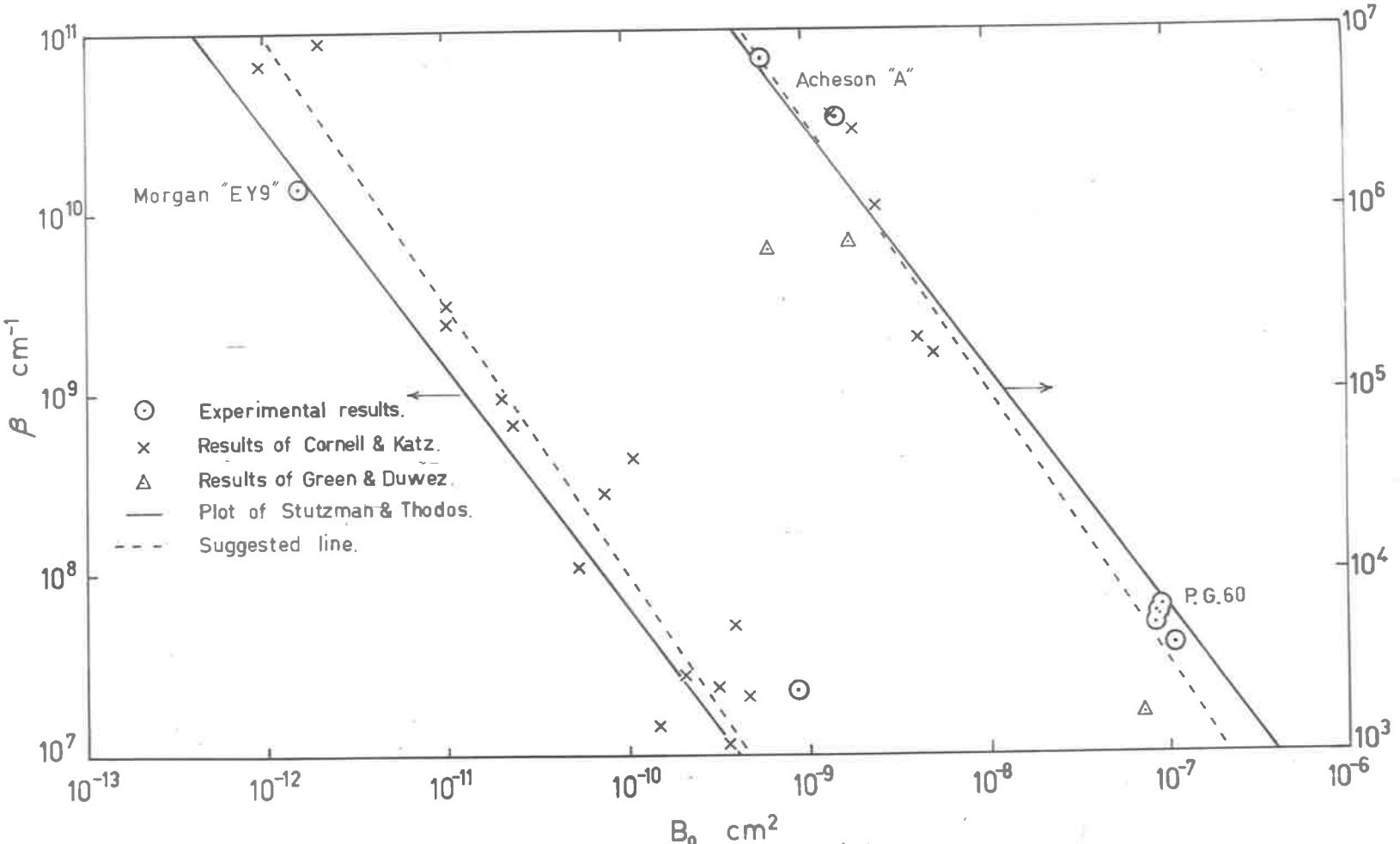

Fig. 5.1-2 The β-B_o Plot of Stutzman and Thodos,[146] showing the Experimental Results for the Reactor Graphite Samples and the Results of Other Authors.[125,126]

(see Table 5.1-3) were plotted in Fig. 5.1-2. The scatter about the mean plot was no greater than that for the results of Cornell and Katz.[125] For Detmns. No. H:3 and No. H:20, the β values agreed quite closely with the $\beta - B_o$ plot at the appropriate values of B_o, but for Detmn. No. H:21, the β value was higher than the predicted value. The β values for P.G. 60 and Morgan "EY9" graphites also closely agreed with the $\beta - B_o$ plot (sections 5.1.1.4 and 5.1.3.6, respectively).

Although β should be a constant for a particular sample, this property was not confirmed by the two scattered values for Rod No. K2A. As the β value (22.4×10^6 cm^{-1}) for hydrogen flow in Rod No. K2A (Detmn. No. H:21) was high (see Fig. 5.1-2) probably because of the small and inaccurate value of the intercept of the $\alpha - \beta$ plot, the value (6.8×10^6 cm^{-1}) obtained for nitrogen flow (Detmn. No. H:3) was taken as the probable value of β for Rod No. K2A. The value of β for a sample whose axis was perpendicular to the graphite extrusion axis (Rod No. K4) was 3.15×10^6 cm^{-1} (Detmn. No. H:20).

Although the values of β obtained for Rod No. K2A were not constant, fairly good agreement was observed between the β values for the flow of different

gases in P.G. 60 Graphite Rod No. K31 (section 5.1.1.4), showing that β could be considered a characteristic coefficient of a porous medium. Cornell and Katz[125] found that the flow results for air, nitrogen, methane, and helium in a sandstone sample all gave the same value of β. Greenberg and Weger[132] showed that β was independent of pressure and temperature in the ranges 60 to 2000 p.s.i. and 15 to 60°C, respectively, for gas flow in porous sintered metals.

(j) The Pore Structure and β

Carman (ref. 5,p.157) has shown that β could be expressed in terms of the porosity ε and surface area S_v if the Kozeny capillary model (section 2.1.3.2(a)) was assumed, e.g.,

$$\beta = \beta_1 S_v / \varepsilon^3; \qquad \ldots (5.1.2\text{-}9)$$

when the tortuosity factor τ was introduced,

$$\beta = \beta_2 \tau^3 / \varepsilon^2 m, \qquad \ldots (5.1.2\text{-}10)$$

where $\beta_1 = \beta_2 \tau^3$, and

β_2 = factor.

Then equation (2.1.7-2), the flow equation uncorrected for slip flow, became equivalent to Ergun's equation[133] (2.1.7-5), with $k_o \tau^2 = 5 \alpha_E$ and $\beta_2 \tau^3 = \beta_E/8$. Ergun[133] deduced that $\beta_1 = 0.29$ for unconsolidated beds. However, Carman (ref.5,p.157) considered that β_1 should be a slowly decreasing

function, i.e.,

$$\beta_1 \simeq 0.4\,(\mu S_v/G)^{0.1} . \qquad \ldots(5.1.2\text{-}11)$$

Cornell and Katz[125] obtained a similar equation to (5.1.2-10). They considered that the factor β_2 was equivalent to the roughness ratio for rough pipes. From their experimental flow results, they correlated $1/\beta_2$ ($= k_2$) against the mean pore diameter d; β_2 ranged from about 3 at d = 30 microns to 400 at d = 0.3 microns.

On the basis of equations (5.1.2-10) and (2.1.4-6), the uncorrected N_{Re} became

$$N_{Re} = \frac{\beta_2 \tau G \quad m}{k_o \ \mu \ \varepsilon} , \qquad \ldots(5.1.2\text{-}12)$$

while the slip-corrected N_{Re} became

$$N_{Re} = \frac{\beta_2 \tau G}{\varepsilon}\left(\frac{m}{k_o \mu} + \frac{4\ \delta_1\ \bar{v}}{3\ k_1\ p_m}\right). \qquad \ldots(5.1.2\text{-}13)$$

When expressed in terms of the pore properties, these groups only apply when the capillary model can be assumed and the Kozeny theory is valid, i.e., for unconsolidated beds. The use of these groups to predict the flow in a porous medium is not satisfactory (see section 2.1.7.2(f)) because of the difficulty of independently measuring the actual values of the pore properties involved in the flow process.

A comparison of the expression for N_{Re}

(equation 5.1.2-12) with the groups employed by other authors (see section 2.1.7.2(c)) showed that the group suggested by MacMullin and Muccini[145] was equivalent to equation (5.1.2-12) but the modified Reynolds number of Blake[142] and Carman[32] should be multiplied by $\beta_2\tau/k_o$ to be consistent with equation (5.1.2-12), i.e., these latter authors did not consider the tortuosity factor τ in their group.

The introduction of the pore size distribution into the β term of the flow equations (5.1.2-5) to (5.1.2-7) in place of ε and m was attempted in the same way as the Kozeny and the Carman-Arnell equations were modified (see section 2.4.3.1) but was found more difficult because of the G^2 term in the equations.

5.1.3 Morgan "EY9" Graphite

5.1.3.1 The Experimental Methods

The results of the low pressure permeability determinations on Morgan "EY9" graphite presented in section 4.1.3.1 indicated that the pressure increase method was the most suitable of the low pressure permeability methods for this graphite. The permeability values obtained by the pressure increase method agreed to about 2% with values obtained by the low pressure flow method. The scatter of the K

values about the K-p_m plots was quite small ($\pm$ 0.5 to 1%) compared with that observed for determinations on Acheson "A" graphite samples by the pressure decay method ($\pm$ 5%).

Although the pressure increase method was not a steady state method since p_o changed with time (see section 2.1.8.2(c)), steady state conditions could generally be assumed as p_o remained less than 1% of p_i for most experiments and straight p_o-t plots were obtained. When curved p_o-t plots were obtained in some determinations because the flow-rate was quite fast or the pressure difference was small, some scatter of the K values was observed as steady state conditions were no longer closely approximated. The values of B_o and K_o determined by the pressure increase method were considered quite accurate, the standard deviations for any determination being generally about 5% and 1%, respectively.

The pressure decay method was unsatisfactory for determining permeability coefficients for Morgan "EY9" graphite samples since the values of K were about 5% lower than those determined by the pressure increase method and were widely scattered about the K-p_m plot because of the inaccuracies in measuring the slope of the decay plot (section 4.1.3.1). For permeability

determinations on Impregnated graphite samples, the difference between the K values obtained by the two methods was much greater (see 5.1.4.1); this difference resulted because of the long time required before steady state flow was attained in the sample after the commencement of flow (about 40 min for nitrogen flow).

For Morgan "EY9" graphite, the time to reach equilibrium flow was not measured. If the observation that the time to reach equilibrium flow was about twice the time-lag ϕ applied for Morgan "EY9" graphite as well as for Impregnated graphite (see section 5.1.4.1 (a)), then the time was from 2 to 4 min for nitrogen flow (Detmn. No. L:24), less than 1 min for hydrogen flow (Detmn. No. L:46), and from 5 to 10 min for xenon flow (Detmn. No. L:45). Equilibrium flow was thus more nearly approached in a decay experiment for Morgan "EY9" graphite than for Impregnated graphite, but the values of K would still be slightly low as was observed. Even the short time of 1 min for equilibrium conditions to be attained for hydrogen flow was sufficient to cause the pressure decay determination to be unsatisfactory (cf. Detmn. No. L:48 with the pressure increase determination No. L:46). This finite time to reach

equilibrium flow would have negligible effect on the pressure increase type experiments where the pressure remained effectively constant with time.

Below about p_m = 300 cm Hg, the high pressure flow method was relatively inaccurate. Flow-rates measured by means of the capillary flow-meter were often in error because the calibration constant decreased below Q_a = 0.03 cm^3/sec and equilibrium flow conditions were not always reached in the capillary; further errors arose from the inaccurate correction of the flow-rate for leakage when p_o was near zero.

5.1.3.2 The Values of B_o and K_o

The agreement between the values of B_o and K_o for the flow of different gases in Rod No. K21 again showed that these coefficients were constant for a particular porous medium. The small maximum variation ($\pm$ 5%) of the individual values from the average values of (4.38 $\pm$ 0.05) x 10^{-12} cm^2 and (2.47 $\pm$ 0.03) x 10^{-7} cm, respectively, and the very low standard deviations demonstrated the relative accuracy of the pressure increase method for measuring permeability coefficients for Morgan "EY9" graphite. Similar variations between the values of B_o and K_o for the flow of different gases in a sample were observed by Ash and Grove[67] for a porous ceramic

(pressure increase method) and Hutcheon et al.[34] for a fine-pore graphite (high pressure flow method), although their results for some gases were more scattered.

In Fig. 5.1-3, the values of the slope b of the $K-p_m$ plots for the different gases are plotted against the reciprocal of the viscosity μ, while, in Fig. 5.1-4, the intercept values a are plotted against $\sqrt{(\mathcal{J}/M)}$. These graphs showed the good linear relations between b and $1/\mu$, and a and $\sqrt{(\mathcal{J}/M)}$ as expected from the theory (section 2.1.4.1). The experimental values fitted straight lines more closely than did the results of Barrer and Grove[65] for flow through a bed of analcite crystals.

The good agreement between the values of B_o and K_o for Morgan "EY9" Rod No. K21 and Morgan "EY9166" Rod No. K24 (about 5% difference) showed the similarity of the pore structure of the "EY9" and "EY9166" grades of Morgan graphite.

The values of B_o and K_o obtained in the high pressure determinations (No. H:5 for Rod No. K22 and No. H:4 for Rod No. K23) were generally about 10% lower than the low pressure values because of the inaccuracy of the high pressure K values below p_m = 300 cm Hg (section 5.1.3.1).

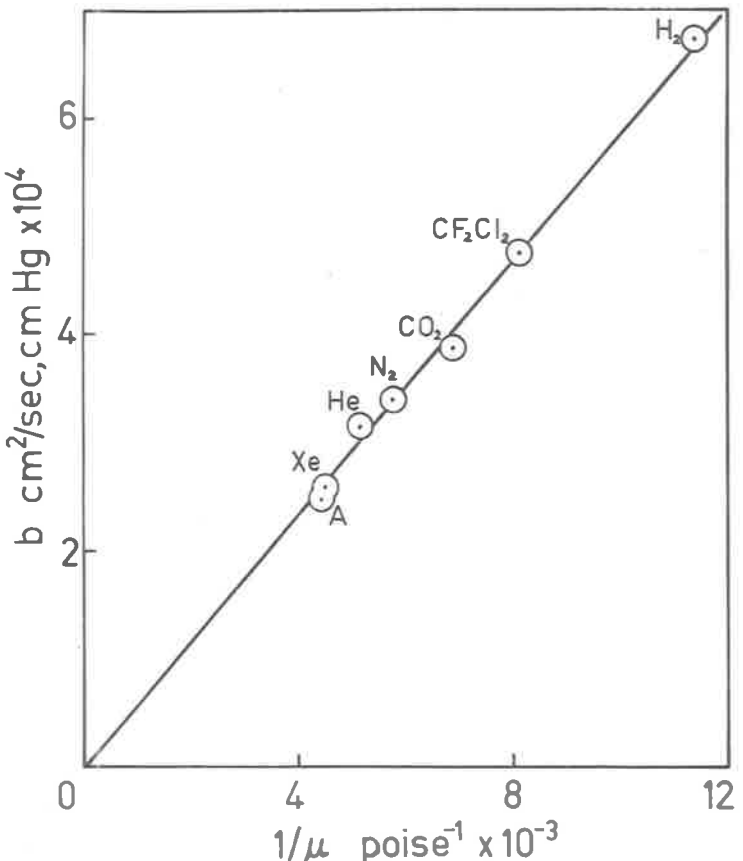

Fig. 5.1-3 Graph of b against $1/\mu$ for the Low Pressure Permeability Results for Morgan "EY9" Graphite Rod No. K21.

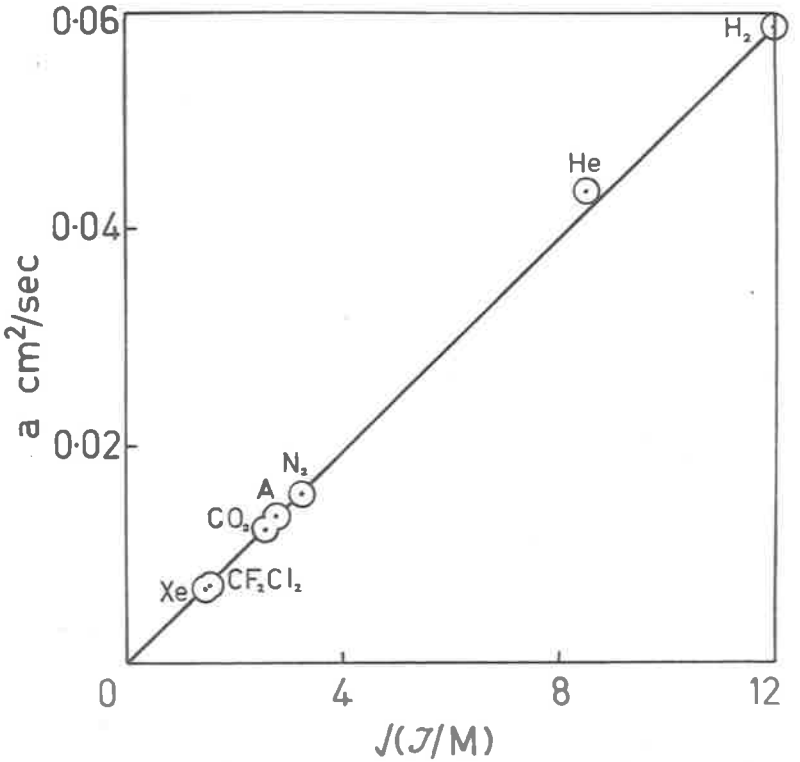

Fig. 5.1-4 Graph of a against $\sqrt{(J/M)}$ for the Low Pressure Permeability Results for Morgan "EY9" Graphite Rod No. G21.

The variation of the values of B_o and K_o for Rod No. K23, whose axis was perpendicular to the graphite extrusion axis, was also quite small (less than ± 5%). The average B_o and K_o values of $(1.64 \pm 0.04) \times 10^{-12}$ cm^2 and $(1.04 \pm 0.04) \times 10^{-7}$ cm (see Table 5.1-1) agreed fairly well with the respective values obtained by Hutcheon et al.[34] for flow perpendicular to the extrusion axis of Morgan graphite samples. The B_o and K_o values determined for the hollow cylindrical sample (No. K25) were much higher than those for Rod No. K23 (section 4.1.3.1) but were suspected to be inaccurate since they were obtained by the pressure decay method.

5.1.3.3 Anisotropy of Morgan "EY9" Graphite

For Morgan "EY9" graphite samples, the permeability values were greater for flow parallel to the extrusion axis of the graphite (Samples K21, K22, and K24) than in the perpendicular direction (Samples K23 and K25). This result was contrary to the results observed for P.G. 60 and Acheson "A" graphites, when the flow in the perpendicular direction was greater (see sections 5.1.1.5 and 5.1.2.3, respectively). However, the anisotropy of Morgan "EY9" graphite was in accordance with the evidence reported in the literature[8,9] for extruded graphites, possibly because this graphite

was finer-pored and of greater density than the P.G. 60 and Acheson "A" graphites and presumably required a higher extrusion pressure in the manufacturing process.

5.1.3.4 Transient Flow Measurements

(a) Time-Lags

For gas flow through Morgan "EY9" graphite samples, the values of the time-lag ϕ were approximately constant or increased slightly with decreasing p_m above about p_m = 4 cm Hg, but increased sharply with decreasing p_m below this pressure (see Fig. 4.1-9). The observed plots of ϕ against p_m closely resembled those obtained by previous investigators[67,101] (see the previous discussion of time-lag measurements given in section 2.1.5.3 (c)), but curved upwards at low p_m for nearly all gases instead of for polar gases only.[67,101]

Since the analysis of time-lag measurements according to Barrer (section 2.1.5.3 (a)) only strictly applied in the Knudsen flow region where the diffusion coefficient was independent of pressure, the intercepts of the ϕ-p_m plots with the ϕ-axis were measured, i.e., the limiting values ϕ_o and ϕ_i at $p_m = 0$ (ϕ_o was the intercept of the extrapolated straight portion of the plot and ϕ_i was the actual intercept made by the curved plot). These values of ϕ for each determination are listed in Table 5.1-4. The values of ϕ_o were readily

obtained from Fig. 4.1-9, and were probably in error by up to $\pm$ 0.1 min because of the scatter of the ϕ values about the plots. On the other hand, the values of ϕ_i were difficult to obtain with much accuracy since the plots approached the ϕ-axis asymptotically and the experimental values of ϕ at low pressures were limited in number and often inaccurate because of the curvature of the p_o-t plots.

The theoretical considerations presented in section 2.1.5.3 (a) showed that $\phi\sqrt{(\mathcal{J}/M)}$ should be a constant for a porous medium provided no adsorption occurred.[67,76,82] For the flow of a range of gases in Rod No. K21, the values of $\phi_o\sqrt{(\mathcal{J}/M)}$ (see Table 5.1-4) were about 3.5 for hydrogen and helium flow but were larger and scattered between 4.6 and 6.0 for the other gases. Even when any possible inaccuracies in the ϕ_o values were allowed for, the values of $\phi_o\sqrt{(\mathcal{J}/M)}$ for hydrogen and helium flow were still lower than those for the other gases. Thus it was suspected that the higher values of $\phi_o\sqrt{(\mathcal{J}/M)}$ for the gases nitrogen, argon, carbon dioxide, freon, and xenon were due to adsorption effects (cf. the results of Barrer and Barrie[82]). Because of the limited number of determinations performed on Rods K23 and K24, no comparisons of the $\phi\sqrt{(\mathcal{J}/M)}$ values were possible.

Table 5.1-4

Limiting Values of the Time-Lags for Morgan "EY9" Samples

Detmn. No.	Sample No.	Gas	ϕ_o min	ϕ_i min	$\phi_o \sqrt{(\mathcal{J}/M)}$	$\phi_o \sqrt{(\mathcal{J}/M)}$
L:46	K21	H_2	0.29	1.6	3.48	19.2
L:44		He	0.42	1.7	3.59	14.6
L:24		N_2	1.43	5.7	4.60	18.3
L:38		A	1.85	10.4	5.07	28.5
L:49		CO_2	2.33	6.5	5.99	16.7
L:47		CF_2Cl_2	3.64	8.5	5.66	13.2
L:45		Xe	3.47	9.4	5.19	14.0
L:35	K23	N_2	1.90	8.1	6.21	26.5
L:37		A	2.48	12.6	6.78	34.4
L:43	K24	N_2	1.20	2.2	3.89	7.2

Table 5.1-5

Calculated Values from Time-Lag Measurements on Morgan "EY9" Samples

Gas	D'_t cm^2/sec	D'_{gt} cm^2/sec	H	K_k* cm^2/sec	$\frac{\varepsilon K_{gs} \eta}{K_{gt}}$	$K_{k_2}\phi_o$ cm^2	$K\phi(av)$ cm^2	$K_{k_2}\phi_i$ cm
H_2	0.607	0.589	-0.03	0.0543	0.092	0.94	1.14	5.20
He	0.419	0.419	0	0.0432	0.103	1.09	1.22	4.41
N_2	0.123	0.158	0.29	0.0155	0.098	1.33	1.51	4.28
A	0.095	0.132	0.39	0.0134	0.101	1.49	1.42	8.37
CO_2	0.076	0.126	0.67	0.0121	0.096	1.69	1.61	4.71
CF_2Cl_2	0.048	0.076	0.58	0.0071	0.093	1.54	1.95	3.60
Xe	0.051	0.073	0.44	0.0069	0.095	1.44	1.70	3.91
N_2	0.061	-	-	0.0069	-	0.79	0.89	3.35
A	0.047	-	-	0.0057	-	0.85	0.91	4.29
N_2	0.075	-	-	0.0162	-	1.17	-	2.14

* From Table 4.1-3

Except for the argon value (80% high), the values of $\phi_i\sqrt{(\mathcal{J}/M)}$ for Rod No. K21 were scattered with a mean value of 16.0 but showed no trend as was observed for $\phi_o\sqrt{(\mathcal{J}/M)}$. The values of ϕ_i were probably too inaccurate for any conclusion to be reached.

(b) Calculation of Diffusion Coefficients by Barrer's Method

Barrer[27] has shown that values of the diffusion coefficient D'_t could be calculated from the values of ϕ by means of equation (2.1.5-8), viz.,

$$D'_t = L^2/6\,\phi. \qquad \ldots(2.1.5\text{-}8)$$

The values of D'_t calculated from ϕ_o for the Morgan "EY9" samples are given in Table 5.1-5. For the flow of a range of gases in Rod No. K21, D'_t decreased as the molecular weight of the gas increased, but not proportionally since the values of the gas phase diffusion coefficient for transient flow D'_{gt}, which were proportional to $1/\sqrt{M}$ and were estimated by means of equation (2.1.5-12) under the assumption that helium was not adsorbed, were greater than the D'_t values.

Equation (2.1.5-10) showed that the difference between the values of D'_{gt} and D'_t was due to the occurrence of adsorption and perhaps surface flow. On the assumption that D'_{st} was negligible, values of the adsorption coefficient H were calculated by means of

equation (2.1.5-10) (see Table 5.1-5). On this basis, adsorption during transient flow was apparently negligible for hydrogen flow (as it was for helium flow), but was significant for the flow of the other gases, being greatest for carbon dioxide flow. If H was greater than zero for helium flow, adsorption would be greater than calculated for all gases but still in the same order as indicated in Table 5.1-5.

It was of interest to estimate the value of τ, the lifetime of a molecule in the adsorbed state, from the equation[101]

$$k_s = \bar{v}\,\tau/4 . \qquad \ldots (5.1.3\text{-}1)$$

With the values of ε and S_v for Morgan "EY9" graphite being 0.15 and 1.03×10^4 cm^2/cm^3, respectively (see section 5.6.2), typical values of the Henry's law constant k_s were calculated (equation 2.1.5-11) as 4.2×10^{-6} for nitrogen and 9.7×10^{-6} for carbon dioxide flow. Then the values of τ were respectively 3.7×10^{-10} sec and 10.4×10^{-10} sec.

The heat of adsorption E_a of the gas on graphite, i.e., the activation energy required by the molecules to be desorbed, was estimated from the period τ_o of the atomic vibrations of the lattice of the graphite by the equation[249]

$$\tau = \tau_o e^{(E_a/RT)} . \qquad \ldots (5.1.3\text{-}2)$$

DeBoer[249] has given τ_o as 5×10^{-14} sec for graphite; then the values of E_a were respectively 5150 and 5750 cal/mol for nitrogen and carbon dioxide adsorption. Because of the assumptions made in the calculations, these values of E_a only indicated the order of magnitude; they were of the same order as those reported previously (ref.5,p.120) for other gas-solid systems.

By means of equation (2.1.5-18), and using the values of K_k(= a) listed in Table 4.1-3, values of the factor $\varepsilon \mathcal{K}_{gs} \eta / \mathcal{K}_{gt} = \varepsilon \mathcal{K}_g$ were calculated for each determination performed on Rod No. K21 (D'_{st} again assumed to be zero); these values, listed in Table 5.1-5, were relatively constant, the average value being 0.097. If η was assumed to equal unity for a first approximation (a reasonable assumption since ε_s/S_s should closely approximate ε/S_v - see equation 2.1.5-15), then the value of ε_s, the pore volume involved in steady state flow per unit bulk volume, was about 0.1 cm^3 for Rod No. K21. The significance of ε_s will be discussed in section 5.6.2.2.

If the calculations described in this section were repeated for the values of ϕ_i , lower values of the diffusion coefficients and an impossible value for ε_s (about 0.4) were obtained. An even greater value of ε_s was obtained when the intercept permeability value K_i

was employed instead of K_k. Hence the use of the extrapolated values ϕ_o in calculating the diffusion coefficients was reasonable.

(c) Assumptions Made in the Calculations

A number of the assumptions made in the Barrer time-lag theory have been discussed previously (section 2.1.5.3 (d)). The theory was only applicable for flow in the Knudsen region where D was independent of concentration (pressure) and time, and its extension to allow for adsorption and surface flow effects was rather dubious. The recommendation has been made (section 2.1.5.3 (d)) that a rigorous mathematical analysis of transient flow should be attempted to allow for all possible flow phenomena.

The diffusion coefficients D'_t calculated in section 5.1.3.4(b) for the Morgan "EY9" graphite samples were effective diffusion coefficients. To calculate the true coefficients D_t, a model pore space must be assumed (ref.5,p.112), e.g., for a capillary pore model,

$$D_t = D'_t \tau^2, \qquad \ldots (2.1.5\text{-}9)$$

where τ = tortuosity factor. Pore properties were calculated from the diffusion coefficients[101] (see section 5.6.1.4) but again the capillary pore model was assumed (equation 2.1.5-13). The structure factor $\mathcal{K}_g$ was readily evaluated but as its true

significance was difficult to assess without the assumption of a generally unsatisfactory pore model, the calculation of ε_s from this factor was not conclusive.

The straight ϕ-p_m plots were extrapolated to zero pressure so that Knudsen flow conditions could be assumed; although the use of the resulting ϕ_o values gave a reasonable value of ε_s, the method of calculation would only be justified as correct when the significance of the ϕ_i values was understood, i.e., when the reason for the upwards curvature of the ϕ-p_m plots at low pressures was explained. Previous investigators[67,101] who observed curved ϕ-p_m plots have employed the values of ϕ_i to make the desired diffusion calculations.

The assumption that H was constant at $p_m = 0$ was probably reasonable since only dilute adsorbed films occurred at very low pressures. However, the validity of the assumption that H = 0 for helium was not so certain; without an independent measurement of H by means of accurate helium adsorption measurements on the graphite, this assumption was necessary in order to calculate the diffusion coefficients. Barrer and Strachan[76] by time-lag measurements, and Maggs et al.[119] by adsorption measurements have shown that helium was

adsorbed to a small extent on carbonaceous materials.

It was suspected that surface flow would be negligible for both transient and steady state flow in the graphites since the surface to volume ratio was too low (see section 2.1.6). As D_{st} must be evaluated by means of equation (2.1.5-10), an independent measurement of H was necessary in order to verify that D_{st} was in fact negligible; the measurement of the adsorption of each gas on the sample at the temperature of the flow experiments would yield the value of the Henry's law constant k_s (and hence H) as the slope of the adsorption isotherm at $p_m = 0$ (cf. the investigations of Barrer and co-workers[76,82,101-103]). If such measurements indicated that D_{st} was not zero, then the values of H would be larger and $\mathcal{K}_g$ smaller than calculated.

Since dead-end pores were expected to occur in both Morgan "EY9" and Impregnated graphites, time effects as discussed in section 2.1.5.3 (b) would presumably affect the results. If the factor a/h introduced by Barrer and Gabor[103] was calculated for helium flow in Rod No. K21, a negative value (-209 sec) was obtained and possibly indicated that the dead-end pores on the average were of larger diameter than the open pores, i.e., η was less than unity.

(d) The Variation of ϕ with p_m

The previous calculations and discussion have been confined to the limiting condition of $p_m = 0$ and the uncertain assumption that H = 0 for helium flow. Previous investigators[67,101] have also confined their considerations to the limiting condition but have employed the intercept ϕ_i in their calculations. At higher pressures, ϕ was definitely dependent upon p_m as shown in Fig. 4.1-9; variation of D'_{gt} and H with p_m was expected at these pressures and possibly caused the slight slope of the ϕ-p_m plots observed above $p_m = 4$ cm Hg. Frisch[108] has given an expression accounting for the concentration-dependence of D but did not consider adsorption effects. At low pressures below $p_m = 4$ cm Hg, the ϕ-p_m plots invariably curved sharply upwards with decreasing p_m and gave an intercept ϕ_i which was greater than ϕ_o.

A comparison of the ϕ-p_m plot with the K-p_m plot for any determination showed that the pressure at which the former plot commenced curving upwards was of the same order as $(p_m)_{min}$, the pressure corresponding to the minimum in the latter plot. For flow in Morgan "EY9" Rod No. K21, the order in which the ϕ-p_m plots commenced curving was from hydrogen and helium at the lowest p_m to xenon and freon at the highest p_m.

This was the same order of variation that was observed for $(p_m)_{min.}$ for the $K-p_m$ plots (see Table 5.1-6). For Impregnated graphite (see 4.1.4.1), the order of variation of p_m for both the $\phi-p_m$ and $K-p_m$ plots was the reverse of that observed for Morgan "EY9" graphite.

The similarity between the plots was significant and possibly indicated that the flow behaviours at low pressures for both transient and steady state flow resulted because of the same effect. Since the high time-lags at low pressures indicated an increased resistance to flow while the high steady state permeability values at similar pressures showed that the resistance to flow had decreased, it appeared that the two effects occurring in the same pressure increase experiment were inconsistent. However, in any experiment at a low pressure (say p_m = 1 cm Hg), the gas took a long time to reach a steady state flow, but when at equilibrium, the gas flow-rate was larger than expected.

(e) Adsorption Effects

Prior to the present transient measurements, the sharp increase in the low pressure values of ϕ with decreasing pressure had only been observed to a limited extent.[67,101] As was noted in section 2.1.5.3(d), the behaviour of the transient flow results is not very well understood. It will be considered in the

following sections.

Barrer and Grove[101] suggested that the sharp increase in the ϕ-p_m plots at low pressures for the flow of the polar gases ammonia and sulphur dioxide through a bed of analcite crystals was due to adsorption of the gases as immobile films; the flattening of the plots at higher p_m was possibly because adsorption ceased to obey Henry's law and approached saturation. For these two gases, they calculated values of the Henry's law constant k_s from the intercept values ϕ_i but did not consider the ϕ values at higher p_m. No adsorption effects were observed for the flow of other gases, since $\phi_i\sqrt{(\mathcal{J}/M)}$ was constant.

According to the suggestion of Barrer and Grove,[101] the adsorption coefficient H (or k_s) decreased as p_m increased, i.e., the adsorption isotherm was not straight but curved concavely towards the pressure axis with increasing adsorption (a Type II or Type IV isotherm of the Brunauer classification[176]). If H became constant above a certain p_m (i.e., the adsorption isotherm became straight), then equation (2.1.5-10) showed that this variation of H would cause D'_t to increase and hence ϕ to decrease with increasing p_m until D'_t and ϕ became approximately constant when H

was constant. Thus the decrease in the value of H with p_m in this manner could lead to a ϕ-p_m plot of the shape observed experimentally.

The adsorption results of Carman and Raal[107] for n-butane on Linde silica at -10°C demonstrated the type of adsorption isotherm and H-p_m plot discussed above (H ≡ Carman's β). Their plots of the effective diffusion coefficient D' against the adsorbate concentration y (y = constant x H p) showed that D' increased initially but then became approximately constant or gave a minimum before increasing sharply in the capillary condensation region. By means of equation (2.1.5-8), values of the time-lag ϕ were back-calculated from D'; the ϕ-p_m plot so derived was found to be approximately straight above p = 10 cm Hg but to curve sharply upwards below this pressure in a similar way to the plots obtained for transient flow in the graphite samples. Even though surface flow occurred for the system of Carman and Raal[107], their results confirmed that the low pressure effect observed for the ϕ-p_m plots could result when the adsorption isotherms were of Type II or Type IV.[176]

Barrer and Strachan[76] reported that the adsorption isotherms for Carbolac porous plugs at about room temperature were approximately linear over their

experimental pressure range and gave constant values of k_s; the ϕ-p_m plots observed for these plugs were then horizontal, and K was also independent of p_m. Thus the manner in which ϕ varied with p_m depended upon the particular shape of the adsorption isotherm, i.e., the way in which the slope of the isotherms varied with p_m.

A comparison of the experimental ϕ-p_m plots for the graphite samples with those derived from the results of Carman and Raal[107] showed that the adsorption isotherms at about 20°C for all gases on Morgan "EY9" graphite were evidently of Type II or Type IV of the Brunauer classification.[176] Even hydrogen and helium showed evidence of adsorption (cf. results of Barrer and Strachan[76]). The results of Barrer and Grove,[101] and Ash and Grove[67] showed that only polar gases were adsorbed to any marked extent for their porous samples.

(f) Application to the Viscous Flow Region

The conclusion that the shape of the ϕ-p_m plot depended upon the variation of H with p_m was based on Barrer's time-lag theory (section 2.1.5.3(a)), for which both D'_t and H should be independent of p_m. Therefore the application of equations (2.1.5-8) and (2.1.5-10) was not strictly valid when these quantities varied with p_m, i.e., in the viscous-slip flow region.

The equation relating the time-lag ϕ to the effective diffusion coefficient D'_t (equation 2.1.5-8) was obtained from the solution to the differential flow equation (2.1.5-6) and was only applicable when D'_t was a constant. Carman and Raal[107] kept Δp small for their experiments so that the theory could be used. Ash and Grove[67] apparently found that equation (2.1.5-8) was applicable for non-sorbed gases in the viscous flow region. However, as it was suspected that ϕ would always be related to D'_t in some way no matter whether D'_t was constant or not, the deductions concerning the shape of the ϕ-p_m plot were qualitatively correct. The solution of the unsteady state flow equation (2.1.5-6) for a variable D'_t as well as for adsorption effects would give the actual relation between ϕ and D'_t.

Carman[107] has pointed out that equation (2.1.5-10) applied when D' and H varied provided Δp was small enough during a measurement to assume the constancy of these quantities. From a consideration of the distribution of pressure in a porous medium (see section 5.1.5.2), it was shown that the permeability equations could be integrated when K was dependent on pressure and Δp was large since at $p = p_m$, $\partial p / \partial x = \Delta p / L$. For similar reasons, it was possible

to derive equation (2.1.5-10) from the expression

$$D'_t \frac{\partial c}{\partial x} = D_{gt} \frac{\partial c_g}{\partial x} + D'_{st} \frac{\partial c_s}{\partial x}, \quad \ldots (5.1.3\text{-}3)$$

where $c = c_g + c_s$.

c_g = gas phase concentration/unit bulk volume,

and c_s = adsorbed phase concentration/unit bulk volume,

for the conditions of variable D' and H and a large Δp, since the gas concentration was directly proportional to the pressure p (equation 2.1.6-3) and $H = \partial c_s / \partial c_g$. The equation only applied at $p = p_m$ and so required values of D' and H at the mean pressure.

Although the application of equation (2.1.5-10) was therefore valid when D'_t and H were pressure-dependent, the validity of equation (2.1.5-8) was doubtful. Hence, until the time-lag theory has been extended to the viscous flow region, the theory must be assumed to apply in this flow region and the derived results considered only qualitatively.

If D_{gc}, the diffusion coefficient for the capillary model, was defined to include a viscous term (cf. equation 2.1.2-9), then equation (2.1.5-18), viz.,

$$K/\varepsilon = \mathcal{K}_g D'_{gt} + \mathcal{K}_s H D'_{st}, \quad \ldots (2.1.5\text{-}18)$$

where $\mathcal{K}_g = \mathcal{K}_{gs} \eta / \mathcal{K}_{gt}$, and

$\mathcal{K}_s = \mathcal{K}_{ss} / \mathcal{K}_{st}$,

was shown to be applicable in the viscous-slip flow region where D' and H were pressure-dependent. The time-lag ϕ was introduced into equation (2.1.5-18) by means of equations (2.1.5-8) and (2.1.5-10) so that

$$6\,K\phi = L^2\,\varepsilon(1 + H)\,\mathcal{K}_g + \varepsilon\phi\,H\,D'_{st}\,(\mathcal{K}_s - \mathcal{K}_g); \quad \ldots (5.1.3\text{-}4)$$

this new equation was dependent upon the validity of equation (2.1.5-8) in the viscous flow region (see above). If $D'_{st} = 0$ or $\mathcal{K}_s = \mathcal{K}_g$, then

$$6\,K\phi = L^2\,\varepsilon(1 + H)\,\mathcal{K}_g. \quad \ldots (5.1.3\text{-}5)$$

When H = 0, equation (5.1.3-5) was equivalent to equation (2.1.5-19), which was obtained[67] for constant D'_t.

(g) The Product $K\phi$

Ash and Grove[67] found that the product $K\phi$ remained substantially constant with p_m for the flow of most gases in a porous ceramic even when the flow was in the viscous-slip region. The values of $K\phi$ tended to be high for some gases at very low pressures and decreased slightly as p_m increased; this variation can be explained from equation (5.1.3-5) by the variation of H with p_m. Their result that adsorption was negligible for all except the polar gases could be in error.

Values of $K\phi$ were calculated for each pressure

increase determination on the Morgan "EY9" graphite samples and the average values taken (see Table 5.1-5). The average values for Rod No. K21 increased as the molecular weight of the gas increased and showed no signs of constancy as observed by Ash and Grove[67]. As the scatter of the individual $K\phi$ values about the average value for any determination was very large ($\pm$ 10 to 20%), any trend of $K\phi$ with p_m was not noted. Below $(p_m)_{min.}$, the values of K and ϕ and hence $K\phi$ increased rapidly with decreasing p_m because H became very large (see section 5.1.3.4(h)); these values of $K\phi$ were not included in the average values.

For any determination, the value of $K_k \phi_o$ (see Table 5.1-5) roughly equalled the average value of $K\phi$. Although the quantity $K_k \phi_o \times 6 \mathcal{K}_{gt} / \mathcal{K}_{gs} \eta \varepsilon L^2$ was about unity for hydrogen and helium flow in Rod No. K21, it did not necessarily indicate that adsorption was negligible (cf. equation 2.1.5-19) since H had already been assumed zero for helium flow. For the other gases, this quantity was greater than unity. The values of $K_k \phi_i$ were much greater than the $K_k \phi_o$ values.

(h) The Adsorption Isotherm

Equation (5.1.3-4) showed that the structure factors $\mathcal{K}_g$ and $\mathcal{K}_s$ could be evaluated if K, ϕ, H, and D'_{st} were known. The values of K, ϕ, and H were measured directly,

while the value of D'_{st} was obtained from equation (2.1.5-10), D'_{gt} being estimated from the time-lag for a non-sorbed gas by means of equation (2.1.5-12). If a capillary pore model was assumed permitting values of the factors $\mathcal{K}_g$ and $\mathcal{K}_s$ to be assessed, then the measurement of K and ϕ by steady state and transient flow determinations on the same porous sample, respectively, enabled the evaluation of H, and hence the plotting of the adsorption isotherm. By similar reasoning, Barrer and Strachan[76] showed that adsorption isotherms in the Henry's law region could be measured by flow methods and were in good agreement with those obtained by direct measurement.

For several of the pressure increase determinations on Morgan "EY9" Graphite Rod No. K21, equation (5.1.3-5) was applied and values of (1 + H) and hence H were calculated from the product $K\phi$ at the p_m for each experiment. Surface flow was assumed to be negligible and $\mathcal{E}\mathcal{K}_g$ was taken as 0.1 (i.e., $\mathcal{E}_s = 0.1$, cf. section 5.1.3.5(b)) so that H was always positive but was negligible for helium flow for p_m = 4 to 10 cm Hg. It was considered that H could not be negative since then gas would be desorbed from the graphite as p_m increased. If $\mathcal{E}\mathcal{K}_g$ was less than 0.1, then H would be greater than the values calculated and would indicate

that more gas was adsorbed. If D'_{st} was not zero, then the values of H would be greater than those calculated.

The plots of H against p_m for helium, nitrogen, and freon flow in Rod No. K21 are presented in Fig. 5.1-5. The values of H decreased rapidly at first as p_m increased, but then passed through a minimum and commenced increasing slowly. These plots were similar in shape to those reported by Carman and Raal[107] although the H values were much less (1 to 3 compared with 100 to 3000). This similarity indicated that the assumptions made in obtaining the H-p_m plots for Morgan "EY9" graphite were reasonable.

The volume of gas adsorbed y (cm^3 at S.T.P/g) was calculated at different p_m by graphical integration of the plots in Fig. 5.1-5. The conversion factor in obtaining the units of y was

$$\Delta y = H \Delta p \, \varepsilon \mathcal{V} / \rho_b \mathcal{R} \mathcal{T} = 1.15 \times 10^{-3} H \Delta p,$$

since $\mathcal{V} = 22.4 \times 10^3$ cm^3/g-mol,

$\varepsilon = 0.16$ cm^3/cm^3 (Table 5.6-5),

$\rho_b = 1.72$ g/cm^3 (Table 5.6-4), and

$\mathcal{R} = 6236$ cm^3, cm Hg/^oK, g-mol.

The resulting cumulative plots of y against p_m were the isotherms for helium, nitrogen, and freon adsorption on Morgan "EY9" graphite near room temperature (see Fig. 5.1-6).

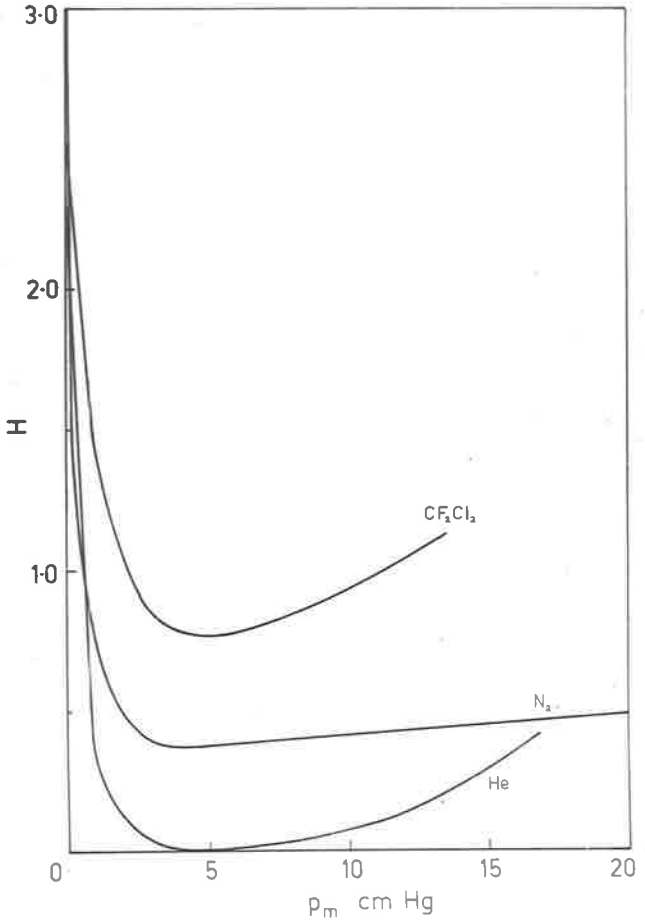

Fig. 5.1-5 Graphs of H against p_m for Helium, Nitrogen, and Freon-12 Adsorption on Morgan "EY9" Graphite Rod No. K21 Derived from the Time-lag Results.

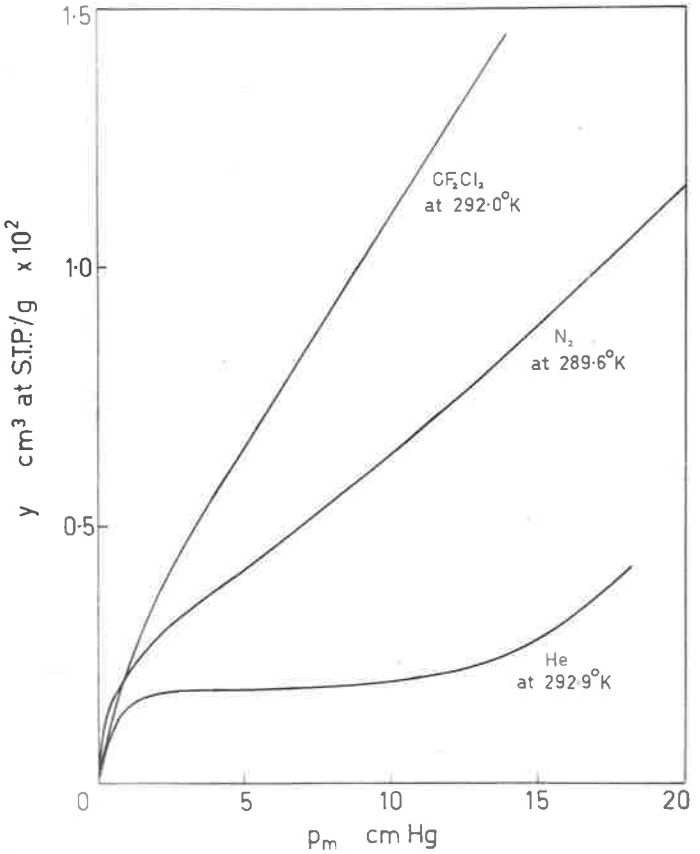

Fig. 5.1-6 Adsorption Isotherms of y against p_m for Helium, Nitrogen, and Freon-12 Adsorption on Morgan "EY9" Graphite Rod No. G21 at Room Temperature.

Of the three gases, freon was adsorbed to the greatest extent and helium to the least, the same order as given in Table 5.1-5. The isotherms were of similar shape to those presented by Carman and Raal[107] for n-butane adsorption on Linde silica at -10°C. They were of Type II or Type IV of the Brunauer classification[176] and showed a hump or knee at about p_m = 2 cm Hg.

The independent measurement* of adsorption isotherms at room temperature for these gases and Morgan "EY9" graphite would confirm the validity of the assumptions made. Generally, the measurement of the adsorption of small gas volumes is difficult[101]; a very sensitive gravimetric method would be required, e.g., for nitrogen adsorption on Morgan "EY9" graphite at room temperature, the apparatus should be able to detect the adsorption of 10^{-6} g of adsorbate /g of graphite.

Since the surface area of the Morgan "EY9" graphite was 0.6 m^2/g (see section 4.3), and the cross-sectional area of the freon molecule σ at room temperature, calculated from the formula[177]

---

* Adsorption measurements with a sensitive gravimetric balance by Mr. D.Williams showed that about 0.1 cm^3 at S.T.P/g of argon were adsorbed by a Morgan "EY9" graphite sample at p = 20 cm Hg. This volume of gas was about 10 times larger than that estimated from the flow measurements possibly because of the more stringent outgassing conditions (heated at 640°C and cooled in argon) for the adsorption measurements.

$$\sigma = 1.091\,(M/N_L\rho_l)^{2/3}\,, \qquad \ldots(5.1.3\text{-}6)$$

where N_L = Avogadro's number, and

ρ_l = bulk density of liquid freon,[250]

was 30.a$Å^2$, the monolayer capacity V_m was calculated from equation (2.3.2-2) to be about 0.07 cm^3 at S.T.P./g. This was much greater than the adsorbed volumes estimated from the flow measurements; for freon flow, V_m would be reached at about p_m = 70 cm Hg or p_m/P_o = 0.17. For krypton adsorption on Morgan "EY9" graphite at - 193°C (see Fig. G.2-1 , Appendix G), V_m was reached at p/P_o = 0.005.

(i) The Physical Significance of the Adsorption Effects

The calculation of the adsorption isotherms for Morgan "EY9" graphite from the values of the product $K\phi$ demonstrated that the low pressure transient behaviour was caused by adsorption effects. These effects could be described mathematically by equation (2.1.5-10); their physical significance is discussed below.

In the pressure increase experiments, the transient or unsteady state flow occurred prior to the attainment of equilibrium steady state flow in the graphite sample. Initially the sample was at a vacuum and so some time was necessary before the steady state pressure and surface concentration distributions were set up. For

viscous-slip flow, the equilibrium pressure distribution was parabolic in shape and was expressed by equation (2.1.1-13) (see section 2.1.1.3).

At any point in the porous medium, the concentration gradient in the adsorbed phase $\partial c_s / \partial x$ was related to the gas phase pressure gradient $\partial p / \partial x$ by

$$\frac{\partial c_s}{\partial x} = \frac{H \varepsilon}{\mathcal{R} \mathcal{T}} \frac{\partial p}{\partial x} \quad . \qquad . \; . \; . \; (5.1.3\text{-}7)$$

If H was constant over the pressure range p_i to p_o in the sample, then $\partial c_s / \partial x$ would be a constant fraction of $\partial p / \partial x$ and the equilibrium surface concentration distribution, plotted dimensionlessly, would be the same as the pressure distribution. However, if H varied, then the surface concentration distribution would be more curved than the pressure distribution. This is demonstrated by the following theoretical considerations.

Dimensionless pressure and surface concentration distributions were calculated for nitrogen flow in a Morgan "EY9" sample (a/b = 50) for the pressure conditions p_i = 1/2, 1, 2, 5, and 10 cm Hg and p_o = 0 cm Hg. The pressure distributions were calculated by means of equation (2.1.1-13) and were almost linear for the pressure conditions considered, the distribution for p_i = 10 cm Hg being the most curved (see Fig. 5.1-7).

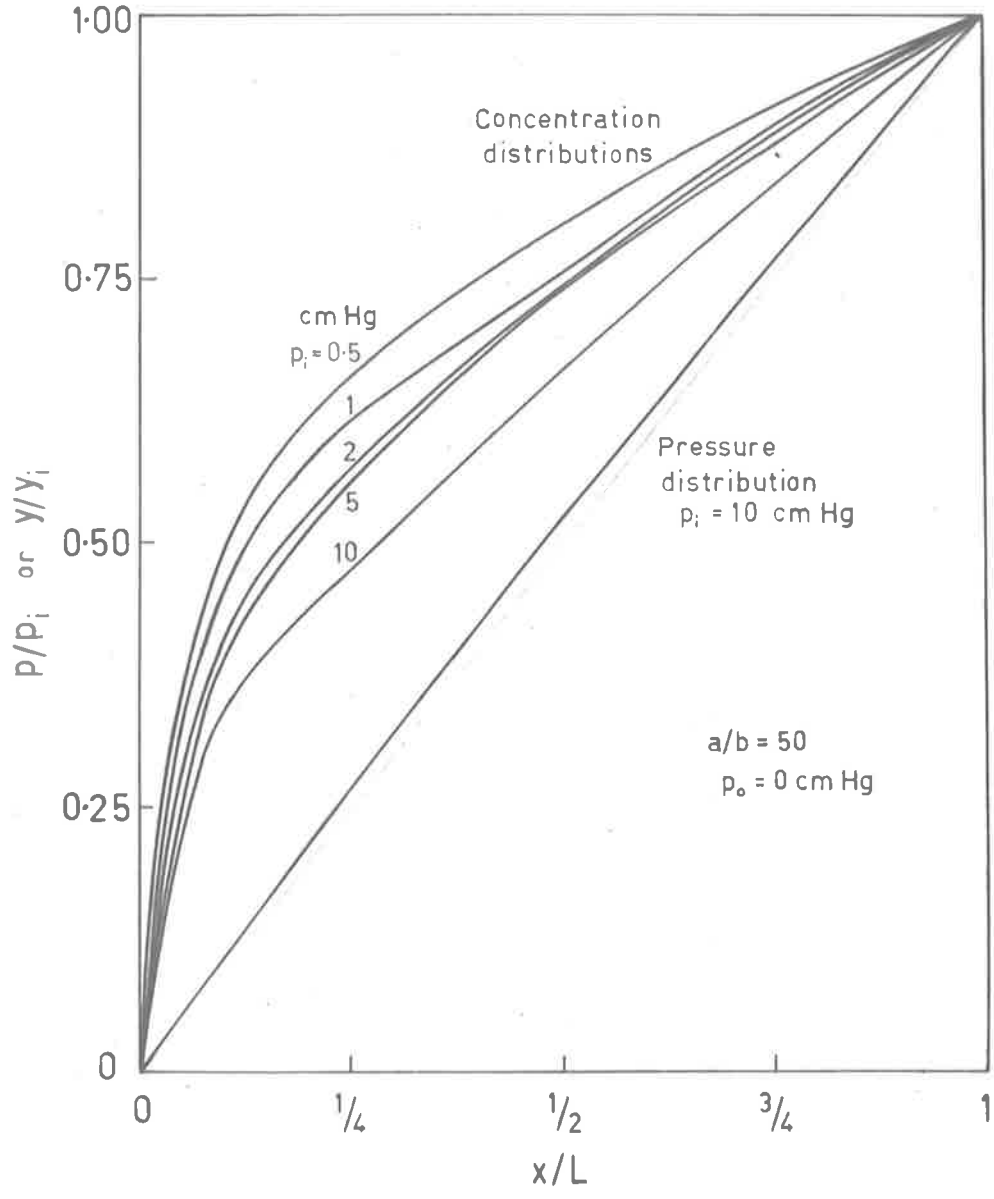

Fig. 5.1-7 Adsorbed-Phase Concentration Distributions in a Morgan "EY9" Graphite Sample (a/b = 50) for Various Pressure Conditions.

The adsorbed phase concentration ($c_s = \rho_b y$) at any point in the sample was estimated from the pressure at that point by means of the adsorption isotherm (Fig. 5.1-6).

Fig. 5.1-7 shows that the surface concentration distributions became more curved as p_i decreased. The rate of change of the curvature of the distributions with pressure became greater as p_i decreased, e.g., the difference in the ratio y/y_i between the curves for $p_i = 1/2$ and $p_i = 1$ cm Hg at $x/L = 1/4$ was about the same as that between the curves for $p_i = 1$ and 2 cm Hg.

To set up the pressure distribution within the sample after the commencement of flow, about the same time was required for the above examples since the distribution did not vary considerably with pressure. However, a much longer time was necessary to set up the adsorbed phase concentration distribution for $p_i = 1/2$ cm Hg than for $p_i = 10$ cm Hg since the concentration at any point in the sample was then greater. If the deviation of the surface concentration distribution from the pressure distribution was taken as a measure of the time-lag and also of the time to reach equilibrium flow, then the time-lags at low pressures were greater than at higher pressures and also the rate of

change of the time-lag with decreasing pressure was greater. That is, a plot of ϕ against p_m would slope upwards as p_m decreased and, at very low pressures, curve sharply upwards because of the more rapid rate of change of y with p at any point in the sample. This larger value of $\partial y / \partial p$ (or $\partial e_s / \partial e_g$) was caused by the large value of H (see Fig. 5.1-5) and hence by the hump in the adsorption isotherm (Fig. 5.1-6).

(j) Deductions from the Discussion on Adsorption Effects

In the calculations of the diffusion coefficients and H given previously (section 5.1.3.4(b)), the rapid increase of H at low p_m was neglected and the extrapolated values of H at $p_m = 0$ were estimated; these values agreed approximately with those obtained by the extrapolation to zero pressure of the straight portions of the H-p_m plots (Fig. 5.1-5) above $p_m = 5$ cm Hg. The isotherms (Fig. 5.1-6) showed that considerable adsorption occurred even though the value of H was zero (e.g., helium flow) or small; H did not therefore always indicate the amount of adsorption, the exception being when Henry's law was obeyed at low pressures. A constant value of H or ϕ did not necessarily mean that Henry's law adsorption had occurred from zero pressure.

The analysis given earlier in section 5.1.3.4(b) was therefore in error, although the calculated values were not markedly incorrect at certain mean pressures. Actually if Barrer's time-lag calculations were performed at about p_m = 5 cm Hg (where H = 0 for helium flow), the calculated values would be correct. The diffusion coefficient D'_t increased sharply with increasing p_m at low pressures and then became fairly constant at about the value given in Table 5.1-5, while D'_{gt} varied proportionally to K according to equation (2.1.5-18).

In calculating the isotherms for gas adsorption on Morgan "EY9" graphite from the Kϕ values, the measured values of K at mean pressures below the minimum were included. If the straight line values of K (= $a + bp_m$) had been used, the H-p_m plots would have still curved upwards at low pressures since ϕ increased in this region, but not as sharply as shown in Fig.5.1-5. The variation of H with p_m possibly explained why minima were observed at low pressures in the K-p_m plots; this will be further discussed in section 5.1.3.5(g).

The explanations of the low pressure transient and steady state phenomena and the proof of the method of obtaining the adsorption isotherms can only become rigorous if confirmed by a theoretical examination of transient flow for pressure-dependent values of D'_t and H.

5.1.3.5 Minima in the K-p_m Plots

(a) Experimental Observations

Definite evidence of minima in the K-p_m plots at low pressures has been obtained (see section 4.1.3.1) for the flow of a number of gases through three samples of Morgan "EY9" graphite (nine determinations). This evidence confirmed the observations of Grove and Ford,[97] Ash and Grove,[67] and O'Neill et al.[68] that permeability minima are obtained for flow in consolidated porous media (see section 2.1.5.2, where the low pressure phenomena are discussed in detail).

The observed minima were not due to experimental errors as the estimated relative error at low pressures was about 8% (see Appendix C.2.3) whereas the K values at the lowest p_m deviated from the straight K-p_m plot by up to 50%. Allowance for the degassing and leakage rate in the apparatus, as determined in a blank experiment, did not significantly change the low pressure K values to eliminate the minimum in any determination.

The approximate values of the mean pressure $(p_m)_{min.}$ corresponding to the minima in the K-p_m graphs (see Table 5.1-6) varied roughly with the molecular weight of the gas since for Rod No. K21, the lowest values occurred for helium and hydrogen flow

Table 5.1-6

Minima Details for Morgan "EY9" and Impregnated Graphites

Sample No.	Gas	$(p_m)_{min.}$ cm Hg	$^+\lambda_{min.}$ cm x 10^4	K_1/K_k	$^+\mu/\sqrt{M}$ at 20°C x 10^7
K21	He	1.0	14.32	1.16	976
	H_2	0.7	13.02	1.20	621
	N_2	1.0	4.85	1.42	331
	N_2	1.4	3.46	1.24	331
	A	2.0	2.59	1.38	352
	CO_2	2.0	1.62	1.40	221
	Xe	$\simeq$ 3.0*	0.96	1.05	196
	CF_2Cl_2	$\simeq$ 2.5*	0.66	1.10	113
K23	N_2	2.5	1.94	1.60	331
	A	1.0	5.17	1.18	352
K24	N_2	0.8	6.06	1.17	331
K42	H_2	1.2	7.58	1.58	621
	N_2	0.5	9.70	1.21	331

* The K-p_m plot commenced to flatten at this p_m.

\+ See Table B.1-1, Appendix B.

and the highest for freon and xenon flow. This variation was contrary to the observations of other authors,[65,67] who found that the deviation from the straight K-p_m plots occurred at the highest pressures for helium, which had the largest mean free path λ, and at lower pressures as the value of λ decreased.

Because of the reversed variation of $(p_m)_{min.}$, the value of $N_{Ku} = \lambda/d$ corresponding to the minimum was not approximately constant as observed by Ash and Grove,[67] but decreased for Rod No. K21 from about 24 for helium flow to about 1 for freon flow. The disagreement between the values of $(p_m)_{min.}$ for the nitrogen and argon determinations for Rods K21 and K23 (see Table 5.1-6) showed that $(p_m)_{min.}$ was not determined very accurately; this inaccuracy perhaps was the reason for the contrary order of variation of the results noted above.

The permeability graphs for hydrogen and helium flow were apparently the most sharply curved at the minimum of all the graphs, while those for nitrogen, argon, and carbon dioxide flow curved more gradually; for freon and xenon flow, the graphs only flattened out at low pressures. Similar variation in the shape of the K-p_m plots for different gases was observed by Ash and Grove.[67]

It was difficult to estimate the actual intercept K_i of the $K-p_m$ plot with the K-axis because of the asymptotic approach of the plot; approximate values of the ratio of K_i to the straight $K-p_m$ line intercept $K_k(=a)$ are given in Table 5.1-6. Generally, for those determinations in which three to six experimental points were obtained below the minimum, K_i/K_k was about 1.4; when the low pressure results were limited or scattered or the $K-p_m$ plot flattened out, lower values of K_i/K_k of less than 1.2 resulted.

(b) Equations of the Permeability Curve

The permeability curve for Detmn. No. L:24 (nitrogen flow in Rod No. K21) was found to be approximately expressed by equations of the forms

$$K = K_k + bp_m + (K_i - K_k)\, e^{-np_m}, \quad \ldots (5.1.3\text{-}8)$$

where the exponent n was about 5, and

$$K = bp_m + K_k\,(9.0p_m + K_i/K_k) \,/\, (9.4\, p_m + 1); \quad \ldots (5.1.3\text{-}9)$$

however, neither equation fitted the experimental results completely no matter what values were chosen for the constants in the correction terms.

The Knudsen-slip term in equation (5.1.3-9) was similar to the equation derived theoretically by Derjaguin and Bakanov[45] (equation 2.1.5-2) for flow in the transition region. The curve calculated from

equation (2.1.5-2) for the theoretical values of the constants differed greatly from the experimental curve.

Because of the relative inaccuracy of the low pressure results below about p_m = 2 cm Hg (see section 4.1.3.1), and the limited number of these results in some determinations, no accurate correlations were possible. The correlations did not assist in discovering the mechanism that caused the minimum in the permeability plot.

(c) Viscosity Effects

The gas viscosity μ is important during viscous flow when the resistance to flow arises from the viscous drag at the pore walls. It therefore occurs in the permeability equation (2.1.4-2); any variation of μ with p_m at low pressure could possibly lead to a permeability minimum.

According to the kinetic theory of gases, μ should be independent of pressure;[251] this is generally true for pressures from a few millimetres of mercury up to several atmospheres since the value of μ varies by less than 0.2% per atmosphere (see Table B.1-1, Appendix B). At low pressures, when the mean free path λ of the gas molecules becomes comparable with the dimensions of the containing vessel, e.g., the diameter of a capillary or pore, the apparent viscosity μ' as determined from the

flow equation, e.g.,

$$GL/\Delta p\ \rho_m = B_o/\mu', \qquad \ldots (5.1.3\text{-}10)$$

is no longer constant but is smaller than the true viscosity because of slippage; in the Knudsen flow region, μ' decreases to zero with pressure.[252]

However, for gas flow in both capillaries and porous media, it is general practice to add a slip-correction term to the viscous term in the flow equation and to take μ as independent of p (see section 2.1.4.1). The variation of the apparent viscosity μ' with decreasing p_m as obtained from the non-corrected flow equation (5.1.3-10) results because of the variation of $G/\Delta p$ with p_m and is thus really caused by the same molecular interaction mechanism that causes K to vary and give a minimum. The variation in μ does not itself determine the minimum in the permeability plot.

(d) Interaction of the Gas Molecules

Some of the suggested causes of permeability minima have been discussed briefly in section 2.1.5.2. The interaction of gas molecules in a fine capillary or pore at low pressures could lead to an increased flow-rate with decreasing p; such molecular interaction is not clearly understood. It is generally considered (see sections 2.1.4 and 2.1.5) that for slip flow, λ is

much less than d and the majority of the molecular collisions occur in the gas-phase, while for Knudsen flow, λ is much greater than d so that gas phase molecular collisions are negligible and collisions with the capillary walls are predominant. It is in the transition region between these two limiting flows that the permeability minima have been observed, i.e., where λ is of the same order as d and both gas-phase and molecule-wall collisions occur.

Very few of the gas molecules on striking a solid surface undergo elastic collisions. Most of them are adsorbed on the surface for a certain finite time (see section 2.1.6) before they are desorbed in completely random directions; such molecule-wall encounters constitute the diffuse reflection of molecules at a surface. For slip flow conditions, there is some evidence (ref.5,p.64) that specular or mirror-like reflections can occur. When an adsorbed film on the solid surface acts like a liquid film, some molecules could possibly be specularly reflected on striking this film.

For flow in fine capillaries at low pressures, the factor f_1 was introduced to account for the fraction of molecules undergoing diffuse reflection (section 2.1.2.1(c)); f_1 approximated to unity for diffuse type

reflection but was lower when specular reflection occurred. In the slip flow region, the value of f_1 depended upon the gas and the nature of the solid surface; it apparently increased as the pressure decreased and the flow passed through the transition region (ref.5,p.64). By analogy with gas flow in capillaries, a similar treatment was applied to gas flow in porous media with the factor δ in the flow equation being equivalent to $(2-f_1)/f_1$ (section 2.1.4.3).

DeMarcus[253] has shown that the use of the factor f_1 gives approximately the correct result for flow in long capillaries (L_c/d_c greater than 100), but claimed it was preferable not to allow for specular reflection for short tubes (and presumably porous media). On the other hand, Lassettre[254] found that the effect of specular reflection on gas transport was marked for a bed of spheres. As the fraction of specular reflections $(1-f_1)$ is difficult to estimate and is influenced by the nature of the solid surface and the occurrence of adsorbed films, the correction of the flow equation for specular reflection by a rather hypothetical factor ranging from 0.6 to 1.0 is of doubtful value.

Because the value of f_1 changed in the transition region between slip and Knudsen flow, the value of the

factor δ in the flow equation also varied;[64] this variation could describe the minimum in the permeability curve as shown by Derjaguin and Bakanov.[45] However, it was suspected that the minimum was caused by a more complex molecular interaction than just the variation in the manner of reflection of the molecules at the pore walls.

(e) The Effect of the Distribution of Pore Sizes

O'Neill, Hey, and Livey[68] showed how to predict a permeability minimum from pore size distribution data. These authors considered that the K-p_m plot would have a minimum if the distribution of pore sizes in the medium was wide, but would only flatten out when the distribution was narrow (see section 2.1.5.2(b)). According to this reasoning, a minimum should be obtained for the flow of all gases in a porous material with a wide pore size distribution provided the factors δ_0 and δ_1 did not vary for each different gas.

However, Ash and Grove[67] observed that the K-p_m plots gave minima for the flow of several gases in a porous ceramic but flattened out for other gases. Similarly, for xenon and freon flow in Morgan "EY9" Graphite Rod No. K21, the K-p_m plots flattened out at low pressures, whereas the flow of other gases in the

same sample gave definite evidence of minima, thus indicating a wide pore size distribution in the graphite. Since there was a gradual trend in the shape of the $K-p_m$ plots at the minimum with increasing molecular weight of the gas (section 5.1.3.5(a)), it was considered that the xenon and freon $K-p_m$ plots probably curved upwards at very low pressures beyond the pressure range studied experimentally. Some of the previously reported $K-p_m$ plots where a flattening was observed were suspected also to curve upwards at extremely low pressures and give a gradually curving minimum (cf. Arnell and Henneberry[85]).

For very fine-pored media with uniform pore structure (Vycor porous glass), no minima have been observed at low pressures since K remained constant with p_m and presumably indicated true Knudsen flow.[82-84] Apparently no attempts have been made to investigate the transition from viscous-slip to Knudsen flow in such media at high pressures. Most investigations on fine-pored media[76,82,83,86] have been confined to pressures below two atmospheres although Kammermeyer and Rutz[84] found that Knudsen flow still occurred up to about 600 cm Hg for gas flow through Vycor porous glass. An increase in surface flow could possibly mask out any contribution due to viscous-slip flow at

high pressures.

It was significant that most observations of permeability minima were for consolidated porous media (see section 2.1.5.2(d)). In such media, the pore size distributions are generally quite large and the porosities low; often the pore distribution is dominated by two main peaks indicating that there are macropores between the solid particles and micropores within the particles themselves (cf. section 5.4.2). The particular pore structure of a porous medium may decide whether or not a permeability minimum will be observed.

The anistropy of the porous medium had no influence on the occurrence of permeability minima since minima were obtained for flow both perpendicular (Sample No.K23) and parallel (Samples K21 and K24) to the extrusion axis of Morgan "EY9" graphite.

(f) Knudsen Flow and Long Flow Paths

Pollard and Present[90] and other authors[91,92] considered that the minimum in the plot of $G/\Delta p$ against p_m for gas flow in a capillary was due to the increased probability of molecules at very low pressures passing through the capillary without collisions (see section 2.1.5.2(a)); they surmised that there were no flow paths long enough in a porous medium for this effect to occur. However, the experimental

evidence for porous media did not always support their theoretical claims, but suggested that long paths could exist in some porous media.[68]

The surmise that no long flow paths were possible in a porous bed resulted from a consideration of the bed as a series of kinked tubes.[90] In a more realistic pore model such as that suggested by Owen[43] (with void spaces separated by fine capillaries), some long flow paths could occur; however, the resulting increase in the flow-rate during Knudsen flow at low pressures was considered very small compared with those required to give the well-defined minima observed for the reactor graphites and other consolidated porous media.[67,68,97]

Because Knudsen flow commenced in a pore or capillary when λ was greater than d, the Knudsen number $N_{Ku} = \lambda/d$ has been taken to characterize the mean pressure $(p_m)_{min.}$ corresponding to the minimum.[67,97] If the value of N_{Ku} at the minimum was approximately constant for any porous medium,[67] then $(p_m)_{min.}$ and also the pressure at which the deviation from the straight $K-p_m$ plot commenced should be proportional to $\mu/\sqrt{M}$.

For Morgan "EY9" graphite, N_{Ku} was not constant for Rod No. K21 and $(p_m)_{min.}$ varied inversely with $\mu/\sqrt{M}$ (see Table 5.1-6). For Impregnated Graphite Sample

No. K42 (see section 5.1.4.4), $(p_m)_{min.}$ was proportional to $\mu/\sqrt{M}$ but the values of N_{Ku} (54 and 69) at the minimum were much greater than those noted previously (between 1 and 25 for different media[67,97]). The value of d (0.14 microns) used to calculate N_{Ku} for Sample No. K42 was possibly low (see Table 5.6-6) so that the values of N_{Ku} were high.

The discordant experimental observations for the reactor graphites indicated that there was apparently no definite relation between N_{Ku} and $(p_m)_{min.}$ and hence no direct evidence of any Knudsen effects as suggested by Pollard and Present.[90] Some mechanism other than that of Pollard and Present might lead to the increased values of K in the Knudsen flow region.

(g) Adsorption and Surface Flow Effects

During the discussion of transient flow (see section 5.1.3.4(d)), the similarity between the $K-p_m$ and the $\phi-p_m$ plots was noted; this similarity possibly indicated that the low pressure flow behaviours for steady state and transient flow were influenced by the same effect. Following a consideration of adsorption effects during transient flow, it was suggested (section 5.1.3.4(j)) that the minima in the $K-p_m$ plots at low pressures were possibly due to adsorption effects.

An examination of equation (5.1.3-5) showed that K could either decrease or increase as p_m decreased or remain constant depending upon whether the product $D_t^! (1 + H)$ decreased, increased, or was constant with decreasing p_m, respectively. If surface flow occurred, K would still vary with p_m in the above manner (cf. equation 5.1.3-4). The variation of ϕ (and hence $D_t^!$) with p_m was due to the particular shape of the $H-p_m$ plot (section 5.1.3.4(e)). It was possible that the variations in ϕ and H cancelled out so that adsorption effects did not influence the values of K. Measurement of the $H-p_m$ and $D_t^! - p_m$ (or $\phi-p_m$) plots for any gas-solid system would indicate the manner in which $D_t^! (1 + H)$ varied with p_m and ascertain whether a minimum resulted from adsorption effects.

However, it was difficult to attach any physical significance to variable adsorption during steady state flow. In the pressure increase experiments, adsorption equilibrium might not have been attained when straight p_o-t plots were observed; however, such non-equilibrium adsorption effects would lower the permeability and were probably negligible anyway.

When surface flow occurred, the product HD'_{st} appeared in equation (2.1.5-18). Even when D'_{st} was very small, the surface flow term in this equation

might become quite significant at low pressures where H was very large so that a minimum in the K-p_m plot was obtained.

Calculations made for nitrogen flow in Morgan "EY9" Graphite Rod No. K21 (Detmn. No. L:24) by means of equation (2.1.5-18) showed that a slight minimum in the K-p_m plot was obtained if D'_{st} was assumed to be 1% of D'_t, but K_i was only 11% greater than K_k (0.0155 cm^2/sec) compared with the experimental difference of about 40%. Values of D'_{st}, estimated from the difference between the observed values of K and K_v (= a + bp_m), were found to increase as p_m decreased; this variation was contrary to previous observations[107,113] when D'_{st} increased with increasing p_m.

The theoretical surface concentration distributions of y/y_i against x/L for Morgan "EY9" graphite (Fig.5.1-7) indicated that surface flow, if it occurred in Morgan "EY9" graphite, could increase as p_m decreased since the surface concentration gradient $\partial y/\partial x$ at the outlet side of the sample increased with decreasing p_m. This increase in surface flow was probably due to the increase in H at low pressures.

(h) Deductions Concerning Permeability Minima

The above discussion showed that a number of effects, viz., the variation in the manner of reflection of gas

molecules at the pore walls, Knudsen flow through any long flow paths, and surface flow effects, could each contribute in a small way to the increased flow-rates observed for flow in porous media at low pressures. However, the explanation of the permeability minima is still far from clear. Apparently, the particular pore structure of the medium (and perhaps its adsorption characteristics) has a considerable influence on the occurrence of permeability minima.

It should be profitable to investigate the flow of gases through porous media with average pore diameters between 100 and 1000 Å, and with both uniform and wide distributions of pore sizes; such media have not been examined very closely.

5.1.3.6 The High Pressure Determinations

Some of the results of Detmn. No. H:4 for nitrogen flow through Rod No. K23 were examined by the Green and Duwez method[126] to determine whether it was applicable to Morgan "EY9" graphite. Previously, the high pressure flow results for gas flow in the transition and turbulent flow regions for P.G. 60 and Acheson "A" graphites were successfully correlated by this method (see section 5.1.2.4). Because of the only slight curvature of the K-p_m plot for this determination (Fig. 4.1-10), the transition was expected to be very

gradual with the largest N_{Re} (at p_m = 1236 cm Hg) not much greater than the critical value of 0.01.

The values of B_o and β calculated from the slope and intercept of the α-β plot were 1.61×10^{-12} cm^2 and 1.35×10^{10} cm^{-1}, respectively. This B_o value agreed with the value of 1.57×10^{-12} cm^2 obtained from the slope of the K-p_m plot for this determination (No. H:4) at low pressures. The value of β agreed quite well with the value predicted by the β- B_o plot (Fig. 5.1-2).

The latter value of B_o, together with the value of β and the intercept value, a = 0.0060 (see Table 4.1-3), were used to calculate values of N_{Re} (slip-corrected) and f for selected experimental results; these values are listed in Appendix K.3. The f-N_{Re} plot agreed quite well with that obtained previously (see Fig.5.1-1), being slightly high in the viscous flow region possibly because of slightly inaccurate results at low pressures when the flow-rates were measured with the capillary flow-meter. Thus the flow in Morgan "EY9" graphite at high pressures was also correlated by the Green and Duwez approach.

Over the mean pressure range of Detmn. No. H:4 (67 to 1236 cm Hg), the values of N_{Re} varied from 0.0009 in the viscous region to 0.09 in the transition

region. At the critical N_{Re} (0.01), the mean pressure was estimated by interpolation to be about 340 cm Hg, while at N_{Re} = 0.05 p_m = 880 cm Hg. The pressure at which the K-p_m plot was observed to commence curving downwards (about p_m = 550 cm Hg or N_{Re} = 0.022) was just greater than the critical p_m (340 cm Hg), thus demonstrating that the curvature of the plot was due to the commencement of inertial flow.

The very gradual change in curvature of the K-p_m plot meant that the flow-rate changed very slowly with pressure for Morgan "EY9" graphite. For the coarser-pored graphites, the flow-rate changed at a faster rate with pressure and the curvature of the plots was more pronounced. No curvature of the high pressure K-p_m plots was observed by Hutcheon et al.[34] for gas flow through Morgan graphites up to p_m = 12 atm (900 cm Hg).

The high pressure flow phenomenon was not observed in the determinations on the Morgan "EY9" graphite rods since separate K-p_m plots for different values of p_o were not obtained (see section 4.1.3.2). By means of equation (5.1.2-5), values of Q_a and K were calculated for Rod No. K23 (Detmn. No. H:4) for p_m = 1013 cm Hg and p_o = 0, 76, and 140 cm Hg. At this p_m, the total variation in the values of Q_a for this range of p_o was 14%, but the corresponding variation in the values of K

was only about 1%, i.e., within the experimental scatter ($\pm$ 1% at p_m = 1000 cm Hg). The calculated values of K agreed to within 1% with the experimental value. For Acheson "A" graphite (Detmn. No. H:3), the total variation in the K values at p_m = 400 cm Hg for the range of p_g from 0 to 130 cm Hg was about 12%.

DISCUSSION

5.1.4 Impregnated Graphite

5.1.4.1 The Low Pressure Experimental Methods

For the permeability determinations on Impregnated Graphite Sample No. K42, the agreement between the results obtained by different methods for nitrogen flow (see section 4.1.4) was generally not very good compared with the agreement observed for the other graphites. The K-p_m plot obtained by the low pressure decay method was 10 to 25% lower than that for the low pressure increase determination, while both plots were about 30 to 40% lower than that determined in the high pressure apparatus by the flow method. These differences arose presumably because of the long time required to reach equilibrium flow in Impregnated graphite after the commencement of flow.

(a) The Time to Reach Equilibrium Flow

In Detmn. No. L:31, it was shown by low pressure flow experiments that the time required to reach a steady state or constant flow-rate after the commencement of flow was less than one hour (about 50 min) for nitrogen flow in Sample No. K42. The pressure increase plots of Detmn. No. L:29 confirmed this long time to reach equilibrium flow; the time ranged from 20 min for

the experiments with p_m about 38 cm Hg up to 50 min when p_m became very small, i.e., it became longer as the mean pressure decreased.

For hydrogen flow (Detmn. No. L:55), the time was much shorter (about 2 min). However, for xenon flow (Detmn. No. L:56), the times required to reach equilibrium flow were extremely long, ranging from about 280 min at p_m = 15 cm Hg to 600 min (10 hr) at p_m = 1.6 cm Hg. For all pressure increase experiments, the time to reach equilibrium flow was about twice the time-lag ϕ (the intercept of the straight p_o-t plot on the t-axis).

Wall[255] has indicated that from 8 to 24 hr were required to reach equilibrium conditions for the flow of methane through Impregnated graphites by a flow method;[152] the permeability of his samples, however, was lower than that for Sample No. K42 (about 0.8×10^{-5} cm^2/sec cf. 1.4×10^{-4} cm^2/sec for nitrogen flow).

(b) <u>The Pressure Decay Determinations</u>

Because the flow of nitrogen through Sample No. K42 took from 20 to 50 min to reach equilibrium flow conditions after commencement of flow, the time depending on the mean pressure, the permeability determinations by the low pressure decay method (Detmn. No. L:30) were not satisfactory; the mean pressure during these

determinations continuously decreased so that equilibrium conditions were never attained. This reason explained why the measured values of K were lower than those determined by other methods (the measured flow was always less than the equilibrium flow).

The very low slope of the K-p_m plot for Detmn. No. L:30 probably resulted from the non-attainment of equilibrium flow conditions in the initially evacuated sample. The observed shape of the K-p_m plot for air flow in Sample No. K41 (Detmn. No. L:23) also resulted from the non-attainment of equilibrium flow, the sample initially being at the inlet pressure for this determination. The time to reach equilibrium flow conditions for Sample No. K41 was probably longer than that for Sample No. K42 because of its higher resistance to flow (lower permeability).

This non-equilibrium effect was also observed for pressure decay determinations for Morgan "EY9" graphite (section 5.1.3.1), but not to the same extent as for Impregnated graphite. For Acheson "A" graphite, equilibrium flow was attained almost instantaneously after any pressure change so that non-equilibrium effects did not arise. For pressure increase type experiments, the non-equilibrium effects were generally not very significant since the pressure in the sample remained

effectively constant with time, and a straight p_o-t plot was obtained after the initial transient period.

(c) The Pressure Increase Determinations

For the pressure increase determinations, the scatter of the K values about the K-p_m plots was generally less than $\pm$ 2%, which was a little larger than that observed for Morgan "EY9" graphite ($\pm$ 0.5 to 1%). In several determinations, curved p_o-t plots were obtained showing that steady state conditions were no longer closely approximated.

Previously (section 5.1.3.1), the low pressure increase method was considered a satisfactory method for determining values of the permeability coefficient; provided p_i was much greater than p_o for any experiment, steady state conditions could generally be assumed. For both Acheson "A" and Morgan "EY9" graphites, the K-p_m plots determined by the increase method have agreed quite closely with the corresponding plots obtained by the low pressure and high pressure flow methods, any differences being attributed to inaccuracies in measurement. However, for Impregnated graphite (Sample No. K42), the values of K determined by the low pressure flow method (Detmn. No. L:31) were 3 to 4½% higher than those obtained by the pressure increase method (Detmn. No. L:29), whereas the relative error

between the two methods was estimated as 2%.

Detmn. No. L:32 showed that either the pressure plots, which were assumed straight after the initial transient period unless obviously curved, were in fact very slightly curved and indicated non-equilibrium flow, or the pressure increases over small time intervals for the flow method were more inaccurate than expected. If equilibrium flow conditions occurred during the pressure increase experiments after the initial transient, the values of K for the flow method could only be consistently higher than the K-p_m plot obtained for for the pressure increase method and not scattered about it if the small time intervals for the flow method were always effectively less than the 2 min intended. No errors resulted from the use of the McLeod gauge to measure the pressure (see Appendix C.2.3).

As the p_o-t plots when plotted with enlarged scales showed a slight curvature, it was suspected that small departures from equilibrium led to the erroneous values of K for Impregnated graphite. Thus the error in the values of K by assuming that steady state conditions were approximated in the pressure increase experiments was indeterminable (probably less than 2%) for Morgan "EY9" graphite, but became greater and more significant for the finer-pored Impregnated graphite,

for which the time to reach equilibrium was greater.

The small disturbances from equilibrium flow were caused by the buildup of pressure p_o in the outlet volume of the apparatus. The low pressure flow method could also lead to slightly erroneous values of K for the above reason since the method depended on the buildup of pressure over a short time interval. The high pressure K-p_m plots for hydrogen and nitrogen flow in Sample No. K42, which were higher than the respective low pressure plots below p_m = 100 cm Hg, were possibly inaccurate at low p_m because of the difficulty in measuring the low flow-rates accurately, but could indicate that the low pressure values were also in error.

(d) Suggested Procedures

Two suggestions were made to permit the accurate determination of low permeability values as obtained for Impregnated graphite: either the low pressure variable volume flow method for determining permeability coefficients (see section 2.1.8.2(b)) should be developed to enable the accurate measurement of low steady-state flow-rates, or rigid equations should be derived to express the flow through a porous sample for the non-equilibrium conditions encountered for the pressure increase experiments in the present apparatus, i.e., the boundary condition that p_o varied with time should

be introduced into the existing equations. The first suggestion involved the construction of a new automatically-controlled apparatus similar to those mentioned previously (section 2.1.8.2(b)); such an apparatus is recommended for future low pressure permeability determinations. Besides permitting accurate measurement of low flow-rates, this apparatus would remove any doubt concerning the use of the McLeod gauge in measuring pressures during the pressure increase experiments (see Appendix C.2.3).

The second suggestion required the use of complex mathematical techniques since the desired equations should provide for a variable permeability (or diffusion) coefficient and for flow in both rods and hollow cylindrical samples. The general differential equation for linear flow in a porous medium is

$$\frac{\partial c}{\partial t} = D \frac{\partial^2 c}{\partial x^2} ; \qquad \ldots (2.1.5\text{-}6)$$

for linear flow, it must be solved for the boundary conditions:

$$\left.\begin{aligned} p &= p_i \text{ at } x = 0 \text{ for all } t, \\ p &= \Phi(x) \text{ for } 0 < x < L \text{ and } t > 0, \\ p &= p_o \text{ at } x = L \text{ for } t = 0, \\ p &= \Phi(t) \text{ at } x = L \text{ for } t > 0, \end{aligned}\right\} \qquad \ldots (5.1.4\text{-}1)$$

where $p = c\,\mathcal{RT}/\mathcal{E}$.

Barrer has given the solution to equation (2.1.5-6) for diffusion (flow) through a porous medium for both the linear[105] and cylindrical[104] systems for appropriate boundary conditions which were similar to those above except that p at x = L was assumed to equal p_o for all t, a condition approximately true only when p_o was very much less than p_i. Barnes[256] and Barrer (ref.257,p.19) have considered the linear system when both p_i and p_o varied with time. The solution for the cylindrical system when p_o varied with time could be obtained from the general solution given by Jaeger.[258] However, none of these solutions were valid when the diffusion coefficent was a function of concentration (pressure).

The effects of adsorption and of dead-end pores in the porous medium should be negligible for the desired solutions when equilibrium flow conditions were closely approached, but would be quite important during the initial transient flow of the pressure increase experiments (see section 2.1.5.3(b)). Solutions of equation (2.1.5-6) for a variable diffusion coefficient may require the use of a computer and are thus beyond the scope of the present author. Co-operation with a mathematician is suggested for any attempt to obtain a solution to this problem.

5.1.4.2 The Values of B_o and K_o

The constancy of the values of B_o and K_o for each sample of Impregnated graphite was not as good as was observed for Morgan "EY9" graphite (see section 5.1.3.2). For the low pressure determinations on Sample No. K42, the considerable variation (about $\pm$ 30%) of the B_o values about the average resulted partly from the very low slopes of the $K-p_m$ plots, since a small change in the intercept value could lead to a large variation in the value of the slope. The values of K at low p_m for xenon flow (Detmn. No. L:56) were possibly low because equilibrium flow was not reached; then the values of B_o and K_o would be respectively lower and higher than obtained.

The average low pressure values of B_o and K_o for Sample No. K42 were therefore considered to be $(1.12 \pm 0.08) \times 10^{-14}$ cm^2 and $(1.89 \pm 0.05) \times 10^{-9}$ cm, respectively. The high pressure values for Sample No. K42 were respectively about 50% lower and 50% greater than the average low pressure values but were in error because of the difficulty of measuring low flow-rates accurately. The absolute accuracy of the low pressure values, however, was in doubt for the reasons mentioned in section 5.1.4.1(c).

For Sample No. K41, the average values of B_o and K_o

as determined in the high pressure apparatus were $(1.10 \pm 0.11) \times 10^{-15}$ cm^2 and $(6.03 \pm 0.29) \times 10^{-10}$ cm, respectively. The variation amongst the values for different gases ($\pm$ 20% and $\pm$ 10%, respectively) was due to the inaccuracy in determining the values of K.

Wall[152] of the Australian Atomic Energy Commission has reported values of $(1.18 \pm 0.02) \times 10^{-15}$ cm^2 for B_o and $(1.32 \pm 0.05) \times 10^{-10}$ cm for K_o as typical permeability results for the flow of labelled methane in Impregnated graphite. His sample was of similar permeability to Sample No. K41 but gave a lower proportion of slip flow.

When the Impregnated graphite samples were prepared for permeability measurements, the outer skin of Sample No. K42 was machined off in the lathe (see Table A.2-1). The outer skin was expected to be more impermeable than the rest of the graphite;[255] Ward and Smith[157] showed that the argon permeability of an impregnated graphite increased by a factor of 3.5 on machining off the outer layer. Hence the removal of the outer skin of Sample No. K42 caused it to have a higher permeability than Sample No. K41. The observed difference in the permeabilities was probably also due to the inconsistency[255] of the A.A.E.C. graphite impregnation process when these samples were treated, resulting in the non-reproducibility

of the permeability between different samples.

The graphite impregnation process[13] developed by the A.A.E.C. has thus reduced the permeability of the Morgan "EY9166" graphite by a factor of about 10^3 for these samples, B_o decreasing from about 4×10^{-12} cm^2 to about 1×10^{-15} cm^2 and K_o from 2.5×10^{-7} cm to about 6×10^{-10} cm. Improvements to the process were expected[13,255] to produce greater reductions in the permeability of later Impregnated graphites than was observed for Samples No. K41 and No. K42.

5.1.4.3 Transient Flow Measurements

(a) Time-Lags

For gas flow in Impregnated Graphite Sample No. K42, the ϕ-p_m plots were generally of similar shape to those obtained for the Morgan "EY9" graphite samples (section 5.1.3.4(a)), the values of ϕ being approximately constant with p_m above p_m = 5 cm Hg, and increasing sharply at low pressures (see Fig. 4.1-14). Below about p_m = 5 cm Hg, the plots for hydrogen, helium, and nitrogen flow dipped downwards slightly and gave a minimum. For nitrogen flow, this minimum was apparently real since the ϕ values were 2 min (13%) lower than the straight plot about which the scatter was only $\pm$ 0.5 min ($\pm$ 4%). The values of ϕ for any gas were much greater than the corresponding values for Morgan "EY9" graphite.

As for Morgan "EY9" graphite (see section 5.1.3.4(a)), the intercept values ϕ_o and ϕ_i were obtained from the ϕ-p_m plots (Fig. 4.1-14); the values for each determination are listed in Table 5.1-7. No ϕ_i values were reported for argon and xenon flow since the determinations for these gases were not continued to low enough pressures. The values of ϕ_i given were probably only approximate because of the difficulty in estimating them accurately. The values of ϕ_o roughly increased with the molecular weight of the gas. Because of the limited number and scatter of the experimental results for helium and argon flow, it was possible that the ϕ-p_m plots were not as drawn in Fig. 4.1-14, but were nearer to horizontal with a dip at about p_m = 2 cm Hg. Then the values of ϕ_o would be approximately 0.65 and 11 min, respectively, for these two gases.

The values of neither $\phi_o \sqrt{(\mathcal{J}/M)}$ nor $\phi_i \sqrt{(\mathcal{J}/M)}$ were constant (see Table 5.1-7) but increased with the molecular weight of the gas. If adsorption effects caused the variation observed, then xenon was adsorbed much more than the other gases.

It was difficult to tell from the values of $\phi \sqrt{(\mathcal{J}/M)}$ whether hydrogen, or even helium, was adsorbed. However, because the hydrogen ϕ values above p_m = 4 cm Hg

Table 5.1-7

Intercept Values of the Time-Lags for Impregnated Graphite Sample No. K42

Detmn. No.	Gas	ϕ_o min	ϕ_i min	$\phi_o\sqrt{(\mathcal{J}/M)}$	$\phi_i\sqrt{(\mathcal{J}/M)}$
L:55	H_2	0.70	2.48	8.38	29.5
L:57	He	0.24 (0.65)	2.35	2.06	20.1
L:29	N_2	15.0	22.0	48.8	71.5
L:58	A	10.0 (11.0)	-	27.3	-
L:56	Xe	300	-	447	-

Table 5.1-8

Calculated Values from Time-Lag Measurements on Impregnated Graphite Sample No. K42

Gas	D'_t cm^2/sec $\times 10^4$	D'_{gt} cm^2/sec $\times 10^4$	H	K_k^* cm^2/sec $\times 10^4$	$\frac{\mathcal{E}\mathcal{K}_{gs}\eta}{\mathcal{K}_{gt}}$	$K_k\phi_o$ cm^2 $\times 10^4$	$K\phi$ (av) cm^2 $\times 10^4$
H_2	30.1	30.1	0	4.18	0.139	175	169
He^+	32.4	21.4	-0.34	3.10	0.145	121	109
N_2	1.41	8.10	4.75	1.26	0.156	1133	1004
A	2.11	6.77	2.21	0.93	0.137	558	604
Xe	0.07	3.74	52.1	0.33	0.088	5940	4750

* From Table 4.1-4

\+ Using ϕ_o = 0.65 min

were constant with p_m and not scattered like the helium results, hydrogen was assumed to be negligibly adsorbed as a basis for the diffusion coefficient calculations.

(b) Calculation of Diffusion Coefficients

The procedure employed in section 5.1.3.4(b) for calculating diffusion coefficients and structure factors for Morgan "EY9" graphite was also followed for Impregnated Graphite Sample No. K42. As shown in later discussion, this procedure was only approximate. Values of the diffusion coefficients D'_t and D'_{gt}, calculated from the values of ϕ_o by means of equations (2.1.5-8) and (2.1.5-12), respectively, are given in Table 5.1-8; hydrogen was assumed to be non-sorbed as mentioned above. Except for helium, the values of D'_{gt} were greater than the values of D'_t.

Actually equation (2.1.5-8) only applied for linear flow in a plane porous medium. For radial flow in a hollow cylindrical sample, a more complex expression given by Barrer (ref.257,p.37) should have been used to calculate values of D'_t from ϕ; simplification of the expression by inserting the values of the diameters d_i and d_o for Impregnated Sample No. K42 showed that the substitution of $(d_i - d_o)/2$ for L in equation (2.1.5-8) caused the values of D'_t to be 6% low.

On the assumption that surface flow was negligible ($D'_{st} = 0$), values of the adsorption coefficient H were calculated by means of equation (2.1.5-10). The values of H (Table 5.1-8) were greater than those for Morgan "EY9" graphite (H less than unity). For helium flow, H was negative but the values of ϕ_o and D'_t were considered inaccurate.

For xenon flow, H was very large and indicated considerable adsorption; the value of the Henry's law constant k_s was 1.29×10^{-4} ($\varepsilon = 0.11$, $S_v = 4.47$ cm^2/cm^3 for Impregnated graphite - section 5.6.2) and was of about the same order as the values of k_s for the flow of sulphur dioxide through a bed of analcite spheres.[101] The lifetime of the xenon molecules in the adsorbed state τ was estimated to be 2.4×10^{-8} sec and the heat of adsorption E_a as 7650 cal/mol (cf. section 5.1.3.4(b)).

The structure factor $\varepsilon K_{gs} \eta / K_{gt} = \varepsilon K_g$ was calculated for each determination by means of equation (2.1.5-18), the values of $K_k (= a)$ being obtained from Table 4.1-4. Except for xenon flow for which the K_k value was low (see 4.1.4.1), the values of the factor agreed quite closely and gave an average value of 0.144. If η was taken as unity, the porosity ε_s for steady state flow was therefore 0.144, which was greater than

the total porosity ε (= 0.11 - see Table 5.6-5). Therefore, either η was greater than one or hydrogen was in fact adsorbed. If the calculations were repeated on the assumption that helium was non-sorbed and its ϕ_o value was 0.65 min, the value of H for each gas was larger and the average value of $\varepsilon\mathcal{K}_g$ was 0.095. The use of the wrong time-lag equation (equation 2.1.5-8) did not affect the values of H but caused the factor $\varepsilon\mathcal{K}_g$ to be 6% high.

The assumptions made in the calculations presented above have been adequately considered for Morgan "EY9" graphite (section 5.1.3.4(c)). Because H varied with p_m as shown in section 5.1.3.4(h), the values of the diffusion coefficients were not constant but also varied with pressure; the extrapolated values at $p_m = 0$ given in Table 5.1-8 represented their order of magnitude for p_m above about 5 cm Hg.

(c) <u>The Xenon Determination</u>

For the xenon determination (No. L:56), very long time-lags were observed (142 to 274 min). Because a number of values of p_o were measured for each pressure increase experiment before steady state flow was attained, the transient portion of the pressure increase plots was well-defined and the method of Call[259] was applied to calculate values of the diffusion coefficient.

In this method, the time was measured for the gas flow-rate through the porous material to become a definite fraction (a half) of the steady state flow-rate; this time was then substituted into a simple equation. However, it was difficult to estimate the time accurately and the values of D differed from those calculated by equation (2.1.5-8) by as much as 12%. Because D varied with p_m, Call's method was not really applicable.

In the xenon determination, the break-through time was about 50 min; this was the time required before any gas appeared at the outgoing side of the graphite after the commencement of the experiment and was caused by an immobile saturated monolayer of adsorbed gas being laid down at all points within the medium reached by the diffusing gas.[260] Barrer[260] has discussed flow in a porous medium when this type of adsorption occurred but only presented a simplified theory for the condition when the break-through time approximated the total time-lag. This method of calculation could not therefore be applied to the xenon experiments where the break-through time was only a small fraction of the time-lag.

(d) <u>The Adsorption Isotherms</u>

For each determination on Impregnated Graphite Sample No. K42, values of the product $K\phi$ were calculated and averaged. The average values, which did not include

the $K\phi$ values below $(p_m)_{min}$, are listed in Table 5.1-8; these values increased approximately with the molecular weight of the gas but the argon value was less than the nitrogen value. The value of $K_k\phi_o$ for each determination agreed fairly closely with the average $K\phi$ value.

Values of H were calculated by means of equation (5.1.3-5) from the individual $K\phi$ values for the experiments in several of the determinations (cf. section 5.1.3.4(h)). Surface flow was assumed to be negligible; εK_g was taken as 0.07 (cf. 0.144, section 5.1.4.3(d)) so that H was positive but very small for helium flow through the sample at p_m = 3 to 5 cm Hg. These assumptions could only be confirmed by independent adsorption measurements.*

The H-p_m plots for hydrogen, nitrogen, and xenon flow in Sample No. K42 are shown in Fig. 5.1-8. For hydrogen and nitrogen adsorption, the values of H decreased sharply with increasing p_m at low pressures but then became approximately constant; for xenon adsorption, the values of H decreased gradually as p_m increased. The shapes of these plots resembled those for the respective ϕ-p_m plots for these gases, with a minimum

---

* Attempts by Mr. D. Williams to measure the adsorption of nitrogen on an Impregnated graphite sample by means of a sensitive gravimetric balance yielded inconclusive results.

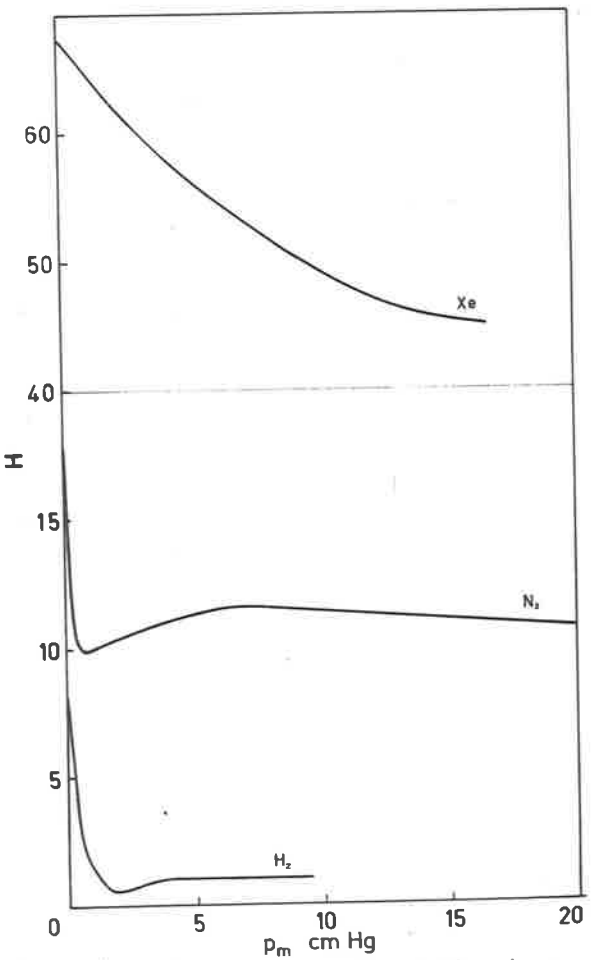

Fig. 5.1-8 Graphs of H against p_m for Hydrogen, Nitrogen, and Xenon Adsorption on Impregnated Graphite Sample No. K42 Derived from the Time-Lag Results.

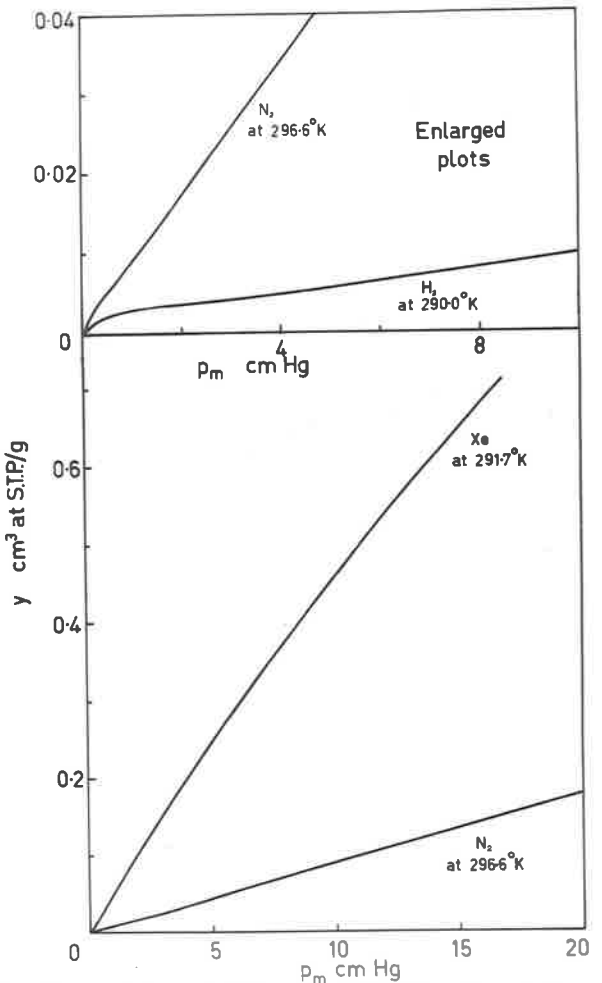

Fig. 5.1-9 Adsorption Isotherms of y against p_m for Hydrogen, Nitrogen, and Xenon Adsorption on Impregnated Graphite Sample No. K42 at Room Temperature.

being obtained at p_m = 1 to 2 cm Hg.

By graphical integration of the H-p_m plots (Fig. 5.1-8), typical adsorption isotherms of the volume of gas adsorbed y against the mean pressure p_m were obtained for hydrogen, nitrogen, and xenon adsorption on Impregnated graphite near room temperature (see Fig. 5.1-9). The conversion factor was

$$\Delta y = 0.80 \times 10^{-3} \; H \, \Delta p \quad cm^3 \text{ at S.T.P/g.}$$

Xenon was adsorbed to the greatest extent and hydrogen the least. The adsorption isotherm was almost straight for hydrogen and nitrogen, but was slightly curved for xenon; at low pressures, however, there was a distinct hump or knee in the hydrogen and nitrogen isotherms (see enlarged plots, Fig. 5.1-9), showing that Henry's law could not be assumed. The isotherms were therefore of Type II or Type IV of the Brunauer classification,[176] and the humps were less distinct than those observed for Morgan "EY9" graphite (Fig. 5.1-6). Possibly the H-p_m plot for xenon flow would have curved more sharply upwards at low p_m and a hump would have been observed in the adsorption isotherm if the xenon permeability determination (No. L:56) had been continued to lower p_m. At any pressure, the amount of nitrogen adsorbed on Impregnated graphite was about 10 times greater than that for Morgan "EY9" graphite.

Since the surface area of the Impregnated graphite was about 2.5 m^2/g (see section 4.3), the monolayer capacity V_m was estimated to be 0.3 cm^3 at S.T.P./g (cf. section 5.1.3.4 (h)). Thus, for Sample No. K42, the monolayer would be completed at about p_m = 6 cm Hg for xenon adsorption and about p_m = 35 cm Hg for nitrogen adsorption, i.e., at much lower relative pressures than for Morgan "EY9" graphite. For krypton adsorption on Impregnated graphite at -193°C, V_m was reached at very low pressures (at about p = 0.001 cm Hg).

5.1.4.4 Minima in the K-p_m Plots

For Impregnated Graphite Sample No. K42, definite evidence of a minimum in the K-p_m plot at low pressures was obtained for hydrogen and nitrogen flow. For argon and xenon flow, the determinations were not continued to low enough pressures for minima to be observed, while for helium flow, the inaccuracy of the values of K at low pressures caused some scatter of the points and no definite indication of a minimum.

For the minima observed, the value of the mean pressure $(p_m)_{min.}$ was greater for hydrogen flow than for nitrogen flow. In contrast to the minima results for Morgan "EY9" graphite (see section 5.1.3.5 (a)), this variation was in accordance with that observed by other authors, since $(p_m)_{min.}$ was directly proportional to

$\mu / \sqrt{M}$ (see Table 5.1-6). The values of $(p_m)_{min.}$ were approximately of the same magnitude as those for Morgan "EY9" graphite (Table 5.1-6) and not higher as was expected for the finer-pored graphite. The values of N_{Ku} corresponding to the minimum, viz., 54 and 69 for hydrogen and nitrogen flow, respectively (d = 0.14 microns for Impregnated graphite - see Table 5.6-6), were much greater than those for "EY9" graphite. Values of N_{Ku} as high as a 50 have not been noted previously in the literature; the values obtained for ceramic samples[67,68,97] were from 1 to 3 while that for a graphite sample[97] was about 25. The ratio of K_i/K_k was greater for hydrogen flow than for nitrogen flow.

There was some indication of a minimum being obtained by the pressure decay method for nitrogen flow in Sample No. K42; however, the results were rather scattered for any definite proof. Generally, the accuracy of K values determined by the pressure decay method was not high at low pressures where a minimum was expected.

5.1.4.5 Flow at High Pressures

The results of the high pressure permeability determinations on Impregnated graphite samples (see section 4.1.4.2) showed that the K-p_m plots were apparently not curved up to mean pressures of about 800 cm Hg.

From the limited number of experiments performed with p_o differing from atmospheric pressure, there was no evidence that the flow phenomenon, which was observed for flow through P.G. 60 and Acheson "A" graphites at high pressures (see section 5.1.2.4), occurred for flow through Impregnated graphite. Thus, as was expected for the relatively fine-pored Impregnated graphite, deviations from viscous type flow only occurred at quite high pressures.

For each sample of Impregnated graphite, a value of β was estimated from the average value of B_o (Table 5.1-1) by means of the graphical correlation of β against B_o (Fig. 5.1-2). For Sample No. K41, $\beta = 2.75 \times 10^{14}$ cm^{-1}; for Sample No. K42, $\beta = 1.25 \times 10^{13}$ cm^{-1} for the low pressure value of B_o (1.12×10^{-14} cm^2) and $\beta = 2.93 \times 10^{13}$ cm^{-1} for the high pressure B_o value (0.59×10^{-14} cm^2).

With these values of β, and the experimental values of B_o and a, it was estimated that $N_{Re} = 0.01$ occurred at about $p_m = 1100$ cm Hg for nitrogen flow in Sample No. K41 (Detmn. No. H:14) and at about $p_m = 450$ cm Hg for nitrogen flow in Sample No. K42 (Detmn. No. H:22). Inertial flow was therefore not observed experimentally in Sample No. K41, but was significant for Sample No. K42 above about $p_m = 450$ cm Hg for nitrogen flow and at much

higher pressures for hydrogen flow (N_{Re} = 0.0057 at p_m = 540 cm Hg for Detmn. No. H:23).

The average K-p_m plot for Detmns. No. H:6 and No. H:22 (nitrogen flow in Sample No. K42) was apparently straight over the pressure range examined (p_m = 130 to 690 cm Hg); however, the K-p_m points below about p_m = 300 cm Hg for Detmn. No. H:6 were slightly lower than those for Detmn. No. H:22 and possibly indicated that the plot did curve slightly and that the points for Detmn. No. H:22 were in error owing to inaccurate measurement of the low flow-rates. Then the high pressure nitrogen results for Sample No. K42 would agree more closely with the low pressure results (Detmn. No. L:29). Unless the hydrogen high pressure results (Detmn. No. H:23) were much more inaccurate than expected, the K-p_m plot for hydrogen flow was still much higher than that determined by the low pressure method (No. L:55).

Accurate values of the permeability coefficient determined in the high pressure apparatus at low mean pressures (p_0 a vacuum) could only be obtained provided the low flow-rates were measured accurately and without difficulty and all leaks in the vacuum system of the apparatus were eliminated.

5.1.4.6 The Freon High Pressure Determination

The results of the high pressure experiments for

freon flow through Impregnated Sample No. K41 (Detmn. No. H:11A) showed that the permeability decreased as the relative partial pressure p_m/P_o of the gas neared unity, i.e., as the pore space became almost completely filled with condensed freon. Thus, at p_m about 370 cm Hg ($p_i/P_o = 1$, $p_o/P_o = 0.75$), the values of the permeability coefficient were only about 20% of those expected by comparison with the determinations for the other gases in the sample, although at about $p_m/P_o = 0.6$, the values of K were approximately as expected (see Fig. 4.1-15) even when p_i was greater than P_o. The variation in K could not be further investigated as the graphite sample became blocked after these experiments.

Apparently the permeability was low when p_m/P_o was greater than about 0.8 and p_i approximated to P_o, but varied with p_m in the normal manner when p_m/P_o was lower even though p_i was greater than P_o. These deductions were drawn from the limited experiments performed and could be in error; no final conclusions were possible until the flow problem was examined in greater detail.

The observation of a decreased permeability at high relative partial pressures was contrary to the findings of Carman[122] for the flow of freon and

sulphur dioxide through a Linde silica plug at -33.1°C. For relative vapour pressures near unity, he obtained permeability values which were much greater than the expected permeability for gas phase flow (see section 2.1.6.2). Similar results were obtained by Gilliland et al.[83] for the flow of isobutane through porous Vycor glass, and by Jones and Isaac[261] for carbon dioxide flow in plugs of lampblack.

However, it has been reported[118,124] that the permeability decreased sharply when the saturation pressure was exceeded because the condensed liquid tended to block the pores and hinder the flow. This was apparently the effect observed experimentally for freon flow in Impregnated graphite (Detmn. No. H:11A). As p/P_o increased, the smallest pores would fill with condensed freon first and then the pores of larger size r in accordance with the Kelvin equation

$$\ln\left\{\frac{P_o}{p}\right\} = \frac{2\gamma M \cos\theta}{r \rho_l \mathcal{R} T} . \qquad \ldots (2.4.4\text{-}2)$$

When the large pores in which the gas phase flow predominated began to fill, the resistance to flow became greater and hence the gas flow-rate and permeability decreased. When p_i was greater than P_o, all the pores were filled and the observed flow was due to the transport of the condensed liquid by viscous flow.[124]

It was not possible to tell from the limited results whether any enhanced flow occurred between p_m/P_o = 0.6 and 0.85 because of the flow of capillary condensate. The experiments of Carman[122] showed that K increased sharply in the region where p_m/P_o was about 0.75. In contrast to the experiments of Carman,[122] and Gilliland et al.,[83] there was no evidence of surface flow of freon in Sample No. K41, the freon probably being held at the pore walls as immobile films.

It was therefore suspected that flow in the condensed phase would make a negligible contribution to the total flow at high relative pressures, and no enhanced flow would be observed. According to Carman (ref.5,p.126), capillary condensate flow should have occurred for freon flow in Impregnated graphite at 20°C and p_m = 360 cm Hg since the ratio of ρ_l/ρ_m, which was a measure of the ratio of the capillary pressure difference to the gas phase pressure difference, was about 55.

The experimental work on freon flow in Sample No. K41 was limited as mentioned previously since the sample became blocked and did not allow further permeability measurements (section 4.1.4.2). Evidently the sudden release of the pressure when the sample was removed from the apparatus caused the condensed freon in the pores to evaporate rapidly; the refrigeration

effect associated with this expansion resulted in the freon and the water vapour in the freon freezing in the pores. This surmise was supported by the observation that the sample and the permeability cell, on removal from the apparatus, were covered with a white powdery deposit and felt cold. Any evaporation of freon would lead to further cooling and freezing of the water so that it was not possible to unblock the sample. A similar phenomenon was observed with a laboratory refrigeration unit when water vapour in the freon -12 refrigerant froze in the expansion valve and prevented successful operation of the unit until a drying tube was added.

5.1.5 Pressure Distribution Measurements

The consideration of the theoretical and experimental aspects of the distribution of pressure in a porous medium during gas flow presented in section 2.1.1.4 showed that very little attention had been given to this subject, especially when the flow was outside the viscous region. The pressure distribution can be quite important for certain flow problems with porous media.

Frequently, the pressure $p_{1/2}$ at the centre of a porous medium has been wrongly assumed to equal the mean pressure p_m instead of a pressure up to 30% higher

than p_m.[19] As a consequence of the pressure distribution theory, the integration of Darcy's law and the application of the permeability equation $K = Q_m p_m L / \Delta p A$ are valid for high Δp when $p = p_m$ (see section 5.1.5.2). The pressure distribution should also be considered when calculating surface diffusion coefficients (see section 2.1.6.1), since the calculation method is not valid when Δp or Δc is large and the adsorption and diffusion coefficients are not constant (cf. section 5.1.3.4(f)).

5.1.5.1 Equations for the Pressure Distribution Curves

By solving the steady state flow equation for gas flow through a porous medium with the appropriate boundary conditions, equations expressing the variation of p with x have been derived (see Appendix E.1). The equation for the distribution of pressure for viscous flow has been mentioned previously in the literature (ref.15,p.680). The equation for viscous and slip flow (equation 2.1.1-13), which was mentioned in section 2.1.1.3, apparently has not been given before. The "ideal" distributions calculated for the pressure distribution results were obtained by means of the latter equation (see section 4.1.5).

As a result of the high pressure flow determinations on P.G. 60 and Acheson "A" graphites

(see section 5.1.2.4(g)), a satisfactory expression (5.1.2-7) was obtained for the flow of gases through reactor graphites when slip, viscous, and turbulent flow all occurred simultaneously in the porous medium. From this expression, a more general solution to the flow equation was attempted to give the distribution equation covering all three flow regions (see Appendix E.1, Condition 4). The resulting equation (equation E.1-11) was complex and difficult to solve for p; however, solutions were possible for special conditions.

When N_{Re} was less than 0.01, i.e., when only viscous and slip flow occurred (Condition 4a), equation (2.1.1-13) was obtained, viz.,

$$p^2 + \frac{2a}{b} p - \left(\frac{a}{b} + p_m\right) 2 \Delta p \frac{x}{L} - p_o^2 - \frac{2a}{b} p_o = 0. \quad \ldots (2.1.1\text{-}13)$$

For complete turbulent flow, i.e., for N_{Re} greater than 100 (Condition 4b), the solution was

$$p^2 - 2p_m \Delta p \frac{x}{L} - p_o^2 = 0. \quad \ldots (2.1.1\text{-}11)$$

As this latter solution was the same as that for viscous flow alone, equation (2.1.1-11) expressed the distribution of pressure for gas flow whenever slip flow was negligible. When the permeability was a constant (Knudsen flow), the pressure distribution was linear (Condition 1).

For flow in the transition region (N_{Re} between 0.01 and 100), analysis of some high pressure results (see Table E.2-2, Appendix E.2) showed that while equation (2.1.1-11) gave the distribution of pressure when no slip flow occurred, it also gave quite satisfactory values of p above N_{Re} = 0.01 when the percentage of slip to viscous flow was less than about 20%. For gas flow in the reactor graphites, slip flow was significant in the transition region, but was less than 20% of the viscous flow. The analysis indicated that equation (2.1.1-13) gave more accurate pressure distributions below N_{Re} = 1.0 than equation (2.1.1-11). As these distributions were almost the same as those calculated from the complex equation (E.1-11), it was thus unnecessary to solve this equation except for the probably very rare occasion when the proportion of slip flow in the transition region was large. Thus the calculation of the "ideal" distributions for the experimental pressure distribution results for the reactor graphites (section 4.1.5) by means of equation (2.1.1-13) did not lead to very large errors when the flow was in the transition region.

The distribution of pressure in a porous medium for all conditions of flow from Knudsen to complete turbulent flow could therefore be expressed mathematically

by equation E.1-11. The theoretical considerations presented here give the first complete analysis and discussion concerning the distribution of pressure in a porous medium, previous work reported in the literature being very limited as shown in section 2.1.1.4.

5.1.5.2 Consequences of the Pressure Distribution Equations

As a consequence of the pressure distribution equations, it was demonstrated (Appendix E.1) that the various forms of Darcy's law (see section 2.1.1.5) could be integrated when Δp was large to give the permeability coefficient at the mean pressure in the medium since, at $p = p_m$, $\partial p/\partial x = \Delta p/L$. Previously, when calculating the coefficients B and K (both dependent on pressure) from the permeability equations, Carman (ref.5,p.2) had stipulated that Δp should be small enough so that the coefficients were effectively constant.

The discussion already given in section 2.1.1.6 indicated that the validity of the permeability equations for large Δp only applied when the permeability coefficient K was a linear function of pressure, i.e., when the flow was in the viscous and slip flow regions. However, the derivation of an expression for the pressure distribution for flow in the transition and

turbulent regions (Appendix E.1, Condition 4) led to the conclusion that this validity of the equations also applied when turbulent flow occurred and K was expressed by equation (5.1.2-7).

Biram[262] has obtained the expression

$$\frac{a}{b} = \frac{\frac{1}{2}(p_i^2 + p_o^2) - p_{\frac{1}{2}}^2}{2p_{\frac{1}{2}} - (p_o + p_i)} \quad \ldots (5.1.5\text{-}1)$$

and proposed that the constants a and b in the expression for K_v ($= a + bp$) could be found by measuring the permeability, and the pressures at the midpoint $p_{\frac{1}{2}}$ and at both ends (p_i and p_o) of a specimen during gas flow. Biram obtained his expression from the pressure distribution, but made no mention of the actual equation or further consequences of the distribution in his note. Biram's expression was readily derived from equation (2.1.1-13) for the pressure distribution in a porous medium for viscous and slip flow.[17] A more general expression for a/b was obtained in terms of the pressure p_N at the point $x/L = N (1 > N > 0)$, e.g.,

$$\frac{a}{b} = \frac{N p_i^2 + (1 - N) p_o^2 - p_N^2}{2\left[p_N - N p_i - (1 - N) p_o\right]} \quad \ldots (5.1.5\text{-}2)$$

The application of Biram's expression to the results of the pressure distribution experiments reported in section 4.1.5 gave values of a/b which

were generally very much less than the experimental values of a/b and were often negative. This considerable difference (up to 140% of the experimental a/b) was due mainly to the inhomogeneity of the graphite (see section 5.1.5.6); the above expressions, (5.1.5-1) and (5.1.5-2), thus only applied to calculate a/b for ideal homogeneous porous media.

5.1.5.3 The Experimental Pressure Distributions

Typical examples of the pressure distribution curves obtained experimentally for gas flow through the P.G. 60, Acheson "A", and Morgan "EY9166" graphite pressure distribution specimens have been given in Figs. 4.1-17 to 4.1-20, section 4.1.5. All the distributions were approximately parabolic in shape; the shape of a particular distribution curve depended upon the variation of the permeability between the individual discs of the specimen and probably resulted from the inhomogeneity of the graphite (section 5.1.5.6).

The distribution curves were plotted dimensionlessly as $(p-p_o)/(p_i-p_o)$ against x/L so that the curves for different experiments could be easily compared. A unique distribution curve covering all experiments was not obtainable. The dimensionless distributions were observed to be more curved as Δp increased when either p_i, p_o, or p_m was held constant, and as p_m

decreased when Δp was constant. In other words, the deviation of the mid-point dimensionless pressure $(p_{½}-p_o)/(p_i-p_o)$ from 0.5 increased as p_o became smaller. These observations were consistent with the predictions from the theoretical distribution equations, and with the observations of Aronofsky and Jenkins.[19]

Consideration of equation (2.1.1-13) showed that the curvature of the distributions increased as the value of a/b decreased for any given pressure conditions of p_i and p_o (see Appendix E.2). For the flow of different gases in the same graphite specimen, a/b was proportional to $\mu(\mathcal{J}/M)$, i.e., the curvature increased in the order of hydrogen, nitrogen, carbon dioxide, and freon-12 flow at constant temperature, and as the temperature decreased for the flow of a given gas. For the flow of the same gas in different graphite specimens, the pressure distributions for Morgan "EY9166" graphite should be the least curved since the a/b ratio was the greatest (81.1 for nitrogen flow) (cf. Appendix E.2).

Unfortunately, only a few comparisons between experiments with different gases or specimens but under almost the same pressure conditions of p_i and p_o were possible because of the difficulty in obtaining set pressures in the different determinations. For the

measurements on the P.G. 60 and Acheson "A" graphite specimens, the distribution curves for different gases under almost the same pressure conditions were very close and no such trend as predicted above was observed (sections 4.1.5.1 and 4.1.5.2) since the values of a/b were small (less than 10) for these graphites. For the Morgan "EY9166" specimen (see section 4.1.5.3), the distributions for freon flow (Detmn. No. G:6) did tend to be more curved than those for carbon dioxide flow (Detmn. No. G:5) in accordance with the theoretical predictions, but the freon measurements were suspected to be inaccurate.

Because of the limited number of comparable experiments, and the variation in the shape of the parabolic distribution curves for the different graphite specimens (due to the inhomogeneity of the graphites), little comparison was possible between experiments on different specimens under the same pressure conditions. The comparisons made, however, did show that the distribution curves for P.G. 60 graphite were more curved than those for Acheson "A" graphite, while the plots for the Morgan graphite specimen were the least curved of all; these observations were in agreement with the theoretical calculations in Appendix E.2.

5.1.5.4 Comparison Between the Experimental and "Ideal" Pressure Distributions

Except for the experiments in Detmn. No. G:1, the "ideal" pressure distribution for any experiment, calculated from the theoretical equation (2.1.1-13), was lower or less curved than the experimental distribution. This difference was attributed to the inhomogeneity of the graphite, which caused the permeabilities of the individual graphite discs of any specimen to vary considerably (see section 5.1.5.6). The use of equation (2.1.1-13) to calculate the "ideal" distributions for the P.G. 60 and Acheson "A" specimens instead of an expression for the transition flow region was shown to be satisfactory in section 5.1.5.1.

As a result of the inhomogeneity of the graphite, the comparison of an experimental distribution curve with the "ideal" curve indicated little except an idea of the variation of the resistances to flow of the individual discs in the specimen. The effect of transition flow (shown theoretically to cause little variation from the "ideal" parabola of equation(2.1.1-13)) and possibly surface flow (e.g., with freon) on the experimental distributions could not be ascertained.

The "ideal" pressure distribution curve for any experiment should represent the distribution if the

porous medium was completely homogeneous in the flow direction. For some of the experiments, distributions were calculated from the experimental results allowing for the inhomogeneity of the graphite; by equating the mass flow-rate through a disc ($K_{disc} \Delta p_{disc}/L_{disc}$) to the mass flow-rate in the overall specimen ($K_{ov} \Delta p_{ov}/L$) when the pressure at one end of the disc was known and K was expressed by equation (5.1.2-7), the unknown pressure at the other end of the disc was estimated. The calculated distributions were very close to the "ideal" distributions, thus showing that the latter represented the distributions for a completely homogeneous porous medium.

5.1.5.5 The Determination of the a/b Values

The value of a/b taken to calculate the "ideal" pressure distributions for each determination was the overall value, i.e., the value obtained from the plot of K_{ov} against p_m. For Morgan "EY9166" graphite, this value was lower than the value of a/b obtained as the average for the discs in the specimen since the experimental K_{av} points lay above the K_{ov}-p_m plots because of the inhomogeneity of the graphite. Because the values of K_{av}, calculated from a theoretical pressure distribution for any value of a/b close to the overall value, agreed closely with the K_{ov}-p_m plot, the overall

value of a/b was used in the calculations.

For the P.G. 60 and Acheson "A" graphite specimens, the choice of the value for a/b was further complicated by the occurrence of some turbulent flow, which caused the $K-p_m$ plots for each graphite to be curved. As insufficient experiments were performed in any determination to obtain a/b from the straight portions of the graphs at low pressures, the straight K_v-p_m plots were estimated from the overall $K-p_m$ values by means of equation (4.1.5-1) (see sections 4.1.5.1 and 4.1.5.2). Values of K_{ov} calculated from these values of a/b checked with the experimental K_{ov} values to within 1%.

The overall values of a and b for Morgan "EY9166" graphite and the estimated values for P.G. 60 and Acheson "A" graphites were generally of the same order as the corresponding values obtained in the low or high pressure permeability determinations; the higher estimated values of a observed for the latter graphites were probably due to an inaccuracy in the estimation method.

By calculating the theoretical pressure distributions for different values of a/b, it was shown that the wrong choice of the value of a/b would probably not cause a very large error in the pressure values.

The variation in the pressure values was greater when p_o = 0 cm Hg than when p_o = 76 cm Hg, and also when x/L = 1/4 than when x/L = 3/4. For a total variation in a/b of 8 for Acheson "A" graphite and 30 for Morgan "EY9166" graphite, the variations in the $p_{1/2}$ values were about 0.2% and 3% when p_o = 76 and 0 cm Hg, respectively.

5.1.5.6 The Inhomogeneity of the Graphite

The distribution measurements (section 4.1.5) showed that the values of K for the individual discs in a given graphite specimen varied considerably at any p_m. This variation indicated that the structure of the original graphite blocks was apparently inhomogeneous in the flow direction. As mentioned before, this inhomogeneity of the specimens led to the differences between the "ideal" and experimental pressure distributions, and the particular shape of each experimental distribution curve. Leakage around the discs of a specimen could have also led to these differences, but this effect was considered negligible (see 5.1.5.7). Inhomogeneity of the graphites was also observed for other permeability measurements (see Table 4.5-1).

For the small discs (1 cm thick x 1.25 cm diameter) employed in the pressure distribution specimens, the

inhomogeneity of the graphite was exaggerated; any local variations in the structure (e.g., cracks) would cause different discs to have widely different permeabilities. In the longer samples used in the permeability studies (5 to 9 cm long x 1.25 cm diameter), local structural variations would not influence the gas flow-rate through a sample to the extent as in the smaller discs; variations in structure would average out so that a smaller difference would be observed between different samples of the same graphite and the inhomogeneity would not be so marked.

For the P.G. 60 graphite specimen, the thickness of the discs was increased from 1.0 cm to 2.5 cm in an attempt to decrease the variation of K between discs.

5.1.5.7 Accuracy of the Distribution Measurements

The accuracy with which the pressure distributions were measured depended upon the errors in the pressure measurements. Mercury manometer pressures were in error by less than 0.12 cm Hg, and capillary depression of the mercury in the two arms of each of the small bore manometers was assumed to cancel out. Errors in the measurement of the values of K were generally less than 6% (see Appendix C.5.3).

Special care was taken when preparing the composite graphite specimens to ensure that no leakage occurred

around a disc or to the atmosphere (see section 3.1.6.1). Leaks to the atmosphere, readily found by applying soap solution when the specimen was pressurized, were sealed with Epoxy resin.

Discontinuities or steps would be observed in the distribution curve if a leak occurred around a disc since the pressure drop would then be reduced and the effective permeability increased. For a very small leak of the order of size of the holes in the graphite, unfortunately only very small discontinuities, of similar shape to those produced by the inhomogeneity of the graphite, would result in the distribution curves. Thus, both small leaks around the discs and the inhomogeneous nature of the graphite could lead to the observed variations between the K values for each disc in a specimen and the deviations from the "ideal" parabolas (cf. section 5.1.5.6).

In order to check for leaks in Specimen No. G1, the specimen was reversed after Detmn. No. G:1 and a further series of experiments conducted (Detmn. No. G:2). The pressure distribution curves were similarly shaped as shown in Fig. 4.1-19, but placed at about equal distances on either side of the "ideal" distribution curve. The high resistance of disc No.4 in the specimen caused the initial large decrease in pressure for

Detmn. No. G:1. Although no satisfactory $K-p_m$ plots were drawn for the individual discs in the specimen because of turbulent flow effects, the rough plots prepared did show that the K_{disc} values for any disc for Detmn. No. G:2 agreed within experimental error with the $K-p_m$ plot for that disc as obtained in Detmn. No. G:1. These rough plots all gave values of a and b in reasonable agreement with those obtained from the corrected K_v-p_m plot.

As no unreasonable or inconsistent $K-p_m$ plots were obtained for any of the specimens, the small discontinuities in the distribution curves were attributed to the inhomogeneity of the graphites and not to leaks in the specimens.

It was really of little consequence whether the observed deviations from ideality were in fact due to inhomogeneity or leakage; as far as could be determined, the experimental distribution results confirmed the predictions obtained from the theoretical considerations.

5.2 The Porosity Measurements

5.2.1 The Accuracy of the Measurements

For the helium displacement measurements, the graphite samples were generally outgassed at about 300°C for about 16 hr (see Table 4.2-1). According to Roberts et al.,[169] outgassing for a few hours at 300°C removed the adsorbed water vapour from graphite samples and raised the helium density by about 1% from the value obtained after outgassing at room temperature; outgassing at 740°C only raised the density a further 0.5%.

The accuracy of determining the dead space volume in the bulb V_D was quite good, but the measurement of the bulb volume V_b proved quite inaccurate as mentioned in section 4.2. Greater accuracy could be achieved if V_b was measured by helium expansion prior to the insertion of the sample into the bulb. A special bulb would be required so that the sample (1.2 cm diameter) could be inserted via a conical joint with the seal being able to withstand the outgassing temperature and the dead space volume being kept to a minimum.

For satisfactory helium displacement measurements, the helium should be negligibly adsorbed (see section 2.2.2.1). The transient flow measurements showed that helium was slightly adsorbed by Morgan "EY9"

and Impregnated graphites (sections 5.1.3.4(e) and 5.1.4.3(d)). From these measurements, the volume of helium adsorbed at p = 20 cm Hg by these graphites during the helium displacement measurements was estimated to be about 0.2% and 0.4% of the total gas volume in the apparatus, respectively; such adsorption would cause errors in the volume V_D of 2% and 4½%, respectively.

However, there was no evidence of adsorption of helium by the graphite during the measurements since equilibrium was attained very quickly after each gas expansion and the total volume of gas at S.T.P. in the apparatus remained almost constant (see section 4.2). The extent to which adsorption of helium actually did occur could only be ascertained by accurate adsorption measurements on the graphite samples.

5.2.2 The Values of the Pore Properties

As was to be expected from the general texture of the graphites, P.G. 60 graphite had the highest porosity (ε = 0.54), with Acheson "A" (0.28), Morgan "EY9" (0.15), and Impregnated (0.11) graphites following in order. For P.G. 60 graphite, the experimental value of ε was higher than that given by the manufacturers (0.48 - see Table A.1-1). Hutcheon et al.[34] found that ε for Morgan graphite was 0.170, while Wall showed that ε = 0.159 ± 0.001 for Morgan "EY9166" graphite.

164

For P.G. 60 and Impregnated graphites, the reproducibility of the values of ε was quite good. However, for Morgan "EY9" graphite, the 27% difference between the two values of ε was due to the inhomogeneity of the graphite and the inaccuracy of the measurements.

The values of the helium density ρ_s (between 1.97 and 2.10 g/cm^3) were lower than the theoretical density of solid graphite ρ_o as determined from X-ray crystallographic data[168] (2.265 g/cm^3). Dresel and Roberts[263] obtained similar density results for synthetic graphites. These low helium densities for graphite showed[168] that a considerable portion of the pore space of graphites either was less than 30Å in radius or contained larger pores blocked or totally closed so that they were inaccessible to helium molecules.

For reactor graphites, Roberts et al.[169] found that 12 to 22% of the total pore volume was inaccessible to helium. For the helium displacement measurements on the graphite samples (see section 4.3), the percentage of unopen pores in the graphites was between 16 and 36%. For the calculation of these percentages (see Appendix F), the density ρ_o was assumed to be 2.265 g/cm^3; this assumption might not be true if any impurities were present in the graphites.

5.3 The Surface Area Measurements

5.3.1 The Accuracy of the Method of Measurement

The graphite samples were outgassed at approximately 300°C for about 16 hr (see section 3.3.3.1). These conditions were sufficient to remove all adsorbed water vapour. For reactor graphite, Roberts et al.[169] found that the measured area after outgassing at 370°C was 35% higher than that after prolonged pumping at room temperature because of the removal of adsorbed water; outgassing at 800°C raised the surface area a further 6% apparently because adsorbed oxygen was removed.

The values of the surface area obtained for the Morgan "EY9" graphite samples differed by 17%. This was good reproducibility when the inhomogeneity of the graphite was considered. The krypton surface area apparatus had previously proved satisfactory for measuring the areas of lead sinters.[237]

Although the apparatus was available, no nitrogen surface areas were determined to check the absolute accuracy of the krypton areas; the inaccuracy of nitrogen surface area measurements below about 5 m^2/g (see section 2.3.2.1(b)) did not warrant the time required to calibrate the apparatus and develop a technique. Generally, satisfactory krypton surface areas have been obtained if the extrapolated liquid

vapour pressure P_o and σ_{Kr} = 19.5Å^2 were used in the calculations (see section 2.3.2.1(c)). A satisfactory krypton area value for a purified Acheson graphite was obtained by McDermot and Lawton[184] using σ_{Kr}= 19.5Å^2.

In the adsorption experiments, straight line B.E.T. plots were observed. If adsorption points had been obtained at smaller p/P_o intervals than was generally achieved in the experiments, a slight curvature in the plot may have been evident; however, because of the scatter amongst the adsorption and desorption points, only a straight line plot was justified. The relatively high values of the B.E.T. C-constant (greater than 100) observed in the experiments indicated that any error in the choice of P_o, resulting in curvature of the B.E.T.plot, would cause only a small error in V_m.[187] Errors due to the non-correction for thermal transpiration effects were negligible (see section 4.3).

In the relative pressure range studied (0 to 0.3), the krypton isotherms were sigmoid-shaped, and apparently belonged to Type II of the Brunauer classification[176] (cf. sections 5.1.3.4(h) and 5.1.4.3(d)). For a graphite sample at 78°K, McDermot and Lawton[184] obtained a similar krypton isotherm but with discontinuities at p/P_o = 0.4 and p = 1.7 x 10^{-3} cm Hg. The upward trend of the present isotherms at p/P_o = 0.3

was possibly due to a similar discontinuity; this possibly could not be confirmed because measurements were not made beyond $p/P_o = 0.3$.

5.3.2 The Surface Area of Acheson "A" Graphite

Values of the surface area were determined for both crushed and bulk samples of Acheson "A" graphite. The initial values of the area (about 1.3 m^2/g) for a crushed sample of graphite were about three times greater than the area (0.43 m^2/g) determined on the same sample (Detmn. No. S:3) approximately three years later (see section 4.3). The area of a bulk sample (Detmn. No. S:4) was 0.71 m^2/g.

Roberts et al.[169] have shown that both oxidation and grinding increased the surface area of a reactor graphite quite considerably (see section 2.3.1). These increases in the area were attributed to the opening-up of previously inaccessible pore spaces during the oxidation and grinding processes. With the exception of the area obtained from the third determination (No. S:3) on the crushed sample, the area results mentioned above for Acheson "A" graphite agreed with the observation of Roberts et al. since the area of the bulk graphite was about a half of the initial area of the crushed sample.

During the three year interval between Detmns. No. S:2 and No. S:3, the apparatus was

reconstructed; however, the same experimental procedure was employed both before and after the reconstruction. Any inaccuracies arising from experimental error or faulty technique did not explain the anomalous B.E.T. plot and low surface area/value for Detmn. No. S:3.

Thomas[190] has indicated that the area of silver films decreased on sintering at 20°C and on chemisorption of oxygen at temperatures up to 20°C. Other authors[264] also showed that the area of a clean catalyst surface decreased on the chemisorption of oxygen and carbon monoxide at room temperature. Therefore, it was believed that the anomalous result for Acheson "A" graphite was caused by some alteration of the graphite surface over the three year interval.

5.3.3 The Surface Area of Impregnated Graphite

The values of the surface area determined for the Impregnated graphite samples differed by 30%. As inaccuracies occurred during both determinations (Nos. S:8 and S:9), the average value of 2.5 m^2/g was taken as an order of magnitude only. Some variation between the area values for different Impregnated samples was to be expected because of the non-reproducibility[255] of the graphite impregnation process.

The average value of the area for Impregnated graphite was over four times greater than that of

Morgan "EY9" graphite. This difference showed that the area of the graphite had increased during the impregnation process (Morgan type graphite was the base material for the Impregnated graphites - see Appendix A.1) possibly because the impregnating material formed a fine honey-comb structure in the pores of the graphite.

In Detmn. No. S:9, the temperature of the liquid nitrogen bath was about 2°K lower than in previous determinations because of the purer liquid nitrogen. This lower bath temperature caused the much slower adsorption rate and the greater amount of krypton adsorbed during this determination compared with other adsorption measurements (see section 4.3).

The method of calculating V_m for Detmn. No. S:9 (see section 4.3) was not very accurate. The assumption that the intercept of the B.E.T. plot was zero was based on the results of the other area measurements. For the final adsorption, when the pressure after 7½hr adsorption was assumed to be the equilibrium value, the error in V_m was negligible if this pressure was 15% too high. Although the B.E.T. theory has been generally considered unsatisfactory[175] below $p/P_o = 0.05$, Gaines and Cannon,[188] and Thomas[190] demonstrated that the theory was applicable at lower relative pressures for krypton. Therefore, even though the maximum value of

p/P_o was less than 0.01, the adsorption results poor, and the method of calculation inaccurate, the value determined for the area of Impregnated Graphite Sample No. S42 was probably quite acceptable.

5.4 The Pore Size Distribution Measurements

5.4.1 Comparison Between the C.S.I.R.O and A.A.E.C. Measurements

The distribution graphs plotted from the tabulated results supplied by the A.A.E.C. were more accurate than the plots received from the C.S.I.R.O. since the agreement between the pore volume estimated from the distribution curve and the volume of mercury entering the graphite samples at the maximum pressure was closer than for the C.S.I.R.O. results. With both sets of graphs, the distributions of pore radii were considered inaccurate below about 200Å (2000Å for P.G. 60 graphite) because of the uncertain compression effects, and at the highest pore sizes because of the dubious contribution of the largest pores. The C.S.I.R.O. results were corrected for the compressibility of the graphite sample at high pressures, but the A.A.E.C. results for the Impregnated samples were not corrected (see section 4.4.2).

A comparison between the distribution graphs for Morgan "EY9" (C.S.I.R.O.) and Morgan "EY9166" (A.A.E.C.)

graphites showed that both distributions ranged between 100 and 100,000Å radii. The peaks were at r = 4000Å and 6000Å, respectively; the latter peak was neither as sharp nor as high as the former. The mean pore radii, estimated from the distribution data, agreed closely, being 0.31 microns and 0.44 microns, respectively.

5.4.2 Significance of the Measurements

The values of γ(= 480 dyn/cm) and θ (= 140°) as used in the pore size distribution calculations were the generally accepted values for most mercury/solid systems (see section 2.4.4.1(a)). Although no nitrogen desorption experiments were performed on the graphites to check the distributions, the results obtained by the C.S.I.R.O. and the A.A.E.C. were presumed to be quite reliable above about r = 200Å. The measurement of nitrogen desorption isotherms and the application of the capillary condensation theory (section 2.4.4.2), although involving tedious calculations, would yield more accurate distribution curves in the micropore range (r less than 200Å).

Because the high pressure mercury penetration method of measuring the pore size distribution of a porous solid yielded the distribution of the largest entrances to the pores, the experimental distribution curve did not represent the true distribution of pore sizes in the graphite but only gave a qualitative

indication of the nature of the pore space (ref.6,p.50).

The graphite samples, especially the fine-pored graphites, almost certainly contained a large number of "ink-bottle" pores. These pores would cause the distribution curve to be weighted towards the lower radii (see section 2.4.4.1(a)). In the true pore size distribution, a portion of the pore volume allotted to small pore radii would be redistributed to larger pore sizes; then the observed peaks occurring in the distribution plots at the larger radii (see Figs. 4.4-2 and 4.4-4) probably would become larger and shifted towards the right, while the peaks at the lower pore sizes would become smaller. Meyer[205] has suggested a method of correcting pore size distributions but tedious calculations were required.

The large peaks at about r = 50Å in the pore size distributions for the Impregnated samples were no doubt due to relatively large voids with fine capillary entrances of radius about 50Å. If the impregnation process (see Appendix A.1) was pictured as the deposition of a graphitized carbon layer upon the pore walls of the base material (Morgan graphite), extremely small pores would be blocked off, while fine pores (less than 0.1 micron) and larger voids would be reduced in size. The distribution graphs (Fig.4.4-4) showed

that the average radius of the largest pores decreased from about 5000Å to about 1000Å during the impregnation process.

A layer of carbon that would reduce the diameter of a fine pore by a half would decrease the diameter and volume of a void by a relatively small amount. In the mercury penetration measurements, the void volume would then be allotted to a smaller radius than for the distribution for Morgan graphite and would cause the large peak observed at about r = 50Å. The large number of "ink-bottle" pores in the Impregnated graphites meant that the pore properties estimated from the distributions were in greater error than those calculated for the other graphites.

It was suggested by the C.S.I.R.O.[240] that the peaks occurring in the distribution curves at r = 20 microns (P.G. 60 graphite), r = 10 microns (Acheson "A" graphite), and r = 0.4 microns (Morgan "EY9" graphite), were due to interparticle voids created during the manufacture of the graphites. The peaks at r = 200Å and 2000Å for Acheson "A" and P.G. 60 graphites, respectively, could be due to the porous structure of the parent carbons.

5.4.3 The Estimation of the Pore Properties from the Pore Size Distribution

The tabulation of the distribution quantities for

each graphite in Table H.2-1, Appendix H.2 showed that, with the exception of P.G. 60 graphite, the largest pores contributed to the total surface area to a negligible extent, while the smallest pores did not considerably influence the total gas flow through the graphites in the viscous and slip flow regions.

Inaccuracies in the distributions below about 200Å (because of uncertain compression effects) would affect the estimated total pore volume and permeability to a negligible extent. However, as the contribution of the smallest pores towards the surface area was often quite appreciable, the surface area estimated from the pore size distribution results was therefore in error. The area estimates obtained represented the area of pores of radius greater than 100Å.

At the highest pore sizes for each graphite, the distribution curve was again considered inaccurate because of the uncertain distribution of these pores. In estimating the pore properties, these large pores made a negligible contribution to the total surface area, but allowed a considerable gas flow. However, they were probably large void spaces which were opened to the surface and enlarged by chipping when the graphite sample was shaped. Their uncertain nature and distribution meant that their contribution to the total estimated

permeability was doubtful. The estimation of the permeability from pore size distribution data was hence of limited value.

Since the measured pore size distributions were weighted towards the lower radii because of "ink-bottle" pores in the graphites (section 5.4.2), the estimated values of the pore properties, with the exception of the porosity, were in error. The estimated mean pore radii and the permeabilities were too low, while the surface areas were too high. The greatest error in these properties occurred for the Impregnated graphite samples because of the larger number of the "ink-bottle" pores. As mentioned by Ritter and Drake,[194] the calculated r_m was actually the average radius of the largest openings to the pores. The estimated values of the pore properties will be compared with values by other methods in section 5.6.

5.5 The Electrical Resistivity Measurements

5.5.1 The Method of Measurement

The d.c. electrical resistivity method, which was a refinement of the method of MacMullin and Muccini[145] and was developed independently of a similar technique described by Stender and Ksenzhek[232] (see section 2.5.6.3), generally proved quite satisfactory for measuring the formation factors for the coarse-pored graphite samples.

As is shown in the justification of the method,[233] no current was conducted by the graphite sample itself but only by the electrolyte in the pores of the sample provided the electrode potentials at the end faces of the sample remained within the range of "ideal polarized" behaviour, i.e., ΔE was less than the decomposition potential E_d for any current flow I. Under such conditions, the effective resistance of the electrolyte in the pores was determined. The use of the four-electrode system avoided the need to correct for electrode polarization or the electrolyte resistance outside the sample. The method was thus superior to that employed by MacMullin and Muccini.[145]

Normal potassium chloride was employed in the majority of the resistivity measurements. Detmns. No. T:1 and No. T:2 on Sample No. T1 showed that two different electrolytes gave effectively the same value of F. However, the use of a number of electrolyte/electrode systems and varying electrolyte concentrations should be studied to determine the optimum conditions for resistivity measurements.

The degassing and saturation of the sample with electrolyte was apparently satisfactory since the application of pressure to the electrolyte in the formation factor cell did not alter the value of F. If the sample was not completely saturated, the measured value of F would be higher than that for 100% saturation.[214] Repeat determin-

ations on reconditioned samples were generally of doubtful accuracy although the agreement obtained was fairly good.

Generally, good plots of ΔE against I were obtained for the coarse-pored P.G. 60 and Acheson "A" graphites with the scatter of the ΔE values at the maximum current being less than $\pm$ 2% (see sections 4.5.1 and 4.5.2). After a step change in I, the equilibrium ΔE value was attained almost immediately for these graphites.

For the determinations on the fine-pored Morgan "EY9" and Impregnated graphites with ΔE less than E_d, ΔE continually drifted with time about a mean value even though the resistance remained approximately constant (section 4.5.4). For zero current flow, ΔE varied with time. The poor stability obtained for these determinations resulted from the very low currents (less than $\pm$ 5 μA) required to keep ΔE less than E_d; such currents were comparable to the leakage current in the graphite and were near the lower limit of the supply circuit. Any instability in the leakage currents could cause the observed drift in the potential drop across the sample.

Dissolved oxygen in the electrolyte was shown[233] to have a negligible effect on the experimental accuracy. By comparison with the permeability studies on the fine-pored graphites (section 5.1.4.1(a)), a large time would

be required to attain equilibrium after any change in I. The method of measurement could be improved by attaching an electrode to the graphite sample so that the drift of the graphite potential could be determined or the potential fixed at a certain value within the range of "ideal polarized" behaviour.

When ΔE was greater than E_d for the fine-pored graphites, i.e., the sample was polarized, no steady readings were obtained (see section 4.5.3); the value of F calculated from the ΔE value after a long time was probably high.

The error in measuring the specific resistance of the electrolyte sample from the formation factor cell was $\pm$ 2%. It was assumed that this sample had the same resistivity as the electrolyte in the pores of the graphite. The measurement of the potentials with the Yew potentiometer was fairly precise (less than 1% error). The error in the current measurements was about $\pm$ 2%. If the slope of the ΔE-I plot was obtained to within $\pm$ 2%, then the error in the calculated values of F was about $\pm$ 7%, which was the order of variation in the F values for the Acheson "A" graphite samples.

5.5.2 The Values of F and q

The values obtained for F for Acheson "A" graphite were rather scattered (see section 4.5.2). The measure-

ment of the nitrogen flow permeability coefficients for a number of the resistivity samples showed that the variation in the F values was due to the inhomogeneous nature of the graphite, the permeability of different samples with the same relation to the extrusion axis varying quite considerably (see Table 4.5-1). Only the magnitude of the values of F (and also q) was therefore meaningful.

The inhomogeneity of the graphite probably became apparent because of the fairly short sample lengths (about 3cm). Previously, inhomogeneity was observed in the pressure distribution specimens (see section 5.1.5.6), but the variation in the permeability of different samples for the permeability studies was quite small (section 4.1).

The F values for the P.G. 60 and Acheson "A" graphite samples whose axes were parallel to the extrusion axis were higher than the values for the perpendicular samples. The resistance was therefore greatest in the parallel direction; this result was in agreement with the anomalous anisotropy observed for these graphites in the permeability determinations (see sections 5.1.1.5 and 5.1.2.3).

The values of q were calculated from the F values using the open porosity values ε. However, because of dead-end pores, the saturated pore volume actually conducting the electric current was smaller than ε and probably equalled the pore volume involved in gas flow (ε_s); then

the calculated values of q would be lower than given in Table 4.5-1.

The q values were the lowest for P.G. 60 graphite (about 1.6) and were of the order observed previously for unconsolidated media (see section 2.5.3). This suggested that P.G. 60 graphite was not consolidated to a very great extent but consisted of sand grains stuck together so that the pore structure of the unconsolidated sand was not altered markedly.

The values of q for Acheson "A" graphite (6 to 11) were of the same magnitude as those obtained for consolidated media by Archie,[217] and Cornell and Katz[125] (section 2.5.3). However, for Morgan "EY9" and Impregnated graphites, the values of F and q, although only approximate, were very much higher than those previously reported.

Obviously these high values of q were not just a measure of the deviousness of the pore paths, but indicated that the pore structure of these graphites was similar to the pore models described by Owen,[43] Flood,[41] and Peterson,[44] i.e., void spaces were connected by narrow constrictions (cf. section 2.5.3). Owen's analysis[43] showed that intersection of the pores, dead-end pores, and contrictions in the pores could cause high values of F and hence q.

Values of the constriction factor P_e , as defined by

equation (2.5.1-6), were calculated for the graphite samples (T taken to equal 2.0) and equalled 0.85 and 0.95 for P.G. 60 graphite, 0.13 to 0.19 for Acheson "A" graphite, and about 0.01 for Morgan "EY9" and Impregnated graphites. According to Owen's theoretical calculations,[43] $P_e = 0.1$ indicated that the size of the voids was about 6 times greater than that of the pore constrictions. For the fine-pored graphites, the pore constrictions were even smaller by comparison with the voids, a fact which was supported qualitatively by the pore size distribution curves for these graphites (see Fig. 4.4-4).

5.5.3 Correlation of F with ε and K

The values of F for the different graphites were correlated with the corresponding values of ε and K (see Fig. 5.5-1). Straight lines with equations

$$F = 0.31\ \varepsilon^{-3.59} \qquad \ldots\ (5.5.3\text{-}1)$$

and

$$F = 123\ K^{-0.58} \qquad \ldots\ (5.5.3\text{-}2)$$

were drawn through the experimental points with the points for Morgan "EY9" and Impregnated graphites deviating from the relations, respectively.

Archie[217] found that F was related to ε by equation (2.5.3-2) with the exponent m being greater than 1.3. Winsauer et al.[213] considered that $F = 0.62\ \varepsilon^{-2.15}$, while Wyllie and Gregory[218] obtained a similar expression with m increasing to 4.2 for consolidated

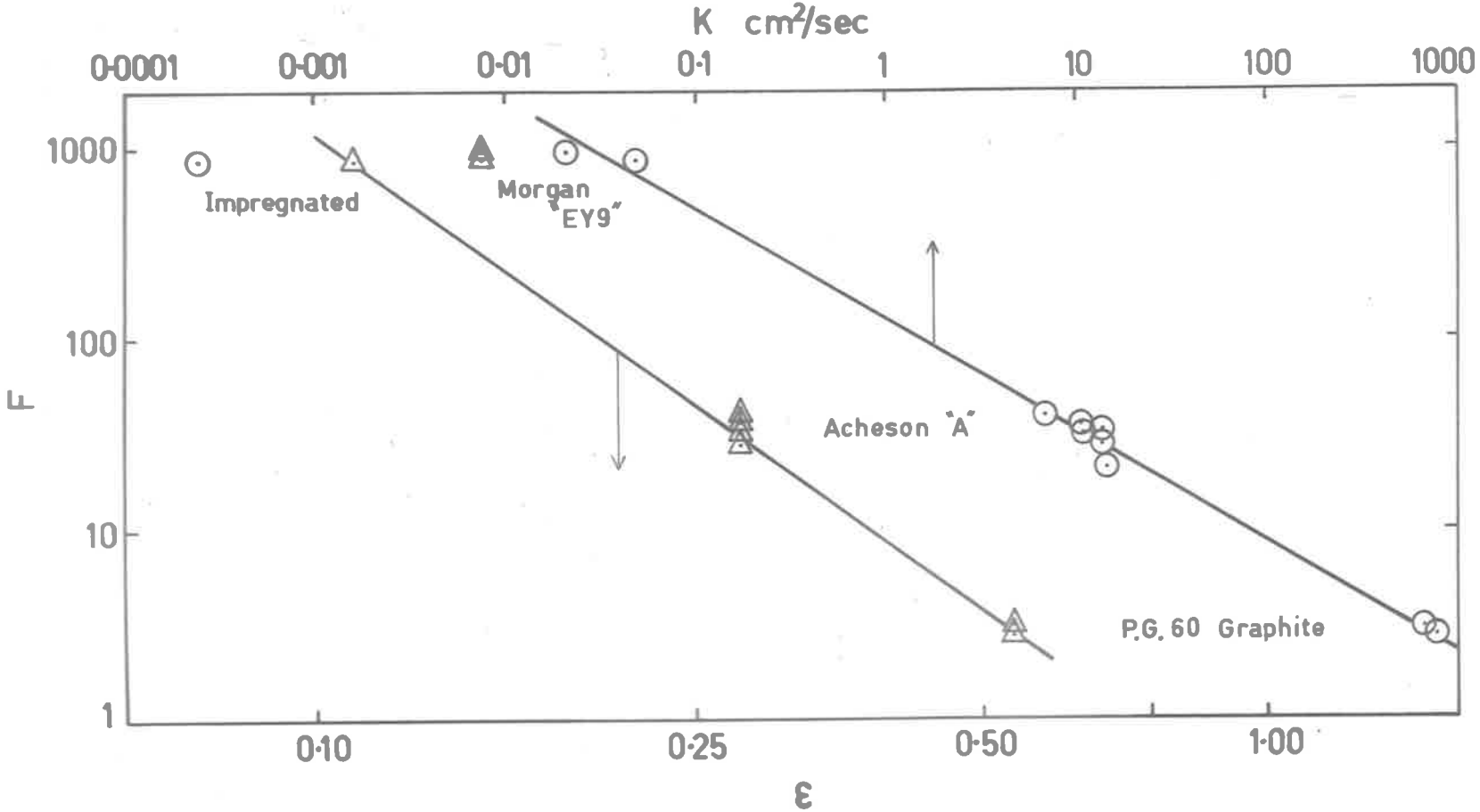

Fig. 5.5-1 Correlations of F with $\mathcal{E}$ and F with K obtained from Electrical Resistivity Measurements on the Graphite Samples.

sandstones. Equation (5.5.3-1) was therefore consistent with previous results for consolidated porous media.

Wyllie and Rose[214] stated that K was proportional to $F^{(1-2m)/m}$, where m was the cementation factor defined by equation (2.5.3-2). From equation (5.5.3-2), m/(1-2m) was equated to the exponent -0.58 and a value for m (3.62) was calculated. This value was in excellent agreement with that obtained from the graph of F against ε, i.e., 3.59, thus apparently giving support to the theory presented by Wyllie and Rose.[214] The physical significance of the relations of F with ε and K is not clearly understood.

5.6 Permeability and the Pore Structure

In the literature survey (section 2.1), it was indicated that many attempts had been made to correlate the permeability of a porous medium with the properties characterising its pore structure. These correlations would permit the calculation of the permeability of a given porous material from its pore properties, or conversely, the estimation of certain pore properties from a permeability determination. Theoretical correlations were of necessity based upon simple pore models (see section 2.1.2) and were often of limited application; constant factors in the derived equations had to be obtained empirically and frequently, especially for consolidated porous media, the values of the pore properties actually involved in the flow

process were different from those measured by independent methods.

In order to examine this problem for flow in the reactor graphites, values of the various pore properties were estimated from the permeability by means of some of the correlations given in section 2.1 and were compared with those obtained by independent measurements.

5.6.1 Calculation of the Pore Properties from the Permeability

Values of the mean pore radius r_m, the surface area S_V, and the tortuosity factor τ were estimated by various methods from the average values of B_o and K_o for flow parallel (par.) and perpendicular (perp.) to the extrusion axis of each graphite (see Table 5.1-1). The graphite samples used were:

P.G. 60	No. K31 (par.) and No. K32 (perp.);
Acheson "A"	Nos. K2, K2A, K3 (par.) and Nos. K4, K5, K6 (perp.);
Morgan "EY9" Impregnated	No. K21 (par.) and No. K23 (perp.); and No. K41 and No. K42 (low pressure results)

For Sample No. K31, the K_o value for nitrogen flow (Detmn. No. H:15) was employed, the average value being high owing to the inaccuracy of measuring low intercept values (section 4.1.1).

5.6.1.1 The Carman-Arnell Equation

The Carman-Arnell[75] equation (2.1.4-6) showed that $B_o = \varepsilon m^2/k$ (section 2.1.4.3). If the Kozeny constant k

was assumed to equal 5.0 (i.e., $\tau^2 = 2$) and the independently measured value of ε employed, then $r_m = 2m$ and $S_v = \varepsilon/m$ could be calculated.[67]

The calculated results given in Table 5.6-1 showed that the values of r_m were less and the values of S_v were greater than those calculated by the method of Hutcheon et al.[34] (section 5.6.1.2). As the tortuosity factor τ^2 calculated by the Hutcheon method became greater than 2, so the differences between the values of r_m and S_v increased. Hence the Carman-Arnell method was only applicable to porous media for which τ^2 was equal to 2, but did not apply for consolidated media because of the limitations of the Kozeny theory (cf. section 2.1.3.2).

5.6.1.2 The Hutcheon, Longstaff, and Warner Method

Hutcheon, Longstaff, and Warner[34] have shown how values of r_m, S_v, and τ^2 could be estimated from permeability results by means of equation (2.1.4-9). The pore properties were given by

$$r_m = 2 B_o k_o \delta_1 / K_o,$$
$$\tau^2 = \varepsilon k_o \delta_1^2 B_o / K_o^2, \text{ and}$$
$$S_v = 2 \varepsilon / r_m.$$

With the shape factors k_o and k_1 taken as 2.5 and 1.0, respectively, and δ_1 assumed to equal 0.8 for consolidated porous media (see section 2.1.4.4), values of the properties were calculated by this method for the various graphite samples (see Table 5.6-1).

Table 5.6-1
Pore Properties Calculated from the Permeability Results

Graphite Sample	ε (Table 5.6-5)	Carman-Arnell method[75] $k_o = 2.5$, $\tau^2 = 2$		Hutcheon et al. method[34] $\delta_1 = 0.8$, $k_o = 2.5$		
		r_m cm x 10^4	S_v cm^2/cm^3	r_m cm x 10^4	S_v cm^2/cm^3	τ^2
P.G. 60 Graphite						
Par.	0.54	17.5	618	24.4	442	3.90
Perp.		19.7	550	21.8	496	2.45
Acheson "A" Graphite						
Par.	0.28	2.50	2240	8.50	660	23.3
Perp.		3.40	1650	11.62	481	23.8
Morgan "EY9" Graphite						
Par.	0.15	0.242	12400	0.708	4240	17.2
Perp.		0.148	20300	0.630	4760	36.4
Impregnated Graphite						
K41	0.11	0.0044	491000	0.073	30200	530
K42		0.0142	156000	0.236	9290	551

The values of r_m and S_v for the parallel and perpendicular samples of each graphite were of approximately the same magnitude. Whereas the value of τ^2 for flow perpendicular to the extrusion axis was less than the value for parallel flow for P.G. 60 graphite but was greater for Morgan "EY9" graphite, the two values of τ^2 for Acheson "A" graphite were almost equal.

From the values of ε, r_m, and τ, it was possible to estimate the value of the factor β_2 from the measured value

of β for each graphite (Table 5.1-1) by means of equation (5.1.2-10), section 5.1.2.4(j). For P.G. 60 graphite, the values of β_2 for flow in the parallel and perpendicular directions were 0.26 and 0.32, respectively. The corresponding values for Acheson "A" graphite were 2.0 and 1.2, while for Morgan "EY9" graphite (perpendicular flow), $\beta_2 = 44$. Thus β_2 increased as the pore size of the graphite decreased in accordance with the correlation obtained by Cornell and Katz.[125]

5.6.1.3 The Adzumi Method

In the Adzumi method[33] (see section 2.1.4.2), $B_o = \pi E_o/8$ and $K_o = \pi \delta_1 F_o/2$. The values of E_o and F_o were calculated from the B_o and K_o values ($\delta_1 = 0.9$) and the quantities $n = F_o^4/E_o^3$, $r = E_o/F_o$, $\varepsilon = n\pi r^2$, and $S_v = 2\pi r n$ were estimated. The values of these properties are given in Table 5.6-2.

The values of r_m agreed quite closely with the corresponding values calculated by the Hutcheon method (Table 5.6-1), but the values of S_v were much less. The values of ε were extremely low and absurd and hence revealed the inadequacy of the method for reactor graphites (cf. section 2.1.4.2). The number of pores n per cm^2 roughly indicated the proportion of flow paths in the samples but did not really mean anything quantitatively.

Table 5.6-2
Pore Properties Calculated by the Adzumi Method

Graphite Sample	n x 10^{-4}	r_m cm x 10^4	ε cm^3/cm^3	S_v cm^2/cm^3
P.G. 60 Graphite				
Par.	0.90	22.0	0.137	124
Perp.	1.81	19.6	0.218	223
Acheson "A" Graphite				
Par.	0.646	7.65	0.0120	31.1
Perp.	0.324	10.63	0.0115	21.7
Morgan "EY9" Graphite				
Par.	67.5	0.64	0.0087	270
Perp.	40.0	0.57	0.0041	143
Impregnated Graphite				
K41	151	0.066	0.00020	62.4
K42	13.8	0.214	0.00020	18.5

Table 5.6-3
The Properties Calculated from Transient Flow Results

Graphite Sample	D'_{gt} cm^2/sec	m/τ^2 cm x 10^6	$S_v\tau^2$ cm^{-1} x 10^{-4}	S_v cm^2/cm^3 x 10^{-4}	r_m cm x 10^4	τ^2
Morgan "EY9" Graphite						
Sample K21	0.419	3.15	4.76	1.03	0.29	4.63
Impregnated Graphite						
Sample K42	0.00324	0.0244	492	5.14	0.047	96

5.6.1.4 The Transient Flow Method

Pore properties were calculated from transient flow results by Barrer's time-lag method[101] (see section 2.1.5.3).

For a non-sorbed gas, equations (2.1.5-13) and (2.1.5-16) gave

$$D'_{gt} = \frac{\mathcal{K}_{gt}}{\tau^2} \quad D_{gc} = \frac{4 \delta \varepsilon \bar{v}}{3 k_1 \tau^2 S_v} \quad ;$$

this expression was based on the capillary pore model and hence was subject to the limitations of such a model. Although helium was shown to be adsorbed on Morgan "EY9" and Impregnated graphites to a small extent (sections 5.1.3.4(h) and 5.1.4.3(d)), the above expression was applied and the magnitude of the quantities m/τ^2 and $S_v \tau^2$ was estimated (see Table 5.6-3) from the values of D'_{gt} given in Tables 5.1-5 and 5.1-8.

The factor δ / k_1 was taken as 0.8 and ε = 0.15 and 0.12 for Morgan "EY9" and Impregnated graphite, respectively. As the surface area calculated by the transient method should approach the B.E.T. surface area[67,101] (see section 2.3.2.3(b)), the values of S_v obtained by adsorption measurements (Table 5.6-7) were used to estimate values of r_m and τ^2 (Table 5.6-3).

5.6.1.5 The Pore Size Distribution Method

Equation (2.4.3-4) expressed the permeability coefficient K in terms of the pore size distribution functions and the tortuosity factor τ. Previously, $K \tau^2$ as a function of p_m was calculated from the pore size distribution data for each graphite by means of this equation

(see section 4.4.3, Table 4.4-1) since values of τ were not known. However, from the values of B_o and K_o for each graphite and with $k_o = 2.5$ and $\delta_1/k_1 = 0.8$, separate values of τ were estimated from the viscous and slip flow terms of the equation; these values are given in Table 5.6-8(section 5.6.2.5).

Generally, the two τ values for flow in any graphite sample were of about the same order, the difference being due to the inaccuracies in the distribution terms; the greatest variation between the values was for Impregnated Graphite Sample No. K42. It was considered (section 5.4.3) that the estimation of the permeability or tortuosity from the pore size distribution was of limited accuracy.

5.6.2 Comparison of the Pore Properties

5.6.2.1 The Bulk Density ρ_b

Values of the bulk density of the graphites were calculated for the porosity samples (see section 4.2, Table 4.2-1) and were also measured by the C.S.I.R.O.[240] prior to the pore size distribution measurements (Table A.5-1, Appendix A.5). These values are compared in Table 5.6-4.

Table 5.6-4
Values of the Bulk Density ρ_b (g/cm^3)

Graphite Grade	Porosity Samples	C.S.I.R.O. Values	Average
P.G. 60	0.952 0.973	0.961 0.971	0.96
Acheson "A"	1.510	1.509 1.541 (3)	1.51
Morgan "EY9"	1.716 1.720	1.721 1.727	1.72
Impregnated	1.787 1.794	-	1.79

The variation in the values of ρ_b for any graphite grade was generally quite small (less than $\pm$ 1%), although three values obtained for Acheson "A" graphite by the C.S.I.R.O.[240] were 2% higher than the preferred value (1.51 g/cm^3) measured for the Acheson "A" porosity sample (No. S2).

5.6.2.2 The Porosity ε

The values of the porosity obtained from the helium density measurements for each graphite (see Table 4.2-1) agreed fairly closely with the corresponding values obtained from the pore size distribution results (see Table 4.4-1). The values estimated by graphical integration of the pore size distribution plots tended to be higher than the values obtained from the pressurizing curve after correction for compression, especially for Acheson "A" graphite. For Morgan "EY9" graphite, the

values obtained by the different methods differed considerably possibly because of the inhomogeneity of the graphite; hence the average of all values was taken (see Table 5.6-5). For Acheson "A" graphite, the helium density value was preferred.

Table 5.6-5
Values of the Porosity $\varepsilon(cm^3/cm^3)$

Graphite Grade	Helium Density	Press'g Curve	Graph Intgr.	Average
P.G. 60	0.546 0.535	0.541	0.545	0.54
Acheson "A"	0.279	0.293	0.332	0.28
Morgan "EY9"	0.168 0.129	0.157 0.140	0.158 0.141	0.15
Impregnated	0.109 0.120 (Sample K42)	0.106 0.104	0.110 0.105	0.11

The values given in Table 5.6-5 were the open porosity values. As mentioned in sections 2.1.4.4 and 2.2.1, the pore volume actually taking part in steady state gas flow was less than the total open pore volume for consolidated porous media since a portion of the pore space consisted of dead-end or blind pores. When the pore properties were estimated from the permeability, a smaller porosity value ε_s should have been used instead of ε. Approximate values of ε_s were obtained from the transient

flow measurements (sections 5.1.3.4(h) and 5.1.4.3(d)) but were based on several uncertain assumptions; these values were 0.10 for Morgan "EY9" graphite and 0.07 for Impregnated graphite, i.e., about two-thirds of the open porosity ε. It was estimated (see section 4.2) that from 16 to 36% of the total pore volume of the graphite samples was unopen, i.e., completely blocked off.

5.6.2.3 The Mean Pore Radius r_m

Although the mean pore radius was not measured directly, values were obtained for each grade of graphite by a number of indirect methods. These values are given in Table 5.6-6.

Table 5.6-6
Values of the Mean Pore Radius r_m (microns)

Graphite Grade	Hutcheon method	Adzumi method	Pore size distribn.	Transient flow method	Adsorp. $\frac{2\varepsilon}{S_v}$	Manufact.
P.G. 60			19		0.99	16
Par.	24	22	-	-	-	
Perp.	22	20	-	-	-	
Acheson "A"			4.5		0.52	5 to 10
Par.	8.5	7.7	-	-	-	
Perp.	11.6	10.6	-	-	-	
Morgan "EY9"			0.31,0.44		0.29	0.5 to 1
Par.	0.71	0.64	-	0.29	-	
Perp.	0.63	0.57	-	-	-	
Impregnated			0.071 (2)		0.058	< 0.5
K41	0.073	0.066	-	-	-	
K42	0.236	0.214	-	0.047	0.047	

Of the steady state permeability methods, the method of Hutcheon et al.[34] was suspected to give the best values of r_m; in the calculations of these r_m values, no assumption was necessary concerning the actual pore volume involved in the flow (see section 5.6.1.2). The permeability r_m values were greater than those estimated from the pore size distribution curves (see Table 4.4-1) but were about the same as those quoted by the manufacturers (Table A.1-1, Appendix A.1).

The calculations of values of r_m by the transient flow method and from the adsorption surface areas (Table 5.6-7) were effectively the same (section 5.6.1.4). The adsorption r_m values ($=2\varepsilon/S_v$) were generally much lower than the permeability values (cf. Ash and Grove[67]), showing that dead-end pore space existed in the graphites. This comparison confirmed the observations of Everett,[51] who showed by a theoretical consideration of a number of geometrical pore models that $2\varepsilon/S_v$ was up to three times lower than r when intersecting pores occurred in the model. For the fine-pored graphites, the adsorption values of r_m agreed with the pore size distribution values.

The values of r_m obtained from the pore size distributions were expected to be low (see section 5.4.3). Fatt[35] considered that r_m calculated from the pore size distribution curve was smaller than the actual r_m depending on

the number and arrangement of the pore intersections in the porous medium.

5.6.2.4 The Surface Area S_g

Values of the surface area of the graphiteswere obtained by direct adsorption measurements (section 4.3, Table 4.3-1), and were estimated from permeability results (section 5.6.1) and pore size distribution data (Table 4.4-1). These values are compared in Table 5.6-7.

Table 5.6-7
Values of the Surface Area $S_g(m^2/g)$

Graphite Grade	Hutcheon Method	Adsorp. B.E.T.	Pore Size Distribn.
P.G. 60	0.046 0.052	1.14	0.15
Acheson "A"	0.044 0.032	0.71	2.5 (0.50 > 500 Å)
Morgan "EY9"	0.25 0.28	0.55 0.65	0.83 0.60
Impregnated	1.7	2.1	4.3 4.9 } >100Å
Sample K42	0.52	2.9	(≃ 2.3 > 500Å)

The B.E.T. adsorption measurements showed that the Impregnated graphite had a surface area about four times that of Morgan "EY9" graphite possibly because a honey-comb type pore structure was formed during the impregnation process (section 5.3.3). P.G. 60 graphite apparently had a higher surface area than Acheson "A" graphite, while both

these graphites had larger areas than Morgan "EY9" graphite according to the B.E.T. results. Usually, the surface area would be expected to increase as the pore size decreased.

Except for P.G. 60 graphite, the surface areas estimated from the pore size distribution curves were greater than the adsorption surface areas. It was suspected that the pore size distribution values were too high (section 5.4.3) because the distributions were weighted towards low radii, i.e., there was too much pore volume at low pore sizes; the surface areas for Acheson "A" and Impregnated graphites for pores greater than 500Å (0.50 and 2.3 m^2/g, respectively) agreed more closely with the adsorption areas than those estimated from the total distribution.

The permeability surface area values calculated by the Hutcheon method[34] were generally much lower than the adsorption area values (cf. Ash and Grove[67]); if the porosity ε_s was employed in the calculations instead of ε, the area values were lower still. This comparison showed that the surface area involved in flow was much less than the total surface area of the graphites because of dead-end pores and internal porosity of the coke particles (cf. section 2.3.2.3(a)).

5.6.2.5 The Tortuosity Factor τ

The values of the tortuosity factor τ determined for the graphites by various methods are reported in

Table 5.6-8.

Table 5.6-8
Values of the Tortuosity Factor τ (cm/cm)

Graphite Grade	Hutcheon Method	Transient Method	Pore Size Distribn. B_o term	Pore Size Distribn. K_o term	Electr. Resisty Msmt.
P.G. 60					
Par.	1.98	-	3.35	2.47	1.22
Perp.	1.57	-	2.97	2.07	1.29
Acheson "A"					
Par.	4.83	-	8.59	5.38	3.30
Perp.	4.88	-	6.75	4.60	2.54 3.00
Morgan "EY9"					
Par.	4.15	2.15	4.00 5.55	3.94 4.49	11.5
Perp.	6.03	-	6.53 9.07	6.06 6.93	12.0
Impregnated					
K41	23.0	-	36.6 26.4	32.1 31.5	9.80
K42	23.5	9.80	11.5 8.27	57.4 56.1	-

The electrical resistivity measurements gave values of the electrical tortuosity factor q from the relation $q = F\varepsilon$ (see section 4.5); τ^2 was equated to q but this assumption might not be correct (see section 2.5.5.1). Resistivity measurements on a perspex model containing a devious circular capillary of known diameter and length showed that $q = (L_o/L)^2$. However, the results for the graphite samples (Table 5.6-8) indicated that there was no obvious relation between the values of q and τ. The values of τ calculated from the permeability and pore size distribution data are

discussed in section 5.6.1.

Because the τ values obtained by different methods for any graphite were quite scattered and of varying accuracy, only the order of magnitude of the values was significant. The values ranged from 1.2 to 3.4 (av. = 2.1) for P.G. 60 graphite, 2.5 to 8.6 (av. = 4.9) for Acheson "A" graphite, 4.0 to 12.0 (av. = 6.3) for Morgan "EY9" graphite, and 8.3 to 60 (av. = 27) for Impregnated graphite, i.e., the values increased as the pore size of the graphite decreased.

The highest values of τ were obtained from the electrical resistivity measurements for Morgan "EY9" graphite but from the pore size distribution method (section 5.6.1.5) for the other graphites. The transient flow method (section 5.6.1.4) gave quite low τ values for the fine-pored graphites. The permeability τ values calculated by the method of Hutcheon et al.[34] (section 5.6.1.2) would be lower than those given in Table 5.6-8 if the porosity ε_s was used instead of ε.

Generally, the values of τ were greater than the value for unconsolidated porous media ($\sqrt{2}$ = 1.41). This confirmed the high tortuosity factors previously observed for consolidated porous media (cf. sections 2.1.4.4 and 2.5.2). The pore structure of the graphites therefore apparently consisted of voids connected by capillaries (see section 5.5.2).

For the P.G. 60 and Acheson "A" graphites, the values of τ for flow in the direction perpendicular to the extrusion axis were lower than those for parallel flow, whereas, for Morgan "EY9" graphite, they were higher. This anisotropy of the graphites was in accordance with the results of the permeability determinations (sections 5.1.1.5, 5.1.2.3, and 5.1.3.3).

5.6.3 Deductions Concerning the Pore Structure

It was not possible to obtain the precise value of any pore property of a graphite because of the inhomogeneity of the pore structure. As the different types of measurements, viz., permeability, porosity-surface area, pore size distribution, and electrical resistivity measurements, were conducted on different pieces of the graphite and were of varying accuracy, only the order of the calculated properties was comparable. Really, for strict comparison, all properties should have been measured for the same sample. For Impregnated Graphite, the surface area and porosity measurements were made on a portion of the permeability sample (No. K42), but even then the comparison of r_m and S_g was not improved since different pore size and area quantities were obtained by the different measurements.

The lack of good agreement between the values of the pore properties calculated from the permeability results and those measured by independent methods indicated that a

portion of the pore volume must have occurred as dead-end pore space, causing the permeability surface area to be less than the adsorption area[67] for any graphite. The use of a lower porosity value to allow for the dead-end pore volume generally did not improve the agreement. The high values of the tortuosity factors indicated that the interconnected pore structure of the graphites consisted of voids and capillaries.

The permeability equations based upon the capillary pore models did not prove adequate even when the modification of Wyllie and Rose[30,58] was employed so that values of τ^2 greater than 2 were possible. The introduction of the pore size distribution functions into the flow equations gave only qualitative results since the distributions were often quite inaccurate (see section 5.4.3).

The correlations between the permeability and the pore structure could be placed on a sounder basis if model pore networks could be readily constructed so that the pore properties and the permeability could be measured for the model as the pore structure was made more complex; however, the production of small holes of about micron size or smaller would be very difficult. Mathematical models based on statistical pore arrangements (section 2.1.2.3) may prove more practicable with the development of computer techniques.

6. CONCLUSIONS

6.1 The Permeability Measurements

1. Permeability coefficients K were determined for the flow of the gases hydrogen, helium, nitrogen, argon, carbon dioxide, freon-12, and xenon through four grades of reactor graphite (viz., P.G. 60, Acheson "A", Morgan "EY9", and Impregnated graphites) at room temperature ($20^{\circ}C \pm 6^{\circ}C$) and at mean pressures p_m from 0.02 cm Hg up to 1236 cm Hg (16.3 atm). A low pressure (vacuum) and a high pressure apparatus were employed.

2. The main methods used to determine the permeability coefficients were the pressure increase and the pressure decay methods for the low pressure apparatus and the flow method for the high pressure apparatus.

3. The pressure increase method was most suitable for determinations on Morgan "EY9" graphite and, to a lesser extent, Impregnated graphite. The pressure decay method, which had not been described in the literature when first used, was applied successfully for determinations on Acheson "A" graphite but was not suitable for the fine-pored graphites because of non-equilibrium effects. The time to reach equilibrium flow was approximately twice the time-lag ϕ and increased as the pore size decreased and the molecular weight of the gas increased. The flow method was employed for P.G. 60 graphite.

4. The plots of K against p_m were generally straight at low pressures but curved towards the p_m-axis at high pressures because of the commencement of turbulent or inertial flow. The flow-rates at the critical Reynolds number N_{Re} (when turbulent flow first became significant) and at the N_{Re} when turbulent flow became fully developed were proportional to μ/M. Experimental results for P.G. 60 graphite confirmed this theory.

5. The permeability results, especially those for Morgan "EY9" graphite, demonstrated that the coefficients B_o and K_o were specific coefficients characterizing each porous medium. High pressure permeability values were not as accurate as the low pressure results.

6. The anisotropy of P.G. 60 and Acheson "A" graphites was anomalous since greater flow was obtained in the direction perpendicular to the extrusion axis; this anomaly probably resulted from some quality of the extrusion process. The anisotropy of Morgan "EY9" graphite was as expected.

7. There was no evidence of surface flow in the graphites. For freon flow in the fine-pored Impregnated graphite, no capillary condensate flow (cf. Carman[122]) was observed at high relative pressures; however, the condensed gas hindered the gas flow thus reducing K.

6.2 High Pressure Flow Results

1. For P.G. 60 and Acheson "A" graphites, a flow phenomenon was observed which had not been reported in the literature previously. At a given p_m, K varied with p_o so that separate K-p_m plots were obtained for each set value of p_o. This phenomenon was shown to be due to the influence of inertia flow effects which became significant above the critical N_{Re}.

2. The high pressure flow results of nine determinations were satisfactorily correlated by the method proposed by Green and Duwez.[126] The dimensionless groups f and N_{Re} were expressed in terms of the coefficients B_o, β, and a, the N_{Re} group of Green and Duwez being redefined to include a slip flow term. Values of B_o and β were obtained more accurately from the α-β plot than from the plot used by Cornell and Katz.[125]

3. The results plotted as an f-N_{Re} graph gave a single curve and showed that gas flow through consolidated media could be satisfactorily correlated by the Green and Duwez method. This method should also be applicable for unconsolidated media and liquid flow.

4. Equations were obtained which described flow over the range from Knudsen flow to complete turbulent flow; these were the first satisfactory expressions available for flow in the transition region between

viscous and turbulent flow. The equations permitted the prediction of the pressure drop for any flow conditions in a porous medium for which the coefficients B_o, β, and a were known.

5. The equation for K fitted the experimental results to within 5% and accounted for the flow phenomenon by means of an inertial resistance term. For rigorous specification of K, two quantities (e.g., p_m and G) must be given instead of the customary mean pressure p_m as for viscous flow.

6. At N_{Re} = 0.01 (the critical N_{Re}), inertia or turbulent flow became significant so that Darcy's law was invalid, while at N_{Re} = 100, viscous flow was negligible and complete turbulence was attained.

7. The experimental values of the inertial resistance coefficient β closely fitted the β-B_o correlation of Katz and Cornell.[147] The results for P.G. 60 graphite showed that β was a characteristic coefficient of a porous medium. The coefficient β was related to the pore properties but the correlation was only of limited application.

8. Slip flow was especially important for the flow through the graphites since it constituted up to 20% of the total flow at N_{Re} = 0.01. These results were apparently the first reported instance where slip

flow and inertial flow occurred simultaneously in a porous medium when the flow was in the transition region. The very wide pore size distributions in the graphites caused this effect.

6.3 Low Pressure Flow Phenomena

1. At very low pressures (p_m less than 2 cm Hg), minima were definitely observed in the K-p_m plots for Morgan "EY9" and Impregnated graphites. These observations confirmed the limited evidence of permeability minima. The Knudsen number N_{Ku} at the minimum ranged between 1 and 70 and was not constant as generally believed.

2. A number of effects including the interaction of the gas molecules at the pore walls, Knudsen flow through long flow paths, the occurrence of an almost negligible amount of surface flow, and the particular pore structure of the medium were considered to contribute to the occurrence of permeability minima.

3. Time-lags ϕ were obtained from the transient flow measurements on Morgan "EY9" and Impregnated graphites. The ϕ-p_m plots increased sharply with decreasing p_m at low pressures for all gases, whereas previously this low pressure behaviour was only observed to a limited extent for polar gases.

4. The transient flow behaviour was due to

adsorption effects, the particular variation of the adsorption coefficient H with p_m leading to the variation of ϕ with p_m. Because a longer time was required to establish the equilibrium adsorbed-phase concentration distribution in the graphites at low pressures, the time-lags became greater.

5. The deductions were only qualitatively correct since the theory depended on assumptions which were not valid when D'_t or H were pressure-dependent. Extension of the time-lag theory and independent measurement of H would check the explanation given for the transient flow behaviour.

6. By means of the derived theory and the transient flow results, isotherms were plotted for the adsorption of gases on Morgan "EY9" and Impregnated graphites at room temperature; the isotherms were of Type II or Type IV.[176] Even helium was adsorbed slightly. Surface flow was assumed to be negligible.

7. The use of Barrer's time-lag theory was limited and gave unsatisfactory results. Adsorption could have occurred even when H = 0.

6.4 The Pressure Distribution Measurements

1. The distributionsof pressure were measured for steady state flow of nitrogen, carbon dioxide, freon-12, and hydrogen through P.G. 60, Acheson "A", and

Morgan "EY9166" graphite specimens for pressures below two atmospheres. The pressure distribution curves were approximately parabolic in shape and tended to be more curved as the pressure drop across a specimen was increased. For viscous flow, the curvature increased as the ratio a/b was decreased (i.e., as the porosity was increased or the ratio $\mu\sqrt{(\mathcal{J}/M)}$ was decreased).

2. Theoretical equations for the variation of p with x in a porous medium, derived by solving the general one-dimensional flow equation for steady state isothermal gas flow through a porous medium for various conditions, showed that the distribution curves were families of parabolas when the permeability coefficient K was a function of p. The expressions for pure viscous flow, viscous and slip flow, and complete turbulent flow were specializations of the general pressure distribution expression for slip, viscous, and turbulent flow occurring simultaneously. Only the first of these expressions has been mentioned previously in the literature, although the second could be obtained from a published equation.

3. The turbulent flow expression, which was identical with that for pure viscous flow, gave the distribution of pressure whenever slip flow was negligible. In the transition region between viscous and turbulent flow, the viscous-slip flow and the non-slip flow

expressions gave pressure distributions which agreed to within 5% for the reactor graphite specimens. Evaluation of the pressure distribution by means of the general distribution expression would only be necessary on rare occasions.

4. As a consequence of the pressure distribution equations, it was shown that Darcy's law could be validly integrated when Δp was large to give the permeability coefficient at the mean pressure. An expression was obtained from the viscous-slip flow distribution expression to calculate the value of a/b from p_i, p_o, and the pressure at any point in a porous medium; this expression only applied when the medium was completely homogeneous.

5. The experimental pressure distributions were generally higher than the "ideal" distributions calculated from the viscous-slip flow distribution equation. This difference was attributed to the observed inhomogeneity of the graphite, although leakage in the specimen would have given the same effect. The "ideal" distributions therefore represented the distributions in a completely homogeneous porous medium. The experimental distributions confirmed the predictions of the theoretical equations despite the inhomogeneity.

6.5 The Pore Properties

1. The porosities and helium densities of the

graphites were determined by helium displacement measurements, while the surface areas were measured by the krypton adsorption method. Pore size distributions of the graphites, obtained by the mercury penetration method, were supplied by other research workers. Electrical formation factors and tortuosity factors were determined on graphite samples saturated with normal potassium chloride by a d.c. resistivity method which was a refinement of previous methods.

2. A considerable portion (16 to 36%) of the pore space of the graphites was inaccessible to gas molecules (i.e., totally blocked off). The pore size distributions indicated that two main groups of pores occurred in the graphites, viz., interparticle voids (r = 0.5 to 20 microns) and internal pores in the coke particles (r less than 2000Å). The high values of the electrical tortuosity factors suggested that the pore structure consisted of voids separated by capillary constrictions (cf. pore model of Owen[43]).

3. Values of the pore properties were estimated from the permeability results and the pore size distribution results. The lack of agreement of these values with the independently measured values showed that a portion of the pore volume occurred as dead-end volume; only about two thirds of the open porosity was estimated to be available for flow. The pore models

were inadequate to relate the permeability to the pore structure. The pore size distribution data was not accurate enough for estimation of the permeability.

6.6 Recommendations

1. For further accurate permeability determinations on the graphites, especially P.G. 60 and Impregnated graphite, the low pressure apparatus should be modified; the steady state low pressure flow method or the variable volume flow method (see section 2.1.8.2) should be developed with a range of flow-measuring devices enabling a wide range of flow-rates to be covered.

2. If pressure increase experiments were to be continued for Impregnated graphite, the solution of the differential flow equation for the non-equilibrium conditions encountered in the experiments and for a variable diffusion coefficient should be obtained to permit accurate analysis of the experimental results.

3. The rigorous extension of the time-lag theory to cover all possible flow phenomena as mentioned in section 2.1.5.3(d) should be considered. Then the validity of the assumptions made in the analysis of the time-lag results (see section 5.1.3.4(f)) could be checked. Independent measurement of the adsorption of the gases on the graphites would provide a check of the

method of obtaining the adsorption isotherms (section 5.1.3.4(h)).

4. Further experimental evidence is required concerning permeability minima. Examination of the low pressure flow of gases through a variety of porous media covering a wide range of mean pore sizes (including fine-pored media with d_m between 100 and 1000Å) should lead to a better understanding of the flow behaviour at low pressures in the Knudsen region. Surface flow effects could also be studied.

5. In order to confirm completely the theoretical pressure distribution equations by means of experimental results, further distribution measurements should be performed on consolidated porous media with homogeneous pore structures, e.g., Vycor porous glass.

6. The variables in the electrical resistivity method for obtaining formation factors should be examined completely. A modified technique with the potential of the graphite fixed would prevent the drifting of the measured potentials.

7. A theoretical and experimental examination of complex pore models would enable better correlations between the permeability and the pore structure to be obtained.

APPENDIX A

THE GRAPHITE SAMPLES

A.1 Details of the Reactor Graphites

The details of the manufacture and the composition of the various grades of reactor graphite supplied by the Australian Atomic Energy Commission are summarized in Table A.1-1. Also included are the forms in which these graphites were supplied. These details were obtained from private communications with the A.A.E.C.[13,244,265]

The Impregnated graphite samples were prepared by the A.A.E.C. by the furfuryl alcohol impregnation process.[13] This process consisted of impregnating Morgan graphite with furfuryl alcohol mixed with a polymerization catalyst, followed by heating to polymerize the alcohol, and then heating at 5°C/hr to 800°C in nitrogen to carbonize the resin.

A.2 The Graphite Samples for Permeability Determinations

A.2.1 Details of the Permeability Samples

In Table A.2-1, details of the graphite samples used in the permeability determinations are presented. For each sample, the relation to the extrusion axis, the dimensions, and the preparation are given.

A.2.2 Description of the Sample Holders

The graphite samples were supported in the perm-

Table A.1-1
Details of the Reactor Graphites

Graphite Grade	Average pore diameter, microns	Details	Form as supplied
Porous Graphite 10 30 40 60	 190 99 69 33	Made by National Carbon Co., Cleveland, Ohio, by extrusion of coke powder of carefully controlled size distribution and a pitch binder, followed by baking and graphitizing. The effective porosity was 48% for all four grades.	Supplied as 7in.dia. x 3in.discs cut from cylinders of the graphite.(265b)
Acheson grade "A"	10-20	Made by British Acheson Electrodes Ltd., Sheffield. It is a very pure graphite, made by extrusion of calcined petroleum coke and coal tar pitch.	Supplied as two rectangular blocks (8in. x 4in. x 3in.) with the direction of extrusion indicated by an arrow on each block.(265a) These blocks were from a larger block (8in. x 8in. x 3in.) of graphite cut in halves.(244) The direction of extrusion was perpendicular to the largest face of the graphite.
Morgan grade 1 - 2 "EY9"		Made by Morgan Crucible Co.Ltd.,London. It was made by extrusion of probably finely ground coke, lampblack, and pitch. It is not of nuclear purity, having a boron content of up to 200 p.p.m.	Supplied as a 3in.dia. x 8in. long disc.(265a)
Morgan grade 1 - 2 "EY9166"		This graphite was identical with the above graphite, except that it was purer with only about 20 p.p.m.boron.	Batch 1: Supplied as cylinders 2in dia. x 8in.long.(13.) Batch 2: Supplied as rods 1in.dia. x 12in. long.(265c)
Furfuryl alcohol Impregnated Morgan "EY9166"	?	This graphite was produced by the A.A.E.C. by the impregnation of Morgan "EY9166" graphite with furfuryl alcohol (see Appendix A.1)	Prepared by impregnation of hollow cylinders of dimensions 8cm long x 2.54cm o.d. x 0.70cm i.d(13.) The average percentage weight increase for seven cylinders was 5.5%.

Table A.2-1
Details of the Graphite Samples for the Permeability Determinations

Graphite Grade	Sample No.	Form	Relation to Extrusion Axis	Dimensions cm l	Dimensions cm x	Dimensions cm d	A^a_2 cm^2	L/A_{-1} cm^{-1}	Coating on Sample	Sample Holder Type
Acheson "A"	K1	Rod	par.	7.366		1.335	1.400	5.262	shellac	(a)
	K2	Rod	par.	7.416		1.260	1.247	5.947	shellac	(a)
	K2A[b]	Rod	par.	6.810		1.260	1.247	5.461	shellac	(a)
	K3	Rod	par.	5.334		1.278	1.283	4.157	shellac	(a)
	K4 [c]	Rod	perp.(1)	6.975		1.305	1.338	5.215	epoxy	(b)
	K5 [c]	Rod	perp.(2)	6.780		1.288	1.303	5.203	epoxy	(b)
	K6	Cyl.	par.	7.888	d_o	2.494	34.10	0.0263	–	(e), (e)
					d_i	0.700				
	K7	Cyl.	par.	7.600	d_o	2.545	33.94	0.0273	–	(e), (e)
					d_i	0.690				
Morgan "EY9"	K21	Rod	par.	7.955		1.280	1.287	6.181	shellac	(a)
	K22	Rod	par.	5.110		1.235	1.198	4.266	epoxy	(b)
	K23	Rod	perp.	6.450		1.290	1.307	4.955	epoxy	(b)
	K25	Cyl.	par.	8.915	d_o	2.638	42.21	0.0234	–	(e)
					d_i	0.713				
Morgan "EY9166"	K24	Rod	par.	5.680		1.310	1.348	4.214	epoxy	(b)
P.G. 60	K31	Rod	par.	7.585		1.305	1.337	5.673	paraffin wax	(b)
	K32	Rod	perp.	8.025		1.321	1.371	6.585	& epoxy	(b)
Impregnated	K41[d]	Cyl.	–	7.770	d_o	2.540	34.47	0.0261	epoxy	(d)
					d_i	0.740				
	K42[e]	Cyl.	–	7.985	d_o	2.490	36.33	0.0240	epoxy	(d)
					d_i	0.748				

Notes: a For the hollow cylinders, the area for flow A was taken as the logarithmic mean area $= (A_o - A_i)/(\ln A_o/A_i)$. Radial flow in the cylinders occurred in the direction perpendicular to the extrusion axis.
b Rod No. K2A was Rod No. K2 decreased in length.
c Rods No. K4 and No. K5 were prepared respectively in two perpendicular directions at right angles to the extrusion axis of the graphite.
d Cylinder No. K41 was Tube No. 1 supplied by the A.A.E.C.
e Cylinder No. K42 was Tube No. 2; the outer skin of this sample was machined off.

eability cells by several types of sample holders. These holders are described below as types (a) to (e). The permeability cells mentioned, viz., the low pressure permeability cells types I and II, and the high pressure permeability cells, are described in sections 3.1.2.1 and 3.1.4.1, respectively. The sample holders and permeability cells are shown diagrammatically in Figs. A.2-1 and A.2-2.

Type (a): For low pressure permeability determinations, a graphite rod was held by sealing it between two glass tubes by means of rubber tubing and Shellac or Epoxy resin* (see Fig. A.2-1(a)). This holder was sealed into the B14 conical joint of the low pressure permeability cell type I with Apiezon black wax "W". For pressure decay type experiments in the type II permeability cell, this sample holder was held by a B14/B19 adaptor.

Type (b): For permeability determinations in the high pressure apparatus, graphite rods were attached to holders prepared from 3/4in. hex. brass rod (see Fig. A.2-2(d)) by means of rubber hose, wire clips, and Epoxy resin. This type of holder was screwed into the high pressure permeability cell and sealed with a neoprene washer. For low pressure experiments, a dural adaptor permitted the sample holder to be placed in the type II cell with the joints being covered with mercury to prevent leakage.

Type (c): For low pressure experiments, some cylindrical samples were sealed into a dural sample holder with black Apiezon "W" wax and held with small springs (see Fig. A.2-1(d)). This holder was supported in the B19 conical joint of the low pressure permeability cell type II, mercury covering the joint to prevent any leakage.

---

* Epoxy resin was prepared by mixing 4 parts of Epikote Resin "828" with 1 part of Epikure "U" Catalyst (Shell Chemical (Aust.) Pty. Ltd.)

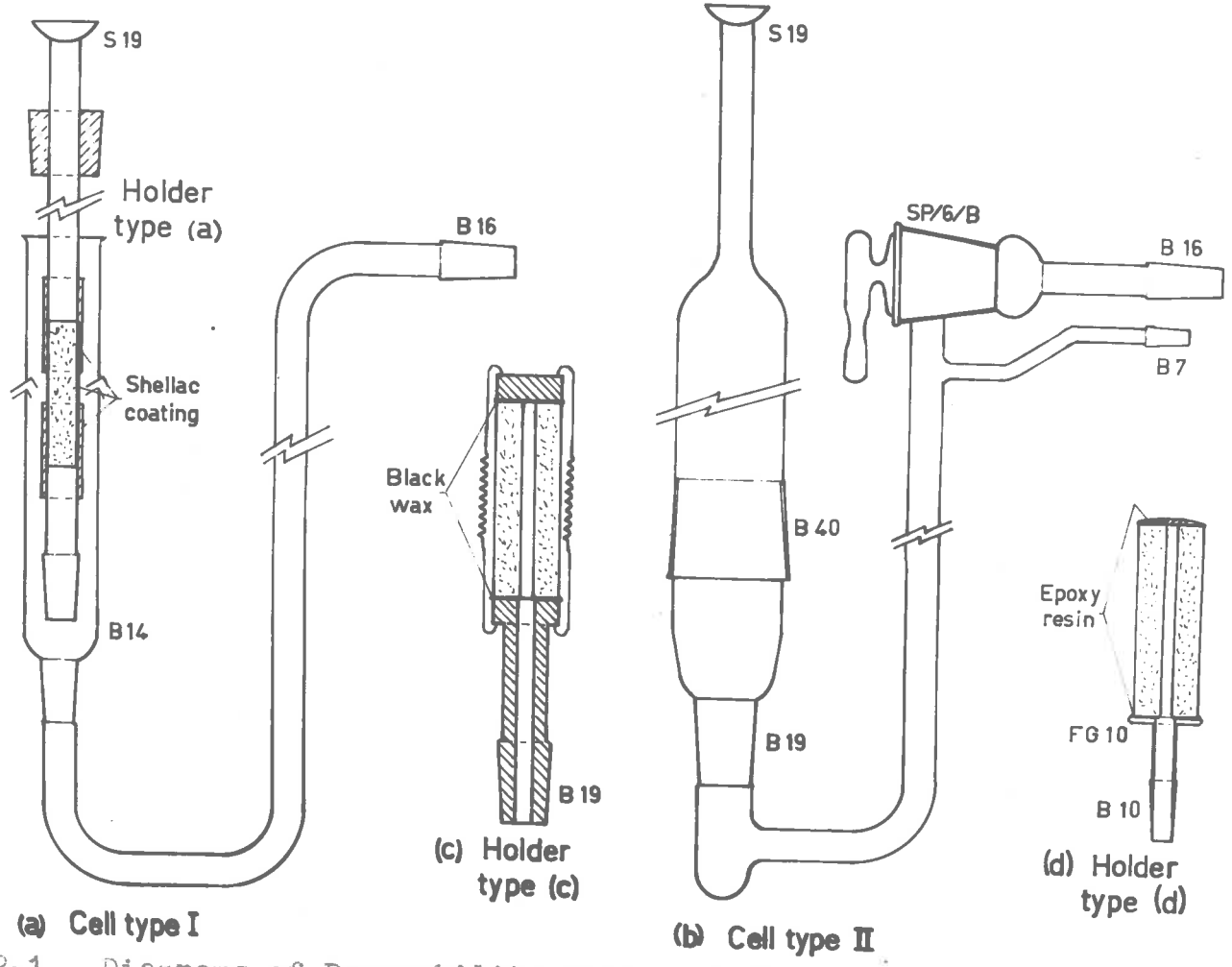

Fig. A.2-1 Diagrams of Permeability Cells and Sample Holders for the Low Pressure Permeability Apparatus.

(a) Permeability Cell Type I with Sample Holder Type (a);
(b) Permeability Cell Type II;
(c) Sample Holder Type (c);
(d) Sample Holder Type (d).

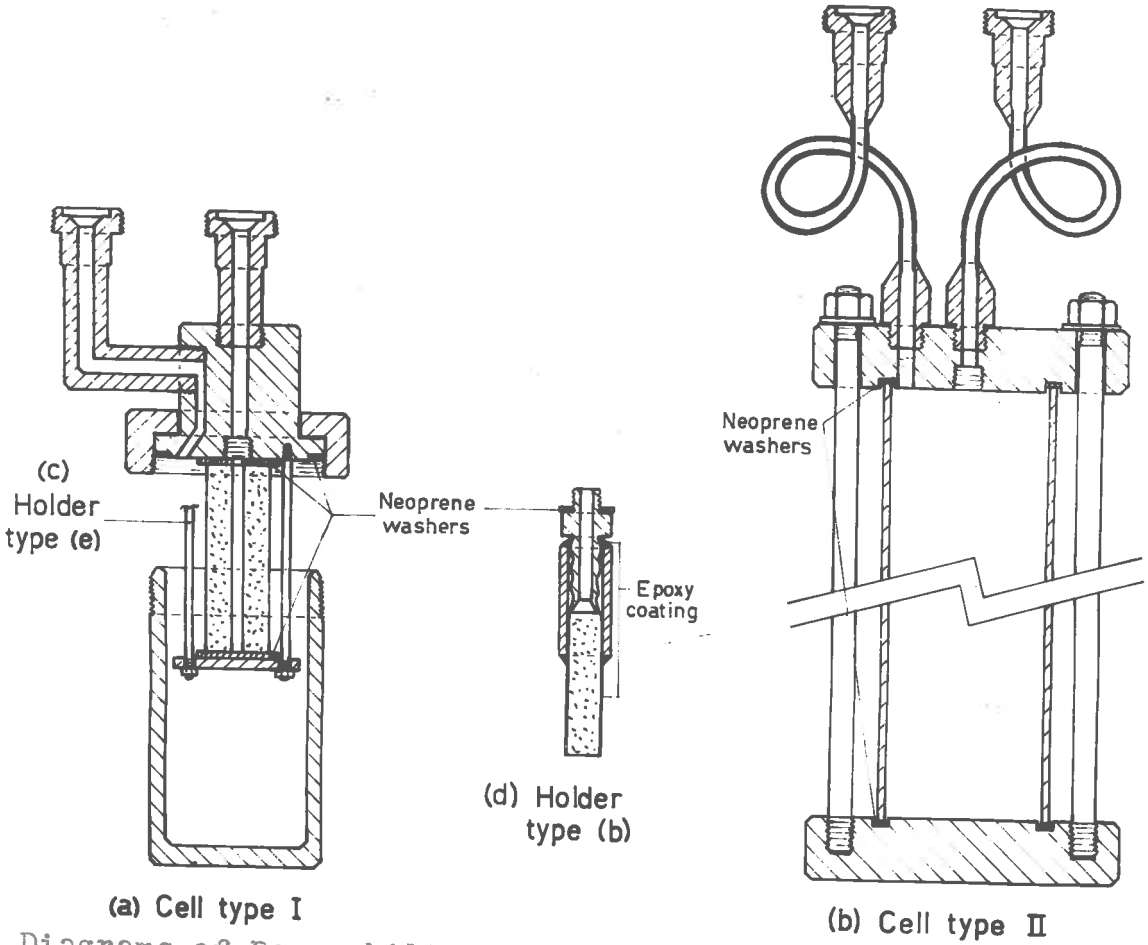

Fig. A.2-2 Diagrams of Permeability Cells and Sample Holders for the High Pressure Permeability Apparatus.
(a) Permeability Cell Type I;
(b) Permeability Cell Type II;
(c) Sample Holder Type (e);
(d) Sample Holder Type (b).

Type (d): Other cylindrical samples were sealed at one end to FG 10 flat joints by Epoxy resin and completely blocked with Epoxy resin at the other (see Fig. A.2-1(d)). These sample holders were attached to B10 conical joints and were supported in the type II low pressure permeability cell and in the high pressure permeability cells by means of adaptors.

Type (e): Originally cylindrical samples were held in the high pressure permeability cell type I by means of a plate held by three bolts with neoprene washers as seals (see Fig. A.2-2(e)). However, this method was only used for two samples as it was difficult to make the seal leakproof.

A.3 The Graphite Specimens for the Pressure Distribution Measurements

The details of the graphite specimens for the pressure distribution measurements are presented in Table A.3-1. The axis of each specimen corresponded to the axis of extrusion of the graphite. The graphite discs in Specimens No. G1 and No. G21 were coated with Epoxy resin, while those in Specimen No. G31 were coated with red sealing wax.

A.4 The Graphite Samples for the Porosity and Surface Area Determinations

The same samples were used for both the porosity and surface area determinations. Details of these samples including their dimensions, bulk volume V_t, and weight w are given in Table A.4-1.

A.5 The Graphite Samples for the Pore Size Distribution Measurements

The details of the graphite samples used in the mercury penetration experiments conducted by the

C.S.I.R.O.[240] are stated in Table A.5-1.

No details were available for the Impregnated graphite samples investigated by the A.A.E.C. (see section 3.4.2.1).

A.6 Details of the Graphite Samples for the Electrical Resistivity Determinations

The dimensions of the graphite samples on which the electrical resistivity measurements were made are presented in Table A.6-1, together with the relation of each sample to the direction of extrusion of the graphite. The cylindrical surfaces of the samples were coated with Epoxy resin generally, although paraffin-wax was applied to the P.G. 60 graphite samples.

Table A.3-1

Details of the Graphite Specimens for Pressure Distribution Measurements.

Specimen No.	Graphite Grade	Disc No.	Dimensions l	x	d	$\frac{L}{K}$ cm^{-1}
				cm		
G1	Acheson "A"	1	0.976	1.236		0.813
		2	0.974	1.236		0.812
		3	0.974	1.236		0.812
		4	0.973	1.236		0.811
		total	3.897	1.236		3.248
G21	Morgan "EY9166"	1	1.096	1.281		0.851
		2	1.107	1.281		0.859
		3	1.109	1.281		0.861
		4	1.051	1.281		0.815
		total	4.363	1.281		3.386
G31	P.G. 60	1	2.414	1.239		2.004
		2	2.548	1.252		2.068
		3	2.551	1.265		2.030
		4	2.535	1.250		2.065
		total	10.048	1.252		8.167

Table A.4-1
Details of the Graphite Samples for Porosity and Surface Area Measurements

Graphite Grade	Sample No.	Form	Dimensions cm l x d		Bulk Volume V_t-cm^3	Weight w g
Acheson "A"	S1	Powder	-14/+18 B.S.S. mesh		variable	
	S2	Cylinder	2.940	1.266	3.701	5.588
Morgan "EY9"	S21	Cylinder	2.814	1.200	3.177	5.464
	S22	Cylinder	2.648	1.201	2.999	5.148
P.G. 60	S31	Cylinder	4.247	1.300	5.633	5.370
	S32	Cylinder	4.230	1.245	5.150	5.012
Impregnated	S41[a]	Cylinder	4.654	0.818	2.446	4.370
	S42[b]	4 irregular pieces	-		3.633[c]	6.517

Notes:
a Sample No. S41 was a portion of Tube No. 4 supplied by the A.A.E.C.

b Sample No. S42 consisted of a diso of about ½ in. thickness cut from permeability sample No. K42. The disc was broken into four irregular pieces so that it would fit into a sample bulb.

c The bulk volume of Sample No. S42 was determined by displacement of water.

Table A.5-1
Details of the Graphite Samples for the C.S.I.R.O Pore Size Distribution Measurements[240]

Graphite Grade	Sample No.	Dimensions cm l x d	Bulk Volume V_t-cm^3	Weight w g	Bulk Density ρ_b-g/cm^3
Acheson "A" (Block 1)	P1	2.586 1.582	5.082	7.665	1.509
"	P2	2.551 1.587	5.053	7.797	1.543
(Block 2)	P3	2.560 1.585	5.057	7.772	1.537
"	P4	2.561 1.584	5.046	7.786	1.543
Morgan "EY9"	P21	2.554 1.587	5.052	8.698	1.721
	P22	2.564 1.585	5.060	8.738	1.727
P.G. 60	P31	2.563 1.577	5.006	4.810	0.961
	P32	2.582 1.582	5.075	4.928	0.971

Table A.6-1
Details of the Graphite Samples for Electrical Resistivity Determinations

Graphite Grade	Sample No.	Relation to Extrusion Axis	Dimensions cm l	x	d	A cm^2	$\frac{L}{A}$ cm^{-1}
Acheson "A"	T1	Par.	5.568	2.685		5.66	0.983
	T2	Perp.	2.144	2.765		6.00	0.357
	T2A[a]	Perp.	1.797	2.765		6.00	0.299
	T3	Par.	1.930	2.749		5.94	0.325
	T4	Perp.	2.428	2.781		6.07	0.400
	T5	Perp.	4.371	2.541		5.07	0.862
	T6	Par.	2.650	2.656		5.54	0.478
	T7	Perp.	4.600	2.740		5.90	0.780
	T8	Par.	3.710	2.645		5.49	0.675
	T9	Par.	4.550	2.447		4.70	0.968
	T10[b]	Perp.(1)	3.795	2.522		5.00	0.760
	T11[b]	Perp.(2)	5.413	2.506		4.94	1.096
Morgan "EY9"	T21	Par.	2.072	2.752		5.95	0.348
Morgan "EY9166"	T22	Par.	2.987	2.592		5.28	0.566
	T23	Perp.	1.754	2.766		6.01	0.292
	T24	Par.	2.407	2.562		5.16	0.467
	T25	Perp.	2.148	2.493		4.88	0.440
P.G. 60	T31	Par.	4.593	2.660		5.56	0.827
	T32	Perp.	4.671	2.450		4.71	0.991
Impregnated	T41[c]	-	1.280	2.080		3.39	0.378

Notes:
a Sample No. T2A was Sample No. T2 decreased in length.
b Samples No. T10 and No. T11 were in perpendicular directions at right angles to the axis of extrusion.
c Sample No. T41 was portion of Tube No. 3 supplied by the A.A.E.C.

APPENDIX B

GAS PROPERTIES

In the following table (B.1-1), the various pertinent properties of the gases used in the permeability determinations are listed. Except for the freon-12 value,[266] the values of the viscosity μ for the gases at 20°C and 1 atm (in poise x 10^7) were obtained from the American Institute of Physics Handbook,[150] together with the increments in the viscosity for a temperature change of 1°C and a pressure change of 1 atm; each viscosity value was the weighted mean of from 8 to 12 experimental values.

The mean free path λ was calculated as a function of the gas pressure p from the viscosity μ by means of the relation (ref.5, p.63)

$$\lambda p = \mu \sqrt{(\pi \mathcal{R} T / 2M)}, \qquad \ldots \text{(B.1-1)}$$

where $\mathcal{R}$ had the value 6236 cm^3, cm Hg/g-mol, °K.

Table B.1-1
Properties of the Gases

Gas	Formula	Molec. Weight M	Viscosity (20°C, 1atm) poise x 10^7 μ	Temperature incr. $\Delta\mu$/°C	Pressure incr. $\Delta\mu$/atm	λp (at 20°C) cm, cm Hg x 10^4
Hydrogen	H_2	2.02	882 ± 1	2.00	0.14	9.10
Helium	He	4.00	1953 ± 5	4.64	0.22	14.32
Nitrogen	N_2	28.02	1750 ± 4	4.55	2.28	4.85
Argon	A	39.94	2225 ± 15	6.37	3.0	5.17
Carbon Dioxide	CO_2	44.01	1463 ± 15	4.50	3.6	3.24
Freon-12	CF_2Cl_2	120.92	1237	2.79	-	1.65
Xenon	Xe	131.3	2246	7.25	-	2.88

APPENDIX C

THE PERMEABILITY DETERMINATIONS

C.1 Volume Calibrations for the Low Pressure Apparatus

The volumes of various sections of the low pressure apparatus were calibrated either by gas expansion from a known volume, or by weighing empty and full of water prior to attachment to the apparatus (see section 3.1.2.5). The volumes of these sections are listed in Table C.1-1 together with the standard deviations. Reference to the line diagram of the apparatus (Fig. 3.1-1) will clarify the position of each section in the apparatus. The volumes of the various adaptors and sample holders were not included in this tabulation.

Generally the volume V of the apparatus involved in permeability determinations by both the pressure increase and pressure decay methods consisted of side 1 of the apparatus and flask I. The maximum error in V was then less than 2%.

C.2 The Pressure Increase/Time-Lag Method

C.2.1 The Theory of the Pressure Increase Method

In permeability determinations by the pressure increase method, gas at essentially a constant inlet pressure p_i flowed through the graphite sample to the initially evacuated outlet side of the apparatus, where the rate of increase of the outlet pressure p_o was

Table C.1-1
Volumes of Sections of the Low Pressure Permeability Apparatus

Section of Apparatus	Volume cm^3	Std. Devn. $\pm cm^3$
Standard volume - flask I	1091	0.2
Standard volume - flask H	1138	1.0
Gas reservoir - flask S_1	6200	210
Gas reservoir - flask S_2	1100	0.5
Gas reservoir - flask S_3	-	-
Gas reservoir - flask S_4	5510	2.0
McLeod gauge bulb and capillary	311	0.6
Inlet arm of McLeod gauge to cut-off point	76.5	1.3
Side I of manometer J	145 + 0.39 p	1.5
Side 2 of manometer J	161 + 0.39 p	0.7
Side I of manometer M	12.7 +0.42 p	0.1
Side I - between stop-cocks and joint a.	265	3.0
Side 2 - between stopcocks	131	-
Gas line F	58	1.2
Side I of permeability cell type I between sample and joint a.	60	0.5
Side 2 of permeability cell type I between sample and stop-cock b.	35	0.8
Side I of permeability cell type II between stopcock c and joint a.	29.5	-
Side I of permeability cell type II between stopcock c and joint d and including side arm to manometer M	55.9	0.5
Side 2 of permeability cell type II between stopcock b and the sample	approx. 200	-

Notes:
1. Joint a refers to the B16 joint by which the permeability cell was attached to side I of the apparatus.
2. Stopcock b is the stopcock in the spherical joint system L.
3. Stopcock c is the Springham SP/6/B stopcock on side I of the permeability cell type II (see Fig. A.2-1(b)).
4. Joint d refers to the B19 joint in which the sample holder was held in the permeability cell type II (see Fig. A.2-1(b)).

observed with a McLeod gauge (see section 3.1.3.1). Provided p_i remained much greater than p_o during an experiment, the volumetric rate of gas flow through the sample Q_m at the mean pressure p_m and temperature $\mathcal{T}_s$ of the sample was obtained from the rate of increase of p_o, (dp_o/dt), in the calibrated outlet side volume V_o of the apparatus.

Over a small interval of time $\delta t = t_2 - t_1$, the pressure in the volume V_o increased from p_{o1} to p_{o2}; then the increase in the number of moles

$$= V_o(p_{o2} - p_{o1})/(\mathcal{R}\mathcal{T}_a),$$

where $\mathcal{T}_a$ = ambient temperature. If δt was very small, the rate of increase in the number of moles

$$= \frac{V_o}{\mathcal{R}\mathcal{T}_a} \frac{dp_o}{dt} \quad . \qquad \ldots (C.2\text{-}1)$$

This rate equalled the gas flow-rate through the sample at that time, viz., $p_m Q_m/(\mathcal{R}\mathcal{T}_s)$ mol/sec. Then

$$p_m Q_m = V_o \frac{dp_o}{dt} \frac{\mathcal{T}_s}{\mathcal{T}_a} \quad . \qquad \ldots (C.2\text{-}2)$$

Hence the permeability coefficient K at p_m and $\mathcal{T}_s$ was given by

$$K = \frac{V_o\, dp_o/dt}{\Delta p} \frac{L}{A} \frac{\mathcal{T}_s}{\mathcal{T}_a} \quad . \qquad \ldots (C.2\text{-}3)$$

The rate of pressure increase dp_o/dt was readily obtained as the slope of the p_o against t plot. Generally, over the time interval during which gas was collected in V_o, this plot was essentially straight; K was then calculated

using the average values of p_i and p_o. However, the p_o-t plot was quite curved for some experiments; then values of the slope were measured for different times during the experiment and the appropriate values of p_i and p_o were employed to calculate K.

The value of the time-lag ϕ was obtained from the intercept of the straight portion of the p_o-t plot with the time axis when extrapolated back to zero pressure. When ϕ was small and difficult to obtain accurately from the graph, it was calculated by means of the expression

$$\phi = t_1 - p_{o1}/(dp_o/dt), \qquad \ldots (C.2\text{-}4)$$

where p_{o1} and t_1 were the pressure and time coordinates, respectively, of the first point on the straight p_o-t plot.

C.2.2 Type Calculation for the Pressure Increase Method

The determination of permeability coefficients for carbon dioxide flow through Morgan "EY9" Rod No. K21 (Detmn. No. L:49) typifies a pressure increase determination. The experimental results for this determination are presented in Table C.2-1. The McLeod gauge pressures were corrected (see section 3.1.2.2) and the values of V_o were obtained by reference to Table C.1-1.

Table C.2-1
Experimental Results for a Pressure Increase Determination
(No. L:49)

Expt. No.	Time min	p_i cm Hg	p_o mm Hg	V_{O_3} cm^3	Temp. $\mathcal{T}_a$	°C $\mathcal{T}_s$
Blank	0		$< 10^{-5}$			
	16		7×10^{-4}			
1	0		$< 10^{-5}$	768.3	20.3	18.4
	1	3.201				
	5		0.0138			
	14		0.063			
	30	av 3.187	0.148			
	46	± 0.014	0.228			
	67		0.335			
	83	3.174	0.416		19.8	18.5
2	0		$< 10^{-5}$	755.6	20.0	18.5
	1	1.386				
	6		0.0071			
	16		0.0295			
	29	av.1.379	0.062			
	60	± 0.007	0.136			
	71		0.162			
	127		0.290			
	146	1.372	0.327		20.2	18.7
3	0		$< 10^{-5}$	755.6	20.3	18.8
	1	0.600				
	5		0.0025			
	18		0.015			
	34	av.0.599	0.030			
	50	± 0.001	0.048			
	77		0.080			
	94		0.098			
	115	0.598	0.121		20.2	18.9

Table C.2-1 (Contd)

4	0		10^{-6}	755.6	19.6	17.8
	1	5.752				
	6		0.036			
	16		0.141			
	33	av.5.732	0.302			
	52	± 0.020	0.486			
	64		0.597			
	74	5.712	0.700		19,6	17.9
5	0		$< 10^{-5}$	755.6	19.7	18.1
	1	10.853				
	5		0.06			
	19	av10.811	0.337			
	32	± 0.042	0.590			
	42		0.786			
	57		1.084			
	72	10.770	1.375		19.5	18.2
6	0		$< 10^{-5}$	1846.7	18.9	17.9
	1	13.976				
	5		0.0375			
	17		0.171			
	29	av.13.940	0.298			
	40	± 0.036	0.415			
	54		0.569			
	66		0.698			
	67	13.904			19.1	18.0
7	0		$< 10^{-5}$	1846.7	19.3	18.0
	1	19.728				
	6		0.071			
	18	av.19.675	0.271			
	36	± 0.054	0.566			
	50		0.798			
	65	19.621	1.042		19.5	18.1

Table C.2-1 (Contd)

8	0		$<10^{-5}$		19.6	18.2
	1	25.875		1846.7		
	6		0.104			
	18	av.25.770	0.382			
	30	± 0.104	0.663			
	42		0.941			
	53		1.195			
	60	25.667	1.360		19.6	18.3
					$\mathcal{T}_s$(av)=	18.2°C

Table C.2-2

Permeability Results for a Pressure Increase Determination (No. L:49)

Expt. No.	p_i cm Hg	p_o cm Hg	p_m cm Hg	Δp cm Hg	dp_o/dt mm/sec x 10^4	K cm^2/sec x 10^2	ø min Graph.	ø min Calc.
1	3.194	0.010	1.602	3.184	0.890	1.320	2.4	2.48
	3.180	0.032	1.606	3.148	0.846	1.269		
2	1.380	0.009	0.694	1.371	0.400	1.356	3.2	2.83
	1.376	0.023	0.700	1.353	0.377	1.294		
3	0.599	0.006	0.303	0.593	0.182	1.426	5.0	-
4	5.732	0.034	2.883	5.698	1.63	1.328	2.2	1.47
5	10.811	0.067	5.439	10.744	3.28	1.419	2.1	1.96
6	13.940	0.035	6.986	13.905	1.80	1.473	1.5	1.63
7	19.675	0.051	9.863	19.624	2.74	1.587	1.6	1.74
8	25.770	0.066	12.918	25.704	3.88	1.715	1.6	1.50

From the experimental results, the p_o-t plot was prepared for each experiment (see Fig. C.2-1); in practice, the scales were chosen for greatest accuracy in measuring the slope. The values of the slope and the intercept on the t-axis obtained from this plot, and the value of the permeability

coefficient K calculated by means of equation (C.2-3) are recorded in Table C.2-2.

The degassing rate of 0.7×10^{-6} mm Hg/sec as obtained in the blank experiment was lower than the maximum permissible rate (1×10^{-6} mm Hg/sec); correction of dp_o/dt at low p_m did not eliminate the minimum in the K-p_m plot. In experiments 3 to 8, straight p_o-t plots were obtained; however curved plots were observed for experiments 1 and 2 and values of K were calculated at two different times (see Appendix C.2.1). The graph of K against p_m, presented in Fig. C.2-2, showed that a minimum was obtained at about p_m = 2 cm Hg (0.027×10^6 dyn/cm^2). The scatter of the K values about the graph was less than $\pm$ 1×10^{-4} cm^2/sec ($\pm$ 0.7%) above p_m = 2 cm Hg, but was greater at lower p_m because of the curved p_o-t plots.

The equation of the straight portion of the K-p_m plot, calculated by the method of least squares, was

$$K = 3.86 \times 10^{-4}\ p_m + 0.0121 \quad (p_m \text{ in cm Hg}).$$

With $\mu = 1455 \times 10^{-7}$ poise at $\mathcal{T}_s$ (see Table B.1-1, Appendix B),

$M = 44.01$,

$\mathcal{T}_s = 18.2^\circ C = 291.4^\circ K$,

$\mathcal{R} = 0.8314 \times 10^8$ gm, cm^2/g-mol, $^\circ$K, sec^2,

$\rho_{Hg} = 13.550$ g/cm^3 at $\mathcal{T}_s$, and

$g_c = 980.665$ cm^2/sec, the values of the coefficients B_o and K_o were calculated,

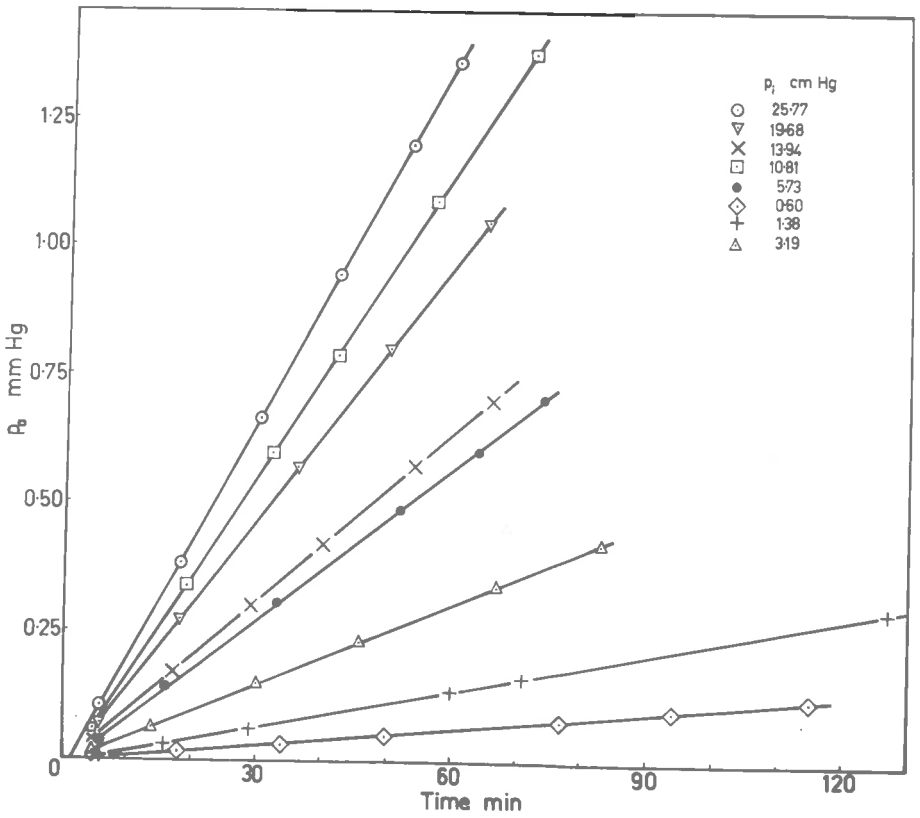

Fig. C.2-1 Pressure Increase Plots of p_o against t for Detmn. No. L:49 (Carbon Dioxide Flow through Morgan "EY9" Rod No. K21).

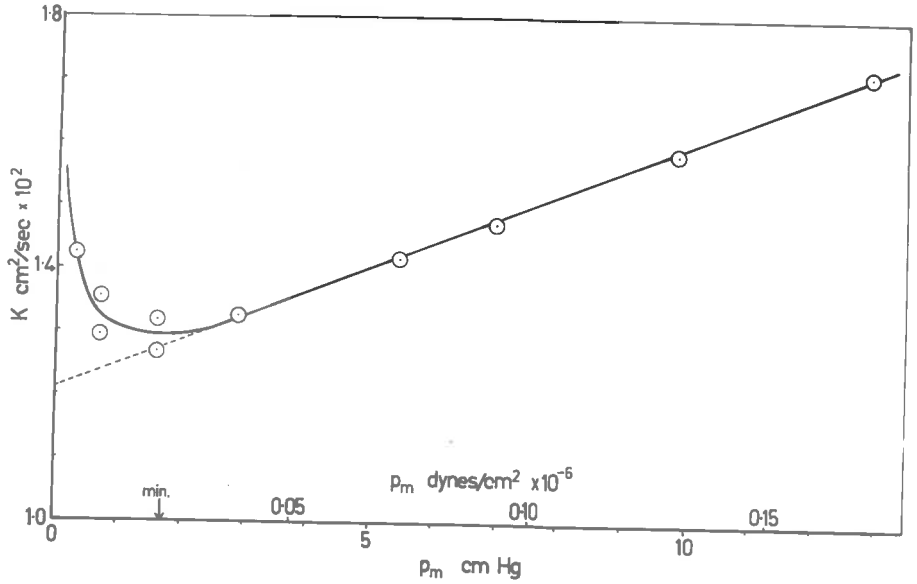

Fig. C.2-2 K-p_m Plot for Carbon Dioxide Flow through Morgan "EY9" Rod No. K21 (Detmn. No. L:49 - Pressure Increase Method).

$$\text{e.g., } B_o = 3.86 \times 10^{-4}\mu = \frac{3.86 \times 10^{-4} \times 1455 \times 10^{-7}}{13.5502 \times 980.665}$$

$$= \underline{4.23 \times 10^{-12} \text{ cm}^2}$$

$$\text{and} \quad K_o = \frac{3}{4} \times 0.0121 \times \sqrt{\left(\frac{\pi M}{8 \mathcal{R} T_s}\right)}$$

$$= \frac{3}{4} \times 0.0121 \times \sqrt{\left(\frac{\pi \times 44.01}{8 \times 0.834 \times 10^{8} \times 291.4}\right)}$$

$$= \underline{2.42 \times 10^{-7} \text{ cm}}$$

C.2.3 Experimental Accuracy

For manometer pressures, the error in a pressure measurement because of the sticking of the mercury in the manometer and the inaccurate alignment and reading of the cathetometer was less than 0.06 cm Hg. This error could be reduced to a minimum by careful measurement. The error in Δp above $p_m = 3$ cm Hg was therefore less than 1%, but became greater as p_m decreased.

McLeod gauge pressure measurement involved a maximum calibration error of 1% and a reading error of less than 1% for p above 10^{-2} mm Hg, i.e., less than 2% error. Below $p = 10^{-2}$ mm Hg, where the error was greater because of the logarithmic scale, the values of p_o could be generally neglected in the pressure increase experiments.

When the mercury in the McLeod gauge was raised to measure p_o, V_o was decreased and the gas compressed for 1 to 2 min; then flow through the sample was possibly upset and faulty K values obtained. Experiments were made to

check the accuracy (see Detmn. No. L:22); the variation in the values of K was quite small, showing that no significant inaccuracies arose from measuring the McLeod gauge pressure. Nevertheless, V_o and the time interval between successive McLeod gauge measurements were made as large as practicable for each experiment for accurate measurement of the flow-rate.

The error in measuring the time of the pressure measurements was less than ½%. Any scatter in the values of p_o was smoothed out when the best-fit straight line was drawn through the p_o-t points. The slope of the p_o-t plot (dp_o/dt) was measured to 3%.

The dimensions of the rod samples were measured to $\pm$ 0.005 cm, i.e., the errors in L and A were about 0.2% and 1½%, respectively. Errors in the measurement of the ambient and sample temperatures were negligible (0.2%). As the change in the ambient temperature during an experiment was generally about 0.2°C, the value of dp_o/dt was negligibly affected.

Hence, for pressure increase experiments, the calculation of values of K by means of equation (C.2-3) involved a maximum overall error of less than 8%, and a relative error of less than 4% for p_m above 3 cm Hg. The estimated errors were larger at lower p_m.

C.3 The Pressure Decay Method

C.3.1 The Theory of the Pressure Decay Method

In the pressure decay method, the rate of decay of the

inlet pressure p_i in the volume V_i was measured while gas flowed through the graphite sample to the outlet side, where the pressure p_o was kept effectively at zero (see section 3.1.3.2). The volumetric rate of gas flow through the sample Q_m at the mean pressure p_m and temperature $\mathcal{T}_s$ of the sample was calculated from the observed rate of pressure decay dp_i/dt in the calibrated inlet volume V_i.

Over a small interval of time $\delta t = t_2 - t_1$, the pressure in V_i decreased from p_{i1} to p_{i2}, i.e., the decrease in the number of moles $= V_i (p_{i1} - p_{i2})/(\mathcal{R}\mathcal{T}_a)$.
If δt was very small, the rate of decrease in the number of moles

$$= -\frac{V_i}{\mathcal{R}\mathcal{T}_a} \frac{dp_i}{dt} . \qquad \ldots (C.3\text{-}1)$$

This rate equalled the gas flow-rate through the sample at that time, viz., $p_m Q_m/(\mathcal{R}\mathcal{T}_s)$ mol/sec. Therefore

$$p_m Q_m = -V_i \frac{dp_i}{dt} \frac{\mathcal{T}_s}{\mathcal{T}_a} . \qquad \ldots (C.3\text{-}2)$$

Hence the permeability coefficient K at p_m and $\mathcal{T}_s$ was given by

$$K = -\frac{V_i \, dp_i/dt}{\Delta p} \frac{L}{A} \frac{\mathcal{T}_s}{\mathcal{T}_a} . \qquad \ldots (C.3\text{-}3)$$

The rate of pressure decay dp_i/dt was obtained as the slope of the plot of p_i against t.

C.3.2 Type Calculation for the Pressure Decay Method

A typical determination of permeability coefficients by the pressure decay method is Detmn. No. L:53, in which values of K are calculated for carbon dioxide flow through Acheson "A" Graphite Rod No. K2A. The experimental results for this determination are given in Table C.3-1.

The determination was discontinued overnight; on recommencement next morning, p_i was increased slightly to overlap the break in the pressure decay. When the rate of pressure decay was less than 0.025 cm Hg/min, V_i was decreased by the removal of the calibrated volume I (point "a" on the decay plot - Fig. C.3-1). The value of V_i was obtained by reference to Table C.1-1. The outlet pressure p_o was derived from the reading indicated on the Pirani gauge.

From the decay plot of p_i against t (see Fig. C.3-1), the slope of the curve dp_i/dt was obtained at different values of p_i. In practice, several p_i-t plots were prepared so that the values of dp_i/dt were obtained with the greatest accuracy. By means of equation (C.3-3), values of K at the different values of p_i were calculated from the values of dp_i/dt (see Table C.3-2).

The graph of K against p_m, shown in Fig. C.3-2, was straight below p_m = 12 cm Hg, but curved slightly downwards above this pressure. The scatter of the values of K about the plot was less than $\pm$ 0.05 cm^2/sec (2½ to 12%).

Table C.3-1
Experimental Results for Detmn. No. L:53

Time min	p_i cm Hg	Temp. °C $\mathcal{T}_a$	$\mathcal{T}_s$
	$V_i = 1845 + 0.842\ p_m$ cm^3		
5	46.378	17.2	16.4
15	41.464		
29	36.044		
51	29.465		
88	22.494	17.2	16.4
113	19.161		
145	16.048	17.5	16.5
Restart			
148	15.878	17.9	16.5
171	14.215		
190	13.031		
213	11.771	19.2	
248	10.163	18.4	16.6
310	8.099	18.5	
350	7.124		
402	6.071	18.8	
405	Remove flask I - point "a", Fig.C.3-1		
	$V_i = 754 + 0.842\ p_m$ cm^3		
423	5.339		
456	4.346		
495	3.483	18.6	16.9
551	2.609		
592	2.169	17.5	
634	1.806		
670	1.552	17.5	17.0

Table C.3-2
Permeability Results for a Pressure Decay Determination (No. L:53)

p_i cm Hg	p_o cm Hg	p_m cm Hg	Δp cm Hg	V_i cm^3	dp_i/dt cm/hr	K cm^2/sec
45	0.01	22.5	45	1864	30.8	1.93
40	0.01	20.0	40	1861	25.1	1.77
35	0.01	17.5	35	1859	19.2	1.54
30	0.01	15.0	30	1857	15.6	1.46
25	0.01	12.5	25	1855	10.85	1.22
20	0.01	10.0	20	1853	7.35	1.03
17.5	0.01	8.75	17.5	1852	5.88	0.941
14	0.01	7.0	14	1851	3.92	0.782
12	0.01	6.0	12	1850	3.19	0.741
10	0.01	5.0	10	1849	2.45	0.684
8	0.01	4.0	8	1848	1.57	0.548
7	0.01	3.5	7	1848	1.30	0.518
5	0.01	2.5	5	756	1.72	0.392
4	0.01	2.0	4	755	1.38	0.393
3	0.01	1.5	3	755	0.948	0.360
2	0.01	1.0	2	754	0.526	0.301

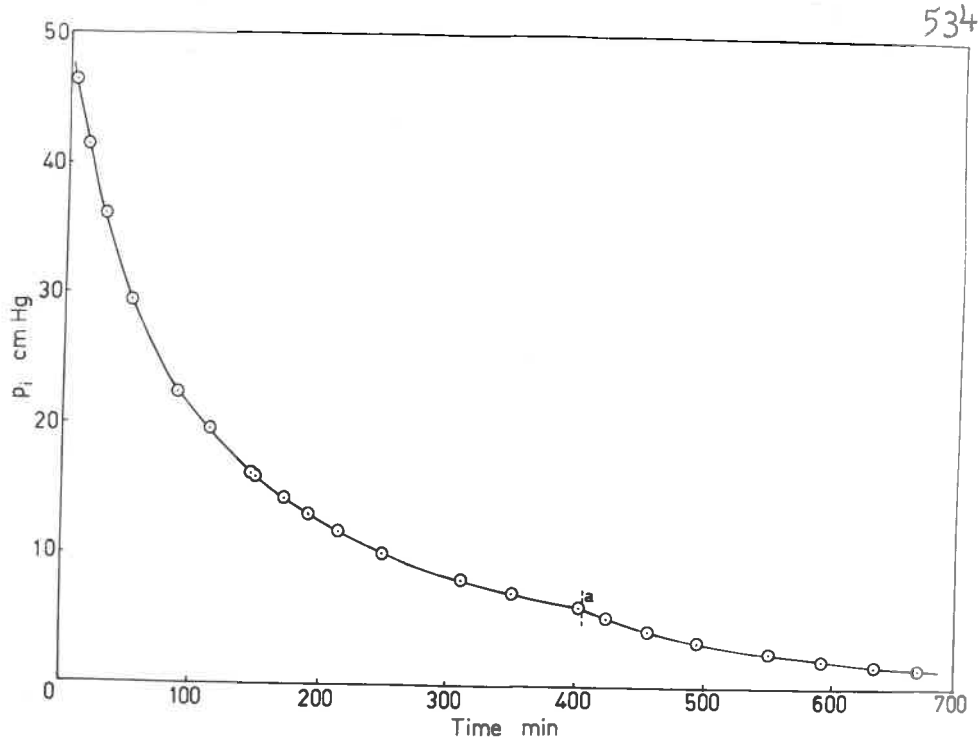

Fig. C.3-1 Pressure Decay Plot of p_i against t for Detmn. No. L:53 (Carbon Dioxide Flow through Acheson "A" Rod No. K2A).

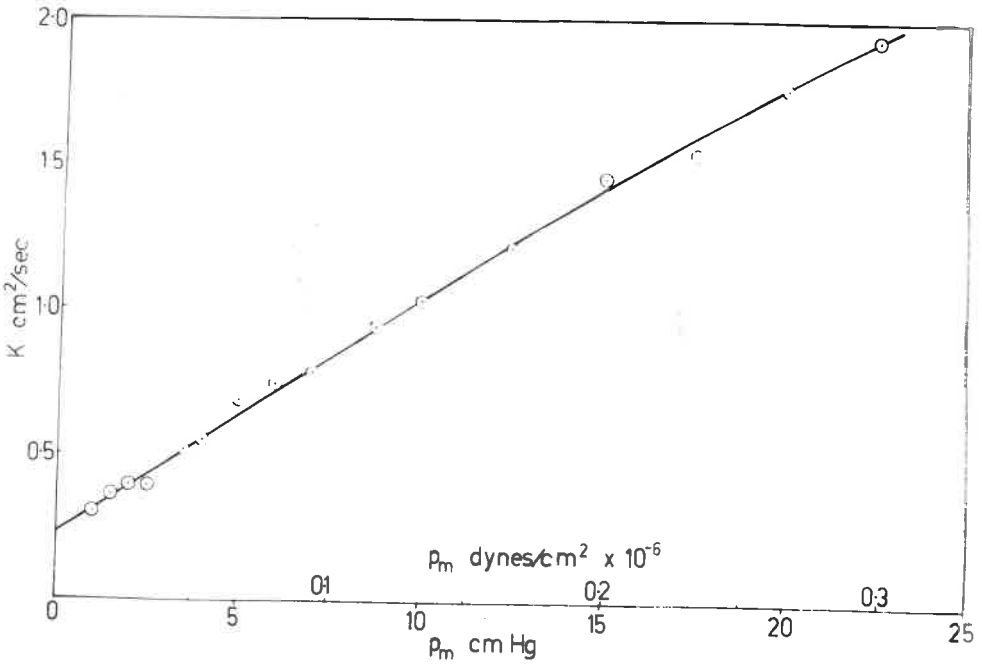

Fig. C.3-2 K-p_m Plot for Carbon Dioxide Flow through Acheson "A" Rod No. K2A (Detmn. No. L:53 - Pressure Decay Method).

The equation of the straight portion of the plot, calculated by the method of least squares, was

$$K = 0.0810\ p_m + 0.230 \quad (p_m \text{ in cm Hg}).$$

By a calculation similar to that in Appendix C.2.2,

$$B_o = \underline{8.82 \times 10^{-10}}\ \text{cm}^2, \text{ and}$$

$$K_o = \underline{4.62 \times 10^{-6}}\ \text{cm}.$$

C.3.3 Experimental Accuracy

The error in the measurement of the pressure by the manometer was less than 0.06 cm Hg, i.e., Δp was in error by less than 1% for p_m above 3 cm Hg (cf. Appendix C.2.3). The error in the time measurement was less than ½%. Any scatter amongst the p_i values was smoothed out when the best-fit curve was drawn through the p_i-t points.

The values of dp_i/dt obtained as the slope of the p_i-t curve were generally not very accurate since it was difficult to draw the curve through the points and to measure the slope accurately with a straight-edge. At each p_i, several values of the slope were measured and the average taken; the observed variation in dp_i/dt was as great as 10%, especially at low p_m (where the curves were replotted with extended scales for greater accuracy), but was generally less than 4%. The numerical procedure of Douglass and Avakian[234] was employed in some experiments to overcome the above difficulties, but the calculations proved to be tedious and often gave little improvement in

the accuracy of the dp_i/dt values.

The errors in the other quantities were the same as mentioned in Appendix C.2.3, viz., V(2%), L(0.2%), A(1½%), $\mathcal{J}_s$(0.2%), and $\mathcal{J}_a$(0.2%). Hence, for pressure decay experiments, the maximum overall error in the values of K calculated by means of equation (C.3-3) was less than 9% above p_m = 3 cm Hg, but was larger at lower p_m.

C.3.4 The Pressure Equalization Method

For experiments by the pressure equalization method, the pressure difference Δp across the graphite sample was measured as a function of time when gas flowed from a closed volume V_i at a high pressure through the sample to an isolated volume V_o at a low pressure (see section 3.1.3.3).

At any time t after the commencement of an experiment, a mass balance over an infinitesimally small time interval dt and comparison with equation (C.3-2) showed that

$$p_m Q_m = - \frac{d(\Delta p)}{dt} \quad \frac{V_o V_i}{V_i + V_o} \quad \frac{\mathcal{J}_s}{\mathcal{J}_a} . \qquad \ldots (C.3-4)$$

The permeability coefficient K at p_m and $\mathcal{J}_s$ was calculated from the equation

$$K = - \frac{V_o V_i}{V_i + V_o} \quad \frac{d(\Delta p)}{dt} \quad \frac{L}{A \Delta p} \quad \frac{\mathcal{J}_s}{\mathcal{J}_a} . \qquad \ldots (C.3-5)$$

It was assumed that the volume of gas in the pores of the graphite sample was negligible compared with V_i and V_o.

The rate of change of Δp ($d(\Delta p)/dt$), was obtained at various values of Δp as the slope of the plot of Δp against t. The volumes V_i and V_o were obtained by reference to Table C.1-1. The mean pressure p_m in the sample was calculated by means of a mass balance.

C.4 The Low Pressure Flow Method

In the low pressure flow method, gas flowed continuously through the graphite sample under steady state conditions and the flow-rate was determined from the increase of pressure p_o in the volume V_o over a certain time interval (2 minutes) after V_o was isolated (see section 3.1.3.4). Since the gas flow-rate through the sample $p_m Q_m/(\mathcal{A}\mathcal{J}_s)$ equalled the rate of increase in the number of moles of gas in V_o (cf.Appendix C.2.1 for the pressure increase method), then

$$p_m Q_m = V_o \frac{\Delta p_o}{\Delta t} \frac{\mathcal{J}_s}{\mathcal{J}_a} . \qquad \ldots . (C.4\text{-}1)$$

Hence the permeability coefficient K at p_m and $\mathcal{J}_s$ was given by the expression

$$K = \frac{V_o \ \Delta p_o/\Delta t}{\Delta p} \frac{L}{A} \frac{\mathcal{J}_s}{\mathcal{J}_a} . \qquad \ldots . (C.4\text{-}2)$$

C.5 The High Pressure Flow Method

C.5.1 The Theory of the High Pressure Flow Method

In permeability determinations by the high pressure flow method, gas at a constant inlet pressure p_i flowed

through the graphite sample under a constant pressure difference Δp, and the volumetric flow-rate of the out-flowing gas Q_a was measured directly with a flow-meter at the pressure p_a and temperature $\mathcal{T}_a$.

Provided there were no leaks in the gas line between the sample and the flow-meter, the mass flow-rate of gas flowing through the graphite sample was equal to the mass flow-rate of gas in the flow-meter under steady state conditions, i.e.,

$$p_m Q_m / \mathcal{T}_s = p_a Q_a / \mathcal{T}_a \quad , \qquad \ldots . \text{(C.5-1)}$$

where Q_m = the volumetric flow-rate through the sample at the mean pressure p_m and temperature $\mathcal{T}_s$ of the sample. The pressure p_a in the flow-meter was generally within a few mm Hg of atmospheric pressure. The permeability coefficient K at p_m and $\mathcal{T}_s$ was then calculated from the equation

$$K = \frac{p_a Q_a}{\Delta p} \frac{L}{A} \frac{\mathcal{T}_s}{\mathcal{T}_a} . \qquad \ldots . \text{(C.5-2)}$$

The flow-rate Q_a was obtained from the flow-meter measurements according to the following equations. For the wet gas test meter, the volume V of gas collected in time t was corrected for the volume of water vapour V_w in the gas, i.e.,

$$Q_a = (V - V_w)/t. \qquad \ldots . \text{(C.5-3)}$$

For the soap-bubble flow-meters, the volume of gas V

collected in time t was corrected to temperature $\mathcal{T}_a$ because the burettes were calibrated at 20°C; then

$$Q_a = (V/t)(293.2/\mathcal{T}_a) . \qquad \ldots . \text{(C.5-4)}$$

With the rotameters, the flow-rate $Q' = Q_{N.T.P.} \sqrt{\mathcal{T}_a}$ was obtained from the rotameter calibration chart of the rotameter float height against Q'. Then

$$Q_a = Q' \sqrt{(\mathcal{T}_a)}/293.2 . \qquad \ldots . \text{(C.5-5)}$$

When the capillary flow-meter was used, the pressure drop Δp across the capillary was measured and the flow-rate Q_a at the mean pressure in the capillary p_a was calculated from

$$Q_a = X \Delta p , \qquad \ldots . \text{(C.5-6)}$$

where X was the capillary flow-meter calibration constant (4.64×10^{-3} cm^3/sec, cm Hg for nitrogen flow above $\Delta p = 7$ cm Hg).

C.5.2 Type Calculation for the High Pressure Flow Method

The determination of permeability coefficients for nitrogen flow through Acheson "A" Graphite Rod No. K4 (Detmn. No. H:20) is a typical high pressure flow determination. The experimental results for this determination are given in Table C.5-1.

The atmospheric pressure p_a was measured for each batch of experiments and was assumed to remain constant while the experiments were performed. Manometer pressure readings (cm Hg units in Table C.5-1) were converted to absolute values where necessary by adding the value of p_a.

Table C.5-1
Experimental Results for a High Pressure Flow Determination
(No. H:20)

Expt. No.	p_i p.s.i.g. or cm Hg	p_o cm Hg	p_a cm Hg	Volume cm^3	Time sec	Q_a cm^3/sec	Temp °C T_s	T_a
	Leakage			7.0	611.8	0.0116		15.4
				7.0	652.8	0.0109		
1	21.1 psi	1.051	75.842	(100 rot.1	21.3	4.75	17.0	17.1
					10.3	4.84		
2	7.941 cm	0.028	75.774	1.8	65.3	0.028	17.6	17.5
3	17.656 cm	0.062	"	1.8	23.25	0.078	17.7	17.7
4	37.560 cm	0.152	"	32	116.6	0.277	17.6	17.6
5	76.181 cm	0.332	"	100	101.4	0.994	17.4	17.4
6	53.8 psi	2.603	75.969	rot.2	(9.7	14.1	16.7	16.8
					(14.45	14.0		
7	75.7 psi	3.853	"	" 2	13.15	21.2	17.0	17.0
8	76.6 psi	77.364	"	" 2	13.10	21.1	17.2	17.2
9	51.4 psi	76.663	"	" 2	(8.92	12.35	17.0	17.0
					(14.02	12.30		
10	20.2 psi	76.187	"	" 1	8.0	3.76	17.0	17.0
11	40.569 cm	0.580	76.515	100	47.1	2.14	17.1	17.2
12	39.442 cm	0.577	"	100	48.0	2.10	17.0	17.0
13	38.266 cm	76.541	76.539	100	88.6	1.14	16.7	16.8
14	8.231 cm	76.401	76.401	30	140.9	0.216	15.9	16.0
15	24.058 cm	76.402	"	100	149.9	0.676	16.0	16.1
16	79.632 cm	76.322	76.304	100	37.1	2.73	16.4	16.4
17	79.537 cm	0.842	"	(100 rot.1	28.8	3.51	16.4	16.5
					7.7	3.54		
18	40.4 psi	76.904	"	" 2	(11.97)	9.07		
					7.27)	8.95	16.2	16.3
19	38.9 psi	2.787	"	" 2	(7.25)	8.95		
					12.0)	9.13	16.2	16.3

Table C.5-2
Permeability Results for a High Pressure Flow Determination
(No. H:20)

Expt. No.	p_i cm Hg	p_o cm Hg	p_m cm Hg	Δp cm Hg	Q_a cm^3/sec	K cm^2/sec
1	185	1.05	93.1	184	4.75	10.19
					4.84	10.38
2	7.94	0.03	3.98	7.9	0.0168*	0.84
3	17.66	0.06	8.86	17.6	0.067*	1.51
4	37.56	0.15	18.9	37.4	0.266*	2.81
5	76.18	0.33	38.3	75.9	0.994	5.18
6	355	2.60	179	352	14.05	15.80
7	469	3.85	236	465	21.2	18.08
8	474	77.36	276	397	21.1	21.03
9	342	76.66	209	265	12.32	18.40
10	181	76.19	129	105	3.76	14.21
11	117.08	0.58	58.8	116	2.14	7.33
12	115.96	0.57	58.3	115	2.10	7.26
13	114.81	76.54	95.7	38.3	1.14	11.89
14	84.63	76.40	80.5	8.2	0.216	10.46
15	100.46	76.40	88.4	24.1	0.676	11.20
16	155.94	76.33	116	79.6	2.73	13.65
17	155.84	0.84	78.3	155	3.52	9.04
18	286	76.90	181	209	9.07	17.28
					8.95	17.05
19	273	2.79	138	270	9.13	13.45
					8.95	13.18

* Corrected for leakage rate

Gauge pressure readings p_g(p.s.i.g. units) were expressed in centimetres of mercury absolute at 20°C by means of the equation $p_{cm\ Hg} = (p_g \times 5.192) + p_a$. The flow-rate Q_a was measured by means of the rotameters (rot.1 = Tube 1A-15-1, rot.2 = Tube 2-15-3, and float heights are recorded in Table C.5-1) and the soap-bubble flow-meter. Equations (C.5-5) and (C.5-4) were therefore applied to calculate Q_a.

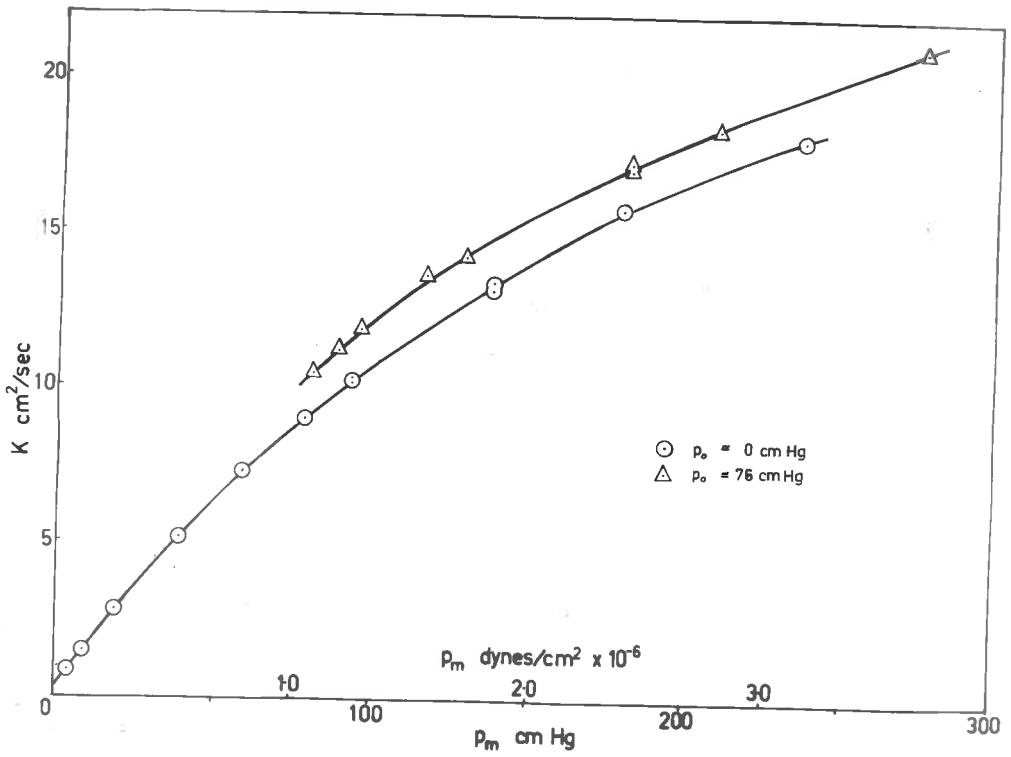

Fig. C.5-1 K-p_m Plot for Nitrogen Flow through Acheson "A" Rod No. K4 (Detmn. No. H:20 - High Pressure Flow Method).

Values of the permeability coefficient K, calculated by means of equation (C.5-2), are tabulated in Table C.5-2. A graph of K against $\bar{p}_m$ presented in Fig. C.5-1 showed that two separate plots were obtained. The plot for p_o about 76 cm Hg (76.2 to 77.4 cm Hg) was higher than that when p_o was about 0 cm Hg (0.03 to 3.9 cm Hg) by about 1.4 cm^2/sec (9.3% at $\bar{p}_m$ = 150 cm Hg where K ≃ 15 cm^2/sec). The plots were slightly curved indicating that some turbulent flow was occurring. The equation of the straight line drawn through the K-$\bar{p}_m$ points for $\bar{p}_m$ below 20 cm Hg, calculated graphically, was $K_v = 0.150\ \bar{p}_m + 0.37$. The values of B_o and K_o estimated from the slope and intercept, respectively, were not as accurate as those obtained by the pressure decay method due to the curved plot, but were of the same order of magnitude.

C.5.3 Experimental Accuracy

Manometer pressures were in error by up to 0.06 cm Hg. The error in pressure measurements with the 0 to 100 p.s.i.g. gauge was 5 cm Hg (1% for full scale deflection), while for the 0 to 600 p.s.i.g. gauge, the error was 10 cm Hg (2% at 100 p.s.i.g.). For p_i less than 2 atm, when both p_i and p_o were measured with the manometer, the error in Δp was 0.5% at high Δp but increased to about 2% at low Δp. When p_i was measured with the pressure gauges, the error in p_o (measured by the manometer) was negligible; the error

in Δp therefore ranged from about 5% at low Δp to 0.5% at very high Δp.

Flow-rate measurement generally involved a calibration and reading error of less than 2% if the flow-rate occurred in the middle portion of each flow-meter range. For the wet gas test meter and soap-bubble flow-meters, flow-rate measurement at the highest and lowest flow-rates for each meter was inaccurate because of the errors in measuring the very short times and the small volumes, respectively.

The error in measuring the atmospheric pressure p_a was less than 0.1%. Any variation in p_a between different experiments only introduced a small error (less than 0.5%). Errors in the temperature measurement were negligible. Generally $\mathcal{J}_s/\mathcal{J}_a$ was taken as unity with little error.

With the errors in L and A for rod samples being 0.2% and 1½%, respectively, the maximum overall error in values of K calculated for high pressure flow experiments by means of equation (C.5-2) was estimated to be less than 6% when the error in Δp was less than 2% but up to 9% when Δp was more inaccurate. The relative errors were correspondingly 4% and 7%.

APPENDIX D

CORRELATION OF THE HIGH PRESSURE FLOW RESULTS

D.1 Theory of the Green and Duwez method

The Green and Duwez procedure[125,126,146] (see section 5.1.2.4(c)) was employed to correlate experimental results for gas flow through the reactor graphites when turbulent flow occurred. For this procedure, the Reynolds number and friction factor were defined as

$$N_{Re} = \beta G (b + a/p_m) \qquad \ldots\ldots (5.1.2\text{-}3)$$

and

$$f = \frac{\rho \Delta p}{\beta G^2 L}, \qquad \ldots\ldots (2.1.7\text{-}11a)$$

a slip correction term having been added to the original N_{Re} group of Green and Duwez[126] so that the flow results were correlated more satisfactorily (see section 5.1.2.4(e)). The factors a and b were the constants in the equation for the viscous-slip flow permeability coefficient K_v ($= a + bp_m$). The inertial resistance coefficient β was defined by the equation

$$\frac{p_m \Delta p \rho_o}{L G} = \alpha \mu + \beta G, \qquad \ldots\ldots (2.1.7\text{-}3)$$

where $\alpha = 1/B_o = 1/b$.

When determining α and β from the experimental results, more accurate values were obtained if a plot of $p_m \Delta p \rho_o/LG^2$ against μ/G was prepared (the α-β plot) instead of the Cornell-Katz plot[125] of $p_m \Delta p \rho_o/L G \mu$ against G/μ (see Appendix D.3).

If ρ_o, L, and μ were incorporated in constants together with conversion factors, and measured quantities were employed, equation (2.1.7-3) became

$$\frac{p_m \Delta p}{(Q_a p_a)^2} = Y \frac{\alpha}{Q_a p_a} + \beta Y Z, \qquad \ldots\ldots (D.1\text{-}1)$$

where $Y = L\mu/(A\, g_o\, \rho_{Hg})$, $\ldots\ldots (D.1\text{-}2)$

$Z = \rho_o/(\mu A)$, $\ldots\ldots (D.1\text{-}3)$

g_o = gravitational conversion factor,

ρ_{Hg} = density of mercury at the flow temperature T_s,

and p_m, Δp were expressed in cm Hg; $p_m \Delta p/(Q_a p_a)^2$ plotted against $1/Q_a p_a$ gave the α-β plot.

The dimensionless groups N_{Re} and f, expressed in terms of the nomenclature of equation (D.1-1), were

$$N_{Re} = Z \beta Q_a p_a \left(B_o + \frac{Y A a}{L p_m} \right) \qquad \ldots\ldots (D.1\text{-}4)$$

and

$$f = \frac{1}{YZ\beta} \frac{\Delta p\, p_m}{(Q_a p_a)^2}. \qquad \ldots\ldots (D.1\text{-}5)$$

Values of N_{Re} and f were calculated from the experimental results by means of these equations.

D.2 Type Calculation of the f-N_{Re} plot

The calculation of values of N_{Re} and f for nitrogen flow through Acheson "A" Graphite Rod No. K4 (Detmn.No. H:20) is described in detail as a typical example of the treatment of high pressure flow results. The method of calculating values of the permeability coefficients for this graphite

rod was illustrated in Appendix C.5.2.

The α-β plot (see Fig. D.2-1(b)) was drawn from the experimental results listed in Table D.2-1. The values of the slope and intercept of the straight line through the six points below $1/Q_e p_a = 0.0015$ were 43.7 and 0.0143, respectively. The values of the quantities required to calculate the constants Y and Z for this determination were:

$L/A = 5.215\ cm^{-1}$,

$A = 1.338\ cm^2$,

$T_s = 16.8^\circ C = 290^\circ K$,

$\mu = 1735 \times 10^{-7}$ poise at T_s (Table B.1-1, Appendix B),

$M = 28.02$,

$z = 1.0$,

$\mathcal{R} = 6236$ cm Hg, $cm^3/^\circ K$, g-mol,

$g_o = 980.665\ cm/sec^2$, and

$\rho_{Hg} = 13.554\ g/cm^3$ at T_s.

Then $\rho_o = M/(z\mathcal{R}T_s) = 1.55 \times 10^{-5}\ g/cm^3$, cm Hg,

$Y = L\mu/(A\, g_c \rho_{Hg}) = 6.81 \times 10^{-8}$ sec, and

$Z = \rho_o/(\mu A) = 6.674 \times 10^{-2}\ sec/cm^4$, cm Hg.

The coefficients α and β were calculated from the slope and intercept, respectively, e.g.,

$\alpha = 43.7/Y = 6.41 \times 10^{-8}\ cm^{-2}$,

and $\beta = 0.0143/YZ = 3.15 \times 10^{-6}\ cm^{-1}$.

The equation of the straight portion of the K-p_m plot for p_m less than 20 cm Hg was (Appendix C.5.2)

Table D.2-1

Typical Calculation of Values of N_{Re} and f for Detmn.No. H:20

Expt. No.	p_m cm Hg	Δp cm Hg	$Q_a p_a$	$\frac{p_m \Delta p}{(Q_a p_a)^2}$	B_o + term $\left[1\ Q_a p_a\right]$	Slip term $\left[m\ Q_a p_a / p_m\right]$	= N_{Re}	f
1	93.10	184.2	361	0.132	0.1182	0.0039	0.122	9.20
2	3.98	7.91	1.28	19.9	0.00042	0.00033	0.00075	1390
3	8.86	17.59	5.09	6.02	0.00167	0.00058	0.00225	421
4	18.86	37.41	20.2	1.73	0.00661	0.00109	0.00770	121
5	38.26	75.85	75.5	0.509	0.0248	0.0020	0.0268	35.5
6	178.8	352	1070	0.0552	0.3500	0.0061	0.356	3.86
7	236.4	465	1610	0.0425	0.5270	0.0069	0.534	2.97
8	275.7	397	1600	0.0425	0.5250	0.0059	0.531	2.97
9	209.3	265	937	0.0632	0.3070	0.0046	0.312	4.41
10	128.6	105	286	0.165	0.0937	0.0023	0.0960	11.5
11	58.83	116.5	163	0.259	0.0533	0.0028	0.0561	18.1
12	58.27	115.4	159	0.265	0.0522	0.0028	0.0550	18.5
13	95.67	38.26	86.6	0.491	0.0284	0.0009	0.0293	34.3
14	80.52	8.23	16.4	2.46	0.00537	0.00021	0.00558	172
15	88.43	24.06	51.4	0.805	0.0168	0.0006	0.0174	56.2
16	116.1	79.61	208	0.215	0.0680	0.0018	0.0698	15.0
17	78.34	155.0	268	0.169	0.0876	0.0035	0.0911	11.8
18	181.4	209	685	0.0809	0.2240	0.0038	0.228	5.65
19	137.9	270	688	0.0787	0.226	0.0051	0.230	5.50

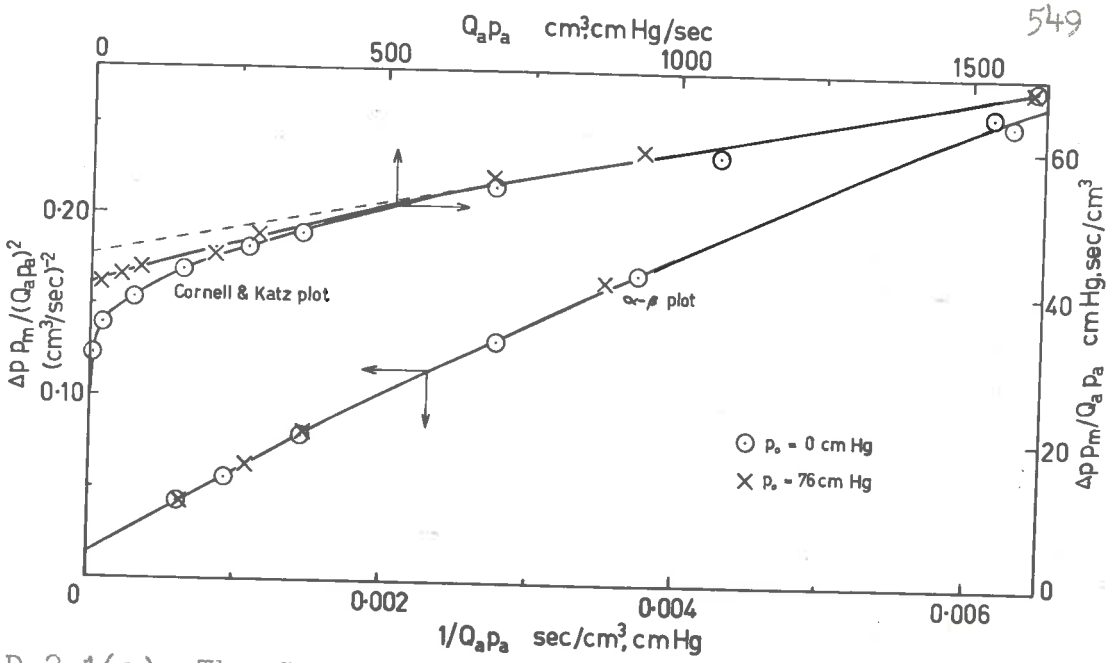

Fig. D.2-1(a) The Cornell-Katz Plot of $p_m \Delta p/Q_a p_a$ against $Q_a p_a$, and

(b) The α-β Plot for $p_m \Delta p/(Q_a p_a)^2$ against $1/Q_a p_a$ for Results of Detmn. No. H:20 (Nitrogen Flow through Acheson "A" Rod No. K4).

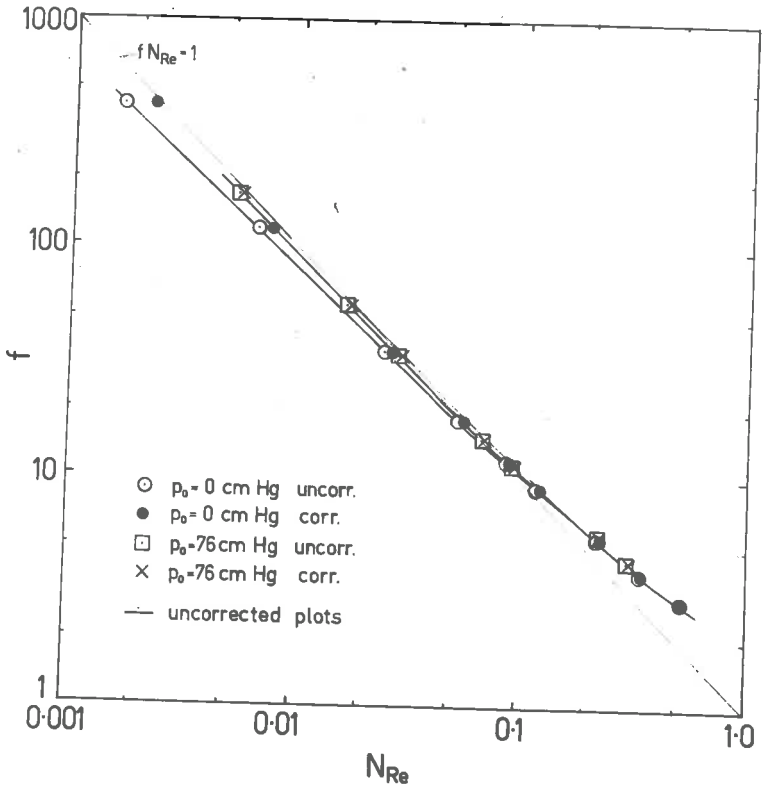

Fig. D.2-2 The Uncorrected and Corrected f-N_{Re} Graphs for Results of Detmn. No. H:20.

$$K_v = 0.130\ p_m + 0.37,$$

i.e., $B_o = 17.0 \times 10^{-10}$ cm^2, and $a = 0.37$ cm^2/sec. However, $B_o = 1/\alpha = 15.6 \times 10^{-10}$ cm^2 as obtained from the $\alpha - \beta$ plot was more accurate than the low pressure value and was therefore employed to calculate N_{Re}.

Values for N_{Re} and f were calculated from the experimental results by means of equations (D.1-4) and (D.1-5), which, on insertion of the values of the constants, reduced to:

$$N_{Re} = 6.67 \times 10^{-2} \times 3.15 \times 10^{-6} \times Q_a p_a \left(15.6 \times 10^{-10} + \frac{6.81 \times 10^{-8} \times 0.37}{5.215 \times p_m} \right)$$

$$= 3.28 \times 10^{-4}\ Q_a p_a + 1.016 \times 10^{-2}\ Q_a p_a / p_m,$$

$$f = \frac{1}{6.81 \times 6.67 \times 3.15 \times 10^{-4}} \frac{\Delta p\ p_m}{(Q_a p_a)^2}$$

$$= 69.9 \frac{\Delta p\ p_m}{(Q_a p_a)^2}.$$

The values of N_{Re} and f are included in Table D.2-1, while the f-N_{Re} graph plotted from these values is shown in Fig. D.2-2. The constants in the expressions for N_{Re} and f for each determinations are given in Table 5.1-3.

D.3 The Deviations Due to Slip Flow

The f-N_{Re} points which were calculated before the slip-correcting term was added to N_{Re} are also shown in Fig. D.2-2. For f = 170 (in the viscous flow region), N_{Re} (uncorrected) was 15% below the corrected value.

The deviation below the theoretical line was greater for the f-N_{Re} values with p_o about 0 cm Hg than those with p_o about 76 cm Hg because of the greater proportion of slip flow; all points lay close to the theoretical line on correction for slip flow.

In Fig. D.2-1(a), the Cornell-Katz plot of $\Delta p\ p_m/Q_a p_a$ against $Q_a p_a$ is presented for comparison with the α-β plot (Fig. D.2-1(b)). In the Cornell-Katz plot, the points for p_o about 76 cm Hg were slightly higher than the p_o about 0 cm Hg points so that it was possible to draw separate curves, especially at low flow-rates where the p_o = 0 cm Hg plot curved sharply downwards. This curvature was due to the occurrence of slip flow (cf. Cornell and Katz,[125] who attributed the low pressure deviation to molecular streaming). Equation (2.1.7-3) only applied when slip flow was negligible, i.e., at high flow-rates. In the Cornell-Katz plot (Fig. D.2-1(a)), slip flow became negligible above $Q_a p_a$ = 700 cm^3, cm Hg/sec; because the points were spread out and scattered, a number of straight lines were possible and considerable variation in the values for the slope (14%) and intercept (7%) resulted.

However, for the α-β plot (Fig. D.2-1(b)), the experimental results were plotted against the reciprocal of the flow-rate so that the values when slip flow was

negligible occurred below $1/Q_a p_a = 0.0015$. Quite accurate values of the slope and intercept were obtained graphically from the straight line plot through these points as less scatter was observed between the $p_o = 0$ cm Hg and $p_o = 76$cm Hg points than for the Cornell-Katz plot. Above $1/Q_a p_a = 0.0015$, the $\alpha - \beta$ plot curved towards the $1/Q_a p_a$-axis.

The above observations concerning the deviations due to slip flow applied to all high pressure flow determinations. For some determinations, a separate $\alpha - \beta$ plot could be drawn for the $p_o = 0$ cm Hg and the $p_o = 76$ cm Hg points; this was particularly observed when the flow-rates were not high enough for slip flow to be negligible. When the variation between the two plots was quite small, the slope and intercept of the mean plot was employed to calculate α and β ; when the variation was larger, the slope and intercept of the $p_o = 76$ cm Hg plot gave better values of α and β since the error due to slip flow was smaller.

APPENDIX E

THE DISTRIBUTION OF PRESSURE FOR GAS FLOW IN POROUS MEDIA

E.1 Derivation of the Equations for the Pressure Distribution

In section 2.1.1.3, it was shown that the general equation for steady state gas flow through a porous medium in the x-direction under isothermal conditions was

$$\frac{\partial}{\partial x}\left(K \frac{\partial p}{\partial x}\right) = 0, \qquad \ldots\ldots (2.1.1\text{-}6)$$

where K = permeability coefficient. The derivation of particular solutions of this equation for various conditions will now be considered.

Condition 1: Knudsen flow region; K constant.

In the Knudsen flow region, which occurs at very low mean pressures, K is presumed to be independent of pressure (section 2.1.5.1). Then equation (2.1.1-6) becomes

$$\partial^2 p/\partial x^2 = 0. \qquad \ldots\ldots (E.1\text{-}1)$$

For the boundary conditions

$$\begin{cases} p = p_i \text{ (inlet pressure) at } x = L, \\ p = p_o \text{ (outlet pressure) at } x = 0, \\ p = \Phi(x) \quad 0 < x < L \text{ for all time,} \end{cases} \qquad \ldots\ldots (2.1.1\text{-}7)$$

the solution of equation (E.1-1) is

$$p = p_o + \Delta p\, x/L, \qquad \ldots\ldots (2.1.1\text{-}8)$$

where $\Delta p = p_i - p_o$ = pressure difference across the sample. Thus, when K is independent of pressure, the variation of

pressure with x/L for gas flow in a porous medium is always linear.

Condition 2: Viscous flow region; $K = B_o \; p/\mu$.

In the viscous flow region only, K can be replaced by $B_o \; p/\mu$ (equation 2.1.1-23). As the viscous flow permeability coefficient B_o is a constant, and μ is assumed independent of pressure,[16] equation (2.1.1-6) becomes

$$\frac{\partial}{\partial x}\left(p \frac{\partial p}{\partial x}\right) = 0,$$

i.e., $$\frac{1}{2} \frac{\partial^2(p^2)}{\partial x^2} = 0. \qquad \ldots . (2.1.1\text{-}10$$

The solution of the differential equation (2.1.1-10) is

$$p^2 = c_1 x + c_2. \qquad \ldots . (E.1\text{-}2)$$

For the boundary conditions (2.1.1-7), the constants c_1 and c_2 in equation (E.1-2) are evaluated and the solution becomes (ref.15,p.680)

$$p^2 - 2 \; p_m \Delta p \; x/L - p_o^{\,2} = 0, \qquad \ldots (2.1.1\text{-}11)$$

where $p_m = (p_i + p_o)/2$ = mean pressure in the sample. Equation (2.1.1-11) is the expression for the variation of pressure in a porous medium for gas flow in the viscous region.

Condition 3: Viscous and slip flow, $K = K_v = a + bp$.

When slip as well as viscous flow occurs, K is a linear function of pressure $K_v = a + bp$, $\ldots (2.1.4\text{-}1)$

where a and b are constants. Then equation (2.1.1-6)

becomes

$$\frac{\partial}{\partial x}\left((a + bp)\ \frac{\partial p}{\partial x}\right) = 0, \qquad \ldots \text{(E.1-3)}$$

i.e., $$a\,\frac{\partial^2 p}{\partial x^2} + \frac{b}{2}\,\frac{\partial^2 (p^2)}{\partial x^2} = 0. \qquad \ldots \text{(E.1-4)}$$

Integration of equation (E.1-4) gives

$$a\,p + b\,p^2/2 = e_3 x + e_4\ , \qquad \ldots \text{(E.1-5)}$$

which, for boundary conditions (2.1.1-7), leads to the solution

$$p^2 + \frac{2a}{b}\,p - \left(\frac{a}{b} + p_m\right) 2\,\Delta p\,\frac{x}{L} - p_o^{\,2} - \frac{2a}{b}\,p_o = 0. \qquad \ldots \text{(2.1.1-13)}$$

Equation (2.1.1-13) expresses the distribution of pressure in a porous medium for gas flow in the viscous and slip flow regions where K is a linear function of p_m. As a direct consequence of this equation, the integration of the various forms of Darcy's law is valid for large Δp (see section 2.1.1.6). The differentiation of the equation for the distribution curve gives

$$2\,\frac{\partial p}{\partial x}\left(p + \frac{a}{b}\right) = 2\left(p_m + \frac{a}{b}\right)\ \frac{\Delta p}{L}\ , \qquad \ldots \text{(E.1-6)}$$

i.e., at $p = p_m$, $\partial p/\partial x = \Delta p/L$, or the slope of the tangent to the distribution curve at $p = p_m$ equals the mean pressure gradient across the medium.

Condition 4: Turbulent and viscous flow.

The solutions of the general flow equation presented above are for specific conditions, and are thus specialize-

tions of a more general solution which covers all flow regions. For gas flow through reactor graphites, the experimental results for simultaneous slip, viscous, and turbulent flow fit the equation (see section 5.1.2.4(g))

$$K = \frac{K_v}{1 + \beta G K_v / p}, \qquad \ldots (5.1.2\text{-}7)$$

where G = mass flow-rate,

β = inertial resistance coefficient, and

$K_v = a + bp.$ $\ldots (2.1.4\text{-}1)$

Insertion of equation (5.1.2-7) into equation (2.1.1-6) results in

$$\frac{\partial}{\partial x}\left\{\left(\frac{a + bp}{1 + b\beta G + a\beta G/p}\right)\frac{\partial p}{\partial x}\right\} = 0. \qquad \ldots (E.1\text{-}7)$$

If $\left.\begin{aligned} e &= 1 + b\beta G \\ d &= a\beta G, \end{aligned}\right\}$ then $\qquad \ldots (E.1\text{-}8)$

$$\left\{p + \frac{a}{be} - \frac{ad}{be(ep + d)}\right\}\frac{\partial^2 p}{\partial x^2} + \left\{1 + \frac{ad}{b(ep + d)^2}\right\}\left(\frac{\partial p}{\partial x}\right)^2 = 0$$

$$\text{or} \quad \frac{\partial^2 (p^2)}{\partial x^2} + \frac{2a}{be}\frac{\partial^2 p}{\partial x^2} - \frac{2ad}{be^2}\frac{\partial^2 \ln(ep + d)}{\partial x^2} = 0 \ldots (E.1\text{-}9)$$

$$\left[\frac{\partial^2 \ln(ep + d)}{\partial x^2} = \frac{e}{(ep + d)}\frac{\partial^2 p}{\partial x^2} - \frac{e^2}{(ep + d)^2}\left(\frac{\partial p}{\partial x}\right)^2\right].$$

Equation (E.1-9) can be solved to give

$$p^2 + \frac{2a}{be}p - \frac{2ad}{be^2}\ln(ep + d) = e_5 x + e_6 \ldots (E.1\text{-}10)$$

which, with the boundary conditions (2.1.1-7), results in

the general solution

$$(p^2 - p_o^2 - 2p_m \Delta p \frac{x}{L}) + \frac{2a}{bc}(p - p_o - \Delta p \frac{x}{L})$$

$$- \frac{2ad}{bc^2} \ln \left(\frac{cp + d}{cp_o + d}\right)\left(\frac{cp_i + d}{cp_o + d}\right)^{x/L} = 0. \qquad \ldots \text{(E.1-11)}$$

Equation (E.1-11) gives the variation of pressure in a porous medium when slip, viscous, and turbulent flow occur simultaneously. Because of the logarithmic term in the equation, the evaluation of p at any x/L is quite complex and involves a trial and error solution. However, the equation can be simplified for the two special conditions of viscous-slip flow (N_{Re} less than 0.01), and complete turbulent flow (N_{Re} greater than 100).

Condition 4a: N_{Re} less than 0.01.

For viscous and slip flow, N_{Re} is less than 0.01, i.e., $N_{Re} = \beta G(b + a/p) < 0.01$. Below $N_{Re} = 0.01$, where G is comparatively small, $b\beta G$ is certainly less than N_{Re} (< 0.01) so that c = 1 to less than 1%. The values of d and the logarithm are generally small (see Appendix E.2) so that the logarithmic term is negligible below $N_{Re} = 0.01$. Then equation (E.1-11) simplifies to equation (2.1.1-13), the equation obtained for viscous-slip flow (Condition 3).

Condition 4b: N_{Re} greater than 100.

When turbulent flow is fully developed (N_{Re} greater than 100), slip flow is negligible, i.e., a/bp_m approximates 0, and $N_{Re} = b\beta G = c > 100$. Then the coefficients of the second and third terms in equation (E.1-11) are less than $0.02a/b$ and $0.02a^2/b^2$, respectively, and tend to zero. Equation (E.1-11) therefore reduces to equation (2.1.1-11), the solution obtained for Condition 2 (viscous flow).

Equations (E.1-11) and (2.1.1-11) show that at $p = p_m$, $\partial p/\partial x = \Delta p/L$. Thus the integrated forms of the equation $G = K \rho_o \partial p/\partial x$ apply when Δp is large for transition and turbulent as well as for viscous and slip flow.

Condition 4c: Slip flow negligible.

The identical solutions of the general flow equation (2.1.1-6) for Conditions 2 and 4b, where slip flow was negligible on both occasions, indicate that equation (2.1.1-11) expresses the distribution of pressure in a porous medium for gas flow whenever slip flow does not occur.

Equation (2.1.1-11) does not apply for liquid flow since the constant m in the equation of state (equation 2.1.1-4, section 2.1.1.2) then equals zero. The general flow equation for incompressible, steady state

liquid flow, for the boundary conditions (2.1.1-7), reduces to $p = p_o + \Delta p\, x/L$, . . . (2.1.1-8) i.e., the distribution of pressure is always linear (cf. Condition 1).

Condition 4d: Transition flow.

When slip flow is significant, i.e., a/bp_m does not equal zero, but the inertial resistance is negligible (N_{Re} less than 0.01), equation (2.1.1-13) is the solution to the general flow equation. When both slip and inertial resistances contribute to the total flow resistance, equation (E.1-11) must be solved to give the pressure at any point in the medium. However, slip flow is often insignificant in the transition and turbulent flow regions (N_{Re} above 0.01); then equation (2.1.1-11) gives the variation of p within the sample. The use of the three equations is examined in the next section (Appendix E.2).

E.2 Comparison of the Pressure Distributions

Examination of equations (2.1.1-11), (2.1.1-13), and (E.1-11) showed that the pressure distributions for non-slip and slip flow conditions became identical when $a/b = 0$. As the a/b ratio was increased, the curvature of the distributions decreased when the flow was in the viscous region (see Fig. E.2-1). This was demonstrated by calculating the theoretical pressures in a specimen from equation (2.1.1-13), e.g.,

$$p = -a/b \pm \sqrt{\{(p_o + a/b)^2 + 2(p_m + a/b)\,\Delta p\, x/L\}} \quad . \quad (E.2\text{-}1)$$

for a/b = 1.2, 5, and 80, and by means of equation (2.1.1-11) when a/b was zero for various inlet and outlet pressure conditions. The pressure values are reported in Table E.2-1 for x/L = 1, 3/4, 1/2, 1/4, 1/8, and 0 and plotted in Fig. E.2-1. The values of a/b approximately equalled the values for the P.G. 60, Acheson "A", and Morgan "EY9" distribution specimens, respectively.

Table E.2-1
Theoretical Pressure Distributions
(in cm Hg)

x/L =	1	3/4	1/2	1/4	1/8	0
(a) p_i = 100, p_o = 10 cm Hg						
a/b = 0	100	86.8	71.1	50.8	36.6	10
a/b = 1.2	100	86.6	70.8	50.3	36.1	10
a/b = 5	100	86.2	70.0	49.1	34.7	10
a/b = 80	100	82.3	62.3	39.0	25.6	10
(b) p_i = 100, p_o = 50 cm Hg						
a/b = 0	100	90.1	79.1	66.2	58.6	50
a/b = 5	100	90.0	78.8	65.9	58.4	50
a/b = 80	100	88.9	77.0	64.2	57.2	50
(c) p_i = 400, p_o = 10 cm Hg						
a/b = 0	400	346.5	283.0	202.2	141.8	10
a/b = 80	400	338.1	265.3	172.4	109.4	10

The distribution curves of these pressure values (Fig. E.2-1) showed that when a/b was small (P.G. 60 and Acheson "A" graphites), the distributions for viscous and

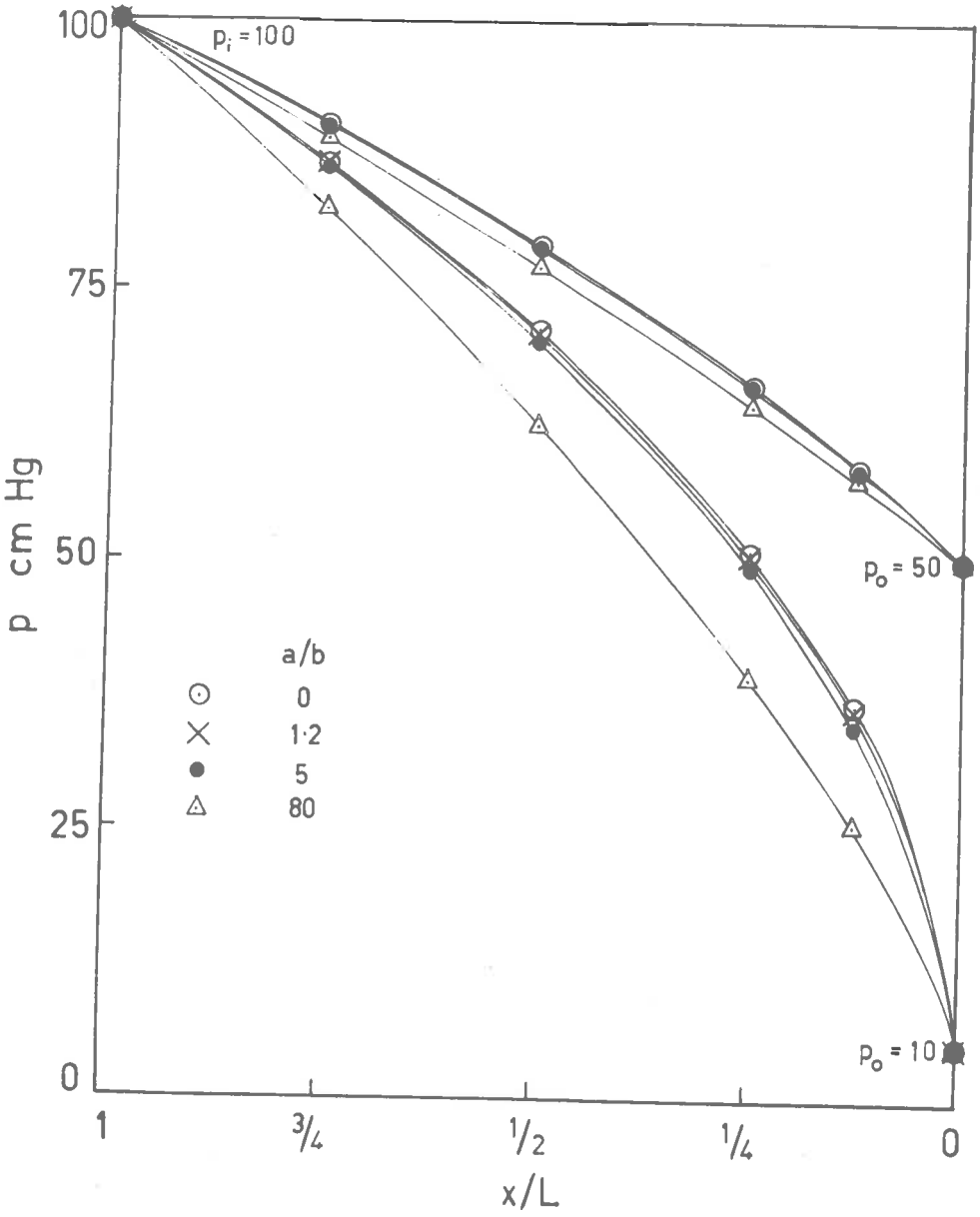

Fig. E.2-1 Theoretical Pressure Distribution Curves showing Variation of Curvature with a/b.

slip flow were less than 5% lower than those calculated from equation (2.1.1-11) for non-slip flow.
However, for Morgan "EY9" graphite, the theoretical pressure distributions for viscous and slip flow were much lower than those for non-slip flow because of the high value for a/b. The percentage difference between the slip and the non-slip distribution curves decreased as p_o increased for constant p_i, and as p_i increased when p_o was constant. A comparison of the theoretical examples with the high pressure flow results showed that the flow in the Morgan "EY9" graphite was in the viscous and slip flow region for all pressure conditions, while the flow in the P.G. 60 and Acheson "A" graphites for conditions (a) and (b) was in the transition region (N_{Re} greater than 0.01). Thus equation (2.1.1-11) gave quite erroneous pressure distributions when the flow was viscous (a/b = 80).

To examine the differences between the pressure distributions further, the pressure $p_{1/2}$ at x/L = 1/2 was calculated by means of the pressure distribution expressions for the results of the high pressure nitrogen flow experiments (section 4.1) when N_{Re} was about 0.01 (see Table E.2-2). When no results were available near this N_{Re}, values of p_m, Δp, and $Q_a p_a$ were obtained by interpolation. Values of $p_{1/2}$ were also calculated for nitrogen flow in P.G. 60 Rod No. K31 at N_{Re} = 0.114 and Morgan "EY9" Rod No. K23 at N_{Re} = 0.222 and

N_{Re} = 1.55, the results for the Morgan "EY9" sample being estimated by means of equation (5.1.2-5).

For N_{Re} = 0.01, the value of $b\beta G$ was from 80 to 97% of N_{Re} with the lowest percentages occurring at low p_m when slip flow was greater than at higher p_m. At higher N_{Re} in the transition region, $b\beta G$ was over 98% of N_{Re} showing that slip flow was then almost negligible. The values of $p_{½}$ calculated from equation (2.1.1-11) at N_{Re} = 0.01 were less than 4% greater than those calculated from the viscous and slip flow expression, equation (2.1.1-13); when the percentage of slip flow was less than 10%, the differences between the two values of $p_{½}$ was negligible (e.g., for Acheson "A" Rods K2A and K4 at p_m = 136 and 83.5 cm Hg, respectively). Because slip flow was negligible at higher N_{Re}, the differences between the values of $p_{½}$ calculated from the two equations were less than 0.5%.

The values of $p_{½}$ calculated from the general equation (E.1-11) neglecting the logarithmic term generally agreed very closely (less than 0.1% difference) with those calculated from equation (2.1.1-13). When the logarithmic term was included in equation (E.1-11), the value of $p_{½}$ changed by less than 0.2% due to the very small values of $2\,ad/bc^2$ and the logarithm; the change was greatest when p_o was very small compared with p_i. Greater differences between the distributions would be observed at lower x/L as

Table E.2-2

Examination of the Pressure Distribution Equations by means of Experimental Results

Graphite Grade	P.G. 60	Acheson "A"	Acheson "A"	Acheson "A"	Morgan "EY9"	P.G. 60	Morgan "EY9"	Morgan "EY9"
Sample No.	K31	K2A	K2A	K4	K23	K31	K23	K23
Detmn.No.	H:15	H:3	H:3	H:20	H:4	H:15	H:4	H:4
a/b cm Hg	1.27	6.20	6.20	2.84	50.4	1.27	50.4	50.4
β cm^{-1}	5.7×10^{3}	6.76×10^{6}	6.76×10^{6}	3.15×10^{6}	1.35×10^{10}	5.7×10^{3}	1.35×10^{10}	1.35×10^{10}
N_{Re}	0.00970	0.0103	0.0115	0.0100	0.0105	0.114	0.222	1.55
p_m cm Hg	10.3*	30.7	136	83.5*	342	44.7	2000+	8000+
Δp cm Hg	19.2*	61.0	22.1	14.1*	684	72.0	3850+	14000+
$Q_a p_a$ cm^3, cm Hg/sec	266*	23.4	31.3	29.5*	6.41	3400	152+	1070+
$b\beta G$	0.00866	0.00820	0.0109	0.00968	0.00915	0.111	0.217	1.54
$a\beta G/p_m$	0.00104	0.00209	0.00063	0.00036	0.00135	0.00315	0.00545	0.0095
$2ad/be^2$ $(cm\ Hg)^2$	0.0276	0.784	1.047	0.0840	45.5	0.290	740	1190
log term	4.64	9.00	0.17	0.17	12.8	2.98	5.42	3.68
$p_{1/2}$ eqn.(2.1.1-11) cm Hg	14.08	43.24	136.5	83.83	483.7	57.41	2776	10630
$p_{1/2}$ eqn.(2.1.1-13) cm Hg	13.76	41.66	136.5	83.81	470.1	57.13	2763	10620
$p_{1/2}$ eqn.(E.1-11) (no log term)	13.77	41.65	136.4	83.83	470.3	57.17	2765	10620
$p_{1/2}$ eqn.(E.1-11) cm Hg	13.78	41.73	136.4	83.83	470.9	57.18	2765	10620

* Obtained by interpolation of experimental results.

\+ Estimated by means of equation (5.1.2-5).

demonstrated by the examples in Table E.2-1, but the conclusions resulting from the above observations would still hold.

Thus the analysis of certain high pressure results presented in Table E.2-2 showed that for the graphites P.G. 60, Acheson "A", and Morgan "EY9", the pressure distributions calculated from the three distribution equations for any experiment when N_{Re} = 0.01 or higher all agreed to less than 5% and could be assumed the same for most practical purposes. Equation (2.1.1-13) gave accurate pressure distributions at all N_{Re} so that it was unnecessary to solve the complex equation (E.1-11) for flow in the transition region. Provided the percentage of slip to viscous flow was less than about 20%, the pressure values obtained by means of equation (2.1.1-11) were quite satisfactory down to N_{Re} = 0.01 since they agreed with values obtained from equation (2.1.1-13). The only occasion when it would be necessary to obtain values of p by solving equation (E.1-11) would be when a large proportion of slip flow occurred in the transition region for any porous medium because of its wide pore size distribution; such an occasion is probably quite rare as slip flow is often quite insignificant in the transition region.

E.3 Reprint of a Published Paper

A reprint of a published paper is included below.

This paper is: "Distribution of Pressure for Flow of Gas through Porous Media",

G.J.Field and H.Watts,

Nature, 192, 1277 (1961).

Field, G. J. & Watts, H. (1961). Distribution of pressure for flow of gas through porous media. *Nature, 192*(4809), 1277-1278.

NOTE:
This publication is included in the print copy
of the thesis held in the University of Adelaide Library.

It is also available online to authorised users at:
http://dx.doi.org/10.1038/1921277b0

APPENDIX F

THE POROSITY DETERMINATIONS

F.1 The Theory of the Porosity Determinations

When the dead space volume V_D in the sample bulb was determined by the helium displacement method (see section 3.2.3.2), the pressure p in the apparatus was measured after each successive expansion. As the total amount of gas in the apparatus remained constant,

$$\frac{p\,V_S}{\mathcal{T}_S} + \frac{p\,V_F}{\mathcal{T}_a} + \frac{p\,V_D}{\mathcal{T}_b} = \text{constant}, \quad \ldots \quad (F.1\text{-}1)$$

where V_S and V_F were the calibrated volumes of the gas burette and free space, respectively, and $\mathcal{T}_S$, $\mathcal{T}_b$, and $\mathcal{T}_a$ were the burette jacket, sample bulb jacket, and ambient temperatures, respectively. Then a plot of $y = (p\,V_S/\mathcal{T}_S) + (p\,V_F/\mathcal{T}_a)$ against $x = p/\mathcal{T}_b$ yielded $(-V_D)$ as the slope. The volume V_D was the volume of the bulb V_b less the volume of solid material V_s of the graphite sample, i.e., $V_D = V_b - V_s$.

The bulb volume V_b was obtained generally from the weight of mercury required to fill the bulb. From the dimensions of the graphite sample, the bulk graphite volume V_t was calculated. Then the pore volume

$$V_p = V_t - V_s$$
$$= V_t - (V_b - V_D). \quad \ldots \quad (F.1\text{-}2)$$

For the fine-pored graphite, where the bulb, still containing the sample, was filled with volume of mercury V_{Hg},

$$V_p = V_D - V_{Hg} . \qquad \ldots (F.1\text{-}3)$$

From the weight w of the graphite sample, and the volumes V_t, V_p, and V_s, the porosity ε, the density of the solid graphite (helium density) ρ_s, the bulk density ρ_b, and the percentage of unopen pores were calculated by means of the equations

$$\varepsilon = V_p / V_t, \qquad \ldots (2.2.1\text{-}1)$$

$$\rho_s = w / V_s, \qquad \ldots (F.1\text{-}4)$$

$$\rho_b = w / V_t, \qquad \ldots (F.1\text{-}5)$$

and the percentage of unopen pores

$$= \left(\frac{1}{\rho_s} - \frac{1}{\rho_c} \right) w \times 100. \qquad \ldots (F.1\text{-}6)$$

For this last relation, it was assumed that the density of the solid graphite ρ_c was equal to the theoretical density[168] of graphite crystallites = 2.265 g/cm^3.

F.2 Type Calculation of the Porosity

For a typical example of the calculation of the porosity, the experimental results obtained for Acheson "A" Sample No. S2 (Detmn. No. D:1) are examined. For the helium displacement measurements, this sample was outgassed at about 310°C for 15 hr. The results of these measurements are presented in Table F.2-1.

From a plot of $(p V_S/\mathcal{T}_S) + (p V_F/\mathcal{T}_a)$ against $p/\mathcal{T}_b$ (see Fig. F.2-1), the slope $= -V_D = -4.076$ cm^3. The bulb volume V_b, measured by filling the empty bulb with mercury, was 6.745 cm^3, i.e., $V_s = V_b - V_D = 2.669$ cm^3. Since $V_t = 3.701$ cm^3 and $w = 5.588$ g, application of the above equations (Appendix F.1) gave $V_p = 1.032$ cm^3, $\varepsilon = 0.279$, $\rho_s = 1.510$ g/cm^3, $\rho_b = 2.093$ g/cm^3, and the percentage of unopen pores = 16.1%.

Table F.2-1
Typical Results of Helium Displacement Measurements
(Detmn. No. D:1)

p	V_S	$\mathcal{T}_S$	$\mathcal{T}_a$	$\mathcal{T}_b$	$\frac{pV_S}{\mathcal{T}_S}=(1)$	$\frac{pV_F}{\mathcal{T}_a}=(2)$	(1)+(2)	$\frac{p}{\mathcal{T}_b}$
cm Hg	cm^3	°K	°K	°K				
39.290	13.003	298.37	290.10	299.15	1.712	1.124	2.836	0.1313
31.243	19.590	298.32	290.12	299.10	2.052	0.894	2.946	0.1045
22.456	32.183	298.28	290.15	299.10	2.423	0.642	3.065	0.0751
17.606	44.521	298.32	290.23	299.10	2.628	0.503	3.131	0.0589
11.626	73.856	298.33	290.22	299.02	2.878	0.333	3.211	0.0389
8.559	104.883	298.36	289.90	299.02	3.009	0.245	3.254	0.0286

$V_F = 8.29$ cm^3, $w = 5.588$g, $V_t = 3.701$ cm^3,

$V_b = 6.745$ cm^3 (sample removed)

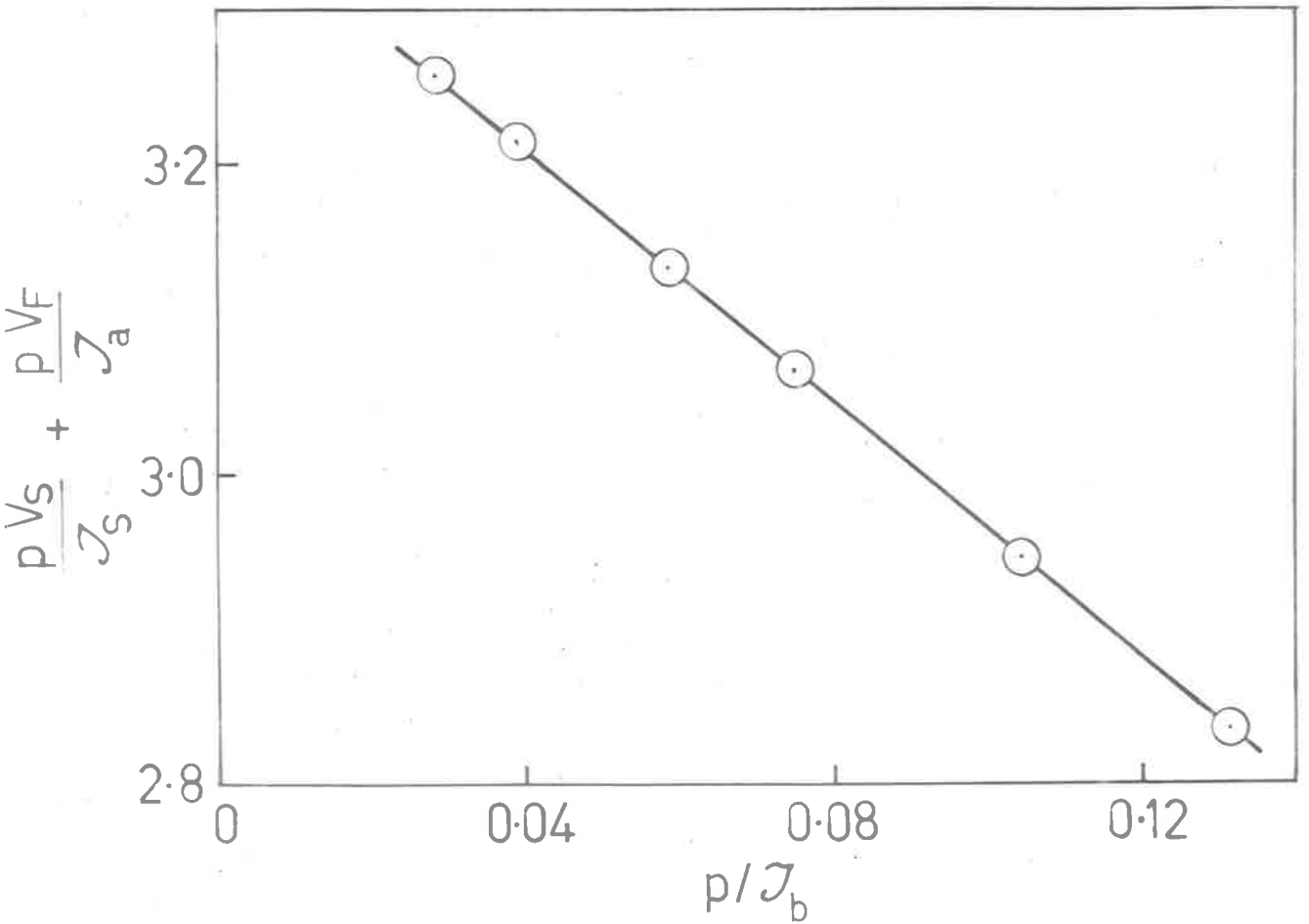

Fig. F.2-1 Plot of $(pV_S/\mathcal{J}_S) = (pV_F/\mathcal{J}_a)$ against $(p/\mathcal{J}_b)$ for calculating the Porosity of Acheson "A" Sample No. S2 (Detmn. No. D:1) from Helium Displacement Measurements.

APPENDIX G

THE SURFACE AREA DETERMINATIONS

G.1 The Theory of the Krypton Surface Area Determinations

In the determination of a Krypton isotherm (see section 3.3.3.3), the initial quantity of gas ($p_1V_G/\mathcal{T}_a$) was expanded from the McLeod gauge (volume V_G) into the apparatus. When the krypton reached equilibrium with the graphite sample and the pressure p_2 was measured, the quantity of gas adsorbed equalled the difference between the total quantity of gas and that contained in the free space volume V_a and the dead space volume in the bulb V_D, i.e.,

$$\left(\frac{pV}{\mathcal{T}}\right)_{ads.} = \left(\frac{pV}{\mathcal{T}}\right)_{total} - \left(\frac{p_2V_a}{\mathcal{T}_a}\right)_{\substack{free\\space}} - \left(\frac{p_2V_D}{\mathcal{T}_b}\right)_{\substack{dead\\space}} \quad \ldots \text{(G.1-1)}$$

where $\mathcal{T}_a$ = ambient temperature, and

$\mathcal{T}_b$ = temperature of the liquid nitrogen bath.

On the addition of more krypton (volume V_G at pressure p_3) to the apparatus, the total amount of gas was:

$$\left(\frac{pV}{\mathcal{T}}\right)_{total} = \left(\frac{pV}{\mathcal{T}}\right)_{ads.} + \left(\frac{p_2V_D}{\mathcal{T}_b}\right)_{\substack{dead\\space}} + \left(\frac{p_3V_G}{\mathcal{T}_a}\right)_{new} \quad \ldots \text{(G.1-2)}$$

On the removal of volume V_a of krypton from the free space

$$\left(\frac{pV}{\mathcal{T}}\right)_{total} = \left(\frac{pV}{\mathcal{T}}\right)_{ads.} + \left(\frac{p_2V_D}{\mathcal{T}_b}\right)_{\substack{dead\\space}} - \left(\frac{p_2V_a}{\mathcal{T}_a}\right)_{\substack{free\\space}} \quad \ldots \text{(G.1-3)}$$

The volume V adsorbed at S.T.P. for each relative pressure p/P_o was computed from $(pV/\mathcal{N})_{ads}$. Then the isotherm of V against p/P_o and the B.E.T. plot of $p/V\,(P_o-p)$ against p/P_o were plotted. The monolayer capacity V_m and the constant C were obtained from the slope and intercept of the B.E.T. plot, e.g.,

$$V_m = (\text{slope} + \text{intercept})^{-1}$$

$$C = (V_m \times \text{intercept})^{-1}$$

The surface area S_g (cm^2/g) was calculated from the equation

$$S_g = \frac{V_m N_L \sigma}{\mathcal{N} w} , \qquad \ldots (2.3.2\text{-}2)$$

where N_L = Avogadro's number,

σ = cross-sectional area of the adsorbate molecule

= 19.5×10^{-16} cm^2/mol for krypton,

$\mathcal{N}$ = molar volume of the gaseous adsorbate, and

w = weight of the sample.

G.2 Type Calculation of the Surface Area

The calculation of the surface area from the krypton adsorption measurements on Morgan "EY9" Sample No. S21 (Detmn. No. S:5) is taken as a type example. The sample was outgassed at about 300°C for 20 hr. The experimental adsorption results for this determination are presented in Table G.2-1.

Calibration of the dead space in the bulb with helium before commencing the adsorption gave $V_D = 5.42$ cm^3. The

pressure p in the apparatus was calculated from the cathetometer readings of the levels in the McLeod gauge by means of equation (3.3.2-1). The temperature of the liquid nitrogen bath $\mathcal{T}_b$ and the vapour pressure p_o of krypton at $\mathcal{T}_b$ were obtained from the respective vapour pressure-temperature tables.[239,186] In the calculation of $(pV/\mathcal{T})_{ads.}$ (see Appendix G.1 and Table G.2-1), V_G = 28.88 cm^3 and V_a = 114.79 cm^3. Correction of the adsorption results for thermal transpiration (section 2.3.2.1(b)) was not necessary as the error involved in $(pV/\mathcal{T})_{ads.}$ was negligible above p/P_o = 0.01 (see Table G.2-1).

From the adsorption results, the krypton isotherm of V against p/P_o (Fig. G.2-1), and the B.E.T. plot of $p/V(P_o-p)$ against p/P_o (Fig. G.2-2) were plotted. Because the slope of the B.E.T. plot was 1.77, and the intercept was -0.01,

$$V_m = 1/(1.77 - 0.01)$$
$$= 0.568 \text{ cm}^3.$$

The weight of the sample w was 5.464 g. Then, with

σ = 19.5 x 10^{-16} cm^2/mol,

N_L = 6.023 x 10^{23} mol/g-mol, and

$\mathcal{N}$ = 22.4 x 10^3 cm^3/g-mol,

the surface area S_g was calculated:

$$S_g = \frac{0.568 \times 6.023 \times 10^{23} \times 19.5 \times 10^{-16}}{22.4 \times 10^3 \times 5.464}$$
$$= \underline{0.545} \text{ m}^2/\text{g}.$$

Table G.2-1

Typical Results of a Krypton Surface Area Determination (Detmn. No. S:5)

Time	Comments	p mm Hg	$\mathcal{T}_a$ °K	$\mathcal{T}_b$ °K	$\frac{pV_a}{\mathcal{T}_a}$	$\frac{pV}{\mathcal{T}_{total}}$	$\frac{pV_D}{\mathcal{T}_b}$ dead space	$\frac{pV}{\mathcal{T}}$ ads.	V cm^3 at S.T.P.	$\frac{p}{P_o}$	$\frac{p}{V(P_o-p)}$
0	Kr added	3.002	289.63		1.1898	1.1898					
1h45m	At equilm.	0.0102 (0.0064)*	290.51	80.52	0.0040 (0.0025)		0.0007 (0.0004)	1.1851 (1.1868)	0.4257 (0.4264)	0.0021 (0.0013)	0.0049 (0.0031)
1h55m	Kr added	3.809	290.56		1.5048	2.6906					
3h10m	At equilm.	1.332	290.58	80.56	0.5263		0.0896	2.0747	0.7453	0.2696	0.4953
	Remove 27.37cm^3	1.332	290.58		0.1255	2.5651					
4h15m	At equilm.	1.111	290.78	80.66	0.4387		0.0747	2.0517	0.7370	0.2206	0.3839
	Remove 114.79cm^3	1.111	290.78		0.4387	2.1264					
5h	At equilm.	0.470	291.34	80.68	0.1853		0.0316	1.9095	0.6859	0.0929	0.1492
	Remove 27.37cm^3	0.470	291.34		0.0442	2.0826					
6h5m	At equilm.	0.398	290.98	80.81	0.1571		0.0267	1.8988	0.6821	0.0767	0.1218
	Remove 114.79cm^3	0.398	290.98		0.1571	1.9255					
6h50m	At equilm.	0.219	290.99	80.83	0.0865		0.0147	1.8243	0.6553	0.0420	0.0670

* Corrected for thermal transpiration[178] - $p_{actual}/p_{measured} \simeq 0.63$; percentage errors were a 0.16% error in V, 58% error in $p/V(P_o-p)$, and < 0.2% error in further calculations.

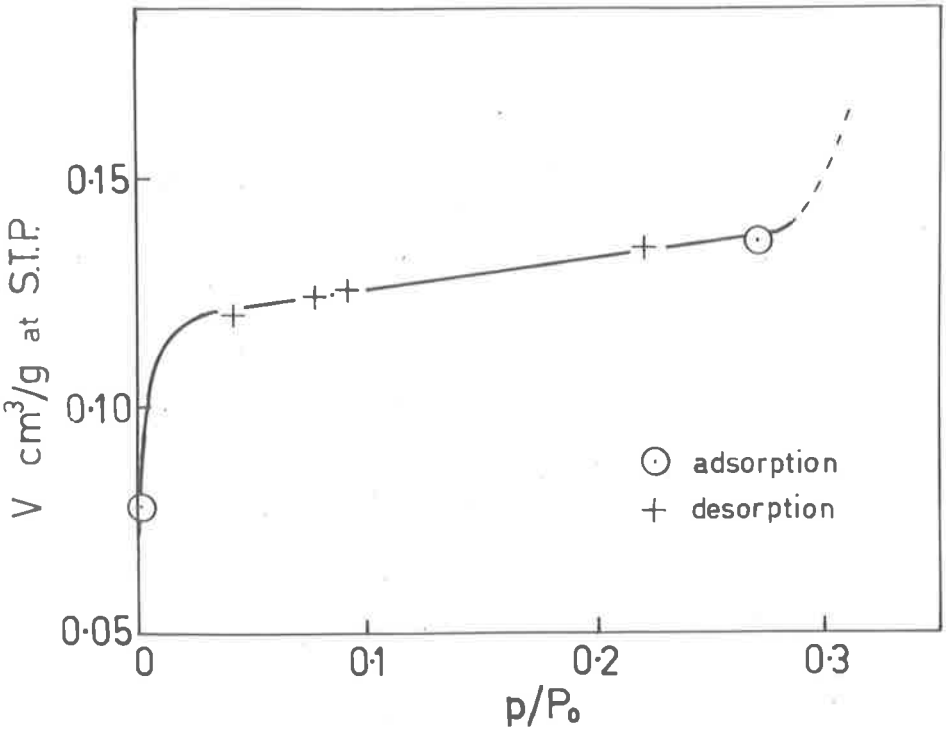

Fig. G.2-1 Krypton Isotherm of V against p/P_o for Morgan "EY9" Sample No. S21 (Detmn. No. S:5).

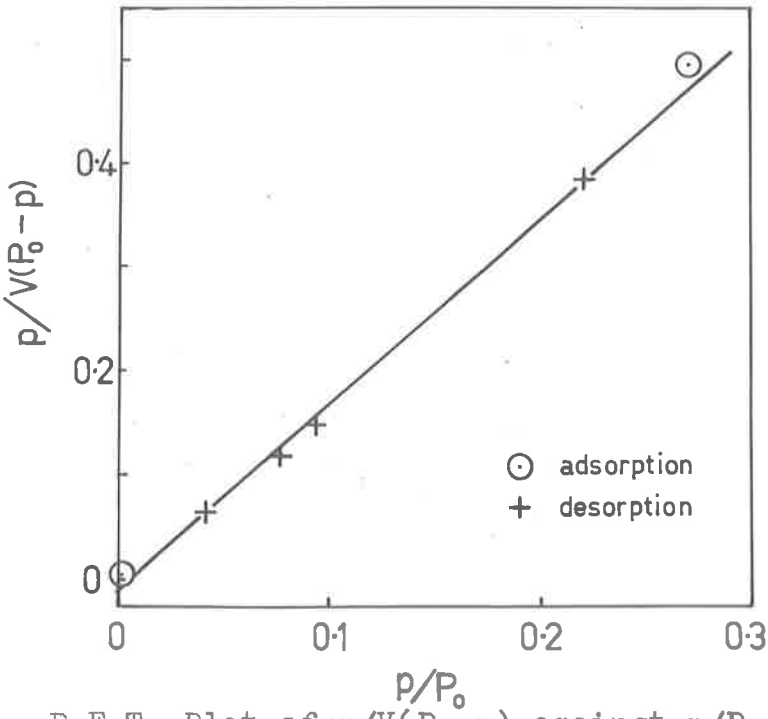

Fig. G.2-2 B.E.T. Plot of $p/V(P_o-p)$ against p/P_o for Determining the Krypton Surface Area of Morgan "EY9" Sample No. S21 (Detmn. No. S:5).

APPENDIX H

THE PORE SIZE DISTRIBUTION MEASUREMENTS

H.1 Theory

In the mercury penetration measurements, the volume of mercury injected into the pores of the graphite was measured as the pressure p_c was increased progressively. The results were plotted as the pressurizing curve of the cumulative volume V(r) against p_c.

The radius r_i of the pore entrances penetrated at any pressure p_{ci} was determined from the equation

$$p_{ci}\, r_i = 2\gamma \cos\theta, \qquad \ldots\ldots (2.4.4\text{-}1)$$

where θ = contact angle between graphite and mercury (140°), and

γ = surface tension of mercury (480 dyn/cm - section 2.4.4.1(a)).

If p_{ci} and r_i were expressed in p.s.i.a. and Å, respectively, then

$$r_i = 1.0667 \times 10^6 / p_{ci}. \qquad \ldots\ldots (H.1\text{-}1)$$

By graphical differentiation of the pressurizing curve at any p_{ci}, the slope $(dV(r)/dp_c)_i$ was obtained. Then the pore entrance size distribution function $D(r_i)$ was calculated from the equation[194]

$$D(r_i) = \frac{p_{ci}}{r_i}\left(\frac{dV(r)}{dp_c}\right)_i, \qquad \ldots\ldots (H.1\text{-}2)$$

The distribution curve of D(r) against r followed.

H.2 Estimation of Pore Properties from the Pore Size Distribution

The area under each pore size distribution curve was

divided into a number of small elements of width δr_i, and the area of each element $D(r_i)\,\delta r_i$ was measured. The width δr_i was not kept constant, but was made as small as practicable. Each elemental area $D(r_i)\,\delta r_i$ was multiplied by r_i, r_i^2, and $1/r_i$, where r_i was the mean pore radius of the element i. Then the summations $\Sigma D(r_i)\,\delta r_i$, $\Sigma r_i\, D(r_i)\,\delta r_i$, $\Sigma r_i^2\, D(r_i)\,\delta r_i$, and $\Sigma D(r_i)\,\delta r_i/r_i$ were made. The summations over a number of intervals of the total radii range and the total sums are summarized for each graphite in Table H.2-1.

From these summations, the pore properties such as the total pore volume V_p, the porosity ε, the mean pore radius r_m, the surface area S_g, and the permeability K were estimated for each graphite by means of the following equations:

$$V_p = \Sigma D(r_i)\,\delta r_i \qquad \ldots (2.4.2\text{-}3)$$

$$\varepsilon = V_p/V_t \qquad \ldots (2.2.1\text{-}1)$$

$$r_m = \Sigma r_i\, D(r_i)\,\delta r_i/V_p \qquad \ldots (2.4.2\text{-}4)$$

$$S = 2\,\Sigma D(r_i)\,\delta r_i/r_i \qquad \ldots (H.2\text{-}1)$$

$$S_g = S/w \qquad \ldots (H.2\text{-}2)$$

$$K = \frac{p_m}{k_o \tau^2 V_t \mu}\,\Sigma r_i^2\, D(r_i)\,\delta r_i + \frac{4\,\delta_l\,\bar{v}}{3\,k_l\,\tau^2\,V_t}\,\Sigma r_i\, D(r_i)\,\delta r_i \qquad \ldots (2.4.3\text{-}4)$$

In the estimation of K, the values assumed for k_o and δ_l/k_l were 2.5 and 0.8, respectively. The values obtained for the pore properties are recorded in Table 4.4-1.

Table H.2-1

Summary of the Pore Distribution Results

Range of r Å		$\Sigma D(r_i)\Delta r_i$	$\Sigma r_i D(r_i)\Delta r_i$	$\Sigma r_i^2 D(r_i)\Delta r_i$	$\Sigma D(r_i)\,\Delta r_i/r_i$
(a) P.G. 60 Graphite - C.S.I.R.O.		cm^3	$cm^4 \times 10^5$	$cm^5 \times 10^{10}$	cm^2
100,000-1,000,000		2.547	512.8	115824	1238
50,000-	100,000	0.052	5.9	297	75
10,000-	50,000	0.081	2.1	67	379
5,000-	10,000	0.025	0.2	1	349
1,000-	5,000	0.039	0.1	0.4	1540
	totals	2.744	519.1	116189	3581
(b) Acheson "A" Graphite - C.S.I.R.O.		cm^3	$cm^4 \times 10^4$	$cm^5 \times 10^{10}$	$cm^2 \times 10^{-2}$
>100,000		0.245	3.363	5915.0	1.5
50,000-	100,000	0.276	2.029	1547.5	5.9
10,000-	50,000	0.706	1.984	634.4	29.5
5,000-	10,000	0.092	0.068	5.2	12.8
1,000-	5,000	0.118	0.030	0.9	57.0
500-	1,000	0.062	0.004	0.04	91.6
100-	500	0.180	0.005	0.01	783.8
	totals	1.679	7.485	8103.1	980.1
(c) Morgan "EY9" Graphite - C.S.I.R.O.		cm^3	$cm^4 \times 10^4$	$cm^5 \times 10^{10}$	$cm^2 \times 10^{-2}$
5,000-	10,000	0.032	0.0192	1.172	5.5
1,000-	5,000	0.731	0.2234	7.769	279.1
500-	1,000	0.022	0.0016	0.013	31.2
100-	500	0.014	0.0005	0.002	44.8
	totals	0.799	0.2447	8.956	360.6

(d) Morgan "EY9166" Graphite - A.A.E.C.

	cm^3/cm^3	cm^4/cm^3 x 10^8	cm^5/cm^3 x 10^{10}	cm^2/cm^3
>50,000	0.00002	1.5	0.0942	0.04
10,000- 50,000	0.0005	8.2	0.1877	2.9
5,000- 10,000	0.0596	358.9	2.1838	1000.5
1,000- 5,000	0.0744	248.9	0.9062	2489.0
500- 1,000	0.0021	1.5	0.0012	294.9
100- 500	0.0039	1.3	0.0004	1347.5
totals	0.1405	620.3	3.3735	5134.8

(e) Impregnated Graphite No. 101 - A.A.E.C

	cm^3/cm^3	cm^4/cm^3 x 10^8	cm^5/cm^3 x 10^{14}	cm^2/cm^3 x 10^{-2}
>10,000	0.0003	8.38	274.90	0.02
5,000- 10,000	0.0003	2.32	16.90	0.05
1,000- 5,000	0.0315	42.80	62.47	23.95
500- 1,000	0.0209	15.59	12.02	28.64
100- 500	0.0283	7.13	2.16	138.79
50- 100	0.0133	0.95	0.07	193.45
10- 50	0.0155	0.54	0.02	476.30
totals	0.1101	77.71	368.54	861.20

(f) Impregnated Graphite No. 112 - A.A.E.C.

	cm^3/cm^3	cm^4/cm^3 x 10^8	cm^5/cm^3 x 10^{14}	cm^2/cm^3 x 10^{-2}
>10,000	0.0002	4.13	79.90	0.01
5,000- 10,000	0.0005	3.21	22.00	0.08
1,000- 5,000	0.0233	36.97	71.68	16.42
500- 1,000	0.0258	19.41	15.10	35.61
100- 500	0.0363	9.56	2.95	168.52
50- 100	0.0150	1.08	0.08	215.75
10- 50	0.0043	0.17	0.007	112.90
totals	0.1054	74.53	191.72	549.29

APPENDIX J

THE ELECTRICAL RESISTIVITY MEASUREMENTS

J.1 The Theory of the Electrical Resistivity Measurements

In the electrical resistivity determinations, the potential drop ΔE across a graphite sample saturated with an electrolyte was measured when a d.c. current I was passed through the sample (see section 3.5.3.3). Provided ΔE was less than the decomposition potential E_d at the current I, no current was conducted by the graphite (section 3.5.3.1). From the slope of a plot of ΔE against I, the resistance R' of the saturated sample was obtained. The specific resistance R_o of the electrolyte was measured independently for each determination.

Then the formation factor F was obtained by means of the equation

$$F = R'/R'_o , \qquad \ldots (2.5.6\text{-}1)$$

where $R'_o = R_o(L/A)$, and $\qquad \ldots (2.5.6\text{-}2)$

L,A = dimensions of the sample.

The electrical tortuosity factor q was calculated from the equation

$$q = F\varepsilon , \qquad \ldots (2.5.1\text{-}3)$$

where ε = the porosity of the sample.

J.2 Type Calculation of the Electrical Tortuosity Factor

The determination of the formation factor and the electrical tortuosity factor for Acheson "A" Graphite

Sample No. T2 when saturated with N KCl (Detmn. No. T:3) is detailed to illustrate the method of calculation. The measured potential drops ΔE are listed for different currents I in Table J.2-1. These results are plotted in Fig. J.2-1. From the slope of the graph, $R' = 102$ ohm.

Table J.2-1
Experimental Results of a Typical Tortuosity Determination (No. T:3)

+ve current		-ve current	
I μA	ΔE mV	I μA	ΔE mV
228	21	0	2
410	41	961	99
608	62	788	81
827	83	589	61
823	82	410	42
961	97	209	21
95	8	94	10

The cell constant C_c for the conductivity cell was obtained by measuring the resistance of an exactly 1 N KCl solution for which the specific conductivity at 25°C was known[267] (0.11180 mho/cm); the resulting value of C_c was 0.827 cm^{-1}. The resistance of the electrolyte R'_s, measured by means of the conductivity bridge, was 7.235 ohm. Then the specific resistance $R_o = R'_s/C_c = 8.75$ ohm-cm.

As L = 2.14 cm and A = 6.00 cm^2 for the graphite sample, $R'_o = R_o (L/A) = 3.12$ ohm.

Hence $F = R'/R'_o = 102/3.12 = \underline{32.7}$.

If the porosity $\varepsilon = 0{,}28$, then $q = F\varepsilon = \underline{9.14}$.

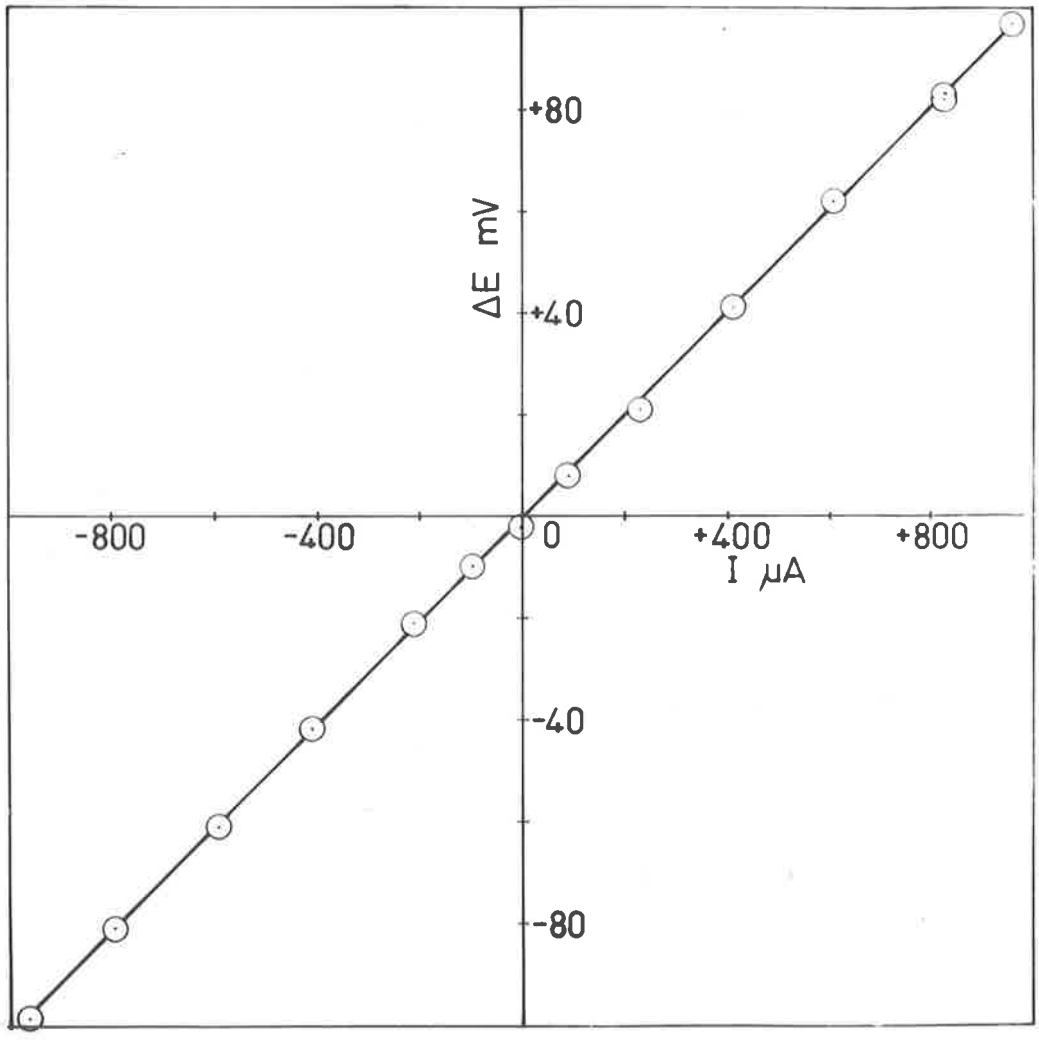

Fig. J.2-1 Plot of ΔE against I for Determining the Formation Factor for Acheson "A" Sample No. T2 (Detmn. No. T:3).

APPENDIX K

DETAILED PERMEABILITY RESULTS

K.1 List of the Permeability Determinations

Table K.1-1
The Low Pressure Determinations

Detmn. No.	Graphite Grade	Sample No.	Gas	Cell Type	Method	Comments
L:1	Acheson "A"	K1	N_2	I	increase	Trial expts.
L:2		K6	N_2	II	increase	
L:3		K2	N_2	I	increase	
L:4		K2	N_2	I	decay	
L:5		K6	N_2	II	flow	Prelim. flow expts.
L:6		K6	N_2	II	flow	
L:7		K2	N_2	I	decay	
L:8		K2	N_2	I	decay	
L:9		K2	N_2	I	decay	
L:10		K2	N_2	I	decay	
L:11		K6	N_2	II	decay	Decay rate fast
L:12	Morgan "EY9"	K21	N_2	I	increase	Leak observed
L:13		K21	N_2	I	increase	
L:14		K21	N_2	I	decay	Very long time
L:15	Acheson "A"	K6	N_2	II	flow	Anomalous results
L:16		K7	N_2	II	flow	
L:17		K3	N_2	I	equalzn.	Results sctrd
L:18		K3	N_2	I	increase	Modfd.method
L:19		K3	N_2	I	decay	
L:20		K3	N_2	I	decay	
L:21		K3	N_2	I	increase	
L:21A		K3	N_2	I	increase	$\mathcal{T}_s$ = 35.5°C
L:21B		K3	N_2	I	equalzn.	Sctrd.result
L:22	Morgan "EY9"	K21	N_2	I	increase	McLeod test
L:23	Impregnated	K41	Air	IIa	decay	Small V_i - trial

Table K.1-1(Contd.)

L:24	Morgan "EY9"	K21	N_2	I	increase	
L:25		K25	N_2	II	decay	
L:26		K25	N_2	II	decay	
L:27		K25	N_2	II	decay	
L:28		K25	N_2	II	increase	
L:29	Impregnated	K42	N_2	II	increase	
L:30		K42	N_2	II	decay	
L:31		K42	N_2	II	flow	Equilm.time
L:32		K42	N_2	II	increase	
L:33	Acheson "A"	K2A	N_2	II	decay	
L:34		K2A	N_2	II	flow	
L:35	Morgan "EY9"	K23	N_2	II	increase	
L:36		K23	N_2	II	flow	
L:37		K23	A	II	increase	
L:38		K21	A	I	increase	
L:39	Acheson "A"	K2A	A	II	decay	
L:40		K5	A	II	decay	
L:41		K5	N_2	II	decay	
L:42		K4	N_2	II	decay	
L:43	Morgan "EY9166"	K24	N_2	II	increase	
L:44	Morgan "EY9"	K21	He	I	increase	
L:45		K21	Xe	I	increase	
L:46		K21	H_2	I	increase	
L:47		K21	CF_2Cl_2	I	increase	
L:48		K21	H_2	II	decay	
L:49		K21	CO_2	I	increase	
L:50	Acheson "A"	K2A	H_2	II	decay	
L:51		K2A	Xe	II	decay	
L:52		K2A	Xe	II	increase	
L:53		K2A	CO_2	II	decay	
L:54		K2A	CF_2Cl_2	II	decay	
L:55	Impregnated	K42	H_2	II	increase	
L:56		K42	Xe	II	increase	
L:57		K42	He	II	increase	
L:58		K42	A	II	increase	

Table K.1-2
The High Pressure Determinations

Detmn. No.	Graphite Grade	Sample No.	Gas	Cell Type	Comments
H:1	Acheson "A"	K6	N_2	I	Prelim.detmn.
H:2		K7	N_2	I	Leakage?
H:3		K2A	N_2	I	
H:4	Morgan "EY9"	K23	N_2	I	
H:5		K22	N_2	I	
H:6	Impregnated	K42	N_2	II	
H:7		K41	N_2	II	
H:8		K41	A	II	
H:9		K41	H_2	II	
H:10		K41	CO_2	II	Leak present
H:11		K41	CF_2Cl_2	II	
H:12		K41	N_2	II	
H:13		K41	N_2	II	
H:14		K41	N_2	II	
H:8A		K41	A	II	
H:9A		K41	H_2	II	
H:11A		K41	CF_2Cl_2	II	Sample blocked
H:15	P.G. 60	K31	N_2	II	
H:16		K31	H_2	II	
H:17		K31	CF_2Cl_2	II	
H:18		K31	A	II	
H:19		K32	N_2	II	
H:20	Acheson "A"	K4	N_2	II	
H:21		K2A	H_2	II	
H:22	Impregnated	K42	N_2	II	
H:23		K42	H_2	II	

Table K.1-3
The Pressure Distribution Measurements

Detmn. No.	Graphite Grade	Specimen No.	Gas	Comments
G:1	Acheson "A"	G1	N_2	order 4 to 1
G:2		G1	N_2	order 1 to 4
G:3		G1	CO_2	order 1 to 4
G:4	Morgan "EY9166"	G21	N_2	
G:5		G21	CO_2	
G:6		G21	CF_2Cl_2	
G:7	P.G. 60	G31	N_2	
G:8		G31	H_2	

K.2 The Low Pressure Determinations

Determinations No. L:1 and No. L:2

Initial pressure increase tests with Acheson "A" Rod No. K1 and Acheson "A" Cylinder No. K6 in the low pressure apparatus showed that nitrogen at about p_i = 20 cm Hg flowed so rapidly through the samples that it was impossible to measure the flow-rate. The need of an external coating on the rod sample was indicated since mercury from the cell oozed through the porous graphite. The sample was discarded as the pores were blocked with mercury.

- - - - - - - -

Determination No. L:3

With Acheson "A" Rod No. K2, p_o increased beyond the range of the McLeod gauge in less than 2 min for p_i about 17 cm Hg. A flow apparatus was therefore considered necessary for permeability determinations on Acheson "A" graphite.

- - - - - - - -

Determination No. L:4

The pressure decay method was tested with Acheson "A" Rod No. K2 in the low pressure apparatus. Below p_i = 2.5 mm Hg, the rate of pressure decay was measured satisfactorily with the McLeod gauge; a manometer was required for measurements at higher pressures.

- - - - - - - -

Determinations No. L:5 and No. L:6

Preliminary flow experiments were made on Acheson "A" Cylinder No. K6 using a temporary apparatus. The inlet pressure was measured with a 0 to 100 p.s.i.g. pressure gauge, and the gas flow-rate with a Fischer and Porter laboratory flow-rator (0 to 600 cm^3/sec). The values of K were inaccurate because K decreased from 8 cm^2/sec at p_m = 88 cm Hg to 5.5 cm^2/sec at p_m = 125 cm Hg, i.e., K was proportional to $1/p_m$ instead of p_m as indicated by theoretical considerations.

- - - - - - - -

Determinations No. L:7 and No. L:8

Details	p_m cm Hg	Δp cm Hg	dp_i/dt cm/hr	V_i cm^3	K cm^2/sec
	5.5	11	5.10	845.6	0.648
	5.0	10	4.46	845.2	0.623
Acheson "A"	4.5	9	3.96	844.8	0.614
Graphite,	4.0	8	3.17	844.4	0.553
	3.5	7	2.64	843.9	0.526
Sample No. K2,	3.0	6	2.12	843.5	0.492
	2.5	5	1.56	843.1	0.435
Nitrogen,	2.0	4	1.20	842.7	0.416
	1.50	3.0	0.827	842.3	0.384
Pressure Decay	1.25	2.5	0.728	842	0.405
Method,	1.00	2.0	0.410	842	0.285
	0.75	1.5	0.281	842	0.261
$\mathcal{T}_s$(av) = 19.6°C.	0.50	1.0	0.202	841	0.281
	0.25	0.5	0.0965	841	0.268
	0.10	0.2	0.0420	841	0.292
	0.10	0.2	0.0420	841	0.292
	0.05	0.1	0.0154	841	0.214

$K = 0.0784\ p_m + 0.241$

Comments: On repeating Detmn. No. L:7 under similar conditions, almost identical values of dp_i/dt were obtained. The average value of several measurements of dp_i/dt at each p_m are recorded above. The pressure p_i decayed from 11.7 cm Hg to 0.1 cm Hg in 22 hr. A straight $K-p_m$ plot was obtained with a maximum scatter of ± 0.04 cm^2/sec in the values of K.

- - - - - - - - -

Determinations No. L:9 and No. L:10

Details	p_m cm Hg	Δp cm Hg	dp_i/dt cm/hr	V_i cm^3	K cm^2/sec
	5.0	10	1.97	1936	0.630
	4.5	9	1.71	1936	0.608
Acheson "A"	4.0	8	1.38	1935	0.552
Graphite,	3.5	7	1.16	1935	0.530
	3.0	6	0.925	1935	0.493
Sample No. K2,	2.5	5	0.672	1934	0.429
	2.0	4	0.533	1934	0.426
Nitrogen,	1.50	3.0	0.375	1933	0.399
	1.25	2.5	0.285	1933	0.364
Pressure Decay	1.00	2.0	0.191	1933	0.305
Method,	0.75	1.5	0.144	1933	0.307
	0.50	1.0	0.103	1932	0.329
$\mathcal{T}_s$ (av) = 20.7°C	0.38	0.75	0.0587	1932	0.250
	0.25	0.50	0.0456	1932	0.291
	0.10	0.20	0.0142	1932	0.227

$K = 0.0776\ p_m + 0.253$

Comments: With V_i greater than for Detmns. No. L:7 and No. L:8, p_i decayed from 10.8 cm Hg to 0.1 cm Hg in 49 hr. The variation of the values of K about the straight $K\text{-}p_m$ plot was less than ± 0.03 cm^2/sec. The values of dp_i/dt recorded above represent the average values of several measurements of the slope of the decay plots obtained for each determination.

- - - - - - - -

Determination No. L:11

Details	p_m cm Hg	Δp cm Hg	dp_i/dt cm/sec	V_i cm^3	K cm^2/sec
	3.70	6.6	0.0960	1942	0.743
Acheson "A"	3.40	6.2	0.0897	1942	0.739
Graphite,	3.05	5.9	0.0803	1942	0.695
	2.81	5.4	0.0717	1941	0.675
Sample No. K6,	2.52	5.0	0.0640	1941	0.659
	2.25	4.5	0.0535	1941	0.607
Nitrogen,	2.00	4.0	0.0434	1941	0.554
	1.50	3.0	0.0260	1941	0.442
Pressure Decay Method,	1.00	2.0	0.0190	1940	0.485
T_s (av) = 25.2°C.	0.50	1.0	0.0070	1940	0.357

$K = 0.1239\ p_m + 0.314$

Comments: Because p_i decreased from 25 to 4 cm Hg in 2 min and from 10 to 1 cm Hg in 4 min, the rate of pressure decay was much too fast for steady state conditions to be assumed. Hence the values of K calculated below p_m = 3.7 cm Hg were considered inaccurate. The maximum scatter about the $K\text{-}p_m$ plot at the lower mean pressures was ± 0.06 cm^2/sec. However, the $K\text{-}p_m$ plot agreed within the experimental scatter with that obtained in Detmn. No. L:41 for Rod No. K5.

- - - - - - - -

Determination No. L:12

For the initial pressure increase experiment in the low pressure apparatus with Morgan "EY9" Rod No. K21, a leak into the outlet side volume developed causing a very large blank rate, which was greater than the actual flow-rate through the sample.

- - - - - - - -

Determination No. L:13

Details	p_m cm Hg	Δp cm Hg	dp_o/dt mm/sec x10^4	V_o cm^3	K cm^2/sec
Morgan "EY9" Graphite,					
Sample No. K21,	8.47	16.75	7.09	695	0.0182
Nitrogen,	8.36	16.56	6.96	695	0.0181
Pressure Increase	5.26	10.46	4.17	695	0.0171
Method,	2.51	5.03	1.90	695	0.0162
$\mathcal{T}_g$ (av) = 18.5°C.	0.43	0.85	0.337	695	0.0170
	14.20	28.16	13.23	695	0.0202

$$K = 0.000341\ p_m + 0.0153$$

Comments: The pressure increase experiments in this determination were generally continued for 30 to 40 min. The degassing rate of about 0.25 x 10^{-5} mm Hg/sec was high; correction of dp_o/dt for this degassing (or leakage) for the experiment with p_m = 0.43 cm Hg still showed that there was evidence of a minimum in the K-p_m plot at about p_m = 1.4 cm Hg. No time-lags were measured as the isolating stopcock in the spherical joint system L had not been added to the apparatus.

Determination No. L:14

Details	p_m cm Hg	Δp cm Hg	dp_i/dt cm/hr	V_i cm^3	K cm^2/sec
	12.5	25.0	0.314	850.8	0.0184
Morgan "EY9"	10.0	20.0	0.243	848.8	0.0177
Graphite,	9.0	18.0	0.214	848.0	0.0173
	8.4	16.8	0.206	847.6	0.0178
Sample No. K21,	7.5	15.0	0.171	846.9	0.0166
	6.0	12.0	0.137	845.7	0.0166
Nitrogen,	5.0	10.0	0.1105	844.9	0.0160
	4.0	8.0	0.0870	844.1	0.0158
Pressure Decay	3.0	6.0	0.0585	843.3	0.0141
Method	2.5	5.0	0.0491	843.0	0.0142
	1.00	2.0	0.0218	841.8	0.0158
$\mathcal{T}_g$(av) = 20.4°C.	0.75	1.5	0.0153	841.6	0.0147
	0.50	1.0	0.0092	841.4	0.0133

$$K = 0.000316\ p_m + 0.0146$$

Comments: For this determination, p_i decreased from 26.6 cm Hg to 0.5 cm Hg in 390 hr. Because of this very slow decay rate, the values of dp_i/dt were considerably inaccurate; the scatter of the K values about the K-p_m above p_m = 4 cm Hg was about ± 0.0004 cm^2/sec (about 2½%), while, below this pressure, the scatter was up to ± 0.0015 cm^2/sec. The pressure decay method

was thus not suitable for determining permeability coefficienets for Morgan "EY9" graphite rods. The K-p_m plot was about 0.001 cm^2/sec (5%) lower than that obtained in Detmn. No. K:13.

Determinations No. L:15 and No. L:16

Further preliminary flow experiments on Acheson "A" Cylinder No. K6 (Detmn. No. L:15) and Acheson "A" Cylinder No. K7 (Detmn. No. L:16) with the same experimental arrangement as employed for Detmns. No. L:5 and No. L:6 gave similar anomalous results, i.e., K proportional to $1/p_m$, even though special care was taken to avoid faulty measurement. These anomalous results could be rectified if the flow-rator calibration chart was corrected to the pressure in the flow-meter. Then K increased from 5.8 cm^2/sec at p_m = 88 cm Hg to 6.2 cm^2/sec at p_m = 125 cm Hg. However, the corrected results were scattered due to inaccurate pressure measurement; further more accurate determinations above 1 atm must be made in a high pressure flow apparatus.

Determination No. L:17

Details	Δp cm Hg	p_m cm Hg	$d(\Delta p)/dt$ cm/sec x 10^3	K cm^2/sec
	V_1 = 1470 cm^3, V_o = 840 cm^3			
Acheson "A" Graphite,	(a)	p_i = 16.1 cm Hg at t = 0		
	12.90	8.50	4.84	0.833
Sample No. K3,	10.25	8.85	4.07	0.881
	8.08	9.15	3.18	0.873
Nitrogen,	6.35	9.38	2.59	0.905
	2.97	9.85	1.17	0.875
Pressure Equalization Method	(b)	p_i = 15.8 cm Hg at t = 0		
	12.40	8.36	4.60	0.825
T_s (av) = 24.7°C.	7.97	8.96	2.95	0.821
	6.24	9.20	2.66	0.944
	3.89	9.52	1.45	0.827
	3.08	9.63	1.22	0.878
	1.53	9.82	0.64	0.928

Comments: The values of K obtained in this determination were scattered about the K-p_m plots obtained in Detmns. L:18 to L:20 by up to ± 0.1 cm^2/sec (± 10%). This large scatter indicated that the pressure equalization method was not as accurate as the other low pressure methods.

Determination No. L:18

Details	p_m cm Hg	Δp cm Hg	dp_o/dt mm/sec x 103	V_o cm3	K cm2/sec
Acheson "A" *	7.90	15.51	43.6	695	0.803
Graphite, *	5.16	9.99	21.6	695	0.625
Sample No. K3,	2.97	5.73	9.40	695	0.464
	3.00	5.61	9.13		0.461
Nitrogen,	1.50	2.82	3.64	695	0.368
	1.53	2.66	3.44		0.369
Pressure Increase Method,	0.44	0.85	0.842	695	0.283
	0.45	0.80	0.787		0.281
$\mathcal{T}_s$ (av) = 26.3°C.*	13.33	26.31	103.0	695	1.118
*	10.07	19.88	64.6	695	0.929

* Modified pressure increase method used.

$K = 0.0650\ p_m + 0.271$

Comments: This determination showed that a modified pressure increase method (see section 3.1.3.1) was suitable for measuring permeability coefficients for Acheson "A" graphite above about $p_m = 4$ cm Hg as the values of K agreed with those from Detmns. No. L:7 to No. L:10. Below $p_m = 4$ cm Hg, the time for the pressure to increase beyond the range of the McLeod gauge was long enough to allow a p_o-t plot to be obtained; this plot was curved and values of K were determined from the slope at two points as mentioned in Appendix C.2.2. The K-p_m plot tended to curve slightly downwards above about $p_m = 8$ cm Hg.

- - - - - - - -

Determinations No. L:19 and No. L:20

Details	p_m cm Hg	Δp cm Hg	dp_1/dt cm/hr	V_1 cm3	K cm2/sec
Acheson "A" Graphite,	13.00	26.0	28.3	851.1	1.060
	11.50	23.0	23.6	850.0	0.999
	10.00	20.0	18.5	848.8	0.900
Sample No. K3,	9.25	18.5	16.6	848.2	0.874
	7.75	15.5	12.3	847.0	0.771
Nitrogen,	7.00	14.0	11.0	846.5	0.762
	6.00	12.0	8.40	845.7	0.679
Pressure Decay Method,	5.00	10.0	6.30	844.9	0.610
	4.00	8.0	4.56	844.1	0.552
	3.00	6.0	2.97	843.3	0.479
$\mathcal{T}_s$ (av) = 23.9°C.	2.50	5.0	2.28	843.0	0.441
	2.00	4.0	1.74	842.6	0.420
	1.50	3.0	1.160	842.2	0.373
	1.00	2.0	0.753	841.8	0.363
	0.50	1.0	0.317	841.4	0.306
	0.25	0.5	0.150	841.2	0.289

$K = 0.0676\ p_m + 0.276$

Comments: In these determinations, p_i decayed from 28 cm Hg to 0.3 cm Hg in 11 hr. Below p_m = 7 cm Hg, a straight K-p_m plot was obtained with a maximum scatter in the values of K of ± 0.03 cm^2/sec. Above this pressure, the K-p_m plot curved downwards slightly; Detmn. No. L:20 confirmed this curvature. The values of dp_i/dt recorded above were average values.

- - - - - - - -

Determination No. L:21

Details	p_m cm Hg	Δp cm Hg	dp_o/dt mm/sec x 10^3	V_o cm^3	K cm^2/sec
	* 16.260	32.220	69.8	1785	1.597
Acheson "A"	4.090	7.840	5.54	1785	0.522
Graphite,	2.992	5.663	3.50	1785	0.457
	2.710	5.057	2.94	1785	0.429
Sample No. K3,	1.744	3.336	1.68	1785	0.372
	1.402	2.685	1.24	1785	0.341
Nitrogen,	1.281	2.491	1.14	1785	0.338
	1.017	1.954	0.842	1785	0.318
Pressure Increase	0.787	1.501	0.625	1785	0.308
Method,	0.563	1.087	0.426	1785	0.289
	0.402	0.787	0.299	1785	0.284
$\mathcal{T}_s$ (av) = 15.8°C.	0.258	0.501	0.184	1785	0.273
	0.200	0.371	0.320	695	0.249
	0.146	0.272	0.227	695	0.242

* Modified pressure increase method.

$$K = 0.0657\ p_m + 0.254$$

Determination No. L:21A

$\mathcal{T}_s$ (av) = 35.5°C.	2.352	4.481	2.43	1785	0.424
	0.505	0.975	0.373	1785	0.302

- - - - - - - -

Comments: In this determination, satisfactory values of K were determined by the pressure increase method for Acheson "A" graphite below p_m = 4 cm Hg even though curved p_o-t plots were observed (cf. Detmn. No. L:18). The K-p_m plot was straight with values of K showing a scatter of ± 0.0005 cm^2/sec (± 1%). Below p_m = 0.25 cm Hg, the K values were about 0.02 cm^2/sec (8%) low. The values of K determined at 35.5°C (Detmn. No. L:21A) were about 7% higher than the K-p_m plot. Time-lags of the order of 3 sec at p_m = 1.5 cm Hg to 20 sec at the lowest p_m were observed, but were too small to measure accurately. The K value at p_m = 16.3 cm Hg determined by the modified pressure increase method was 23% too high.

- - - - - - - -

Determination No. L:21B

Details	Δp cm Hg	p_m cm Hg	$d(\Delta p)/dt$ cm/sec x 10^3	K cm^2/sec
Acheson "A" Graphite, Sample No. K3,	V_i = 1507 cm^3, V_o = 1785 cm^3, p_i = 30.54 cm Hg at t = 0			
Nitrogen, Pressure Equalization Method, $\mathcal{T}_s$ (av) = 15.6°C.	24.93	15.53	8.51	1.159
	22.48	14.93	7.72	1.171
	20.32	14.84	6.73	1.123
	18.38	14.75	5.99	1.105

Comments: The scattered results of this experiment again showed that the pressure equalization method was inaccurate (cf. Detmn. No. L:17). The values of K were 5% lower than the K-p_m plot obtained in Detmn. No. L:33.

Determination No. L:22

This pressure increase determination was performed to discover whether any significant inaccuracies arose when the McLeod gauge was raised to measure p_o with the consequent decrease in V_o and compression of the gas for 1 to 2 min (see Appendix C.2.3). For three almost identical experiments for nitrogen flow through Morgan "EY9" Graphite Rod No. K21, each of 30 min duration, the McLeod gauge was read at 2 min, 4 min, and 30 min intervals, respectively. A 3% variation between the values of K was observed, showing that the measurement of the pressure with the McLeod gauge had little effect on the determination of K. The average value of K (0.0174 cm^2/sec at p_m = 12.3 ± 0.1 cm Hg) was about 10% lower than the value at the same p_m for Detmn. No. L:13.

Determination No. L:23

Because of the low flow-rates which were expected for Impregnated graphites, two trial pressure decay experiments were made on Impregnated Graphite Cylinder No. K41 with V_i about 15 cm^3. With air as the permeating gas and p_o a vacuum, p_i decreased from 76 to 3 cm Hg in about 10 hr. The two experiments gave values of K which agreed by about 0.5×10^{-5} cm^2/sec (10%). The K-p_m plots were approximately linear above p_m = 25 cm Hg, but below this pressure, the slope decreased sharply so that K was almost constant at about 2×10^{-5} cm^2/sec for p_m less than 15 cm Hg.

Determination No. L:24

Details	p_m cm Hg	Δp cm Hg	dp_o/dt mm/sec x 10^3	V_o cm^3	K cm^2/sec	ϕ min
Morgan "EY9" Graphite,	31.215	62.099	1.46	1804	0.0261	1.08
	25.433	50.618	1.10	1804	0.0241	1.10
	20.585	41.169	0.827	1804	0.0223	1.20
Sample No. K21,	16.778	33.556	0.645	1804	0.0213	1.16
	13.638	27.167	0.490	1804	0.0201	1.29
	11.053	22.021	0.377	1804	0.0191	1.29
Nitrogen, *	9.029	17.993	0.285	1804	0.0176	1.25
	7.056	14.062	0.225	1804	0.0178	1.25
Pressure	5.727	11.414	0.179	1804	0.0175	1.43
Increase	4.173	8.319	0.127	1804	0.0170	1.33
Method,	2.428	4.841	0.072	1804	0.0165	1.40
	1.978	3.916	0.145	713	0.0163	1.55
J_s (av) =	1.091	2.154	0.0775	713	0.0158	1.75
16.40C.	0.376	0.743	0.0280	713	0.0165	2.20
	0.179	0.357	0.0141	713	0.0173	2.40

* Liquid air bath on trap K.

Determination No. L:24A

	0.141	0.283	0.0113	713	0.0174	2.75
J_s (av) =	0.091	0.183	0.00723	1804	0.0174	4.10
27.20C.	0.066	0.132	0.00676	713	0.0224	3.40
	0.039	0.078	0.00324	713	0.0182	3.37
	0.029	0.058	0.00283	713	0.0214	4.00

$$K = 0.000336\ p_m + 0.0155$$

Comments: The degassing rate was about 0.10×10^{-6} mm Hg/sec for Detmn. No. L:24 and 0.22×10^{-6} mm Hg/sec for Detmn. No. L:24A. The pressure increase experiments were generally continued for about an hour and straight p_o-t plots were obtained. The K values were scattered about the straight K-p_m plot by less than $\pm$ 0.0001 cm^2/sec ($\pm$ ½%). A definite minimum was observed in the K-p_m plot at about p_m = 1 cm Hg since the value of K at p_m = 0.03 cm Hg was of the same order as that found with p_m = 20 cm Hg. In Detmn. No. L:24A, the very low inlet pressures were measured with the McLeod gauge prior to the commencement of each experiment, and the values of dp_o/dt obtained from the p_o-t plots were corrected to allow for the degassing rate. Time-lags were measured and ranged from 1 to 4 min, increasing as p_m decreased. For experiment no. 7 (*), a cold bath was placed around a trap K in the outlet side volume and the value of K was found to be 5% lower than the K-p_m plot.

- - - - - - - -

Determination No. L:25

Details	p_m cm Hg	Δp cm Hg	dp_1/dt cm/hr	V_1 cm^3	K cm^2/sec
Morgan "EY9" Graphite,	15.00	30.0	25.55	1972	0.01089
	12.50	25.0	20.65	1970	0.01054
	8.75	17.5	13.65	1967	0.00993
Sample No. K25,	7.50	15.0	11.15	1966	0.00946
	6.25	12.5	9.43	1965	0.00959
Nitrogen,	5.00	10.0	7.30	1964	0.00928
	4.00	8.0	5.63	1963	0.00894
Pressure Decay	3.50	7.0	4.86	1962	0.00882
Method,	3.00	6.0	4.19	1962	0.00887
	2.50	5.0	3.41	1962	0.00867
T_s (av) = 26.4°C.	2.00	4.0	2.67	1961	0.00848
	1.50	3.0	2.00	1961	0.00847

$K = 0.000183\ p_m + 0.00824$

Determination No. L:26

	15.00	30.0	25.60	1972	0.01091
	12.50	25.0	20.50	1970	0.01046
T_s (av) = 24.7°C.	11.25	22.5	18.20	1969	0.01030
	10.00	20.0	15.60	1968	0.00993
	7.50	15.0	11.55	1966	0.00979
	6.25	12.5	9.10	1965	0.00925
	5.00	10.0	7.20	1964	0.00914
	3.50	7.0	4.97	1962	0.00902
	3.00	6.0	4.13	1962	0.00874
	2.50	5.0	3.45	1962	0.00877
	2.00	4.0	2.70	1961	0.00857
	1.50	3.0	1.98	1961	0.00838

$K = 0.000179\ p_m + 0.00825$

Comments: Detmn. No. L:26 was a repeat of Detmn. No. L:25 and excellent agreement was obtained. The pressure p_1 decayed from 35 cm Hg to 0.5 cm Hg in 6 hr. Straight K-p_m plots were obtained with the K values being scattered by less than ± 0.0002 cm^2/sec (2%). At very low pressures (below p_m = 1.5 cm Hg), the values of K, not reported above, were very scattered (± 0.001 cm^2/sec or ± 12%) and no sign of a minimum was observed.

- - - - - - - -

Determination No. L:27

Details	p_m cm Hg	Δp cm Hg	dp_1/dt cm/hr	K cm^2/sec
Morgan "EY9" Graphite,	15.63	31.25	7.00	0.01187
	15.00	30.00	6.79	0.01200
	13.75	27.50	6.15	0.01185
Sample Cylinder No. K25,	13.13	26.25	5.76	0.01164
	12.50	25.00	5.30	0.01124
Nitrogen	11.87	23.75	5.05	0.01127
	11.25	22.50	4.75	0.01119

Pressure Decay Method,	10.00	20.00	4.14	0.01097
	9.00	18.00	3.68	0.01085
$\mathcal{T}_s$ (av) = 24.3°C,	8.00	16.00	3.14	0.01040
	7.00	14.00	2.71	0.01026
V_1 = 8200 cm^3.	6.00	12.00	2.30	0.01016
	5.00	10.00	1.86	0.00986
	~~4.50~~	~~0.00~~	~~1.86~~	~~0.00986~~
	4.50	9.00	1.68	0.00989
	3.50	7.50	1.39	0.00982

$$K = 0.000194\ p_m + 0.00899$$

Comments: For this determination, the inlet volume V_1 was made four times larger than that in the previous determinations (Nos. L:25 and L:26) by the inclusion of a reservoir bulb. The pressure p_1 then decayed from 33.5 cm Hg to 7.4 cm Hg in 7½ hr. Because V_1 was so large, no correction was made for the changing volume in the manometer. The maximum scatter of the K values about the linear K-p_m plot was ± 0.0002 cm^2/sec (2%). The K-p_m plot was about 0.0009 cm^2/sec (9%) higher than those for Detmns. No. L:25 and No. L:26.

Determination No. L:28

Details	p_m cm Hg	Δp cm Hg	dp_o/dt mm/sec x 10^4	V_o cm3	K cm^2/sec
Morgan "EY9"	0.382	0.552	11.09	1812	0.00852
Graphite,	0.214	0.310	6.19	1812	0.00847
Sample No. K25,	0.092	0.133	2.65	1812	0.00844
Nitrogen,	0.0508	0.0734	1.49	1812	0.00863
Pressure Increase	0.0317	0.0452	0.906	1812	0.00850
Method,	0.0173	0.0250	0.512	1812	0.00868
$\mathcal{T}_s$ (av) = 22.5°C.					

Comments: These experiments were performed at quite low pressures below p_m = 0.4 cm Hg. Except for the first experiment, the initial values of p_1 were measured with the McLeod gauge, while the final p_1 were estimated from the change in pressure in V_o. As curved p_o-t plots were obtained, values of K were calculated at several times during each experiment; the average values are reported above. The blank rate was about 0.2 x 10^{-6} mm Hg/sec. The values of K only varied slightly and were 0.0002 cm^2/sec (2.4%) higher than the K-p_m plot for Detmn. No. L:25; however, they did show that the K-p_m plot curved upwards below about p_m = 0.08 cm Hg. Only very small time-lags of less than a minute were observed for this determination.

Determination No. L:29

Details	p_m cm Hg	Δp cm Hg	dp_o/dt mm/sec x 10^4	V_o cm3	K cm^2/sec x 10^4	ϕ min
	38.039	75.596	26.54	1820	1.528	9.6
Impregnated	30.358	60.235	20.62	1820	1.487	10.3
Graphite,	23.740	47.041	15.88	1820	1.474	11.8
	15.256	30.138	9.75	1820	1.404	12.9
Sample No.	12.009	23.688	7.39	1820	1.355	12.9
K42,	9.481	18.502	5.74	1820	1.345	13.2
	5.100	10.064	3.01	1820	1.297	13.85
Nitrogen,	2.425	4.738	1.39	1820	1.268	13.3
	1.989	3.635	2.68	729	1.277	13.5
Pressure	0.692	1.309	0.950	729	1.266	12.5
Increase	0.345	0.653	0.480	729	1.286	13.3
Method,	0.173	0.330	0.254	729	1.341	16.7
	0.062	0.116	0.094	729	0.411	19.0
$\mathcal{J}_s$ (av) =	18.268	36.073	11.52	1820	1.384	11.7
23.40C.	10.321	20.149	6.23	1820	1.346	13.9
	7.754	15.145	4.58	1820	1.314	14.1
	3.988	7.797	2.26	1820	1.258	13.7,14.6
	32.285	64.064	21.91	1820	1.481	10.9
	25.389	50.221	16.76	1820	1.452	12.3
	19.949	39.324	12.85	1820	1.417	12.6 *

* p_o initially 1.15 mm Hg instead of 10^{-6} mm Hg.

$$K = 7.46 \times 10^{-7} p_m + 12.61 \times 10^{-5}$$

Comments: The degassing rate for this determination was about 0.2×10^{-6} mm Hg/sec. Below p_m = 12 cm Hg, the pressure increase experiments were continued for about two hours instead of the customary one hour because up to 50 min were required to attain steady equilibrium flow and hence a straight p_o-t plot. The values of K were generally scattered about the K-p_m plot by less than $\pm 0.1 \times 10^{-5}$ cm^2/sec ($\pm$ 0.8%) although the maximum scatter was $\pm 0.3 \times 10^{-5}$ cm^2/sec ($\pm$ 2.3%). A definite minimum was observed in the plot at about p_m = 0.5 cm Hg. Time-lags from 10 to 19 min were observed.

- - - - - - - - -

Determination No. L:30

Details	p_m cm Hg	Δp cm Hg	dp_1/dt cm/hr	V_1 cm3	K cm^2/sec x 10^{-4}
Impregnated	32.5	65	10.15	112.6	1.166
Graphite,	30.0	60	9.18	110.5	1.121
	27.5	55	8.65	108.4	1.130
Sample No. K42,	25.0	50	8.03	106.2	1.131
	22.5	45	7.39	104.1	1.134
Nitrogen,	20.0	40	6.67	102.0	1.128
	17.5	35	5.98	99.9	1.132

Pressure Decay Method,	15.0	30	5.26	97.8	1.137
	12.5	25	4.46	95.7	1.132
	10.0	20	3.60	93.6	1.117
$\mathcal{T}_s$ (av) = 22.2°C.	7.0	14	2.60	91.1	1.122
	5.0	10	1.96	89.4	1.162
	4.0	8	1.54	88.6	1.131
	3.0	6	1.225	87.7	1.187
	2.0	4	0.806	86.9	1.161
	1.5	3	0.593	86.5	1.134

Comments: On the reduction of V_i to about 100 cm^3, p_i decayed from 69 to 2 cm Hg in 19 hr for this pressure decay determination on the Impregnated graphite sample. The values of K remained approximately constant at 1.13×10^{-4} cm^2/sec over most of the pressure range studied (scatter about $\pm 0.01 \times 10^{-4}$ cm^2/sec or ± 1%); below p_m = 5 cm Hg, the K values increased slightly although they were quite scattered (5%). The K-p_m plot was much lower than that obtained in Detmn. No. L:29 by the pressure increase method (10% lower at low p_m and 25% at p_m = 30 cm Hg).

Determination No. L:31

Details	Av. p_m cm Hg	Av. Δp cm Hg	t min	$Q_{S.T.P.}$ $cm^3/sec \times 10^3$	K $cm^2/sec \times 10^4$
	11.56	23.12	20	1.32	-
	± 0.05	± 0.10	45	1.63	1.356
Impregnated Graphite,			75	1.67	1.391
			135	1.67	1.397
			240	1.69	1.407
Sample No. K42,			290	1.69	1.407
			1411	1.67	1.400
			1451	1.69	1.405
Nitrogen,			1718	1.67	1.402
			av.	1.68	1.401
Low Pressure Flow Method,	31.25	62.54	20	4.36	-
	± 0.20	± 0.40	140	5.02	1.541
			192	4.96	1.523
$\mathcal{T}_s$ (av) = 18.0°C.			1216	4.91	1.535
			1277	4.96	1.531
			av.	4.96	1.532
	36.45	72.89	148	5.87	1.554
	± 0.07	± 0.15	248	5.86	1.559
			290	5.90	1.574
			av.	5.88	1.562
	18.50	37.00	61	2.71	1.423
	± 0.03	± 0.06	183	2.74	1.435
			228	2.74	1.430
			av.	2.73	1.429
	5.30	10.61	131.5	0.757	1.385
	±0.02	± 0.04	177	0.744	1.358
			287	0.739	1.345
			av.	0.747	1.363

Comments: These experiments showed that steady state flow conditions were attained less than one hour after the commencement of flow for Impregnated graphite. The flow-rate Q (at S.T.P.) then remained constant with time with a scatter of less than ± 1%. The sample time was generally 2 min. The values of K were about 0.05×10^{-4} cm^2/sec (3.5%) higher than the K-p_m plot obtained for this sample by the pressure increase method (Detmn. No. L:29).

Determination No. L:32

Details	p_m cm Hg	Δp cm Hg	dp_o/dt mm/sec x 10^4	V_o cm^3	K cm^2/sec x 10^4
Impregnated	5.403	10.481	7.25	755	1.246
Graphite,	2.677	5.202	3.57	755	1.233
Sample No. K42,	28.063	55.838	45.67	755	1.473
Nitrogen,	28.110	55.871	18.72	1846	1.477
Pressure Increase	36.930	73.539	25.50	1846	1.532
Method,	22.846	45.417	14.71	1846	1.427
$\mathcal{T}_s$(av) = 17.5°C.	12.520	24.765	7.52,7.55	1846	1.345,1.351

$K = 7.67 \times 10^{-7} p_m + 12.54 \times 10^{-5}$

Comments: Because of the difference between the values of K for Detmns. No. L:29 and No. L:31, further experiments were performed. With the sample at equilibrium flow conditions at t = 0 as for a low pressure flow experiment, the flow-rate Q at any p_m was calculated from the change in pressure Δp_o in the outlet volume over progressively longer time intervals Δt after the isolation of V_o from the vacuum pump (t = 0). The values of Q and K were found to decrease as t increased. When $t = \Delta t$ = 2 min (i.e., a flow experiment), the value of K at any p_m agreed with the value from Detmn. No. L:31; when Δt was longer than 10 min, the values of K agreed with the K-p_m plot of Detmn. No. L:29. If p_o-t plots were prepared as for a pressure increase experiment, the values of K so obtained (recorded above) also agreed with those of Detmn. No. L:29. The p_o-t plots, when drawn with enlarged scales, curved very slightly as p_o increased. The degassing rate was 0.04×10^{-6} mm Hg/sec.

Determination No. L:33

Details	p_m cm Hg	Δp cm Hg	dp_i/dt cm/hr	V_i cm^3	K cm^2/sec
Acheson "A"	35.0	70	14.20	7534	2.30
Graphite,	32.5	65	12.24	7532	2.13
Sample No. K2A,	30.0	60	10.77	7529	2.03
Nitrogen,	27.5	55	9.24	7527	1.90
Pressure Decay	25.0	50	7.91	7525	1.79
Method,	22.5	45	6.67	7523	1.68
$\mathcal{T}_s$(av) = 17.1°C.	20.0	40	5.26	7521	1.49

17.5	35	4.12	7519	1.33
15.0	30	3.27	7517	1.23
12.5	25	2.28	7515	1.030
10.00	20.0	7.51	1466	0.829
8.75	17.5	6.19	1465	0.778
7.50	15.0	4.88	1463	0.715
6.25	12.5	3.59	1462	0.631
5.00	10.0	2.57	1461	0.565
4.00	8.0	1.83	1461	0.502
3.00	6.0	4.76	369	0.439
2.50	5.0	3.64	368	0.403
2.00	4.0	2.68	368	0.370
1.50	3.0	1.86	367	0.342
0.50	1.0	2.46	71.9	0.266
0.25	0.5	1.12	71.7	0.241

$K = 0.0631\ p_m + 0.240$

Comments: In this determination, the inlet side volume was decreased when dp_i/dt became less than about 2.0 cm Hg/hr in order to increase the accuracy of measurement at lower pressures. A total time of 16 hr was required for p_i to decay from 73 cm Hg to 0.1 cm Hg. The K-p_m plot was straight up to about p_m = 22 cm Hg, but curved downwards at higher p_m. The values of K were scattered about the plot by generally much less than the maximum variation of ± 0.05 cm^2/sec.

Determination No. L:34

Details	p_m cm Hg	Δp cm Hg	$\Delta p_o/\Delta t$ cm/min	V_o cm^3	K cm^2/sec
Acheson "A"	8.832	17.664	0.0882	1832	0.827
Graphite,	8.847	17.695	0.0897		0.840
Sample No. K2A,	15.124	30.248	0.217	1832	1.188
Nitrogen,	15.128	30.257	0.218		1.190
Low Pressure	15.143	30.286	0.217		1.186
Flow Method,					
$T_s(av) = 25^oC.$					

Sample time Δt = 1 min

Comments: These two low pressure flow experiments showed that the values of K differed from the K-p_m plot obtained in Detmn. No. L:33 by less than 0.05 cm^2/sec (5%), which was the maximum scatter observed in Detmn. No. L:33. The flow-rate remained almost constant with time, varying by much less than ± 1%.

- - - - - - - -

Determinaion No. L:35

Details	p_m cm Hg	Δp cm Hg	dp_o/dt mm/sec x 10^4	V_o cm^3	K cm^2/sec x 10^3	ϕ min
Morgan "EY9"	38.200	76.050	9.79	1832	11.50	1.38
Graphite,	29.770	59.290	6.98	1832	10.55	1.50
Sample No. K23,	23.770	47.354	5.20	1832	9.81	1.62
Nitrogen,	17.690	35.249	3.59	1832	9.11	1.55
Pressure	11.590	23.107	2.14	1832	8.30	1.52
Increase	4.794	9.522	1.96	741	7.44	1.80
Method,	2.267	4.500	0.92	741	7.40	2.15
$\mathcal{T}_{s(av)}$ =	0.975	1.935	0.404	741	7.55	2.10
26.1°C.	0.428	0.850	0.195	741	8.27	5.0
	0.152	0.303	0.0857	741	10.23	7.0

$K = 0.000122\ p_m + 0.00690$

Comments: The measured blank rate was about 0.5×10^{-6} mm Hg/sec. The experiments were continued for about an hour, and straight p_o-t plots were obtained. The K-p_m plot was straight with a definite minimum at $p_m = 2.5$ cm Hg; the scatter of the K values about the plot was $\pm 0.05 \times 10^{-3}$ cm^2/sec (½%). The outlet volume V_o was decreased during the determination so that the rate of pressure increase did not become too slow. Time-lags ranging between 1.4 and 7.0 min were observed.

Determination No. L:36

Details	p_m cm Hg	Δp cm Hg	$\Delta p_o/\Delta t$ cm/min x 10^3	V_o cm^3	K cm^2/sec x 10^3
Morgan "EY9"	22.926	45.851	7.57	741	9.97
Graphite,	23.122	46.245	3.06	1832	9.88
Sample No. K23,	10.913	21.827	3.05	741	8.43
Nitrogen,	10.939	21.877	3.07	741	8.47
Low Pressure Flow	10.951	21.902	3.05	741	8.41
Method,					
$\mathcal{T}_{s(av)}$ = 27.7°C.					

Sample time Δt = 10 min

Comments: These two low pressure flow experiments showed that the K values at both p_m were about 2% higher than the K-p_m plot obtained in Detmn. No. L:35 by the pressure increase method (cf. Detmn. No. L:31). The flow-rate in each experiment remained almost constant with time after the first flow measurement was made at about t = 1 hr.

- - - - - - - -

Determination No. L:37

Details	p_m cm Hg	Δp cm Hg	dp_o/dt mm/sec x 10^5	V_o cm^3	K cm^2/sec x 10^3	ϕ min
Morgan "EY9"	18.141	36.012	75.3	741	7.54	2.07
Graphite,	14.305	28.390	56.5	741	7.16	2.18
	10.189	20.237	37.4	741	6.71	2.24
Sample No. K23,	6.445	12.803	22.2	741	6.32	2.34
	2.935	5.836	9.63	741	6.00	3.14
Argon,	1.185	2.355	4.01	741	6.17	3.30
	0.406	0.809	1.30	741	5.83	3.90
Pressure Increase	0.794	1.571	2.60	741	6.00	3.50
Method,	0.168	0.337	0.512	741	5.51	5.50
*	0.167	0.305	0.544	741	6.45	2.00
$\mathcal{T}_s$(av) = 25.0°C.	0.069	0.136	0.228	741	6.10	9.70

* p_o initially 10^{-2} mm Hg instead of 10^{-5} mm Hg.

$$K = 0.000103\ p_m + 0.00568$$

Comments: Experiments were generally conducted for about an hour, although the experiments at the lowest pressures, where the initial p_i was measured with the McLeod gauge, were continued for a longer time. The p_o-t plots were straight and indicated time-lags from 2 to 10 min. The blank degassing rate was about 0.5×10^{-6} mm Hg/sec. The K values were scattered about the K-p_m plot by less than 2.5×10^{-5} cm^2/sec (0.6%). Although the very low pressure points were much more scattered, a minimum was observed in the K-p_m plot at about p_m = 1 cm Hg with five of the six points lying above the straight plot. Several of these low pressure K values were inaccurate because the p_o values were measured on an inaccurate portion of the McLeod gauge scale; the initial p_o was increased from 10^{-5} mm Hg to 1×10^{-2} mm Hg for one experiment to overcome this difficulty.

Determination No. L:38

Details	p_m cm Hg	Δp cm Hg	dp_o/dt mm/sec x 10^4	V_o cm^3	K cm^2/sec x 10^2	ϕ min
Morgan "EY9"	14.833	29.503	4.54	1804	1.70	1.47
Graphite,	10.511	20.913	3.03	1804	1.60	1.42
Sample No. K21,	6.728	13.378	1.81	1804	1.49	1.40
Argon,	2.761	5.498	0.723	1804	1.45	2.00
Pressure	1.108	2.192	0.708	713	1.41	2.30
Increase	0.378	0.748	0.259	713	1.51	3.80
Method,	0.167	0.334	0.124	713	1.62	7.50
$\mathcal{T}_s$(av) =	4.181	8.327	1.10	1804	1.46	1.78
26.9°C. *	3.801	7.518	2.43	713	1.42	1.30

* p_o initially 2.1×10^{-3} mm Hg instead of 10^{-5} mm Hg

$$K = 0.000246\ p_m + 0.0134$$

Comments: The degassing rate was about 0.3×10^{-6} mm Hg/sec. Straight p_o-t plots were observed with time-lags ranging from 1.3 to 7.5 min. The scatter of the K values about the K-p_m plot was ± 0.0002 cm^2/sec (± 1.3%), with one value deviating by 0.0004 cm^2/sec; the scatter of the points at low pressures led to some inaccuracy in the values of B_o and K_o. A minimum was obtained at about p_m = 2 cm Hg.

Determination No. L:39

Details	p_m cm Hg	Δp cm Hg	dp_i/dt cm/hr	V_i cm^3	K cm^2/sec
Acheson "A" Graphite, Sample No. K2A, Argon, Pressure Decay Method, $\mathcal{T}_s$ (av) = 26.3°C.	30.0	60	10.39	7529	1.97
	27.5	55	8.55	7527	1.77
	25.0	50	6.87	7525	1.56
	22.5	45	5.67	7523	1.43
	20.0	40	4.53	7521	1.29
	17.5	35	3.35	7519	1.087
	15.0	30	2.59	7517	0.980
	12.5	25	1.88	7515	0.854
	10.00	20.0	6.17	1466	0.683
	7.50	15.0	4.03	1463	0.594
	5.00	10.0	2.17	1461	0.479
	4.00	8.0	1.47	1461	0.407
	3.00	6.0	3.85	369	0.357
	2.00	4.0	2.33	368	0.324
	1.50	3.0	1.45	367	0.268
	1.00	2.0	0.95	367	0.264
	0.50	1.0	2.05	71.9	0.223
	0.25	0.5	0.97	71.7	0.213

$$K = 0.0509\ p_m + 0.206$$

Comments: The pressure p_i decayed from 76 cm Hg to 0.2 cm Hg in 18½ hr. Below p_m = 15 cm Hg, the K-p_m plot (equation given above) was straight and the scatter of the K values about the plot was less than ± 0.03 cm^2/sec. Above p_m = 15 cm Hg, the K values tended to be high and the plot curved upwards. Faulty experimental technique or a leak from the inlet side of the apparatus possibly caused this upward curvature of the K-p_m plot at high p_m.

Determination No. L:40

Details	p_m cm Hg	Δp cm Hg	dp_i/dt cm/hr	V_i cm^3	K cm^2/sec
Acheson "A" Graphite, Sample No. K5, Argon,	32.5	65	18.73	7536	3.11
	30.0	60	16.55	7533	2.98
	27.5	55	13.73	7531	2.70
	25.0	50	11.60	7529	1.51
	22.5	45	9.66	7527	2.32
	20.0	40	7.59	7525	2.05
	17.5	35	6.31	7523	1.95

Details	p_m cm Hg	Δp cm Hg	dp_i/dt cm/hr	V_i cm^3	K cm^2/sec
Pressure Decay Method,	15.0	30	4.71	7521	1.69
	12.5	25	3.55	7519	1.53
	10.00	20.0	2.31	7517	1.24
$\mathcal{T}_s$ (av) = 24.40C.	7.50	15.0	6.72	1462	0.941
	5.00	10.0	3.52	1461	0.7 38
	4.00	8.0	2.49	1461	0.652
	3.00	6.0	1.76	1460	0.614
	2.00	4.0	3.63	368	0.479
	1.50	3.0	2.45	367	0.430
	1.00	2.0	1.48	367	0.389
	0.50	1.0	3.30	71.9	0.340

$K = 0.0952\ p_m + 0.281$

Comments: In 13½ hr, p_i decreased from 70 cm Hg to 1.0 cm Hg. The K-p_m plot was linear below p_m = 17 cm Hg, but curved downwards at higher mean pressures. The maximum scatter of the experimental points about this graph was ± 0.07 cm^2/sec.

- - - - - - - -

Determination No. L:41

Details	p_m cm Hg	Δp cm Hg	dp_i/dt cm/hr	V_i cm^3	K cm^2/sec
Acheson "A" Graphite,	30.0	60	20.75	7043	3.50
	27.5	55	17.80	7041	3.28
	23.8	47.5	13.50	7038	2.88
Sample No. K5,	20.0	40	9.91	7035	2.51
	17.5	35	7.97	7033	2.30
Nitrogen,	15.0	30	5.99	7031	2.02
	12.5	25	4.24	7029	1.71
Pressure Decay Method,	10.00	20.0	2.81	7026	1.42
	7.50	15.0	1.76	7024	1.185
$\mathcal{T}_s$ (av) = 24.8°C.	5.00	10.0	4.35	1461	0.914
	4.00	8.0	3.04	1460	0.798
	3.00	6.0	2.18	1460	0.762
	2.50	5.0	1.53	1459	0.642
	1.50	3.0	2.94	367	0.518
	1.00	2.0	1.73	367	0.456
	0.50	1.0	0.80	366	0.421

$K = 0.1095\ p_m + 0.364$

Comments: In this determination, p_i decreased from 76 cm Hg to 0.1 cm Hg in about 14 hr. The K-p_m plot was straight below p_m = 20 cm Hg, but curved downwards above this pressure. The maximum scatter of the values of K about the plot was ± 0.05 cm^2/sec.

- - - - - - - -

Determination No. L:42

Details	p_m cm Hg	Δp cm Hg	dp_1/dt cm/hr	V_1 cm3	K cm^2/sec
Acheson "A"	32.5	65	27.25	7045	4.26
Graphite,	30.0	60	23.50	7043	3.98
	27.5	55	20.35	7041	3.75
Sample No. K4,	25.0	50	16.85	7039	3.42
	22.5	45	13.83	7037	2.12
Nitrogen,	20.0	40	11.06	7035	2.80
	17.5	35	8.90	7033	2.58
Pressure Decay	15.0	30	6.83	7031	2.31
Method,	12.5	25	4.87	7029	1.97
	10.00	20.0	3.46	7026	1.75
$\mathcal{T}_s$ (av) = 24.0°C.	7.50	15.0	1.98	7024	1.34
	5.00	10.0	4.96	1461	1.044
	4.00	8.0	3.39	1460	0.892
	3.00	6.0	2.32	1460	0.812
	2.00	4.0	2.46	755	0.670
	1.50	3.0	1.58	755	0.573
	1.00	2.0	0.94	754	0.511
	0.50	1.0	0.41	754	0.445

$K = 0.1337\ p_m + 0.375$

Comments: The inlet pressure p_1 decayed from 74 cm Hg to 1.0 cm Hg in 14 hr. The values of K were scattered about the K-p_m plot by less than ± 0.05 cm^2/sec. The plot commenced curving downwards at p_m = 10 cm Hg after being linear below this pressure. - - - - -

Determination No. L:43

Details	p_m cm Hg	Δp cm Hg	dp_o/dt mm/sec x 10^4	V_o cm3	K cm^2/sec x 10^2	ϕ min
Morgan "EY9"	4.144	8.208	1.88	1832	1.760	1.00
Graphite,	1.478	2.902	1.55	741	1.660	1.20
Sample No. K24,	0.299	0.582	0.325	741	1.740	2.00
Nitrogen,	7.459	14.774	3.51	1832	1.835	0.75
Pressure	12.557	24.828	6.41	1832	1.991	0.51
Increase	17.077	33.788	9.46	1832	2.156	0.82
Method,	21.430	42.460	12.56	1832	2.277	0.54
$\mathcal{T}_s$(av) = 22.0°C.						

$K = 0.000309\ p_m + 0.0162$

Comments: The values of K were scattered about the K-p_m plot by ± 1.5 x 10^{-4} cm^2/sec (less than ± 1%). A minimum was indicated in the plot at about p_m = 0.8 cm Hg. Experiments were generally of an hour's duration and gave time-lags from 0.5 to 2.0 min. The blank rate was 1 x 10^{-6} mm Hg/sec.

- - - - - - - -

Determination No. L:44

Details	p_m cm Hg	Δp cm Hg	dp_o/dt mm/sec x 10^4	V_o cm^3	K cm^2/sec x 10^2	ϕ min
Morgan "EY9"	1.442	2.769	2.75	713	4.36	0.48
Graphite,	0.190	0.359	0.375	713	4.59	1.14
Sample No. K21,	3.793	7.456	2.99	1804	4.94	0.33
Helium,	(7.910	(15.589	(6.43	1804	(4.58	0.40
Pressure	(7.891	(15.251	(6.30		(4.59	
Increase	12.958	25.557	10.90	1804	4.74	0.49
Method,	15.715	31.050	13.40	1804	4.80	0.47
$\mathcal{T}_s$(av) = 19.7°C.	9.890	19.459	8.09	1804	4.63	0.40

$K = 0.000313\ p_m + 0.0432$

Comments: Some of the p_o-t plots for this determination were slightly curved; time-lags were between 0.4 and 1.1 min. The blank rate was 0.06×10^{-6} mm Hg/sec. The K-p_m plot was straight with the values of K being scattered by less than $\pm 1.5 \times 10^{-4}$ cm^2/sec (± 0.35%). A minimum was observed at about p_m = 1 cm Hg.

- - - - - - - -

Determination No. L:45

Details	p_m cm Hg	Δp cm Hg	dp_o/dt mm/sec x 10^4	V_o cm^3	K cm^2/sec x 10^3	ϕ min
Morgan "EY9"	2.499	4.958	0.872	713	7.71	3.6
Graphite,	0.777	1.540	0.267	713	7.61	5.5
Sample No. K21,	0.281	0.560	0.0352	1804	6.98	8.0
Xenon,	4.170	8.280	1.50	713	7.95	3.3
Pressure	7.154	14.208	2.84	713	8.79	3.3
Increase	12.695	25.171	5.91	713	10.30	2.9
Method,	18.625	37.100	3.89	1804	11.65	2.4
$\mathcal{T}_s$(av) = 17.6°C.	16.240	32.361	3.24	1804	11.14	2.5
	* 1.389	2.649	0.446	713	7.40	5.35
	** 0.273	0.481	0.078	713	7.13	- 5.1

* p_o initially 0.488 mm Hg
** p_o initially 0.291 mm Hg

$K = 0.000258\ p_m + 0.00693$

Comments: The measured degassing rate was 0.07×10^{-6} mm Hg/sec. Time-lags ranged from 2.4 to 8.0 min. Above p_m = 4 cm Hg, the K values were scattered about the K-p_m plot by less than ± 0.0001 cm^2/sec (about ± 1%); below this pressure, four of the five experimental points deviated from the plot by up to +0.0002 cm^2/sec, while the fifth point was 0.0005 cm^2/sec high. Although these low pressure points indicated that the plot tended to flatten out, there was no definite evidence of a minimum. Additional experiments performed at low pressures with the initial p_o greater than zero did not elucidate the nature of the low pressure deviation from the K-p_m plot.

- - - - - - - -

Determination No. L:46

Details	p_m cm Hg	Δp cm Hg	dp_o/dt mm/sec x 10^4	V_o cm^3	K cm^2/sec x 10^2	ϕ min
Morgan "EY9"	8.288	16.236	9.27	1804	6.39	0.29
Graphite,	8.301	16.262	(9.44 9.51	1804	(6.45 6.50	0.29
Sample No. K21, Hydrogen, Pressure	4.008	7.856	(4.32 4.37	1804	(6.11 6.19	0.13
Increase	4.908	9.609	5.40	1804	6.24	0.22
Method,	12.136	23.896	14.40	1804	6.68	0.29
$J_s(av)$ = 18.1°C.	(1.917	(3.835	(2.05	1804	(5.93	0.08
	(1.912	(3.676	(2.00		(6.04	
	(0.762	(1.524	(1.97	713	(5.68	-
	(0.784	(1.413	(1.91		(5.93	
	(0.276	(0.552	(0.783	713	(6.22	0.72
	(0.282	(0.505	(0.670		(5.82	
	(0.230	(0.461	(0.661	713	(6.30	0.90
	(0.235	(0.429	(0.574		(5.88	
	(0.240	(0.400	(0.553		(6.07	

$K = 0.000675\ p_m + 0.0587$

Comments: For this determination, the p_o-t plots were curved, especially for the experiments at the lowest pressures; values of dp_o/dt were obtained at several points on each curved plot and values of K calculated using the appropriate values of p_i and p_o. The scatter of the K values about the K-p_m plot above p_m = 1 cm Hg was ± 0.0007 cm^2/sec (± 1.1%). Below this pressure, the values of K at any p_m varied by about 7% due to the curved p_o-t plots but did indicate that a minimum occurred in the K-p_m plot at about p_m = 0.7 cm Hg. Time-lags were small (less than 1.0 min). The degassing rate was 0.07 x 10^{-6} mm Hg/sec. - - - -

Determination No. L:47

Details	p_m cm Hg	Δp cm Hg	dp_o/dt mm/sec x 10^4	V_o cm^3	K cm^2/sec x 10^3	ϕ min
Morgan "EY9"	3.015	5.982	1.16	713	8.53	3.8
Graphite,	1.255	(2.500	(0.481	713	(8.43	5.4
Sample No. K21,		(2.480	(0.449		(7.93	
Freon-12,	0.272	0.538	0.0941	713	7.70	7.15
Pressure	5.570	11.057	2.45	713	9.73	3.2
Increase	7.661	15.263	1.46	1804	10.62	2.6
Method,	10.998	21.900	2.43	1804	12.33	2.9
$J_s(av)$ =	13.099	26.088	3.14	1804	13.33	2.7
18.8°C.	0.573	1.139	0.204	713	7.88	5.8

$K = 0.000477\ p_m + 0.00706$

Comments: The degassing rate was 0.025 x 10^{-6} mm Hg/sec. The scatter of the K values about the straight K-p_m plot was less than ± 5 x 10^{-5} cm^2/sec (about ± 0.5%). Below about p_m = 2 cm Hg, the plot tended to flatten out even though some variation of the K values was obtained in this region because of the slightly curved p_o-t plots. The time-lags ranged from 2.6 to 7.2 min. - - - - - - - -

Determination No. L:48

Details	p_m cm Hg	Δp cm Hg	dp_i/dt cm/hr	V_i cm^3	K cm^2/sec x 10^2
Morgan "EY9"	13.0	26	2.54	391.7	6.55
Graphite,	12.0	24	2.30	390.9	6.41
	11.0	22	2.09	390.1	6.34
Sample No. K21,	9.0	18	1.67	388.4	6.17
	8.0	16	1.48	387.5	6.13
Hydrogen,	6.5	13	1.19	386.3	6.05
	5.0	10	3.76	90.5	5.82
Pressure Decay Method,	4.0	8	3.00	89.7	5.76
	3.5	7	2.60	89.2	5.67
$\mathcal{T}_s$(av) = 18.7°C.	2.5	5	1.88	88.4	5.69
	1.5	3	1.00	87.6	5.00
	1.0	2	0.59	87.1	4.40

$$K = 0.000838\ p_m + 0.0543$$

Comments: This determination was performed to observe whether a minimum could be obtained for Morgan "EY9" Graphite by the pressure decay method; hydrogen was used since this gas would flow faster and reach equilibrium conditions at any pressure more quickly than the other gases. The pressure p_i decayed from 27.7 cm Hg to 0.5 cm Hg in 21 hr. The K values were considerably scattered because of the inaccuracy of the calculating method, the maximum variation about the K-p_m plot above p_m = 2 cm Hg being ± 0.002 cm^2/sec (about ± 3½ %). Below p_m = 2 cm Hg, no minimum was obtained as the K values rapidly became smaller as p_m decreased; it was suspected, however, that the experimental technique was faulty in this low pressure range. The K-p_m plot was about 0.004 cm^2/sec (4 to 6%) lower than the plot obtained in Detmn. No. L:46 by the pressure increase method. - - -

Determination No. L:49

Morgan "EY9" Graphite,
Sample No. K21, Carbon Dioxide, Pressure Increase Method,
$\mathcal{T}_s$ (av) = 18.2°C.

The details of this determination are included in Appendix C.2.2 as a typical example of a pressure increase permeability measurement.

$$K = 0.000385\ p_m + 0.0121$$

- - - - - - - -

Determination No. L:50

Details	p_m cm Hg	Δp cm Hg	dp_1/dt cm/hr	V_1 cm^3	K cm^2/sec
Acheson "A" Graphite,	18.75	37.5	11.30	8119	3.70
	17.50	35.0	10.12	8117	3.55
	15.00	30.0	7.89	8115	3.23
Sample No. K2A,	12.50	25.0	6.27	8113	3.08
	10.00	20.0	4.37	8111	2.68
Hydrogen,	7.50	15.0	2.82	8109	2.30
	6.00	12.0	2.06	8108	2.10
Pressure Decay	5.00	10.0	1.50	8107	1.84
Method,	4.50	9.0	1.33	8107	1.81
	3.00	6.0	3.22	1847	1.50
$\mathcal{T}_s$(av) = 18.8°C.	2.50	5.0	2.62	1847	1.46
	1.50	3.0	1.28	1846	1.19
	1.00	2.0	0.786	1845	1.10
	0.75	1.50	0.607	1845	1.13
	0.50	1.00	0.377	1845	1.05
	0.25	0.50	0.198	1845	1.10
	0.20	0.40	0.147	1845	1.02

$K = 0.1760\ p_m + 0.982$

Comments: In this determination, 16½ hr were required for p_i to decrease from 44 cm Hg to 0.3 cm Hg. The K-p_m plot was linear up to about p_m = 8 cm Hg, but curved downwards at higher p_m. The scatter of the values of K about the plot was less than ± 0.05 cm^2/sec.

- - - - - - - -

Determination No. L:51

Details	p_m cm Hg	Δp cm Hg	dp_1/dt cm/hr	V_1 cm^3	K cm^2/sec
Acheson "A" Graphite,	18.0	26.0	12.97 12.42	1860	1.013 0.970
	16.0	32.0	9.90	1858	0.869
Sample No. K2A,	14.0	28.0	8.41	1856	0.843
	12.0	24.0	6.28 6.08	1855	0.734 0.711
Pressure Decay Method,	10.0	20.0	4.48	1853	0.628
	8.0	16.0	3.18	1851	0.556
Xenon,	6.0	12.0	1.94	1850	0.453
	5.0	10.0	1.32	1849	0.369
$\mathcal{T}_s$ (av) = 18.6°C.	4.0	8.0	0.970	1848	0.339
			2.29	757	0.328
	3.0	6.0	1.51	756	0.288
	2.0	4.0	0.790	755	0.226
	1.5	3.0	0.551	755	0.210
	1.25	2.5	0.425	755	0.194
	1.0	2.0	0.318	754	0.181

$K = 0.0528\ p_m + 0.127$

Comments: About 16 hr were required for pi to decrease from 36 cm Hg to 2 cm Hg. The xenon was recovered from the outlet

side of the sample by freezing it into trap Q so that p_o remained less than 0.01 cm Hg throughout the determination. The K-p_m plot was straight up to p_m = 9 cm Hg with a maximum scatter of the values of K about the plot of ± 0.02 cm^2/sec. Above this pressure, the plot curved downwards and greater scatter (± 0.04 cm^2/sec) was observed.

Determination No. L:52

Details	p_m cm Hg	Δp cm Hg	dp_o/dt mm/sec x 10^4	V_{o_3} cm^3	K cm^2/sec	ϕ min
Acheson "A"	2.172	4.332	10.5	1832	0.241	0.01
Graphite,	2.154	4.000	9.75		0.243	
	2.144	3.684	8.70		0.235	
					0.240 av.	
Sample No. K2A,						
	0.815	1.627	2.80	1832	0.172	0.11
Xenon,	0.810	1.520	2.65		0.174	
	0.806	1.419	2.50		0.176	
					0.174 av.	
Pressure						
Increase	0.334	0.666	2.35	741	0.142	0.24
Method,	0.350	0.537	2.04		0.153	
					0.147 av.	
$\mathcal{T}_s$(av) =	0.162	0.323	1.130	741	0.141	0.74
16.9°C.	0.168	0.273	0.946		0.140	
	0.023	0.045	0.154	741	0.137	2.14

Comments: In order to observe whether a minimum was obtained in the K-p_m plot for xenon flow through Acheson "A" graphite at pressures lower than could be investigated by the pressure decay method (Detmn. No. L:51), this determination was performed by means of the pressure increase method. The p_o-t plots were curved (cf. Detmn. No. L:18) and values of K were calculated at several points during each experiment. The K-p_m plot was identical with that of Detmn. No. L:51 at the lowest mean pressures; no minimum was observed above p_m = 0.023 cm Hg. Time-lags were observed but were generally small and difficult to measure.

Determination No. L:53

Acheson "A" Graphite, Sample No. K2A,
Carbon Dioxide, Pressure Decay Method, $\mathcal{T}_s$ (av) = 16.6°C.

The details of this determination are included in Appendix C.3.2 as the type calculation for pressure decay permeability measurements.

$$K = 0.0810\ p_m + 0.230$$

Determination No. L:54

Details	p_m cm Hg	Δp cm Hg	dp_i/dt cm/hr	V_i cm^3	K cm^2/sec
Acheson "A"	12.50	25.0	11.50	1855	1.289
Graphite,	10.00	20.0	7.42	1853	1.038
	7.50	15.0	4.47	1851	0.833
Sample No. K2A,	6.25	12.5	3.51	1850	0.784
	5.00	10.0	2.18	1849	0.609
Freon-12,	4.50	9.0	1.83	1848	0.567
	4.00	8.0	1.38	1848	0.481
Pressure Decay	3.00	6.0	2.26	756	0.430
Method,	2.00	4.0	1.21	755	0.345
	1.50	3.0	0.770	755	0.293
$\mathcal{T}_s$ (av) = 16.5°C.	1.00	2.0	0.432	754	0.246
	0.75	1.5	0.306	754	0.232
	0.50	1.0	0.156	754	0.178

$K = 0.0901\ p_m + 0.159$

Comments: During this determination, p_o was maintained at a low value by freezing out the freon in trap Q. In 13 hr, p_i decayed from 27 cm Hg to 1 cm Hg. Within the mean pressure range of the determination, no curvature of the K-p_m plot was observed. The maximum scatter of the values of K about the plot above p_m = 5 cm Hg was ± 0.05 cm^2/sec; below this pressure, the scatter was less (± 0.02 cm^2/sec).

Determination No. L:55

Details	p_m cm Hg	Δp cm Hg	dp_o/dt mm/sec x 10^4	V_o cm^3	K cm^2/sec x 10^4	ϕ min
Impregnated	2.797	5.595	5.43	1851	4.29	0.6
Graphite,	2.794	5.164	5.08		4.35	
	0.475	0.951	1.067	1851	4.95	1.3
Sample No. K42,	0.490	0.853	0.854		4.41	
	0.188	0.376	1.103	760	5.32	1.9
Hydrogen,	0.220	0.309	0.935		5.48	
	4.557	9.114	0.873	1851	4.23	0.7
Pressure	4.476	8.799	0.855		4.29	
Increase	7.272	14.545	14.2	1851	4.31	0.7
Method,	9.131	18.263	18.0	1851	4.35	0.7
	1.504	3.008	2.84	1851	4.17	0.6
$\mathcal{T}_s$(av) = 16.8°C.	1.505	2.859	2.65		4.10	

$K = 1.99 \times 10^{-6}\ p_m + 4.18 \times 10^{-4}$

Comments: The degassing rate was 0.6 x 10^{-6} mm Hg/sec. Below p_m = 5 cm Hg, the p_o-t graphs were curved; above p_m = 1 cm Hg, the variation between the two values of K calculated at any p_m was about 0.07 x 10^{-4} cm^2/sec, but below p_m = 1 cm Hg, the variation was greater. Nevertheless, a straight K-p_m plot was obtained with a scatter of ± 0.1 x 10^{-4} cm^2/sec (± 2.3%) and a minimum was observed at about p_m = 1.2 cm Hg. Time-lags ranged between 0.6 and 1.9 min. Pressure increase experiments were not possible above p_m = 10 mm Hg as p_o then reached the limit of the McLeod gauge after about 30 min.

Determination No. L:56

Details	p_m cm Hg	Δp cm Hg	dp_o/dt mm/sec x 10^4	V_o cm3	K cm^2/sec x 10^5	ϕ min
Impregnated Graphite,	14.204	27.779	2.94	1851	4.67	142
	8.641	16.490	3.82	773	4.27	180
Sample No. K42,	4.204	8.194	0.712	1864	3.86	235
Xenon,	1.590	2.939	0.536	760	3.32	274
Pressure Increase	15.563	30.337	3.43	1851	4.99	142
Method,						

$\mathcal{T}_s$(av) = 18.5°C.

$$K = 1.065 \times 10^{-6}\ p_m + 0.328 \times 10^{-5}$$

Comments: In this determination, the observed time-lags were extremely high (142 to 274 min), while the time to reach steady equilibrium flow was about 5 hr for the experiments at the highest p_m and about 10 hr when p_m = 1.59 cm Hg. Because of the length of time required for these experiments (11½ hr maximum), they were only continued until an apparently straight p_o-t plot was obtained or p_o was beyond the range of the McLeod gauge. Thus, for some experiments, the value obtained for dp_o/dt might not have been the equilibrium flow value; the observed scatter of ± 0.1 x 10^{-5} cm^2/sec (± 2 to 3%) of the values of K about the K-p_m plot resulted from this inaccuracy. There was no evidence of a minimum in the K-p_m plot above p_m = 1.59 cm Hg. The blank rate of 4 x 10^{-6} mm Hg/sec was high as difficulty was encountered in reducing the xenon pressure in the apparatus. - - - - -

Determination No. L:57

Details	p_m cm Hg	Δp cm Hg	dp_o/dt mm/sec x 10^4	V_o cm3	K cm^2/sec x 10^4	ϕ min
Impregnated Graphite,	1.005	1.873	3.32	760	3.20	1.20
	1.028	1.749	3.06		3.16	
Sample No. K42,	0.482	0.900	1.52	760	3.05	1.40
Helium,	0.498	0.871	1.46		3.03	
Pressure	0.198	0.382	0.667	760	3.15	1.70
Increase Method,	0.204	0.335	0.546		2.94	2.15
$\mathcal{T}_s$ (av) =	2.845	5.490	3.92	1851	3.14	0.40
20.1°C.	4.777	9.218	6.62	1851	3.16	0.48
	7.338	14.317	10.40	1851	3.20	0.75
	9.424	18.468	13.52	1851	3.22	0.64
	0.655	1.235	2.17	760	3.17	0.70
	0.630	1.109	1.94		3.16	

$$K = 1.26 \times 10^{-6}\ p_m + 3.10 \times 10^{-4}$$

Comments: The degassing rate was 0.3 x 10^{-6} mm Hg/sec, and slightly curved p_o-t graphs were obtained in this determination. The scatter of the values of K about the K-p_m plot above p_m = 2.5 cm Hg was only ± 0.2%, but was greater (± 3%) below this pressure. For the experiments at p_m = 0.49 and 0.20 cm Hg,

a leak into the inlet volume was suspected; the resulting low values of K meant that there was insufficient evidence for a minimum in the K-p_m plot at low pressures. Time-lags ranged from 0.4 to about 2 min.

- - - - - - - -

Determination No. L:58

Details	p_m cm Hg	Δp cm Hg	dp_Q/dt mm/sec x 10^4	V_Q cm^3	K cm^2/sec x 10^4	ϕ min
Impregnated Graphite,	16.054	31.761	7.49	1851	1.039	10.7
Sample No. K42,	9.970	19.674	4.45	1851	0.998	10.2
Argon,	4.933	9.747	2.13	1851	0.970	10.9
Pressure Increase Method,	1.997	3.940	0.835	1851	0.936	9.7
$\mathcal{T}_{s(av)}$ = 23.1°C.	0.410	0.780	0.408	760	0.945	9.9

$$K = 0.702 \times 10^{-6}\ p_m + 0.928 \times 10^{-4}$$

Comments: The scatter of the values of K about the K-p_m plot was ± 0.01 x 10^{-4} cm^2/sec (± 1%). There was no definite evidence of a minimum in the plot above p_m = 0.41 cm Hg. The observed degassing rate for these experiments was 0.04 x 10^{-6} mm Hg/sec and time-lags were between 9.7 and 11 min.

- - - - - - - -

K.3 The High Pressure Determinations

Determination No. H:1

From calibration measurements performed in the high pressure apparatus, values of K for nitrogen flow through Acheson "A" Cylinder No. K6 were calculated for p_m between 20 and 105 cm Hg and p_o either about 1 atm or a vacuum. For p_m = 100 cm Hg and p_o about 86 cm Hg, K = 9.25 cm^2/sec; however, for p_o less than 1 atm, the values of K were much lower than the K-p_m plot obtained for p_o greater than 1 atm. Because some quantities were not measured accurately, the values of K were approximate and served only as a guide for further determinations.

- - - - - - - -

Determination No. H:2

Permeability coefficients were determined in the high pressure apparatus for nitrogen flow through Acheson "A" Cylinder No. K7 for p_m between 80 and 136 cm Hg and p_o greater than 76 cm Hg. The measured pressures were corrected for the pressure losses in the apparatus (section 3.1.4.1). Between p_m = 90 cm Hg and 130 cm Hg, the plot of K against p_m was linear with an intercept on the K-axis of 2.57 cm^2/sec. However, at lower p_m, the values of K were about 5% higher than the K-p_m plot; when the outlet flow was restricted so that p_o increased, the values of K were about 13% high. Since it was difficult to make the seals in the sample holder (type (e)) leakproof, the results were of questionable accuracy.

Determination No. H:3

Details	p_m cm Hg	Δp cm Hg	Q_a cm^3/sec	K cm^2/sec	p_o cm Hg	N_{Re}	f
	187	118.5	2.52	8.83	127.7		
Acheson	142	132	2.23	7.01	76.0	0.052	18.4
	118	84.0	1.248	6.17	76.0		
"A"	126	87.5	1.39	6.57	81.8	0.0327	27.7
	95.0	139	1.68	5.05	25.4		
Graphite,	103	125	1.61	5.39	40.1		
	161	165	2.98	7.59	78.3	0.0692	14.5
Sample	193	228	4.70	8.70	78.9		
	201	244	5.06	8.74	79.0	0.117	9.16
No. K2A,	208	257	5.33	8.73	79.1		
	224	288	6.36	9.28	79.2		
Nitrogen,	231	303	6.62	9.19	79.3		
	232	241	5.62	9.82	111.0		
High	219	219	5.01	9.53	109.2		
	210	202	4.49	9.28	108.7		
Pressure	181	144	2.91	8.45	109.7		
	160	102	1.90	7.77	109.2		
Flow	171	125	2.50	8.35	108.7		
	167	73.6	1.49	8.51	130.1		
Method,	177	97.0	2.04	8.84	128.9	0.0471	20.2

$\mathcal{J}_s$ (av) = 16.1°C.

215	175	3.93	9.44	128.1	0.0907	11.9
229	203	4.79	9.93	127.8	0.110	9.93
239	213	5.19	10.23	132.7		
261	267	6.59	10.36	127.2	0.151	7.82
239	322	7.39	9.49	78.1	0.169	6.90
248	339	7.95	9.69	78.2	0.182	6.51
262	366	8.81	9.95	78.4		
274	389	9.60	10.21	78.5	0.219	5.65
290	423	10.60	10.36	78.7		
313	468	12.56	11.09	79.0	0.285	4.55
325	491	13.66	11.50	79.1		
343	528	15.02	11.76	79.4	0.340	3.93
226	295	6.51	9.21	78.5	0.149	7.70
182	208	4.08	8.19	78.2	0.0943	11.10
372	583	17.22	12.33	80.4	0.390	3.57
386	610	18.1	12.40	80.7		
412	662	20.2	12.75	80.2		
434	710	22.2	13.07	79.4	0.500	3.06
458	756	24.7	13.65	79.7	0.555	2.79
294	431	11.06	10.71	78.3		
476	731	24.8	14.17	110.3		
441	666	21.2	13.30	108.3		
399	581	18.0	12.94	108.7		
376	534	16.24	12.69	108.9		
270	322	8.20	10.61	108.7		
290	366	9.67	11.02	107.1		
230	247	5.75	9.55	106.8		
309	406	11.0	11.14	105.8		
328	444	12.65	11.73	106.4		
342	467	13.75	12.11	108.1		
362	508	15.5	12.55	107.9		
422	627	19.8	12.99	108.3		
212	418	8.61	8.52	3.0	0.198	5.84
221	435	9.10	8.69	3.2		
248	489	10.83	9.19	3.8	0.248	5.05
276	544	13.07	9.98	4.4	0.300	4.31
291	573	14.41	10.44	4.7	0.329	3.91
340	667	18.2	11.32	6.0	0.413	3.36
374	734	21.0	11.85	6.8	0.475	3.05
396	778	22.8	12.16	7.2	0.515	2.90
413	810	24.4	12.50	7.8	0.550	2.76
92.5	183	2.20	4.99	0.9	0.0528	17.1
84.7	168	1.87	4.62	0.8	0.045	20.0
110	217	2.91	5.55	1.1	0.0691	13.9
136	268	4.14	6.41	1.5	0.0968	10.4
161	318	5.43	7.09	2.0	0.126	8.53
164	312	5.43	7.22	8.2		
105	137	1.95	5.89	36.8	0.0464	18.6
164	252	4.55	7.46	37.4	0.106	9.56
213	349	7.20	8.55	38.2		
251	427	10.00	9.70	37.2		
305	535	14.3	11.06	37.6		
358	641	18.3	11.82	36.9	0.414	3.36
404	735	21.5	12.08	36.7	0.485	3.14

430	788	24.0	12.61	36.4	0.541	2.88
245	233	5.80	10.28	128.1		
292	330	9.00	11.26	127.0	0.205	5.83
349	442	13.5	12.61	128.3	0.306	4.14
399	540	18.0	13.78	128.9	0.406	3.28
437	620	20.6	13.75	127.5	0.464	3.14
474	692	24.0	14.34	128.3	0.540	2.79
97.5	42.8	0.595	5.74	76.0		
60.2	121.0	1.043	3.57	0.1		
41.6	83.3	0.544	2.70	0.1	0.0143	57.6
82.1	10.0	0.118	4.91	77.1	0.0029	289
68.6	37.4	0.368	4.09	49.9	0.0091	93.0
62.7	49.4	0.449	3.78	38.0	0.0112	75.4
54.0	67.6	0.535	3.29	20.3		
30.7	61.0	0.308	2.10	0.2	0.0086	96.7
49.4	24.1	0.180	3.11	37.4	0.0046	180
18.1	36.1	0.121	1.39	0.1	0.0038	218
72.5	143.3	1.43	4.15	0.9	0.0351	25.2
92.5	111.4	1.38	5.16	36.8	0.0328	26.6
110	66.4	0.986	6.16	76.8	0.0234	36.8
128	36.6	0.636	7.21	110.0	0.0150	56.5
136	22.1	0.411	7.72	124.7	0.0096	87.5
117	8.9	0.149	6.95	112.7		
81.0	86.7	0.968	4.65	37.7		
73.6	102.0	1.040	4.24	22.7	0.0255	34.0
90.2	26.4	0.336	5.30	77.0	0.0081	103
105	56.6	0.814	5.98	77.0		
122	22.4	0.377	7.00	111.0		
143	29.4	0.557	7.88	128.0		
98.2	121.0	1.57	5.38	37.6	0.0375	23.7
121	85.2	1.34	6.56	77.9		

$K_v = 0.058\ p_m + 0.36$ (graphically)

Comments: Altogether about 160 experiments were performed in this determination; only the results of the most reliable experiments are recorded above. Flow-rates were determined by the soap-bubble flow-meter for Q_a between 0.12 and 3.0 cm^3/sec and by the rotameters at higher Q_a.

With the first experiments, a considerable scatter of the K values was observed at any p_m (cf. Detmn. No. H:2). To investigate this variation fully, further experiments were performed for set values of p_o (viz., 0, 37, 78, 109, and 128 cm Hg) and various p_1 between 36 cm Hg and 11 atm (150 p.s.i.g.). Although the adjustment of p_o to an exact value was quite difficult, p_o was kept to within ± 2 cm Hg of the set values for the different experiments. For each p_o value, a separate curved K-p_m plot was obtained. At a given p_m, the value of K increased with increasing p_o. The maximum variation in K at any p_m over the range of p_o from 0 to 128 cm Hg was about 1.2 cm^2/sec (15% at p_m = 150 cm Hg), while the difference between the p_o = 78 cm Hg plot and the p_o = 0 cm Hg plot was about 0.5 cm^2/sec (7%). The scatter of the values of K about any plot was less than ± 0.3 cm^2/sec. Below about

p_m = 100 cm Hg, the plots converged into a single line which agreed quite closely below p_m = 30 cm Hg with the K-p_m plot obtained in Detmn. No. L:33. When the graphs were replotted with Δp as the parameter, the value of K and the slope of the plot both decreased at any p_m as Δp increased.

Determination No. H:4A

Details	p_m cm Hg	Δp cm Hg	Q_a cm³/sec	K cm²/sec x 10^2	N_{Re}	f
Morgan "EY9"	321	490	0.0565	4.34	0.0074	144
	354	556	0.0718	4.86		
Graphite,	378	603	0.0814	5.08		
	411	670	0.0978	5.49		
Sample No. K23,	471	789	0.130	6.17		
	518	883	0.158	6.70	0.0188	53.8
Nitrogen,	585	1018	0.199	7.32		
	632	1110	0.232	7.80	0.0271	38.2
High Pressure Flow	686	1220	0.274	8.40		
	723	1293	0.303	8.78		
Method,	775	1400	0.348	9.32	0.0403	26.3
	851	1550	0.420	10.15		
$\mathcal{T}_s$ (av) = 19.6°C.	547[a]	1094	0.214	7.33		
	614[a]	1230	0.255	7.78		
	674[a]	1347	0.299	8.04		
	737[a]	1470	0.351	8.92		
	809[a]	1620	0.419	9.69		
	474[a]	948	0.157	6.20		
	412[a]	824	0.122	5.55		
	342[a]	684	0.0844	4.67	0.0105	96.1
	421[a]	841	0.125	5.62		
	452[a]	903	0.142	5.95	0.0171	59.5
	555[a]	1109	0.210	7.04		
	627[b]	965	0.196	7.56		
	627[c]	953	0.198	7.73		
	279	406	0.0415	3.81		
Determination No. H:4B[+]						
$\mathcal{T}_s$ (av) = 19.9°C.	294	416	0.0442	4.03		
	180	200	0.0143	2.72		
	144[a]	288	0.0173*	2.28	0.0025	427
	226	289	0.0248	3.23	0.0032	334
	115	76	0.0042	2.06		
	72.0[a]	144	0.0054*	1.41		
	67.3[a]	135	0.0048*	1.34	0.0009	1200
Determination No. H:4C						
$\mathcal{T}_s$ (av) = 25.9°C.	832	1512	0.390	9.68	0.0447	24.4
	969	1790	0.530	11.14		
	1096	2040	0.674	12.40		
	1236	2320	0.848	13.72	0.0958	11.7
	384	615	0.0811	4.95		

524	896	0.158	6.62		
627	1100	0.222	7.57		
967	1780	0.530	11.17	0.0605	17.9
1013	1870	0.584	11.70	0.0666	16.3
1182	2210	0.789	13.39	0.0891	12.3

* Corrected for leakage rate in vacuum lines, 0.003 cm^3/sec.

+ For Detmn. No. H:4B, Q_a has been corrected from the mean pressure in the capillary flow-meter (about 80 cm Hg) to atmospheric pressure.

a p_o = 0 to 0.25 cm Hg
b p_o = 144 cm Hg
c p_o = 150.6 cm Hg
otherwise p_o = 1 atm.

$$K = 0.000119\ p_m + 0.0060 \text{ (graphically)}$$

Comments: Flow-rates were measured by means of the soap-bubble flow-meter except for Detmn. No. H:4B, when the capillary flow-meter was employed. The K-p_m plot was slightly curved, being 0.008 cm^2/sec (7%) lower at p_m = 1000 cm Hg than the extrapolated straight line plot through the low pressure points. The scatter of the values of K about the plot was generally less than ± 0.001 cm^2/sec and certainly less than ± 0.002 cm^2/sec. The K values determined when p_o was not about one atmosphere agreed with the p_o = 1 atm plot. The plot at low mean pressures agreed reasonably well with the plot obtained in Detmn. No. L:35.

Determination No. H:5A

Details	p_m cm Hg	Δp cm Hg	Q_a cm^3/sec	K cm^2/sec x 10^2
Morgan "EY9" Graphite,	344	534	0.190	11.60
	370	588	0.224	12.45
Sample No. K22,	407	660	0.270	13.34
	464	775	0.354	14.94
Nitrogen,	524	895	0.455	16.60
	588	1022	0.555	17.72
High Pressure Flow Method,	651	1150	0.681	19.32
	717	1281	0.829	21.11
$\mathcal{T}_s$ (av) = 19.1°C.	788	1423	1.001	22.94
	804[a]	1607	1.187	24.00
	845	1538	1.168	24.73
	872[b]	1450	1.132	25.43
	332[c]	352	0.114	10.52
	292	431	0.127	9.60
	253[a]	505	0.139*	8.84
	343	535	0.189	11.42
	419	686	0.284	13.38
	528	904	0.461	16.49
	258	366	0.095	8.31
	263[d]	339	0.093	8.78
	683	1215	0.773	20.36
	620[a]	1238	0.721	18.98
	656	1159	0.704	19.84

Determination No. H:5B+

$\mathcal{T}_s$ (av) = 19.8°C.				
	290	384	0.1140	9.65
	174	181	0.0360	6.51
	151	141	0.0257	5.82
	150	139	0.0250	5.78
	121	84	0.0128	4.97
	81.5[a]	163	0.0194*	3.87
	62.2[a]	124	0.0129*	3.37
	119.2	73	0.0110	4.88

Determination No. H:5C

$\mathcal{T}_s$ (av) = 28.3°C.				
	811	1470	1.060	23.47
	963	1775	1.500	27.51
	1058	1963	1.815	30.00
	1216	2280	2.390	34.01

* Corrected for leakage rate in vacuum lines, 0.003 cm^3/sec.

\+ For Detmn. No. H:5B, Q_a has been corrected from the mean pressure in the capillary flow-meter (about 80 cm Hg) to atmospheric pressure.

a p_o = 0 to 0.37 cm Hg
b p_o = 147 cm Hg
c p_o = 156 cm Hg
d p_o = 93 cm Hg
otherwise p_o = 1 atm.

$$K = 0.000285\ p_m + 0.0155 \text{ (graphically)}$$

Comments: Except for Detmn. No. H:5B, when the capillary flow-meter was used, flow-rates were measured by means of the soap-bubble meter. The K-p_m plot was slightly curved as the deviation below the extrapolated low pressure straight line was 0.018 cm^2/sec (6½%) at p_m = 1000 cm Hg. The scatter of the values of K about the plot was less than ± 0.004 cm^2/sec with the values determined when p_o did not equal atmospheric pressure agreeing with the plot for p_o = 1 atm within the experimental scatter. At low p_m (less than 30 cm Hg), the plot was slightly lower than that obtained in Detmn. No. L:24.

- - - - - - - - -

Determination No. H:6

Details	p_m cm Hg	Δp cm Hg	Q_a cm^3/sec	K cm^2/sec x 10^4
Impregnated Graphite,	290	403	0.0692*	3.12
	180	197	0.0275*	2.53
Sample No. K42,	237	303	0.0470*	2.81
	395	638	0.127	3.61
Nitrogen,	392	633	0.124	3.57
	488	825	0.188	4.14
High Pressure Flow Method,	655	1158	0.310	4.86

$\mathcal{T}_s$ (av) = 28.7°C.

* Gas flow-rates were measured by means of the capillary flow-meter in these experiments; the soap-bubble flow-meter was used in the other experiments.

Comments: Values of K determined with p_o a vacuum were 0.25×10^{-4} cm^2/sec (6%) higher than the K-p_m plot for p_o = 1 atm and indicated a small leak in the vacuum system. The sample holder was unfortunately broken while the leak was being located and the determination could not be completed immediately, but was continued later as Detmn. No. H:22.

- - - - - - - -

Determination No. H:7

(see Determination No. H:14)

- - - - -

Determination No. H:8A (No. H:8)

Details	p_m cm Hg	Δp cm Hg	Q_a cm^3/sec x 10^2	K cm^2/sec x 10^5
Impregnated Graphite,	(415 (419	(677 (685	(1.94 (2.00	(5.68 (5.79
Sample No. K41, Argon,	576	1001	3.38	6.70
High Pressure Flow Method,	218	283	0.637	4.46
$\mathcal{J}_s$ (av) = 19.8°C.				

$$K = 0.626 \times 10^{-7} p_m + 3.10 \times 10^{-5}$$

Comments: Because a leak had been discovered in the graphite sample holder (see Detmn. No. H:14), Detmn. No. H:8 was repeated (Detmn. No. H:8A). The straight K-p_m plot was lower than that for the original determination by about 0.3×10^{-5} cm^2/sec (6% at p_m = 300 cm Hg). Flow-rates were measured with the soap-bubble flow-meters and p_o was atmospheric pressure.

- - - - - - - -

Determination No. H:9A (No. H:9)

Details	p_m cm Hg	Δp cm Hg	Q_a cm^3/sec x 10^2	K cm^2/sec x 10^4
Impregnated Graphite,	367	581	6.05	2.06
Sample No. K41,	163	173	1.42	1.63
Hydrogen,	266	380	3.50	1.83
High Pressure Flow Method,	426	701	7.56	2.14
$\mathcal{J}_s$ (av) = 19.2°C.				

$$K = 1.99 \times 10^{-7} p_m + 1.31 \times 10^{-4}$$

Comments: In Detmn. No. H:9, the K values increased by 100% over four days and then remained steady to give a straight K-p_m plot. It was suspected that this variation in the results was due to leakage in the sample holder (see Detmn. No. H:14) and so the determination was repeated (Detmn. No. H:9A). The redetermined K-p_m plot was about 1.8×10^{-5} cm^2/sec (10%) lower than that for Detmn. No. H:9 showing that leakage partially caused the variation of results in Detmn. No. H:9. The scatter of the K values about the plot was less than ± 0.25×10^{-5} cm^2/sec (± 1.0 to 1.5%). Flow-rates were measured with the soap-bubble flow-meter and p_o was kept at atmospheric pressure.

- - - - - - - -

Determination No. H:10

In this determination, carbon dioxide flow through Impregnated Graphite Cylinder No. K41 was investigated by the high pressure flow method. As the maximum gas pressure that could be supplied from the gas cylinder was limited to about 140 p.s.i.g. and the low flow-rates were difficult to measure accurately, considerable scatter of the values of K about the mean K-p_m plot was observed ($\pm$ 0.8 x 10^{-5} cm^2/sec or $\pm$ 13% at p_m = 300 cm Hg). However, the results were in error because of the leak in the sample holder (see Detmn. No. H:14). No repeat determination was possible since the graphite sample was ruined in Detmn. No. H:11A, which was conducted prior to a carbon dioxide repeat determination. Therefore, from the K-p_m plot observed in Detmn. No. H:10, the equation of the plot for carbon dioxide flow in Sample No. K41 for no leakage conditions was estimated to be

$$K = 1.05 \times 10^{-7} p_m + 2.80 \times 10^{-5}.$$

Determination No. H:11A (No. H:11)

Details	p_m cm Hg	Δp cm Hg	Q_a cm^3/sec x 10^3	K cm^2/sec x 10^5	p_m/P_o
Impregnated Graphite, Sample No. K41, Freon-12, High Pressure Flow Method, $\mathcal{T}_s$ (av) = 19.9°C.	244[a]	336	5.13	3.03	0.58
	360[b]	134	0.587 0.415	0.87 0.62	0.85
	366[b]	118	0.963 0.763	1.62 1.28	0.86
	377[b]	98	0.555	1.12	0.89
	259[a]	366	5.97 6.71	3.24 3.64	0.61

a p_o = 76 cm Hg, b p_o 300 cm Hg.

Comments: In Detmn. No. H:11, values of K were determined for p_m between 100 and 220 cm Hg and the scatter about the K-p_m plot was less than $\pm$ 0.25 x 10^{-5} cm^2/sec ($\pm$ 6 to 10%). However, because of the leak found in the sample holder (see Detmn. No. H:14), a repeat determination was commenced (No. H:11A).

Experiments were attempted at high pressures with p/P_o from 0.6 to 0.9 (the saturation vapour pressure p_o of freon-12 at 20°C = 425 cm Hg[250]). When p_m was about 250 cm Hg (p_m/P_o = 0.59), the values of K were approximately 1.5 x 10^{-5} cm^2/sec (30%) lower than the K-p_m plot for Detmn. No. H:11; the equation of the K-p_m plot for no leakage conditions was then estimated to be

$$K = 1.20 \times 10^{-7} p_m + 0.22 \times 10^{-5}.$$

However, with p_1 = 425 cm Hg (p_m about 370 cm Hg, p_m/P_o = 0.87), p_1/P_o was unity and the values of K were only about 20% of those predicted by the above equation. The values of K at any p_m varied by up to 30% because of the difficulty of accurately measuring the low flow-rates.

When the pressure was released and the sample removed from the cell, it was noticed that the sample was covered with a white deposit. On replacement of the sample and reapplication of the pressure, no flow through the graphite was obtained, even when the graphite was heated and when nitrogen pressure (p_1 = 250 p.s.i.g.) or a vacuum was applied to the sample. The sample was apparently blocked and did not permit further permeability determinations.

- - - - - - - -

Determinations No. H:12 and No. H:13

(see Detmn. No. H:14).

- - - - - - - -

Determination No. H:14 (H:7, H:12, and H:13)

Details	p_m cm Hg	Δp cm Hg	Q_a cm^3/sec x 10^2	K cm^2/sec x 10^5
Impregnated Graphite, Sample No. K41,	359	566	(1.905 (1.955	(6.67 (6.85
Nitrogen,	194	235	0.638	5.38
High Pressure Flow Method,	515	877	3.55	8.03
$\mathcal{T}_s$ (av) = 20.0°C.	260	369	(1.115 (1.092	(5.97 (5.89
	638	1124	4.89	8.63
	701	1250	5.66	8.98
	424	696	2.54	7.24
	471	789	2.98	7.49
	(549 (545	(946 (939	(3.87 (3.78	(8.11 (7.98

$$K = 7.15 \times 10^{-8}\ p_m + 4.13 \times 10^{-5}$$

Comments: This determination was a continuation of Detmns. H:7, H:12, and H:13. When the series of Determinations H:7 to H:11 had been completed, Detmn. No. H:7 was repeated (Detmns. H:12 and H:13) in order to observe whether the results were reproducible since the results for hydrogen flow through the sample (Detmn. No. H:9) had varied with time. However the values of K were about 35% higher than the K-p_m plot for Detmn. No. H:7, and showed that a leak had developed in the graphite sample holder. Detmn. No. H:14 was therefore performed when the sample holder was repaired to show if a leak had been present during Detmn. No. H:7. The values of K for Detmn. No. H:14 were scattered about the straight K-p_m plot by less than ± 0.15 x 10^{-5} cm^2/sec (about ± 2%) and agreed quite closely with the plot for Detmn. No. H:7. However, the latter plot was apparently curved downwards below p_m = 400 cm Hg probably because of the scatter of the results and perhaps a small leak.

Only the results of the final determination (No. H:14) are reported above and considered in the discussion. In all the nitrogen flow determinations on Impregnated Graphite Cylinder No. K41, the flow-rate Q_a was measured with the soap-

bubble flow-meters. The outlet pressure p_o was generally atmospheric pressure; the three values of K determined with p_o corresponding to 0 or 225 cm Hg during Detmn. No. H:7 were within experimental scatter of the K-p_m plot for p_o = 1 atm.

- - - - - - - - -

Determination No. H:15

Details	p_m cm Hg	Δp cm Hg	Q_a cm^3/sec	K cm^2/sec	N_{Re}	f
P.G. 60	81.38	8.90	11.02	537	0.0276	36.8
Graphite,	86.88	18.27	23.2	551	0.0580	18.3
	80.10	6.64	8.18	534	0.0205	49.3
Sample No. K31,	79.31	5.34	6.46	525	0.0162	62.9
	17.28	30.79	8.76	124	0.0232	42.9
Nitrogen,	12.86	23.34	5.05	94	0.0137	72.7
	23.76	41.38	15.7	164	0.0408	24.8
High Pressure	28.52	48.76	21.6	192	0.0556	18.5
Flow Method	34.50	57.75	28.7	216	0.0734	15.0
	49.04	78.17	52.6	292	0.133	8.59
$\mathcal{T}_g$ (av) =	84.95	120.5	121.7	439	0.305	4.27
16.6°C.	70.81	102.9	92.2	389	0.232	5.31
	1.70	3.21	0.14*	19	0.0006	1730
	7.94	14.74	2.08*	61	0.0059	168
	6.04	11.36	1.28*	49	0.0038	260
	24.36	42.53	16.6	169	0.0431	23.4
	44.67	71.95	44.7	269	0.114	9.96
	59.35	90.37	70.7	339	0.178	6.64
	92.59	30.02	38.2	551	0.0955	11.80
	97.72	38.57	51.0	573	0.127	8.98
	103.4	47.67	64.9	590	0.162	7.27
	123.4	52.29	82.2	681	0.205	5.90
	118.9	47.12	71.2	666	0.183	6.84
	107.5	51.89	72.4	614	0.181	6.59
	122.3	72.65	107.9	654	0.269	4.74
	137.6	92.50	142.1	676	0.354	3.91
	150.3	106.7	170.9	704	0.425	3.41
	170.2	126.1	211.1	736	0.525	2.99
	102.2	143.7	158.8	486	0.397	3.61

* Corrected for leakage rate of 0.01 cm^3/sec.

$K_v = 6.6\ p_m + 8.4.$

Comments: Flow-rates were measured by means of the soap-bubble flow-meter (Q_a less than 5 cm^3/sec), the rotameters (Q_a = 5 to 25 cm^3/sec), and the wet gas test meter (Q_a greater than 25 cm^3/sec). Two curved K-p_m plots were obtained, with the plot for p_o near one atmosphere (76.6 to 107.2 cm Hg) being about 110 cm^2/sec (25%) higher at p_m = 80 cm Hg than that when p_o was a vacuum (0.1 to 30.4 cm Hg). As the revolving of the wet gas test meter caused fluctuations in the flow through the sample, the outflow from the permeability cell was restricted. The increasing resistance of the flow lines and meter with increasing flow-rate resulted in the large variation in the values of p_o. At about

p_m = 120 cm Hg, two K-p_m values were 3% higher than the plot; this difference was because p_o for these values was greater than p_o for the value on the line (96 cm Hg cf. 86 cm Hg).

Determination No. H:16

Details	p_m cm Hg	Δp cm Hg	Q_a cm^3/sec	K cm^2/sec	N_{Re}	f
P.G. 60	3.36	6.19	1.15*	81	0.00072	1530
Graphite,	5.26	9.59	2.34	107	0.00119	890
	11.20	19.66	8.01	179	0.00317	330
Sample No. K31,	39.60	47.78	57.5	530	0.0187	55.1
	1.70	3.18	0.47*	64	0.00044	2360
Hydrogen,	1.71	3.19	0.50*	68	0.00047	2100
	3.70	6.84	1.52*	96	0.00092	1050
High Pressure	6.59	12.53	3.81	132	0.00177	546
Flow Method,	10.99	20.55	8.36	177	0.00333	312
	15.61	26.64	14.2	232	0.00523	199
$\mathcal{T}_s$ (av) =	20.33	33.58	21.9	283	0.00769	137
16.4°C.	23.41	37.81	27.2	312	0.00936	116
	30.11	45.83	41.5	393	0.0139	77.2
	49.69	59.63	85.4	624	0.0273	39.1
	40.63	51.26	61.0	518	0.0198	53.9
	56.55	65.78	105.9	701	0.0336	32.0
	60.35	68.97	117.6	743	0.0371	29.0
	69.39	76.48	144.7	841	0.0454	24.4
	81.34	9.08	21.0	1006	0.00652	159
	85.71	17.63	42.4	1046	0.0132	81.1
	89.42	24.77	62.4	1097	0.0193	55.6
	94.32	34.05	89.3	1141	0.0277	38.6
	98.98	42.66	116.5	1188	0.0359	30.0
	103.80	51.38	146.5	1241	0.0451	23.2
	111.50	64.82	194.0	1303	0.0595	18.4

* Corrected for leakage rate of 0.01 cm^3/sec.

$$K_v = 11.7\ p_m + 48.$$

Comments: The soap-bubble flow-meter was used for measuring flow-rates less than 8.0 cm^3/sec, while the wet gastest meter was used for higher flow-rates. The two K-p_m plots for this determination were curved, but not to the same extent as those for Detmn. No. H:15. The plot for p_o about 1 atm (76.9 to 79.1 cm Hg) was about 40 cm^2/sec (4%) higher at p_m = 80 cm Hg than the plot when p_o was a vacuum (0.1 to 31.2 cm Hg). At low p_m (less than 20 cm Hg), the K-p_m values were scattered about the plot by ± 5 cm^2/sec.

Determination No. H:17

Details	p_m cm Hg	Δp cm Hg	Q_a cm^3/sec	K cm^2/sec	N_{Re}	f
P.G. 60	25.40	41.67	17.9	184	0.361	4.16
Graphite,	18.68	34.09	(12.84	(161	0.271	4.75
			(13.15	(165		
Sample No. K31,	13.34	23.35	6.74	124	0.149	8.64
	7.37	13.55	2.59*	82	0.0656	18.7
Freon-12,	5.32	9.84	1.51*	66	0.0424	28.8
	5.30	9.81	1.49*	65	0.0419	29.4
High Pressure	3.51	6.58	0.84*	55	0.0280	41.1
Flow Method,	9.70	17.29	3.68	91	0.0868	15.5
	80.64	8.98	13.10	625	0.245	5.31
$\mathcal{T}_s$ (av) =	88.60	22.60	30.4	577+	0.567	2.72
17.6°C.	36.84	58.20	30.9	228	0.601	2.83
	31.14	50.02	24.7	212	0.487	3.21
	78.47	4.72	6.86	626	0.129	9.90
	13.65	23.91	6.44	116	0.141	9.90
	17.35	29.50	9.76	143	0.206	6.76

* Corrected for leakages rate of 0.01 cm^3/sec.

\+ p_o estimated - apparently too low.

$$K_v = 7.1\ p_m + 29.$$

Comments: Flow-rates were measured with the wet gas test meter for Q_a greater than 6.0 cm^3/sec and with the soap-bubble flow-meter for lower Q_a. The K-p_m plot for p_o about 0 cm Hg was much more curved than similar plots obtained for other determinations on P.G. 60 graphite; the intercept of the plot was about 10 times greater than expected. At p_m = 80 cm Hg, the p_o = 1 atm plot was estimated to be about 300 cm^2/sec (100%) higher than the p_o = 0 cm Hg plot. Because only a limited supply of gas was available from each freon can, and the flow-rate was quite fast, steady state conditions were difficult to maintain, especially at high pressures; this difficulty resulted in the 5% scatter of the points about the plot for p_o about 0 cm Hg and the variation of the points when p_o was near 1 atm.

Determination No. H:18

Details	p_m cm Hg	Δp cm Hg	Q_a cm^3/sec	K cm^2/sec	N_{Re}	f
P.G. 60	3.40	6.39	0.36*	24.7	0.0014	712.0
Graphite,	13.52	24.91	4.43*	77.4	0.0134	74.2
	7.31	13.69	1.43*	45.5	0.0047	211.0
Sample No. K31,	20.61	37.15	(8.95	(104.8	0.0288	34.1
			(9.85	(115.4		
Argon,	32.51	56.41	21.2	164	0.0607	17.7
	41.38	69.89	32.1	200	0.0911	12.1
High Pressure	52.95	86.57	48.7	245	0.1370	8.4
Flow Method,	78.25	2.71	2.57	412	0.0072	138.0
	89.11	23.23	22.8	429	0.0636	17.3
$\mathcal{T}_s$ (av) = 16.40°C.	105.35	50.61	55.1	475	0.1530	7.6

* Corrected for leakage rate of 0.01 cm^3/sec.

$K_v = 5.2\ p_m + 7.1$.

Comments: Flow-rates were measured with the soap-bubble flow-meter for Q_a less than 4.4 cm^3/sec, and with the wet gas test meter for higher Q_a. Two slightly curved K-p_m plots were obtained. The plot for p_o about 1 atm was estimated to be about 75 cm^2/sec (20%) higher at p_m = 80 cm Hg than that when p_o was near 0 cm Hg. The scatter of the K-p_m values about the plots was less than $\pm$ 5 cm^2/sec.

Determination No. H:19

Details	p_m cm Hg	Δp cm Hg	Q_a cm^3/sec	K cm^2/sec	N_{Re}	f
P.G. 60	3.80	7.20	0.60*	42.	0.0017	600
Graphite,	7.67	14.33	2.05*	72	0.0050	206
	16.69	31.10	8.54	143	0.0192	54.0
Sample No. K32,	26.29	45.65	18.9	209	0.0417	26.4
	42.32	69.03	43.1	315	0.0929	12.3
Nitrogen,	62.28	95.05	80.8	429	0.1720	7.1
	86.32	16.15	21.6	675	0.0455	23.6
High Pressure	85.13	16.37	20.6	635	0.0434	25.8
Flow Method,	114.68	63.67	95.8	759	0.2010	8.0
	94.49	34.20	46.7	682	0.0983	11.6
$\mathcal{T}_s$ (av) = 16.6°C.	86.17	19.67	25.2	641	0.0531	21.0

* Corrected for leakage rate of 0.01 cm^3/sec.

$K_v = 7.9\ p_m + 12$.

Comments: The soap-bubble flow-meter, the rotameter, and the wet gas test meter were used to measure the flow-rate. The K-p_m plots were curved. At p_m = 80 cm Hg, the plot for p_o about 1 atm was about 100 cm^3/sec (18%) higher than that for p_o about 0 cm Hg. - - - - - - - -

Determination No. H:20

Acheson "A" Graphite, Sample No. K4,
Nitrogen, High Pressure Flow Method, $\mathcal{T}_s$ (av) = 16.8°C.

Details of this determination are included in Appendix C.5.2 as the type calculation for high pressure flow measurements.

$K_v = 0.130\ p_m \pm 0.37$ (graphically).

Determination No. H:21

Details	p_m cm Hg	Δp cm Hg	Q_a cm^3/sec	K cm^2/sec	N_{Re}	f
Acheson "A"	154.8	158.8	6.84	17.75	0.110	11.0
Graphite,	110.4	218.4	6.88	12.98	0.114	10.7
	193.0	380.1	18.04	19.55	0.288	4.72
Sample No. K2A,	232.0	313.5	17.58	23.10	0.279	4.94
	104.8	59.1	2.03	14.15	0.0339	31.6
Hydrogen,	58.0	115.0	2.40*	8.56	0.0432	24.3

High Pressure	30.8	61.04	0.79*	5.32	0.0162	63.1
Flow Method,	186.1	219.9	10.67	20.16	0.171	7.53
	149.0	294.0	11.76	16.62	0.191	6.64
$\mathcal{T}_s$ (av) =	125.9	99.7	3.76	15.67	0.0620	18.5
16.0°C.	78.8	156.0	4.08	10.88	0.0703	15.4
	93.7	34.8	1.09	13.03	0.0184	57.4
	79.6	6.6	0.18	11.53	0.0031	331
	12.3	24.4	0.18*	3.01	0.0051	202

* Corrected for leakage rate of 0.011 cm^3/sec.

$K_v = 0.125\ p_m + 1.44$ (graphically).

Comments: Flow-rates were measured by means of the soap-bubble flow-meter for Q_a less than 4.0 cm^3/sec, and by the wet gas test meter for higher Q_a. The first two values of K were slightly low probably because the sample was still being purged. Curved K-p_m plots were obtained with the plot for p_o about 76 cm Hg being about 0.6 cm^2/sec (3½%) higher at p_m = 150 cm Hg than the p_o = 0 cm Hg plot. The graph below p_m = 20 cm Hg agreed with that obtained in Detmn. No. L:50.

Determination No. H:22. Continuation of Detmn. No. H:6.

Details	p_m cm Hg	Δp cm Hg	Q_a cm^3/sec	K cm^2/sec x 10^4
$\mathcal{T}_s$ (av) = 24.8°C.	666	1162	0.316	4.94
	443	737	0.151	3.72
	433	716	0.146	3.70
	196	242	0.0394	2.95
	129	106	0.152	2.61
	128	105	0.145	2.51
	473	794	0.178	4.07
	687	1222	0.340	5.06
	538	925	0.220	4.33
	331	511	0.0912	3.24
	253	355	0.0589	3.01
	214	276	0.0489	3.22

$K = 4.24 \times 10^{-7}\ p_m + 1.99 \times 10^{-4}$

Comments: The gas flow-rates were measured by means of soap-bubble flow-meters. The scatter of the K values about the straight K-p_m plot was ± 0.2×10^{-4} cm^2/sec (± 5 to 7%) with the maximum scatter being observed at low p_m where the flow-rate was more difficult to measure. The values of K below p_m = 250 cm Hg were about 0.3×10^{-4} cm^2/sec higher than the K-p_m plot obtained in Detmn. No. H:6 ($K = 5.0 \times 10^{-7}\ p_m + 1.62 \times 10^{-4}$). The K-$p_m$ plots below p_m = 100 cm Hg for Detmns. No. H:6 and No. H:20 were much higher (about 50%) than that obtained for this sample by the low pressure methods (e.g., Detmn. No. L:29).

- - - - - - - -

Determination No. H:23

Details	p_m cm Hg	Δp cm Hg	Q_a cm^3/sec	K cm^2/sec x 10^4
Impregnated Graphite,	474	796	0.455	10.42
Sample No. K42,	398	644	0.337	9.54
Hydrogen,	302	451	0.210	8.49
High Pressure Flow Method,	231	310	0.138	8.11
θ_g (av) = 23.6°C.	241	330	0.151	8.34
	359	565	0.283	9.13
	540	929	0.556	10.91

$$K = 0.917 \times 10^{-6}\ p_m + 5.94 \times 10^{-4}.$$

Comments: A soap-bubble flow-meter was employed to measure the gas flow-rates. The scatter of the values of K about the K-p_m plot was ± 0.2 x 10^{-4} cm^2/sec (± 2 to 3%). The plot below p_m = 150 cm Hg was higher than that obtained for the same sample by the low pressure increase method (Detmn. No. L:55), the intercept values differing by about 40%.

- - - - - - - -

K.4 The Pressure Distribution Measurements

Q_a cm3/sec	Pressure Distrib. cm Hg	$(p_m)_{disc}$ cm Hg	K_{disc} cm^2/sec	Δp_{ov} cm Hg	p_m cm Hg	K_{ov} cm^2/sec	Ideal Distrib. cm Hg
Determination No. G:1							
Acheson "A" Graphite, Specimen No. G1 (order 4 to 1), Nitrogen, T_s (av) = 21.7°C.							
1.33	120.07						120.1
	108.90	114.48	7.41				110.7
	98.76	103.83	8.05	44.17	97.99	7.38	100.4
	87.57	93.17	7.32				88.9
	75.90	81.69	7.03				75.9
		98.29	7.45	av.			
2.20	121.96						122.0
	101.55	111.76	6.66				105.0
	81.50	91.53	6.81	121.21	61.36	4.50	84.8
	55.04	68.27	5.15				58.6
	0.75	27.90	2.52				0.8
		74.86	5.28	av.			
1.02	111.05						111.1
	101.99	106.52	6.92				103.3
	93.90	97.95	7.77	34.97	93.57	7.19	95.0
	85.03	88.47	7.07				86.0
	76.08	80.56	7.03				76.1
		93.37	7.20	av.			
1.99	113.42						113.4
	94.45	103.94	6.41				97.5
	75.81	85.13	6.53	112.75	57.04	4.33	78.7
	51.16	63.48	4.94				54.3
	0.67	25.91	2.42				0.7
		69.62	5.07	av.			
1.23	86.89						86.7
	72.32	79.60	5.18				74.5
	57.85	65.09	5.22	86.44	43.67	3.50	59.9
	38.81	48.33	3.95				41.0
	0.45	19.63	1.97				0.5
		53.16	4.08	av.			
0.835	69.69						69.7
	57.90	63.80	4.32				59.7
	46.21	52.06	4.36	69.31	35.04	2.95	46.9
	30.86	38.54	3.32				32.5
	0.39	15.62	1.68				0.4
		42.50	3.42	av.			
0.555	55.71						55.7
	46.22	50.97	3.61				47.6
	36.73	41.48	3.62	55.39	28.02	2.49	38.0
	24.37	24.55	2.78				25.6
	0.32	12.34	1.43				0.3
		32.33	2.86	av.			

Q_a cm^3/sec	Pressure Distrib. cm Hg	$(p_m)_{disc}$ cm Hg	K_{disc} cm^2/sec	Δp_{ov} cm Hg	p_m cm Hg	K_{ov} cm^2/sec	Ideal Distrib. cm Hg
1.16	97.44						97.4
	85.50	91.47	5.99				87.3
	74.27	79.88	6.36	51.20	71.85	5.60	76.0
	61.21	67.74	5.49				62.8
	46.25	53.73	4.80				46.3
		73.21	5.66	av.			
1.19	120.12						120.1
	110.28	115.20	7.45				111.7
	101.50	105.89	8.35	37.91	101.16	7.74	102.8
	91.87	96.69	7.60				93.1
	82.20	87.04	7.59				82.2
		101.21	7.75	av.			
2.43	144.45						144.5
	125.72	135.08	7.95				128.9
	108.34	117.03	8.59	81.17	103.86	7.35	111.2
	87.61	97.97	7.20				90.3
	63.28	75.44	6.16				63.3
		106.38	7.48	av.			
2.10	118.20						118.2
	98.71	108.46	6.62				101.9
	79.75	89.23	6.80	106.32	65.04	4.85	82.9
	54.89	67.32	5.18				58.2
	11.88	33.38	3.00				11.9
		74.60	5.40	av.			

Determination No. G:2

Acheson "A" Graphite, Specimen No. G1 (order 1 to 4), Nitrogen, $\mathcal{T}_s$ (av) = 20.5°C.

2.17	120.55						120.6
	105.97	113.26	9.19				104.0
	87.46	96.72	7.20	108.43	66.33	4.92	84.6
	64.43	75.95	5.79				59.5
	12.12	38.28	2.55				12.1
		81.05	6.18	av.			
1.43	123.12						123.1
	114.20	118.61	9.90				113.0
	103.86	109.03	8.51	46.88	99.68	7.54	102.1
	92.37	98.11	7.67				90.1
	76.24	84.30	5.45				76.2
		102.51	7.88	av.			
2.29	125.89						125.9
	111.40	118.64	9.71				109.5
	93.21	102.30	7.72	98.32	76.73	5.73	90.3
	70.98	82.09	6.31				66.2
	27.57	49.27	3.24				27.6
		88.08	6.75	av.			

Q_a cm^3/sec	Pressure Distrib. cm Hg	$(p_m)_{disc}$ cm Hg	K_{disc} cm^2/sec	Δp_{ov} cm Hg	p_m cm Hg	K_{ov} cm^2/sec	Ideal Distrib. cm Hg
1.94	125.72						125.7
	113.58	119.65	9.89				111.9
	98.84	106.21	8.11	71.86	89.79	6.68	96.3
	81.48	90.16	6.52				77.9
	53.86	67.67	4.32				53.9
		95.92	7.21	av.			
1.36	125.69						125.7
	117.49	121.59	10.29				116.5
	107.86	112.68	8.74	42.77	104.30	7.88	106.4
	97.37	102.62	8.02				95.3
	82.92	90.14	5.81				82.9
		106.76	8.22	av.			
0.915	71.82						71.8
	62.70	67.26	6.21				61.6
	51.26	56.97	4.94	70.96	36.33	3.19	49.4
	36.83	44.04	3.91				33.6
	0.85	18.84	1.57				0.9
		46.78	4.16	av.			

Determination No. G:3

Acheson "A" Graphite, Specimen No. G1 (order 1 to 4), Carbon Dioxide, θ_s (av) = 22.6°C.

2.25	119.01						119.0
	104.48	111.75	9.62				102.2
	86.10	95.29	7.60	118.19	59.92	4.72	82.1
	63.29	74.70	6.10				56.0
	0.82	32.05	2.24				0.8
		78.45	6.39	av.			
1.45	120.40						120.4
	112.04	116.22	10.72				110.8
	102.26	107.15	9.15	44.05	98.38	8.15	100.6
	91.54	96.90	8.34				89.2
	76.35	83.95	5.89				76.4
		101.06	8.52	av.			
1.58	122.72						122.7
	113.83	118.28	10.87				112.6
	103.38	108.60	9.21	47.36	99.04	8.24	101.5
	91.84	97.61	8.35				89.3
	75.36	83.60	5.84				75.4
		102.02	8.57	av.			
1.86	102.62						102.6
	90.09	96.36	9.10				87.9
	76.83	83.46	8.59	101.93	51.66	4.48	70.4
	54.38	65.60	5.07				47.8
	0.69	27.54	2.12				0.7
		68.24	6.22	av.			

Q_a cm^3/sec	Pressure Distrib. cm Hg	$(p_m)_{disc}$ cm Hg	K_{disc} cm^2/sec	Δp_{ov} cm Hg	p_m cm Hg	K_{ov} cm^2/sec	Ideal Distrib. cm Hg
3.15	166.60						166.6
	149.40	158.00	11.39				148.7
	130.91	140.15	10.57	90.16	121.52	8.66	129.2
	110.02	120.47	9.35				105.9
	76.44	93.23	5.81				76.4
		127.96	9.28	av.			
3.91	165.16						165.2
	143.07	154.12	10.98				140.3
	118.19	130.63	9.72	163.99	83.17	5.91	113.1
	87.53	102.86	7.89				77.9
	1.17	44.35	2.80				1.2
		107.99	7.85	av.			

Determination No. G.4

Morgan "EY9166" Graphite , Specimen No. G21, Nitrogen, $\mathcal{T}_s$ (av) = 29.8°C.

x 10^2			x 10^2			x 10^2	
1.56	168.19						168.2
	152.14	160.17	6.34				149.2
	133.97	143.06	5.65	88.58	123.90	4.56	128.6
	102.39	118.18	3.25				102.9
	79.61	91.00	4.28				79.6
		128.10	4.88	av.			
0.546	59.06						59.1
	50.52	54.79	4.15				46.9
	39.45	44.99	3.23	59.05	29.54	2.39	33.4
	19.39	29.42	1.79				18.1
	0.02	9.70	1.75				0.0
		34.72	2.73	av.			
0.826	133.85						133.9
	122.97	128.41	4.92				121.3
	110.84	116.91	4.45	55.83	105.94	3.82	108.0
	91.37	101.11	2.78				93.6
	78.02	84.69	3.86				78.0
		107.78	4.00	av.			
1.73	136.65						136.7
	117.99	127.32	5.92				111.8
	94.12	106.06	4.66	136.54	68.38	3.22	83.2
	48.32	71.22	2.44				48.5
	0.11	24.21	2.20				0.1
		82.20	3.81	av.			

Q_a cm^3/sec x 10^2	Pressure Distrib. cm Hg	$(p_m)_{disc}$ cm Hg	K_{disc} cm^2/sec x 10^2	Δp_{ov} cm Hg	p_m cm Hg	K_{ov} cm^2/sec x 10^2	Ideal Distrib. cm Hg
Determination No. G:5							
Morgan "EY9166" Graphite, Specimen No. G21, Carbon Dioxide, $\mathcal{T}_s$(av) = 27.0°C.							
1.372	127.96						128.0
	110.66	119.31	5.20				101.7
	88.75	99.70	4.15	127.89	64.02	2.81	72.6
	46.87	67.81	2.18				39.5
	0.07	23.47	1.85				0.1
		77.57	3.35	av.			
0.630	124.93						124.9
	115.43	120.18	4.31				113.7
	104.79	110.11	3.86	48.04	100.91	3.38	102.0
	88.12	96.46	2.48				89.8
	76.89	84.50	3.48				76.9
		102.81	3.53	av.			
0.375	39.75						39.8
	33.70	36.73	4.09				30.4
	26.09	29.89	3.27	39.71	19.89	2.48	20.9
	12.63	19.36	1.86				10.8
	0.04	6.33	1.88				0.0
		23.08	2.78	av.			
Determination No. G:6							
Morgan "EY9166" Graphite, Specimen No. G21, Freon-12, $\mathcal{T}_s$ (av) = 29.3°C.							
0.891	127.17						127.2
	118.00	122.59	6.39				115.8
	107.25	112.62	5.50	49.36	102.49	4.72	103.9
	89.97	98.61	3.43				91.3
	77.81	83.89	4.63				77.8
		104.43	4.99	av.			
0.622	121.79						121.8
	105.99	113.89	2.58				99.3
	86.53	96.26	2.12	121.77	60.91	1.34	73.4
	48.78	67.65	1.10				42.3
	0.02	24.40	0.81				0.0
		75.55	1.65	av.			
0.635	121.93						121.9
	112.51	117.22	4.44				111.7
	102.77	107.64	4.29	44.70	99.58	3.69	100.9
	87.61	95.19	2.76				89.5
	77.23	82.42	3.83				77.2
		100.62	3.83	av.			

Q_a	Pressure Distrib.	$(p_m)_{disc}$	K_{disc}	Δp_{ov}	p_m	K_{ov}	Ideal Distrib.
cm^3/sec	cm Hg	cm Hg	cm^2/sec	cm Hg	cm Hg	cm^2/sec	cm Hg
Determination No. G:7							
P.G. 60 Graphite, Specimen No. G31, Nitrogen, ϑ_s(av) = 26.5°C.							
36.7	112.83						112.8
	105.46	109.14	759				105.1
	98.15	101.80	789				96.6
	88.04	93.10	560	35.68	94.99	639	87.4
	77.15	82.60	529				77.2
		96.66	659	av			
84.9	155.61						155.6
	141.33	148.47	905				140.9
	127.05	134.19	934				124.4
	106.60	116.82	639	73.48	118.86	717	105.3
	82.12	94.36	544				82.1
		123.46	755	av			
108.2	153.81						153.8
	134.68	144.25	861				133.2
	114.09	124.38	826				109.1
	81.40	97.74	510	131.70	87.96	510	78.2
	22.11	51.75	287				22.1
		106.53	621	av.			
98.2	152.97						153.0
	135.79	144.38	871				134.9
	117.78	126.79	856				114.1
	90.62	104.20	558	100.55	102.70	606	88.5
	52.43	71.52	404				52.4
		111.72	672	av.			
67.5	152.99						153.0
	142.31	147.65	964				141.6
	131.39	136.85	994				129.2
	116.43	123.91	696	53.07	126.46	790	115.0
	99.93	108.13	641				99.9
		129.14	824	av.			
Determination No. G:8							
P.G. 60 Graphite, Specimen No. G31, Hydrogen, ϑ_s (av) = 25.4°C.							
189	155.73						155.7
	141.20	148.47	1850				140.5
	126.35	133.78	1870				123.4
	104.89	115.62	1268	76.61	117.42	1430	103.5
	79.12	92.00	1077				79.1
		122.47	1516	av.			
219	151.36						151.4
	133.32	142.34	1848				132.6
	114.42	123.87	1820				110.8
	85.46	99.94	1168	109.10	96.80	1244	83.6
	42.25	63.86	795				42.3
		107.50	1408	av.			

BIBLIOGRAPHY

1. Lockett, E.E., in "Industrial Carbon and Graphite", (Soc. Chem. Ind., London, 1958), p.493.

2. 40-MW(E) Prototype High-Temperature Gas-Cooled Reactor Research and Development Program, Report to Dec. 31st, 1959, U.S.A.E.C. Report No. GA-1235, p.viii.

3. Fortescue, P., Nicoll, D., Rickard, C., and Rose, D., Nucleonics, 18, 86 (1960).

4. Huddle, R.A.U., Arragon, P.A.P., and Price, M.S.T., Nuclear Eng., 5, 314 (1960).

5. Carman, P.C., "Flow of Gases Through Porous Media," (Butterworths, London, 1956).

6. Scheidegger, A.E., "The Physics of Flow Through Porous Media,"(Univ. of Toronto Press,1957).

7. Hader, R.N., Gamson, B.W., and Bailey, B.L., Ind. Eng. Chem., 46, 2 (1954).

8. Currie, L.M., Hamister, V.C., and MacPherson, H.G., in Proc. 1st. Int. Conf. on Peaceful Uses of Atomic Energy, (United Nations, Geneva,1955), 8,451.

9. Davidson, H.W., G.E.C. Atomic Energy Rev., 1,130 (1958).

10. Boyland, D.A., G.E.C. Atomic Energy Rev., 2, 44 (1959).

11. Watt, W., Bickerdike, R.L., Brown, A.R.G., Johnson, W., and Hughes, G., Nuclear Power, 4, no.34, 86 (1959).

12. Anon., Brit. Chem. Eng., 5, 606 (1960).

13. Warner, R.K., Private communication from A.A.E.C., June 8th, 1959.

14. Darcy, H.P.G., Les fountaines publiques de la ville de Dijon, (Victor Dalmont, Paris, 1856) (cited by Carman - ref.5,p.1).

15. Muskat, M., "The Flow of Homogeneous Fluids Through Porous Media,"(McGraw Hill, New York, 1937).

16. Aronofsky, J.S., J.Appl. Phys., 25, 48 (1954).

17. Field, G.J., and Watts, H., Nature, 192, 1277 (1961) (Reprint given in Appendix E.3).

18. Barrer, R.M., Proc. Phys. Soc., 58, 321 (1946).

19. Aronofsky, J.S., and Jenkins, R., in Proc. 1st. U.S. Nat. Congr. Appl. Mech.,(Amer.Soc. Mech.Engrs., New York, 1952), p.763.

20. Jenkins, R., and Aronofsky, J.S., J. Appl. Mech., 20, 210 (1953).

21. Aronofsky, J.S., and Ferris, O.D., J. Appl. Phys., 25, 1289 (1954).

22. Muskat, M., and Botset, H.G., Physics, 1, 27 (1931).

23. Heatherington, C.P., MacRoberts, D.T., and Huntingdon, R.L.,Trans. Amer. Inst. Min. Engrs., 146, 166 (1942).

24. Vetrov, B.M., Petrenko, I.I., and Todes, O.M., Soviet Phys. - Tech. Phys., 4, 930 (1960).

25. Žagar, L., Arch. Eisenhüttenw., 26, 777 (1955).

26. McCabe, W.L., and Smith, J.C., "Unit Operations of Chemical Engineering", (McGraw Hill, New York, 1956), pp.65 to 68.

27. Barrer, R.M., Discuss. Faraday Soc., 3, 61 (1948); J.Phys. Chem., 57, 35 (1953).

28. Purcell, W.R., Trans. Amer. Inst. Min. Engrs., 186, 39 (1949).

29. Burdine, N.T., Gournay, L.S., and Reichertz, P.P., Trans. Amer. Inst. Min. Engrs., 189, 195 (1950).

30. Wyllie, M.R.G., and Spangler, M.B., Bull, Amer. Assoc. Petrol. Geol., 36, 359 (1952).

31. Kozeny, J., Sitzungsber. Akad. Wiss. Wien, Abt IIa, 136, 271 (1927) (cited by Carman - ref.5,p.11).

32. Carman, P.C., Trans. Inst. Chem. Engrs., 15, 150 (1937).

33. Adzumi, H., Bull. Chem. Soc. Japan, 12, 304 (1937).

34. Hutcheon, J.M., Longstaff, B., and Warner, R.K., in "Industrial Carbon and Graphite", (Soc. Chem.Ind., London, 1958),p.259.

35. Fatt, I., Trans. Amer. Inst. Min. Engrs., 207, 144, 160, 164 (1956).

36. Childs, E.C., and Collis-George, N., Proc. Roy. Soc., 201A, 392 (1950).

37. Marshall, T.J., Nature, 180, 664 (1957); J. Soil Sci., 9, 1 (1958).

38. Wyllie, M.R.J., and Gardner, G.H.F., World Oil, 146, 121, 210 (1958).

39. Millington, R.J., and Quirk, J.P., Trans. Faraday Soc., 57, 1200 (1961).

40. Flood, E.A., Tomlinson, R.H., and Leger, A.F., Canad. J. Chem., 30, 372 (1952).

41. Flood, E.A., in "The Structure and Properties of Porous Materials", Eds. Everett, D.H., and Stone, F.S., (Butterworths, London, 1958), p.151.

42. Seldin, E.J., and Mrozowski, S., in Proc. 3rd. Conf. on Carbon, Univ. of Buffalo, 1958, (Pergamon, New York, 1959), p.687.

43. Owen, J.E., Trans. Amer. Inst. Min. Engrs., 195, 169 (1952).

44. Peterson, E.E., Amer. Inst. Chem. Engrs. J., 4, 343 (1958).

45. Derjaguin, B.V., and Bakanov, S.P., Soviet Phys. - Tech. Phys., 2, 1904 (1957).

46. Evans, R.B., Watson, G.M., and Mason, E.A., J. Chem. Phys., 35, 2076 (1961).

47. Emersleben, O., Phys. Z., 26, 601 (1925) (cited by Scheidegger - ref. 6, p.108).

48. Brinkman, H.C., Appl. Sci. Res., Hague, 1A, 27 (1947).

49. Iberall, A.S., J. Res. Nat. Bur. Stand., 45, 398 (1950).

50. Rose, W., Tung, H.C., and Newman, C., J. Phys. Chem., 65, 1440 (1961).

51. Everett, D.H., in "The Structure and Properties of Porous Materials," Eds. Everett, D.H., and Stone, F.S., (Butterworths, London, 1958), p.95.

52. Scheidegger, A.E.,J. Appl. Phys., 25, 994 (1954).

53. Carman, P.C., Discuss. Faraday Soc., 3, 72 (1948).

54. Sullivan, R.R., J. Appl. Phys., 12, 503 (1941).

55. Dallavalle, J.M.,"Micromeritics", (Pitman, New York, 1948), 2nd edition.

56. Arthur, J.R., Linnett, J.W., Raynor, E.J., and Sington, E.P.C., Trans. Faraday Soc., 46, 270 (1950).

57. Ergun, S., Analyt. Chem., 23, 151 (1951).

58. Wyllie, M.R.J., and Rose, W.D., Nature, 165, 972 (1950).

59. Wyllie, M.R.J., and Gregory, A.R., Ind. Eng. Chem., 47, 1379 (1955).

60. Johnson, W.E., and Hughes, R.V., Producers Monthly, 13, no.1,17 (1948) (cited by Scheidegger - ref.6,p.66).

61. Walker, P.L., Rusinko, F., and Raats, E., Nature, 176, 1167 (1955).

62. Klinkenberg, L.J., A.P.I. Drill. Prod. Pract., 200 (1941) (cited by Carman - ref.5,p.69).

63. Schwertz, F.A., J. Appl. Phys., 20, 1070 (1949).

64. Carman, P.C., Proc. Roy. Soc., 203A, 55 (1950).

65. Barrer, R.M., and Grove, D.M., Trans. Faraday Soc., 47, 826 (1951).

66. Kraus, G., Ross, J.W., and Girifaloo, L.A., J. Phys. Chem., 57, 330 (1953).

67. Ash, R., and Grove, D.M., Trans. Faraday Soc., 56, 1357 (1960).

68. O'Neill, J.S., Hey, A.W., and Livey, D.T., J. Nuclear Materials, 3, 125 (1961).

69. Rigden, P.J., J. Soc. Chem. Ind., 66, 130 (1947).

70. Muskat, M., "Physical Principles of Oil Production", (McGraw Hill, New York, 1949), p.126.

71. Flood, E.A., Tomlinson, R.H., and Leger, A.E., Canad. J. Chem., 30, 348 (1952).

72. Arnell, J.C., Canad. J. Res., 24A, 103 (1946); 25A, 191 (1947).

73. Carman, P.C., Nature, 160, 301 (1947).

74. Lea, F.M., and Nurse, R.W., Symp. on Particle Size Analysis, (Inst. Chem. Engrs. and Soc. Chem. Ind., London, 1947), p.47.

75. Carman, P.C., and Arnell, J.C., Canad. J. Res., 26A, 128 (1948).

76. Barrer, R.M., and Strachan, E., Proc. Roy. Soc., 231A, 52 (1955).

77. Carman, P.C., and Malherbe, P. le R., J. Appl. Chem., 1, 105 (1951).

78. Scheidegger, A.E., Geofis. Pura Appl., 30, 17 (1955) (cited by Scheidegger - ref.6, pp.139, 146).

79. Knudsen, M., Ann. Physik, 28, 75 (1909) (cited by Carman - ref.5, p.63).

80. Rutz, L.O., and Kammermeyer, K., U.S.A.E.C. Report No. AECU-3921 (1958).

81. Adzumi, H., Bull. Chem. Soc. Japan, 12, 292 (1937).

82. Barrer, R.M., and Barrie, J.A., Proc. Roy. Soc., 213A, 250 (1952).

83. Gilliland, E.R., Baddour, R.F., and Russell, J.L., Amer. Inst. Chem. Engrs. J., 4, 90 (1958).

84. Kammermeyer, K., and Rutz, L.O., Chem. Eng. Progr. Symp., 55, no.24, 163 (1959).

85. Arnell, J.C., and Henneberry, G.O., Canad. J. Res., 26A, 29 (1948).

86. Dacey, J.R., and Fendley, J.A., in "The Structure and Properties of Porous Materials", Eds., Everett, D.H., and Stone, F.S., (Butterworths, London, 1958), p.142.

87. Berman, A.S., and Lund, L.M., in Proc. 2nd. Int. Conf. on Peaceful Uses of Atomic Energy, (United Nations, Geneva, 1958), 4, 359.

88. Gaede, W., Ann. Physik, 41, 289 (1913).

89. Timofeev, D.P., Russ. Chem. Rev., 29, 180 (1960).

90. Pollard, W.G., and Present, R.D., Phys. Rev., 73, 762 (1948).

91. Eberhardt, W.H., U.S.A.E.C. Report No. K-992 (1953) (cited by Rutz and Kammermeyer - ref.80, p.24).

92. Hiby, J.W., and Pahl, M., Z.Naturforsch., 7a, 542 (1952) (cited by Carman - ref.3,p.67).

93. Hirsch, E.H., J. Appl. Phys., 32, 977 (1961).

94. Monroe, A.E., and Gaffee, D.I., Nature, 178, 197 (1956).

95. Wicke, E., and Vollmer, W., Chem. Eng. Sci., 1, 282 (1952).

96. Amonenko, V.M., and Vasutinsky, B.M., Ukrain. Fiz. Zhur., 6, 263 (1961).

97. Grove, D.M., and Ford, M.G., Nature, 182, 999 (1958).

98. Talaev, M.V., Colloid J. (U.S.S.R.), 22, 699 (1960).

99. Maidanik, G., Trans. Faraday Soc., 56, 118 (1960).

100. Daynes, H.A., Proc. Roy. Soc., 97A, 286 (1920).

101. Barrer, R.M., and Grove, D.M., Trans. Faraday Soc., 47, 837 (1951).

102. Barrer, R.M., and Gabor, T., Proc. Roy. Soc., 251A, 353 (1959).

103. Barrer, R.M., and Gabor, T., Proc. Roy. Soc., 256A, 267 (1960).

104. Barrer, R.M., Trans. Faraday Soc., 36, 1235 (1940).

105. Barrer, R.M., Trans. Faraday Soc., 35, 628, 644 (1939)

106. Kraus, G., and Ross, J.W., J. Phys. Chem., 57, 334 (1953).

107. Carman, P.C., and Raal, F.A., Trans. Faraday Soc., 50, 842 (1954).

108. Frisch, H.L., J.Phys. Chem., 61, 93 (1957); 62, 401 (1958).

109. Frisch, H.L., J.Phys. Chem., 63, 1249 (1959).

110. Fatt, I., J. Petrol. Technol., 11, no.12, (1959). 66

111. Goodknight, R.C., Klikoff, W.A., and Fatt, I., J.Phys. Chem., 64, 1162 (1960).

112. Goodknight, R.C., and Fatt, I., J. Phys. Chem., 65, 1709 (1961).

113. Carman, P.C., and Raal, F.A., Proc. Roy. Soc., 209A, 38 (1951).

114. Babbitt, J.D., Canad. J. Res., 28A, 449 (1950).

115. Wicke, E., and Voigt, U., Angew. Chem., B19, 94 (1947).

116. Tomlinson, R.H., and Flood, E.A., Canad. J. Res., 26B, 38 (1948).

117. Carman, P.C., Nature, 163, 684 (1949).

118. Carman, P.C., and Malherbe, P. le R., Proc. Roy. Soc., 203A, 165 (1950).

119. Maggs, F.A.P., Schwabe, P.H., and Williams, J.H., Nature, 186, 956 (1960).

120. Jones, W.M., Trans. Faraday Soc., 47, 381 (1951).

121. Ross, J.W., and Good, R.J., J. Phys. Chem., 60, 1167 (1956).

122. Carman, P.C., Proc. Roy. Soc., A211, 526 (1952).

123. Rutz, L.O., and Kammermeyer, K., U.S.A.E.C. Report No. AECU-4328 (1959).

124. Rutz, L.O., and Kammermeyer, K., Ref. 80, p.56.

125. Cornell, D., and Katz, D.L., Ind. Eng. Chem., 45, 2145 (1953).

126. Green, L., and Duwez, P., J. Appl. Mech., 18, 39 (1951).

127. Bakhmeteff, B.A., and Feodoroff, N.V., J. Appl. Mech., 4, A97 (1937).

128. Lapple, C.E., Chem. Eng. Progr., 43, 544 (1947).

129. Forchheimer, P., Z. Ver. dtsch. Ing., 45, 1782 (1901) (cited by Scheidegger - ref.6,p.127).

130. Lindquist, E., Proc. Premier Congrés Grandes Barrages, Stockholm, 5, 81 (1933) (cited by Scheidegger - ref.6,p.128).

131. Ergun, S., and Orning, A.A., Ind. Eng. Chem., 41, 1179 (1949).

132. Greenberg, D.B., and Weger, E., Chem. Eng. Sci., 12, 8 (1960).

133. Ergun, S., Chem. Eng. Progr., 48, 89 (1952); Ind. Eng. Chem., 45, 477 (1953).

134. Wagstaff, J.B., and Nirmaier, E.A., Ind. Eng. Chem., 47, 1129 (1955).

135. Smith, K.L., and Roper, G.H., Austral. J. Chem. Engrs., 1, no.4, 5 (1960).

136. Chilton, T.H., and Colburn, A.P., Ind. Eng. Chem., 23, 913 (1931).

137. Brownell, L.E., and Katz, D.L., Chem. Eng. Progr., 43, 537 (1947); Brownell, L.E., Dombrowski, H.S., and Dickey, C.A., Chem. Eng. Progr., 46, 415 (1950).

138. Leva, M., Chem. Eng. Progr., 43, 549 (1947); Leva, M., and Grummer, M., Chem. Eng. Progr., 43, 633, 713 (1947).

139. Rose, H.E., and Rizk, A.M., Proc. Inst. Mech. Engrs., 160, 493 (1949).

140. Hudson, H.E., and Roberts, R.E., Proc. 2nd. Midwestern Conf. on Fluid Mechanics (1952) in Ohio State Univ. Eng. Series 31, no.3,p.105.

141. Leva, M., Weintraub, M., Grummer, M., Pollchik, M., and Storch, H.H.,U.S. Bur. Min. Bull. no. 504 (1951).

142. Blake, F.C., Trans. Amer. Inst. Chem. Engrs., 14, 415 (1922).

143. Burke, S.P., and Plummer, W.B., Ind. Eng. Chem., 20, 1196 (1928).

144. Brownell, L.E., Gami, D.C., Miller, R.A., and Nekarvis, W.F., Amer. Inst. Chem. Engrs. J., 2, 79 (1956).

145. MacMullin, R.B., and Muccini, G.A., Amer. Inst. Chem. Engrs. J., 2, 393 (1956).

146. Stutzman, L.F., and Thodos, G., J. Petrol. Technol., 8, no.11, 59 (1956).

147. Katz, D.L., and Cornell, D., "Flow of Natural Gas from Reservoirs", College of Eng., Univ. of Michigan (1955) (cited by Stutzman and Thodos - ref.146).

148. Rose, H.E., Proc. Inst. Mech. Engrs., 153, 141, 148, 154 (1945).

149. Grootenhuis, P., J. Appl. Mech., 18, 426 (1951).

150. Lindsay, R.B., in "American Institute of Physics Handbook", Ed. Gray, D.E., (McGraw Hill, New York, 1957), p.2-207.

151. Barr, G., J. Sci. Instr., 11, 321 (1934).

152. Wall, G.C., A.A.E.C. Report No. AAEC/E73 (1961).

153. Carlson, A.J., and Eastman, M.C., Petrol. Technol., 3, no.2, T.P. 1196 (May 1940).

154. Carman, P.C., and Malherbe, P. le R., J. Soc. Chem. Ind., 69, 134 (1950).

155. Hodgins, J.W., Flood, E.A., and Dacey, J.R., Canad. J. Res., 24B, 167 (1946).

156. Leiby, C.C., and Chen, C.L., J. Appl. Phys., 31, 268 (1960).

157. Ward, W.T., and Smith, N.V., in Gas-Cooled Reactor Project Quarterly Progress Report to Dec. 31st, 1960, U.S.A.E.C. Report No. ORNL-3049, p.297.

158. Rigden, P.J., J. Soc. Chem. Ind., 62, 1 (1943).

159. Blaine, R.L., Amer. Soc. Testing Materials Bull. no. 123, 51 (1943).

160. Whiteway, S.G. Amer. Ceram. Soc. Bull., 39, 677 (1960).

161. Davies, L.J., and Booth, H., Amer. Ceram. Soc. Bull., 40, 744 (1961).

162. Žagar, L., Arch. Eisenhüttenw., 27, 657 (1956).

163. Wheeler, A., Catalysis, 2, 105 (1955).

164. Wall, G.C., A.A.E.C. Report No. AAEC/TM 86 (1961).

165. Schumb, W.C., and Rittner, E.S., J. Amer. Chem. Soc., 65, 1692 (1943).

166. Smith, J.W., Chem. and Ind., no.28, 885 (1958).

167. Howard, H.C., and Hulett, G.A., J. Phys. Chem., 28, 1082 (1924).

168. Ubbelohde, A.R., and Lewis, F.A., "Graphite and its Crystal Compounds", (Oxford Univ. Press, London, 1960), pp.37,38.

169. Roberts, L.E.J., Harper, E.A., and Small, C.T., U.K.A.E.A. (Harwell) Report No. AERE C/R 882 (1958).

170. Connor, P., Ind. Chemist, 37, 178, 224 (1961).

171. Emmett, P.H., J. Phys. Chem., 63, 449 (1959).

172. Brunauer, S., Emmett, P.H., and Teller, E., J. Amer. Chem. Soc., 60, 309 (1938).

173. Brunauer, S., Deming, L.S., Deming, W.E., and Teller, E., J. Amer. Chem. Soc., 62, 1723 (1940).

174. Harkins, W.D., and Jura, G., J. Amer. Chem. Soc., 66, 1366 (1944).

175. Harkins, W.D., "The Physical Chemistry of Surface Films", (Reinhold, New York, 1952), pp. 228 to 231.

176. Brunauer, S., "The Adsorption of Gases and Vapours", Vol.I,(Oxford Univ. Press, London, 1943), p.150.

177. Emmett, P.H., and Brunauer, S., J. Amer. Chem. Soc., 59, 1553 (1937).

178. Haul, R.A.W., Angew. Chem., 68, 238 (1956).

179. Rosenberg, A.J., J. Amer. Chem. Soc., 78, 2929 (1956).

180. Beebe, R.A., Beckwith, J.B., and Honig, J.M., J. Amer. Chem. Soc., 67, 1554 (1945).

181. Bloecher, F.W., Mining Eng., 3, 255 (1951).

182. Gulbransen, E.A., and Andrew, K.F., Ind. Eng. Chem., 44, 1039 (1952).

183. Kington, G.L., and Holmes, J.M., Trans. Faraday Soc., 49, 417 (1953).

184. McDermot, H.L., and Lawton, B.E., Canad. J. Chem., 37, 54 (1959).

185. Sing, K.S.W., and Swallow, D., J. Appl. Chem., 10, 171 (1960).

186. Meihuitzen, J.J., and Crommelin, C.A., Physica, 4, 1 (1937).

187. Haynes, J.M., J. Phys. Chem., 66, 182 (1962).

188. Gaines, G.L., and Cannon, P., J. Phys. Chem., 64, 997 (1960).

189. Malden, P.J., and Marsh, J.D.F., J. Phys. Chem., 63, 1309 (1959).

190. Thomas, J., Nature, 189, 134 (1961).

191. Cannon, P., and Gaines, G.L., Nature, 190, 340 (1961).

192. Mathews, D.H., J. Appl. Chem., 7, 610 (1957).

193. Brooks, C.S., and Purcell, W.R., Trans. Amer. Inst. Min. Engrs., 195, 289 (1952).

194. Ritter, H.L., and Drake, L.C., Ind. Eng. Chem., Analyt., 17, 782 (1945).

195. Faris, S.R., Gournay, L.S., Lipson, L.B., and Webb, T.S., Bull. Amer. Assoc. Petrol. Geol., 38, 2226 (1954); 39, 268 (1955).

196. Wiggs, P.K.C., in "Industrial Carbon and Graphite", (Soc. Chem. Ind., London,1958), p.252.

197. Wiggs, P.K.C., in "The Structure and Properties of Porous Materials," Eds. Everett, D.H., and Stone, F.S., (Butterworths, London, 1958), p.183.

198. Henderson, J.H., Producers Monthly, 14, no.1,32 (1949) (cited by Scheidegger - ref.6,p.99).

199. Washburn, E.W., Proc. Nat. Acad. Sci. U.S.A., 7, 115 (1921).

200. Drake, L.C., and Ritter, H.L., Ind. Eng. Chem., Analyt., 17, 787 (1945).

201. Drake, L.C., Ind. Eng. Chem., 41, 780 (1949).

202. Cameron, A., and Stacy, W.O., Austral. J. Appl. Sci., 9, 283 (1958).

203. Thurstan, E.G., and Wall, G.C., A.A.E.C. Report No. AAEC/TM85 (1961).

204. Joyner, L.G., Barrett, E.P., and Skold, R., J. Amer. Chem. Soc., 73, 3155 (1951).

205. Meyer, H.I., J. Appl. Phys., 24, 510 (1953).

206. Ingles, O.G., Austral. J. Appl. Sci., 9, 120 (1958).

207. Cameron, A., and Stacy, W.O., Chem. and Ind., no.9, 222 (1960).

208. Carman, P.C., Proc. Roy. Soc., 209A, 69 (1951).

209. Barrett, E.P., Joyner, L.G., and Halenda, P.P., J. Amer. Chem. Soc., 73, 373 (1951).

210. Derjaguin, B.V., in Proc. 2nd. Int. Congr. on Surface Activity, (Butterworths, London, 1957), 2, 153.

211. Cochran, C.N., and Cosgrove, L.A., J.Phys. Chem., 61, 1417 (1957).

212. Rose, W., and Bruce, W.A., Trans. Amer. Inst. Min. Engrs., 186, 127 (1949).

213. Winsauer, W.O., Shearin, H.M., Masson, P.M., and Williams, M., Bull. Amer. Assoc. Petrol. Geol., 36, 253 (1952).

214. Wyllie, M.R.G., and Rose, W.D., Trans. Amer. Inst. Min. Engrs., 189, 105 (1950).

215. Hoogschagen, J., Ind. Eng. Chem., 47, 906 (1955).

216. Hedley, W.H., "Diffusion of Gases Through Porous Media," D.Sc. Thesis, Washington Univ., 1957.

217. Archie, G.E., Trans. Amer. Inst. Min. Engrs., 146, 54 (1942).

218. Wyllie, M.R.J., and Gregory, A.R., Trans. Amer. Inst. Min. Engrs., 198, 103 (1953).

219. Klinkenberg, L.J., Bull. Geol. Soc. Amer., 62, 559 (1951)

220. Penman, H.L., J. Agric. Sci., 30, 437, 570 (1940).

221. Piret, E.L., Ebel, R.A., Kiang, C.T., and Armstrong, W.P. Chem. Eng. Progr., 47, 405 (1951).

222. Michaels, A.S., Amer. Inst. Chem. Engrs. J., 5, 270 (1959).

223. Street, N., Austral. J. Chem., 11, 607 (1958).

224. Perkins, F.M., Osoba, J.S., and Ribe, K.H., Geophysics, 21,1071 (1956).

225. Wyllie, M.R.J., Bull. Amer. Assoc. Petrol. Geol., 39, 266 (1955).

226. Lorenz, P.B., Nature, 189, 386 (1961).

227. Rust, C.F., Trans. Amer. Inst. Min. Engrs., 195, 217 (1952).

228. Dunlap, H.F., Bilhartz, H.L., Shuler, E., and Bailey, C.R., Trans. Amer. Inst. Min. Engrs., 186, 259 (1949).

229. Patnode, H.W., and Wyllie, M.R.J., Trans. Amer. Inst. Min. Engrs., 189, 47 (1950).

230. Wyllie, M.R.J., and Southwick, P.F., J. Petrol. Technol., 6, no.2, 44 (1954).

231. Sauer, M.C., Southwick, P.F., Spiegler, K.S., and Wyllie, M.R.J., Ind. Eng. Chem., 47, 2187 (1955).

232. Stender, V.V., and Ksenzhek, O.S., J. Appl. Chem. (U.S.S.R.), 32, 111 (1959).

233. Denholm, W.T., Field, G.J., and Watts, H., Paper to be published in Austral. J. Appl. Sci.

234. Mickley, H.S., Sherwood, T.K., and Reed, C.E., "Applied Mathematics in Chemical Engineering," (McGraw Hill, New York, 1957), 2nd edition, p.25.

235. Gilmont, R., Analyt. Chem., 23, 157 (1951).

236. Culver, R.V., "Activation and Adsorption Studies on Saran Charcoals", Ph D. Thesis, Univ. of Adelaide, 1954.

237. Ward, D.H., "The Properties of Lead Blast Furnace Sinters: Surface Area and Reducibility Studies", M.E.Thesis, Univ. of Adelaide, 1959.

238. Joyner, L.G., in "Scientific and Industrial Glass Blowing and Laboratory Techniques", Eds. Barr, W.E., and Anhorn, V.J., (Instruments Publ. Co., Pittsburgh, 1949), p.276.

239. Yost, D.M., and Russell, H., "Systematic Inorganic Chemistry of the Fifth- and- Sixth- Group Non-Metallic Elements", (Prentice Hall Inc., New York, 1946), p.258.

240. Brown, H.R., Private communication from Division of Coal Research, C.S.I.R.O., reference M.156 (July, 1959).

241. Wall, G.C., Private communication from A.A.E.C., June 22nd, 1961.

242. Eusner, G.R., and Shapland, J.T., J. Amer. Ceram. Soc., 42, 459 (1959).

243. Truitt, J., Evans, R.B., Smith, N.V., and Watson, G.M., in Reactor Chemistry Progress Report to Jan.31st, 1960, U.S.A.E.C. Report No. ORNL-2931, p.149.

244. Wall, G.C., Private communication from A.A.E.C., June 6th, 1961.

245. Backofen, W.A., J. Metals, 13, 206 (1961).

246. Hill, R., "The Mathematical Theory of Plasticity", (Oxford Univ. Press, London, 1960), p.317.

247. Wallick, G.C., J. Petrol. Technol., 5, no.11, 20 (1953).

248. Calhoun, J.C., and Yuster, S.T., A.P.I. Drill. and Prod. Pract., 335 (1946) (cited by Wallick - ref.247).

249. DeBoer, J.H., "The Dynamical Character of Adsorption", (Oxford Univ. Press, London, 1953), p.35.

250. Perry, J.H., "Chemical Engineers' Handbook", Ed. Perry, J.H., (McGraw Hill, New York, 1950), 3rd edition, p.261.

251. Loeb, L.B., "Kinetic Theory of Gases", (McGraw Hill, New York, 1927), 1st edition, p.187.

252. Chapman, S., and Cowling, T.G., "The Mathematical Theory of Non-uniform Gases", (Cambridge Univ. Press, London, 1939), p.102.

253. De Marcus, W.C., U.S.A.E.C. Report No. K-1302, pt.IV (1956).

254. Lassettre, E.N., U.S.A.E.C. Report No. K-1258 (1956).

255. Wall, G.C., Private communication from A.A.E.C., April 6th, 1960.

256. Barnes, C., Physics, 5, 4 (1934).

257. Barrer, R.M., "Diffusion in and through Solids," (Cambridge Univ. Press, London, 1951).

258. Jaeger, J.C., J. Proc. Roy. Soc. New South Wales, 74, 342 (1940).

259. Call, F., J. Appl. Chem., 6, 298 (1956).

260. Barrer, R.M., Brit. J. Appl. Phys., Suppl. no.3, S41 (1954).

261. Jones, W.M., and Isaac, P.J., Trans. Faraday Soc., 55, 1947 (1959).

262. Biram, J.G., Nature, 187, 865 (1960).

263. Dresel, E.M., and Roberts, L.E.J., Nature, 171, 170 (1953).

264. Stone, F.S., and Tiley, P.F., Nature, 167, 654 (1951).

265. Warner, R.K., Private communication from A.A.E.C.,
(a) June 26th, 1958;
(b) August 6th, 1958;
(c) May 27th, 1960.

266. Benning, A.F., and Markwood, W.H., Refrig. Eng., 37, 243 (1939).

267. "Handbook of Chemistry and Physics", Ed. Hodgman, C.D., (Chemical Rubber Publ. Co., Cleveland, Ohio, 1953), 35th edition, p.2363.

GLOSSARY OF SYMBOLS

a	a constant; a constant in the permeability equation (2.1.4-1), i.e., the intercept of the K_v-p_m plot on the K-axis.
A	a constant.
A	cross-sectional area; cross-sectional area of a porous medium to flow (A_i, A_o) (also A_1, A_2).
A_p	cross-sectional area of a pore.
b	a constant in the equation of state (2.1.1-4).
b	a constant in the permeability equation (2.1.4-1), i.e., the slope of the K_v-p_m plot.
B	a constant.
B	mass permeability coefficient.
B_o	viscous flow permeability coefficient in cm^2 (B_{on}, B_{ox}, B_{oy}).
B_1	volume permeability coefficient.
c	a constant (also c_1, c_2, c_3, c_4, c_5, c_6).
c	variable factor ($= 1 + b\beta G$).
c	concentration of gas or adsorbate per unit bulk volume of a porous medium (c_g, c_i, c_s).
Δc	concentration difference across a porous medium.
C	a constant; a constant in the B.E.T. equation (2.3.2-1).
C	constriction factor of Owen[43].
C	concentration of gas in moles per unit volume of the gas phase.
C_c	cell constant of the conductivity cell.
d	differential operator.
d	variable factor ($= a\beta G$).

d	diameter (d_o); diameter associated with a porous medium or pore diameter.
d	diameter of a graphite sample (d_1, d_o).
d_p	external diameter of a particle.
D	a constant.
D	diffusion coefficient (D_{gs}, D_{gt}, D_{ss}, D_{st}, D_t, D_s - e.g., D_{gs} is the gas phase diffusion coefficient for steady state flow).
D'	effective diffusion coefficient or diffusion coefficient in an actual porous medium ($= D/\tau^2$).
D_b	diffusion coefficient of a gas in the bulk phase.
D_e	effective or apparent diffusion coefficient of a gas diffusing through a porous medium.
D_{go}	gas phase diffusion coefficient for the capillary pore model.
D_o	diffusion coefficient at $\varepsilon = 0$.
D(r)	pore size distribution function ($D(r_1)$).
e	exponential function.
ΔE	potential drop across a porous sample saturated with electrolyte.
E_a	heat of adsorption of a gas on a solid.
E_d	decomposition potential of a graphite/electrolyte half cell.
E_o	a constant in Adzumi's equation (2.1.4-5).[33]
f	friction factor; friction factor of Green and Duwez.[126]
f', f"	modified friction factors.
f_1	fraction of gas molecules diffusely reflected at capillary or pore walls.

F	electrical formation factor or formation resistivity factor of a porous medium ($= q / \varepsilon$).
F_f	empirical correction factor of Brownell[137] for f.
F_{Re}	empirical correction factor of Brownell[137] for N_{Re}.
F_o	a constant in Adzumi's equation (2.1.4-5).[33]
g	gravitational acceleration.
g_o	gravitational conversion factor.
G	mass rate of flow in g/cm^2, sec (G_o).
h	a constant.
h_1, h_2	measured heights in the McLeod gauge.
H	adsorption coefficient ($= \partial C_s / \partial C_g$).
I	current flow.
k	Kozeny constant for viscous flow ($= k_o \tau^2$).
k'	complex shape factor for slip or Knudsen flow ($= k_1 \tau^2$).
k_o	shape factor for viscous flow (k_{ox}, k_{oy}).
k_s	Henry's law constant.
k_1, k_2	empirical constants of Cornell and Katz.[125]
k_1	shape factor for slip or Knudsen flow.
K	permeability coefficient in cm^2/sec (K_g, K_s, K_{av}, K_{disc}, K_{ov}).
K_a	apparent permeability coefficient.
K_i	actual intercept of the K-p_m plot on the K-axis.
K_k	permeability coefficient for steady state Knudsen flow (= a).
K_o	specific permeability coefficient for slip or Knudsen flow.

K_t	permeability coefficient for turbulent flow ($= p_m/\beta G$).
K_v	permeability coefficient for viscous-slip flow ($= a + bp_m$).
l	a constant ($= Z\beta B_o$).
l	length of a graphite sample.
L	length (L_o); geometric length of a porous medium in the flow direction.
L_p	average length of a flow path through a porous medium.
m	a constant in the equation of state (2.1.1-4); a constant ($= YZAa\beta/L$).
m	hydraulic radius (m_g, m_x, m_y); mean hydraulic radius of a pore ($2\varepsilon/S_v$).
m	cementation factor.
M	molecular weight of a gas.
n	an exponent; a constant ($= 1/YZ\beta$).
n	number of capillaries of radius r per unit area of cross-section.
n	number of equal fractions of the total pore volume.
N	distribution function of Flood.[41]
N_{Ku}	Knudsen number ($= \lambda/d$).
N_L	Avogadro's number ($= 6.023 \times 10^{23}$ mol/g-mol).
N_{Re}	Reynolds number; Reynolds number of Green and Duwez.[126]
N_{Re}', N_{Re}''	modified Reynolds numbers.
p	pressure of gas (p_a, p_i, p_m, $(p_m)_{av}$, p_o).
Δp	pressure difference across a porous medium (Δp_{ov}).

p_a atmospheric pressure or pressure in a flow-meter.

p_c capillary pressure of liquid in a capillary or pore ($= 2\gamma \cos\theta/r$) (p_{ci}).

p_g measured gauge pressure.

$(p_m)_{min.}$ mean pressure corresponding to the minimum in the K-p_m plot.

p_N gas pressure at any point N in a porous medium.

p_{vi} vapour pressure at a liquid-vapour meniscus in pores of radius r_i.

$p_{½}$ gas pressure at $x/L = 1/2$ in a porous medium.

P constriction or convergence factor (P_d, P_e, P_p refer to diffusion, electrical resistivity, and permeability measurements, respectively).

P_o saturation vapour pressure of an adsorbate.

q electrical tortuosity factor (q_x, q_y).

Q volumetric flow-rate in cm^3/sec (Q_a, Q_c, Q_m, Q_{mc}).

Q' measured flow-rate through a rotameter.

r radius of a pore (r_i, r_m) (also r_1, r_2, r_3, ... r_m).

R resistivity of a porous medium saturated with electrolyte.

R' resistance of a saturated porous medium ($= R(L/A)$).

R_o resistivity or specific resistance of an electrolyte.

R_o' resistance of an electrolyte ($= R_o(L/A)$).

R_s' measured resistance of the electrolyte.

$\mathcal{R}$ universal gas constant.

s_i degree of saturation of pores of radius $\geqslant r_i$.

S	internal surface area of a porous medium (S_t, S_g).
S_g	internal surface area per unit weight of a porous medium.
S_o	specific surface or internal surface area per unit volume of the solid material of a porous medium.
S_v	internal surface area per unit bulk volume of a porous medium.
t	time.
Δt	time of a sample.
T	tortuosity of a porous medium ($= (L_p/L)^2$).
$\mathcal{T}$	absolute temperature of a gas ($\mathcal{T}_a$) ($\mathcal{T}_s$, $\mathcal{T}_b$ are temperatures of portions of the helium displacement apparatus).
$\mathcal{T}_s$	temperature at the sample.
v	superficial linear velocity of gas flow.
$\bar{v}$	mean thermal molecular velocity of a gas ($= \sqrt{(8\mathcal{R}\mathcal{T}/\pi M)}$).
V	volume (V_1, V_2) (V_a, V_b, V_p, V_r, V_s, V_1, V_2 are volumes of portions of the helium displacement and surface area apparatus).
V	volume of gas adsorbed by a porous medium at pressure p.
V_c	volume of flow channels in a porous medium.
V_{Hg}	volume of mercury.
V_m	monolayer capacity or the volume of adsorbate required to give a uni-molecular layer on the surface of an adsorbent.
V_p	volume of the pore space in the porous medium (V_{pi}).
V_s	volume of the solid material of a porous sample.

V_t total or bulk volume of a porous medium.

V_v volume of the dead-end pore space in a porous medium.

V_w volume of water vapour in a gas.

$V(r_1)$ cumulative pore volume of pores of radius $\geq r_1$.

$\mathcal{V}$ molar volume of a gas (= 22.4 x 10^3 cm^3/g-mol).

w weight of a porous sample.

x length coordinate.

X calibration constant of the capillary flow-meter.

y concentration in adsorbed phase per unit weight of adsorbent (= ϵ_g/ρ_b) (y_1).

Y a factor (= $L\mu/(Ag_c\rho_{Hg})$).

z compressibility factor (= 1.0).

Z a factor (= $\rho_g/(\mu A)$).

Greek Letters

α parameter of Flood.[41]

α (= λ_w/λ_g).

α viscous resistance coefficient (= $1/B_o$).

α_E viscous flow parameter in Ergun's equation (2.1.7-5).[133]

β inertial resistance coefficient.

β_E kinetic energy parameter in Ergun's equation (2.1.7-5).[133]

β_1, β_2 roughness and shape factors for inertial flow in a porous medium.

γ parameter of Flood.[41]

γ surface tension at a gas-liquid interface.

δ	a small increment.
σ	a dimensionless parameter allowing for the proportion of diffuse to specular reflections of gas molecules at capillary or pore walls.
δ_l	dimensionless parameter corresponding to slip flow.
δ_o	dimensionless parameter corresponding to Knudsen flow.
Δ	a finite difference (e.g., Δe, ΔE, Δp, Δt).
ε	porosity of a porous medium (ε_i, ε_s, ε_t, ε_x, ε_y).
$\varepsilon(r_i)$	cumulative porosity for pores of radius $\geq r_i$.
η	factor ($= \varepsilon_g S_v / \varepsilon S_s$).
θ	angle of contact.
θ	average angle which flow paths make with overall direction of flow.
κ	structure factor (κ_g, κ_{gs}, κ_{gt}, κ_s, κ_{ss}, κ_{st}).
κ_l	structure factor for slip flow ($= \delta_l / k'$).
κ_o	structure factor for Knudsen flow ($= \delta_o / k'$).
λ	mean free path of a gas molecule.
λ_g	mean free path of a gas molecule at p_m.
λ_w	mean free path of a gas molecule between collisions with the pore walls.
μ	viscosity of a gas.
μ'	apparent viscosity of a gas.
π	numerical constant (= 3.1416).
ρ	density of a gas (ρ_m).
ρ_b	bulk density of a porous medium.

ρ_c	theoretical density of solid graphite crystallites.
ρ_{Hg}	density of mercury at $\mathcal{T}_s$.
ρ_l	density of a liquid.
ρ_o	density of a gas at unit pressure (= $M/(z\mathcal{R}\mathcal{T})$).
ρ_s	helium density or density of the solid material of a porous medium.
σ	cross-sectional area of an adsorbate molecule (e.g., σ_{N_2}, σ_{Kr} refer to the nitrogen and krypton molecules).
Σ	summation sign.
τ	permeability tortuosity factor (τ_1).
$\uparrow$	time of residence of adsorbed molecules at a surface.
τ_o	period of atomic vibrations of a solid lattice.
ϕ	time-lag or intercept of the straight portion of the p_o-t plot on the t-axis.
ϕ_i	actual intercept of the ϕ-p_m plot on the ϕ-axis.
ϕ_o	intercept of the extrapolated straight portion of the ϕ-p_m on the ϕ-axis.
Φ	"function of".
χ	diffusion tortuosity factor (= ε/ψ).
ψ	diffusibility (= D_e/D_b).
∂	partial differential operator.

Subscripts

a	measured quantity at ambient conditions (e.g., p_a, Q_a, $\mathcal{T}_a$).
c	property for a capillary or tube (e.g., d_c, D_{gc}, G_c, L_c, m_c, Q_c, Q_{mc}).

g	property for the gas phase (e.g., θ_g, D_{go}, D_{gs}, D_{gt}, K_g, $\mathcal{K}_g$, $\mathcal{K}_{gs}$, $\mathcal{K}_{gt}$).
i	property referring to the inlet side of the sample (e.g., θ_i, P_i, V_i, y_i).
i	internal dimension of the hollow cylindrical sample (e.g., A_i, d_i).
i	refers to the set of pores i (e.g., $D(r_i)$, p_{oi}, p_{vi}, r_i, V_{pi}, ε_i, τ_i).
m	property at the mean pressure p_m and temperature $\mathcal{T}_s$ in a porous medium (e.g., Q_m, Q_{mo}, ρ_m).
m	mean value of a property (e.g., P_m, r_m).
n	property in the n-direction (e.g., B_{on}).
o	property referring to the outlet side of the sample (e.g., P_o, V_o).
o	external dimension of the hollow cylindrical sample (e.g., A_o, d_o).
s	property for the adsorbed or surface phase (e.g., θ_s, D_{ss}, D_{st}, K_s, $\mathcal{K}_s$, $\mathcal{K}_{ss}$, $\mathcal{K}_{st}$).
s	property for steady state flow conditions (e.g., D_s, D_{gs}, D_{ss}, S_s, $\mathcal{K}_{gs}$, $\mathcal{K}_s$, $\mathcal{K}_{ss}$).
t	property for transient flow conditions (e.g., D_{gt}, D_{st}, D_t, S_t, $\mathcal{K}_{gt}$, $\mathcal{K}_{st}$, $\mathcal{K}_t$).
x	property in the x-direction (e.g., B_{ox}, k_{ox}, m_x, q_x, $\mathcal{E}_x$).
y	property in the y-direction (e.g., B_{oy}, k_{oy}, m_y, q_y, $\mathcal{E}_y$).
av	property averaged for the discs in a pressure distribution specimen (e.g., K_{av}, $(p_m)_{av}$).
disc	property of a disc in a pressure distribution specimen (e.g., K_{disc}).
ov	property for the overall pressure distribution specimen (e.g., K_{ov}, Δp_{ov}).